with saturated clay, which is more difficult. The strain path (b) is essentially the same as in Fig. 1.1b for stages 0 - 1 - 2, practically volume-conserving during a rapid wall rotation 2 - 3 - 4, and accompanied by volume changes during a subsequent fully drained slow rotation. The stress path (c) deviates, with the onset of wall rotation, from σ_1 = const until the excess pore pressure is fully dissipated. In the active case, the pore pressure decreases so that σ_1 increases; the opposite happens in the passive case. A volume increase (4 - 5) is accompanied by an increase of σ_2 in the active case, and a volume decrease with σ_2-increase in the passive case. Close to the limiting states (4) narrow shear zones arise. Delays reveal a marked influence of pore-water flow and viscosity of the grain skeleton.

A bearing capacity problem with dry sand is represented by Fig. 1.4. It is helpful to consider at lease one soil element under the centre of a strip foundation (A) and one under the neighboured free surface (B). Sedimentation and unloading by erosion are the same for A and B, the paths corresponding to Fig. 1.1. The strains (b) due to strip loading are first contractant, later dilatant. The stress paths (c) tend towards limiting states earlier in A than in B. For equilibrium reasons σ_1 is nearly constant in B and σ_2 is roughly equal in A and B. In strain space A corresponds to the active and B to the passive case of Fig. 1.2. Narrow shear zones occur in the vicinity of limit states (4).

Fig. 1.5 shows the corresponding problem with saturated clay. After uniform precompression the strains (b) are nearly volume-conserving during rapid load application, and afterwards, with sufficient drainage time, contractant in A and dilatant in B. The effective stress paths (c) are governed by pore pressure increase in A and decrease in B which is dissipated slowly so that the paths tend to the same statical conditions as in Fig. 1.4. Slip surfaces can occur.

Fig. 1.1 to 1.4 may suffice to represent typical boundary

value problems of foundation engineering. Other and more complicated problems can only be mentioned here:

- dams, slopes, cuts and cavities imply other shapes of boundaries;
- walls and foundations of other shapes and other foundation bodies imply other boundaries and kinematical conditions;
- layers, faults and tectonic stresses produce other initial states than the ones of Figs. 1.1 to 1.5;
- loads and displacements imposed to the earth body can be very rapid, transient, repeated, or cyclic;
- hydraulic, chemical, thermal or electrical processes can play an important rôle.

We leave these aspects aside not as they are unimportant but as the existing constitutive relations do not even cover yet all the cases described by Figs. 1.1 to 1.5 in a satisfactory manner. Another class of boundary value problems has to be dealt with here, however. It arises when soil bodies are sollicitated in order to detect their material properties. Numerous field and laboratory tests can serve, without being element tests (i.e. implying uniform stress and strain in the soil body), to check constitutive assumptions and to determine material constants defined by one or the other constitutive relation. Preferably such boundary value problems should yield closed-form solutions.

The expansion of a vertically cylindrical cavity by a pressuremeter is represented by Fig. 1.6. The strain path (b) of a surrounding soil element is practically volume-conserving with saturated clay (c), and first contractant than dilatant with dry sand (s). The effective stress path (c) tends to a limit state with decreasing σ_2 and σ_1 with soft clay, whereas σ_1 increases with sand (and hard clay). Unfortunately, the initial state (1 in Fig. 1.6) is not well-defined and at best

produced by a process as in Fig. 1.1 which implies a plane of strains orthogenal to the one of Fig. 1.6. Thus even the best pressuremeter and associated theory cannot yield more than crude estimates of material parameters.

Fig. 1.7 shows a sample in a triaxial apparatus. Even with a perfect end lubrication and non-rotating end plates bulging (a) can occur. This bifurcation conceals the true stress-strain curve (dashed) from a certain point (B) onwards. It can be prevented by use of flat samples, where a necking under triaxial extension is always occurring if the confining stress σ_2 is produced by fluid pressure. Localized modes of bifurcation (narrow shear bands and cracks) cannot even be avoided with purely strain-controlled tests. Evaluation of test results as if diffuse or localized modes of bifurcation had not occurred leads to wrong conclusions with respect to constitutive relations and parameters.

Another important group of boundary value problems is associated with so-called undisturbed samples. Extracting a soil element from the ground and inserting it into a testing apparatus adds a complicated and rarely well-defined history to the one of Fig. 1.1. If a constitutive relation does not reflect this procedure its practical application can be rather unrealistic.

Physical model tests, possibly with artificially increased gravity, can reproduce such processes as depicted in Figs. 1.1 to 1.6. Constitutive relations are the clue to model laws which are needed for the transfer of results to prototypes. Thus constitutive relations should represent similarity properties of the material. (Another use of model tests - and large scale tests - will be discussed in Sec. 3).

2. Properties to be represented

Strictly speaking, material properties are defined by constitutive relations (irrespective of their analytical or

graphical representation). We here denote by properties relations for certain very restricted processes of soil elements represented by certain types of graphs or functions as far as they have been corroborated by element tests. Such relations do not suffice to solve boundary value problems but serve as a kind of frame for constitutive relations.

The stress and strain paths represented in Figs. 1.1 to 1.6 can be decomposed into monotonic sections separated by sharp bends or even reversals. A monotonic section can be straight in stress or strain space, but not generally both. We consider paths with 0, 1 or 2 sharp bends. The influence of viscosity is suppressed by assuming constant magnitudes of strain rates first; this simplification will be dropped at the end of this section.

Monotonic paths without sharp bends occur during sedimentation and, more generally, in the laboratory. They have been studied in strain-controlled cuboidal tests with sand (Goldscheider 1976) and biaxial tests with clay (Kuntsche 1982). When starting with zero stress, proportional strain and stress paths are associated (Fig. 2.1). We consider three distinguished strain path directions (a): isotropic (A), uniaxial (B), and so that the soil element remains practically unstressed (C). The latter cannot precisely be determined and is therefore replaced, in Fig. 2.1, by a closely neighboured path. It is contractant for clay, nearly isochoric for loose sand, and dilatant for dense sand. The physically possible sector of strain paths is delimitated by type C directions.

The associated stress paths (b) are also hydrostatic in case A, and have an inclination $\sigma_2/\sigma_1 = K_o$ in case B; K_o is the so-called earth pressure coefficient at rest. The nearly stress-free path is close to the inclination $\sigma_2/\sigma_1 = K_a$, K_a being the coefficient of active earth pressure. The relationship among stress and strain path directions is nearly independent of the material (not depicted). K_o and K_a in case of clay are independent of density, but increase with initial density in case of sand.

The representation is completed by a plot of void ratio e versus mean effective stress $\bar{\sigma}$ (c). The curves for clay do not strongly depend of the path direction. They can scarcely be determined for $\bar{\sigma} \to 0$ and evidently show $e \to 0$ for $\bar{\sigma} \to \infty$. The void ratio of sand at $\bar{\sigma} = 0$ can be produced by placement of the grains. With increasing $\bar{\sigma}$, the change of e is markedly different from the one of clay. With type A and B paths, the compressibility is drastically reduced by an increase of grain hardness and density (although the asymptote $e \to 0$ for $\bar{\sigma} \to \infty$ remains valid). Type C paths are abnormal by leaving e constant with loose sand and implying an increase of e with dense sand. These relations are partly veiled by the scatter of results: it is not possible to exactly reproduce a certain initial void ratio.

We now turn to paths with one sharp bend. The first sections may be as in Fig. 2.1, the second ones straight either in strain or stress space. Due to their wide variety only narrow subgroups of such paths have been studied experimentally. The material properties outlined in the sequel are subject to some doubt as they have not generally been checked.

Consider four bilinear strain paths (Fig. 2.2a). The associated stress paths (b) of the second sections are curved. They tend towards these stress paths which had been produced by the strain path direction of the second section from the very beginning. This property of both sand (Gudehus et al. 1977) and clay (Kuntsche 1982) holds for strain paths within the possible sector of Fig. 2.1a; path II of Fig. 2.2 is one example. States during proportional stress and strain paths are called swept-out-memory- or SOM-states as they do not bear the memory of more complicated histories. It appears that SOM-states are produced by any monotonic strain paths of sufficient amount. If the strain path direction is outside the physically possible sector (cf. Fig. 2.1a) the stress path comes back to the origin (e.g. IV), i.e. the soil element tends to decay. Certain path directions (e.g. III) lead to the SOM states

associated with the sector limits of Fig. 2.1 and leave the stress state unchanged then. These are limit states both in the statical and the kinematical sense (Goldscheider 1976).

Fig. 2.3 illustrates that identical strain paths are associated with geometrically similar stress paths, if the latter start close to zero stress. This kind of self-similarity is characteristic of sand and clay. It holds also for unstressing paths, as shown in Fig. 2.4 with an initial uniaxial compression (cf. Fig. 1.1). (Zero stress has to be excluded in order to avoid contradictions.)

Fig. 2.5 shows a special case of the properties outlined by means of Figs. 2.2 and 2.3: constant-volume cylindrical compression (C) and extension (E) of clay after isotropic compression; such processes occur in undrained triaxial tests. The stress paths (b) imply a reduction of mean stress up to the limit states (in this case called critical states). Limit states are not clearly reached under extension with confining fluid pressure due to necking of the sample. Note that such stress paths are very special as compared with the ones in the field (cf. Figs. 1.3 and 1.5). It appears that only the SOM and similarity rules as outlined above remain valid.

Similar properties are revealed with bilinear stress paths. We will refer here to results of triaxial compression tests only as with other triaxial tests of this kind uniform sample deformations have rarely been secured. Typical sand results by Hettler are plotted in Fig. 2.6. Two geometrically similar stress paths (b) produce identical strain paths (a). After an isotropic compression of negligible amount there is first uniaxial compression ($\dot{\varepsilon}_2 = 0$). The relative dilation $\dot{\varepsilon}_2/\dot{\varepsilon}_1$ at the limit state is the same as the one which produces a limit state in the sense of Fig. 2.2 if the density is equal.

Fig. 2.7 shows corresponding results for clay (drained triaxial compression). The stress paths (b) differ from the ones for sand only by the stress ratio σ_1/σ_2 reached at limit states. The strain paths (a) are nearly vertical ($\dot{\varepsilon}_2 \approx 0$) first;

the relative volume change $\dot{\varepsilon}_2/\dot{\varepsilon}_1$ comes close to -1/2, i.e. constant volume, when reaching the limit states.

A generalization of these properties to other bilinear stress paths requires some caution. The observation of $\dot{\varepsilon}_2 = 0$ at the onset of cylindrical compression (not made with conventional tests) is certainly restricted to cylindrical symmetry. A change from contractancy to dilatancy is typical of the strain paths. More generally, it has been found that immediately after any sharp bend of a bilinear stress path there is a volume decrease (Goldscheider 1975, Kuntsche 1982).

The similarity property has to be relaxed for large amounts of pressure, presumably due to deformation and fracture of grains. Strain paths with higher initial stress reach limit states with lower dilatancy and stress ratios and higher amounts of strain. Conversely, stress paths with higher pressure level produce higher strain and compression amounts. However, this effect is practically negligible if the stress components do not exceed ca. 1 MN/m^2.

Rather little is known about paths with <u>two sharp bends</u> because of their wide variety. Some features of sand behaviour under plane strain are illustrated by Fig. 2.8a and b. After the second sharp bend (point 2) a straight stress path section may turn back (A) or be orthogonal to the previous section (B, sometimes called loading to the side). With any density the strain path is contractant immediately after the bend (Goldscheider 1975). From a certain stress point (3) onwards the subsequent strains develop as if the previous stress path had been proportional (i.e. 0 - 3 straight). The then required path length (2 - 3) increases with the deviation of the path directions before and after the bend. Observations indicate that the similarity rule as outlined above holds again.

It appears that sufficiently long monotonic paths after the second bend lead to SOM-states again. There are states in between (2 - 3), however, which cannot only be characterized by stress and density. (In a rather vague sense, not yet defined

for arbitrary paths with two sharp bends, they are frequently called overconsolidated or preloaded states.)

Similarity and memory properties can also explain the repeatability of test results with not more than one scheduled sharp bend: remnants of more path bends at low stress level inevitably encountered at the beginning of the test are swept out by subsequent monotonic paths.

Stress paths of the same kind imposed upon clay produce strain paths as shown in Fig. 2.8c. The volume changes differ from the ones of sand both in quality and quantity. Volume decrease is more prenounced, and increase is almost inevitably localized in shear bands (dashed path section). It appears that larger monotonic strains than with sands are needed to reach SOM-states. The similarity rules seem to hold again.

Finally, some notes on soil viscosity are suited. Its influence can be represented by associated plots of strain and stress paths with absolute time labels. The experimental results are restricted to very few types of paths. The importance of viscous effects increases with the relative amount of water in the diffuse double layers around the soil particles. The following restriction to clay should not veil the fact that qualitatively the same viscous properties are observed with sand and silt.

Proportional stress paths with different rates are associated with different proportional strain paths (Fig. 2.9). A reduction of stress rates by orders of magnitude causes only slight changes of strain ratios and amounts. Isochoric strain paths with different rates are associated with different effective stress paths of the same type (Fig. 2.10, cf. Fig. 2.5). The change is only noticeable if the rates vary by orders of magnitude.

It appears that the similarity and memory properties outlined above are not affected if the rates of stress or strain remain within one order of magniture. Stronger changes of rates affect both directional and intensity (stiffness) properties, however.

3. Manageability

A constitutive relation should be conceived and represented in such a manner that one can reasonably work with it. As this seemingly trivial requirement is by no means always satisfied it will be specified in the sequel. To sum up, the representation should be tractable, the determination of the required material constants should be technically and economically feasible, and the equations should be analytically and/or numerically well-posed and economically feasible. All these requirements are only necessary, not sufficient.

Tractability of a paper can effectively be tested by having it worked through by a reader who is willing and able to understand but not familiar with details of the concept. If he obtains the same analytical relations from the given set of assumptions, and the same figures from given sets of data, the paper is tractable. As such tests, made by the author and some of his co-workers, produced negative results with more than 3/4 of the papers tested, it is of reason to give some hints here. (Their necessity reflects how complicated the field of constitutive relations has become.)

The used set of assumptions should be completely outlined. Logical completeness, as with a set of axioms, is only desirable. More important is a hierarchical order of presentation so that the reader can more easily look for possible inconsistencies. Following K. Popper, one should strictly distinguish contradictions of the assumptions among each other and versus observations. Even oversimplified assumptions may be justified for engineering approaches, if they are clearly stated as such. It is helpful, though not indispensable in the sense of tractability, to justify the assumptions by observations (this is not yet a strict validation).

All the quantities occurring in the proposed relations should be completely defined. Of course, stress and strain definitions can be taken from the literature on continuum mechanics. Notations and sign conventions are not yet standardized, unfortu-

nately, but this is only a minor source of confusion. New quantities should be introduced by showing how to work with them analytically and numerically, i.e. by working definitions. Functionals, functions, variables, parameters and constants should be clearly discerned. The reader can learn their meaning with a well-organized typology and some significant examples. (It is sometimes required that all the quantities should have 'physical meaning'; this will be achieved if the reader can get familiar with the proposed relations by working with them.)

A complete procedure for determining the material constants should be given. This implies a description of

- required sampling and testing equipment and procedure,
- evaluation of test results and typical range of constants.

The tractable description should enable the reader to repeat the procedure and to judge the range of applicability of the proposed relations. Thus it will turn out whether the proposal is technically and economically feasible.

Some sophisticated constitutive relations imply material constants which can only be determined by element tests with rarely available equipment (such as a truly triaxial apparatus) or not yet existing machines (such as for general shear deformation). This has to be clearly stated together with recommended values of such constants. This shortcoming cannot be avoided: simpler constitutive relations tacitly imply fixed values of such constants (e.g. by neglecting the effects of third and mixed invariants). If the mathematical formulation is well-posed, such assumptions can be checked by comparing solutions of boundary value problems with model test results.

The economical aspect cannot easily be judged as simplicity is not a measurable notion. The number of constants is certainly not a relevant measure, except for the required human and artificial memory. A rough economical measure is the required sum of expenses for sampling, testing, and evaluation. If

constitutive relations are thought for practical application, required working duration and qualification of equipment and staff should be given (note that with a non-tractable description the duration would be infinite). As with any data acquisition in the light of safety and economy, such an information cannot be sufficient, however; engineering judgment is also needed.

Constitutive relations are analytically and numerically well-posed if

- they lead to solutions of boundary value problems which can be physically realized (existence);
- they lead to one solution if there is only one in reality (uniqueness);
- the solutions with small deviations of material constants show small deviations only if this is also the case in reality (stability).

As relevant constitutive relations of soils are represented by nonlinear or sector-wise linear sets of differential equations these requirements cannot generally be checked by the presently available methods of functional analysis. They can as yet only be tested by numerical experiments which will be indicated in the sequel. Note that the above requirements are only necessary and imply some rather general hypotheses of continuum mechanics (local action, simple material).

The numerical tests should begin with soil elements under uniform stress and strain, i.e. with simulated element tests. One has a set of ordinary (not partial) differential equations then. Within the intended range of application, characterized by path directions and strain rates, histories should be systematically scanned by means of numerical integration. Graphical representations (as by response envelopes, e.g. Gudehus 1979) are recommended for rapid discrimination. The reader can easily follow these tests if flow charts or even programs are given.

This procedure should precede any publication. It will help the respective author to eliminate improper formulations and to delimitate the range of applicability. The class of histories must not be restricted to element tests available to the author (such as triaxial compression only, say). The examples of Figs. 1.1 to 1.7 show that the complete range has to be tested. Numerical stability should be checked first. If this has been achieved (and tractably demonstrated), the range of uniqueness should be ascertained. Note that non-uniqueness of the response of soil elements has not been observed experimentally (which is not to be confused with bifurcation of samples). Non-existence should only occur with certain continuations from limit states.

If the proposed constitutive relation has passed this numerical element test it should be further tested with boundary value problems implying only one or two spatial derivatives. Examples are

- expansion and compression of a cylindrical or spherical cavity;
- expansion and compression of a cylinder or cuboid with deviations from uniform strain;
- rotation of a wall with uniform backfill around its feet;
- shear of a thin layer between two rigid plates.

Some reference experiments are available for such cases. A few numerical and physical aspects will be outlined now.

The moment of truth during such tests arises with sudden changes of path directions. They occur in reality if imposed boundary stresses or displacements are reversed, and in case of bifurcations. A sensitive change of intensity response to change of path direction, especially in the vicinity of limit states, is characteristic of soils and has thus to be modelled by relevant constitutive relations. If the equations are sectorwise incrementally linear (as elastoplastic laws, e.g.), the switch conditions needed for changes of sectors

can destroy numerical stability. Completely nonlinear foundations (as some rate-type laws) have to be linearized by a kind of Newton-Raphson method the convergence of which is by no means guaranteed. Many of the published constitutive relations cannot pass such tests even with only one spatial derivative (cavity expansion and compression, e.g.).

Economy of the proposed equations should be tested as outlined above for material constants. Although the sum of expenses for hardware and staff is not a sufficient measure estimated figures for it are helpful; they should rely upon the solution of real boundary value problems.

It is noted once more that the criteria of manageability are necessary and not sufficient altogether. As with any theory, comparison of predictions with acceptable experimental results is an indispensable part of validation.

References

Goldscheider, M. (1975): Dilatanzverhalten von Sand bei geknickten Verformungswegen. Mech. Res. Comm., 2, p. 143 - 148.

Gudehus, G., Goldscheider, M. and Winter, H. (1977): Mechanical Properties of Sand and Clay and Numerical Integration Methods: Some Sources of Errors and Bounds of Accuracy. In: Finite Elements in Geomechanics (Ed. G. Gudehus), Wiley, p. 121 - 150.

Gudehus, G. (1979): A comparison of some constitutive laws for soils under radially symmetric loading and unloading. Proceed. 3rd Int. Conf. Num. Meth. Geomech. (Ed. W. Wittke), Aachen, Balkema, p. 1309 - 1323.

Kuntsche, K. (1982): Materialverhalten von wassergesättigtem Ton bei ebenen und zylindrischen Verformungen. Veröffentl. Inst. f. Bodenmech. u. Felsmech. Karlsruhe, Heft 91.

Vardoulakis, I. (1979): Bifurcation Analysis of the Triaxial Test on Sand Samples. Acta Mechanica, 32, p. 35 - 54.

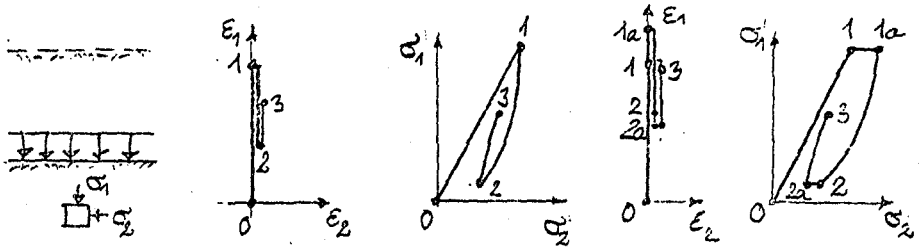
1,1
a)
b)
c)
d)
e)

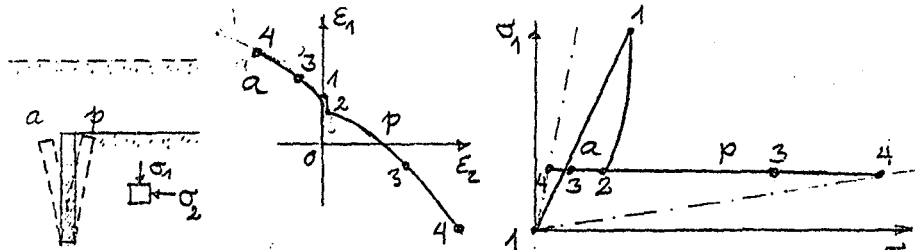
1,2
a)
b)
c)

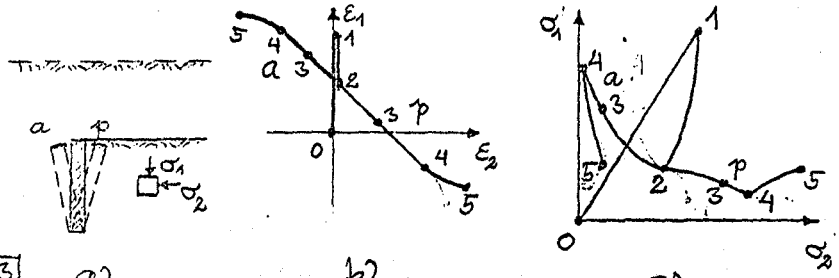
1,3
a)
b)
c)

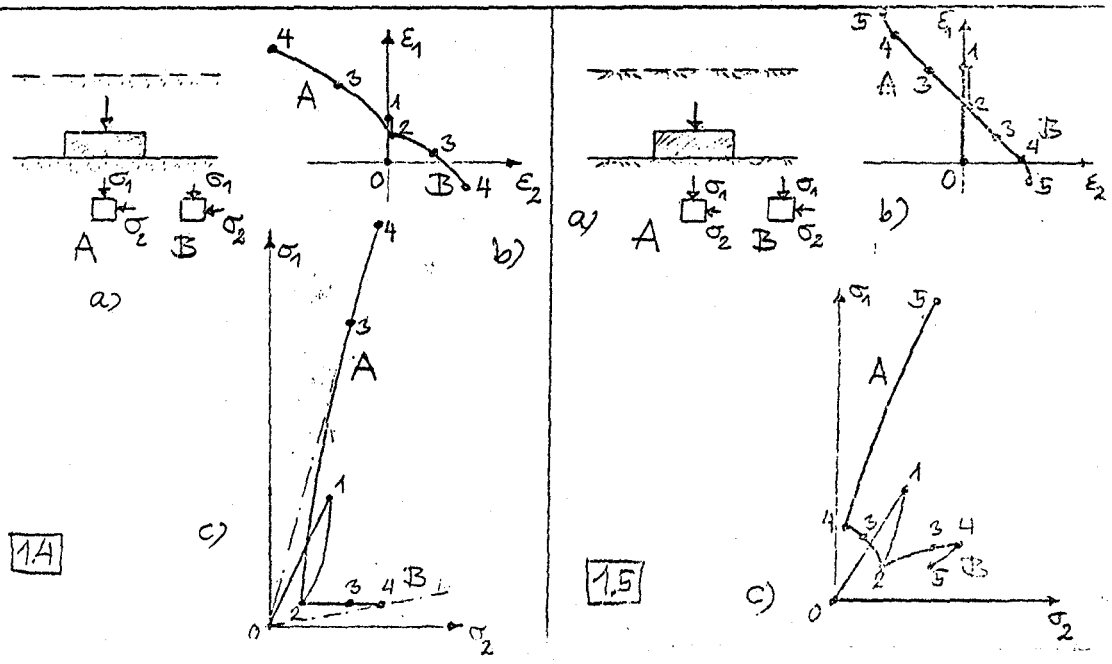
1,4
a)
b)
c)
1,5
a)
b)
c)

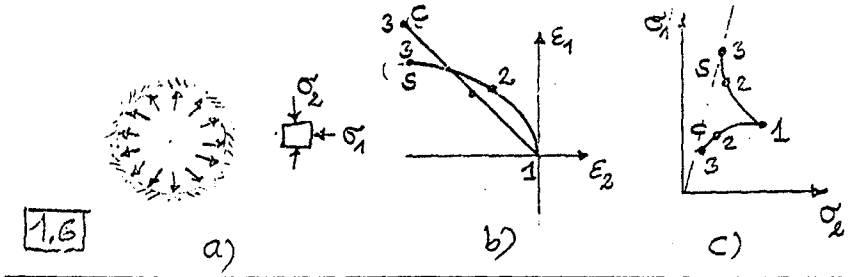
3
C
3
S
2
1
ε_1
ε_2
σ_2
σ_1
σ_1'
σ_2'
a)
b)
c)

1.6

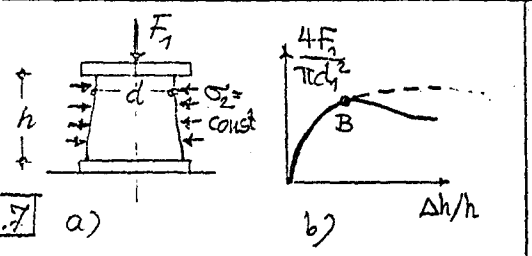
F_1
d
h
σ_2' = const
$\frac{4F_1}{\pi d_1^2}$
B
$\Delta h/h$
a)
b)

1.7

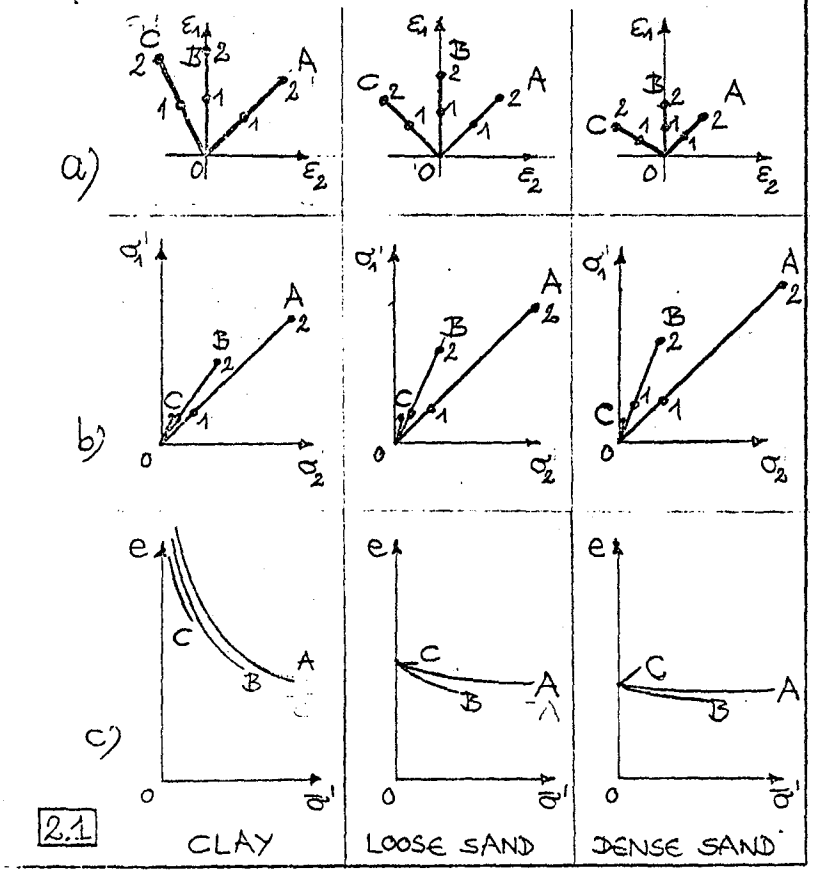
a)
b)
c)
ε_1
ε_2
σ_1'
σ_2'
e
A
B
C
0
CLAY
LOOSE SAND
DENSE SAND

2.1

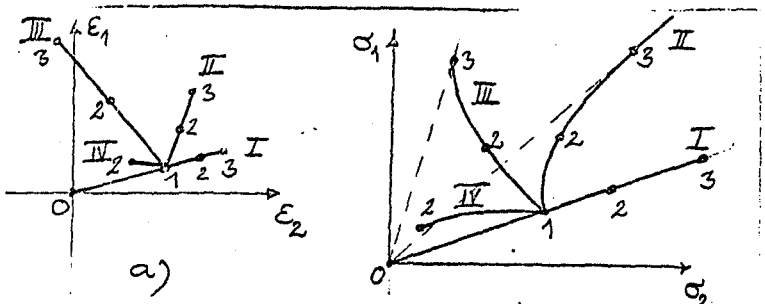
III
ε1
II
I
IV
ε2
a)
σ1
σ2
b)

2.2

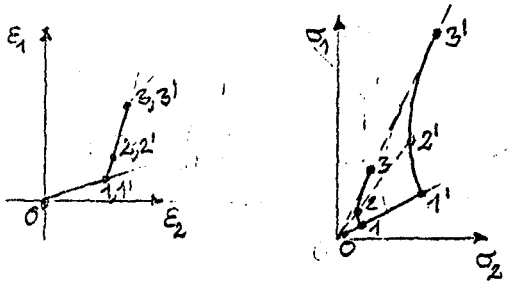
ε1
ε2
a)
σ1
σ2
b)

2.3

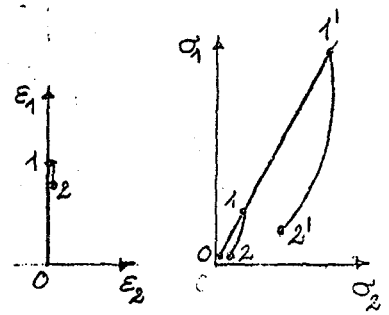
ε1
ε2
σ1
σ2

2.4

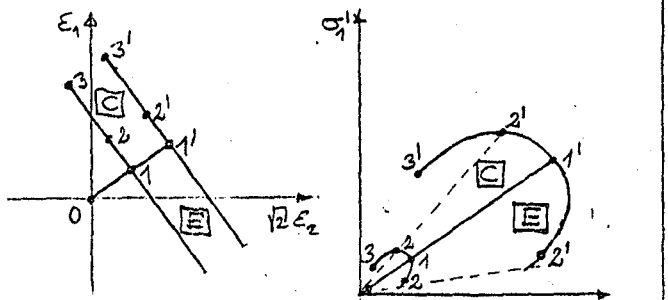
ε1
C
E
√2 ε2
σ1'
√2 σ2'
a)
b)

2.5

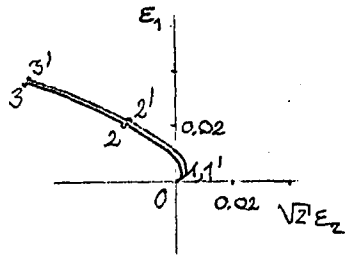

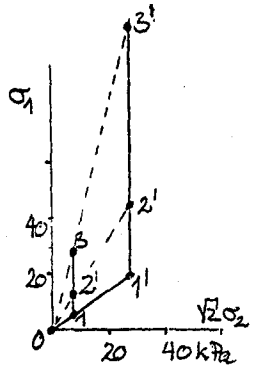

2.6 a) b)

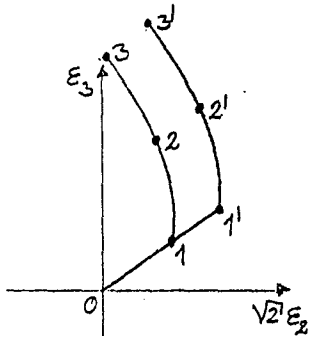

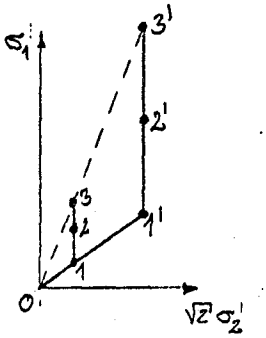

2.7 a) b)

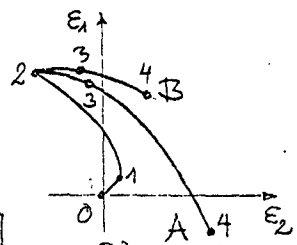

a)

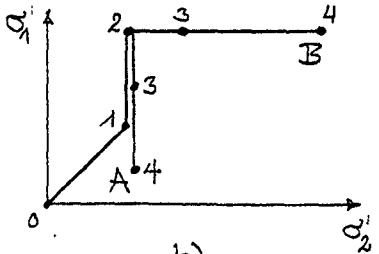

b)

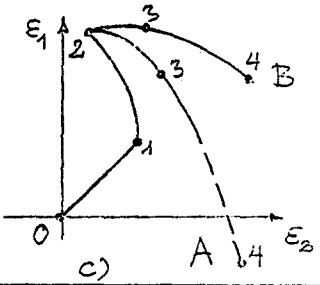

c)

2.8

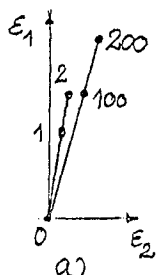

a)

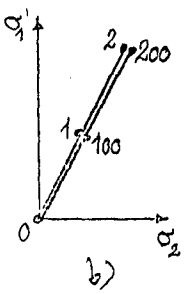

b)

2.9

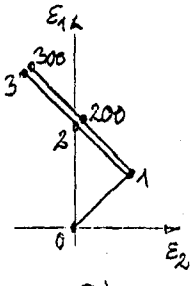

a)

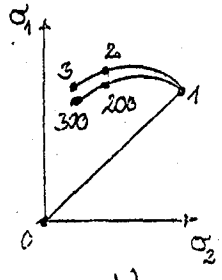

b)

2.10

INELASTIC PROPERTIES OF SOLIDS WITH RANDOM CRACKS

Y.V. ZAITSEV

ALL-UNION POLYTECHNICAL INSTITUTE (VZPI)

MOSCOW, USSR

INELASTIC PROPERTIES OF SOLIDS WITH RANDOM CRACKS

Yu.V.Zaitsev

VZPI, Moscow, USSR

I. Introduction

Geological materials can often have microstructures composed of coherent grains (monocrystals), sometimes with only weak bonding forces between them, or of granules in an unbonded aggregate. When nominally coherent, they typically have pores and/or cracks, randomly distributed in the volume of a solid. (Nikolaevskii and Rice, I979)

Concrete is one of the most complex construction materials consisting of randomly distributed inclusions embedded in a continuous relatively softer porous matrix (hardened cement paste) the properties of which depend on time. The effect of this heterogeneity is to cause non-uniform internal strains, and both the process of cracking and failure in such a material become complex and discontinuous. (Swamy and Sriravindrarajah, I982). The aggregate-matrix interface in such a system becomes critical and the weakest link; pre-existing microcracks in this area create nuclei of potential crack propagation, inelastic behaviour and failure of concrete.

There are many models which allow to describe the behaviour of random cracks in a material such as rocks and concrete under various load conditions. Mathematical treatment of the problem of random cracks in a three-dimensinal body is very complicated. Therefore in most of theories this problem is reduced to the

problem of random cracks in a two-dimensional body.

Let us at first analyse models in which a material with random cracks is supposed to be quasihomogenious. These models are mainly used to describe the behaviour of rocks and hardened cement paste (hcp). After that the models which take the significantly inhomogenious structure of a material (such as concrete) into consideration will be analysed.

2. Models of quasihomogenious solids (rocks, hcp) with random cracks.

2.I. Uniaxial tension, biaxial loading (tension+tension, tension +compression).

For such loading conditions opening mode cracks (Mode I) are typical. Carpinteri, Di Tomasso and Viola (I978) have analysed a part of solid body - a thin plate with random cracks . The plate is subjected to the biaxial tension (or compression with tension) σ_1, σ_3 . The length of cracks is assumed to be small as compared to the plate dimensions. The interaction of cracks is neglected. It is assumed that propagation of the most dangerous crack leads to the failure of the solid. To estimate the load value when the crack starts to propagate, formulae of fracture mechanics are used. By various values of σ_3 / σ_1 different values of crack inclination β are decisive for strength of the solid (see fig.I)

Fig.I

A similar model was analysed by Panasjuk et al (I976).

It has been shown that the interaction of n existing random cracks can in principle be taken into consideration with the help of a system of integral equations. However difficulties of the computation prevent the estimation of the interaction of more than two random cracks. Results for two random cracks according to

Fig.2-5 Panasjik et al (I976) are given in fig.2-5.

Here dash lines correspond to the left tips of cracks, and solid lines - to the right tips. Curves I and 2 correspond to cracks No.I and No.2. From fig.2 one can see that by $0 < \beta < 7\pi/30$ fracture begins from internal tips and by $\beta > 7\pi/30$ from external tips. Critical load p_* is minimal by $\beta \cong 5\pi/36$. By $\beta = \pi/3$ the critical load is the same as by an isolated crack ($p_* = p_0$), oriented perpendicular to the external stress.

From fig. 2 one can see that the angles θ_* of the initial crack propagation are negative by $0 < \beta < \pi/6$ and $5\pi/12 < \beta \leq \pi/2$. It means that fracture propagates not in the direction to the nearby crack but in the direction away from it.

On fig. 3 the minimal critical load corresponds to $\beta \cong 5\pi/36$ again. Fracture begins from the left (internal) tip of the crack No.2. By increase of β -value the initiative of fracture goes over to the right tip (and then to the left one) of crack No.I. Fig. 3 shows the corresponding angle of the initial crack propagation too.

From fig. 4 one can see that by $\alpha < 7\pi/36$ fracture initiates from the left (internal) tip of the 2nd crack, and by $\alpha > 7\pi/36$ from the right (internal) tip of the Ist crack.

Fig. 4 also shows the effect of orientation of the second crack on the direction of initial propagation of the Ist crack. By deviation of the 2nd crack from coplanarity, the fracture from the right (internal) tip of the Ist crack will propagate in the direction to the more distant tip of the 2nd crack.

From fig. 5 one can see that by such crack position nearly by any orientation of the 2nd crack, the critical load is higher than for an isolated crack ($p_*/p_0 > 1$), oriented perpendicular to the external stress.

It is remarkable that curves for p/p_0 on fig. 2-5 qualitatively differ only little from the curves for an isolated crack of random orientation (dotted lines).

Failure criteria for a solid with random cracks subjected to biaxial tension (or compression with tension) have been also investigated by Panasjuk et al (1976). It was assumed that all random cracks interact but this interaction takes place only in pairs. It means that in a solid there are some pairs of interacting cracks, moreover, distance between pairs is so large that the pairs may be considered isolated pairs. For each pair the crack length 2l and the distance d between centres of cracks are given. For such a model fig.1 shows failure criterion by plane state of stress by $\lambda = 2l/d = 0,5$ (curve 1). Curve 2 shows the same failure criterion for a body with only one isolated crack of a related length; this length is chosen from the condition that uniaxial tensile strength of the body with one isolated crack and with pairs of interacting cracks is the same. One can see from fig. 1 that the interaction of cracks qualitatively only slightly affect the failure criteria by plane state of stress.

There are also some theories which pay attention not so much to geometrical arrangement of random cracks as to probabilistic concept of crack formation and crack propagation. H.Mihashi (1983) has assumed, that failure processes of brittle materials may be regarded as a kind of markoff process, because the probability of cracking is influenced only by the state of the previous instant but it is independent of the motion preceding the time instant t. Markoff

process is characterized by a transition probability $\bar{\rho}_{01}(t)$ representing the probability that the state of the element is changed from state 0 (non-fracture) to state I (fractured) (Fig.6a). Since the fracture of brittle materials is caused by cracking, the transition probability may be equal to the rate of crack initiation $\rho(t)$. When an element is composed of n units, the rate of crack initiation which leads to the fracture of the element is given by the following equation:

Fig.6

$$\bar{\rho}(t) = n\bar{\mu}(t)$$

where $\bar{\mu}(t)$ is the mean value of $\mu(t)$ for a large number of n, $\mu(t)$ is the probability of fracture initiation at the momemn t.

According to the theory of stochastic process:

$$\frac{dP_0(t)}{dt} = -\bar{\rho}_{01}(t)P_0(t)$$

where $P_0(t)$ means the probability that no fracture occurs before the time t in any units. The variable t may have other meanings but time: for example, stress under a monotonically increasing load, the number of cycles under a repeated load.

Failure process of a solid is composed of a series of local brittle fracture (that is assumed to be cracking). The number

of units n might be connected with the number of some kinds of rather large microcracks (Fig. 6b) A large number of 'n' may describe a very porous solid. The theory of Mihashi provides a basis for mathematical formulation of the influence of some factors of strength: the rate of loading, enviromental temperature, size of the specimens, age of the specimens and the upper stress of repeated load.

However, by this model, as by all the models described above, the following question still remains open: how to calculate tensile macrostrain of a solid with respect on crack formation and crack propagation, i.e. how to estimate the real inelastic behaviour of a solid with random cracks.

There are some attempts to evaluate deformation of a body with respect to defects (pores and cracks) with help of effective modulus E of elasticity and effective Poisson's ratio ν . This values may be expressed as follows (R.Salganik, 1974):

$$E = E_0 (1 - k\pi\Omega/4); \quad \nu = \nu_0 (1 - k\pi\Omega/4),$$

where Ω is a little parameter, $\Omega = N\ell^2$, N - number of defects in a volume unity, l - defect size, E_0 and ν_0 - values of E and ν in a body without defects; k = 3 for pores and k = I for cracks. It is assumed in this approach that defects are isotropically distributed on the body and that defects are small as compared to dimension of the body. It must be noted that such assumptions restrict the use of this model for concrete and rocks, because propagating cracks in these materials are oriented with respect to the external load (parallel to load by compression or perpendicular to it by tension), and crack dimensions near to ultimate load are comparable to dimen-

sions of a sample. Therefore it seems to be appropriate for calculation of inelastic deformation to take into account cracks of the real length and of the real orientation.

Budiansky and O'Connel (I976) have proposed an analytical metod for estimation of effective elastic moduli for a solid containing random cracks of different shape. Calculations are made for the case of ellyptical cracks.

Effect of orientation and number of cracks on the strength and other properties of a solid was analysed by Ikeda, Kabayashi and Sakurai (I973). A model of microstructure with cracks using statistical methods, including generalization of the model by Walsh for the multiaxial state of stress, has been developed by Brady (I969,I970, I973).

More precise estimation of inelastic behaviour of a solid with random cracks can be made with the help of the model shown on fig. 7a; it was assumed that the centres of cracks are statistically uniformly distributed on the area in fig 7a which represents the specimen size (Zaitsev, I980, I982; Zaithev and Wittmann, I98I). The length of cracks is uniformly distributed on the interval $[a,b]$. The angle of crack orientation α with respect to the external load is also uniformly distributed on the interval $[0,2\pi]$. For every crack the interaction with only one nearby crack was taken into account; this was made according to the results given in fig. 2-5. The random structure has been created by a computer program. The possibility of crack arrest by crack crossing was taken into consideration.

Fig.7

Taking the opening of cracks into consideration, the

contribution of cracks to the longitudinal strain ε can be found, if we assume the linear superposition of the two components

$$\varepsilon_1 = \varepsilon_1' + \varepsilon_1''$$

where ε_1' is the contribution of the elastic unfractured material, ε_1'' is the inelastic component caused by the displacement of crack edges. According to Panasjuk, Savruk, Dazyshin (I976), the half width v of a crack of the length 2l in a material with modulus of elasticity E subjected to tensile stress p (perpendicular to the cracks, $\alpha = \pi/2$) can be found as follows:

$$v(x,0) = \frac{2p}{E}\sqrt{l^2 - x^2}$$

whereby the maximal half-width is equal to

$$v_{max} = 2pl/E.$$

If the angle between crack direction and load direction $\alpha \neq \pi/2$, i.e. a crack is inclined with respect to load direction, these expressions may be rewritten as follows:

$$v(x,0) = 2p\sin^2\alpha\sqrt{l^2 - x^2}/E;$$

$$v_{max} = 2pl\sin^2\alpha/E$$

The effect of shear stress $\tau = p\sin\alpha\cos\alpha$ on the crack opening is neglected.

The component ε_1' is equal to σ/E, while the component ε_1'' can be found if we assume that elongation caused by the displacement of the crack edges is "smeared" on the volume of the sample. Thus for one crack we have

$$\varepsilon_1'' = 2\int_0^{2\ell} v(\xi)\,d\xi / bh$$

and for all the n cracks

$$\varepsilon_1'' = 2\sum_{i=1}^{n}\int_0^{2\ell_i} v(\xi)\,d\xi = \frac{4P}{E}\sum_{i=1}^{n}\sin^2\alpha_i \int_0^{2\ell_i}\sqrt{\ell_i^2-\xi^2}\,d\xi$$

Fig.7b shows stress-strain curves in uniaxial tension according to the results of simulation of crack propagation in a sample. (See fig. 7a).

Damage approach for concrete in uniaxial tension has been developed by Loland (1980), Lorrain and Loland (1983). Damage (ω) denotes the relative portion of the nominal fracture area (A in fig.8 a) which is not mechanically intact. Damage includes pores (1) and all kinds of cracks (2). It is suggested that the initiation of cracking is more depended on strains than on atresses.

Fig.8

When straining a specimen, damage will occur within the total length of the strained body when strain (ξ) is less than the strain capacity (ε_{cap}). Above this strain level, damage will develope in the fracture zone only as shown in Fig. 8 b. Fig. 8c shows a summary of damage approach for concrete in uniaxial tension.

2.2. Uni- and multiaxial compression.

The models with opening-mode cracks (Mode I) can describe the behaviour of solids subjected mainly to the uniaxial tension, sometimes also to the biaxial tension or tension with compression. By uniaxial compression (typical for concrete) and especially by multiaxial compression (which is typical for rocks), propagation of shear cracks (Mode II) must be also taken into consideration.

Rong and Xiao-Xiu (I980) have studied behaviour of gabbro under triaxial compression. The development of microcracks was studied under the microscope. It was found that under low stresses, the microcracks occur within the crystal grains of the rock minerals and their orientation is determined principally by the configuration of the crystals. When the applied stress reaches about 70-80% of the ultimate strength, the cracks become more concentrated in the central part near one diagonal of the sample. At this time there appear a few microfaults which pass through several crystal grains. The orientation of these microfaults depends obviously on the direction of the external stress, which makes an angle less than 40° with the direction of maximum stress. The volume changes in the rock samples were also measured and compared with the observations in the microcracks. It is found that the development of the microcracks and their influence on other physical properties of the rock are dependent on the dimensions of the crystal grains.

In a paper by Simmons and Richter (I976) results are given of the petrographical studies of microcracks in rock. The length of microcracks is usually of 10^{2} mm range but may be of some meters length. Data on structure and propagation of pores and microcracks are given also by Brace et al. (I972), Gash (I97I) and other investigators.

Microcrack closure in rocks under increasing stress was observed directly by Batzle (I980) with a scanning electron

microscope. Uniaxial stresses to 300 bars were applied to specimens of granite, both unheated and previously heat-cycled to 500°, and diabaze, heat cycled to 700° . An assumption was made, that numerous factors influence the behaviour of cracks under stress including orientation, shape, source, and the proximity of other fractures. In general, fractures oriented perpendicular to the maximum stress direction close, and those oriented parallel tend to open. These trends, however, are often changed by the other factors. Natural cracks have walls that are irregular, etched and pitted, and poorly matched. Closure is incomplete with many portions of the crack remaining open and interconnected. A single fracture may partially close, forming numerous smaller cracks.

Experimental results have been summerized by Nikolaevskii (I982) on the diagram, giving a classification for fracture
Fig.9 of rocks (fig. 9). One can see on fig. 9 fracture surface BB', surface of onset of dilatancy (inelastic volume change due to microcracking) AA', zone of dilatancy (shaded area) and OO' - line of the Coulomb condition $\tau = \mu\sigma$, with friction coefficient μ .

The numbers on fig.9 correspond to granite. To the left from the point O' (0,5 GPa, 400°C) rocks fail brittle, to the right - plastic. By low confining pressure (I) cracks propagate parallel to the axial compression (vertical) as the opening mode cracks. By increasing confining pressure crack edges closed (2), crack propagate now as inclined cracks, and angle of inclination in the respect to the axial load depends on the principal stress ratio and some other factors

In the interval from the point 0,2 GPa, 200° C to the point O' shear bands (3) are formed due to the localization of dilatancy cracks. Then one can see pseudoplastic (cataclastic) fracture 4 (due to formation of a large number of little cracks) and plastic (dislocation) fracture 5. To the right from the point IGPa (or I,5 GPa, 500° C, or 0,7 GPa, 800° C) there are no cracks, rocks become waterproof.

Fig.IO An idealized model for rocks (see Fig.IOa) consists, after Nikolaevskii and Rice (I979), of a solid with a random array of flat Griffith cracks that are closed under compressive principal stresses and which can begin to slip when the Coulomb condition $\tau = \mu\sigma$ is met based on locally-resolved shear (τ) and normal (σ) stresses. If the crack surfaces are flat so that slippage is not accompanied by dilatant uplift at asperities, and if no local tensile fissures are opened at the crack tips, there is no plastic dilatancy.

The idealized model of Fig.IOa suffices also for an examination of subsequent yield surfaces. In particular, as illustrated in Fig.IO b, the macroscopic yield surface can be considered as the inner envelope of an essentially infinite family of yield surfaces for individual fissures of all possible orientations (Nikolaevskii and Rice, I979). Initially, these individual yield surfaces have the form $\tau = \mu\sigma$ where the orientation of an individual crack enters in the calculating τ and σ from the macroscopic stress state.

Later, as slips Δu develop, a kind of "hardening" occurs since not all of the nominally applied shear stress τ is actually carried by the crack surface.

In Fig. IO c limit surfaces representative of coherent rock, e.g. granite, are given after Nikolaevskii and Rice (I979). Here the zone of dilatancy is located between the line of onset of dilatancy and the limit failure curve. Inside, the response can be modelled by rule of nonassociative plasticity, although on the microlevel the cracking is brittle.

In Fig.IO d the case of porous limestone is illustrated. Under high σ the response is similar to that of porous metals, due to the effects of plastic flow around pores. This gives the capped form of yield surface of the entire material, where the region at lower σ corresponds to inter-pore shearing. At limit conditions these shears combine to a macroscopic surface of localization.

The localization of previously homogeneous deformation into narrow shear band is a common feature of geological materials that are loaded to failure under multiaxial compression. Rudnicky and Rice (I975) explained the onset of localization as a bifurcation into a localized mode that is predictable in terms of the non-elastic constitutive relations prevailing up to the moment of localization.

The onset of localization may be important to the inception of earth faulting and also to the concentration of deformations into narrow shear zones in a variety of geotechnical problems, e.g., in landslides on slopes. What is missing in the theoreti-

cal description thus far developed is the explanation of what happens as deformations proceed within the localized zone.

Using method of Geniev, Kissjuk and Tjupin (I974), in papers by Kozachevskij (I98I), Kozachevskij and Zjazin (I982) a dilatancy model of theory of plasticity is developed. This model is based on the non-linear behaviour of concrete not only by shear deformation, but also by volume deformation, taking into account cracking connected with dilatancy.

Dilatancy as a result of cracking can be explained with the help of model by Stavrogin (I969), Stavrogin and Protasenja (I979). Statistical ideas of this model are explained on Fig. II (a,b,c,d) where 4 different cases of loading with stresses σ_1, σ_2 are shown, whereby the value of $C = \sigma_2/\sigma_1$ increase by transition from "a" to "d". Statistically distributed defects by loading of the body cause shear on the microareas, which coincide with defects. Defects are distributed uniformly with mean distance "b". Density of defects N increase by increase of C. If shear stress on microareas has reached a critical value, shear deformation occurs, which leads to fracture on vertical microarea (see Fig. II,e). Macroscopically a rough shear surface ω is formed, and the part I of the body moves with respect to the part 2. Fracture on vertical microareas causes the increase of volume of a body.

Fig.II

It can be calculated on this model (see fig.II f,g) that with respect to crack formation ν -value is equal to $\nu = \varepsilon_1/\varepsilon_2 = 1/2 tg\alpha$.

Influence of cracks on effective elastic moduli in compression have been studied by many investigators. In papers by Walsh (1965a, 1965 b, 1980), Walsh and Brace (1968, 1972) rock is considered to be elastic and isotropic, containing pores or elliptical cracks of random orientation. Non-linear stress-strain behaviour and hysteresis due to cracks are analyzed. Cracks close under increasing compressive stress, causing an increase in Young's modulus. Modulus may not be equal to that of solid material since frictional sliding at crack faces can occur.

If the fluid is not permitted to enter the pores by a plastic barrier, the effective compressibility must also include a term to account for the resulting decrease in porosity.

Expressions for effective compressibility of rocks having various shapes of pores, including spherical, penny-shaped, and elliptical, are given. The pressure required to close a crack is of the order of $E\alpha$ where E is Young's modulus and α is the aspect ratio. Cracks having an aspect ratio of 1/1000 can be closed by moderate pressure.

Results of investigation of all elastic moduli have been published by Warren and Washner (1976).

Mechanical properties of rocks and rock masses have been considered by Bernaix (1974) as depending on presence and behaviour of cracks (fissures). Fissure reaction mechanisms are investigated using models, covering plane fissures to fissures with random asperities. Rock behaviour is analysed with reference to these basic mechanisms and it is found that, under some confining stresses, fissures develop gradually under load from stable to unstable.

Models described above allow to describe inelastic deformation of a quasihomogeneous material under multiaxial compression, which is typical for rocks. The second quasihomogeneous material considered in this lecture is hardened cement paste, which in most cases is subjected to the state of stress close to uniaxial compression. By such conditions the propagation of longitudinal opening cracks (splitting cracks) is typical - see fig. 9 , region I.

Mihashi has modified his model mentioned above (see fig.6) for this case.

The case of compressive failure (Fig.6 d) may be described by two different types of models . . . . . If the failure process is modelled by two states (i.e. non-fractured state and fractured state), Type A model is available even for compressive fracture (see fig.6a). When the first step of failure process does not mean the fracture of a specimen, Type B should be used (fig.6c). It is also possible to make much more complex models only by means of increasing the number of states. However, the equation

becomes very comlpex and it is not easy to define the coefficients rationally.

It must be noted that the theory of Mihashi does not allow to estimate macrostrain of a solid with respect on crack formation and crack propagation.

Bažant (I980) has suggested that there are basically two types of inelastic strains - plastic and fracturing. The plastic strains, $d\epsilon_{ij}^{pl}$, are due to plastic slip which takes place at constant stress and does not affect elastic stiffness and the fracturing strains $d\epsilon_{ij}^{fr}$ are due to microfracturing or microcracking which is accompanied by a stress drop and result in a degradation of material stiffness.

$$de_{ij} = \frac{ds_{ij}}{2G} + de''_{ij} ; \qquad de''_{ij} = de^{pl}_{ij} + de^{fr}_{ij} ;$$

$$de^{fr}_{ij} = \frac{\partial \Phi}{\partial e_{ij}} dk ; \qquad de^{pl}_{ij} = \frac{1}{2G} \frac{\partial \Psi}{\partial e_{ij}} d\varsigma ,$$

in which Ψ and Φ are the plastic and fracturing loading functions; G - elastic shear modulus, introduced for dimensional convenience; $s_{ij} = \sigma_{ij} - \delta_{ij}\sigma$ = stress deviator; $\sigma = \sigma_{kk}/3$ = volumetric stress; $e_{ij} = \epsilon_{ij} - \delta_{ij}\epsilon$ = strain deviator; $\epsilon = \epsilon_{kk}/3$ = volumetric strain; δ_{ij} = Kronecker delta; de^{pl}_{ij} = plastic strain increments, de^{fr}_{ij} = fracturing strain increments.

For data fitting, a computer program has been developed. Small loadig steps are used to integrate the constitutive relation numerically for specified forms of materials functions and given material parameters.

Problems of application of fracture mechanics to concrete and hcp

have been studied by many authors, for instance, Bažant (I979), Cappinteri, Di Tomasso and Viola (I978), Desay (I977), Dias and Hilsdorf (I973), Hillerborg(I983), Mindess (I983), Moavenzadeh and Kuguel (I969), Sauoma,Ingraffea and Catalano (I980), Slate, Jaguot, Lierse, Ringkamp, Rastogi, Terrien (I983), Shah (I97I, I979), Shah and McGarry (I97I), Wittmann(I983), Ziegeldorf (I983) and others.

Non-linear behaviour of concrete has been experimentally investigated by many authors, for instance, Basoul and Naso (I982), Desay (I977), Dias and Hilsdorf (I973), Evanse and Marathe (I968) Gerstle, Aschl, Belotti, Bertacchi, Kots'ovos, Hon-Jim, Linse, Newman, Rossi, Schickert, Taylor, Traina, Winkler and Zimmermann (I980), Hsu, Slate, Sturman, Winter (I963), Jonston (I970), Lott and Kesler (I966), Stroeven (I973), Ziegeldorf (I983) and others.

In a model of Zaitsev (I969 to I982), Zaitsev and Wittmann (I97I to I98I), Wittmann and Zaitsev (I972 to I98I) it was assumed that hardened cement paste has pre-existing defects in form of pores and cracks. First of all the interaction of two pores with cracks (Fig. I2) has been studied with help of methods of fracture mechanics. Main results are shown in Fig. I3. First stages at crack propagation are stable. The presence of neighbouring holes causes the unstable fashion of crack propsgation (by $\Psi = \Psi_2$ and $\sigma_{1*}^{o} = \sigma_{1*}^{max}$, see curves 2 on Fig. I3); curves 2a correspond to irreversible cracks and curves 2b - to reversible cracks. The calculations for different c/r-values have shown that the related crack length (at the end of the length of stable crack propagation) Ψ_2 is nearly constant ($\Psi_2 = 0.69 \div 0.73$ for internal cracks and $\Psi_2 = 0.5I \div 0.55$ for external cracks). The related crack length Ψ_1 ,

Fig.I2
Fig.I3

which corresponds to q_*^{max} (one pore with two coplanar cracks) on the line Ia, can also be regarded as a constant ($\Psi_1 = 0,46 \div 0,47$).

The process of crack propagation discussed above will lead to the joining of two internal cracks and formation of a new crack, crossing both holes (see dotted lines on Fig. I2). The results, which were obtained in a similar way, are given in Fig. I3 (line 4). A comparison of curves 2 and 4 shows that if the load has reached the value q_*^{max} (i.e. cracks have entered into the zone of unstable propagation), both interacting cracks join at once and the λ-value "jumps" from curve 2 to curve 4 (wave line).

The following stage of crack propagation, when three, four and more coplanar cracks interact, is a process having a statistical nature, because this interaction depends significantly on the distribution of distance between pores. This process can be simulated using Monte-Carlo-Methods. The results of the simulation described by Zaitsev (I97I, I974), Zaitsev and Wittmann (I97I,I974) show a satisfactory agreement with existing experimental results.

In the model described above it is assumed that all the cracks are coplanar. It is, however, well known that real hardened cement paste has cracks oriented at random. Therefore a more complicated model has been analysed. It was assumed that all pores are statistically uniformly distributed on the area in Fig.I4a , which represents the specimen size. Each pore has two pre-existing cracks, the length of which is uniformly distributed within the range $0 < \ell/r < 2$. The angle of crack orientation α_i with respect to the external load is also uniformly distributed within the limits of 0 and 2π .

Fig.I4

The interaction of cracks was taken into account by the assumption that two cracks (i = I; 2) will interact and coalesce if α_1 and α_2 are both below $\pi/6$ (above $5\pi/6$) . The random structure has been created by a computer program.

Simulation of crack propagation as described above makes it possible to estimate the effect of pore size distribution on the fracture mechanism, mechanical strength and strain behaviour of hardened cement paste. In particular, it was found (Zaitsev, I980) that by increasing the mean size of pores while keeping the quantity constant, the ultimate load will decrease. Increasing the maximum size of pores but keeping a constant mean size and a constant quantity of pores will decrease the ultimate load too.

Fig. 14 b shows stress-strain curves in uniaxial compression of a sample (see Fig.14a) according to results of simulation of crack propagation, by ε_1'' according to results of paragraph 2.I.

3. Models of significantly inhomogeneous solids with random cracks (concretes).

3.I. Uniaxial tension.

Phenomenological aspects of the inelastic properties of concrete in uniaxial tension may be summarized as follows. The $\sigma-\varepsilon$ diagram is linear up to stresses of about 80% of the ultimate stress. The deviation of the $\sigma-\varepsilon$ diagram from the straight line is connected with enlargement of preexisting bond cracks. At higher loads continuous cracks (i.e.

cracks combining some bond cracks and mortar cracks) are formed. Some propagating cracks can be arrested by aggregate particles. About the origin of pre-existing bond cracks different views exist. Usually such crack formation is explained by shrinkage of the hydrating cement paste. However, according to Ziegeldorf (1983), shrinkage cracks must emanate radially from aggregates. The second point of view is related to the observation, that water lenses develop under coarse aggregates during setting of the fresh concrete, and the crack density is greatest in the horizontal direction at all stress levels. It seems that both effects (shrinkage and bleeding) are responsible for pre-existing cracks, and the crack pattern
Fig.15 according to fig. 15, a must be expected in concrete (Ziegeldorf, 1983).

Model of Mihashi described above can also be applied to the case of concrete in tension.

Application of methods of fracture mechanics may be very useful for such problems. However, Bažant (1979) has shown that methods of linear fracture mechanics can be applied to concrete (regarded as a quasihomogenious solid) only by crack dimensions in order of magnitude of some meters, which is significantly more than dimensions of real cracks in concrete structures. Therefore, by investigation of crack propagation in concrete with help of methods of fracture mechanics it is necessary to analyse concrete as as a multiphase system consisting of quasihomogenious matrix (hardened cement paste) and inclusions (aggregate particles). Such an approach has also an important advantage: it gives the possibility to evaluate the effect of quantity, shape of particles, K_{Ic} and E -values of aggregate on inelastic behaviour of concrete.

Let us now analyse crack propagation in concrete subjected to uniaxial tension, according to the model of Wittmann-Zaitsev. We shall investigate the problem of crack propagation in an elastic plate of relative thickness 1 containing circular inclusions (coarse aggregate particles). Each inclusion has one pre-existing bond crack; the dimension of the most dangerous crack in the matrix (hardened cement paste), defining its strength, is small as compared to the dimension of the inclusions. We shall assume also that the value of K_{IC} for inclusions is greater than the value of K_{IC} for the matrix, and the value of K_{IC} for the matrix is greater than the value of K_{IC} for the interface, i.e.

$$K_{IC}^{INCL} > K_{IC}^{M} > K_{IC}^{IF}.$$

With these assumptions, this problem has been solved by Cherepanov. He has found the following relationship between the external tensile load q_* and the angle θ, which defines the dimension of the crack:

$$q_* = K_{IC}^{IF} F(\theta) \sqrt{R};$$

$$F(\theta) = \frac{4(3-\cos\theta)/\sqrt{\pi}}{\sqrt{\sin\theta(44+12\cos\theta+12\cos^2\theta-4\cos 4\theta+\sin^4\theta)}}$$

Fig.I6 Line I on Fig. I6 shows this relationship; on the y-axis values of the related load $q^0_{IF} = q_* \sqrt{2R/\pi} / K_{IC}^{IF}$ are given. Where $\theta < \theta_0$ $(\theta_0 = \pi/4)$ a crack propagates in an unstable fashion (descending part of the curve), but

when $\theta > \theta_o$ the crack becomes stable (ascending part of the curve). The crack can propagate in a stable fashion only before the external load has reached a definite critical value, corresponding to the appearance of matrix branches of the crack according to Fig. I6 (above), which will again lead (by $\theta > \theta_2$) to an unstable fashion of crack propagation. The precise value of θ_2 depends on the value of K_{IC}^{IF} / K_{IC}^{M} : the greater this value is, the less the angle θ_2 is. By $K_{IC}^{IF} / K_{IC}^{M} = 0{,}6$ (which is near to the experimental results of Alexander, Hillermaier and Hilsdorf, Ziegeldorf and Hilsdorf, etc) $\theta_2 = \pi/2$. This situation is shown in Fig. I6 , where line 3 gives the values of the related load for the interfacial part of the crack $q_M^o = q_* \sqrt{2R/\pi} / K_{IC}^{M}$ (i.e. $q_M^o = 0{,}6\, q_{IF}^o$), and line 2 gives the values of the related load for the crack in the matrix. the last values have been found in an approximative way as for a Griffith's crack of the length $2(\ell + R)$. The load value q_o (beginning of the stable stage of crack propagation along the interface) is equal to approximately 80% of the value of q_2 , which corresponds to the beginning of the unstable stage of crack propagation in the matrix. The following stages of crack propagation in concrete can be analysed in an analogous way.

Now we can simulate the structure of concrete and the crack propagation using Monte-Cerlo-Methods. Typical examples of one
Fig.I7 of the computer realisations are shown in Fig. I7. For the simulation, 50 circular inclusions have been produced, and each of them is assumed to have one pre-existing interfacial crack.

It was also supposed that there are pre-existing cracks in the matrix. It was assumed that the centres of cracks in the matrix and the centres of aggregate particles are uniformly distributed on the area of the sample. The length of pre-existing matrix and interfacial cracks as well as the diameter of aggregate particles are assumed to have a Gaussian distribution.

Taking the opening of cracks into consideration, the contribution of cracks to the longitudinal deformation ε_1 can be found, if we assume linear superposition of the two components (see page 8).

Fig.I8 Fig. I8 shows stress-strain curves for concrete according to the results of simulation of crack propagation. On the X-axis, values of the related strain $\varepsilon/\varepsilon^*_{el}$ are given ($\varepsilon^*_{el} = \sigma_{ult}/E$, σ_{ult} is the fracture stress), and on the Y-axis values of related load $q^o_* = q_* \sqrt{2\bar{R}/\pi} / K^M_{IC}$, where $\bar{R}$ is mean value of the diameter of aggregate particles.

The simulated $\sigma-\varepsilon$ curves for concrete in tension may be divided into the three regions shown in figure I8. In the region I, which corresponds to the crack pattern in figure I7a, the external load is less than the q_o-value (see Fig. I6) for each of the pre-existing cracks. This means that cracks do not propagate and there is only very little extension (widening) of these cracks. The $\sigma-\varepsilon$ diagram (line 2 in Fig. I8) is linear, but it has a little bit greater declination as compared to the line 1, which corresponds to a material without cracks; this difference is due to the crack extension(widening) mentioned above.

In the region 2, cracks according to Fig.I7a begin to propa-

gate in a stable fashion, which corresponds to external load values greater tnan the q_o-value (see Fig. I6) for the most dangerous cracks. The corresponding $\sigma - \varepsilon$ curves become slightly non-linear (see lines 3 in Fig. I8, each line corresponds to one realization of the Monte-Carlo-Method.)

In region 3 (see Fig. I7 b,c) cracks begin to propagate through the matrix between the aggregate particles. The $\sigma - \varepsilon$ curves become significantly non-linear (see line 3 in Fig. I8 , upper parts.) Finally, failure of the sample occurs (see Fig. I7d). It was found that region I corresponds to $\sigma < 0{,}65\,\sigma_{ult}$; region 2 to $0.65\,\sigma_{ult} < \sigma < 0{,}9\,\sigma_{ult}$, and region 3 to $\sigma > 0{,}9\,\sigma_{ult}$. It was also found that, by assumed parameters of crack redistribution, the critical load for pre-existing matrix cracks (according to paragraph 2.I) was higher than σ_{ult} for concrete, thus the failure of concrete in this case only depends on the propagation of pre-existing interfacial cracks.

Fig.I9 Fig. I9 shows the mean value (from 20 realizations) of the summarized length of cracks (related to the area of the sample) as a function of the related strain $\varepsilon/\varepsilon_*$. Lines I and 2 correspond to interfacial and matrix cracks. Lines 3 and 4 are given according to experimental results. All results of simulation of crack propagation in concrete described above are in reasonable agreement with existing experimental results.

3.2. Uniaxial compression

Phenomenological aspects of inelastic properties of concrete subjected to the uniaxial compression may be summarized

as follows. The pre-existing bond cracks initially do not propagate. From external stress of 30-40% of the ultimate stress, the bond cracks begin to propagate in a stable manner along the interface, then mortar cracks appear. At 70-80% of the ultimate stress there is a significant increase in the number of mortar cracks, and by joining with nearby bond cracks, these begin to form continuous cracks. Their orientation is mainly parallel to the direction of the external load.At all stress levels bond cracks predominate whereby failure of the contact zone of sand particles rarely occurs. For higher strength concretes the strain-stress curve is linear up to a higher stress-strength ratio than in normal concretes because of a decrease in the amount and extent of bond cracking (Ziegeldorf, I983).

The phenomenological description of the fracture process of concrete has delivered valuable information. But many fundamental problems are still unsolved. In particular, the experimental results concerning the effect of aggregate concentration on concrete strength are rather contradictory, the effect of aggregate -paste bond strength on concrete strength is not well understood.

What generally is missimg is a theoretical basis capable of explaining such effects.

Model of Mihashi, model of Zaitsev-Wittmann described above can be applied to the case of concrete in compression too.

In the model of Zaitsev-Wittmann for the case of concrete in compression a problem of crack propagation in an elastic

plate of thickness I, containing inclusions (coarse aggregate particles) is analysed. Inclusions having in this case random polygonial shape are randomly distributed in a matrix. The size and shape distribution and the volume content of the inclusions can be varied in order to simulate different concrete mix proportions. Each inclusion has one pre-existing bond crack; the dimension of the most dangerous crack in the matrix (hardened cement paste), defining its strength, is small as compared to the dimension of the inclusions.

We begin with the simplest case of a randomly inclined crack in an elastic plate loaded at infinity. In Fig.20 an initial crack having a length of 2ℓ, and an inclination of α with respect to the direction of external compressive load $q(q<0)$ is shown. This crack might propagate along the same inclined line as a shear crack (Mode II). It can be shown, however, that in our example at the tips of the initial crack, two branching cracks of Mode I (splitting, or opening cracks) are created (Dias and Hilsdorf (1973), Desay (1977)). By introducing simplifying assumptions the crack length ℓ_2 according to Zaitsev (1977), Zaitsev and Wittmann (1977) can be expressed as follows:

Fig.20

$$P/\sqrt{\pi\ell^2} = K_{Ic}$$

where $P = T \sin\alpha$ and T is the resulting force of shear stress $\tau_{\xi\eta}$, causing sliding of two opposite sides of the inclined crack. Taking the coefficient of friction ϱ into consideration, T can be expressed as follows:

$$T = 2\ell_1\tau_{\xi\eta} = 2\ell_1 q\,(\sin\alpha\cos\alpha - \varrho\sin^2\alpha)$$

From these equations we can obtain (crack of Mode I in matrix):

$$q_I^M = -\frac{\sqrt{\pi \ell_2}}{2\ell_1} \frac{K_{IC}^M}{A(\alpha,\rho)}$$

where $A(\alpha,\rho) = \sin^2\alpha\cos\alpha - \rho\sin^3\alpha$. From the lower equation one can see that the propagation of such a crack is stable, i.e. ℓ_2 will steadily increase as $|q|$ increases. A similar stable propagation of such cracks has been observed experimentally.

After analysing this simplest case, we shall now consider a homogeneous matrix with one polygonial inclusion, representing an aggregate particle in an infinite matrix. An initial interfacial crack with length $2\ell_1$ is assumed to be located along one side AB (see Fig.2Ia). This problem can be treated in a similar way as the one with an inclined crack in a homogeneous matrix, taking into consideration, however, concentration of shear and normal stress in the interface. This can be done by introducing coefficients of stress concentration k_τ , k_σ . It can be shown that the initial shear crack spreads (mode II) in an unstable fashion as soon as the critical load q_{II}^{IF} (Mode II, interface) is reached:

Fig.2I

$$q_{II}^{IF} = -\frac{K_{IIC}^{IF}}{\sqrt{\pi \ell_1}\, D_{IF}(\alpha,\rho)}$$

where $D = k_\tau \sin\alpha\cos\alpha - k_\sigma \rho \sin^2\alpha$. The shear crack reaches the length $2L_1$ (see Fig.2Ib) and stops, because further crack propagation in the same inclined direction would take place through the matrix, where $K_{IIC}^M \gg K_{IIC}^{IF}$

If, however, the external load is increased to a higher critical value q_I^M :

$$q_I^M = - \frac{\sqrt{3/4}\ K_{IC}^M}{\sqrt{\pi L_1}\ D_{IF}(\alpha,\rho)}$$

branching cracks in the matrix will develop (see Fig.2I c). The actual crack length in the matrix can be given as a function of load analogously with the case of a homogeneous material treated alone:

$$q = - \frac{\sqrt{\pi \ell_2}}{2L_1} \quad \frac{K_{IC}^M}{A_{IF}(\alpha,\rho)}$$

where $A_{IF}(\alpha,\rho) = D_{IF}(\alpha,\rho)\sin\alpha$, and ℓ_2 corresponds to the distance AA' as shown in Fig. 2Ic.

Fig.22 In Fig.22 the situation as shown in figure 21c is repeated, but now it is assumed that the branching crack AA' meets a second inclusion as it propagates. Further crack growth will either take place through the inclusion maintaining the same direction, or the crack has to follow the same inretface MN, but as a crack of Mode II (see Fig. 22c). To know which path will be followed, three critical load values must be compared:

$$q_I^{INCL} = - \frac{\sqrt{\pi \ell_2}}{2L_1} \quad \frac{K_{IC}^{INCL}}{A_{IF}(\alpha,\rho)}$$

$$q_I^{INT} = - \frac{2 K_{IC}^{IF} \sqrt{\pi \ell_2}/L_1}{A_{IF}(\alpha,\rho)\left\{3\cos\frac{\beta}{2} + \cos\frac{3\beta}{2}\right\} - 3B_{IF}(\alpha,\rho)\left\{\sin\frac{\beta}{2} + \sin\frac{3\beta}{2}\right\}}$$

$$q_{II}^{INT} = - \frac{2 K_{IC}^{IF} \sqrt{\pi \ell_2}/L_1}{A_{IF}(\alpha,\rho)\left\{\sin\frac{\beta}{2} + \sin\frac{3\beta}{2}\right\} + B_{IF}(\alpha,\rho)\left\{\cos\frac{\beta}{2} + \cos\frac{3\beta}{2}\right\}}$$

The index INCL denotes that values are valid for the crack propagation through the second inclusion; ℓ_2 corresponds to the distance AA' as shown in Fig. 22b and $B_{IF}(\alpha,\rho)$ is equal to:

$$B_{IF}(\alpha,\rho) = D_{IF}(\alpha,\rho)\cos\alpha$$

From the expressions for $q_{V_I}^{INCL}$, $q_{V_I}^{INT}$, $q_{V_{II}}^{INT}$ it is evident that the further crack path depends on the relationship between interface and inclusion characteristics K_{IC}^{INCL}, K_{IC}^{IF}, K_{IIC}^{IF} as well as on the geometry of the crack path A'-ABB' (see expressions for $A_{IF}(\alpha,\rho)$, $B_{IF}(\alpha,\rho)$) and the inclination of the interface MN.

For further discussion of these theoretical predictions we shall look into three different cases:

- normal concrete (where $K_{IC}^{IF} << K_{IC}^{INCL}$)
- high strength concrete (where $K_{IC}^{IF} \approx K_{IC}^{INCL}$)
- lightweight concrete (where $K_{IC}^{IF} >> K_{IC}^{INCL}$)

These three cases shall be dealt with separately.

In the case of normal concrete a crack will propagate mainly along the interface MN, because the critical $q_{V_I}^{INCL}$-value will be too high as a result of high K_{IC}^{INCL}-values. Whether crack propagation according to Mode I or to Mode II will take place, depends significantly on the sign of β (see Fig.22). If $\beta<0$ a crack of Mode I is to be expected but if $\beta>0$ (as in Fig.22), a crack of Mode II is more probable.

It must be noted that shear cracks (Mode II) are facilitated by shear components of external pressure, whereas the presence of normal confining components of external compression makes the formation of opening cracks in the interface (Mode I by $\beta<0$) less likely as compared to the formation of shear cracks (Mode II by $\beta>0$). This theoretical prediction has been verificated experimentally (Zaitsev and Wittmann, 1981). As a consequence, in a material with randomly distributed inclusions (where the probability of occurence of positive and negative

values of β are equal) new interfacial cracks will propagate mainly according to Mode II by $\beta > 0$. This means that a resulting crack running through the total specimen will contain some interfacial parts, which deviate largely in the same direction ($\beta > 0$!) from the external load direction (see also Fig. 22). Thus, the resulting crack will be slightly inclined and not exactly parallel to the external load direction.

In the case of high-strength concrete a crack as shown in figure 22 will propapagate either according to the mechanics described above (i.e. along the interface), or it will penetrate into the inclusion. With increasing values of β crack propagation along an interface occurs at higher loads.

Above a critical value β_* of the angle of inclination of the interface side β, cracks will choose their way through inclusions. The critical value, β_*, is practically independent of α and/or ρ and depends only on the ratio χ_1 of K_{Ic}^{INCL} and K_{Ic}^{IF}. In particular, by $\chi_1 = K_{Ic}^{INCL}/K_{Ic}^{IF} = 1$ we obtain $\beta_* = \pi/3$. Crack propagation in the inclusion also depends on the ratio χ_1. If $\chi_1 < 1$, cracks grow more rapidly and if $\chi_1 > 1$ they grow more slowly as compared to the homogeneous matrix. Thus, for hihg-strenght concrete the probability of crack deviation from the direction of the external load is much less as compared to the case of normal strength concrete.

In the case of lightweight concrete, where the interface strength is much higher than the matrix strength, fracture surfaces run across the matrix and aggregate patticles. For this case the model of crack initiation at pores according to paragraph 3.I can be used. It has been shown that such cracks

propagate in lightweight concrete in a stable fashion analogous to the case of hardened cement paste discussed above. After a crack has reached an inclusion it propagates into the inclusion. This popagation becomes instable because of the small K_{IC}^{INCL} -values as compared to corresponding K_{IC}^{M} -values. When the crack, after having passed through the inclusion, reaches the matrix again, it stops. After further increase of the external load (depending on $\chi_1 = K_{IC}^{INCL} / K_{IC}^{M}$ -value) the crack will propagate through the matrix again as if it were a homogeneous material.

After describing all essential elements of crack propagation in a two-phase material, we can simulate the structure of concrete and the crack propagation using Monte-Carlo-Methods. Typical examples of computer realizations of the structure of
Fig.23 normal and lightweight concrete are shown in Fig.23. In the case of normal concrete 30 polygonal inclusions have been produced. Each particle is supposed to have one interfacial crack. The structure can also be used to study crack propagation in high strength concrete. In this case the geometrical arrangement is maintained, but the fracture mechanics parameters are modified. The random structure of lightweight concrete is simulated by 20 round inclusions and small pores spread over the matrix.

As the load in the computer experiment is increased, first the most critical cracks will propagate. Further increase of the load produces a characteristic crack pattern and finally one crack will run throuh the total specimen. This is defined to be failure of the material.

Different load levels and corresponding crack patterns are
Fig.24-26 found by means of a computer experiment as shown in fig.24-26. A discussion of this result is published by Zaitsev and Wittmann (I98I), Wittmann and Zaitsev (I98I). Cracks in normal concrete do not penetrate aggregates, thus they contain some interfacial parts which mostly have an angle of inclination of the same sign, and the resulting "over-all" crack will be slightly inclined. To the author's knowledge, this often observed behaviour is now theoretically explained for the first time.

Fig.27 Fig. 27 shows stress-strain curves in uniaxial compression according to the results of simulation of crack propagation for normal concrete after Zaitsev and Kazatskij (I982). The effect of K_{IC}- and E- values of aggregates on the shape of σ-ε -curves of concrete have been studied. K_{IC} - and E- values for matrix were equal to 0,3 MPa.$m^{1/2}$ and 27 GPa respectively.

K_{IC} - and E -values for aggregates were equal to 0,33 MPa.$m^{1/2}$ and 29,7 GPa (curve I), 0,45 MPa.$m^{1/2}$ and 40,5 GPa (curve 2), 0,57 MPa.$m^{1/2}$ and 51,3 GPa (curve 3), 0,8I MPa.$m^{1/2}$ and 72,9 GPa (curve 4). Geometrical arrangement of simulated structure of concrete, including pre-existing cracks was the same for all realizations. As we can see from Fig. 27, computer experiments give a possibility to evaluate the effect of aggregate properties on inelastic behaviour and strength of concrete and provide a solid basis for further systematic investigations. Differing material structures as well as failure under a multiaxial state of stress can be studied in a similar way. Time-dependent processes such as failure under high sustained load can be included in this type of investigation too.

REFERENCES

Ashrabov A.A. and Zaitsev Y.V. (I98I). 'Elements of fracture mechanics of concrete' (in Russian). Ukituvchi, Tashkent.

Bascoul A., Maso J.C. (I982) 'Influence of the spatial strain gradient on the cracking limit state of concrete' in Proc. Int. Symp. Bonds between cem. paste and oth. materials. INSA, Toulouse, I7-I9 Nov. I982, pp. C.47-C.45.

Bazant Z.P. (I974). 'A new approach to inelasticity and failure of concrete, sand and rock: endochronic theory.' Proc. IIth Ann.Meet. Soc. of Engng. Sci., Duke University, Durham, N.C., Nov. I974 (Ed. G.J.Dvorak), pp.I58-I59.

Bažant Z.P. (I980) 'Hysteretic fracturing endochronic theory for concrete', Journal of the Engeneering Mechanics Division. Proceedings of the ASCF, v. I06, No.EM5.

Bažant Z.P. (I982) 'Methematical models for creep and shrinkage of concrete.' in Creep and Shrinkage in Concrete Structures (Eds. Z.P.Bazant and F.H.Wittmann), pp.I63-256, Wiley.

Bažant Z.P. (I979) 'Material behaviour under various types of loading.' in High Strength Concrete (Ed. S.P.Shah), Proc. of a Workshop held at the Univ. of Ill. at Chicago Circle, Chicago, I979, pp.79-92

Batzle M.L., Simmons G. and Seigfried M.W. (I980). 'Microcrack closure in rocks under stress: direct observation.' J. of Geophysical Research, vol. 85, 7072-7090.

Bernaix J. (I974). 'Properties of Rock and Rock Masses', Advances in rock mechanics. Vol. I, Part A, Proceedings of the Third Congress of the International Society for Roch Mechanics. Washington, D.C., I974, p.9-38.

Brace W.F., Silver E., Hadley K., Goetze C. (I972). 'Cracks and pores: a closer look.' Science, vol.I78, I62-I64.

Brady B.T. (I969) 'The non-linear mechanical behaviour of brittle rock', Int. J. Rock Mech. and Mining Sci., vol. 6, 2II-225 and 30I-3I0.

Brady B.T. (I970) 'A mechanical equation of state for brittle rock' Part I, Int. J. Rock Mech. and Mining Sci. vol.7, 385-42I.

Brady B.T. (I973) 'A mechanical equation of state for brittle rock'. Part II, Int. J. Rock Mech. and Mining Sci. vol.I0,29I-309.

Budiansky B. and O'Connel J. (I976) 'Elastic moduli of a cracked solid,' Int. J. Solids and Struct. Vol. I2, No.2, 8I-97.

Carpinteri A., Di Tomasso A. and Viola E. (I978). 'Stato limite di frattura nei materiali fragili. Modelli meccanici teorici per l'interpretazione della fratura nei caliectruzzi e nelle rocce'. Publicazione n. 38, Universita di Bologna, Instituto di scienza delle construzioni, Bologna.pp.1-24.

Desay P. (I977). 'Fracture of concrete in compression', Materiaux et constructions', v.I0, I39-I43.

Dias S., Hilsdorf H.K. (I973) 'Fracture mechanisms of concrete under compressive loads', Cem. Concr. Res.,vol.3, No.4,pp

Dougill J.W. (I982).'Mechanics of concrete systems: current approaches to assesing material behaviour and some possible extensions', in Creep and Shrinkage in Concrete Structures (Eds. Z.P.Bazant and F.H.Wittmann), pp. 23-49, Wiley.

Dougill J.W., Rida M.A. (I980) 'Further consideration of progressively fracturing solides', J.Engng. Mech. Div. ASCE, I02I-I038.

Evans R.H. and Marathe M.S. (I968).'Microcracking and stress-strain curves for concrete in tension',Materiaux et Constructions,

vol. I, No. I, 6I-64

Gash P.J. (I97I) 'A study of surface features related to brittle and semibrittle fracture', Tectonophysics, vol. I2, 349-39I.

Gerstle K.H., Aschl H., Belotti R., Bertacchi P., Kots'ovos M.D., Hon-Jim Ko, Linse D.,Newman J.B., Rossi P., Schickert G., Taylor M.A., Traina L.A., Winkler H., Zimmerman R.M. (I980) Behaviour of concrete under multiaxial stresses', -Journal of the Engineering Mechanics Division, , vol. I06, No EM6, pp. I383-I403.

Genijev G.A., Kissjuk V.N., Tjupin G.A. (I974) 'Theory of plasticity of concrete and reinforced concrete' (in Russian), Strojizdat, Moscow.

Hillerborg A. (I983). 'Analysis of a single crack', in Fracture Mechanics of Concrete (Ed. F.H.Wittmann), Elsevier, A msterdam.

Hsu T.T.C., Slate F.O., Sturman G.M. and Winter G. (I963) 'Microcracking of plain concrete and the shape of the stress-strain curve.', J.Amer. Concr. Inst., vol.60, No.2,209-224.

Ikeda K., Kabayashi Y. and Sakurai T. (I973). 'Effect of flows on the strength of rocks', Quart. Repts. Railway Techn. Res. Inst., vol. I4, No.2, 6I-64.

Jonston C.D. (I970) 'Deformation of concrete and its constituent materials in uniaxial tension', Highway Res. Rec, No. 324, .

Kozachevskij A.I. (I98I).'About relations of deformation theory of plasticity for concrete with respect on structural anisotrophy', in Resistance of Materials and Theory of Structures (in Russian), vol. 39, Budivelnik,Kiev,pp.84-88.

Kozachevskij A.I. and Zjazin A.M. (I982) 'Study of non-linearity of dilatancy model of deformation theory of plasticity for concrete', in Static and Dynamic of Sophisticated Building Structures (in Russian). LISI, Leningrad, pp.38-45.

Loland K.E. (I980).'Continuous damage model for load-response estimation of concrete', Cem. Concr. Res., v.IO, 395-402.

Lorrain M. and Loland K.E. (I983) 'Damage theory applied to concrete', in Fracture Mechanics of Concrete (Ed. F.H. Wittmann), Elsevier, Amsterdam.

Lott J., Kesler C.E. (I966).'Crack propagation in plain concrete', in Symp. on Structure of Portland Cement Paste and Concrete, Spec. Rep. 90, Highw. Res. Board,Washington, D.C., pp. 204-2I8.

Mihashi H. (I983) 'A stochastic theory for fracture of concrete', in Fracture Mechanics of Concrete (Ed. F.H.Wittmann), Elsevier, Amsterdam.

Mindess S. (I983) 'Application of fracture mechanics to hardened cement paste and concrete.- A historical review', in Fracture Mechanics of Concrete (Ed. F.H.Wittmann), Elsevier, Amsterdam.

Mindess S. and Diamond S. (I980). 'A preliminary SEM study of crack propagation in mortar', Cem. Concr. Res. vo. IO, No.4, pp.509-5I9.

Moavenzadeh F. and Kuguel R. (I969). 'Fracture of concrete,' J. of Materials, vol.4, No. 3,pp. 497-5I9.

Nikolaevskii V.N. (I982) 'Deformation of geomaterials and porous media', Proc. USSR Acad. Sci., Mechanics of Solid, No.2 96-I09. (in Russian).

Nikolaevskii V.N. and Rice J.R. (I979)'Current topics in the nonelastic deformation of geological materials', in High pressure Sci. and Technol, Vol. 2, pp.455-464, Plenum,New York.

Panasjuk V.V. (I968) 'Limit equilibrium of brittle bodies with cracks', Naukova Dumka, Kiev. (in Russian)

Panasjuk V.V., Savruk M.P. and Dazyshin A.P. (I976),'Stress distribution around cracks in plates and shells',(in Russian) Naukova Dumka, Kiev.

Rice J.R. and Rudnicki J.W. (I980)'A note on some features of the theory of localization of deformation', Internat. J. Solids Struct., v.I6, 597-605.

Rong.C., Xiao-Xin (I979) 'Studies of the fracture of gabbro', Internatinal Journal of Rock Mechanics and Mining Sciences and Geomechanics Abstracts, v.I6, I87-I93.

Rudnicki J.W. and Rice J.R. (I975)'Conditions for the localization of deformation in pressure-sensitive dilatant materials', J.Mech. Phys. Solids, v.23, No.6, 37I-394.

Ruetz W. (I966) 'Das Kriechen des Zemensteins im Beton uns seine Beeinflussung durch gleichzeitiges Schwinden', Dtsch. Ausschuss Stahlbeton, Schriftenr. Heft I83, Wilhelm Ernst & Sohn, W.-Berlin.

Salganik R.L. (I973). 'Mechanics of bodies with great number of cracks' ,Proc. USSR Acad. Sci., Mech. of Solid, No.4, I49-I58 (in Russian).

Sauoma V.E., Ingraffea A.R. and Catalano D.M. (I980) 'Fracture toughness of concrete - K_{Ic} revisited', Rep.80-9, Department of Struct. Engng, Cornell Univ.,Ithaca,New York.

Shah S.P. and McGarry F.J. (I97I) 'Griffith fracture criterion and concrete', J. Engng. Mech. Div., ASCE, vol.97, No.EM6, I663-I676.

Shah S.P. (I979) 'Whither fracture mechanics in concrete design?' Proc. Engng. Foundation Conf. on Cement Production and Use, Rindge, June 25-29, I979, pp. I87-I99.

Sellevold E.J. (I976) 'Low frequency internal friction and short-time creep of hardened cement paste: an experimental correlation', Proc. Conf. on Hydraulic Cement Pastes: Their Structure and Properties. Sheffield, pp.330-334.

Simmons G., Richter D. (I976) 'Microcracks in rocks,' Phys. and Chem. Miner. and Rocks. London,ppI05-I37.

Slate F.O., Jaquot P., Lierse J., Ringkamp M., Rastogi P.K. and Terrien M. (I983) 'Experimental methods for detection and analysis of cracks in concrete', in Fracture Mechanics of Concrete (Ed. F.H.Wittmann), Elsevier, Amsterdam.

Stavrogin A.N. (I969) 'Research on limit state and deformation of rocks', Proc. USSR Acad. Sci., Physics of the Earth, No. I2, 3-I7.

Stavrogin A.N. and Protosjenja A.G. (I979). Plasticity of rocks, Nedra, Moscow. (in Russian)

Stroeven P. (I973) 'Some aspects of the micromechanics of concrete', Ph.D. Thesis, Delft.

Swamy K.N. (I983) 'Experimental methods to determine fracture mechanics parameters - mortar and concrete', in Fracture Mechanics of Concrete (Ed. F.H.Wittmann), Elsevier, Amsterdam.

Swamy R.N. and Sriravindrarajah R. (I982),'Influence of time on the aggregate-matrix bond under sustained load', Proc.

Int. Symp. Bonds between cement paste and other materials, INSA, Toulouse, I7-I9, Nov. I982, pp. C.66-C.78.

Walsh J.B. (I965a) 'The effect of cracks on the compressibility of rock ' J. Geophys. Res., v.70, No.2, 38I-389.

Walsh J.B. (I965 b) 'The effect of cracks on the uniaxial elastic compression of rocks', J. Geophys. Res., Vol. 70, No. 2, 399-4II.

Walsh J.B. (I965c) 'The effect of cracks on Poisson's ratio' J. Geophys. Res., vol. 70, No.20, 5249-5257.

Walsh J.B. (I980) 'Static deformation of rock', J. Engng. Mech. Div. ASCE, I005-I0I9.

Walsh J.B., Brace W.F. (I968) 'Elasticity of rock: a review of some recent theoretical studies', Felsmech. und Ingenieurgeol., vol. 44, No.4, 283-297,

Walsh J.B., Brace W.F. (I972). 'Elasticity of rock in uniaxial strain', Int. J. Rock. Mech. and Mining Sci.,vol.9, No. I, 7-I5.

Warren N., Nashner R. (I976) 'Theoretical calculation of compliences of a porous medium', in Phys. and Chem. Miner. and Rocks,London.

Wang P.T., Shah S.P. and Naaman A.E. (I978). 'Stress-strain curves of normal and lightweight concrete in compression', J. of Amer. Concr. Inst., vol.75, No.II, 603-6II.

Wittmann F.H. (I982) 'Creep and shrinkage mechanisms' in Creep and Shrinkage in Concrete Structures (Eds. Z.P.Bazant and F.H.Wittmann), pp. I29-I6I, Wiley.

Wittmann F.H. (I983) 'Structure of concrete with respect to crack formation', in Fracture Mechanics of Concrete (Ed. F.H.Wittmann), Elsevier, Amsterdam.

Wittmann F.H. and Zaitsev Y.V. (I972) 'Behaviour of hardened cement paste and concrete under high sustained load', Mechanical Behaviour of Materials, Proc. of the I97I Int. Conf. on Mech. Behaviour of Materials, Kioto, Japan, pp.84-95.

Wittmann F.H. and Zaitsev Y.V. (I976) 'Concrete - a visco-elastic porous body'. Proc. 2nd Int. Conf. on Mech. Behaviour of Materials, Boston, USA, August I6-20, I976, pp.I63-I67.

Wittmann F.H. and Zaitsev Y.V. (I98I) 'Crack propagation and fracture of composite materials such as concrete', Proc. 5th Int. Conf. on Fracture, Cannes, March 29 - April 3, I98I.

Zaitsev Y.V. (I969) 'Limit equilibrium of a compressed plate containing a circular hole and cracks' (in Russian), USSR Acad. Sci., Journ. Appl. Mech. and Techn. Phys., No.5, I00-I0I.

Zaitsev Y.V. (I97Ia) 'Deformation and failure of hardened cement paste and concrete subjected to short term load', Cem. Concr. Res., v. I, I23-I37.

Zaitsev Y.V. (I97Ib) 'Deformation and failure of hardened cement paste and concrete under sustained load', Cem. Concr. Res. v.I, 329-344.

Zaitsev Y.V. (I97Ic) 'Experimental investigation to determine the behaviour of hardened cement paste and plaster of Paris under high load', Cem. Concr. Res. v.I, 437-447.

Zaitsev Y.V. (I974) 'Propagation of opening mode cracks in brittle materials subjected to compression' (in Russian) Proc. USSR Acad. Sci., Mech. of Solid, No.4, II8-I25.

Zaitsev Y.V. (I975) 'Consideration of micro- and macro-structure of a material and its pshysical non-linearity in problems of crack propagation in concrete' (in Russian),

Izvestija Vuzov, Stroitelstvo i Architectura, No. II, I5-20.

Zaitsev Y.V. (I977) 'Fracture mechanism of concrete under compression' (in Russian), Beton i Zhelezobeton, No.7,35-37.

Zaitsev Y.V. (I980) 'Influence of structure on fracture mechanism of hardened cement paste', Proc. 7th Int. Congr. on Chemistry of Cement, Paris, June 30 - July 4, I980, pp. VI-I76 - VI-I80.

Zaitsev Y.V. (I98I) 'Fracture mechanism and strength of concrete under triaxial compression', Proc. 5th Int. Conf. on Fracture, Cannes, March 29 - April 3, I98I.

Zaitsev Y.V. (I982) Simulation of deformation and strength of concrete with help of methods of fracture mechanics' (in Russian), Stroiizdat, Moscow.

Zaitsev Y.V. and Wittmann F.H. (I97I) 'Zur Dauerfestigkeit des Betons unter konstanter Belastung', Der Bauingenieur, 46 Jahrg., 84-90.

Zaitsev Y.V. and Wittmann F.H. (I973) 'Fracture of porous viscoelastic materials. Proc. 3rd Int. Conf. on Fracture, Munich, FRG, IX - 323.

Zaitsev Y.V. and Wittmann F.H. (I974). 'Verformung und Bruchvorgang poröser Baustoffe bei kurzzeitiger Belastung und Dauerlast', Deutcher Ausschuss für Stahlbeton, Schriftenr. Heft 232, Wilhelm Ernst und Sohn, W.-Berlin, pp. 65-I45.

Zaitsev Y.V. and Wittmann F.H. (I977) 'Crack propagation in a two-phase material such as concrete', Proc. 4th Int. Conf. on Fracture, Waterloo, Canada, June I9-24, I977, pp.II97-I203.

Zaitsev Y.V. and Wittmann F.H. (I98I) 'Simulation of crack propagation and failure of concrete', Materiaux et Constructions, v. I4, 357-365.

Zaitsev Y.V. and Kazatskij M.B. (I982) 'Evaluation of crack resistance of concrete under uniaxial compression using methods of fracture mechanics', in Evaluation and security of safety of hydotechnical structures, Proc. of Conferences and Meetings on hydraulic engineering, Energija, Leningrad.

Ziegeldorf S. (I983) 'Phenomenological aspects of the fracture of concrete', in Fracture Mechanics of Concrete (Ed. F.H.Wittmann), Elsevier, Amsterdam.

FIGURE CAPTIONS

Fig. I. Failure criteria in biaxial tension for a solid with random cracks.

Fig. 2-5. Interaction of two random cracks.

Fig. 6. Stochastic model for hardened cement paste; a - transition line graph of a stochastic process for tension; b - scheme of fracture in tension; c - transition line graph for compression; d - scheme of fracture in compression.

Fig. 7. Consequent stages of crack propagation in a quasihomogeneous porous solid under tension and stress-strain curves according to results of crack propagation.

Fig. 8. Damage approach for hardened cement paste and concrete in tension; a - fracture zone with pores (I) and cracks (2); b - net contours (net area A_n) of a specimen with reference to the load-elongation curve; c - net stress S, damage ω and nominal stress σ, related to strain ε.

Fig. 9. Classification of fracture for rocks. I - stress path; 2 - yield surface for individual fissure; 3 - elastic zone; 4 - post-loading limit surfaces; 5 - failure; 6 - dilatancy zone; 7 - brittle, 8 - ductile.

Fig. IO. Model of rocks with random cracks.

Fig. II. Model of rocks with a geometrical arrangement of cracks.

Fig. I2. Schematic representation of two pores and coplanar cracks in hardened cement paste.

Fig. I3. Relationship between related external load and related crack length near two pores: a) $c/r = 2$ b) $c/r = IO$

I - relationship for two cracks (Ia) and one (Ib) isolated crack (without interaction) 2 - relationship for interacting external cracks. 3 - relationship for interacting internal cracks.

Fig. I4. Consequent stages of crack propagation in a quasi-homogeneous porous solid under compression and stress-strain curves according to results of simulation of crack propagation.

Fig. I5. Cracks in concrete in compression. a - cracks in unloaded concrete; b - consequent stages of crack propagation and stress-strain relationship; I - aggregate, 2 - mortar, 3 - interface cracks, 4 - cracks between aggregates.

Fig. I6. Relationship between related external tensile load and related length og an interfacial crack; I - interfacial crack (load is related to K_{IC}^{IF}) 2 - interfacial crack (load is related to K_{IC}^{M}) 3 - interfacial crack and additional matrix (load is related to K_{IC}^{M}).

Fig. I7. Crack pattern for different load level in concrete. Cracks originating from interfaces run around aggregates.

Fig. I8. Stress-strain curves for concrete in tension according to results of simulation of crack propagation; I - linear for a material without cracks; 2 - linear for a material with pre-existing cracks which do not propagate; 3 - non-linear taking into account crack propagation; 4 - experimental curves for concrete in tension.

Fig. I9. Summarized length of cracks as a function of related strain $\varepsilon/\varepsilon_x$;,I - simulated (interface cracks); 2 - simulated (matrix cracks), 3 - experimental (interface cracks), 4 - experimental (matrix cracks).

Fig. 20. Schematic representation of the development of branching cracks and definition of symbols used in corresponding equations.

Fig. 2I. An initial crack with length $2\ell_1$ (a) grows in an unstable fashion along an interface AB (b) and finally stable branching cracks AA' and BB' are created as the load is increased.

Fig. 22. A crack path as shown in Fig. 2I, in the vicinity of the second inclusion (a); the crack meets the second inclusion (b); finally the crack will propagate along the interface MN (c).

Fig. 23. Typical computer realization of random structure; a - normal concrete; b - lightweight concrete.

Fig. 24! Crack pattern for two different load levels in normal concrete. Cracks are running around inclusions.

Fig. 25. Crack pattern for two different load levels in high strength concrete. Some cracks penetrate through inclusions.

Fig. 26. Crack pattern for two different load levels in lightweight concrete. Cracks originating from pores run through inclusions

Fig. 27. Stress-strain curves for concrete according to results of simulation of crack propagation.

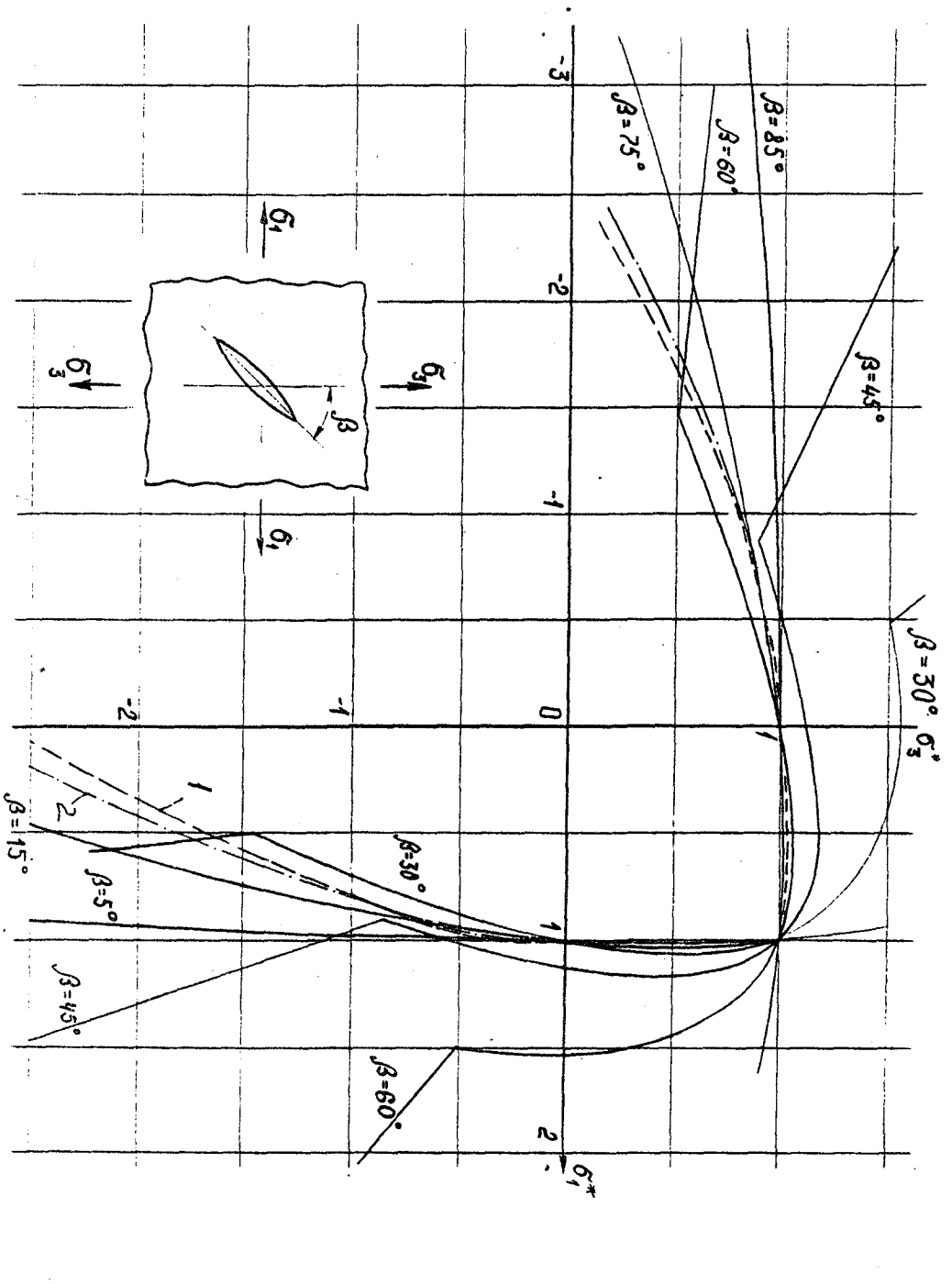

Fig. 1

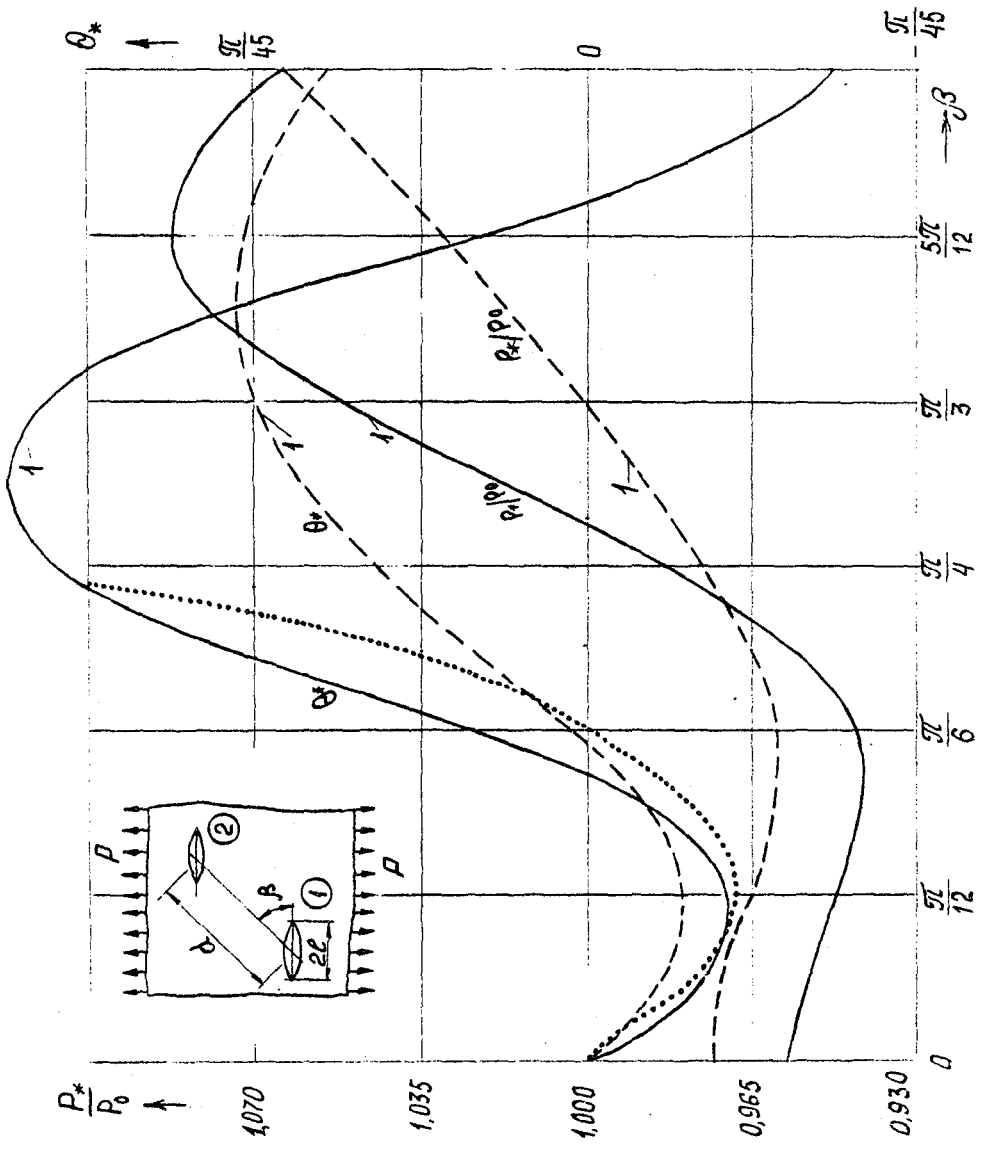
θ*
π/45
0
-π/45
β
π/12
π/6
π/4
π/3
5π/12
P*/P₀
1,070
1,035
1,000
0,965
0,930
P+ρ₀
P₁/ρ₀
θ*
1
2
2ℓ
d
P
p

Fig. 2

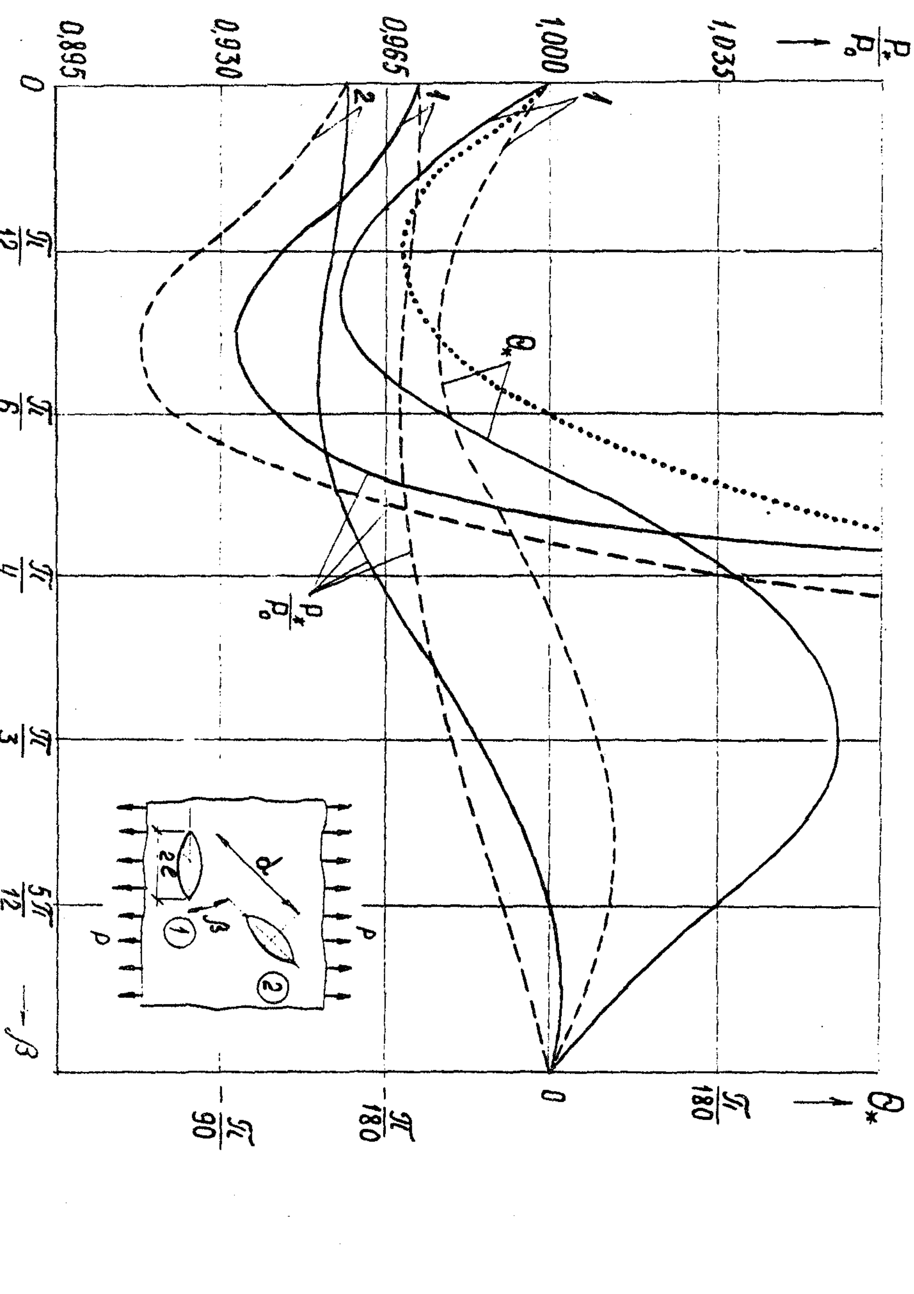

P_*/P_0
0,895
0,930
0,965
1,000
1,035
0
π/12
π/6
π/4
π/3
5π/12
β
Θ_*
0
π/180
π/90
π/180
1
1
2
Θ_*
P_*/P_0
α
2ℓ
β
P
P
1
2

Fig. 3

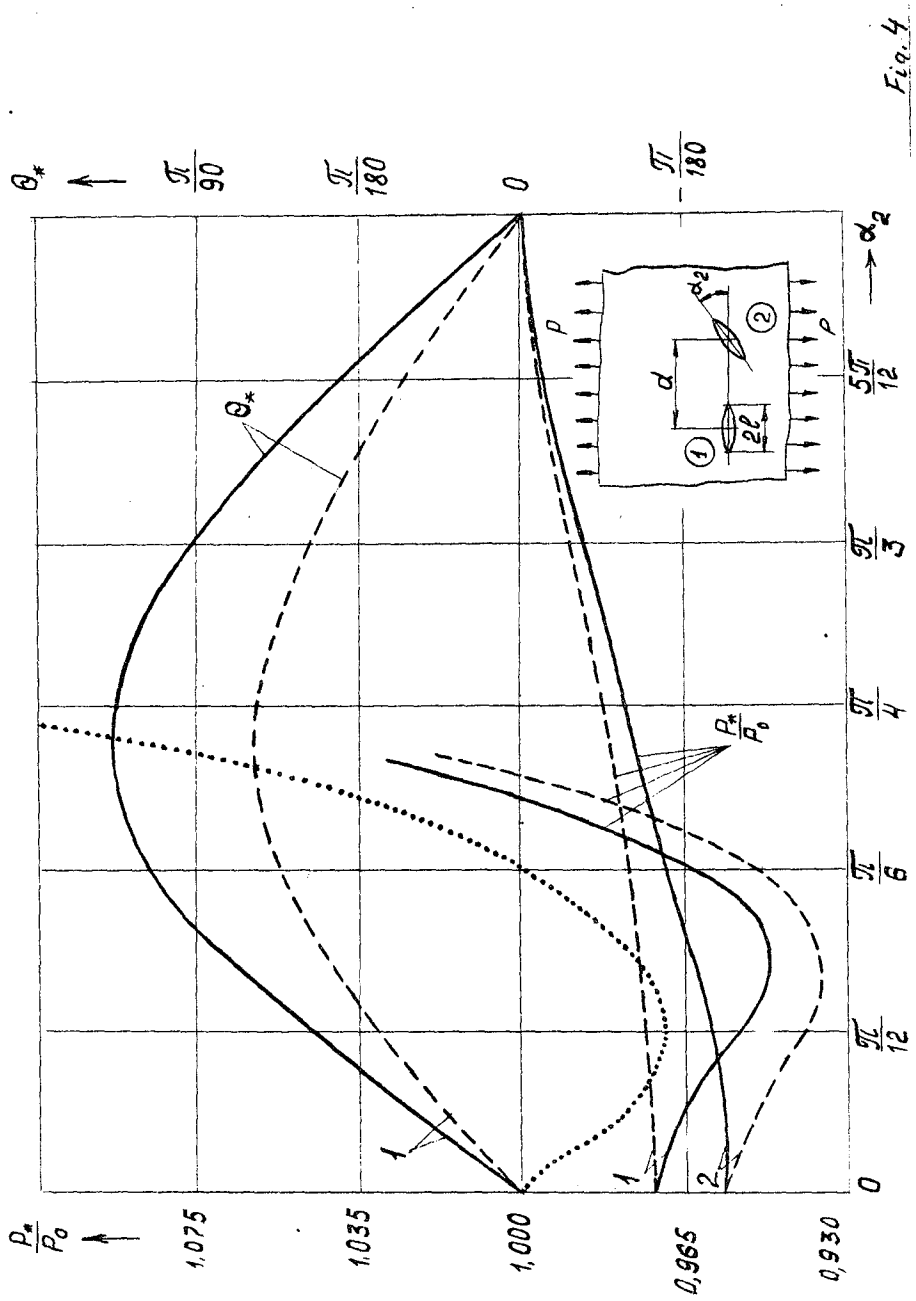
θ*
π/90
π/180
0
-π/180
α₂
5π/12
π/3
π/4
π/6
π/12
0
P*/P₀
1,075
1,035
1,000
0,965
0,930
1
2
d
2ℓ
p

Fig. 4

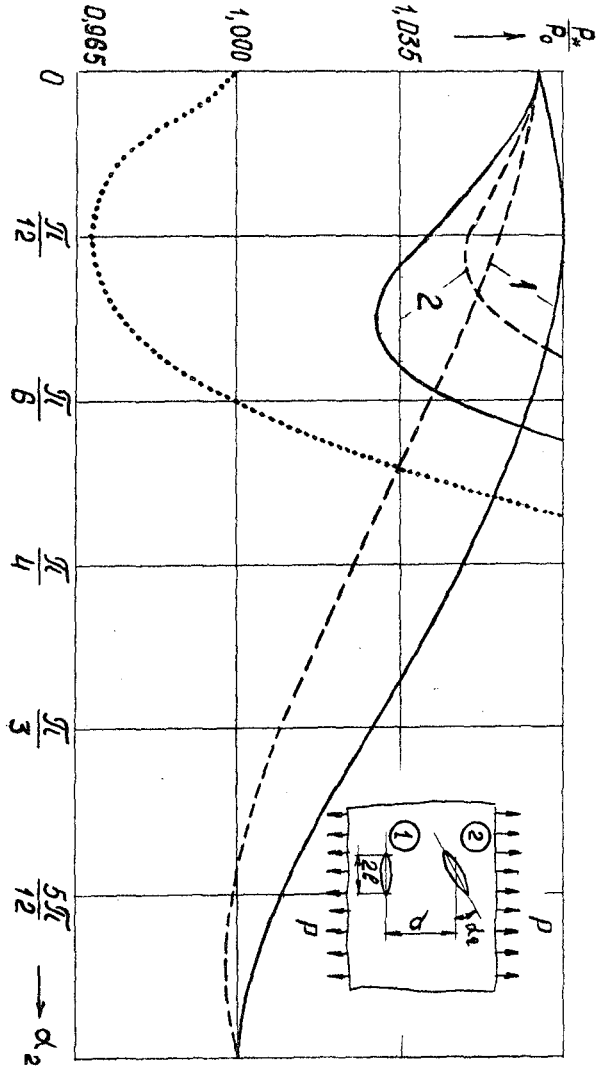
$\frac{p_*}{p_0}$
0,965
1,000
1,035
0
$\frac{\pi}{12}$
$\frac{\pi}{6}$
$\frac{\pi}{4}$
$\frac{\pi}{3}$
$\frac{5\pi}{12}$
α_2
1
2
p
p
d
dα
22

Fig. 5

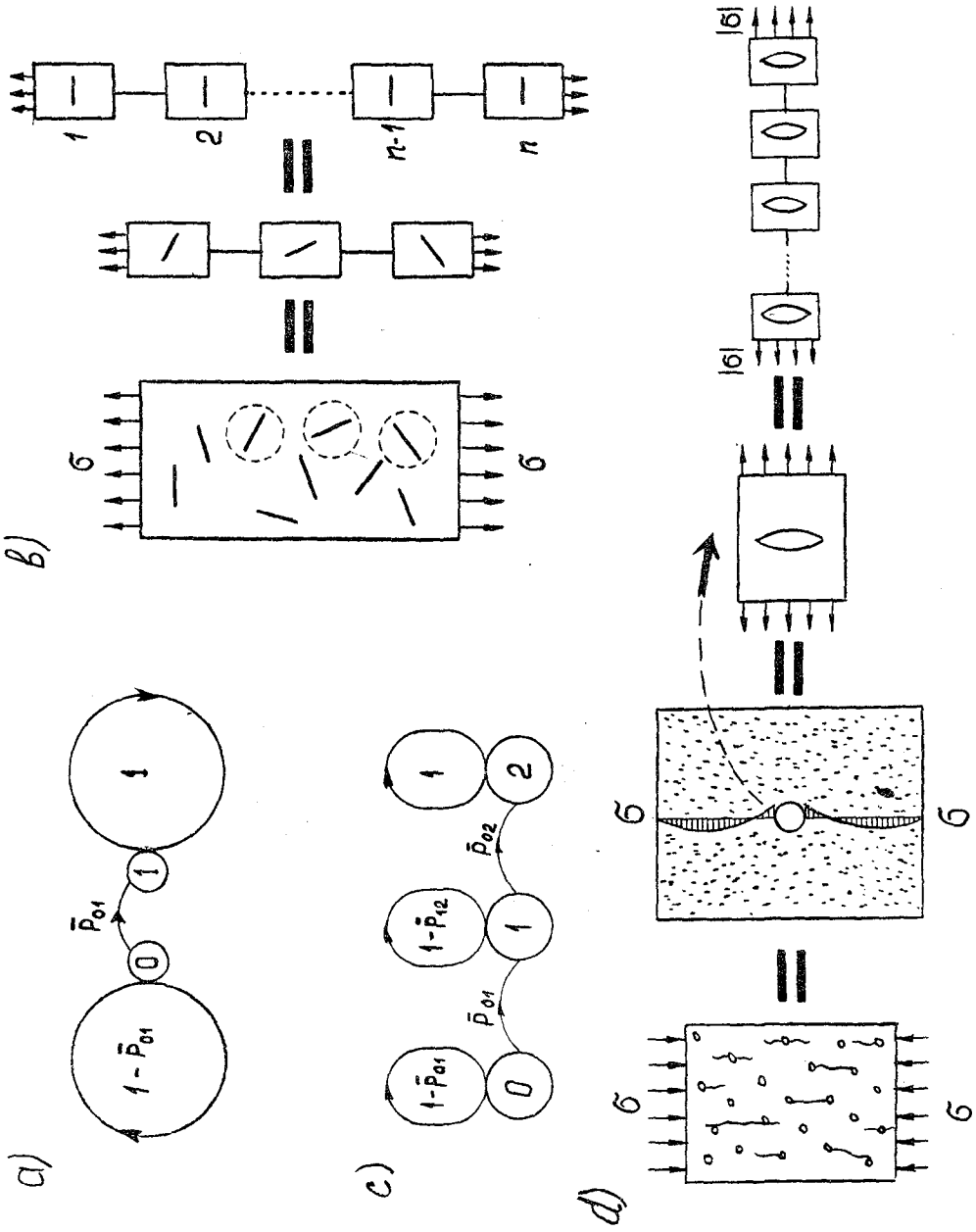
a)
1
1
$\bar{P}_{01}$
0
$1-\bar{P}_{01}$
b)
1
2
n-1
n
6
6
c)
1
2
$\bar{P}_{02}$
$1-\bar{P}_{12}$
1
$\bar{P}_{01}$
$1-\bar{P}_{01}$
0
d)
161
161
6
6
6
6

Fig. 6

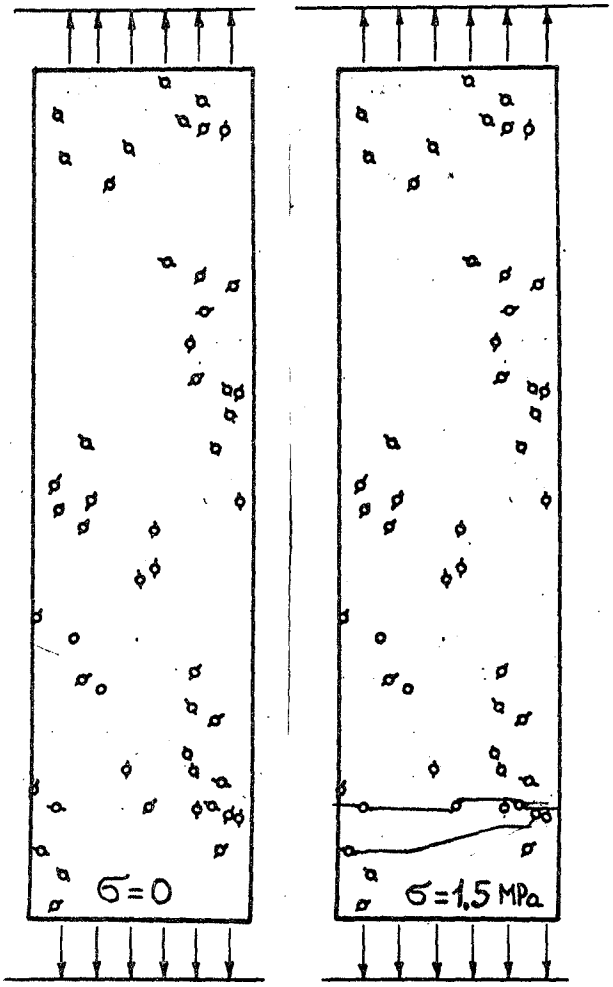

Fig. 7a

в)

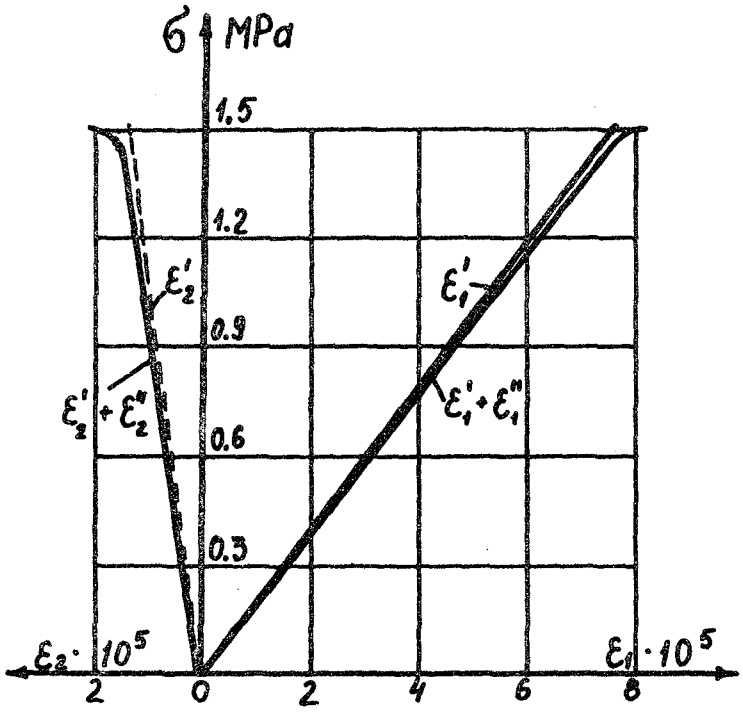
σ MPa
1.5
1.2
0.9
0.6
0.3
$\varepsilon_2' + \varepsilon_2''$
ε_2'
ε_1'
$\varepsilon_1' + \varepsilon_1''$
$\varepsilon_2 \cdot 10^5$
$\varepsilon_1 \cdot 10^5$
2
0
2
4
6
8

Fig 7(6)

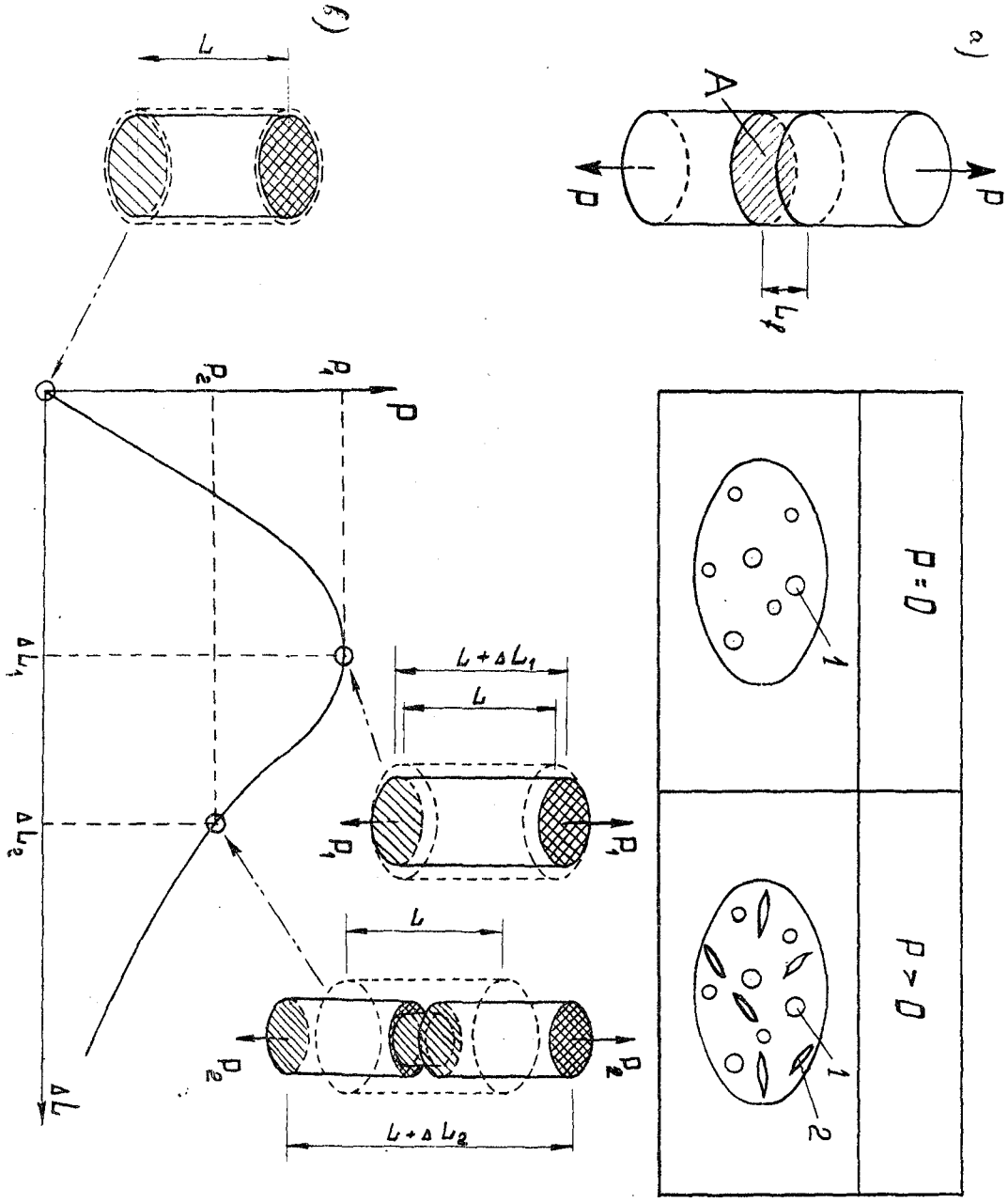
а)
A
P
P
ΔL_1
б)
L
P_2
P_1
P
ΔL_1
ΔL_2
$L+\Delta L_1$
L
P_1
P_1
L
P_2
P_2
$L+\Delta L_2$
ΔL
P = 0
P > 0
1
1
2

Fig. 8.6(б)

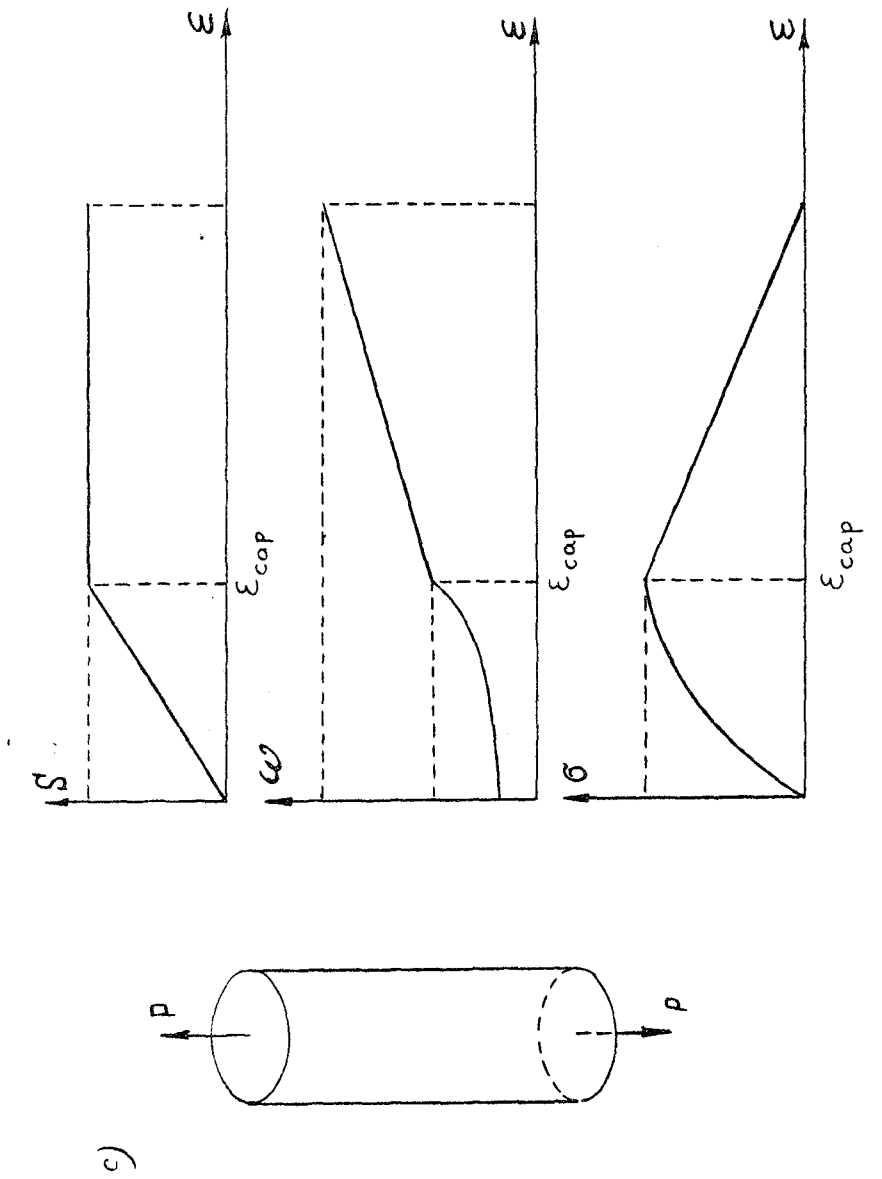

Fig. 8(c)

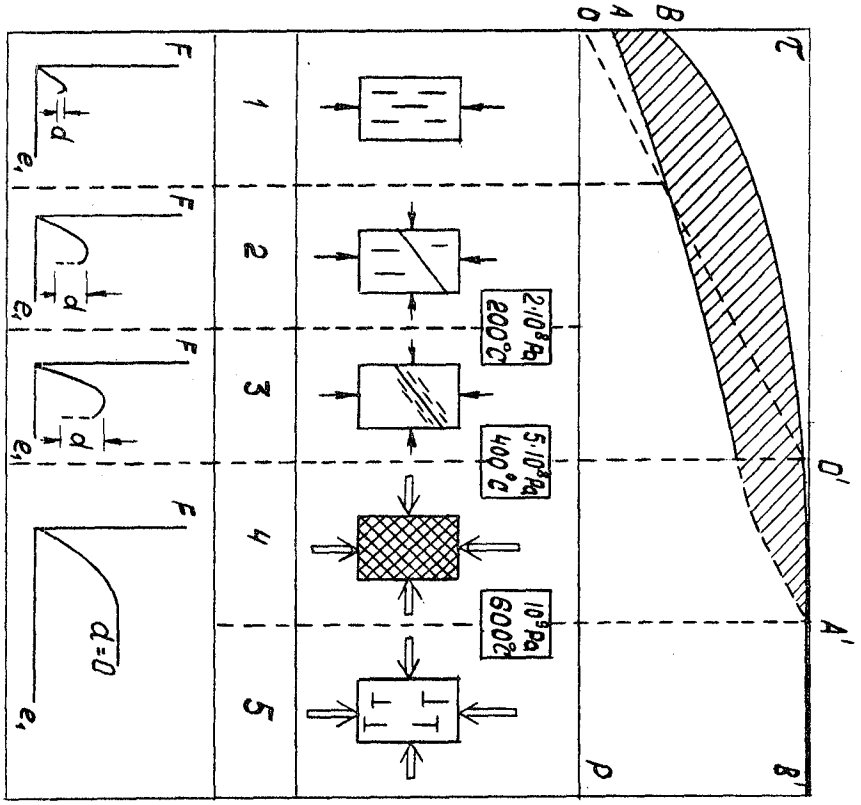

Fig. 9

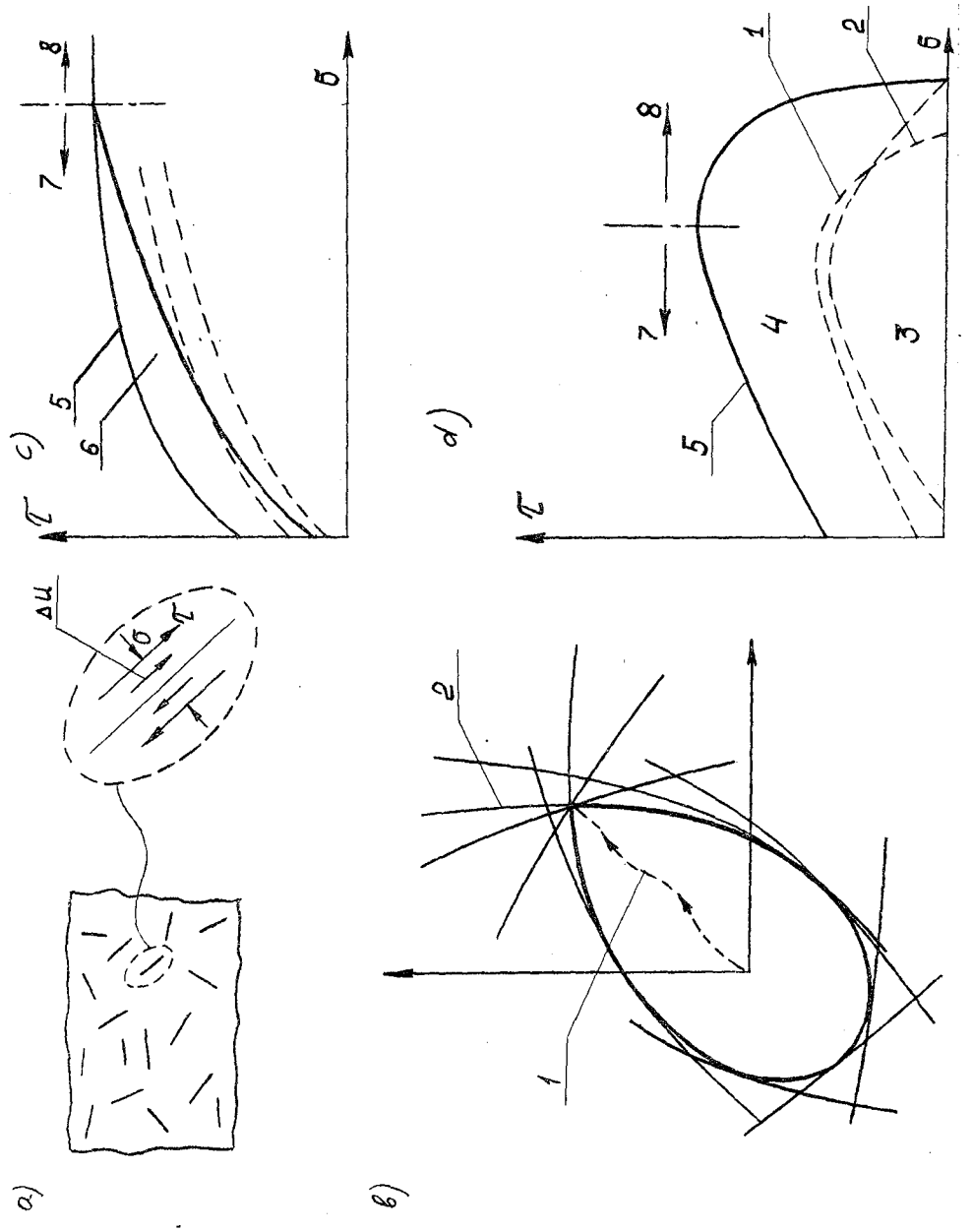

Fig 10

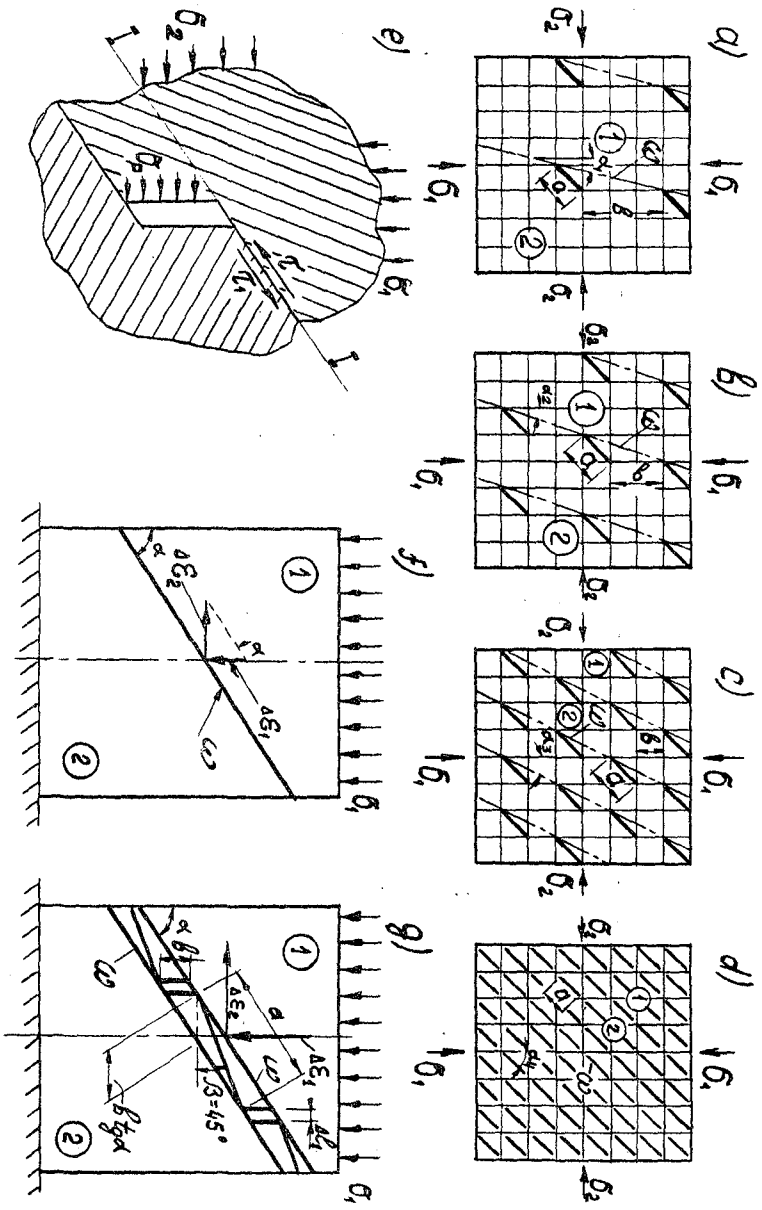

Fig. 11

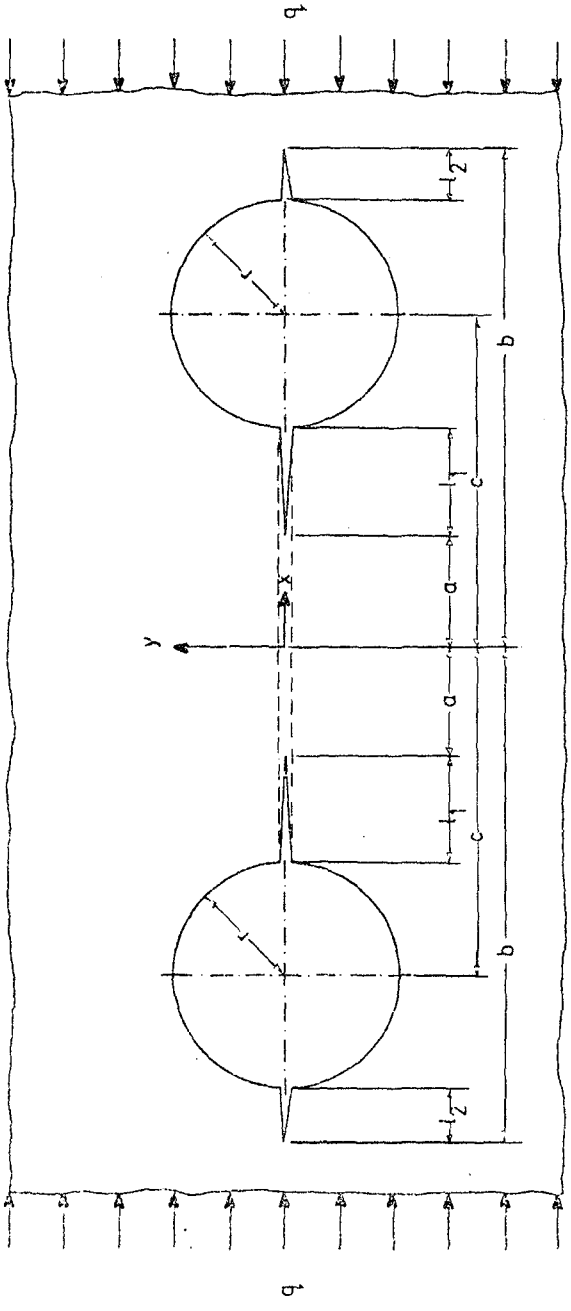

Fig. 12.

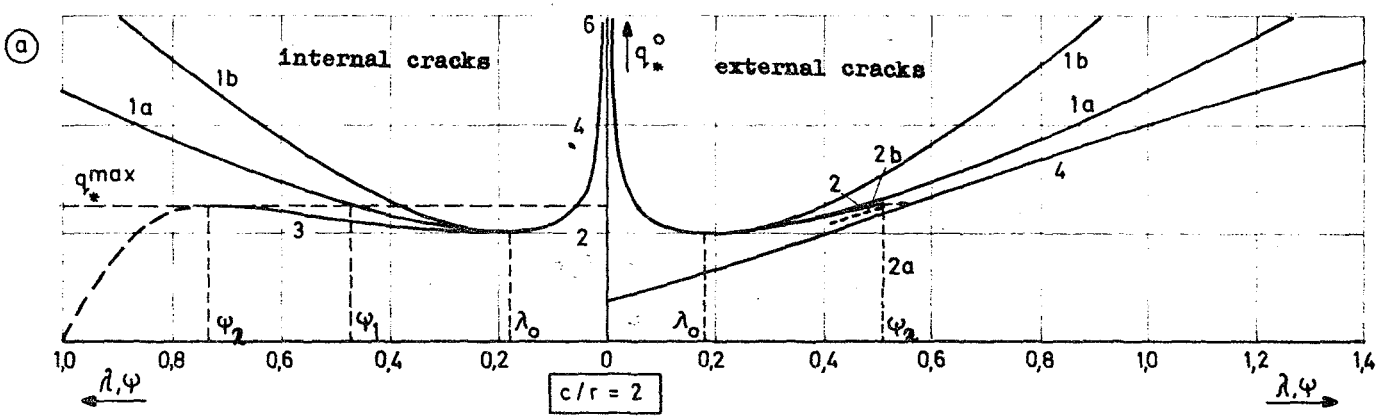
a
internal cracks
external cracks
1a
1b
2
2a
2b
3
4
q_*^{max}
q_*^0
φ_2
φ_1
λ_0
c / r = 2
λ, φ
b
internal cracks
external cracks
$\varphi = \frac{l_i}{c-r}$
$\lambda = l_i / r$
c / r = 10

Fig. 13

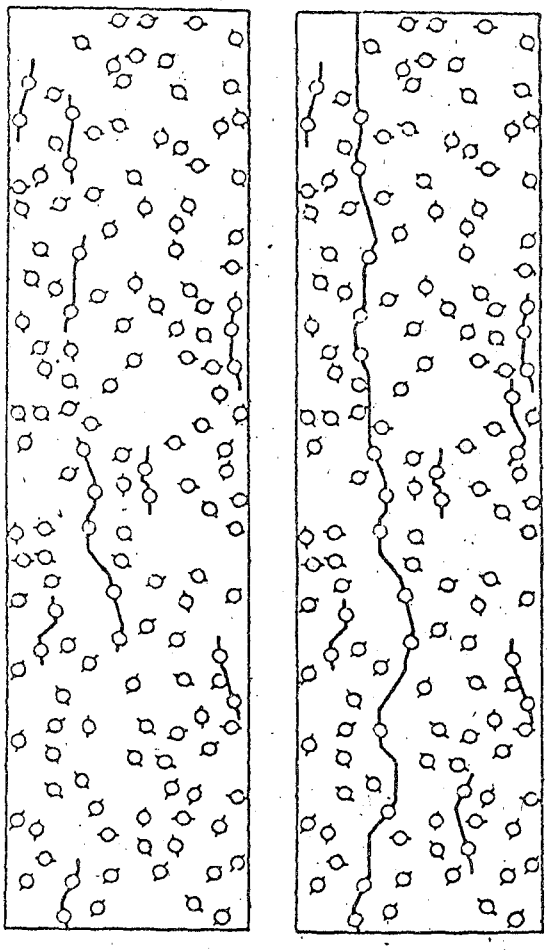

Fig. 14,a

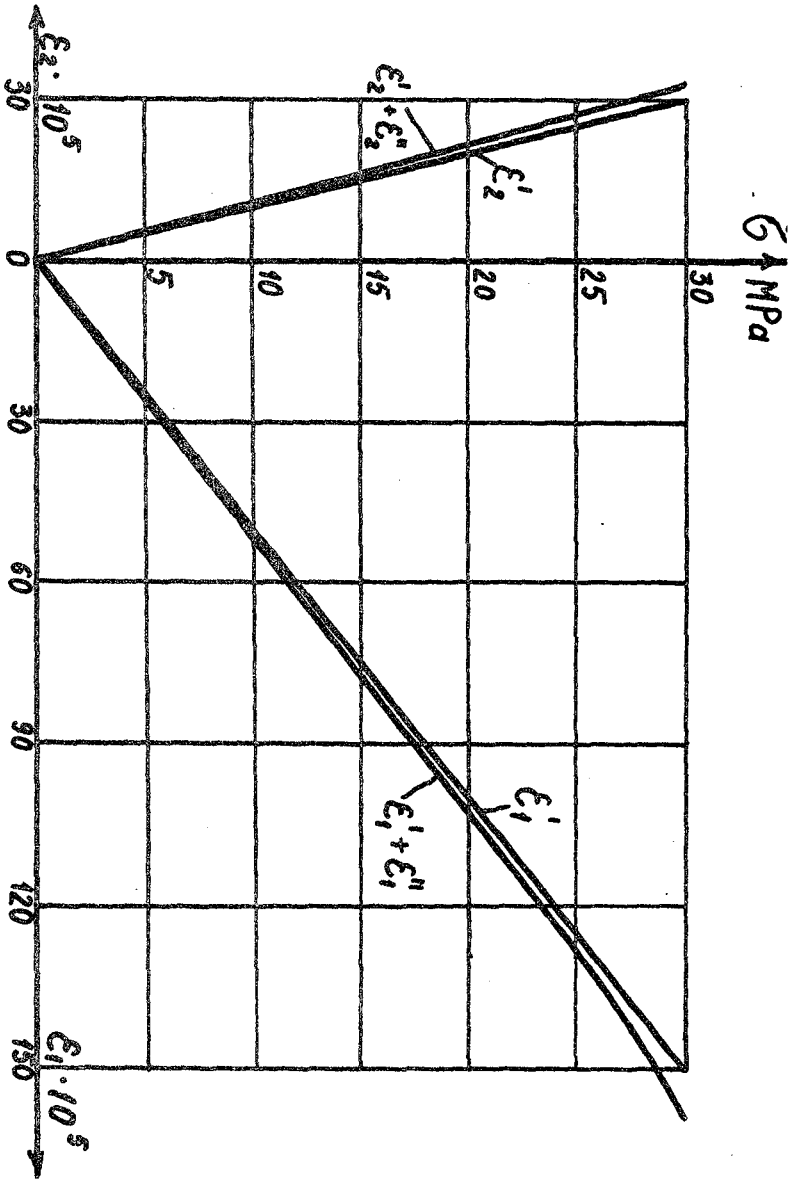
б)
σ MPa
0
5
10
15
20
25
30
$\varepsilon_2 \cdot 10^5$
30
0
30
60
90
120
150
$\varepsilon_1 \cdot 10^5$
$\varepsilon_2' + \varepsilon_2''$
ε_2'
$\varepsilon_1' + \varepsilon_1''$
ε_1'

Fig. 14(б)

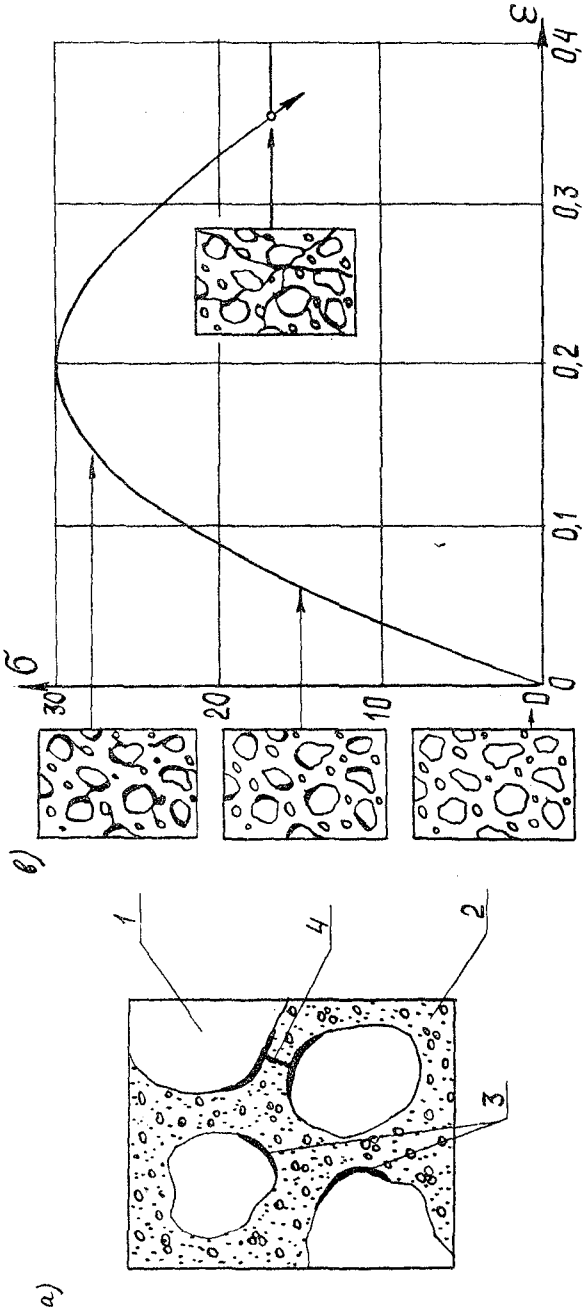

Фиг. 15

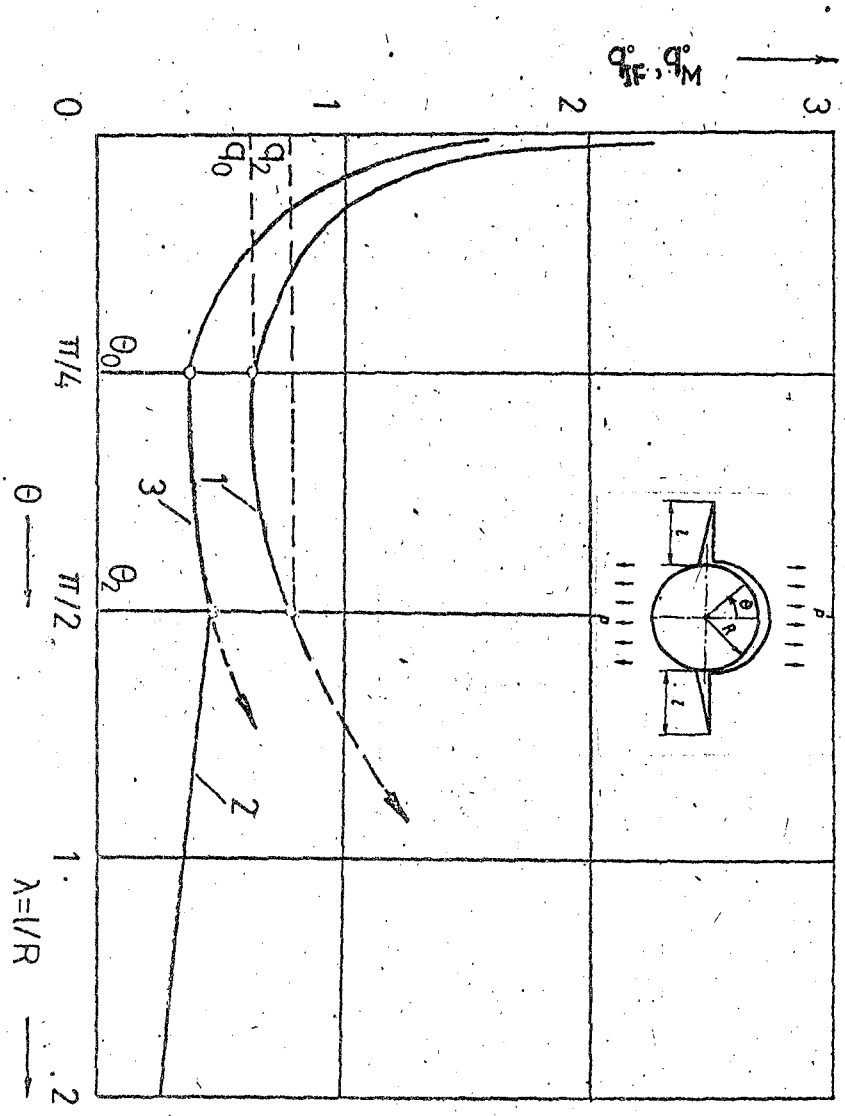
0
1
2
3
$q^{\circ}_{1F}, q^{\circ}_{M}$
q_2
q_0
$\pi/4$
θ_{01}
θ
$\pi/2$
θ_2
1
2
3
1.
.2
$\lambda = l/R$
l
l
θ
R
R

Fig 16

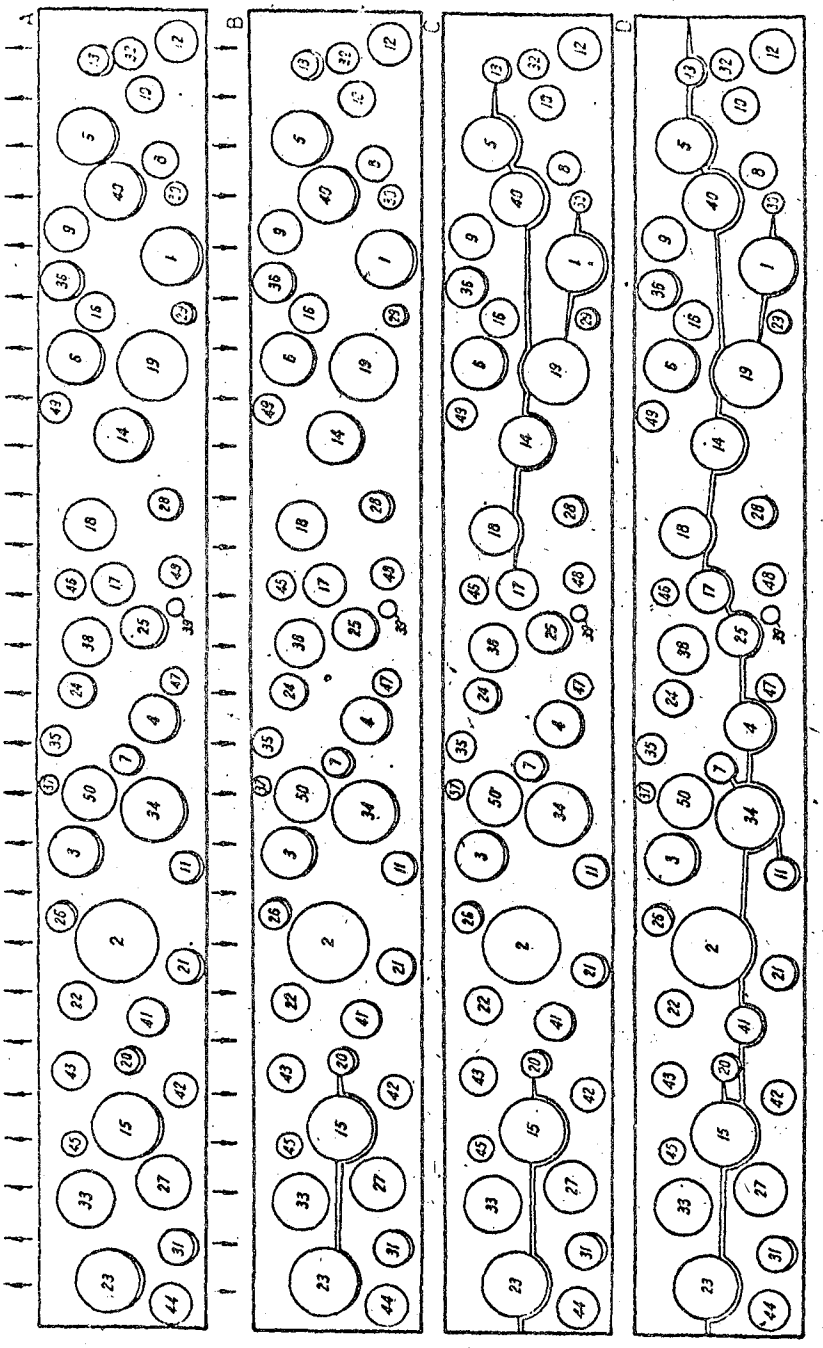

Fig. 17.

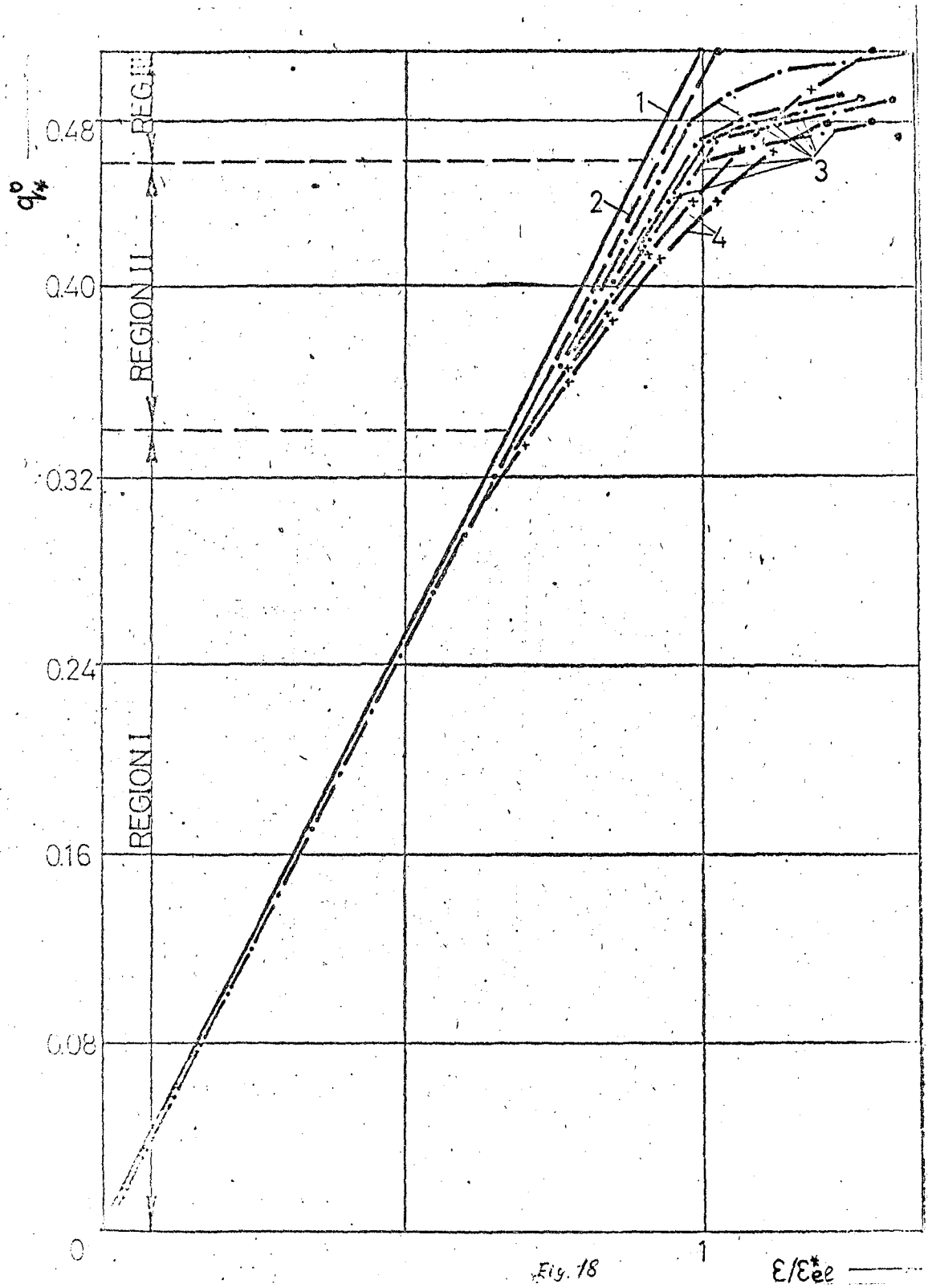
REGION III
REGION II
REGION I
0.48
0.40
0.32
0.24
0.16
0.08
0
1
2
3
4
1
$\varepsilon/\varepsilon^*_{ee}$

Fig. 18

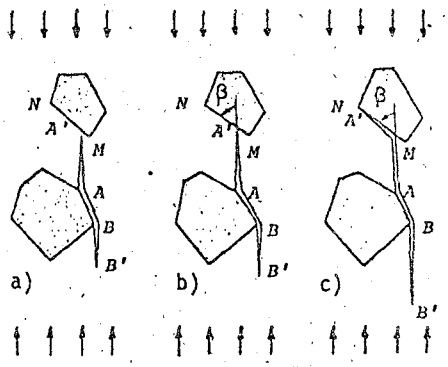

Fig. 22

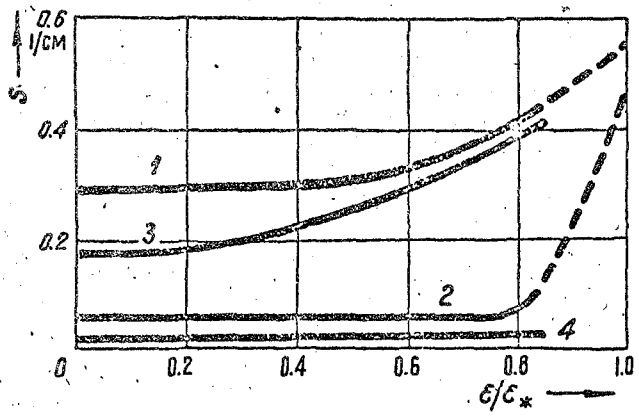

Fig. 19

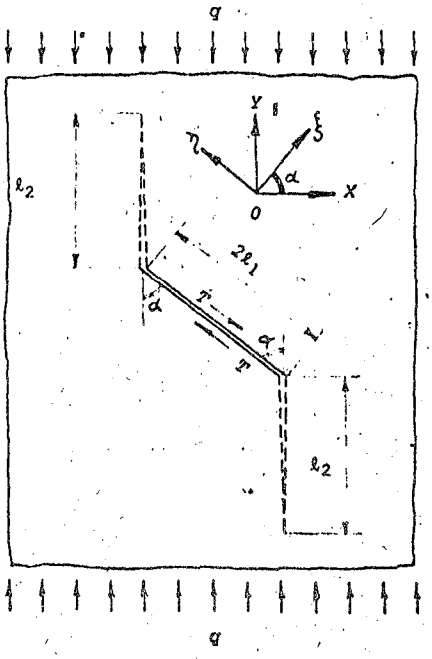

Fig. 20

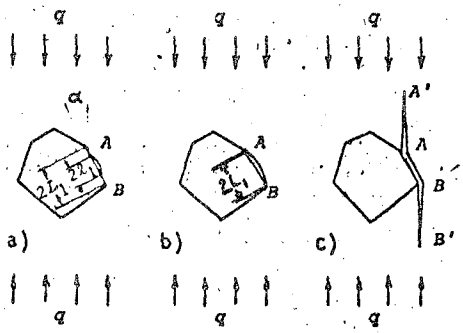

Fig. 21

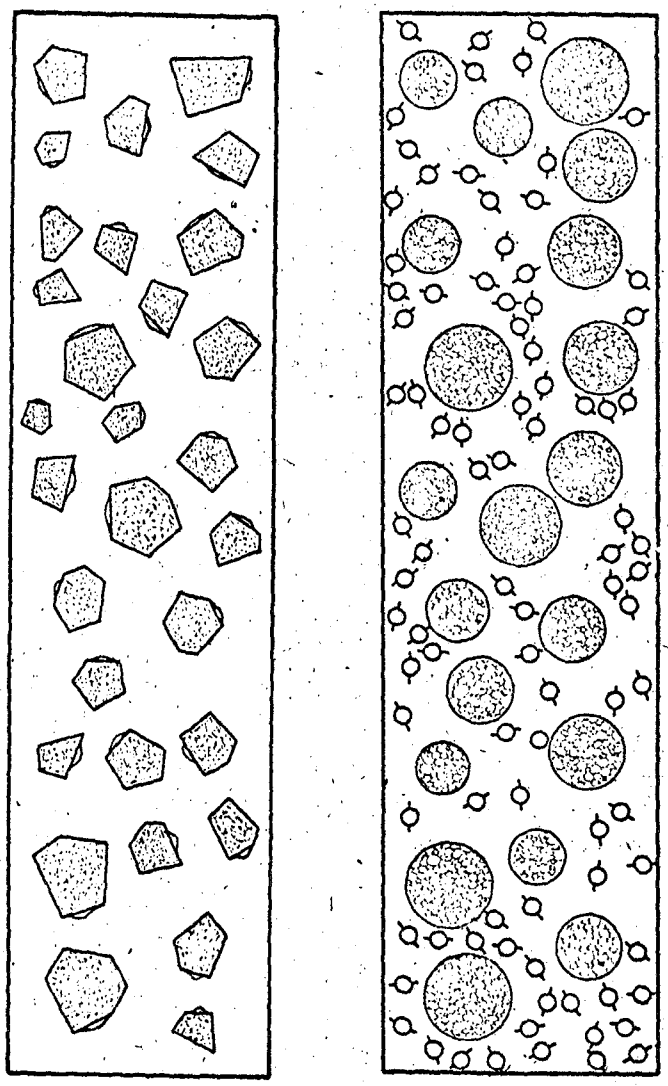

a b

Fig. 23

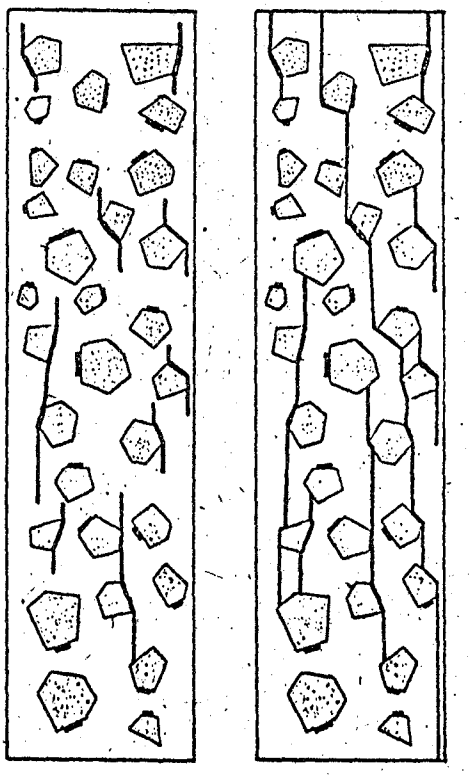

Fig. 24

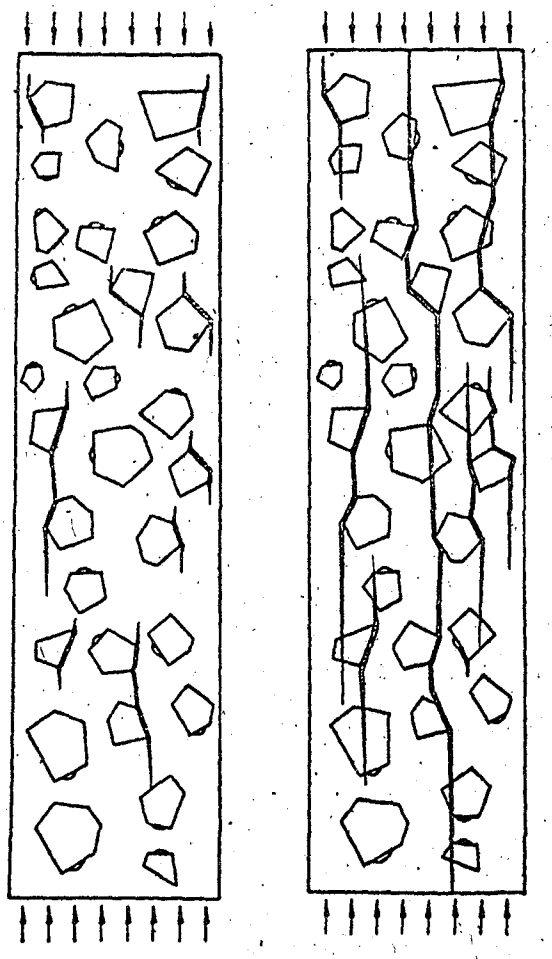

Fig. 25

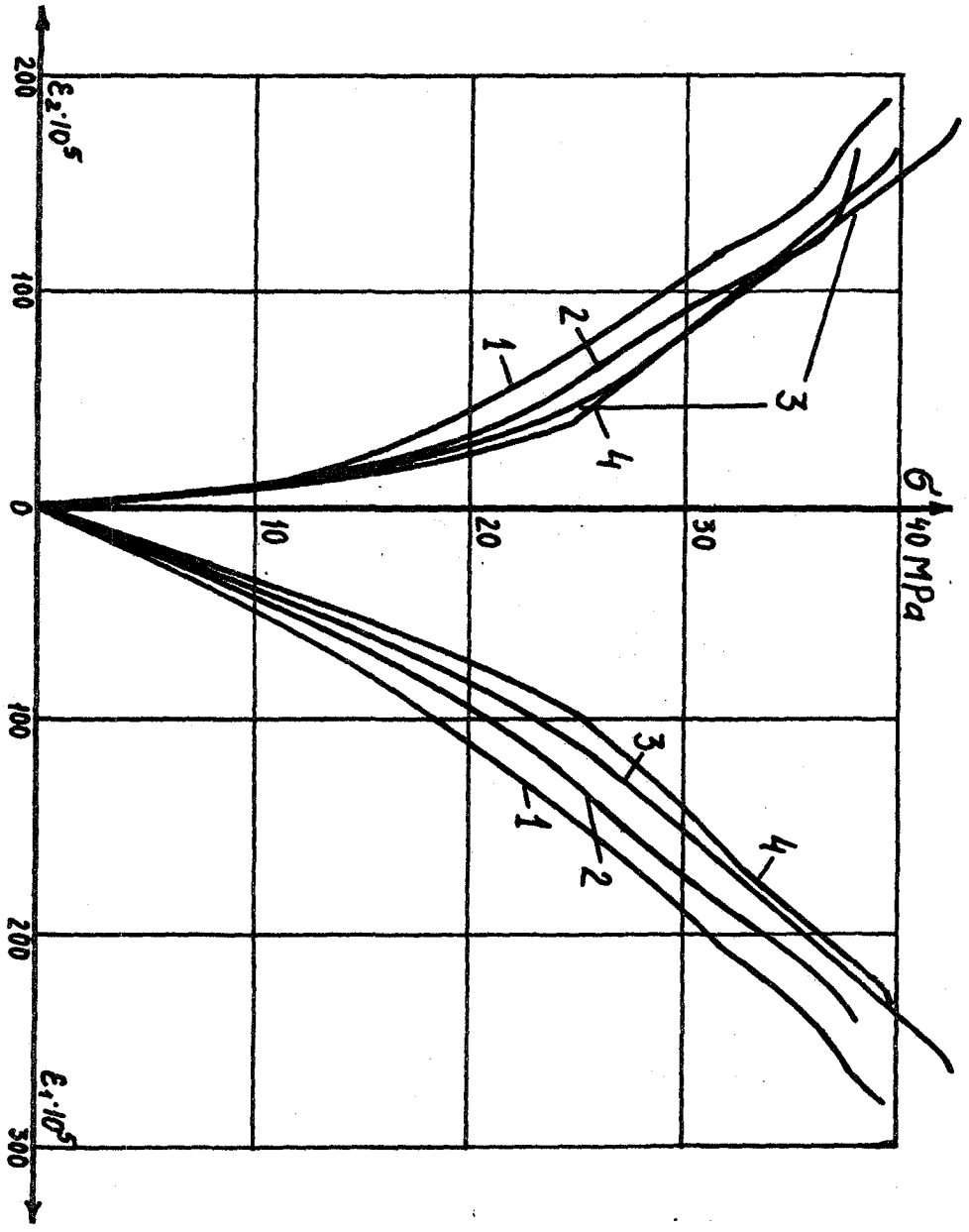
200
100
0
100
200
300
$\varepsilon_2 \cdot 10^5$
$\varepsilon_1 \cdot 10^5$
10
20
30
40 MPa
σ
1
2
3
4

Fig 27

*The Mechanics of Fracture Under High-Rate Stress Loading**

Dennis Grady
Thermomechanical & Physical Division, 1534
Sandia National Laboratories
Albuquerque, New Mexico 87185

Abstract

The fracture properties of brittle materials subjected to impulsive or high rate loading is considered. Fracture is viewed as a microstructural process through the activation, growth and coalescence of a system of interacting cracks. The loading rate dependence of fracture stress is explained in terms of inertia of isolated cracks. The number of cracks participating in the fracture process, and the number and size of fragments in the failed material are related to both the inherent flaw structure and the rate of energy application required to sustain the system of growing cracks. Differences in loading conditions leading to material failure can result in vastly different fragment size distributions. These differences are compared with physically based statistical laws and possible relations to the loading conditions are explored. Lastly, continuum modelling of dynamic fracture focused toward computational analyses of complex applied problems is covered.

---

* This work performed at Sandia National Laboratories supported by the U.S. Department of Energy under contract number DE–AC04–76DP00789.

1 Introduction

The response of a single crack to both static and impulsive loading has received considerable attention over the past several decades and is reasonably well understood. The mechanics of a system of such cracks under impulsive or stress-wave loading and how this cooperative response relates to the transient strength and ultimate failure of a solid body is less well understood, and has been under study in several laboratories over the previous several years. Experimental studies of fracture under high rate loading have revealed unusual features associated with the phenomena such as greatly enhanced material strength and fracture stress dependence on loading conditions. Although such observations have lead to the postulation of rate dependent material properties, most of these features can be understood in terms of fundamental fracture concepts when considered in terms of a system of interacting cracks.

In applications of the concepts of dynamic fracture, or the theories which purport to describe such fracture, there are a number of features worthy of prediction. Perhaps the first, and most fundamental, is the transient strength, or ability to support an impulsive load, either without sustaining fracture damage, or else sustaining fracture damage within some tolerable level without permitting total failure. In partially fractured bodies the spacing or fabric of the cracking may be of importance along with the void volume and extent of intersection, which will relate to the permeability of the crack system. In completely failed bodies the degree of fragmentation is of interest in many applications. The size and velocity of ejected fragments is of concern, and the distribution in fragment sizes and how this relates to the conditions of loading is also of importance.

The present paper reviews several of the features of dynamic fracture and fragmentation which have come to light over the past several years. In the second section, the concept of dynamic fracture strength is treated. Experimental studies have shown that solids subjected to high rate or impulsive loading exhibit dramatically enhanced material strength. A number of criteria have been proposed to account for this effect over the years. Recently, the strength properties of a single crack subjected to stress-wave loading have been explored and found to relate well with the behavior of a system of cracks within a body as a whole. Earlier criteria appear to be similar statements of the same behavior.

In the third section the properties of the material and the conditions of loading which lead to the number of fractures participating in the fracture process and the number and size of fragments resulting in the failed body are considered. Two interrelated concepts are important here. First is the inherent

distribution of flaws or sites of weakness in the body which constitute the points of fracture activation. The second relates to the energy or the rate of energy application required to sustain the system of growing cracks. Although the inherent flaw distribution, a material property, has been used to determine fracture number and fragment size in most previous work, it has been found that in numerous applications a kinematic energy condition appears to govern the fracture fabric.

The following section is concerned with the mechanical and statistical conditions which determine the distributions in fragment size resulting from catastrophic fracture events. This is an interesting, diverse, and extremely complex topic about which very little is currently known. Two statistical concepts which have been proposed in the earlier literature for determining fragment size distributions are considered. The first is based on Poisson statistics while the second is a unique application of Boltzmann energy statistics. They lead to vastly different distributions and each appears to have application in certain circumstances. There is evidence that both the mode and the multiplicity of the dynamic fracture event is important in determining the shape of the distribution.

In the final topical section a brief review of the various approaches to continuum modelling of dynamic fracture currently under consideration is presented. Such modelling represents a necessary final goal in that the complexities of stress loading, geometry, and the interaction of stress and relief waves necessitate the use of wave-propagation codes to address realistic problems.

2 Dynamic Fracture Strength

The dependence of the dynamic fracture strength of rock on the rate of loading can be studied through the response of an isolated crack under the action of constant tensile strain-rate loading. Illuminating studies on the strength of a body due to stress concentrating effects of cracks under static loading have emerged from the concepts initiated by Griffith [1920]. The impact response of an elastic solid containing a crack and subjected to an abrupt tensile loading normal to the crack surface has also been well characterized and is extensively discussed by Chen and Sih [1977], while response of a solid to more general loading functions applied to the crack has been considered by Freund [1973]. Application of these methods to constant tensile strain-rate loading have been explored in detail by Kipp et al. [1980] and provide an understanding of many of the features observed in the dynamic fracture of rock.

2.1 The Dynamic Stress Intensity Factor

The theory of linear elastic fracture mechanics applied to the dynamic loading of an isolated crack has provided a clear understanding of the response of cracks to transient tensile loads. The response to various types of Heaviside loading has been outlined by Chen and Sih [1977] and the Heaviside response function may be employed as a Green's function for other dynamic pulse shapes [Freund, 1973].

In particular, if a Heaviside tensile stress of magnitude σ_o is applied to a crack with a characteristic dimension a, then the functional form of the stress intensity factor, K_I at the crack tip, is

$$K_I(a,t) = \sigma_o \sqrt{\pi a} f(c_s t/a)\,, \tag{1}$$

where c_s is the shear wave velocity. The response to an arbitrary stress loading function, $\sigma(t)$, may then be expressed as [Freund, 1973],

$$K_I(a,t) = \sqrt{\pi a} \int_0^t \sigma'(s) f(c_s(t-s)/a) ds\,. \tag{2}$$

A convenient loading function for comparison with experimental data on the dynamic fracture strength of rock is that of constant strain rate loading [Kipp et al., 1980]. For linear elastic response the constant strain rate, $\dot{\epsilon}_o$, and stress rate, $\dot{\sigma}_o$, are related through the elastic modulus of the material. Under this special loading condition Equation (2) becomes,

$$K_I(a,t) = \dot{\sigma}_o \sqrt{\pi a} \int_0^t f(c_s/a) ds\,. \tag{3}$$

Fracture is expected to initiate at a time, t_c, when the stress intensity factor in Equation (3) achieves the critical stress intensity factor. At this time the applied stress will have achieved the fracture stress level, σ_c, related to t_c through $\sigma_c = \dot{\sigma}_o t_c$. Thus,

$$K_{Ic} = \dot{\sigma}_o \sqrt{\pi a} \int_0^{\sigma_c/\dot{\sigma}_o} f(c_s s/a) ds\,, \tag{4}$$

provides an implicit relation for the fracture initiation stress and the dependence on both the crack size and the critical stress intensity factor.

2.2 A Strain Rate Dependent Fracture Criterion

Before discussing the dynamic fracture process it is important to recall the form of the function, $f(c_s s/a)$. An elastic analysis of the Heaviside loading has been considered by Chen and Sih [1977]. Solutions for both the penny-shaped crack and the plane crack exhibit the familiar square root singularity in time at the crack tip for the stress intensity factor, followed by overshoot and oscillating convergence to the static value.

To achieve an explicit relation for the strain rate dependence of the fracture stress, a solution expected to be valid at high loading rates has been used [Grady and Kipp, 1979a; Kipp et al., 1980]. Assuming the solution for penny-shaped crack response to Heaviside loading valid for small normalized time,

$$K_I(t) = N\frac{2}{\sqrt{\pi}}\sigma_o\sqrt{a}\sqrt{c_s t/a}\,, \tag{5}$$

and, as before, using Equation (5) as a Green's function for constant strain- rate loading of a crack results in the crack-size independent relation for the stress intensity factor,

$$K_I(t) = N\frac{2}{\sqrt{\pi}}\sqrt{c_s}\dot{\sigma}_o\frac{2}{3}t^{\frac{3}{2}}\,. \tag{6}$$

Here N is a geometric coefficient equal to 1.12 for the penny-shaped crack. As in Equation (4), a relation among the critical stress intensity factor, the fracture stress, and the fracture time can be established and results in the strain-rate dependent fracture stress,

$$\sigma_c = \left(\frac{9\pi E K_{Ic}^2}{16N^2 c_s}\right)^{\frac{1}{3}}\cdot\dot{\epsilon}_o^{\frac{1}{3}}\,. \tag{7}$$

Equation 7, of course, corresponds to the stress level required to initiate fracture on an isolated, normally-oriented circular crack which is sufficiently large relative to the loading conditions specified by the strain rate, $\dot{\epsilon}$. In a body with a distribution of flaws under similar loading conditions, fracture initiation within some population of this distribution would be expected, providing flaws spanning a characteristic size of the order $a \sim (c_s K_{Ic}/E\dot{\epsilon}_o)^{\frac{2}{3}}$, were contained within the distribution . Assuming that the material is sufficiently flawed, Equation 7 might be expected to provide a reasonable measure of the dynamic strength of the body.

2.3 Experimental Measurements of the Fracture Strength of Rock

Explosive or percussive rock breakage involves dynamic fracture in the sense that transient waves or the interaction of transient waves with local free surfaces carry regions of rock into tension, initiating fracture and fragmentation. It has been known since the early studies of Rinehart [1965] that the dynamic fracture strength of rock can exceed the static strength by as much as one order of magnitude. This observation has been substantiated by later studies and has attained fairly wide acceptance. In rock blasting calculations, the known static fracture strength is often arbitrarily increased by a factor of seven or eight to account for dynamic conditions.

A fairly substantial body of experimental data exists in which loading rates comparable to impulsive rock breakage applications have been simulated. These data tend to support the discrepancy between static and dynamic strength. Dynamic laboratory measurements using compressive [Kumar,1968; Green and Perkins, 1968; Lindholm et al.,1974; Lundberg, 1976; Lankford,1976], torsional [Lipkin et al.,1977], and tension [Birkimer, 1971] Hopkinson bar techniques have identified rate sensitive rock fracture. Plate impact induced spall in rock has also been studied [Shockey et al.,1974; Grady and Hollenbach, 1979; Grady and Kipp,1979; Cohn and Ahrens,1981]. Rock fracture through magnetic stress loading methods has also been pursued [Forrestal et al.,1978].

Fracture toughness measurements [Oucherlony, 1980] have been obtained on some of the rocks for which dynamic strength as measured by plate impact spall experiments is also available. In figure 1, comparison of dynamic spall data with the dynamic fracture relation in Equation 7 illustrates a reasonable correlation, and the practical applicability of this relation in providing estimates of dynamic rock strength. In the spall experiments a nominal strain rate of $\dot{\epsilon}_o \simeq 10^4/s$ was achieved and used in the calculation. Figure 2 illustrates a similar comparison of the strain rate dependence of Equation 7 with data obtained with both Hopkinson bar and plate impact experiments [Grady and Lipkin,1980]. Although in reasonable agreement in both rate dependence and magnitude for most rocks, the relatively rate independent response of Solenhofen limestone, which has also been observed by others [Green and Perkins,1968], is noted. It is believed that the relatively small flaw size and homogeneity of this rock leads to the observed rate independence over the $10^2/s$ to $10^4/s$ strain rate regime. The behavior of Solenhofen limestone emphasizes that caution should be exercised in generally applying Equation 7 to dynamic rock strength predictions.

2.4 Comparison With Other Dynamic Fracture Criteria

In past years other dynamic fracture criteria have been established to describe observed dynamic strength behavior. In general, these studies have lead to criteria similar in form to the expression in Equation 7. Tuler and Butcher [1968] proposed a criteria for incipient dynamic fracture damage of the form

$$\int_0^\tau (\sigma - \sigma_t)^\lambda dt = c\,, \tag{8}$$

where σ and τ are the tensile pulse amplitude and duration, respectively, and σ_t is the stress threshold for damage growth. They found that $\lambda = 2$ provided the best agreement with spall data on aluminum. Assuming that σ is significantly larger than σ_t and considering constant strain rate loading, Equation 8 leads to a cube root dependence on strain rate similar to Equation 7.

Birkimer [1971], in an attempt to explain Hopkinson bar fracture data on quartzite and concrete proposed that fracture occurred when the work on the fracture plane,

$$w = A \int \sigma dx\,, \tag{9}$$

achieved a critical value. σ is the stress and A is the area of the bar. Using the relation $dx = (c\sigma/E)dt$ (c is the wave velocity), and assuming constant strain rate loading results in the relation.

$$\sigma_c = \left(\frac{3E^2W}{AC}\right)^{\frac{1}{3}} \cdot \dot{\epsilon}_o^{\frac{1}{3}}\,. \tag{10}$$

Steverding and Lehnigk [1976] developed a relation described as a least action law for fracture initiation,

$$\int \sigma^2 dt = \frac{\pi\gamma E}{c}\,. \tag{11}$$

Here, γ is the specific surface energy for crack growth. It is apparent that their proposed fracture criterion will also lead to a cube root dependence on strain rate. A similar spall fracture criterion has been discussed by Ivanov and Mineev [1978].

Because of the importance of the state of fracture damage created in rock breakage, it is useful to consider a seemingly different criteria related to rock fracture due to Von Rittinger [1867]. This relation states that the energy required to fragment a body is inversely proportional to the size modulus, x, of the resulting fragment distribution, namely;

$$U = \frac{b}{x}, \tag{12}$$

where b is a constant. As far as can be determined, no physical basis has been put forth for Rittinger's law. Application of this relation has been actively debated in the field of grinding and crushing[e.g., Charles,1957; Faddeenkov,1975] and has given rise to alternative relations such as those of Kick [1885] and Bond [1952]. Conditions of multiple particle breakage during crushing and grinding are complex. Bergstrom et al.,[1961], however, has shown that in single breakage Equation 12 is obeyed for numerous brittle materials.

In single breakage the energy to fracture the material is initially stored as elastic energy and if the specimen supports a stress σ at fracture then the energy in Rittinger's relation (Equation 12) is of the order $\sigma^2/2E$. In brittle catastrophic fracture, crack propagation will rapidly approach a terminal growth velocity, c_g. If cracks coalesce to form fragments at a time, t_c, then the nominal fragment size will be on the order of $x \sim c_g t_c$. Applying these relations to Equation 12 and assuming constant strain rate loading results in

$$\sigma_c = \left(\frac{2bE^2}{c_g}\right)^{\frac{1}{3}} \dot{\epsilon}_o^{\frac{1}{3}} \tag{13}$$

suggesting that the fragmentation behavior noted by Rittinger may have a similar physical basis.

3 Energy Concepts In Catastrophic Fragmentation

The damage created in severe impulsive tensile fracture events in rock or rock like material is a complexity of intersecting cracks which may reflect both the intensity and the orientation of the applied tensile stress field. As an example, the fracture damage of an explosion placed in a deep borehole consists of severe

comminution to small particle sizes in the rock immediately adjacent to the explosion and grading to larger fragments with increasing distance. Further from the charge the fracture damage reduces to a small number of radial cracks which may propagate a considerable distance before arresting. In many applications of explosive or percussive rock breakage the production of optimum and uniform fragment sizes is either the objective or is important to the efficiency of the process. Consequently an understanding of the fracture effects governing the intensity of cracking and fragment size is needed.

3.1 Inherent Flaw Effects in the Dynamic Fracture Process

As pointed out in the previous section, by adjusting the rate of loading, different levels of tensile stress can be achieved in the material before catastrophic failure occurs. This behavior is understood by hypothesizing that the virgin material contains a distribution of flaws with various sizes and orientations [Grady and Kipp,1980]. The flaws become active and grow when subjected to tensile loads of various magnitudes. The active flaws grow during the period of load application and eventually coalesce, causing material failure. When a load is applied slowly, only those flaws which become active at low stress levels actually contribute to the fragmentation process because these flaws grow and coalesce, and failure occurs, before the applied load reaches a level of stress high enough to activate other flaws. This results in a low apparent threshold for material failure and comparatively large fragments because the number of contributing flaws is small. When the load is applied more rapidly, a higher level of stress is achieved before flaw coalescence occurs; thus, a greater number of flaws participate, causing the fragment dimensions to be smaller and the apparent threshold for material failure to be higher.

It is also recognized that a specific amount of energy is required to create a new fracture surface during the fracture event, and this energy must come from the loading stress wave. This surface energy is of the order $K_{Ic}^2/2E$, where K_{Ic} is a measure of the fracture toughness and E is the elastic modulus. If the material is loaded at a rate such that a stress σ_c is achieved before failure occurs then an elastic energy of order $\sigma_c^2/2E$ is stored in the body and available for fragmentation. A consideration of energy balance suggests that a fragment size of approximately $d \sim (K_{Ic}/\sigma_c)^2$ might be achieved in the dynamic fragmentation event with a corresponding fragment surface area per unit volume of $A \sim 6/d$. Direct observation has shown that this energy balance is never achieved, and

measured fragment surfaces are typically one or more orders of magnitude below this energy limit.

Consequently, based on this observation, previous studies have assumed that fragment sizes achieved in dynamic fracture events are flaw rather than energy governed and considerable effort has been focused on characterizing the flaw distribution in rock material, through direct observation [Shockey et al.,1974], or other indirect methods [Grady and Kipp,1980; Margolin,1983]. Usually the flaw distribution has been related to the stress level of flaw activation with $N(\sigma)$ providing the number of flaws per unit volume which activate at or below a stress, σ. Thus, if a threshold stress σ_c is achieved before failure, the nominal fragment size predicted is $d \sim N(\sigma_c)^{-\frac{1}{3}}$.

3.2 Kinetic Energy Considerations

Although accurate characterization of the flaw structure appears to be important, there is evidence that such characterization alone is not sufficient to explain all of the observed effects in dynamic fracture and fragmentation. Energy balance principles still appear to play a significant role. As described earlier, the dynamic fracture stress appears to be governed largely by fracture energy considerations. Also, the fragmentation studies of Rittinger[1867], Charles[1957], and Bergstrom[1961] reflect, at least qualitatively, energy aspects in the breakage process.

There is another way to model the dynamic fracture process which leads to an energy balance governing the average fragment size [Grady,1982a]. In this approach kinetic energy rather than elastic strain energy is considered to be the important energy fueling the fracture process. The model is thought to be most reliable in extremely catastrophic fragmentation events, however, in application it has been found quite useful over a fairly broad range of fracture rates.

Consider a body which has previously been compressed by some means and is currently in a state of rapid expansion. The instantaneous kinematic state will be determined by the density, ρ, and the density rate, $\dot{\rho}$, which will be assumed uniform over a sufficiently large region encompassing the point of interest. Conceptually, one might consider an elastic sphere which has been compressed uniformly and suddenly released and is currently in a state of rapid outward expansion. The kinetic energy associated with the outward motion is responsible for the fracturing forces and surface tension associated with newly created fractures resists the fracture process. It is equally intuitive that, after

fragmentation, particles will continue to fly apart at high velocities. Thus, the production of fragment surface area cannot simply be governed by a balance of kinetic energy and surface energy, since a large portion of the kinetic energy remains after fragmentation.

An expression for the kinetic energy available for fragmentation can be determined by considering an element of the expanding body with a volume of the order of the fragment size expected from the event. With reference to a specific coordinate system, the kinetic energy of this element can be decomposed into a center-of-mass kinetic energy, T_{cm}, and the kinetic energy relative to a coordinate system referenced to the center of mass, T'. Assuming average response, forces acting on the element during fragmentation should, due to symmetry, exert no net impulse and, consequently, both the center-of-mass velocity and kinetic energy of the particle should remain invariant during fragmentation. Thus in a decomposition of the kinetic energy, the center-of-mass kinetic energy, T_{cm}, of the fragments must be conserved during fragmentation and only the kinetic energy relative to the center of mass, T', is available to fuel the breakage process. This latter energy may be regarded as a local kinetic energy which is available for fragmentation without violating local momentum conservation.

An explicit expression for the local kinetic energy can be obtained by considering a spherical mass element of radius, a, expanding uniformly at a density rate, $\dot{\rho}$. The kinetic energy about the center of mass for this single sphere is,

$$T' = \frac{2\pi}{45} \frac{\dot{\rho}^2}{\rho} a^5 . \tag{14}$$

Dividing by the volume of the spherical element and expressing in terms of the fragment surface area to volume ratio, $A = 3/a$, a measure of the local kinetic energy density, in terms of the surface area created by fragmentation is obtained

$$T = \frac{3}{10} \frac{\dot{\rho}^2}{\rho A^2} . \tag{15}$$

The new fragment surface energy density is simply,

$$\Gamma = \gamma A , \tag{16}$$

and the total energy is given by,

$$U = \frac{3}{10} \frac{\dot{\rho}^2}{\rho A^2} + \gamma A . \tag{17}$$

We will assume that during the catastrophic fragmentation process, forces brought about will seek to minimize the energy in Equation 17 with respect to the fracture surface area. This approach assumes that the coordinate, A, is available or free to vary during the fracture process and, consequently, requires a sufficient supply of flaws or sites of fracture initiation during the process, although precise requirements are not yet clearly understood.

At equilibrium, $dU/dA = 0$, and the equilibrium fracture surface area is,

$$A = \left(\frac{3\dot{\rho}^2}{5\rho\gamma} \right)^{\frac{1}{3}} . \tag{18}$$

Equation 18 provides a quantitative measure of the fragment surface area created in the fracture process in terms of fundamental thermodynamic and kinematic properties. Typically a nominal fragment size, rather than surface area, is of interest. Assuming spherical fragments of equal size, the fragment diameter is related to the surface area through, $d = 6/A$.

If Equation 18 is used along with, $\dot{\epsilon} = \dot{\rho}/3\rho$, and, $\gamma = K_{Ic}^2/2\rho c^2$, an expression for the nominal fragment diameter for dynamic fragmentation in a brittle material is obtained,

$$d = \left(\frac{\sqrt{20} K_{Ic}}{\rho c \dot{\epsilon}} \right)^{\frac{2}{3}} , \tag{19}$$

where, $\dot{\epsilon}$, is the linear strain rate and, K_{Ic}, is the fracture toughness. Nominal fragment size data for oil shale have been obtained as a function of strain rate [Grady and Kipp, 1980]. Material properties for the oil shale studied are, $K_{Ic} = 0.9\ MN/m^{\frac{3}{2}}$, $p = 2300\ kg/m^3$, and $c = 4000\ m/s$. The prediction of Equation 19 is shown to provide a reasonable description of the data in Figure 3. Further work [Grady,1982a;1982b; Grady and Benson,1983; Costin and Grady,1983] are showing that Equation 18 or 19 provide a useful predictive relation for numerous dynamic fragmentation applications and that energy rather than flaw considerations govern the fragmentation. It also suggests that kinetic energy rather than strain energy is more important in many cases in determining fragment sizes.

3.3 Application to Well Shooting

An interesting and perhaps useful application of the fragment size expression derived from the model based on energy principles can be found in the

process known as well shooting or the dynamic stimulation of wellbores through explosive or propellant loading [Warpinski et al, 1979; Schmidt et al., 1981]. The multiple fracturing of wellbores holds promise for stimulating naturally fractured reservoirs through intersection with the pre-existing fracture network. The use of high-strength explosives have been found to have detrimental effects, however, through crushing and plastic flow near the borehole which can result in a residual compressive stress field and a tightly locked formation rather than the desired multiple fracture pattern and enhanced permeability [Smith et al., 1978]. Extensive experiments by Schmidt et al.[1981] in Nevada Test Site tuff have shown that propellants with appropriate burning rates can produce stress loading behavior which optimizes the dynamic multifracturing process without excessive crushing or plastic damage. They conclude that perhaps the most crucial parameter is the initial stress loading rate in the wellbore.

Certain aspects of this problem can be understood in terms of the energy expression for fragment size determined in the previous section. By assuming a geometry more appropriate to the radial cracking process occurring in the dynamically loaded wellbore, an expression similar to that of Equation 18 or 19,

$$N = \left(\frac{\rho c \dot{\epsilon}}{6 K_{Ic}} \right)^{\frac{2}{3}}, \tag{20}$$

can be obtained for the number of fractures per unit length occurring at a strain rate, $\dot{\epsilon}$. Assuming a wellbore diameter, D, the number of cracks initiating from the wall is predicted to be,

$$N_D = \pi D \left(\frac{\rho c \dot{\epsilon}}{6 K_{Ic}} \right)^{\frac{2}{3}}. \tag{21}$$

This relation can be compared with the experiment of Schmidt et al.[1981] in NTS tuff in which an intermediate burning rate propellant provided a loading rate of $20\, psi/\mu s$, to a peak pressure of $13,800\, psi$. This translates to a circumferential strain rate at the wellbore wall of approximately, $\dot{\epsilon} = 30/s$. Using the material properties for tuff of, $\rho = 1600\, kg/m^3$, $c = 2000\, m/s$, $K_{Ic} = 0.3\, MN/m^{\frac{3}{2}}$, and a wellbore diameter, $D = 0.15\, m$, Equation 21 provides a fracture number of, $N_D = 6.7$. This compares well with the seven major fractures and several minor fractures actually observed by mine back methods in this experiment.

Although the agreement is encouraging and well shooting is an interesting application of the energy balance approach to predicting fracture spacing in

dynamic fracture, this is only one aspect of a complex pulse tailoring problem. Extensive calculations have been performed by Swenson[19] focused on optimizing all aspects of wellbore stimulation by multiple fracturing.

Considering the relatively gentle loading rates associated with wellbore stimulation, it is not presently clear why an energy balance considering only kinetic energy and fracture surface energy while ignoring the strain energy should be successful in predicting fracture spacing. It would also seem from dimensional considerations that the wellbore diameter might enter the relation in a more complicated way. The calculation clearly suggests, however, that the fracture process is not simply predicted by a description of inherent flaws in the neighboring rock. A complete theory of the multiply fracturing event should also include the energy concepts identified here.

4 Particle Size Distributions Occurring in Dynamic Fragmentation

In the opening section of this report concepts relating to the transient strength and dynamic fracture stress of brittle solids subjected to impulsive stress-wave loading were considered. The following section provided a discussion of flaw structure and energy factors governing the new fracture surface area created in catastrophic fragmentation. It remains to consider a concept which is frequently the end concern in numerous impulsive fracture applications, namely, the distribution in sizes of the particles created in the event.

Numerous areas in science and everyday experience can be cited. One current application is concerned with recovery of oil from oil shale. Economic recovery requires effective fragmentation and distribution of void volume through explosive blasting methods [Boade et al., 1981]. More generally, aspects of fragmentation and resulting fragment distributions are important to a number of explosive or percussive rock breakage applications including deep drilling [Varnado, 1978], explosive or propellant stimulation of gas and oil wells [Warpinski et al., 1979], and quarry, mining and construction blasting [Langefors and Kihlstrom,1967]. On a less technical chord, theories concerned with the accretion of planetary bodies have been proposed which depend on impact fragmentation and resulting fragment distributions [Matzui and Mitzutani,1977]. Distributions of iron particles on the ocean floor, apparently resulting from the catastrophic ablation of meteorites entering the earth's atmosphere [Yamakashi et al.,1981], and the natural occurrence of the explosive eruption of a volcano or the catastrophic

impact of a major meteorite [O'Keefe and Ahrens,1976] involve processes of fragmentation which can distribute debris through the earth's atmosphere.

Because of the continuing practical interest in material fragmentation, studies on various aspects of the problem can be traced through the literature for more than a century. The statistical nature of fragmentation was recognized early and stimulated efforts in identifying size distribution relations which correctly described the resulting fragmentation. Various standard distributions such as Poisson [Lienau,1936; Bennett,1936], binomial [Gaudin and Meloy,1962], log normal [Kolmogorov,1941], and Weibull [Rosin and Rammler,1933], have been used and functions associated with the names of Rosin and Rammler[1933], Schuhmann[1940], and Gaudin and Meloy[1962] have acquired popularity in certain applications.

The strictly statistical approaches to fragmentation, however, tacitly ignored the dynamics of the fragmentation event and did not provide a means of correlating energy, or some other measure of the loading conditions, with the fragment distribution. These ideas appear to have first been explored in the studies of Mott[,1947] and have been pursued more recently by Grady[1981a,b]. In this approach more significance is attributed to the dynamics of fracture activation and growth, including the nucleation process and the influence of material deformation properties. Mott[1947], in considering a restricted geometry, combined the spatial randomness of the fracture process with the growth of plastic tensile release waves and predicted fragment distributions dependent on both dynamic and material properties. More recent studies [Shockey et al.,1974; Dienes, 1978; Margolin,1983] have focused on developing physically founded laws governing the nucleation, growth and coalescence of fracture during one- and two-dimensional stress-wave propagation. A different approach to the statistics of fragmentation has been proposed by Griffith [1943], where particle fracture surface energy is related to the distribution through a unique application of classical Boltzmann statistics concepts.

4.1 The Weibull Distribution

The statistical representations which have been used to describe fragment size distributions are almost as numerous as the fragmentation phenomena. Most were selected from classical statistical formulas. The Weibull representation is a flexible two-parameter analytic formula which has been found successful in describing a large body of fragmentation data. Application of the Weibull

formula to fragment distributions appears to have been first suggested by Gates [1915]. The most extensive comparisons of empirical data with this statistical representation was made by Rosin and Rammler[1933] in terms of mining and ore reduction applications.

Considerable effort has focused on supplying a theoretical framework for a Weibull description of fragmentation. Bennett[1936], Gilvarry[1961], and Kuznetsov [1975] have focused significant efforts in this direction, however, a clear theoretical basis has yet to be demonstrated. In fact, exact applicability of a Weibull representation to fragmentation has theoretical problems at the fine end of the distribution in terms of divergence of expressions for the fragment number and fragment surface area.

The purpose here is not to provide theoretical support for a Weibull description of fragmentation. A Weibull distribution has been found very successful in terms of describing fragmentation over the range of available data and is used here as a convenient means for examining systematic features of fragmentation phenomena.

According to the Weibull representation of fragmentation, the cumulative distribution of fragment volume fraction (or mass fraction) finer than size, x, is

$$V(x) = 1 - e^{-\left(\frac{x}{\sigma}\right)^n} . \tag{22}$$

The volume density distribution is provided by the derivative of Equation 22,

$$v(x) = \frac{n}{\sigma}\left(\frac{x}{\sigma}\right)^{n-1} e^{-\left(\frac{x}{\sigma}\right)^n} . \tag{23}$$

In Equation 22 or 23, σ, is the scale parameter and is closely related to the mean fragment size. The shape parameter, n, determines the variance and the skewness of the distribution. The Weibull representation has the flexibility of describing a very flat distribution with, $n \simeq 1$, to a strongly centered distribution for large values of n.

The exponential expression in Equation 22 and 23 provides the cutoff for the large particle upper end of the distribution. If attention is focused only on the fine portion of the distribution (ie., x sufficiently smaller than σ), then simple power representations are obtained with,

$$V(x) = \left(\frac{x}{\sigma}\right)^n , \tag{24}$$

and

$$v(x) = \frac{n}{\sigma}\left(\frac{x}{\sigma}\right)^{n-1} . \tag{25}$$

This distribution is frequently convenient in application and has further convenience in the present paper where comparison with other distributions which are not Weibull in their upper end behavior is desired.

Experimental evidence indicates that the shape parameter, n, can range from as low as 0.5 to an upper limit of about 5. A theoretical upper limit of $n = 6$ is suggested by one statistical approach [Grady and Kipp,1983]. Behavior of the distribution shape over various methods of fragmentation is typified by the plot in Figure 4. A large body of fragmenting munitions data, exemplified by the work of Weimer and Rogers[1979] show values of n ranging from about 4 to 5. Direct impact fragmentation experiments show n from about 2 to 3 [Shockey et al.,1974] and in tension Hopkinson bar tests, where substantial shearing fragmentation occurs, values from about 1.2 to 1.8 are typical [Grady et al.,1981; Costin and Grady,1983]. A large and diverse body of fragmentation data show distributions with n equal or close to unity. Ball milling comminution of minerals results in distributions with n near one [Rosin and Rammler, 1933]. Explosive crushing experiments on glass spheres also provide values of n very close to unity [Bergstrom et al.,1962]

Several examples can be cited from the geophysical literature. Perkins and Tilles[1968] have suggested that interplanetary debris, presumably due to comet disintegration or to asteroid break up is best described by, $n \simeq 1$, at least for the fine particles, While Matsui and Mizutane[1977] have found this particular distribution appropriate in calculations of planetesimal fragmentation. Yamakashi et al.[1981] have shown that magnetic spherules in deep sea sediments attributed to atmospheric ablation or to earlier fragmentation of iron meteorites, are also well described with a particle size distribution with n near unity.

The data available are far from complete, or systematic, but evidence is mounting which suggests that the rather broad range of the distribution parameter, n, may be related, at least in part, to the type or method of fragmentation. It appears that single tensile fragmentation leads to fragment size distributions with large values of n. In contrast, fragmentation with significant shearing and continued comminution leads to lower values, with indications that $n = 1$ may be a limiting value.

4.2 The Single Fracture (Poisson) Limit

In fragmentation phenomena, events in which abrupt, single or initial one-time fragmentation occurs, as opposed to events in which continued reduction of already broken fragments occurs, can be identified. For instance, a rapidly expanding spherical shell of material will undergo an abrupt fragmentation process when the tensile strength is reached. Individual fragments will continue to fly outward on roughly radial trajectories and no further breakage will occur. The distribution in fragment size is determined by the physics and statistics of the process at the time of failure. In contrast, when a brittle solid is deformed in shear, the initial fracture event is followed by continued comminution as fragments roll and tumble and repeatedly impact one another. As another example of continued comminution, if the spherical shell in the first example were a ductile solid or liquid and if the initial fragments were ejected at a sufficiently high velocity into a finite atmosphere, further fragmentation of these particles would occur through aerodynamic breakup, ablation, or burning processes. The final size distribution of particles is observed to reflect this multiplicity of breakup processes.

The present section will focus on theoretical concepts leading to the fragment size distributions which result from the first example, namely, that of single fracture. The added effect of continued comminution will be considered in the following section.

With one notable exception, which will be addressed later [Griffith,1943], theories focused on predicting fragment size distributions have started with the fundamental premise of a randomly cracked body. This immediately invokes concepts of Poisson statistics which were central to the developments of Bennett [1936], Lienau [1936], Gilvarry [1961], and Mott [1943]. The approaches differ and that of Lienau and Mott, who apparently were not biased by a desire to arrive at a Weibull representation, appear to be the more correct application of the concepts. Extension of the statistical concepts to two and three dimensions proposed by Mott can be questioned, however, and an alternative method has been pursued by Grady and Kipp[1983]. The concepts are most readily appreciated in one dimension, however, where fractures are considered to be points distributed randomly on an infinite line.

Consequently, consider, after the fracture event, an infinite one-dimensional line or rod along which fractures occur randomly with an expected or average size, x_o. Randomly distributed points on an infinite line obey Poisson statistics and the probability of finding, n, fractures in a length, x, is given by,

$$P(n,x) = \left(\frac{x}{x_o}\right)^n e^{-\frac{x}{x_o}}/n! \,. \tag{26}$$

To determine the probability distribution in fragment lengths, we first obtain the probability of a length, x, having no fractures in it,

$$P(o,x) = e^{-\frac{x}{x_o}} \,, \tag{27}$$

and then the probability of finding one fracture in a length, dx,

$$P(1,dx) = \frac{1}{x_o} dx \,. \tag{28}$$

Then, the probability of finding a fragment of length, x, within a range of x to $x + dx$ is given by,

$$dP = P(o,x)P(1,dx) = \frac{1}{x_o} e^{-\frac{x}{x_o}} \, dx \,, \tag{29}$$

which provides an exponential fragment size probability distribution of the form [Lienau,1936],

$$p(x) = \frac{1}{x_o} e^{-\frac{x}{x_o}} \,. \tag{30}$$

The dynamic ductile fracture of radially expanding thin metal rings which closely approximates the one-dimensional fragmentation process has been found to be well described by the predicted exponential distribution [Grady et al.,1983].

Mott[1943] recognized the applicability of the development of Lienau [1936] and used it as the basis for deriving the well-known Mott distribution for the fragmentation of thin shells. He reasoned that Equation 30 might still apply to two-dimensional fragmentation (and, by logical extension to three dimension) and related the linear measure of the random variable to the fragment mass through, $x \sim m^{\frac{1}{2}}$. A change of variables then provides the probability distribution,

$$p(m) = \frac{1}{2\sqrt{\mu m}} e^{-\sqrt{m/\mu}} \,, \tag{31}$$

where, μ, is the expected value of the fragment mass. Integration provides the familiar Mott cumulative fragment number distribution,

$$N(m) = N_o\left(1 - e^{-\sqrt{m/\mu}}\right), \tag{32}$$

against which a large body of exploding shell data have been compared.

Grady and Kipp[1983] have argued that, in the application of Poisson statistics to two and three dimensional fragmentation, a measure of area, or volume, respectively, should be selected as the random variable. For volume fragmentation an exponential probability density distribution in the fragment volume,

$$p(v) = \frac{1}{v_o} e^{-\frac{v}{v_o}} , \tag{33}$$

is obtained.

When related to the cumulative mass distribution shown in Figure 5 the Mott development leads to a shape parameter of, $n = 4$, while that of Grady and Kipp provide, $n = 6$. It is currently believed that an upper limit of, $n = 6$, corresponds to truly random fragmentation. It is not yet clear, however, whether natural fragmentation is a strictly random statistical process, at least in the sense discussed here.

4.3 The Multiple Fracture (Boltzmann) Limit

As pointed out earlier, experimental values for the shape parameter, seem to range from about 1 to 5, and although not yet well understood, there are indications that the more complex the fragmentation event in terms of opportunities for fragments to experience repeated breakage, the closer the value of n is to unity. For example, in the process of mineral reduction through ball milling [Rosin and Rammler,1933], resulting distributions show values of n very close to one, and numerous further examples exist, some of which were cited earlier.

There are some immediate theoretical problems with a cumulative mass fraction distribution of the form, $M(x) = x/\sigma$ (compare with Equation 24). The mass fraction density distribution is, $dM/dx = 1/\sigma$, while the fragment number and area distributions should behave as, $dN/dx \sim x^{-3}/\sigma$, and $dA/dx \sim x^{-1}/\sigma$, respectively. Due to the behavior of the distribution at small particle size both the integrated fragment number and area are infinite. Consequently, a theory which explains the flat, $n = 1$, distribution should also account for a cutoff at small particle size.

A theoretical approach which holds some promise for explaining both features was suggested Griffith [1943]. This study was not pursued and has lain

dormant for a number of decades. Never-the-less its appeal to fundamental concepts is attractive and the ideas warrant further investigation. This approach is based on equipartition of energy concepts where the energy of interest is the new fracture surface energy created in the fragmentation event [Griffith,1943]. The basic premise is the same as that used in the development of classical Boltzmann statistics. Namely, the number of material elements in an energy state is determined by the most probable distribution of all the material elements over the available energy states consistent with the total energy. The most probable number of elements is found to be,

$$n_j = g_j e^{-\alpha-\beta\epsilon_j} , \tag{34}$$

where the parameters α and β are determined by the total number, N, and energy, E, of the system and g_j is the density of states corresponding to the energy level, ϵ_j. In the present application the energy, E, corresponds to the new fracture surface energy. It is not clear that recourse to temperature is either necessary or has meaning. Since the surface energy of a fragment will be of the order, γx^2, and the volume, of the order, x^3, a relation between a particle energy state and size, of proportionality, $1/x$, is arrived at. Griffith [1943] arrived at a distribution of the form,

$$\frac{dM}{dx} = Be^{-\frac{b}{x}} , \tag{35}$$

where B and b are constant parameters of the distribution. In that development a uniform density of states was assumed which is not obvious and is one feature of the theory which should be considered more deeply. Never-the-less, the resulting distribution leads to a flat, $n = 1$, behavior at large particle size and has an exponential cutoff for small x.

Grady and Varga [1983] have carefully analyzed the particle size distribution resulting from an explosively shocked quartz sample to a shock pressure of approximately $8\,GPa$. A photometric apparatus was used to accurately determine the particle size distribution down to less than $1\,\mu m$. The particle size distribution is compared with the theoretical distribution of Equation 35 in Figure 5. For values of $B = 0.004\,\mu m^{-1}$ and $b = 4.5\,\mu m$, the theoretical expression provides a remarkably good description of the data including the rollover between 1 and $10\,\mu m$, the relatively flat, $n = 1$, behavior between about 10 and $200\,\mu m$, and the large particle cutoff at $250\,\mu m$. From the reasonably good agreement with the present fragment data, it would seen that the statistical energy theory of Griffith [1943] warrants more serious attention. The agreement may be fortuitous, however. The application is significantly different from the usual physical

processes described by Boltzmann statistics and the treatment of the density of states is open to question.

5 Continuum Modelling of Dynamic Fracture

Practical application of the concepts of dynamic fracture mechanics typically involve complex loading situations where the stresses and stress rates vary in both space and time over the region of interest. Applications to consider which illustrate the complexity of problems of interest include explosive blasting in single or multiple boreholes, with or without nearby free surfaces; impact or explosive cratering; and percussive or drag bit drilling, to name a few. Such applications involve unique stress-wave propagation geometries leading to the dynamic fracture process and are difficult to evaluate by strictly analytic methods.

With the advance of high-speed computer methods, efforts have been directed toward developing continuum descriptions of the fracture, fragmentation, and wave propagation to evaluate complex fracturing events. Davison and Stevens [1973] have established the fundamental concepts necessary in a thermodynamically consistent continuum description of dynamic fracture. Several groups have pursued models based on the activation, growth and coalescence of inherent distributions of fracture-producing flaws to predict crack and fragment size spectra in brittle fracture [Shockey et al.,1974; Grady and Kipp,1980; Dienes, 1980; Margolin,1982]. Other workers have preferred to apply well developed concepts from plasticity to the problem of fracture [Butkovich,1976; Johnson,1978; Glenn,1976], predicting regions and levels of damage, nonrecoverable void volume, and tensile or shear fracture. The most appropriate approach has not yet been identified.

5.1 Directions In Continuum Modelling

The present discussion of continuum modelling of dynamic fracture is not intended to be an exhaustive review. Rather, it points out the variety of approaches which have been, and are still being, pursued to provide methods for calculating dynamic fracture phenomena. Such work is still quite active and considerable effort appears to remain before the best approaches emerge as mature calculational techniques.

One of the earliest, and simplest, methods for establishing a state of dynamic fracture within a stress-loaded body was to specify a tensile stress threshold (or spall threshold) at which point the corresponding elements were assumed to instantaneously fractured. The technique did illustrate certain of the stress-wave propagation features characteristic of fracturing bodies, however, it is now recognized that a fracture threshold independent of the size of the body and rate of loading is not a physical property.

Davison and Stevens [1973] studied the application of high intensity and short duration loads to brittle materials which results in intense local fracturing or spalling of the body. They introduced a concept of fracture damage in terms of a vector field describing the size and orientation of distributed penny-shaped cracks throughout the region of fracture. Damage was allowed to incur gradually according to some specified law of growth determined by the changing stress state at the point of fracture.

This general idea has been pursued by others. Curran and coworkers in a series of papers [Shockey et al., 1974; Seaman et al., 1976; Curran et al., 1977] have developed a theory of dynamic brittle fracture based on the nucleation and growth of penny-shaped crack fracture damage which evolves gradually to full coalescence of fragments. The inherent distribution of fracture-producing flaws is regarded as observable and petrographic methods are described in their work for determining such distributions. Laws based on the current stress state are specified to drive fracture nucleation and growth. The model has been implemented in two-dimensional stress wave codes and has been used extensively in several geo-engineering related applications.

A model of continuum fracturing devoted primarily to explosive fragmentation of oil shale was developed by Grady and Kipp [1980]. The general framework followed that of Davison and Stevens [1973] in that fracture damage represented a scalar variable measure of crack-like defects which could grow under appropriate tensile stress loading. Physics of the activation and growth process, however, was guided by a dynamic application of Weibull statistical concepts which leads to the known size dependence of fracture stress observed in static testing [Jaeger and Cook, 1969]. This approach allowed the fracture damage activation parameters to be determined directly from experimental measured fracture stress and fragment size dependence on strain rate [Grady and Kipp 1979,1980].

A Bedded Crack Model of dynamic fracture for brittle and quasibrittle materials has been developed by Margolin and coworkers [Dienes, and Margolin, 1980; Margolin and Adams, 1982; Margolin, 1983]. Fracture damage is based on a microphysical description of fracture following the Griffith theory and con-

siderable care in consistently relating damage and material integrity through an effective modulus theory was achieved. The model is amenable to computational simulation and dynamic fracture features such as rate dependent fracture strength appear naturally within the workings of the model.

A somewhat different approach to stress-wave induced fracture is represented in the work of Butkovich [1976] developed to calculate underground explosive fracture and induced permeability in coal. The method is more akin to conventional elastic-plastic calculations in that stress-space surfaces of yield or failure are established to determine onset of fracture. Fracture due to shearing is explicitly treated and two parameters are associated with fracture damage; a shearing related distortional strain and a tensile induced cracking or porosity which is related to the permeability.

A similar plasticity model of dynamic fracture has been described by Johnson [1978] and applied to explosive fracture in oil shale. A scalar fracture damage parameter is related to the damage-induced reduction in the unconfined yield stress of the material, although the parameter is a mathematical concept rather than a measured property. Damage growth is related to the over stress in excess of a pressure dependent yield surface, with no damage growth above a brittle-ductile transition point on the yield surface. Computer simulations of explosives placed in boreholes provided successful descriptions of extent and regions of fracture damage and dependence on explosive energy and geometrical features.

5.2 An Application of Continuum Fracture Modelling

Computer simulation of a complex dynamic fracture application can be illustrated by calculations performed in support of large scale explosive fragmentation experiments conducted in the colony Oil Shale Mine near Grand Junction, Colorado [Harper and Ray,1981]. The computer model used was that of Grady and Kipp [1980] and various extended applications have been considered by Boade et al. [1981] and Chen et al. [1983]. In this model stress and strain are related through,

$$\sigma_{ij} = K(1-D)\epsilon\delta_{ij} + 2G(1-D)\left(\epsilon_{ij} - \frac{1}{3}\epsilon\delta_{ij}\right), \tag{36}$$

where K and G are the intrinsic moduli of the oil shale and the time changing effective moduli are determined by a scalar measure of the fracture damage, D.

the constitutive description in tension is provided by two rate equations for the fracture damage and fracture surface area,

$$\dot{D} = (36\pi)^{\frac{1}{3}}[n(\epsilon)]^{\frac{1}{3}} C_g D^{\frac{2}{3}}(1-D)\,, \tag{37}$$

$$\dot{A} = (48\pi^2)^{\frac{2}{3}}[n(\epsilon)]^{\frac{2}{3}} C_g D^{\frac{1}{3}}(1-D)\,, \tag{38}$$

where the specific forms are determined by physical considerations of internal cracks to high rate loading and the Weibull crack statistics concepts noted earlier [Grady and Kipp,1979,1980]. The parameter C_g is a crack propagation velocity and $n(\epsilon)$ is a crack activation law specified by the Weibull fracture theory.

The complexity of the stress waves generated by explosive charges, and the appearance of relief waves that emanate from free surfaces or regions previously fractured, necessitate the use of wave-propagation codes to address realistic problems. The codes numerically integrate the conservation equations of mass, momentum,and energy, along with the constitutive equations for the material. The fracture model described above was incorporated into the Lagrangian two-dimensional wave code, TOODY-IV [Swegle,1978].

A calculation is illustrated for one Colony Mines fragmentation experiment in Figure 6. This experiment involved the detonation of a 5.2 kg, 0.75 m long charge of AN-FO at the bottom of a 0.1 m diameter, 2.0 m deep borehole drilled into the floor of the mine. Profiles of the excavated crater measured at 90° intervals around the axis of the borehole are shown in the figure. Based on earlier experiments [Grady et al.,1980], a damage level of 0.2 had been selected as a criterion for fracture damage levels sufficient for ejection. The numerical calculation established the damage contours and domains of fragment size shown in Figure 6 and are regarded as a reasonably good simulation of the cratering experiment. This type of calculation has been extended to evaluate concepts in explosive blasting [Boade et al.1981]. Multiple charges with variations in placement and timing have been accessed. Optimization of charge decking in the same borehole has also been performed by calculation.

6 Summary

There appears to be a clear relation between the fracture threshold of a single crack subjected to high strain rate loading and the response of a crack system in determining the transient strength and fracture stress of a rapidly loaded body. Although certain conditions pertaining to the density and distribution of flaws are apparently required, studies on rocks over a variety of material conditions and strain rates seem to support this observation.

Perhaps one of the most interesting and important observations which is emerging from current studies on the bulk or continuum fracture properties of materials subjected to very rapid or impulsive loading is the importance of some measure of the fracture surface energy. A fracture toughness or strain energy release rate appears to be a necessary ingredient fundamental to both the dynamic strength of materials and in determining the number of cracks participating in the fracture process along with the final fragment size in the failed material.

This concept has been noticeably absent in the large body of continuum and computer modelling which has appeared in the literature to date. Considerably more emphasis has been focused on describing an initial condition of the body in terms of inherent flaws and weaknesses; perhaps more than is warranted. The ideas which are emerging suggest that both inherent flaw properties and energy conditions are probably important, but at the higher loading rates the latter effect becomes increasingly dominant.

Lastly, the description fragment size distributions resulting from fracture events and relating these distributions to the different geometries, material properties, and loading conditions is an interesting and complex problem which, at present, is very poorly understood. Distributions are observed to range from sharply centralized to broadly dispersed and there are indications that these differences may relate to the mode and multiplicity of fracture. Physically based statistical laws including those of Poisson and Boltzmann are being compared with fragmentation data, however, observations and conclusions at the present time are very tentative.

7 Figure Captions

Figure 1. Spall fracture strength of selected rocks.

Figure 2. Strain-rate dependent fracture strength of several rocks.

Figure 3. Strain-rate dependence of average fragment size in oil shale.

Figure 4. Behavior of the fragment size distribution dispersion parameter over various fragmentation methods.

Figure 5. Particle size distribution from shock fragmentation of quartz.

Figure 6. Computational calculation of (a) fracture damage and, (b) mean fragment size, about an explosively loaded borehole in oil shale.

8 Bibliography

Bennett, J. G., Broken Coal, *J. Inst. Fuel*, **10**, 22-39, 1936.

Bergstrom, B. H., C. L. Sollenberger, and W. Mitchell, Jr., Energy Aspects of Single Particle Crushing, *Trans. AIME* **220**, 267-372, 1961.

Bergstrom, B. H., C. L. Sollenberger, and W. Mitchell, Energy and Size Distribution Aspects of Single Particle Crushing, *Proc. U. S. Symp. Rock Mech. 5th*, 155-172, 1962.

Birkimer, D. L., A Possible Fracture Criterion for the Dynamic Tensile Strength of Rock, *Proc. 12th Symp. on Rock Mech.*, G. B. Clark, ed., **573**, 1971.

Boade, R. R., M. E. Kipp, and d. E. Grady, "A Blasting Concept for Preparing Verticle Modified in Situ Oil Shale Retorts," Report SAND81-1255, Sandia National Laboratories, Dec. 1981.

Bond, F. C., Third Theory of Comminution, *Trans. AIME*, **193**, 484-494, 1952.

Butkovich, T. R., Calculation of Fracture and Permeability Enhancement from Underground Explosions in Coal, *Proc. Am. Soc. Mech. Eng.*, Mexico City, Sept. 19-23, 1976.

Charles, R. J., Energy-Size Reduction Relationships in Comminution, *Trans. AIME*, **208**, 80-88, 1957.

Chen, E. P. and G. C. Sih, *Elastodynamic Crack Problems*, G. C. Sih, editor, Noordhoff International Publishing, 1977.

Chen, E. P., M. E. Kipp, and D. E. Grady, A Strain-Rate Sensitive Rock Fragmentation Model, *Mechanics of Oil Shale*, K. T. Chang and J. W. Smith, editors (Applied Science Limited) Chapt. 10, 1983.

Cohn, S. N. and T. J. Ahrens, Dynamic Tensile Strength of Lunar Rock Types, *J. Geophys. Res.*, **86**, 1794-1802, 1981.

Costin, L. S. and D. E. Grady, Dynamic Fragmentation of Brittle Materials Using the Torsional Kolsky Bar, (to be published) *Proc. Third Int. Conf. on Mech. Properties of Materials at High Rates of Strain*, Oxford, England, April, 1984.

Curran, D. R., L. Seamann, and D. A. Shockey, Dynamic Failure in Solids, *Phys. Today*, **30**, 46-55, 1977.

Dienes, J. K. and L. G. Margolin, A Computational Approach to Rock Fragmentation, *Proc. U.S. Symposium on Rock Mech. 21st*, Rolla, Missouri, May, 1980.

Faddeenkov, N. N., Distribution of Fragment Sizes in Block-Type Solid Rock Crushing by Blasting, *Sov. Min. Sci.* **11**, 660-664, 1975.

Davison, L. and A. L. Stevens, Thermomechanical Constitution for Spalling Bodies, *J. Appl. Phys.*, **44**, 588-674, 1973.

Forrestal, M. J., D. E. Grady, and K. W. Schuler, An Experimental Method to Estimate the Dynamic Fracture Strength of Oil Shale in the 10^3 to 10^4 s^{-1} Strain Rate Regime, *Int. J. Rock Mech. Min. Sci.*, **15**, 263-265, 1978.

Freund, L. B., Crack Propagation in an Elastic Solid Subject to General Loading - III. Stress Wave Loading, *J. Mech. Phys. Solids*, **21**, 47-61, 1973.

Gates, A. O., *Trans. Am. Inst. Mining, Petrol, Engrs.* **52**, 875 (1915).

Gandin, A. M., and T. P. Meloy, Model and a Comminution Distribution Equation for Single Fracture, *Trans. Soc. Min. Eng. AIME* **223**, 40-50, 1962.

Gilvarry, J. J., Fracture of Brittle Solids, I, Distribution Function for Fragment Size in Single Fracture (theoretical), *J. Appl. Phys.*, **32**, 391-399, 1961.

Glenn, L. A., The Fracture of a Glass Half-Space by Projectile Impact, *J. Mech. Phys. Solids*, **24**, 93-106, 1976.

Grady, D. E. and R. E. Hollenbach, Dynamic Fracture Strength of Rock, *Geophys. Res. Letters*, **6**, 73-76, 1979.

Grady, D. E. and M. E. Kipp, Oil Shale Fracture and Fragmentation at Higher Rates ofLoading, *Proc. U.S. Symp. Rock Mech., 20th*, 403-406, Austic, TX, 1979.

Grady, D. E. and M. E. Kipp, The Micromechanics of the Impact Fracture of Rock, *Int. J. Rock Mech. Min. Sci.*, **16**, 293-302, 1979.

Grady, D. E. and J. Lipkin, Criteria for Impulsive Rock Fracture, *Geophys. Res. Letters*, **7**, 255-258, 1980.

Grady, D. E. and M. E. Kipp, Continuum Modelling of Explosive Fracture in Oil Shale, *Int. J. Rock Mech. Min. Sci.*, **17**, 147-157, 1980.

Grady, D. E., Fragmentation of Solids Under Impulsive Stress Loading, *J. Geophys. Res.*, **86**, 1047-1054, 1981a.

Grady, D. E., Application of Survival Statistics to the Impulsive Fragmentation of Ductile Rings, *Shock Waves and High-Strain-Rate Phenomena in Metals*, M. A. Meyers and L. E. Murr, editors, 181-192, 1981b.

Grady, D. E., J. Lipkin, and L. S. Costin, Energy and Particle Size Effects in the Fragmentation of Oil Shale with a Torsional Split Hopkinson Bar, *Proc. U.S. Symp. on Rock Mech., 22nd*, MIT, Cambridge, MA, 1981.

Grady, D. E., Local Inertial Effects in Dynamic Fragmentation, *J. Appl. Phys.*, **53**, 322-325, 1982a.

Grady, D. E., "Analysis of Prompt Fragmentation in Explosively Loaded Uranium Cylindrical Shells," SAND82-0140, Sandia National Laboratories, Albuquerque, New Mexico, February, 1982b.

Grady, D. E. and D. A. Benson, Fragmentation of Metal Rings by Electromagnetic Loading, *Exp. Mech.* (in press) 1983.

Grady, D. E. and M. E. Kipp, Statistical Size Distribution in Random Single Fracture (in preparation) 1983.

Grady, D. E. and K. S. Varga, Shock Comminution of Crystalline Quartz (in preparation) 1983.

Grady, D. E., D. A. Benson, and M. E. Kipp, Energy and Statistical Effects in the Dynamic Fragmentation of Metal Rings (to be published) *Third Int. Conf. on Mechanical Properties of Materials at High Rates of Strain* Oxford, England, April, 1984.

Green, S. J. and R. D. Perkins, Uniaxial Compression Tests at Varying Strain Rates on Three Geologic Materials, *Symp. on Rock Mech.*, K. E. Gray, editor, 35-54, Austin, Texas, 1968.

Griffith, A. A., The Phenomena of Rupture and Flow in Solids, *Phil. Trans. Royal Soc., A*, **34**, 137-154, 1920.

Griffith, L., A Theory of Size Distribution of Particles in a Comminuted System, *Can. J. of Res.*, **21**, 57-64, 1943.

Harper, M. D. and J. M. Ray, "Experimental Design and Crater Profiles of Intermediate Scale Experiments in Oil Shale," Los Alamos National Laboratory, Rpt. LA-8553-PR, June, 1980.

Ivanov, A. G. and V. N. Mineev, Scale Effects in Fracture, *Expl. Comb. and Shock Waves*, 617-638, 1980.

Johnson, J. N., "Explosive Produced Fracture of Oil shale, Los Alamos Scientific Laboratory," Rpt. LA-7357-PR, 38-45, 1978.

Kick, F., Das Gesetz Der Proportionalem Widerstand and Seine Anwendung, Leipsig, 1885.

Kipp, M. E., D. E. Grady, and E. P. Chen, Strain-Rate Dependent Fracure Initiation, *Int. J. Fracture 16,* 471-478, 1980.

Kolmogorov, A. N., On the Log-Normal Law of Distribution of Fragment Dimensions in Crushing (in Russian), *Dokl. Akad. Nank. SSSR*, **31**, 99, 1941.

Kuznetsov, V. M. and N. N. Faddeenkov, Fragmentation Schemes, *Fiz. Gor. Vzr.*, **11**, 637-645, 1975.

Kumar, A., The Effect of Stress Rate and Temperature on the Strength of Basalt and Granite, *Geophysics*, **33**, 501-510, 1968.

Langstors, V., and B. Kihlstrom, *The Modern Technique of Rock Blasting*, 2nd ed., John Wiley, New York, 1967.

Lankford, J., Dynamic Strength of Oil Shale, *soc. Pet. Eng. J.*, **16**, 17-22, 1976.

Lienau, C. C., Random Fracture of a Brittle Solid, *J. Franklin Inst.*, **221**, 485-494, 674-686, 769-783, 1936.

Lindholm, U .S., L. M. Yeakley and A. Nagy, The Dynamic Strength and Fracture Properties of Dresser Basalt, *Int. J. Rock Mech. Min. Sci*, **11**, 181-191, 1974.

Lipkin, J., D. E. Grady, and J. d. Cambell, Dynamic Flow and Fracture of Rock in Pure Shear, *18th U.S. Sym. on Rock Mech.*, Keystone, Colorado, 3B2-1, June, 1977.

Lundberg, B., A Split Hopkinson Bar Study of Energy Absorption in Dynamic Rock Fragmentation, *Int. J. Rock Mech. Min. Sci.*, **13**, 187-197, 1976.

Margolin, L. G. and T. F. Adams, Numerical Simulation of Fracture, *Proc. U.S. Sym. Rock Mech., 23rd*, Berkeley, CA, August, 1982.

Margolin, L. G., Numerical Simulation of Fracture, *Proc. Int. Conf. on Constitutive Laws for Engineering Materials* C. S. Desai and R. H. Gallagher, editors, 567, Tucson, Arizona, 1983.

Matzui, T., and W. Mitzutani, Why is a Minor Planet Minor?, *Nature*, **270**, 506-507, 1977.

Mott, N. F. and E. H. Linfoot, "A Theory of Fragmentation," Extra-Mural Research No. F72/80, *Ministry of Supply* (England), January, 1943.

Mott, N. F., Fragmentation of Shell Cases, *Proc. R. Soc. London*, **300**, 300-308, 1947.

O'Keefe, J. D. and T. J. Ahrens, Impact Ejecta on the Moon, *Proc. Lunar Sci. Conf. 7th*, 3007-3025, 1976.

Oucherlony, F., "Review of Fracture Toughness Testing of Rock," Report DS 1980:15, Swedish Detonics Research Foundation, Stockholm, Sweden, 1980.

Parkins, D. W. and D. Tilles, Influx Measurements of Extra-Terrestrial Material, *Science*, **159**, 936-946, 1968.

Rinehart, J. S., Dynamic Fracture Strengths of Rocks, *Proc. Seventh Symp. Rock Mech.*, Pennsylvania State University, 1965.

Rosin, P., and E. Rammler, The Laws Governing the Fineness of Powdered Coal, *J. Inst. Fuel*, **7**, 29-36, 1933.

Schuhmann, R., Principles of Comminution, in Size Distribution and Surface Calculations, *Mining Technology*, Rpt. AIME TP 1189, 1-11, Am. Inst. Min., Metall., and Pet. Eng., New York, July, 1940.

Schmidt, R. A., N. R. Warpinski, S. J. Finley, and R. C. Shear, "Multi-Frac Test Series Final Report," SAND81-1239, Sandia National Laboratories, Albuquerque, New Mexico, November, 1981.

Seaman, L., D. R. Curran, and D. A. Shockey, Computational Models for Ductile and Brittle Fracture, *J. Appl. Phys.*, **47**, 4814-4826, 1976.

Shockey, D. A., D. R. Curran, L. Seaman, J. T. Rosenberg, and C. F. Petersen, Fragmentation of Rock Under Dynamic Loads, *Int. J. Rock Mech. Min. Sci.*, **11**, 303-317, 1974.

Smith, C. W., R. C. Bass, and L. D. Tyler, Puff'n Tuff, a Residual Stress - Gas Fracturing Experiment, *Proc. U.S. Sym. Rock Mech., 19th*, Stateline, Nevada, 1978.

Steverding, B. and S. H. Lehnigk, The Fracture Penetration Depth of Stress Pulses, *Int. J. Rock Mech. Min. Sci.*, **13**, 75-80, 1976.

Swegle, J. W., "TOODY IV - A Computer Program for Two-Dimensional Wave Propagation," SAND78-0522, Sandia National Laboratories, 1978.

Swenson, D. V. and L. M. Taylor, A Finite Element Model for the Analysis of Tailored Pulse Stimulation of Boreholes, *Num. Anal. Methods in Geomech.*, (to be published), 1983.

Tuler, F. R., and B. M. Butcher, A Criterion for the Time Dependence of Dynamic Fracture, *Int. J. Frac. Mech.*, **4**, 431-437, 1968.

Varnado, S., "Geothermal Drilling and Completion Technology Development," Report 78-0670C, Sandia National Laboratories, July, 1978.

Von Rittinger, P. r., Lehrbuch Der Aufbereitungskunde, (Ernst und Korn, Berliln, 1867), 19.

Warpinski, N. R., R. A. Schmidt, and P. W. Cooper, High-Energy Gas Frac: Multiple Fracturing in a Wellbore, *20th Proc. U.S. Sym. Rock Mech.*, 143-152, 1979.

Weimer, R. J. and H. C. Rogers, Dynamic Fracture Phenomena in High-Strength Steels, *J. Appl. Phys.*, **50**, 8025-8030, 1979.

Yamakashi, K., K. Nogami and t. Shimamura, Size Distribution of Siderophile Element Concentrations in Black Magnetic Spherules from Deep-Sea Sediments, *J. Geophys. Res.*, **86**, 3129-3132, 1981.

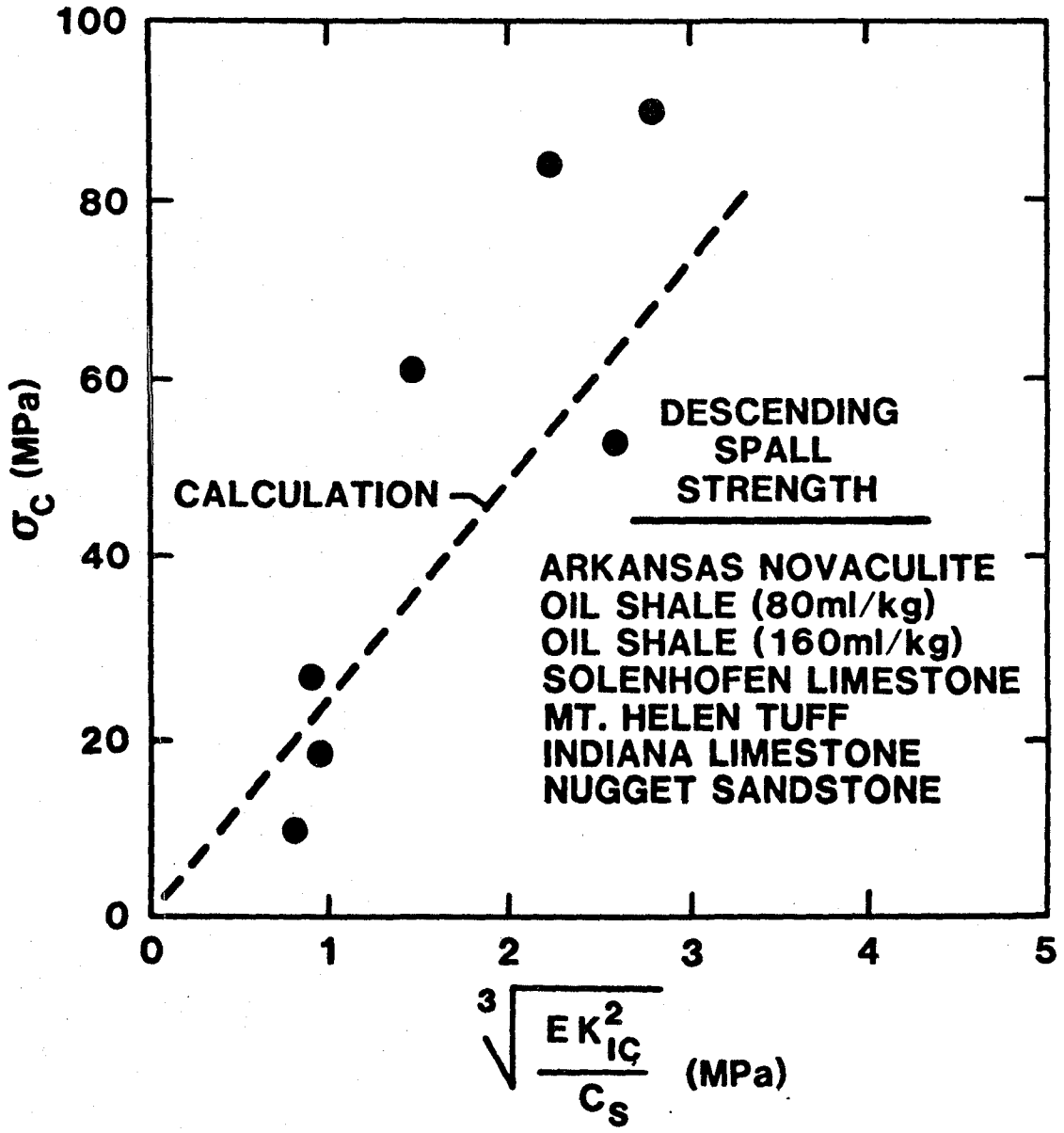
100
80
60
40
20
0
σ_c (MPa)
0
1
2
3
4
5
$\sqrt[3]{\frac{EK_{IC}^2}{C_S}}$ (MPa)
CALCULATION
DESCENDING SPALL STRENGTH
ARKANSAS NOVACULITE
OIL SHALE (80ml/kg)
OIL SHALE (160ml/kg)
SOLENHOFEN LIMESTONE
MT. HELEN TUFF
INDIANA LIMESTONE
NUGGET SANDSTONE

Figure 1.

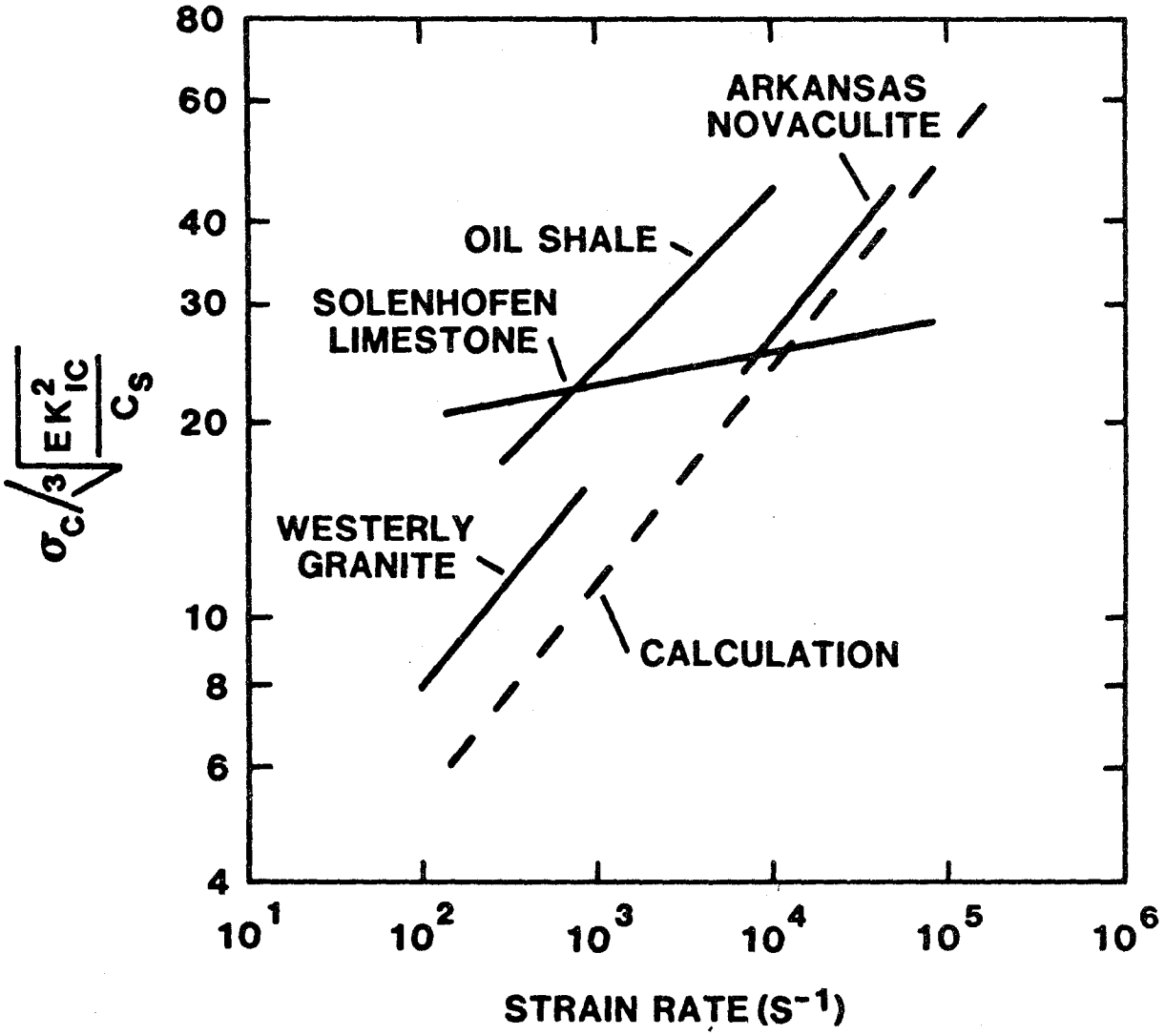
80
60
40
30
20
10
8
6
4
ARKANSAS NOVACULITE
OIL SHALE
SOLENHOFEN LIMESTONE
WESTERLY GRANITE
CALCULATION
$\sigma_c/3\sqrt{EK_{IC}^2/C_s}$
10^1
10^2
10^3
10^4
10^5
10^6
STRAIN RATE (S^{-1})

Figure 2.

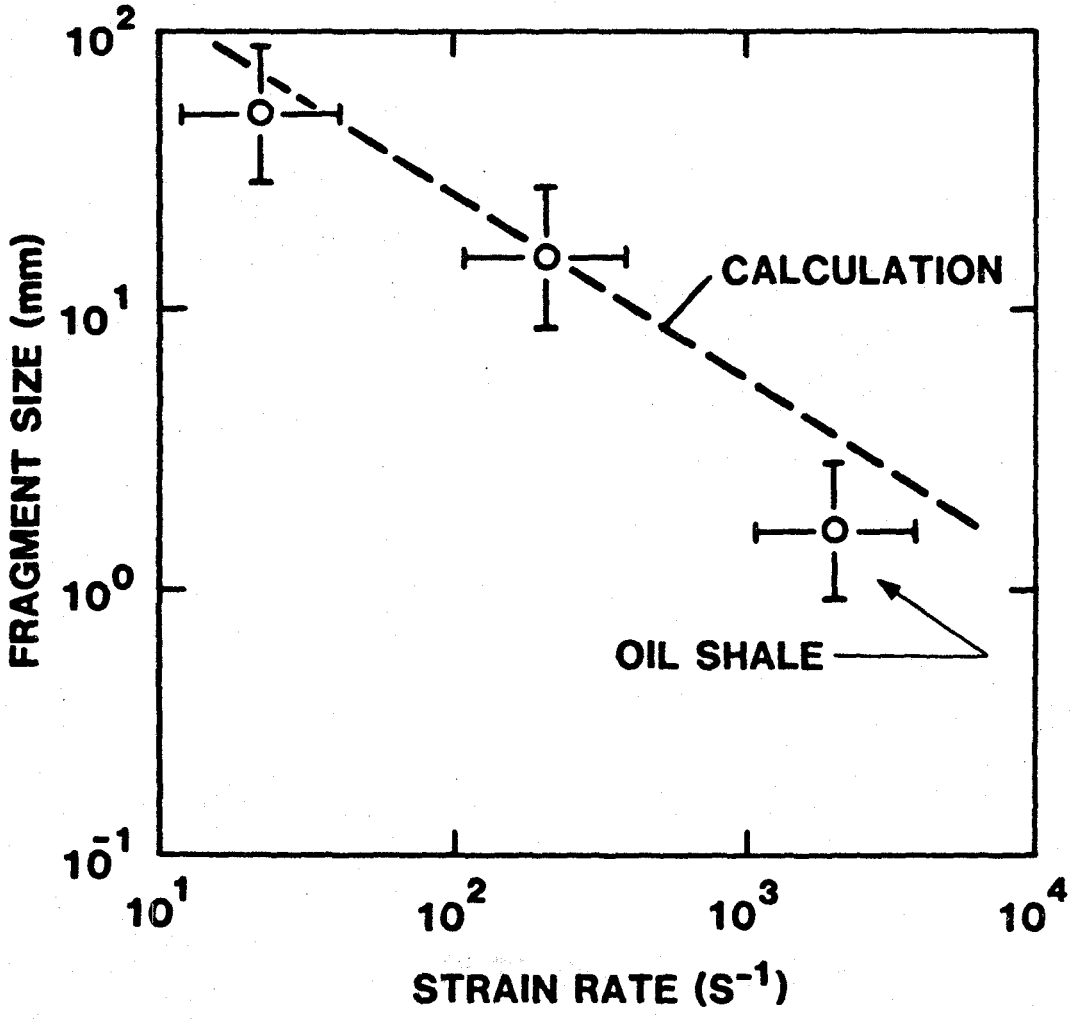
FRAGMENT SIZE (mm)
10^2
10^1
10^0
10^{-1}
CALCULATION
OIL SHALE
10^1
10^2
10^3
10^4
STRAIN RATE (S^{-1})

Figure 3.

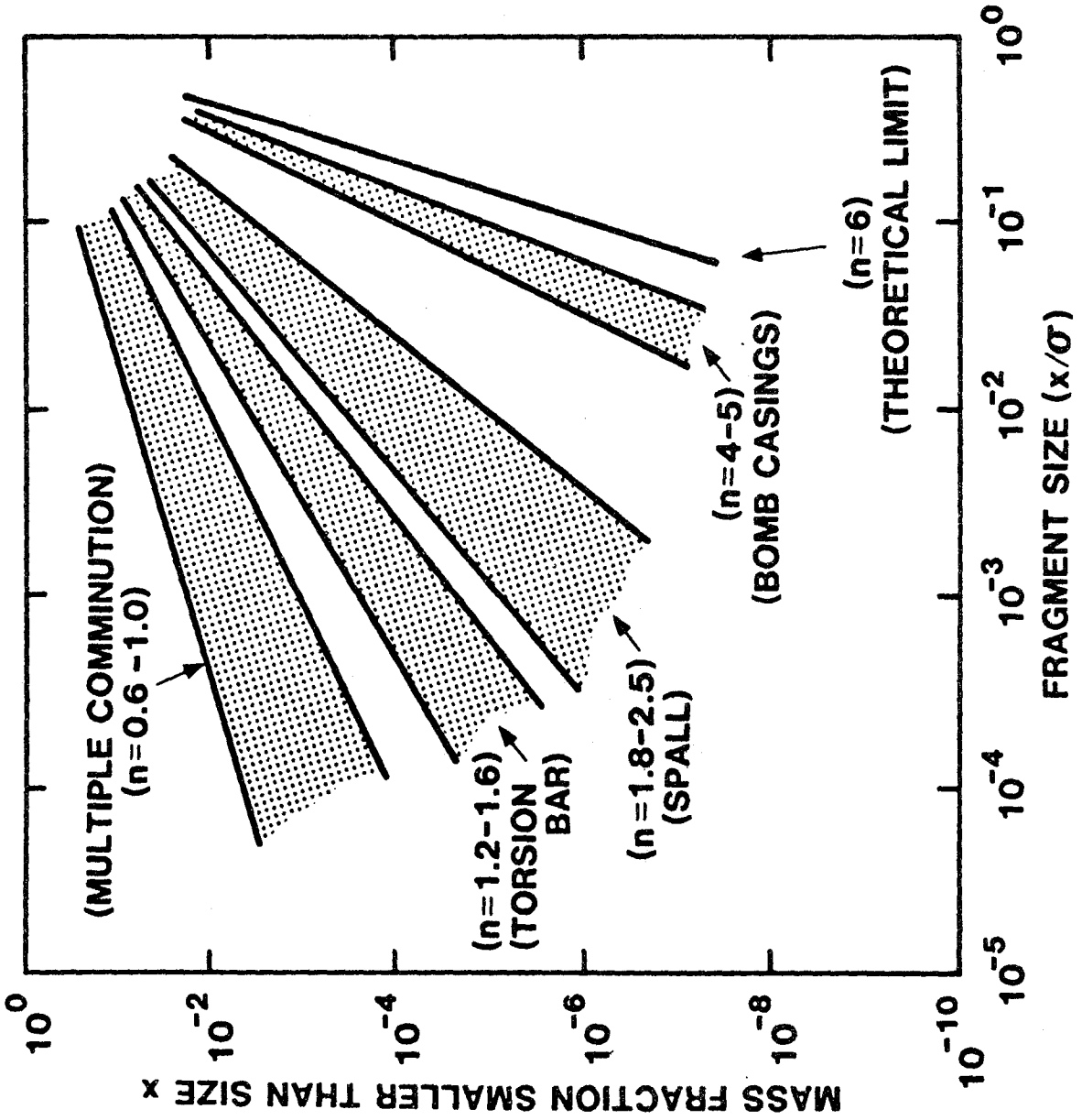
MASS FRACTION SMALLER THAN SIZE x
FRAGMENT SIZE (x/σ)
(MULTIPLE COMMINUTION)
(n=0.6 -1.0)
(n=1.2-1.6)
(TORSION
BAR)
(n=1.8-2.5)
(SPALL)
(n=4-5)
(BOMB CASINGS)
(n=6)
(THEORETICAL LIMIT)

Figure 4.

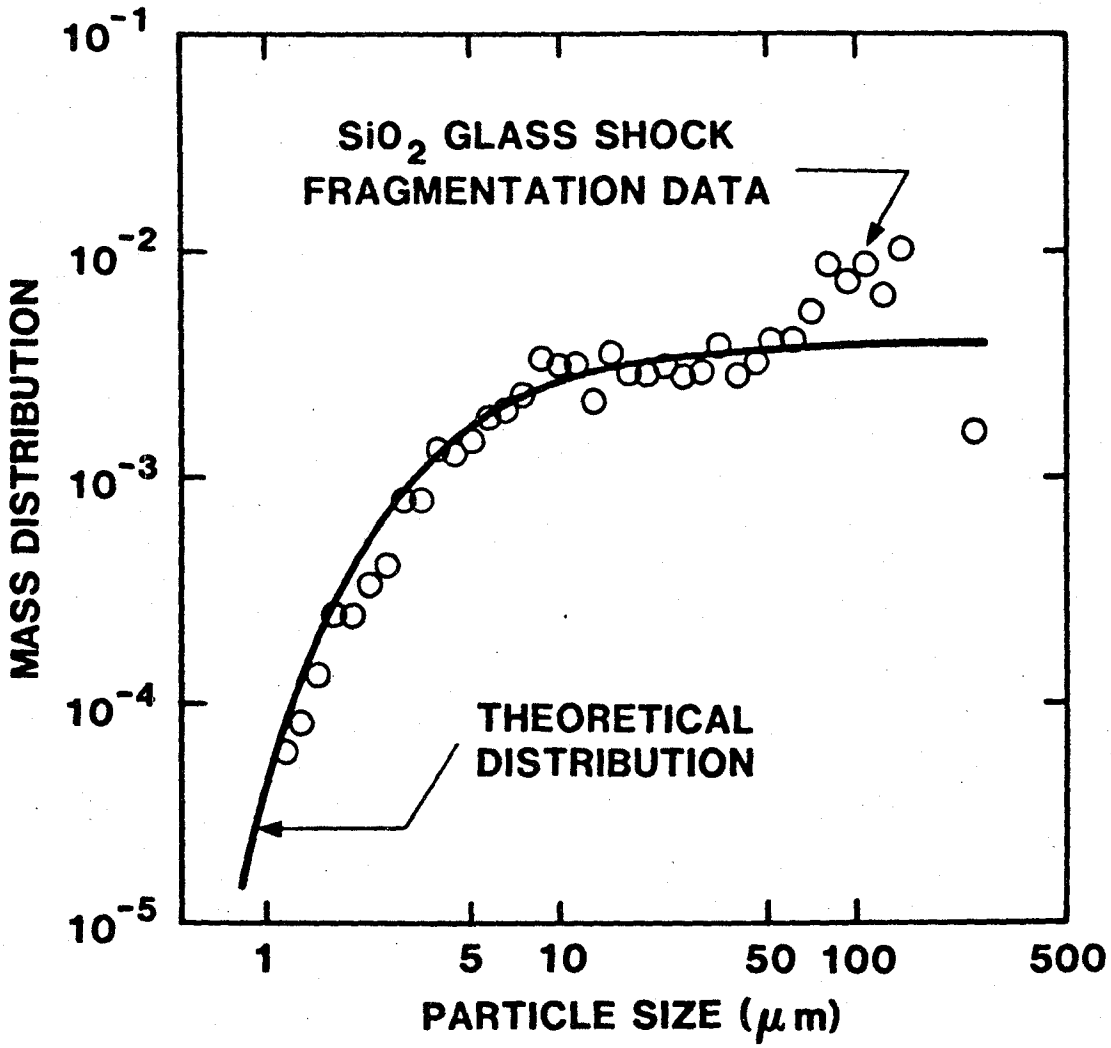
10^{-1}
10^{-2}
10^{-3}
10^{-4}
10^{-5}
MASS DISTRIBUTION
SiO_2 GLASS SHOCK
FRAGMENTATION DATA
THEORETICAL
DISTRIBUTION
1
5
10
50
100
500
PARTICLE SIZE (μm)

Figure 5.

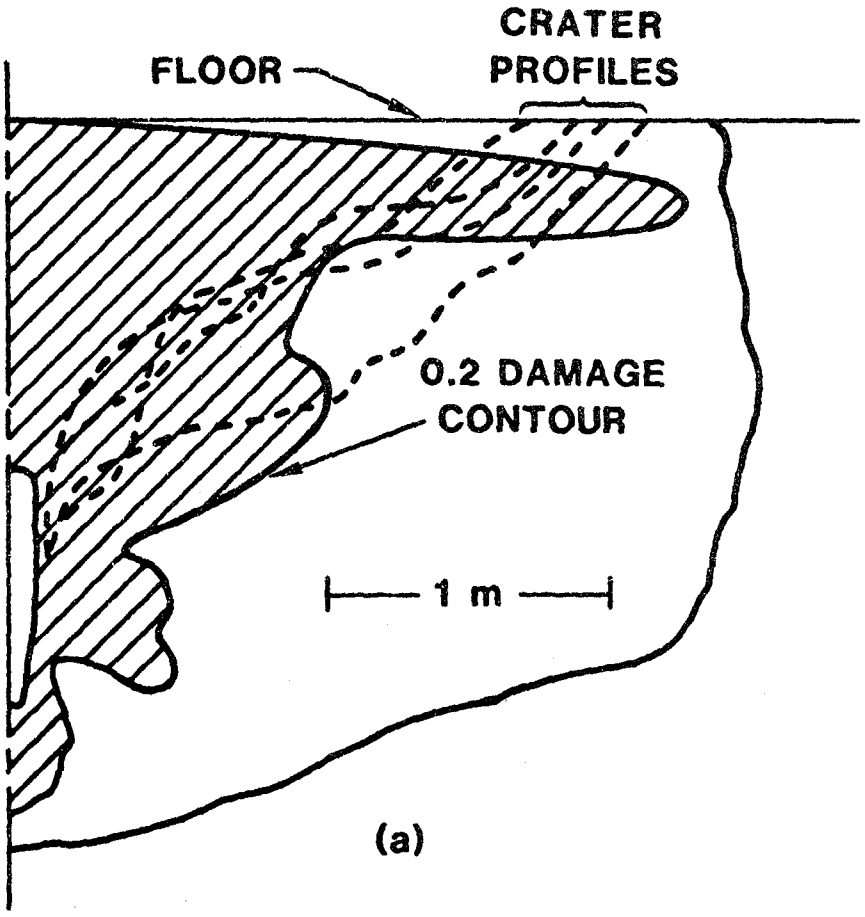

Figure 6.

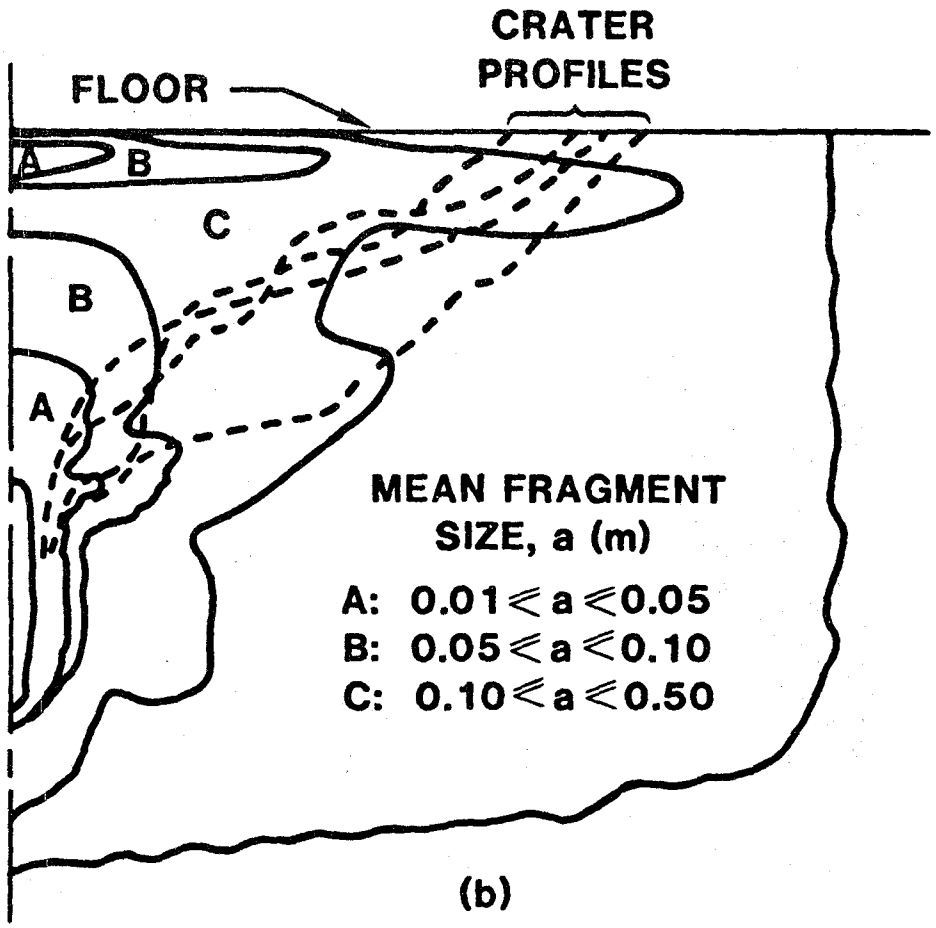
CRATER
PROFILES
FLOOR
A
B
C
B
A
MEAN FRAGMENT
SIZE, a (m)
A: 0.01 ⩽ a ⩽ 0.05
B: 0.05 ⩽ a ⩽ 0.10
C: 0.10 ⩽ a ⩽ 0.50
(b)

Figure 6.

CONSTITUTIVE RELATIONS FOR FRICTIONAL SLIP

Andy Ruina
Assistant Professor of Theoretical and Applied Mechanics
Cornell University
Ithaca, NY 14853, U.S.A.

Summary

This presentation discusses the mechanical description of the interface between two adjoining solids, rocks in particular. The macroscopic mechanical variables of interest here are the shear stress τ, the normal stress σ, the slip δ and the surface separation D. The possibility of slip in more than one direction, the relative rotation of neighboring surfaces, or the effects of in plane stress components are not included. Also neglected are the effects of transient changes in temperature, chemical environment and fluid pressure.

A 'continuum point', a concept that is not necessarily applicable in all situations, refers to a region that includes the adjoining surfaces as well as a thin layer of solid. It must be large enough to average the hetorogeneous micro-mechanisms, yet small enough that deformation of the adjoining solids is macroscopically homogeneous. The deformation variables δ and D can be defined by the separation of material points on opposite sides of the surface and somewhat removed from it. The slip δ, for example, is the shear displacement not accounted for by the bulk deformation of an equivalent quantity of solid with the same stress state.

Interest in the description of frictional constitutive relations has been motivated by the two general questions of 1) strength and 2) stability. Most constitutive descriptions are primarily concerned with strength, the largest shear stress τ, for a given normal stress σ as slip proceeds a macroscopic distance. Constitutive relations aimed at understanding stability of slip are centered on conditions under which τ decreases with δ. We will emphasize this latter class of constitutive laws, especially the state variable laws that have followed from the work of Dieterich.

SHEAR LOCALIZATION IN ROCKS INDUCED BY TECTONIC DEFORMATION

Brian Evans*
and
Teng-fong Wong**

*Deaprtment of Geological and Geophysical Sciences
Princeton University
Princeton, N. J. 08455

**Department of Earth and Space Sciences
State University of New York
Stony Brook, N. Y. 11974

Abstract

Geologic materials show localization on all scales from centimeters to kilometers, at all metamorphic grades and for extended periods of geologic history. We review here the analyses of shear localization for two end members of possible rheologies: 'brittle faulting' which is pressure-sensitive and relatively rate-sensitive, and 'fully plastic' flow instability which is temperature- and rate-sensitive and relatively pressure-insensitive.

Localization in a pressure-sensitive, dilatant material has been analyzed as an instability in the constitutive relation of homogeneous deformation. Prediction from such bifurcation analyses is compared with recent laboratory and field observations. Difficulties still exist with regard to the appropriate representation of the complex micromechanical processes within a continuum framework, and the scaling from laboratory specimen to geologic dimension.

Shear zone formation in the fully plastic region involves strain weakening which may be caused by thermal weakening, transition in flow mechamisms, weakening due to metamorphic reactions or several other causes. Our current understanding of the weakening processes is qualitative at best, and further theoretical treatment of the instability is limited by lack of quantitative field and laboratory data.

Introduction

Shear localization is observed in geologic materials on scales ranging from the size of thin sections up to zones that are hundreds of kilometers long and perhaps 30 km or so in width. Geologic deformation occurs over a broad spectrum of temperature, pressure, and time scales. At one end of the

spectrum, localization results in shear bands commonly referred to as 'faults', in which case the onset of localization occurs with relatively little inelastic strain (typically not more than a few percent) and insignificant dislocation activity. On the other hand, 'shear zones' are quite common in geologic settings for which deformation is believed to have occurred at temperature and pressure high enough for crystal plasticity and possible steady state creep processes to be operative over the time scale involved.

It is well known that predictions from localization analyses are very sensitive to the details of the constitutive equations used. In general the inelastic behavior of rock is expected to be pressure, temperature and rate sensitive with varying degrees of strain softening or hardening under the pressure and temperature range of geophysical interest (Figure 1). Therefore, relevant instability analysis can be carried out only for situations for which inputs on mechanical behavior from detailed laboratory and field studies are available.

Since geologic materials are so rich in examples of strain localization, we will not attempt to present a comprehensive review of the whole subject. The transition from the brittle to the ductile field is extremely complex (Carter and Kirby, 1978; Paterson, 1979). While a localization analysis in this context is well worth study, our current understanding of rock rheology in the transitional regime is too limited for developing a meaningful theoretical framework. We will therefore limit our scope and focus on two end members: brittle faulting where the deformation is highly pressure-sensitive and relatively rate-insensitive, and shear zone formation where the deformation is highly rate-senstive and basically pressure-insensitive. Following current rock mechanics usage, the latter mode of deformation will be

referred to as 'fully plastic.'

Recent development in theoretical, field and laboratory work have allowed new insights into the brittle faulting process. An active research area in continuum mechanics is the analysis of shear localization as a bifurcation phenomenon. Such an approach for a rate-insentive, but pressure-sensitive and dilatant material have provided a unified framework for the continuum description of faulting (Rudnicki and Rice, 1975). On a microscopic scale, systematic electron microscopy studies (Wong, 1982) detail the complexity of the micromechanical processes and provide a comparison with the continuum description. At the same time, detailed mapping of geologic faults (Segall and Pollard, 1983; Aydin and Johnson, 1983) and seismological study of mining-induced earthquakes (McGarr et al., 1979) highlights some difficulties regarding the scaling question. The presence of water can have significant effects on the brittle behavior of rocks. This subject is discussed in another presentation (Rudnicki, 1983); we will focus our discussion on brittle faulting in dry rocks.

An analysis of flow instability has to take into account the strain-rate sensitivity, activation enthalpy, strain hardening (or softening) and adiabatic heating (Argon, 1973; Jonas, et al., 1976). One major advance in rock rheology study in the past decade has been in the careful determination of the flow laws for steady state creep of materials thought to be constituents of the upper mantle and lower crust (Goetze, 1978; Kirby, 1980). Such experimentally determined constitutive relations have provided the essential input parameters for basically all the theoretical analyses of ductile shear zone formation. Mechanisms proposed include 'thermal runaway' (Yuen et al., 1978; Fleitout and Froidevaux, 1980), 'plastic instability' (Poirier et al., 1979) and 'chemical weakening' (Sorensen, 1983).

Another advance has been through the extensive use of transmission electron microscopy and chemical microanalysis techniques in the study of deformation-induced microstructures. Systematic sampling in the field and comparison of the microstructures seen in field samples with those in laboratory specimens have provided important constraints on the operative mechanisms (Christie and Ord, 1980; Kohlstedt and Weathers, 1980; White et al., 1980).

In a certain sense, the analysis of shear localization for geologic materials proceeds along lines similar to earlier developments in applied mechanics for metal, polymer and metallic glass. This parallel development does not appear to be broadly appreciated nor fully exploited. We will try to emphasize such parallel developments where appropriate in the following discussion.

Localization Analysis for Frictional, Dilatant Materials

When loaded under compressive stresses in the brittle field, a rock fails by development of a localized shear band. This process, commonly called 'faulting' in a geologic context has been extensively studied, and a comprehensive review was recently given by Paterson (1978). We will first summarize recent theoretical results from bifurcation analyses of constitutive relations proposed for pressure-sensitive, dilatant materials and then compare them with experimental observations.

The theory of localization of plastic deformation was reviewed by Rice (1976), and results pertinent to geologic materials such as rock and soil were summarized by Cleary and Rudnicki (1976). Since then, there have been several papers proposing constitutive relations for rock-like materials (e.g., Bazant and Kim, 1979; Nemat-Nasser and Shokooh, 1980). Most of these involve pressure-dependent yielding and dilatancy but otherwise one similar in spirit

to the flow theory of metal plasticity. We will focus on the following relation proposed by Rudnicki and Rice (1975) for brittle rock which has the essential features of this class of constitutive relations with the least complication:

$$D_{ij} = \frac{1}{2G} \left(\overset{\nabla}{\sigma}_{ij} - \frac{\nu}{1+\nu} \overset{\nabla}{\sigma}_{kk} \delta_{ij} \right) + \frac{1}{h} P_{ij} Q_{kl} \overset{\nabla}{\sigma}_{kl} \qquad (1)$$

with

$$P_{ij} = \sigma'_{ij}/2\tau + \beta/3 \, \delta_{ij}$$

$$Q_{ij} = \sigma'_{ij}/2\tau + \mu/3 \, \delta_{ij}$$

where D_{ij} is the symmetric part of the rate of deformation, and $\overset{\nabla}{\sigma}_{ij}$ is the spin-invariant Jaumann rate of Cauchy stress. The first term in bracket represents the usual Hookean behavior, whereas the second part is the inelastic contribution. σ'_{ij} is deviatoric part of the stress tensor, and τ is the square root of the second stress invariant J_2. Note that the inelastic deformation is described by 3 parameters: a hardening modulus h, a dilatancy parameter β, and a frictional parameter μ.

The deformation is therefore rate-insensitive, and the relation reduced to the classical Prandtl-Reuss relation when the pressure dependence of yielding and dilatancy are insignificant. Rudnicki and Rice (1975) argued on physical grounds that subsequent yield surfaces should have a vertex structure. Non-normality coupled with yield surface vertices render the analysis to be more involved than that in classical metal plasticity. Recently, Needleman (1979) presented a detailed plane-strain analysis of the incompressible case. Rudnicki and Rice (1975) neglected terms of the order stress divided by shear modulus in their final computation. Vardoulakis (1980) and Anand and Spitzig (1982) recently suggested that such terms can be important in certain situations, and compare predictions from the more involved calculation with experimental data on granular sand.

Fitting stress-strain data for brittle rock, Rudnicki and Rice (1975) estimated μ to range from 0.4 to 0.9 and β from 0.2 to 0.4. For such materials, the bifurcation analysis predicts a localized zone inclined at about 30^{o} to σ_1 (the maximum principal compressive stress) for a sample loaded to fracture under axisymmetric compression. This is in general agreement with experimental observations (Paterson, 1978). For a fixed μ and β, the critical value of h at onset of localization is strongly dependent on the loading configuration. In general, localization under plane-strain deformation has to occur at the hardening stage (Anand and Spitzig, 1982). For a wide range of μ and β, the critical h for axisymmetric compression is generally predicted to be very negative (well into strain softening). The result is modified if the influence of yield surface vertex (Rudnicki and Rice, 1975) and stress-induced anisotropy (Rudnicki, 1977) are included.

Micromechanics of Brittle Faulting

Earlier experiments with strain gauges (Hadley, 1975), acoustic emission (Lockner and Byerlee, 1980), and holography (Soga et al, 1978) indicate pre-failure localization of strain at a hardening stage. Direct microscopic observation requires samples deformed stably through the post-failure region with displacement control. Using a testing machine of high stiffness and special loading-unloading technique (Wawersik and Brace, 1971), Wong (1982) obtained complete suites of pre- and post-failure samples of Westerly granite for scanning electron microscope (SEM) study.

The SEM observation points out the complexity of the localization process in this relatively isotropic, low porosity (about 1%) rock. Inception of faulting in the sense of localized deformation extending over two or more grains is quite evident in samples stressed to just beyond peak stress. The micromechanical processes leading to the formation of a through going fault

include a number of mechanisms dependent on mineralogy and grain orientation. These include three types of geometric instability well known to the material scientists: microbuckling of slender columns in grains segmented by microcrack arrays (Figure 2), with characteristic dimension of a grain size (Evans and Adler, 1978); kinking in biotite grains (Figure 3) which have reached the plastic yield stress (Frank and Stroh, 1952); rotation and crushing of 'joint blocks' formed by pore-emanated cracks in plagioclase (Figure 4), with characteristic dimension dictated by the pore spacing (Goodman, 1976). In addition, shear slip along cracks at high angle to σ_1, favorable for frictional displacement is evident in the post-failure samples (Figure 5).

A continuum description such as (1) of the brittle behavior of a complicated, polycrystalline material such as rock is probably adequate over a continuum element large enough for the effects of grain scale inhomogeneity and anisotropy to average out. The SEM observation shows that the mineral quartz, comprising about one-third by volume of the granite, has limited participation in the localization process in the initial post-failure stage. In other words, localized deformation extending over a continuum element with grains of all major mineral types is not observed until the sample has been deformed well into the post-failure stage. In this limiting sense, the SEM observation agrees with the theoretical prediction discussed above.

Physical Theory of Dilatancy in Brittle Rock

A number of physical theories have been developed aiming to determine the macroscopic stress-strain behavior of a brittle rock in terms of the micromechanical processes. A group of models, commonly referred to as 'sliding crack models' postulate that frictional sliding along grain boundaries or cracks inclined at high angle to σ_1 pull open other tensile

cracks, causing the latter to extend parallel to σ_1 and giving rise to dilatancy (Kachanov, 1982; Moss and Gupta, 1982). Kachanov's approach is in a sense similar to the slip theory of Batdorf and Budiansky (1949). His results show that there is limited path-independence for stress histories which do not depart too much from proportional loading, and elaborate on the development of yield surface corners. Important qualitative insights have emerged from such micromechanical models on phenomenological descriptions represented by (1) which are motivated by a physical model analogous to the 'sliding crack.'

On the other hand, Stevens and Holcomb (1980) argued on the basis of SEM observations and their own study of hysteresis in stress cycling tests that the 'sliding crack' is unrealistic. SEM studies of Tapponier and Brace (1976) concluded that dilatancy is primarily a consequence of two types of cracking: (1) widening and extension of pre-existing discontinuities, such as grain boundaries, cracks and pores; (2) initiation and propagation of cracks at localities with high contrast in elastic moduli, such as at transverse grain boundaries between different minerals. Recently, Kranz (1979) and Batzle et al. (1980) suggested that geometric irregularities such as asperities at grain boundaries may be important in the initiation of stress-induced cracks.

A conclusion common to all the SEM studies is that the stress-induced cracks are in general 'mode I' tensile cracks. The crack orientation has a highly anisotropic distribution, and is mostly at low angles (say, less than 15°) to σ_1. Neither Tapponier and Brace (1976) nor Kranz (1979) found a significant number of inclined cracks. Although Wong (1982) did observe a number of cracks inclined at high angles to σ_1 in granite samples deformed under pressure and temperature higher than previous work, no appreciable mode II or III deformation along such cracks are evident in the pre-failure samples.

A number of mechanisms have been proposed as alternatives to the 'sliding crack.' Stevens and Holcomb (1980) suggested the 'reversible Griffith crack', and Janach and Guex (1980) proposed the 'shear bubble' model which hinges on the behavior of interfacial cracks with different elastic properties on either side. The implications of such alternative micromechanical models on phenomenological descriptions have not been quantitatively explored in detail.

There are, however, some recent observations in agreement with the 'sliding crack model.' Focal mechanism study of acoustic emission from brittle rock undergoing dilatancy concludes that many of the emission sources can not be adequately represented by a tensile crack (Sondergeld and Estey, 1982), strongly suggesting that shear slip has to be involved. Tensile opening of microcracks is easily resolved under the SEM. Whereas recognition of appropriate 'strain markers' helps one to identify shear displacement discontinuity in the field, no unambiguous approach is available for identifying shear cracks under the SEM.

The Scaling Problem

The size effect is of particular importance in rock mechanics because of the large span in dimension between laboratory samples and rock mass involved in engineering practice or tectonic processes. Most of the data available are in cm-size cylindrical specimens deformed in a conventional triaxial configuration. Several laboratories are interested in developing large-scale testing facilities, and the progress was reported in a recent workshop (Cook and Heard, 1981).

The size effect for uniaxial compressive strength has been investigated to an extent. The ratio of laboratory to field strengths for several relatively weak rocks can be as high as 10, and it seems that there is a critical size of about 1 m such that larger specimens suffer no further

decrease in strength (Singh, 1981; Brace, 1981). It is fair to say that more thorough studies, both theoretical and experimental, are necessary before a more definitive conclusions can be drawn.

A question naturally arises as to the relevance of laboratory results to the understanding of large scale faulting. There are not many comprehensive field studies of the evolution of brittle faulting. Two recent studies on different scales concluded that the mechanical processes in the field are very similar to the laboratory observation. McGarr et al. (1979) reported that the localized deformation due to mining-induced earthquakes possesses features quite similar to those seen by Hallbauer et al. (1973) in laboratory specimens of the country rock stressed to failure. A careful mapping of the Navajo and Entrada sandstones in Utah was carried out by Aydin and Johnson (1983), who concluded that many of their observations can be adequately interpreted by Rudnicki and Rice's model.

However, a recent field study by Segall and Pollard (1983) concluded that the laboratory observation may not be universally applicable in the field. Their observation of faulting in granodiorite in the central Sierra Nevada indicates that faults are nucleated on pre-existing joints (large scale tensile cracks). The joints subsequently act collectively as a weak zone and undergo significant shear motion probably induced by a stress field rotated over time. More careful field studies of this nature are needed to clarify how applicable such a localization process is to other geologic settings.

Localization of Flow in the Plastic Regime

Lapworth (1985) was the first to describe a fine-grained, well-laminated rock along the Moine Thrust zone in Scotland and named it mylonite. Since then, geologists have recognized that mylonites indicate shear zones of localized deformation which may extend to continental dimensions (Figure 6).

Mylonites in such shear zones usually show grain size reduction, and some times show evidence of melting. The deformation mechanism is inferred to be rate-sensitive plastic flow in many instances.

A convenient (but not necessarily exact) criterion commonly used for the localization analysis of rate-sensitive materials is that the onset of localization occurs if the load bearing capacity decreases with strain (Backofen, 1972; Argon, 1973). Recently, there have been some studies (e.g., Bai, 1982; Steif et al., 1982) to explicitly consider the development of runaway instability of strain associated with an initial imperfection.

There are two important differences between the usual material science and the geologic analysis of strain localization in this context. First, the change of area with loading is an important consideration especially with regard to the development of necking in metals. Although there are extensional tectonic settings for which necking seems to be important (Taopponier and Francheteau, 1978) most of the shear zones occur at geologic settings for which the loading can be approximated as simple shear and therefore the area variation needs not be considered.

Second, although thermal softening induced by adiabatic heating is of importance to metals only for dynamic loading (Culver, 1973; Costin et al., 1979) it can be significant for geologic materials with a much lower thermal diffusivity. As a matter of fact, most of the theoretical analyses have aimed to assess the possible contribution of thermal softening. Poirier (1980) recently presented a comprehensive analysis with the geologic problem in mind. He considered a constitutive relation for simple shear of the following form:

$$\sigma = M^{(1+n+m)} \tau_o \varepsilon^n \dot{\varepsilon}^m \exp\left(\frac{mQ}{RT}\right) \qquad (2)$$

where M is the Taylor factor (Kochs, 1958), τ_o is a constant possibly weakly dependent on temperature, ε is the strain, $\dot{\varepsilon}$ is the strain rate, n is the

strain hardening coefficient ($n = \frac{\partial \sigma}{\partial \varepsilon}\Big|_{\dot{\varepsilon},\, T}$), m is the strain rate sensitivity ($\frac{\partial \sigma}{\partial \dot{\varepsilon}}\Big|_{\varepsilon,\, T}$), and Q is the activation energy.

He took for convenience the criterion for onset of localization that:

$$\frac{\partial \ln \sigma}{\partial \varepsilon} = (1+n+m)\,\frac{d\ln M}{d\varepsilon} + \frac{d\ln \tau_o}{d\varepsilon} + \frac{n}{\varepsilon} - m\frac{d\ln \dot{\varepsilon}}{d\varepsilon} - \frac{mQ}{RT^2}\frac{dT}{d\varepsilon} = 0 \qquad (3)$$

From left to right, the contributions from the different terms are referred to as 'geometric softening,' 'structural softening,' 'strain softening,' 'strain rate softening,' and 'thermal softening,' respectively. Of course, they will be referred to as 'hardening' with the signs reversed.

It is quite evident from field evidence that metamorphism and deformation are often concurrent (Beach, 1980). Chemical reactions between minerals, influx or egress of water, and thermal perturbation can all alter the coefficients above. Although we discuss separate softening mechanisms below, it is important to recognize that the decoupling of processes is strictly pedagogical.

Thermal Softening

Among the mechanisms proposed for shear zone formation, thermal softening is probably the most thoroughly analysed from a theoretical point of view. Most of the geologic studies follow the approach of Gruntfest (1963) who showed that thermal runaway occurs under constant stress (σ_o) boundary conditions if the parameter:

$$Gu = \frac{a\sigma_o^2 l^2}{k\eta_o} \qquad (4)$$

archieves a critical value. Here, η_o is the viscosity at temperature T_o, l is the characteristic dimension, and k is the thermal conductivity. The viscosity η at temperature T is given by $\eta = \eta_o \exp(-a(T-T_o))$. Gruntfest's formalism has been adapted to analyze the instability of magma flow (Fujii and

Uyeda, 1974) and glaciers (Clark et al, 1977).

Although an instability condition such as (3) can in principle be applied to materials with a wide range of rheology, our current understanding of flow behavior of rock is limited. A fair amount of experimental studies have been performed on steady state creep of rocks (Goetze, 1976; Kirby, 1980), but; although the brittle-ductile transition is an area of active research (Tullis and Yund, 1977; Caristan, 1982), quantitative results on the flow behavior are too limited to be of much use for such an analysis.

Yuen et al. solved the 1-dimensional problem of coupled heat transport and deformation of two half-spaces with an instantaneous stepwise increase in slip at the interface. The rheology was taken to be Newtonian viscous, with the effective viscosity adjusted to agree with experimentally determined power law creep results. An important conclusion is that thermal runaway probably is uncommon with constant velocity boundary conditions (which is considered to be the more realistic situation for geologic application). In fact, the shear zone broadens out to a dimension that scales as the square root of time.

If a characteristic dimension is introduced into the problem by specifying a width for a pre-existing weak zone (e.g., induced by a thermal anomaly), a transient stage is possible with strain gradually localized towards the center (Fleitout and Froidevaux, 1980). As expected, the subsequent long-term behavior will be similar to that considered by Yuen et al. (1978).

Poirier et al. (1979) considered a more realistic rheology by including transient creep behavior extrapolated from Goetze's (1971) experimental data for Westerly granite. An initial imperfection with a flow stress lower than the surroundings (at the same temperature and strain rate) is introduced. No runaway instability is possible with constant velocity boundary condition even

for total adiabaticity. As a matter of fact, the long term response of the weakened zone is to deform uniformly at a strain rate which scales as the initial strength defect and the inverse of strain rate sensitivity.

A common conclusion to all these studies is that the thermal anomaly characteristically extends to a dimension wider than that for strain concentration, which can be significant in the field comparison of mineral assemblages and strain data. However, the degree of strain concentration predicted by the model calculations is not as drastic as some of the field observations. The results may be modified if one performs the computation for a 2- or even 3-dimensional geometry. Necking, for example, is sensitive to the geometry and loading configuration (Backofen, 1972). However, the major weakness is probably the inadequacy of the constitutive relations used. We will discuss below the field and laboratory observations which all point to the complexity of softening mechanisms. A quantitative description of these mechanisms is urgently needed before a more realistic consideration of shear zone formation is possible.

Geometric, Structural and Strain Softening

In addition to the inference that plastic flow has occurred, three elements seem to be intrinsic to the definition of a mylonite: 1) occurrence of a planar zone, narrow with respect to the surrounding undeformed rock, 2) reduction of grainsize from protolith to mylonite zone, 3) enhanced foliation or lineation (Tullis *et al.*, 1982). The first of these elements is, of course, the evidence for localization of shear (Ramsay, 1980). However, it is important to remember that while the field evidence certainly indicates at least transient strain localization, the steady state shear zone structure is not known. In fact, Sorenson (1983) has argued, on the basis of field evidence, that strain softening of the rocks may indeed be followed by strain

hardening.

It is generally believed that the grain size reduction in shear zones occurs by recrystallization during deformation, i. e., dynamic recrystallization (Bell and Etheridge, 1973; White, 1977; Christie and Ord, 1980; Kohlstedt and Weathers, 1980) although small grain sizes could also result from the formation of new minerals (Robin, in Tullis et al., 1982). Experiments on dynamically recrystallizing metals document weakening of 0.20 of the yield stress or more at the onset of recrystallization (Glover and Sellars, 1973; Sellars, 1978; Ion et al., 1982). Micrographs of these experiments show newly formed grains along previously existing grain boundaries. There is a striking similarity between the textures in the dynamically recrystallized metals and in materials deformed in the superplastic regime on the one hand, and the progression of textures in a mylonitic shear zone on the other hand. For example, compare micrographs from Glover and Sellars (1973) or Ion et al., (1982) with Figure 7 (from Kohlstedt and Weathers, 1980). Thus it has been suggested that the strain localization in the shear zone results from strength differences between the coarse grained protolith and the fine-grained mylonite. The difference may result from geometric weakening due to preferred orientation of the dynamically recrystallized grains, or from structural weakening induced by increased recovery due to recrystallization from enhanced grain boundary sliding (see White, 1977 for a review) or a transition to diffusional superplastic flow (Boullier and Gueguen, 1975). An additional source of structural weakening may derive from the strength differences due to rearrangement of the geometric distribution of the phases in polymineralic rocks (Poirier, 1980).

Although comparisons between the dynamically recrystallized metals and textures in geologic shear zones are intuitively and esthetically appealing,

recent experiments on dynamically recrystallizing rocks are equivocal. Post (1977) has observed localized zones of finely recrystallized grains in a series of mechanical tests on Mt. Burnett dunite. The formation of recrystallized zones was sometimes associated with stress drops of 0.3 - 0.6 of the peak stress. Those stress drops have been ascribed to either the onset of grain-size sensitive flow (Twiss, 1976; Goetze, 1978) or transient creep effects (Post, 1977; Zeuch, 1982, 1983). However, other experiments in peridotite (Chopra and Paterson, 1981), quartzite, (Christie et al., 1983) and limestone (Schmid, Paterson, and Boland, 1980) deformed to large strains do not show strain weakening during recrystallization.

Recent experiments on peridotites (Chopra and Paterson, 1981) and halite (Guillope and Poirier, 1979) may provide important keys to reconciling these results: Chopra and Paterson showed that the presence of water promotes recrytallization and have suggested that the decreased strength of 'wet' samples is due to stress relaxation along grain boundaries. Guillope and Poirier (1979) have demonstrated that dynamic recrystallization may occur either by progressive subgrain rotation or grain boundary migration. Poirier (1980) has suggested that no weakening would be expected during the operation of the former mechanism. Thus, on the basis of present experimental data, the presence of finely recrystallized material cannot necessarily be presumed to be causative of strain weakening. It is possible that both the production of fine grains and the operation of strain weakening may depend critically on the introduction of water or some other chemically weakining agent (Etheridge and Wilkie, 1979; Sorenson, 1983).

Metamorphic Reactions and Strain Softening

It has long been recognized that deformation in shear zones commonly is accompanied by metamorphic reactions (Teall, 1885; Beach, 1980). Often times,

petrologic examination reveals that the shear zone was an open chemical system and that minerals in the zone have undergone extensive hydration (Kerrich et al., 1977; Beach, 1980). However this need not always be true, since in at least some cases, localized strain may develop in rocks undergoing prograde reactions (e.g., Brodie, 1980,1981).

Mechanical tests on metals, ceramics and minerals alike show that both brittle and plastic strength may depend on the chemical environment. For instance, deformation by pressure solution is strongly dependent on the chemical properties of an intergranular fluid (Robin, 1978). Deformation of quartz by dislocation and diffusional mechanisms is dramatically affected by the presence of water (see a review by Paterson and Kekulawala, 1979) and perhaps by the activity of other chemical species as well (Hobbs, 1981). Furthermore exothermic metamorphic reactions (e.g., retrograde hydration reactions) will provide an additional heat source.

The metamorphism may also cause structural weakening since the reaction products form a new mineral assemblage which may be weaker than the unreacted rock (White and Knipe, 1978); this is particularly so in the case of hydration of feldspar to form phyllosilicates. In addition, new minerals dispersed throughout the matrix may inhibit grain growth allowing grain size sensitive mechanisms including diffusional flow, pressure solution or grain boundary sliding to operate with enhanced strain rates (Etheridge and Wilkie, 1979).

It is clear that chemical reactions may profoundly affect the mechanical strength of rocks; apparently the converse is equally true. Reduction of the grain size of a potential reactant will increase the grain boundary area available as a reactant site (Mitra, 1978; Wintsch, 1975) and can potentially greatly increase the metamorphic reaction rate. Deformation may also increase the rate of introduction of water, either through dilatancy enhanced

permeability (Sibson, et al, 1975) or by plastic strain. It has been shown that the temperature of the α-β phase transition in quartz is affected by nonhydrostatic stress (Coe and Paterson, 1969) and it is probable that other mineral equilibria will also be affected (Yund and Tullis, 1980; Wintsch, 1975, 1981). Finally, chemical potential gradients due to non-hydrostatic stresses may well couple with gradients between reactants and products to cause increased diffusion rates (Brodie, 1980) or to provide favorable nucleation sites for new minerals (Knipe, 1979). Thus concurrent metamorphic and deformation processes are tightly coupled, and to understand the mechanical behavior of reacting mineral assemblages will require the consideration of both sets of phenomena.

Conclusion

We reviewed here the study of shear localization in geologic materials in two contexts. An interesting observation is that our understanding of the two phenomena, brittle faulting and shear zone formation, seem to have followed quite different lines of development.

Laboratory studies of dilatancy and fracture in brittle rock have been very active in the past twenty years or so. The quantitative evaluation of the stress-strain relationship as well as microscopy study of stress-induced microstructures have motivated seminal work on the formulation of constitutive equations incorporating dilatancy and pressure-sensitivity. The subsequent bifurcation analyses provide insight on the importance of both loading configurations and physical parameters on the onset of localization.

In contrast, only limited field study with a quantitative approach has been made, although the phenomenon is widely observed in tectonic settings. As a result, a number of important questions concerning the scaling problem remain unanswered.

On the other hand, the tectonics study of shear zones has been an active area of research. Field evidence frequently indicates that fluids have entered sheared regions and that metamorphism and deformation are concurrent and, quite probably, intricately coupled processes. Geometric, structural and strain softening may result from spatial redistribution of a weak phase, refinement of grain size and subsequent transition to grain size sensitive creep, reduction of the Taylor factor due to the production of preferred orientation, or increased recovery due to transient creep effects.

In contrast, quantitative study of this problem in the laboratory is very limited, partly due to the experimental difficulty and partly due to the complexity of the process. Although a generalized framework can be adapted from materials science, the advance in theoretical interpretation is relatively slow in the absence of appropriate constitutive equations for strain softening specialized to geologic materials. Thermal softening is one problem analyzed theoretically to some detail, and thermal runaway appears to be unlikely unless imperfection with drastic strength reduction is present or the boundary condition is approximated by constant stress.

References

Anand, L., Spitzig, W. A. (1982), 'Shear-band Orientations in Plane Strain,' Acta Metall, 30, 553-561.

Argon, A. S. (1973), Stability of plastic deformation, in The Inhomogeneity of Plastic Deformation, ASM, 161-189, 1973.

Aydin, A., Johnson, A. M. (1983), 'Analysis of Faulting in Porous Sandstones,' J. Structural Geol., 5, 19-31.

Backofen, W. A. (1972), 'Deformation Processing,' Addision Wesley, Reading Mass.

Bai, Y. L. (1982), 'Thermo-plastic Instability in Simple Shear,' J. Mech. Phys. Solids, 30, 195-207.

Batdorf, S. B., Budiansky, B. (1949), 'A Mathematical Theory of Plasticity Based on the Concept of Slip,' Technical note 1871, Nat. Adv. Committee on Aeronautics.

Batzle, M., Simmons, G., Siegfried, R. W. (1980), 'Microcrack Closure in Rocks Under Stress,' J. Geophys. Res., 85, 7072-7090.

Bazant, Z. P., Kim, S. S. (1979), 'Plastic-fracturing Theory for Concrete,' J. Eng. Mech. Div. ASCE, 105, 407-428.

Bell, T. H., Etheridge, M. A. (1973), 'Microstructure of Mylonites and Their Descriptive Terminology,' Lithos, 6, 337-348.

Boullier, A. M., Gueguen, Y. (1975), 'SP-Mylonites: Origin of Some Mylonites by Super-plastic Flow,' Contrib. Mineral Petrol., 50, 93-104.

Brace, W. F. (1981), 'The Effect of Size on Mechanical Properties of Rock,' Geophys. Res. Lett., 8, 651-652.

Beach, A. (1980), 'Retrogressive Metamorphic Processes in Shear Zones,' J. Struct. Geol., 2, 257-263.

Brodie, K. H. (1980), 'Variations in Mineral Chemistry Across a Phlogopite

Peridotite Shear Zone,' J. Struct. Geol., 2, 265-272.

Brodie, K. H. (1981), 'Variation in Amphibole and Plagioclase Composition with Deformation,' Tectonophysics, 78, 385-402.

Caristan, Y. (1982), 'The Transition From High Temperature Creep to Fracture in Maryland Diabase,' J. Geophys. Res., 87, 6781-6790.

Carter, N. L., Kirby, S. H. (1978), 'Transient Creep and Semibrittle Behavior of Crystalline Rocks,' Pageogh, 116, 807-839.

Chopra, P. N., Paterson, M. S. (1981), 'The Experimental Deformation of Dunite,' Tectonophysics, 78, 453-473.

Christie, J. M., Koch, P. S., Ord, A., George, R. P. (1983), 'The Effect of Water on the Rheology and Microstructures of Experimentally Deformed Quartzite,' J. Geophys. Res., in press.

Christie, J. M., Ord, A. (1980), 'Flow Stress from Microstructures of Mylonites: Example and Current Assessment,' J. Geophys. Res., 85, 6253-6262.

Clarke, G. K. C., Nitzan, U., Paterson, W. S. B. (1977), 'Strain Heating and Creep Instability in Glaciers and Ice Sheets,' Rev. Geophys. Space Physics, 15, 235-247.

Cleary, M., Rudnicki, J. (1976), 'On the Initiation and Propagation of Dilatant Rupture Zones in Geological Materials,' in The Effect of Voids on Material Deformation, ASME.

Coe, R. S., Paterson, M. S. (1969), 'The α-β Inversion in Quartz: A Coherent Phase Transition Under Non-hydrostatic Stress,' J. Geophys. Res., 74, 4921-49-48.

Cook, N. G. W., Heard, H. C. (1981), 'NSF-UC Berkely Workshop on Large Scale Laboratory Testing in Geomechanics,' Geophys. Res. Lett., 8, 645-723.

Costin, L. S., Crisman, E. E., Hawley, R. H., Duffy, J. (1979), 'On the

Localization of Plastic Flow in Mild Steel Tubes Under Dynamic Torsional Loading,' in Mechanical Properties at High Rates of Strain, (J. Harding, ed.), pp. 90-100.

Culver, R. S. (1973), 'Thermal Instability Strain in Dynamic Plastic Deformation,' in Metallurgical Effects at High Strain Rates, (R. W. Rhde et al, eds.), pp. 519-530.

Etheridge, M. A., Wilkie, J. C. (1979), 'Grain Size Reduction, Grain Boundary Sliding and the Flow Strength of Mylonites,' Tectonophysics, 58, 159-178.

Evans, A. G., Adler, W. F. (1978), 'Kinking as a Mode of Structural Degradation in Carbon Fiber Composites,' Acta Mett., 26, 725-738.

Fleitout, L., Froidevaux, C. (1980), 'Thermal and Mechanical Evolution of Shear Zones,' J. Struct. Geol., 2, 159-164.

Frank, F. C., Stroh, A. N. (1952), 'On the Theory of Kinking,' Proc. Phys. Soc., B65, 811-821.

Fujii, N., Uyeda, S. (1974), 'Thermal Instabilities During Flow of Magma in Volcanic Conduits,' J. Geophys. Res., 79, 3367-3370.

Glover, G., Sellars, C. M. (1973), 'Recovery and Recrystallization During High Temperature Deformation of α-iron,' Met. Trans., 4, 765-775.

Goetze, C. (1971), 'High Temperature Rheology of Westerly Granite,' J. Geophys. Res., 76, 1223-1230.

Goetze, C. (1978), 'The Mechanics of Creep in Olivine,' Phil. Trans. Roy. Soc. London, A288, 99-119.

Goodman, R. E. (1976), 'Methods of Geological Engineering,' West, St. Paul, 472 pp.

Gruntfest, I. J. (1963), 'Thermal Feedback in Liquid Flow, Plane Shear at Constant Stress,' Trans. Soc. Rheol., 7, 195-207.

Guillope, M., Poirier, J. P. (1979), 'Dynamic Recrystallization During Creep

of Single Crystalline Halite: An Experimental Study,' J. Geophys. Res., 84, 5557-5567.

Hadley, K. (1975), 'Azimuthal Variation of Dilatancy,' J. Geophys. Res., 80, 4845-850.

Hallbauer, D. K., Wagner, H., Cook, N. G. W. (1973), 'Some Observations Concerning the Microscopic and Mechanical Behavior of Quartzite Specimens in Stiff, Triaxial Compression Tests,' Int. Journ. Rock Mech. Min. Sci., 10, 713-726.

Hobbs, B. E. (1981), 'The Influence of Metamorphic Environment Upon the Deformation of Minerals,' Tectonophysics, 78, 335-383.

Ion, S. E., Humphreys, F. J., White, S. H. (1982), 'Dynamic Recrystallization and the Development of Microstructure During the High Temperature Deformation of Magnesium,' Acta. Metall., 30, 1909-1919.

Janach, W., Guex, L. H. (1980), 'In-plane Propagation of shear Microcracks in Brittle Rocks Under Triaxial Compression,' J. Geophys. Res., 85, 2543-2553.

Jonas, J. J., Holt, R. A., Coleman, C. E. (1976), 'Plastic Stability in Tension and Compression,' Acta Metall., 24, 911-918.

Kachanov, M. L. (1982), 'A Microcrack Model of Rock Inelasticity,' Mech. Mat., 1, 19-41.

Kerrich, R., Fyfe, W. S., Gorman, B. E., Allison, I. (1977), 'Local Modification of Rock Chemistry by Deformation,' Contrib. Mineral Petrol., 65, 183-190.

Kirby, S. H. (1980), 'Tectonic Stresses in the Lithosphere: Constraints Provided by the Experimental Deformation of Rocks,' J. Geophys. Res., 85, 6353-6363.

Kohlstedt, D. L., Weathers, M. S. (1980), 'Deformation-induced Microstructures, Paleopiezometers and Differential Stresses in Deeply Eroded

Fault Zones,' J. Geophys. Res., 85, 6269-6285.

Knipe, R. J. (1979), 'Chemical Changes During Slaty Cleavage Development,' Bull. Mineral., 102, 206-209.

Kocks, U. F. (1958), 'Polyslip in Polycrystals,' Acta Metall., 6 85-94.

Kranz, R. L. (1979), 'Crack Growth and Develpment During Creep in Westerly Granite,' Int. J. Rock Mech. Min. Sci., 16, 23-36.

Lapworth, C. (1885), 'The Highland Controversy in British Geology: Its Causes, Course and Consequences,' Nature 32, 558-559.

Lockner, D. A., Byerlee, J. D. (1980), 'Development of Fracture Planes During Creep in Granite,' in Proc. of 2nd Conf. on AE/Microseismic Activity in Geological Structures, and Materials, (H. R. Hardy, Jr. and F. W. Leighton, eds.) Trans. Tech. Pub., Clausthal, Germany.

McGarr, A., Spottiswoode, S. M., Gay, N. G., Ortlepp, W. D. (1979), 'Observations Relevant to Seismic Driving Stress, Stress Drop, and Efficiency,' J. Geophys. Res., 84, 2251-2261.

Mitra, G. (1978), 'Ductile Deformation Zones and Mylonites: The Mechanical Processes Involved in the Deformation of Crystalline Basement Rocks,' A. J. Sci., 1057-1084.

Moss, W. C., Gupta, Y. M. (1982), 'A Constitutive Model Describing Dilatancy and Failure in Brittle Rock,' J. Geophys. Res., 87, 2985-2990.

Needleman, A. (1979), 'Non-normality and Bifurcation in Plane Strain Tension and Compression,' J. Mech. Phys. Solids, 27, 231-254.

Nemat-Nasser, S., Shokooh, A. (1980), 'On Finite Plastic Flows of Compressible Materials with Internal Friction,' Int. J. Solids Struct. 16, 495-514.

Paterson, M. S. (1978), Experimental Rock Deformation - The Brittle Field, Springer Verlag, N. Y., 254 pp.

Paterson, M. S. (1979), 'The Mechanical Behavior of Rock Under Crustal and

Mantle Conditions,' in The Earth: Its Origin, Structure and Evolution (M. W. McElhinny, ed.), 469-489.

Paterson, M. S., Kekulawala, K. R. S. S. (1979), 'The Role of Water in Quartz Deformation,' Bull. Mineral., 102, 92-98.

Poirier, J. P. (1980), 'Shear Localization and Shear Instability in Materials in the Ductile Field,' J. Struct. Geol., 2, 135-142.

Poirier, J. P., Bonchez, J. L., Jonas, J. J. (1979), 'A Dynamic Model for Aseismic Ductile Shear Zones,' Earth and Planet. Sci. Lett., 43, 441-453.

Post, R. L. (1977), 'High Temperature Creep of Mt. Burnett Dunite,' Tectonophysics, 42, 75-110.

Ramsay, J. G. (1980), 'Shear Zone Geometry: A Review,' J. Struct. Geol., 2, 83-99.

Rice, J. R. (1976), 'The Localization of Plastic Deformation,' in Theoretical and Applied Mechanics (W. T. Koiter, ed.), North-Holland.

Robin, P. Y. F. (1978), 'Pressure Solution at Grain-to-Grain Contacts,' Geochim. Cosmochim. Acta, 42, 1383-1389.

Rudnicki, J. W. (1977), 'The Effect of Stress-induced Asisotropy on a Model of Brittle Rock Failure as Localization of Deformation,' Proc. 18th U. S. Symposium on Rock Mechanics.

Rudnicki, J. W., Rice, J. R. (1975), 'Condtions for the Localization of Deformation in Pressure-Sensitive Dilatant Materials,' J. Mech. Phys. Solids, 23, 371-394.

Schmid, S. M., Paterson, M. S., Boland, J. N. (1980), 'High Temperature Flow and Dynamic Recrystallization in Carrara Marble,' Tectonophysics, 65, 245-280.

Segall, P., Pollard, D. D. (1983), 'Nucleation and Growth of Strike Slip Faults in Granite,' J. Geophys. Res., 88, 555-568.

Sellars, C. M. (1978), 'Recrystallization of Metals During Hot Deformation,' Phil. Trans. R. Soc., 135, 513-516.

Sibson, R. H., Moore, J. Rankin, A. H. (1975), 'Seismic Pumping - A Hydrothermal Fluid Transport Mechanism,' J. Geol. Soc. Lond., 131, 653-659.

Singh, M. M. (1981), 'Strength of Rock,' in Physical Properties of Rocks and Minerals (Y. S. Toulonkian and C. Y. Ho, eds.) pp. 83-121.

Soga, N., Mizutani, H., Spetzler, H. Martin, R. J., III (1978), 'The Effect of Dilatancy on Velocity Anisotropy in Westerly Granite,' J. Geophys. Res., 83, 4451-4458.

Sondergeld, C. H., Estey, L. H. (1982), 'Source Mechanisms and Microfracturing During Uniaxial Cycling of Rock,' Pageogh, 120, 151-166.

Sorensen, K. (1983), 'Growth and Dynamics of the Nordre Stromfjord Shear Zone,' J. Geophys. Res., 88, 3419-3438.

Steif, P. S., Spaepen, F., Hutchinson, J. W. (1982), 'Strain Localization in Amorphous Metals,' Acta Metall. 30, 447-455.

Stevens, J. L., Holcomb, D. J. (1980), 'A Theoretical Investigation of the Sliding Crack Model for Dilatancy,' J. Geophys. Res., 85, 7091-7100.

Tapponier, P., Brace, W. F. (1976), 'Development of Stress-induced Microcracks in Westerly Granite,' Int. Journ. Rock Mech. Min. Sci., 13, 103-112.

Tappoiner, P., Francheteau, J. (1978), 'Necking of the Lithosphere and the Mechanics of Accreting Plate Boundaries,' J. Geophys. Res., 83, 3955-3970.

Teall, J. J. H. (1885), 'The Metamorphism of Dolenite into Hornblende Schist,' Q. Jour. Geol. Soc., 41 133-145.

Tullis, J., Snoke, A. W., Todd, V. R. (1982), 'Significance and Petrogenesis of Mylonitic Rocks,' Geology, 10, 227-230.

Tullis, J., Yund, R. A. (1977), 'Experimental Deformation of Dry Westerly Granite,' J. Geophys. Res., 82, 5705-5718.

Vardoulakis, I. (1980), 'Shear Band Inclination and Shear Modulus of Sand in Biaxial Tests,' Int. J. Num. Analy. Meth. Geomechanics, 4, 103-119.

Wawersik, W. R., Brace, W. F. (1971), 'Post Failure Behavior of a Granite and a Diabase,' Rock Mech., 3, 61-85.

White, S. A., Burrows, S. E., Carreras, J., Shaw, N. D., Humphreys, F. J. (1980), 'On Mylonites in Ductile Shear Zones,' J. Struct. Geol., 2, 175-187.

White, S. (1977), 'Geological Significance and Recrystallization Processes in Quartz,' Tectonophysics, 39 143-170.

White, S. H., Knipe, R. J. (1978), 'Transformation and Reaction Enhanced Ductility in Rocks,' J. Geol. Soc., London, 135, 513-516.

Wintsch, R. P. (1975), 'Feldspathization as a Result of Deformation,' Bull. Geol. Soc. Amer., 86, 35-38.

Wintsch, R. P. (1981), 'Syntectonic Oxidation,' Am. J. Sci., 281, 1223-1239.

Wong, T-F. (1982), 'Micromechanics of Faulting in Westerly Granite,' Int. J. Rock. Mech. Min. Sci., 19, 49-64.

Yuen, D. A., Fleitout, L., Schubert, G., Froidevaux, C. (1978), 'Shear Deformation Zones Along Major Transform Faults and Subducting Slabs,' Geophys J. Royal Astro. Soc., 54, 93-119.

Yund, R. A., Tullis, J. (1980), 'The Effect of Water, Pressure, and Strain on Al/S: Order Disorder Kinetics in Feldspar,' Contin. Min. and Pet., 72, 297-302.

Zeuch, D. H. (1982), 'Ductile Faulting, Dynamic Recrystallization, and Grain Size Sensitive Flow of Olivine,' Tectonophysics, 83, 293-308.

Zeuch, D. H. (1983), 'On the Inter-relationship Between Grain Size Sensitive Creep and Dynamic Recrystallization of Olivine,' Tectonophysics, 93, 151-168.

Figure Captions

Figure 1. Schematic drawing of a two layer model of a large fault zone (after Sibson).

Figure 2. Axial crack arrays in microcline (mi) and quartz (qtz) observed in a sample retrieved just after loaded to the peak stress ($\sigma_1-\sigma_3$ = 1.21 GPa). The confining pressure (σ_3) was 250 MPa and temperature was 150°C. The microcline grain has segmented into slender columns and incipient microbuckling is evident. Mineral at the top is plagioclase (pg). Maximum compression (σ_1) was vertical.

Figure 3. Kinking in a biotite grain located right next to the shear band in a post-failure sample deformed at 250 MPa and 150°. Note the cracks along the easy slip planes. Maximum compression was vertical.

Figure 4. Pore emanated cracks in a plagioclase grain in a post-failure sample. The spacing of the pores seems to dictate the characteristic dimension of the 'block' structures which undergo rotation and crushing to accomodate strain localization. Maximum compression was vertical.

Figure 5. Coalescence of a crack array in quartz (qtz) and a crack network in plagioclase (pg) with a grain boundary (g) to form a throughgoing fault. The long axial cracks in quartz outline slender columns that were continuous and have buckled during the instability process, wehreas not many well-defined elongated columns can be traced in the plagioclase grain. At high magnification, the longer cracks in the latter can be seen to be joining up with pores. Shear slip along the grain boundary is evident. Maximum compression was vertical.

Figure 6. Aeiral photograph of the Nordre Stromfjord shear zone in Greenland. The rocks above the fjord are largely undeformed while those below the fjord have suffered strains about 6.0. The total offset along the 120 km long feature is about 15 km. The width of the fjord in the photograph is about 3 km.

Figure 7. Transmitted light photomicrographs of the development of microstructure in a quartzite from the Idaho Springs-Ralston shear zone showing progressively larger amounts of dynamic recrystallization towards the center of the shear zone. The similarity of these textures to dynamically recrystallized metals is striking. (From Kohlstedt and Weathers, 1980, permission of American Geophysical Union).

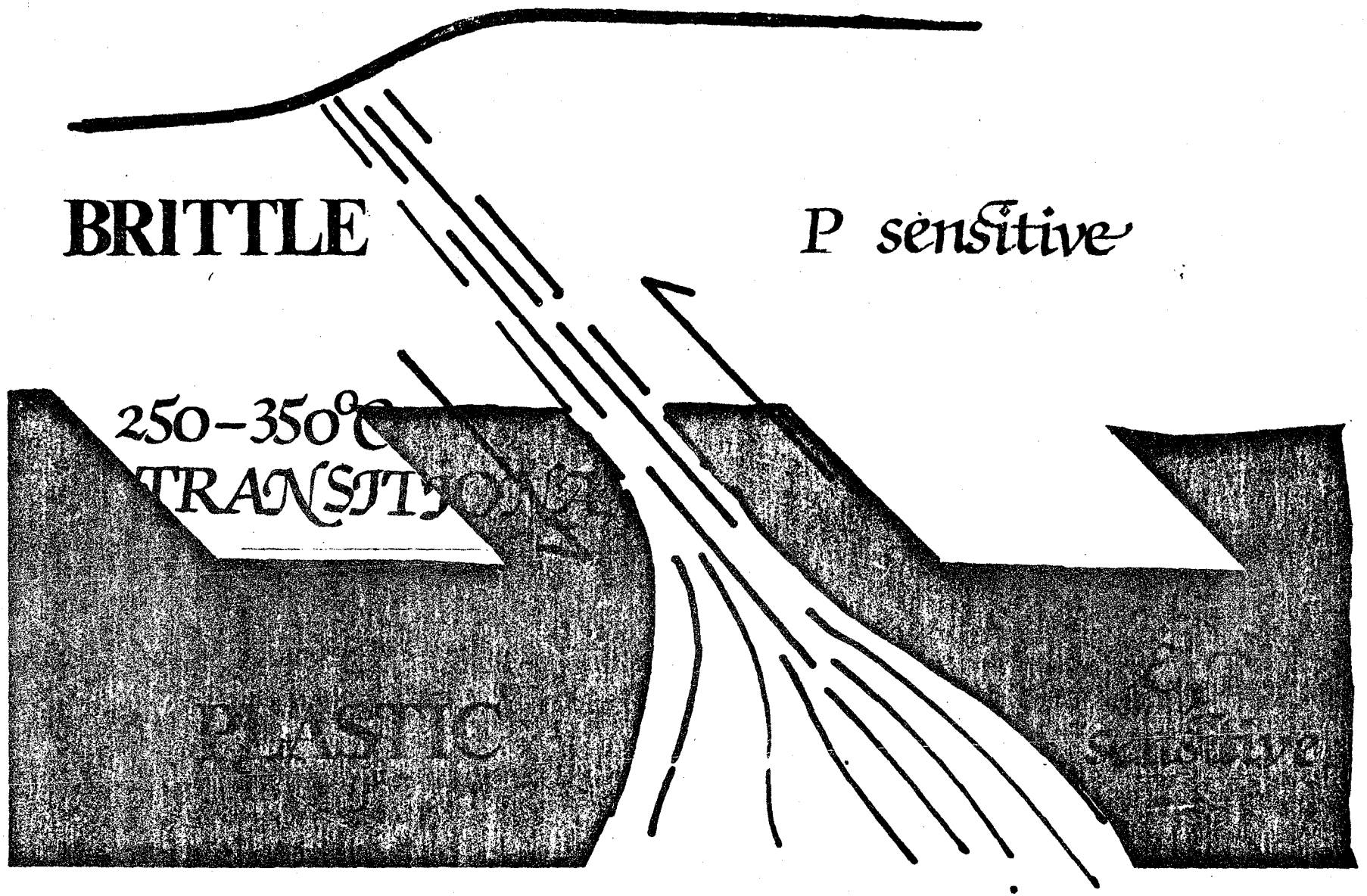
BRITTLE
P sensitive
250-350°C
TRANSITIONAL

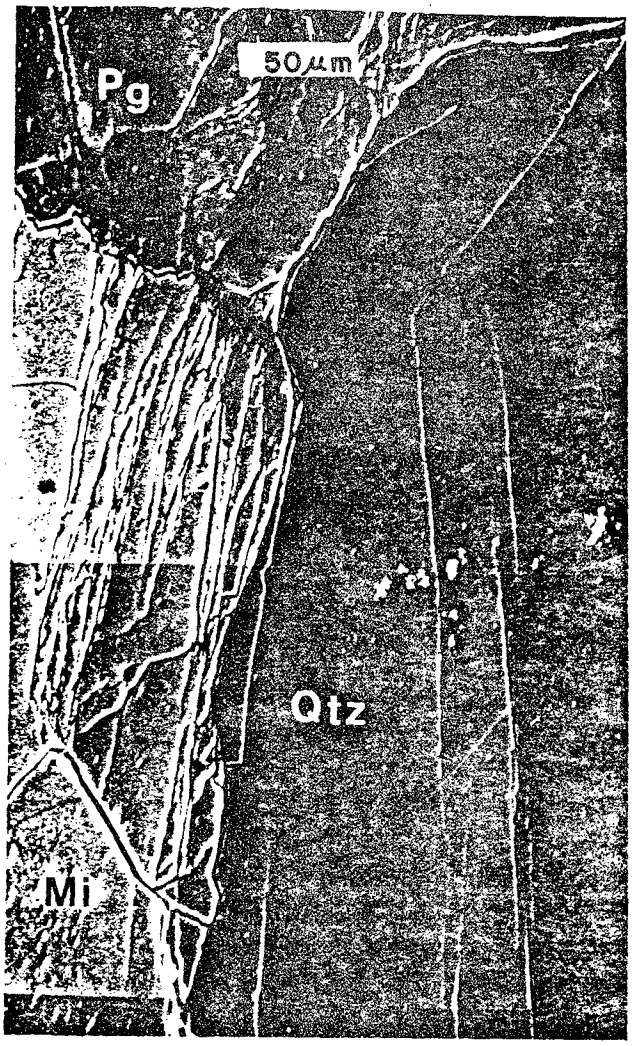

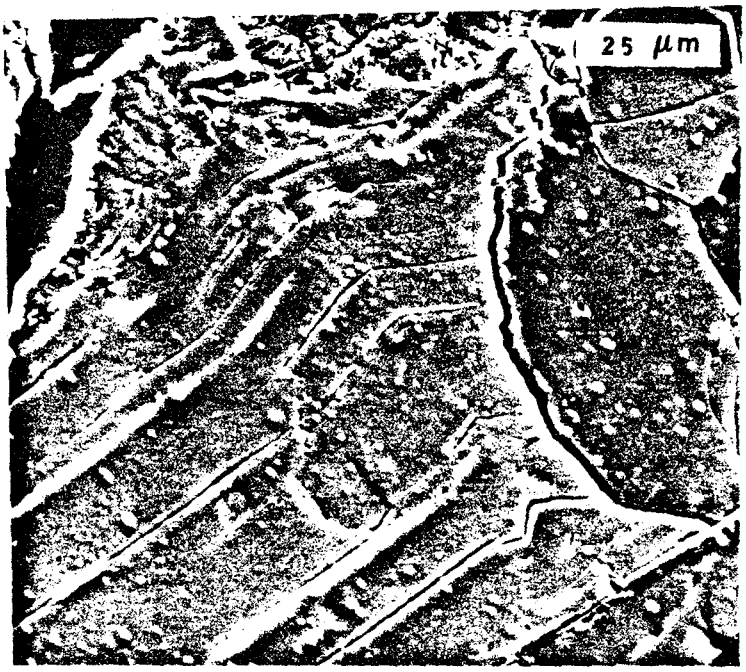
25 μm

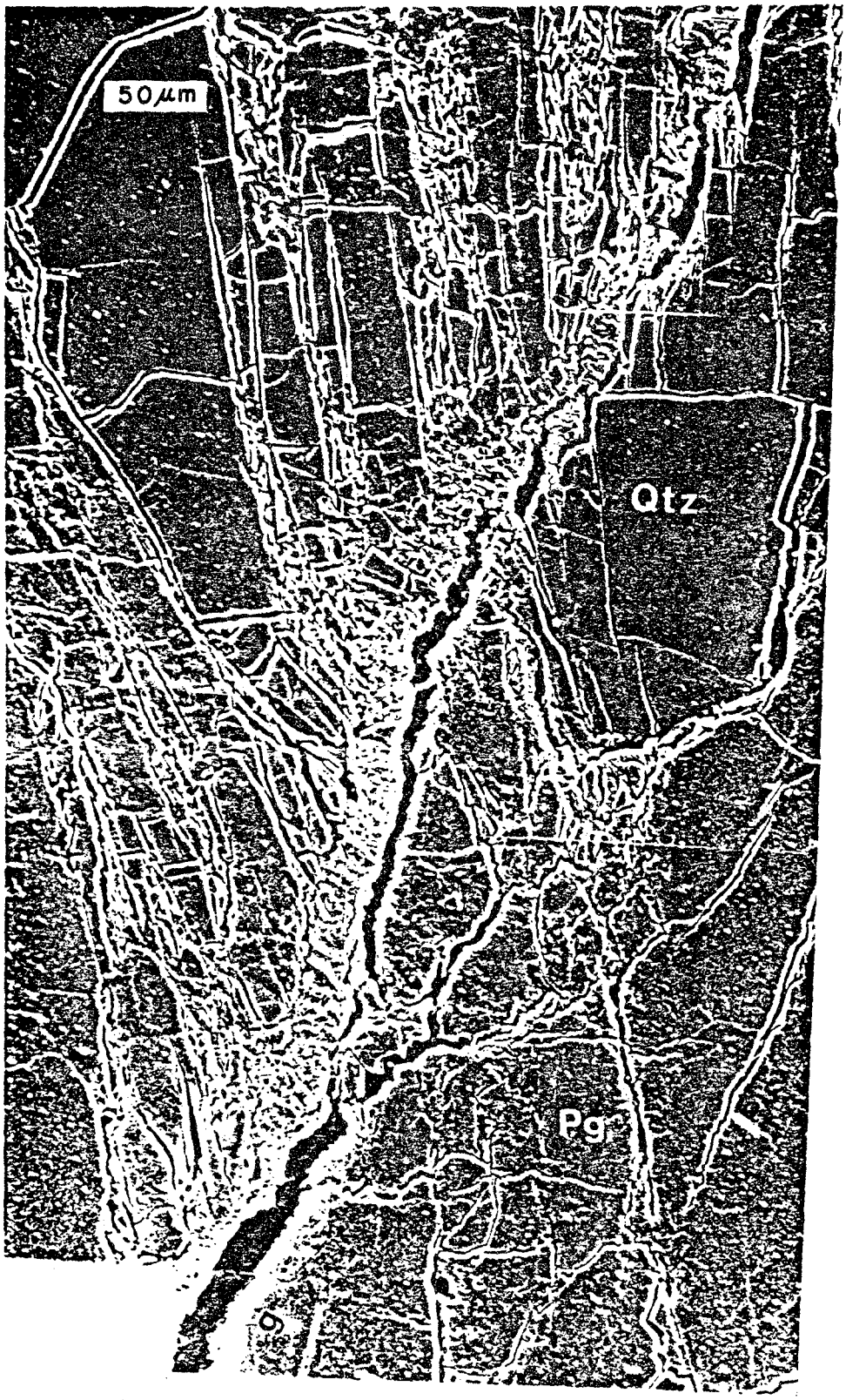
50μm
Qtz
Pg

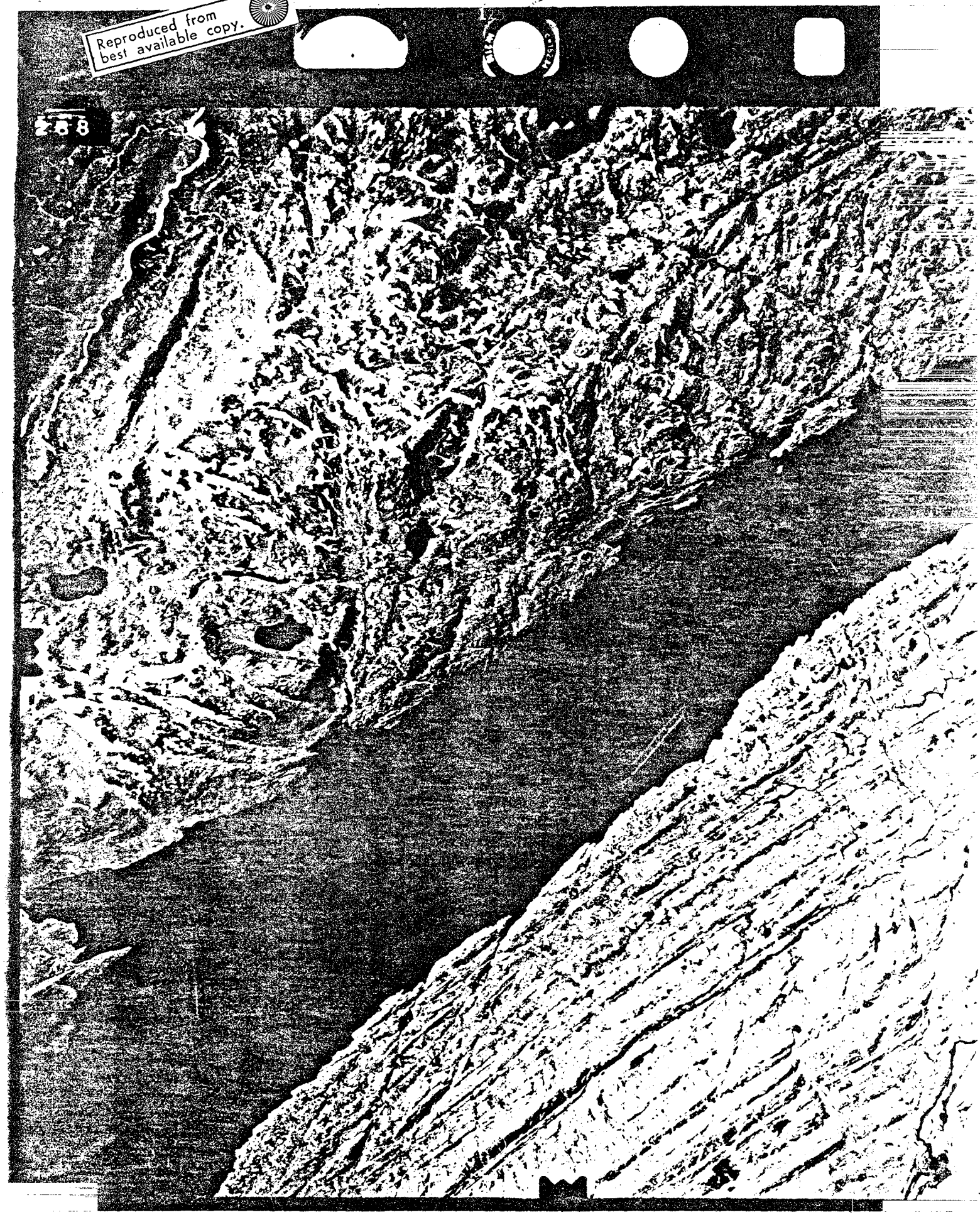

A 0.1 mm

B 0.1 mm

C 0.1 mm

FRACTURE PROPAGATION IN ROCK

A. R. Ingraffea
Associate Professor of Structural Engineering
Cornell University
Ithaca, New York 14853, U.S.A.

1. INTRODUCTION

Suppose one wants to predict numerically the stability and trajectory of a set of discrete cracks in rock or a rock mass. Further, suppose one wants to apply a rigorous, fracture-mechanics-based approach to this situation. Two problems immediately present themselves. First, how does one measure, accurately and inexpensively, the fracture toughness of the rock? Second, how does one formulate a numerical model which captures all the physics required by fracture mechanics as applied to rock?

The intent of this paper is to answer both of these questions. A survey of actual and potential applications of fracture mechanics principles to the problem of crack propagation in rock is unnecessary. One has only to scan the Proceedings of the United States National Symposia on Rock Mechanics over the past decade to understand that such applications range over virtually all time and distance scales of interest to geotechnical, structural, and materials engineers. An excellent starting point for such a perusal is the excellent keynote paper by Fairhurst and Cornet [1].

Again, rather than summarizing all developments in fracture toughness testing of rock, this paper will detail a single method which is likely to become a practical standard. The reader is referred to excellent summaries by Barton [2] and Ouchterlony [3] for range and background on this topic.

While other, more exotic numerical methods are being brought to bear on the modelling problem, approaches based on standard finite and boundary

element formulations are detailed here. The reader will surely find counter-point to these methods in the accompanying Discussion to this paper.

Finally, what of the synergism between computer and numerical method in the area of rock fracture modelling? State-of-the-art interactive graphic techniques can, as will also be shown here, greatly facilitate the solution to this difficult class of problem.

2. FRACTURE TOUGHNESS TESTING

As part of his activity with the ASTM Subcommittee E24.07 on Fracture of Brittle Non-Metallic Materials, the proposer conducted an international survey of fracture toughness testing techniques for rock. Results of that survey, conducted in 1979, indicated that no fewer than ten different specimen geometries had been employed for this purpose. Since then, interest has continued to grow rapidly as evidenced by the recent compilations by Ouchterlony and Barton mentioned above. Together, these summaries of test results indicate that at least 70 rock types have been tested using no fewer than two dozen different geometries.

Evolution of Practical Fracture Toughness Testing Specimens

Selection of the most appropriate geometry for practical application, as opposed to basic research, testing can be approached by applying the following constraints. The specimen must:

1. Be easily and inexpensively prepared from core with minimal wastage. It is anticipated that a large number of tests would be required to accommodate in a statistically meaningful way variation in test parameters and lithologies. This constraint in itself effectively eliminates from consideration geometries requiring many and accurate machining operations. In the writer's best judgment, the only candidate geometries remaining after application of this constraint

are core-based; these are the hollow pressurized cylinder (PC) [4], the short-rod (SR) [5], the single-edge-cracked (or chevron-edge-notched) round-bar-in-bending (SECRBB, CENRBB) [6], and the disc-shaped compact specimen (DC(T)) [7]. Figure 1 shows how it would be possible, using the last three geometries, to use a single length of core to measure toughness in three mutually perpendicular directions [8]. It is apparent that if there is not a large anisotropy in toughness, the more-difficult-to-test DC(T) specimen would be superfluous.

2. Be able to produce valid fracture toughnesses with one dimension as small as two inches. Since only preliminary testing can indicate minimum dimension requirements for valid results, it is difficult to say whether this constraint would, a priori, eliminate any of the candidates listed above with the common NX core size. It should be noted, however, that only one of those geometries, the short-rod, offers the possibility of testing cracks longer than the core diameter.
3. Be easily instrumented and loaded, even at high temperatures. This constraint effectively eliminates the HPC from consideration because of the effect of high temperature on the pressurizing fluid and pressure seals. Monitoring crack length in the CCD would also present a problem. Loading and instrumentation on the SECRBB/CENRBB and SR are straightforward at room temperature, but require some modification for high temperature testing.
4. Possess a firm analytical basis in the form of compliance and stress intensity factor calibration. The SR [9,10,11], the SECRBB/CENRBB [6,12], and the DC(T) [7] meet this constraint.

5. Have a proven track record of use on rock. The writer [13,14], Barker [5], and Atkinson [15] have together tested at least 30 different rock types using the SR. The SECRBB/CENRBB has also seen extensive use on rock [6,16].

Other constraints may well arise. For example, if available core is subject to discing, the SECRBB/CENRBB may not be suitable in that, with its crack propagating in the direction of the discing planes, it might produce biased toughness measurements.

Application of these constraints and observations indicates that only two candidate specimens currently exist, the SECRBB/CENRBB and the SR. Actually, of the two RBB specimens, only the CENRBB should receive further consideration since, like the SR, it has the distinct advantages of a chevron notch design. These considerable advantages are:

1. No fatigue precracking is required since a natural crack is produced during the stable growth phase of loading.
2. Neither crack length nor displacement measurements are required if the specimen conforms to LEFM size restrictions. Even if small-scale inelasticity is permitted, that is, the specimen is used for J_{Ic} or K^{p}_{Ic} (defined below) measurement, crack length is still not required.
3. To evaluate K_{Ic} on specimens meeting size restrictions, only the maximum load applied by a soft testing machine is required.

In a comparison between the SR and CENRBB specimens, the CENRBB is easier to prepare, while for the SR substantially less core length is required, load-line-displacement is easier to measure and, as noted above, much longer natural crack lengths are available.

The author has used the SR extensively in fracture toughness testing of a wide variety of rocks at Cornell University [13,14]. In the next section experience with the SR is detailed with descriptions of specimen calibration, testing technique, and result interpretation is presented.

The Short-Rod Testing System

Considerable effort has been expended in establishing complete testing systems built around the short-rod [17,14]. The starting point for such a system is accurate compliance and stress-intensity factor calibration of the specimen. An entire symposium [14,18] was recently held on this topic. A proposed standard short-rod geometry, Figure 2, very similar to that used in all testing at Cornell, was analyzed by a number of workers using both finite and boundary element techniques. The results of these analyses can be expressed as follows. For critical stress-intensity factor,

$$K_{Ic} = \frac{P_{max}\ \overline{Y}_{min}}{B\ \sqrt{W}} \tag{1}$$

where,

P_{max} = maximum applied load

B = specimen diameter

W = specimen length

and $\overline{Y}_{min}$ is the minimum value of the average, normalized stress intensity factor given by,

$$\overline{Y} = \frac{K_I\ B\ \sqrt{W}}{p} = \sqrt{W}\ \left[\frac{1}{2b}\ \frac{d(CEB)}{d(a/B)}\right]^{1/2} \tag{2}$$

here,

b = length of the crack front

a = crack length

C = compliance at point 1 in Figure 2

The $\overline{Y}_{min}$ value found in the author's analyses is 28.3 and occurs at a critical crack length, a_c, of 0.83B. This value is in excellent agreement with those obtained analytically and experimentally by other workers [10,18].

A least-squares fit to computed compliances produced the following expression,

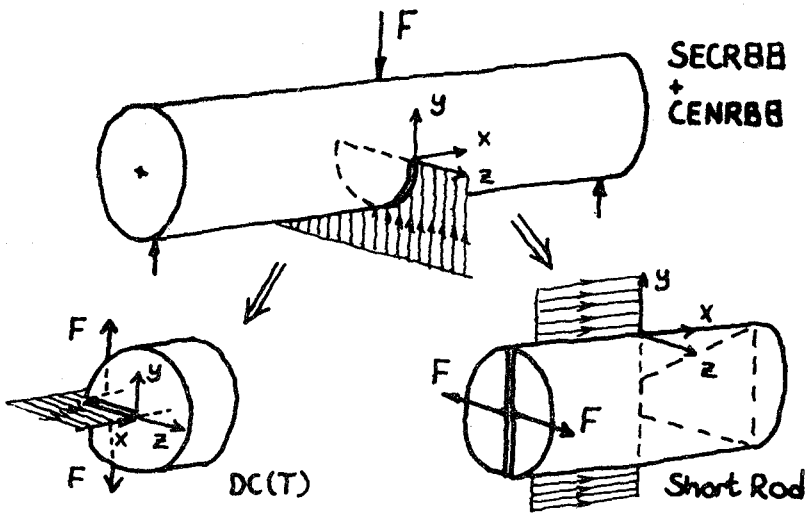

Fig. 1 Three core-based test specimens from one piece of core. From Ref. 8.

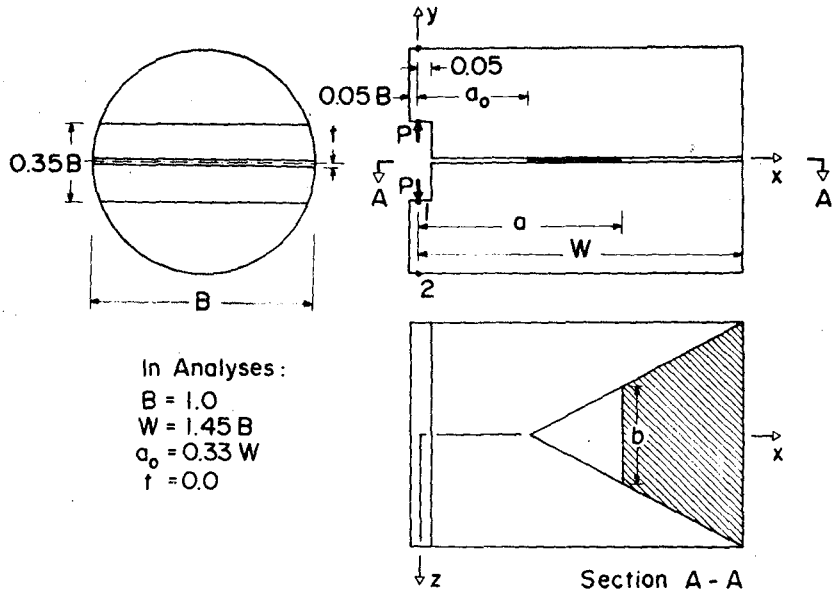

Fig. 2 Preferred short-rod specimen geometry and nomenclature. From Ref. 11.

$$CEB = -3049 + 20124.7(a/B) - 52052.3(a/B)^2 + 67368.7(a/B)^3 - 43334.7(a/B)^4 + 11192.9(a/B)^5 \quad (3)$$

which is valid for $0.65 < a/B < 1.1$. Equations 1 through 3 are valid if LEFM restrictions are met by the specimen size in use. The short-rod can also be used, however, to produce J_{Ic} or J_{Ic}-like measures of toughness through simple calculations described later.

A practical testing system should not involve time consuming, expensive specimen preparation procedures. Three simple operations are used to prepare a short-rod specimen directly from rock cores. First, the specimen is cut to a nominal length of 1.45B using a standard, water-cooled, rock cut-off saw. The ends are made parallel by proper adjustment of the core guide prior to cutting. Second, the diametral cuts are made. The specimen is held at the proper angle for each of two cuts necessary to produce the chevron notch by a simple fixture which prohibits core rotation about its axis between cuts. Lastly, metal end plates are epoxied to the top surfaces to act as loading lines for the splitting force. The use of plates as opposed to the groove shown in Figure 2 was chosen for load transfer because the latter method would require a grinding operation. Preparation time is such that a technician with minimal training can prepare 20-30 specimens a day from rock cores. A prepared specimen is shown in Figure 3.

The method of testing of a short-rod is also straightforward and involves application of an opening load to the mouth of the specimen. As the load is increased, a crack initiates at the point of the chevron slot and advances longitudinally in a stable manner, tending to split the specimen in half, Figure 3, right. If microcracking and plasticity effects are negligible, the opening load reaches a maximum when the crack reaches a critical location; thereafter, the crack-advancing load decreases with further crack growth.

The maximum load is linearly related to the fracture toughness, K_{Ic}, from fundamental principles of linear elastic fracture mechanics by way of Equation 1.

In tests at Cornell the splitting force is applied with a simple mechanical testing apparatus. The loading device is hand held and operated and is shown in Figure 3. Turning the actuating knob creates the splitting force which is read directly on an integral force gage. General test procedure consists of inserting the jaws of the loading device between the end plates, turning the knob, and recording the failure load which is given by a following needle on the gage.

Testing of a range of rock types showed that application of the splitting force sometimes caused horizontal shearing failure in specimens with weak bedding planes when these planes were close to perpendicular to the expected fracture plane, Figure 4, lower right. The method used to eliminate this phenomenon was an application of an axial pressure prior to testing. This pressure serves to give the bedding planes greater shearing resistance. The clamps used to apply the pressure were calibrated. Accordingly, a known torque on the clamps produced a known pressure. The modification to the general testing procedure for axial loading involved applying and tightening the clamps to give the desired axial pressure prior to insertion of the jaws of the loading device. As before, the failure load is recorded and is substituted into a relationship like Equation 1 which has been corrected for axial pressure [14]. Figure 4 shows the clamps attached to a specimen ready for testing.

If the crack tip process zone, which might be experiencing microcracking and/or plasticity, is too large relative to the crack length to be negligible, but still sufficiently small compared to other specimen dimensions, the measured critical stress intensity assumes the role of K_Q. An inelasticity

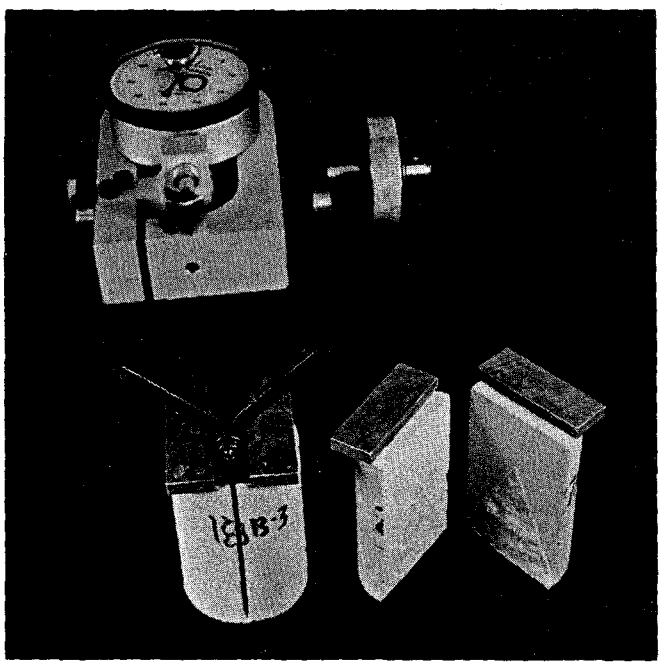

Fig. 3 NX size short-rod specimens of Indiana limestone. Prepared for test, left. After test, right.

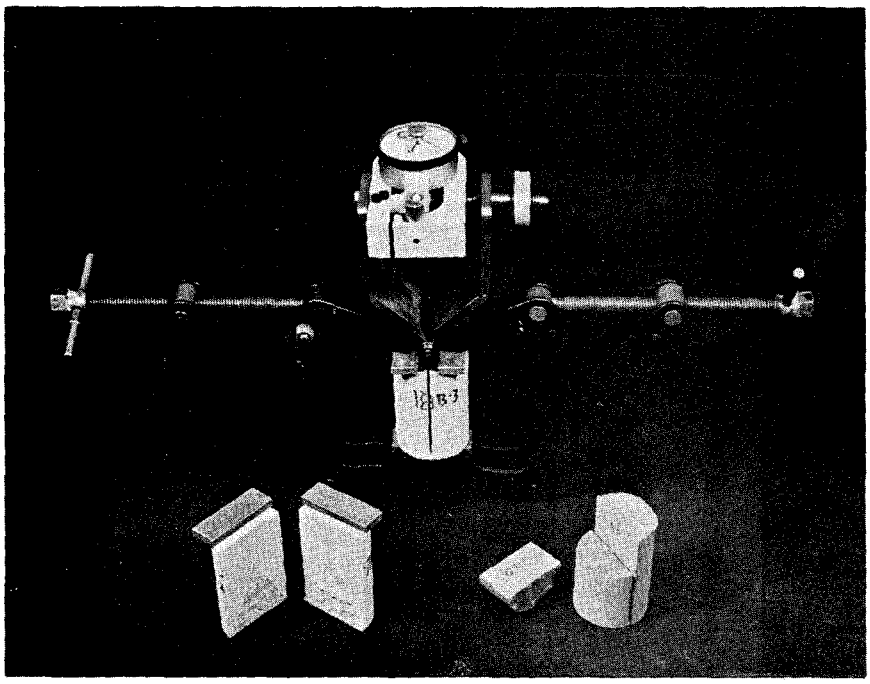

Fig. 4 Premature failure of specimen, lower right. Calibrated clamps on specimen, rear.

correction factor can then be applied to K_Q to produce a K_{Ic}^P value. Hereafter K_{Ic}^P is used to denote the "elasto-plastic K_{Ic}" whose meaning and measurement were first described by Barker [19]. K_{Ic}^P is similar to J_{Ic} in that it is a value of toughness which would be equal to a K_{Ic} obtained from a specimen large enough to meet LEFM restrictions. There are substantial differences between the two and also certain advantages in using the K_{Ic}^P approach. These are discussed by Barker [19] who used a K_{Ic}^P approach to obtain valid K_{Ic} values for Indiana limestone from specimens which were too small to produce K_{Ic} from LEFM calculations [20].

If the specimen is sub-size, a record of load versus any displacement proportional to the load-line displacement is required to measure K_{Ic}^P. The equation proposed by Barker [19] for computing K_{Ic}^P is,

$$K_{Ic}^P = \left(\frac{1 + p}{1 - p}\right)^{1/2} K_Q \tag{4}$$

where

K_Q = critical stress intensity as computed from Equation 1, where, for this case, P_{max} is replaced by the load corresponding to the critical crack length, $a_c = 0.83B$.

p = inelasticity correction index

The correction index is computed from a load-displacement plot, such as the hypothetical example shown in Figure 5, by way of,

$$p \equiv \frac{\Delta x_o}{\Delta x} \tag{5}$$

The reader should study Reference 19, and for justification of Equations 4 and 5.

Figure 6 is a plot of apparent toughness, K_Q, versus crack length for over 100 tests on Indiana limestone. Four investigators and five specimen geometries were used over a period of ten years to generate these results.

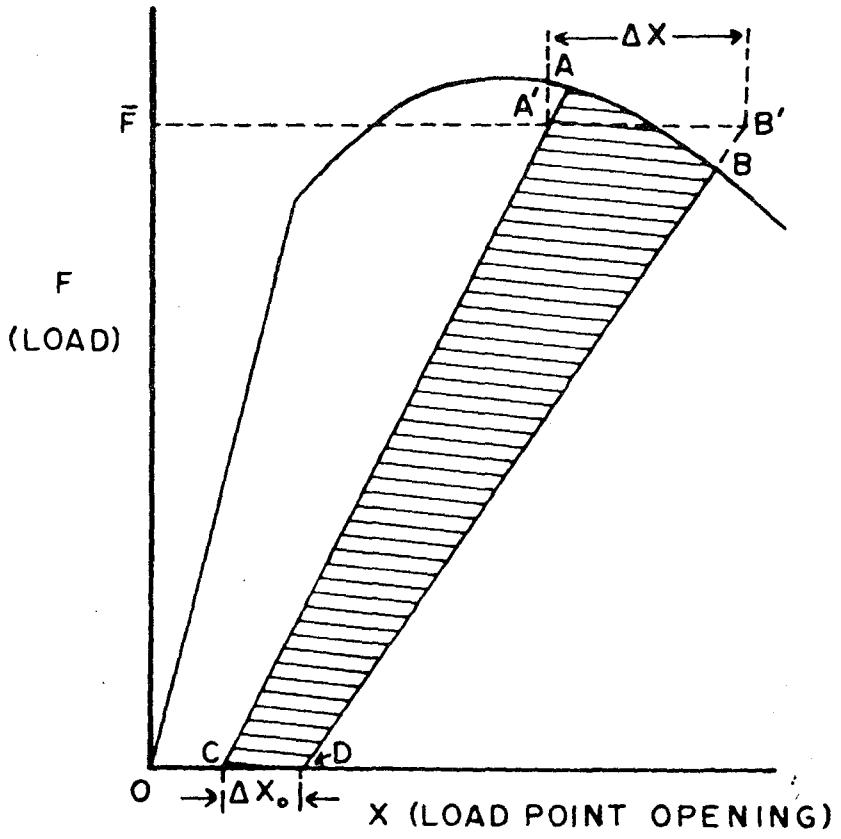

Fig. 5 Idealized load versus load point opening loading cycle for short-rod specimen with small scale inelasticity. From Ref. 19.

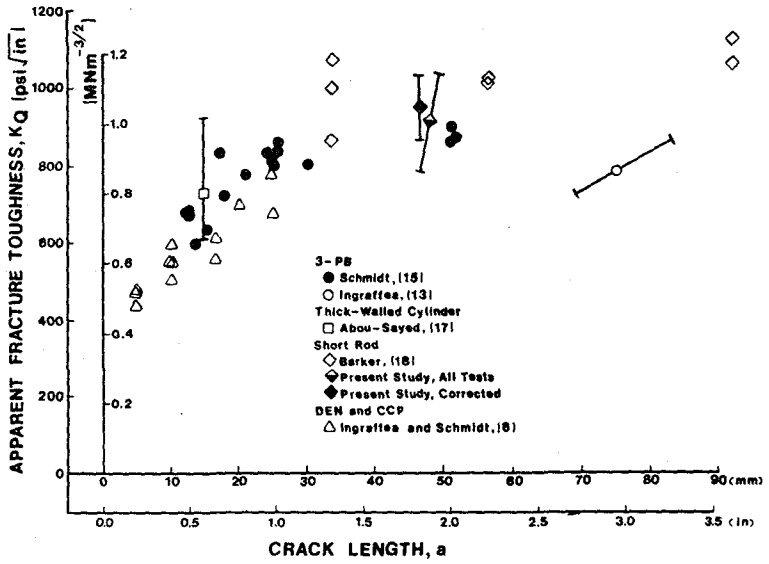

Fig. 6 Summary of K_Q versus crack length test results for Indiana limestone. References cited and figure itself are in Ref. 14.

Of special interest here are the short-rod results from Cornell, labeled as present study, and by Barker. Results from 34 tests at Cornell (slightly corrected for deviation from nominal dimensions) plot well within the K_Q vs a trend established by other geometries. Barker's results are actually values of K_{Ic}^P and indicate that, for Indiana limestone, the NX core size used for the Cornell tests is not quite large enough for LEFM use.

It is certainly safe to say that, with the introduction of the short-rod testing system, toughness measurements, even when limited by available core size, are now practical. With information controlling the behavior of a discrete crack available from testing, it follows that techniques for emloying such information in an analytical model should be addressed.

3. NUMERICAL MODELLING OF DISCRETE CRACK PROPAGATION

Why should one study fracture propagation? Is not prediction of fracture initiation the object of fracture mechanics? In his papers on rupture under tensile and compressive loading, Griffith [21,22] proposed conditions for fracture initiation which he presumed to be coincident with structural instability. The vast majority of the fracture mechanics research since Griffith has addressed the problem of predicting structural failure as the immediate consequence of fracture initiation. Yes, considerable attention has been focused on sub-critical crack growth as in fatigue and ductile fracture. However, the amount of propagation before fracture initiation in these cases is typically small compared to that which potentially occurs after. Why, then, should one be interested in modelling propagation: where a crack goes, what it does along the way, and how much energy it takes to get there?

There is nothing in the rules of rock mechanics (or fracture mechanics, either) which says that a fracture, once initiated, is always unstable. It may stop. Where? Why? What was its trajectory? What must be done to get it going again? Moreover, these questions must be addressed for each crack since

in rock mechanics study of the propagation of a single crack is not often the case. So, already one has:

Observation #1: Fracture propagation can be stable in the load control sense. Assuming linear elastic fracture mechanics (LEFM) conditions (unless otherwise noted), this implies that stress-intensity is decreasing with increasing crack length. As shall be seen, this situation is generally due to the preponderance of compressive in situ stresses and loadings in geotechnical engineering. Obviously, it will not be sufficient just to compute stress-intensity factors for an initial crack configuration. A good numerical model should be able to update stress-intensity factors as crack length changes.

Observation #2: Propagation of multiple cracks is common in realistic problems of rock mechanics. A numerical model should be versatile enough to accommodate propagation of many cracks.

This latter observation leads to another difficulty in modelling of fracture propagation. With each growth increment of a given crack, a new boundary value problem is generated. Displacement and traction boundary conditions may change, stress trajectories are altered, even loading may change in direction and intensity. As a consequence, propagation of one crack may cause initiation of another, and cracks may influence each other's stability and trajectory. This is clearly the case in dynamic fracture because of stress wave reflections. But without a periodic "look" at the full stress field during quasi-static propagation, one might overlook:

Observation #3: Each increment of fracture changes the structure. One should be able to predict the effects of this change on the stress field and on other cracks.

With the possibility of multiple cracks propagating quasi-statically one

must dispense with another simplification often applied in fracture mechanics, that of self-similar propagation. Curvilinear (mixed-mode, to some people) crack propagation is common in rock mechanics. Therefore, one must have:

Observation #4: Cracks curve during propagation in response to a change the stress field. A numerical model should be able to predict a changing crack trajectory.

Moreover, if one accepts that mixed-mode stress intensity factors, for example K_I and K_{II}, can be present along a crack front, then there follows:

Observation #5: Theoretically, mixed-mode fracture initiation can occur when $K_I \leq K_{Ic}$. Consequently, a numerical model must incorporate an interaction theory which accurately predicts the critical mixture of stress intensity factors which will cause the next increment of propagation.

Of course, fracture can be foe as well as friend to the geotechnical engineer. Mine, tunnel, dam abutment, and rock foundation instability problems are often the result of unpredicted fracture propagation. A numerical model which can predict the likelihood of a roof fall or rock burst, and can suggest a method of fracture stabilization or an alternate form of energy release can be an invaluable design tool.

Clearly, the problems of crack propagation modelling, even with the simplifying assumptions of LEFM, are manifold. The problem begins with fracture initiation, so one has to go a bit further than simple stress-intensity factor solutions. This is the purpose of the present section. Within the context of modern techniques of stress analysis, the finite and boundary element methods (FEM and BEM), the following topics are addressed:

1. A method for efficient, accurate calculation of stress intensity factors for substitution into,

2. Mixed-mode fracture initiation theories for critical mixture and angle change predictions.
3. Methods for crack increment length prediction for a given load change, or, conversely, the prediction of the load required to drive a crack a given distance.
4. Algorithms for incorporating the above into efficient computer programs.
5. Techniques for efficient remeshing to accommodate discrete crack growth.
6. The use of interactive computer graphics in the highly adaptive, nonlinear field of fracture propagation modelling.

This will be accompanied with example problems whenever possible. The first of these will be presented in the next section to provide a physical basis for the observations particular to rock fracture just presented.

The Nature of Fracture Propagation in Rock

The following example problem will serve a number of purposes. It will lend physical insight into characteristics particular to fracture propagation in rock. It will clarify some misconceptions and their implications regarding the theoretical fracture resistance of rock structures. Finally, it will serve as a basis for development and comparison on the techniques required for modelling fracture propagation.

Example 1: Observations on Fracture Propagation Under Compression

The problem is shown in Figure 7 and is recognized to be that addressed by Griffith in his second paper [22]. Rock plates like those shown in Figure 7 were tested by the author [23,24,25] with the following results:

1. As predicted by Griffith [22], first crack growth occurs from points initially under tensile stress concentration on the notch (see Figure 8). This set of two, symmetrically placed cracks was labelled primary.
2. Primary crack trajectory was curvilinear.
3. In contrast to what Griffith [22] expected, propagation of primary cracks was observed to be stable: an ever increasing load was required to increase crack length.
4. After considerable primary crack propagation, a second set of two, symmetrically placed, cracks appeared. These were labelled secondary and originated in the interior of the plate in a newly formed tensile stress zone (see Figure 9).
5. Failure of the plate, defined as a through-going rupture, was a result of unstable secondary crack propagation, Fig. 8, at a load level in the range of 3 to 5 times the primary crack initiation load.

These observations were typical for plates of Indiana limestone and St. Cloud charcoal granodiorite, with $30° \leq \beta \leq 90°$.

Observations 2 and 3 differentiate the observed fracture response of this configuration from that usually observed in tension-loaded structures. Stable primary crack propagation indicates that, within the assumption of LEFM, the associated energy release rate, G, decreases with increasing crack length for a constant load. The curvilinear nature of the primary crack path is a result of a variable, mixed-mode stress intensity being applied to the incrementally advancing crack tip.

Items 3 through 5, above, deserve special attention. The often quoted, and quite incorrect, theoretical ratio of compressive to tensile strength of rock is based on the supposition that the initiation of what are here called primary cracks is synonymous with rupture. That such is not the case has

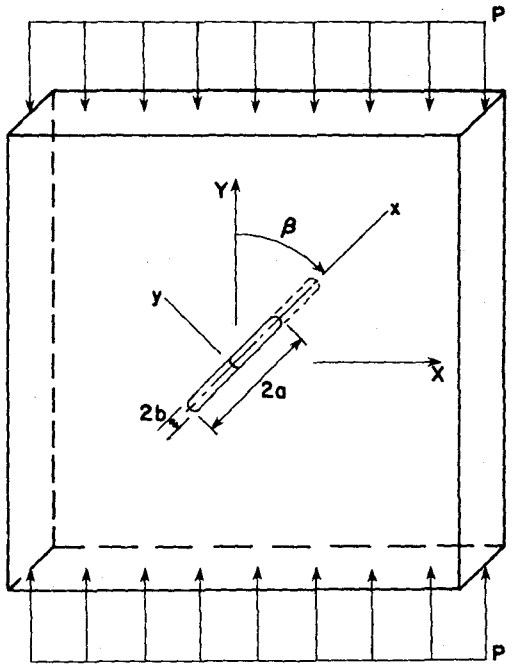

Fig. 7 Angle-notched plate loaded in uniaxial compression. From Ref. 23.

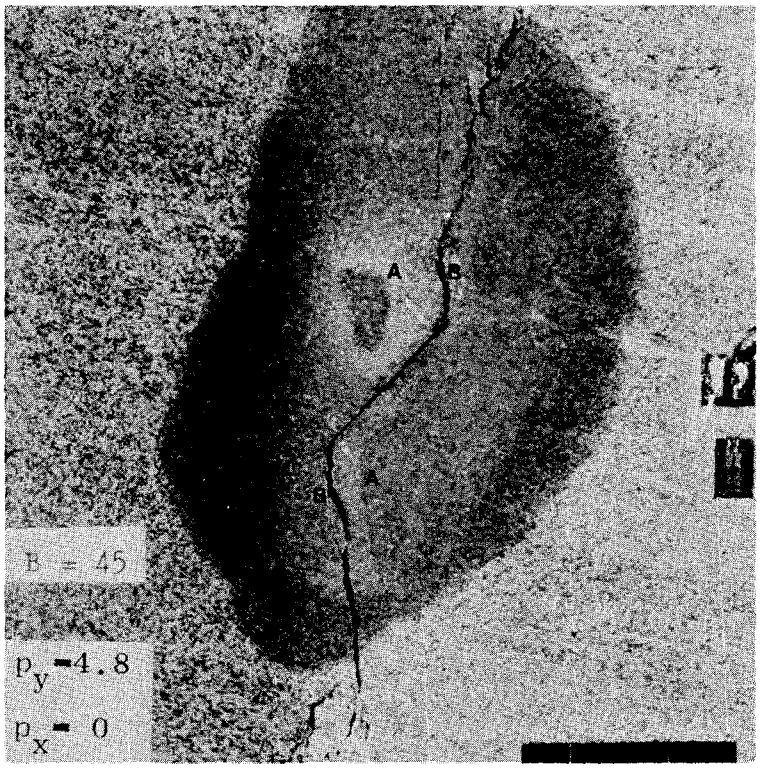

Fig. 8 Results of test on Indiana limestone plate. Primary cracks to points A. Secondary cracks nucleated near points B. From Ref. 23.

been observed by many experimentalists (e.g. 26,27,28) and digested by few of anybody else: sub-critical crack growth can occur under ideal LEFM conditions and monotonically increasing load.

Observations 4 and 5 are particular to rock. In tests on glass, polymethylmethacrilate (PMMA) and CR39 in the same configuration [26,27,28], only primary cracking was evident and rupture did not occur. This phenomenon is shown in Figure 10 which depicts the primary crack behavior of a PMMA plate loaded to near its compressive yield stress. Results 4 and 5 therefore indicate a fundamental difference in the fracture response of rock structures as compared to glass, plastic, and metals. As we shall see later, the high (though not theoretically predictable!) compressive to tensile strength ratio of rock compared to those materials leads to what the author has called the strength ratio effect [29]. This effect explains the initiation of what are called secondary cracks in the present problem, and is the proximate cause of rupture in this as well as many other problems in rock fracture. The strength-ratio effect is actually a corollary to Observation #3 mentioned earlier, but bears individual emphasis:

> Observation #6: Due to fracture propagation, new regions of tensile stress can be generated. Although the magnitude of those tensile stresses may be low compared to an applied compressive stress, the relatively low tensile strength of rock makes such regions potential sites for nucleation of additional cracks. A model for fracture propagation should be capable of predicting formation of such sites.

With these experimental observations, and with a list of requirements for modelling of fracture propagation in hand, one can begin model formulation.

Stress Intensity Factor Computation

The prediction of load level, angle change, and length corresponding to

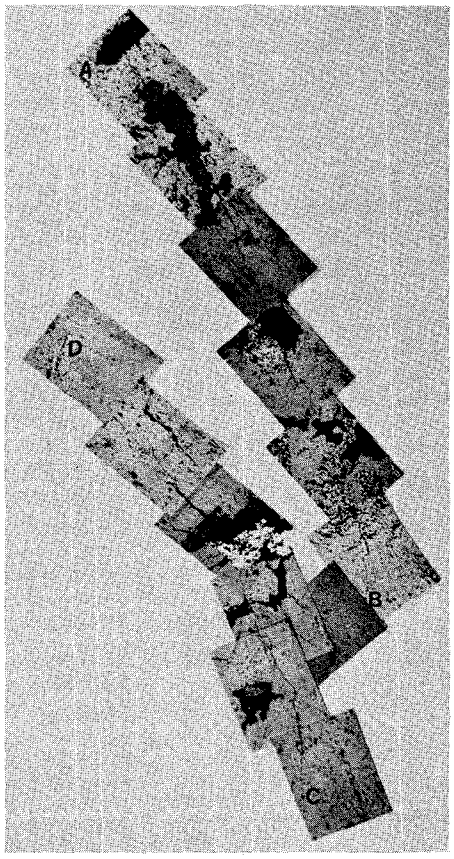

Fig. 9 Composite micrograph of granodiorite fractures. Notch tip, A; primary crack tip, B; nucleating secondary crack, C to D. From Ref. 23.

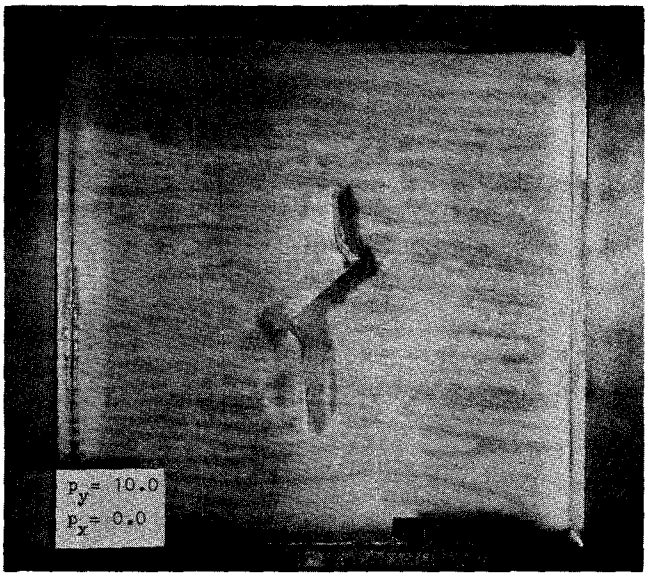

Fig. 10 Results of test on PMMA plate. Primary cracking only; no rupture occurs. From Ref. 23.

each increment of fracture propagation requires accurate computation of mixed-mode stress intensity factors. Their efficient computation is also desirable since, as noted above, many analyses may need to be performed in a single problem. Virtually all of the numerical methods applicable to elastostatics have been used for stress intensity factor computation. A particularly simple yet accurate method which does not depart from standard FEM and BEM approaches is available. This method is described in detail elsewhere [30,31,32]; however it will be briefly summarized here.

Consider the typical crack-tip region shown in Figure 11. Assume that the region has been discretized with standard, isoparametric, linear-strain triangles and that two of these are arrayed as shown. It has been shown that these elements will reproduce the LEFM-predicted displacement and stress fields if, as shown in Figure 11, the mid-side nodes of all element sides emanating from the crack tip are moved to the quarter-point position. Shih et al [33] have further shown that the displacements computed at the labeled nodes in Figure 11 can be correlated with the theoretical displacements at their positions with the stress intensity factors as weight functions. Solving for the stress-intensity factors loads directly to,

$$K_I = \frac{\sqrt{2\pi}}{L}\frac{G}{\kappa+1}\left[4(v'_B - v'_D) + v'_E - v'_C\right]$$

$$K_{II} = \frac{\sqrt{2\pi}}{L}\frac{G}{\kappa+1}\left[4(u'_B - u'_D) + u'_E - u'_C\right] \qquad (6)$$

in which,

L = length of singularity element side along the ray,

v' = crack-opening nodal displacements,

u' = crack-sliding nodal displacements.

$\kappa = (3 - 4\nu)$ for plane strain

The primes indicate that the global-coordinate nodal displacements have been transformed to the crack-tip coordinate system defined in Figure 11. The

above procedure has been generalized to the three-dimensional case by Ingraffea and Manu [34]. This approach is also available, with only slight modification, for BEM codes which use isoparametric element formulations [35,36]. For studies on the accuracy of the method the reader should see References 30, 31, 34.

Algorithmically, the displacements and coordinates of the crack face nodes belonging to the quarter-point FEM or BEM elements need to be flagged and retrieved for each crack increment solution. These are then transferred to a simple subroutine which codes Equations 6. In a crack propagation analysis, this computation would be done for each crack tip after each load or growth increment. The computed stress intensity factors would determine the stability and angle change of each crack tip according to one of the theories outlined in the next section.

Theories of Mixed-Mode Fracture

The determination of fracture initiation from an existing flaw in combined Mode I and Mode II requires knowledge of the stress intensity factors, determined analytically and functions of geometry and load, and the appropriate fracture toughness, a material state property, determined experimentally. These parameters combine in a theoretical mixed-mode fracture initiation function analogous to a multi-axial stress state yield function of plasticity. A number of theories are available which produce such a function [37,38,39]. Only one of these theories will be briefly summarized here.

The $\sigma(\theta)_{max}$ theory was first formulated by Erdogan and Sih [37]. The parameter governing fracture initiation in their theory is the maximum circumferential tensile stress, $\sigma(\theta)_{max}$, near the crack tip.

Given a crack under mixed-mode conditions, the stress state near its tip can be expressed in polar coordinates as,

$$\sigma_r = \frac{1}{\sqrt{2\pi r}} \cos\frac{\Theta}{2}\left[K_I\left(1 + \sin^2\frac{\Theta}{2}\right) + \frac{3}{2}K_{II}\sin\Theta - 2K_{II}\tan\frac{\Theta}{2}\right] + \ldots$$

$$\sigma_\Theta = \frac{1}{\sqrt{2\pi r}} \cos\frac{\Theta}{2}\left[K_I\cos^2\frac{\Theta}{2} - \frac{3}{2}K_{II}\sin\Theta\right] + \ldots \qquad (7)$$

$$\tau_{r\Theta} = \frac{1}{\sqrt{2\pi r}} \cos\frac{\Theta}{2}\left[K_I\sin\Theta + K_{II}(3\cos\Theta - 1)\right] + \ldots$$

The $\sigma(\Theta)_{max}$ theory states that:

1. Crack extension starts at the crack tip and in a radial direction.
2. Crack extension starts in a plane normal to the direction of greatest tension, i.e., at Θ_0 such that $\tau_{r\Theta} = 0$.
3. Crack extension begins when $\sigma_{\Theta_{max}}$ reaches a critical, material constant value.

The theory is stated mathematically using Eqs. (7),

$$\sigma_\Theta\sqrt{2\pi r} = \text{constant} = \cos\frac{\Theta_0}{2}\left[K_I\cos^2\frac{\Theta_0}{2} - \frac{3}{2}K_{II}\sin\Theta_0\right] = K_{Ic} \qquad (8)$$

or

$$1 = \cos\frac{\Theta_0}{2}\left[\frac{K_I}{K_{Ic}}\cos^2\frac{\Theta_0}{2} - \frac{3}{2}\frac{K_{II}}{K_{Ic}}\sin\Theta_0\right] \qquad (9)$$

and,

$$\tau_{r\Theta} = 0 \Rightarrow \cos\frac{\Theta_0}{2}\left[K_I\sin\Theta_0 + K_{II}(3\cos\Theta_0 - 1)\right] = 0. \qquad (10)$$

Equations (9) and (10) are the parametric equations of a general fracture initiation locus in the K_I-K_{II} plane, shown in Figure 12. Also, the direction of the initial fracture increment, Θ_0, can be found from Eq. (10) which gives,

$$\Theta_0 = \pm\pi \text{ (trivial)}$$

$$K_I\sin\Theta_0 + K_{II}(3\cos\Theta_0 - 1) = 0. \qquad (11)$$

In summary, the governing equations of the $\sigma(\theta)_{max}$ theory are (9) and

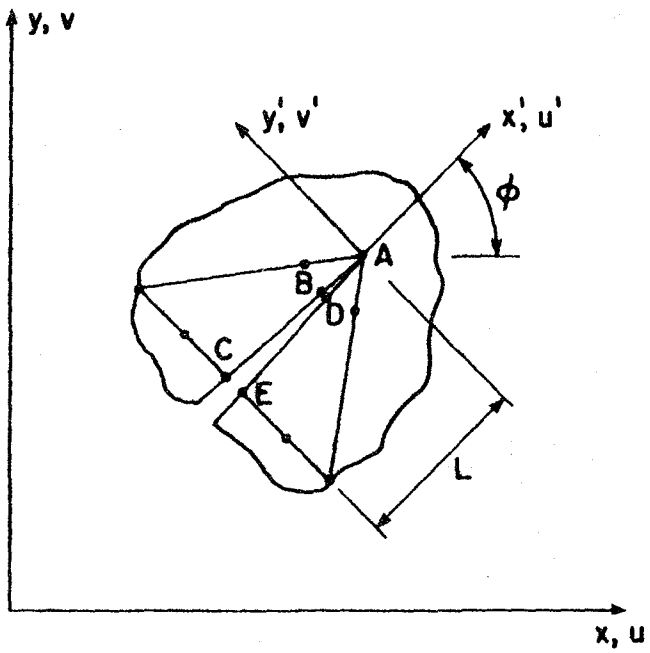

Fig. 11 Nodal lettering for stress intensity factor computation using equ. 6.

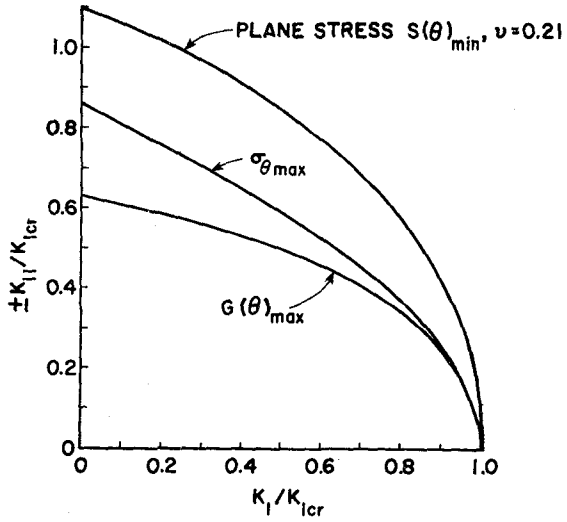

Fig. 12 Fracture initiation loci for mixed-mode theories.

(10). Algorithmically, the stress intensity factors for a given crack tip location and loading are first substituted into Eq. (10) to obtain the new angle of propagation, Θ_0. The stress intensity factors and the angle θ_0 are are then substituted into Eq. (9). If it is not satisfied, the stress intensity factor pair plots either within or outside the fracture locus shown in Figure 12. If within, then that crack cannot propagate without a sufficient increase in stress intensity factors. If outside, then the crack is unstable and can continue to propagate until it reaches a free surface or until the stress intensity factor pair returns to within the locus.

In a quasi-static fracture propagation analysis the governing equations for one of the theories would be applied at the end of each growth step or load step. Recall Observation #3: It may not be necessary to increase loads to bring the stress intensity factors of previously stable crack tip onto the fracture locus. The propagation of another crack may cause the same effect. Algorithmically, this implies that the interaction factor for each crack tip, the right-hand-side of Eq. (9), be updated in memory after each crack or load increment. As shall be seen later, depending on the mode of interaction between the program and the user, the former or the latter will use the interaction factors to decide which one or more of the crack tips should be propagated in a given fracture step.

Comparison of Mixed-Mode Fracture Theories

Figure 12 compares the interaction effects predicted by the $\sigma(\theta)_{max}$, $S(\Theta)_{min}$, and $G(\theta)_{max}$ theories. It can be seen that the $S(\theta)_{min}$ theory is the least conservative of the three shown. It also predicts that the Mode II fracture toughness of most rocks ($\nu < 0.3$) is larger than K_{Ic}, while the other theories predict a smaller value.

How does theory compare to experiment? References 23 and 40 contain much data and lengthy discussion relevant to this question, but the comparisons are

all based on materials other than rock. The author has performed wide spectrum, mixed-mode fracture initiation tests on Indiana limestone and Westerly granite [41]. The results are shown in Figure 13a and 13b for the limestone and granite, respectively. It appears, based on this somewhat limited data, that the $S(\theta)_{min}$ theory is the most accurate of the three theories used for comparison.

It should be emphasized, however, that a crack finding itself under substantial Mode II loading does not long remain in the high K_{II}/K_I domain of interaction. Such a crack quickly changes trajectory to minimize or eliminate the K_{II} component. Consequently, the life of a crack propagating quasi-statically is spent in the high K_I/K_{II} region of the interaction plane where the differences among the theories are minimal. It is the author's opinion that, except for fracture increments under high K_{II}, use of any of the refer enced theories would result in substanially the same trajectory and load history. This will be seen in example problems to follow.

Predicting Crack Increment Length

Previous sections showed how to compute stress intensities, and how to use them to predict local stability and angle change. However, Observation #1 is a reminder that to complete a fracture propagation model one must also be able to predict either, a) the length of a fracture increment for a given load change, or, b) the load change required to drive a crack a specified length. These predictions are relatively simple and straightforward.

The fundamental principle here is that a fracture, once initiated, will continue to propagate as long as there is sufficient energy or, equivalently, effective stress intensity, available. Effective stress intensity, K^*, here refers to a mixed-mode case and is the combination of Mode I, II, and III stress intensity factors required by the particular mixed-mode theory in use. The right-hand side of Equation (9) can, therefore, be viewed as normalized effective stress intensity factors.

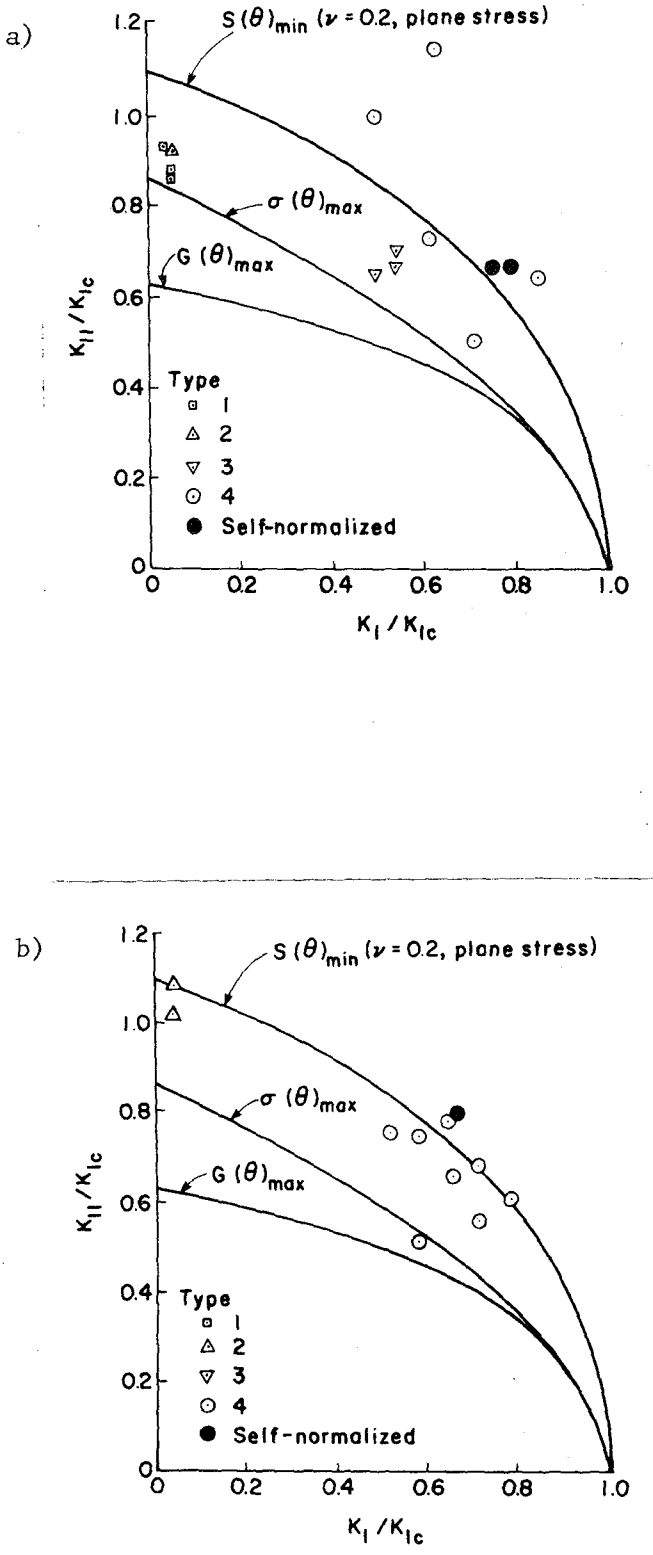

Fig. 13 Results of mixed-mode fracture initiation tests. a) Indiana limestone; b) Westerly granite. From Ref. 41.

One must consider a number of possible stability cases in creating an algorithm for predicting fracture increment length. These possibilities will be addressed through Figures 14 and 15. For simplicity, assume that LEFM applies for all crack lengths. Further assqme that one is investigating propagation along some predicted direction θ_0.

Case 1: Effective stress intensity increases monotonically with crack length, curve OA in Fig. 14. If the initial flaw size is less than a_i, no propagation occurs. For $a = a_i$, propagation can occur and it will continue at $P = P_i$; that is, a condition for local instability has been met. Of course, an algorithm could be written which would place such a scenario in displacement or crack-length control: A crack increment, Δa, could be specified and the load decrement required to just bring the crack tip to a $a_i + \Delta a$ could be computed. This situation is depicted by curve OA' in Figure 14. To compute P recall that LEFM specifies that at instability,

$$K_{Ic} = \sqrt{\alpha_i P_i} \quad a_i = \alpha_{i+1} P_{i+1} \sqrt{a_{i+1}} \tag{12}$$

where,

α = factor depending on geometry and interaction theory

Therefore,

$$P_{i+1} = \frac{\alpha_i}{\alpha_{i+1}} P_i \frac{\sqrt{a_i}}{a_{i+1}} \tag{13}$$

Equation (13) is only directly useful, however, if the α_{i+1} coefficient is known at Step i. For arbitrary problems, this is certainly not the case. An alternative is to propagate the fracture an amount Δa in the direction θ_0 and compute K^*_{i+1} at load level P_i. The new load level is then,

$$P_{i+1} = \left(\frac{K_{Ic}}{K^*_{i+1}}\right) P_i \tag{14}$$

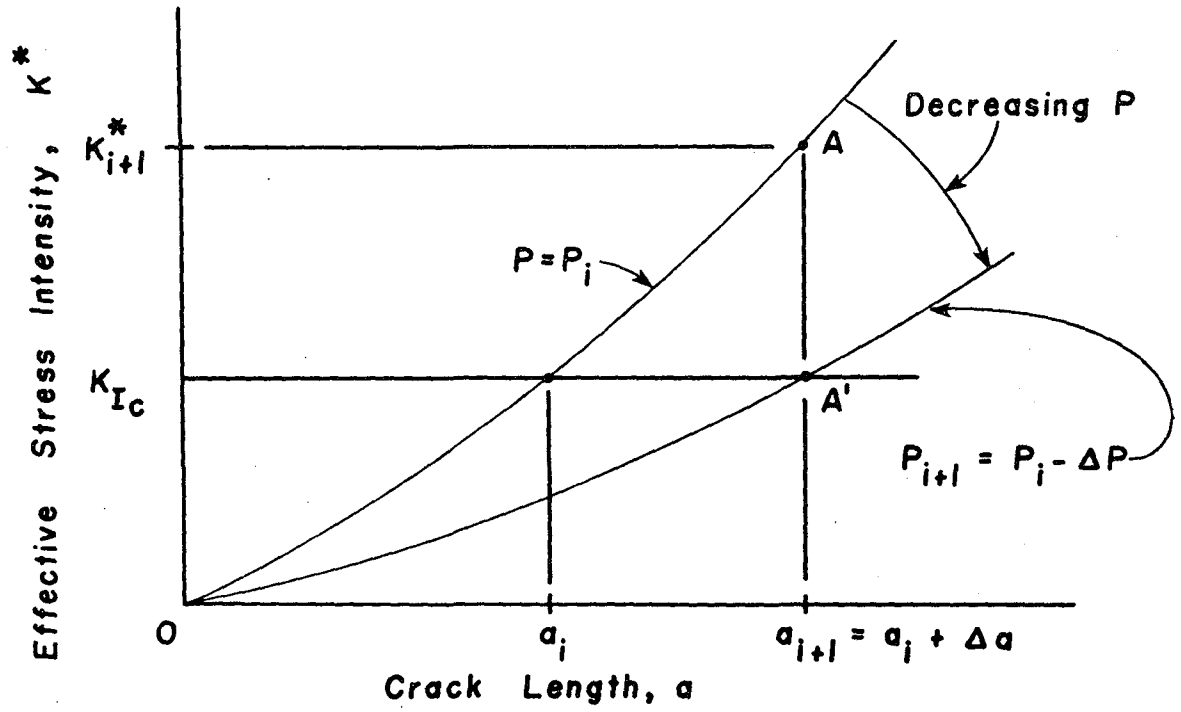

Fig. 14 Stress intensity factor variation for Case 1.

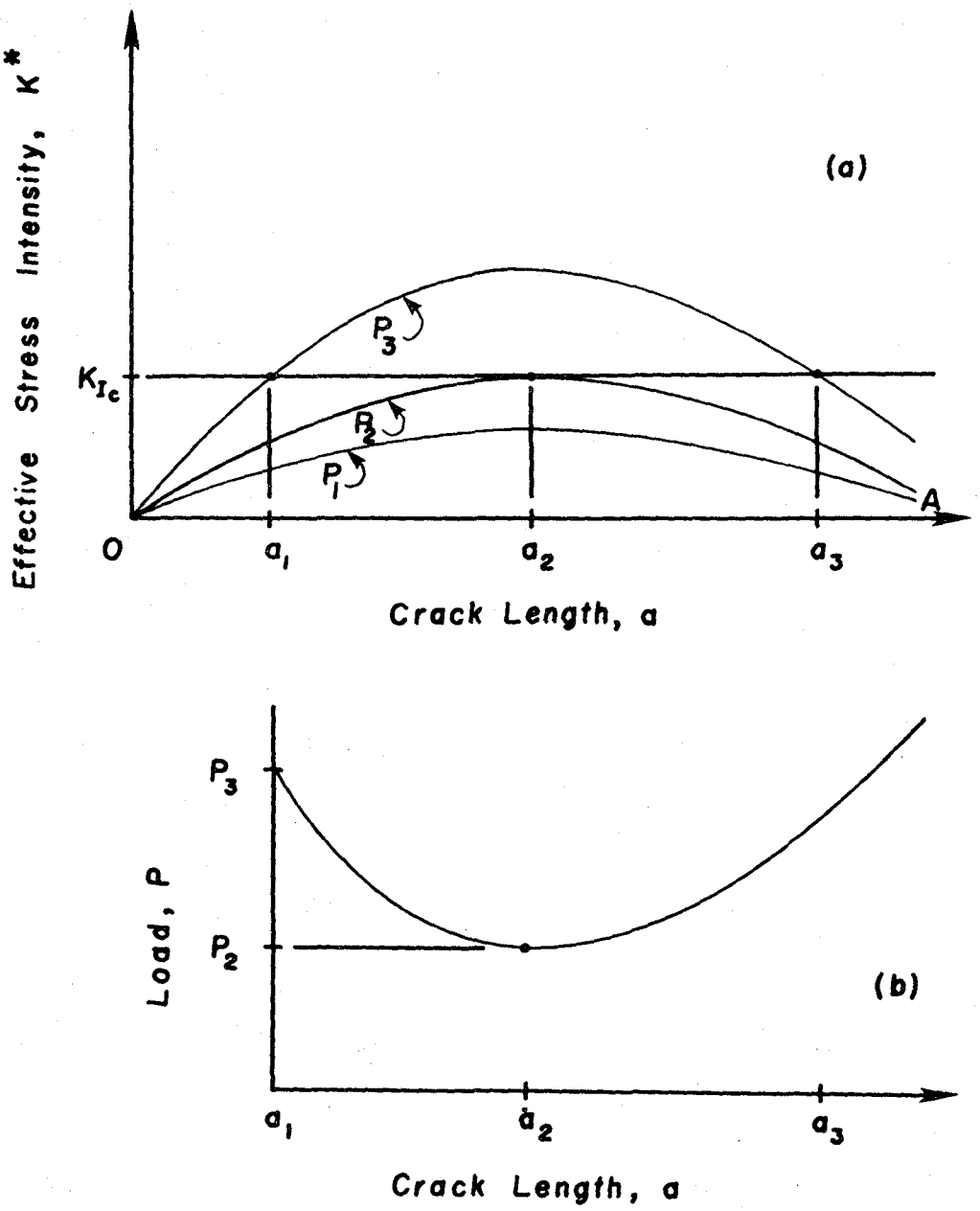

Fig. 15 Stress intensity factor variation for Case 2; b) load variation for Case 2.

as can be seen in Figure 14. Behavior described in this case is typical of many of the Mode I fracture specimens used to measure K_{Ic} of rock. It can also occur in a variety of circumstances in practical rock fracture problems.

Case 2: Effective stress intensity increases, reaches a maximum value, and then decreases with increasing crack length, curve OA in Figure 15a. For the value of K_{Ic} shown and at load level P_1, no crack propagation is possible. At load level P_2, propagation is possible only at crack length $a = a_2$, but the corresponding, theoretical fracture increment length is $\Delta a = 0$. At load level P_3, propagation can occur for a crack of length a_1, and it would be unstable in load control. Again, as in case 1, above, using a crack length or displacement control algorithm the crack of initial length a_1 could be propagated stably to length a_2 by decreasing the load incrementally from level P_3 to level P_2, as shown in Figure 15b.

For crack lengths longer than a_2, fracture propagation is stable in the load control sense. An effective stress intensity monotonically decreasing with increasing crack length implies that a monotonically increasing load is required for continued propagation. In Figure 15, it can be seen that if the load is again increased to P_3 propagation to crack length a_3 is possible.

An example of this behavior for a pure Mode I case is shown in Figure 16 which is taken from a study on fracture propagation around underground openings [29]. Cracks are induced at crown and invert of a circular opening in plate under the indicated biaxial compression. The computed K^* (here $K_I^* = K_I$) versus crack length relationship at two load levels is shown. Although it was assumed that the effective toughness, K_Q, increased with crack length, the propagation scenario is the same as described above. Propagation is unstable at first, but ceases each time the K_I and K_Q curves intersect. This type of propagation behavior is very common in rock mechanics. It occurs, for example, in hydrofracturing.

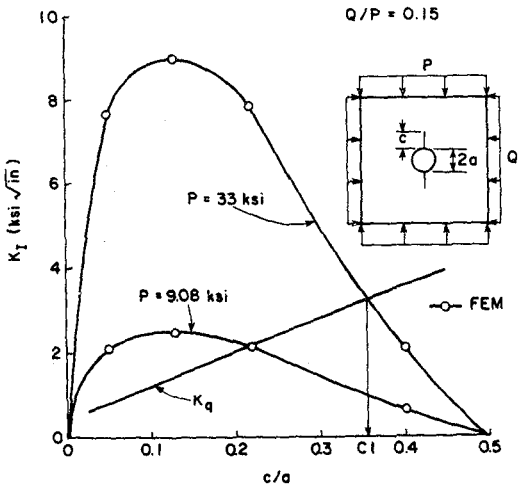

Fig. 16 Stress intensity factor variation for crack propagating from circular hole. (1 ksi = MPa, 1 ksi $\sqrt{in}$ =1.1 MPa $\sqrt{m}$) From Ref. 29.

If one is starting with crack length a_1, and load level P_3 (Figure 15), the prediction technique is the same as described under Case 1: Propagate the fracture an amount Δa in the direction θ_0 at load P_3, compute the effective stress intensity for the new crack length, and apply Equation (14).

Suppose, however, that one is at load level P_2 and crack length a_2. One can still use the same algorithm: the only difference is that the quantity in parentheses in Equation (14) will now always be less than one.

The reverse of Case 2 is also possible: Effective stress intensity can at first decrease and then begin to increase with increasing crack length. (See, for example, References 42 and 43.) This implies nothing new algorithmically, however, since the implications of this situation are handled by the techniques described in Cases 1 and 2.

A number of alternative numerical techniques for fracture increment length prediction are available [23,44,45]. Some are based on energy balance, some are more approximate than others. The simple technique described here is theoretically exact for pure Mode I, colinear propagation. Recalling Observation #4, however, we can see that any technique which employs finite, straight fracture increments will be approximate. One is updating effective stress intensity incrementally, rather than continuously. A curvilinear trajectory is being modeled piecewise by straight segments. Stress intensity factors and angle changes will be somewhat in error. The error depends on the specified length of the fracture increment.

The analogy here is with dynamic analysis where the time step controls accuracy and stability of the solution. It is the author's experience with his codes that predicted trajectories sometimes oscillate about an average path. This is a manifestation of error in K_{II} simulation which is a result of "kinking" the crack path rather than allowing it to continuously curve. Spuriously high K_{II} values are computed which, alternating in sign with each

increment, zig-zag the crack. However, it is quite possible that if too large an increment is used divergence of predicted trajectory could occur.

All the theoretical ingredients for fracture propagation modelling under mixed-mode, LEFM assumptions have now been presented. These ingredients have been combined in computer programs developed by the author and his students at Cornell University. In the next section, some general observations concerning these programs will be presented.

4. FRACTURE PROPAGATION PROGRAMS

Research and application thrusts into fracture propagation modelling at Cornell University can be divided into areas of numerical method and user-computer interface.

Numerical Methods

Incremental fracture propagation codes have been developed using both the finite and boundary element methods. As will be shown, each of these methods has characteristics which make it the appropriate choice for given structure, dimensionality of model, or interface hardware.

In general, the boundary element method as used here is suited to elastic, homogeneous structures containing few propagating cracks. The boundary element method is superior in efficiency and accuracy to the finite element method for modelling of three-dimensional crack propagation problems. Since only the boundaries of the structure, including the crack faces, need to be discretized, the data base for a boundary element method analysis is much smaller than that of a finite element method analysis. Also, since perspective views of three-dimensional meshes are not encumbered with all the interior nodes and elements of a finite element mesh, effective user-computer interface can be obtained with low-level computer graphics equipment.

A two-dimensional code, Boundary Element Fracture Analysis Program, BEFAP [44,46], is operational, and an example of its use is described later.

The three-dimensional version is under development in connection with the Cornell Program for Computer Graphics for use with high-level computer graphics hardware (see next section for description of high- and low-level computer graphics hardware).

For problems involving inhomogeneities, interfaces, or many cracks, BEFAP currently is not suitable. For problems of this type, as well as those involving material nonlinearity, the Finite Element Fracture Analysis Program, FEFAP [45,47], has been developed. Again, the two-dimensional version of FEFAP is operational, and the three-dimensional version is being implemented in a high-level interactive computer graphics environment. Examples of problems solved using FEFAP will also be presented later.

User-Computer Interface

Three levels of user-computer interfacing are available for operation the BEFAP/FEFAP group:

1. Interactive Without Graphics: the standard keyboard entry of data, editing of files, and spooling of output to a printer.
2. Low-Level Interactive Computer Graphics: storage tube graphic display devices. Display of initial mesh, deformed mesh, principal stress vectors, crack increment trajectories, G curves, and load displacement curves. Interactive programming capability, meaning that the user participates in the real time solution of the problem by, for examples, editing each mesh update, or selecting the length of a crack increment or magnitude of a load increment.
3. High-Level Interactive Computer Graphics: vector refresh graphic display devices. With high-level graphics, all of the capabilities of low-level exist but the display is continually updated. This means that selected regions of the display can be changed nearly instantaneously without the necessity for redraw of the entire

display. The mesh can be "zoomed" or panned to highlight detail, and three-dimensional objects can be translated and rotated to enhance the user's perception of a complex object and its mesh.

The operational version of BEFAP currently operates only in the interactive mode, while FEFAP operates in interactive, low-level, and high-level interactive graphic modes.

In the example problems to follow, one will notice an evolution in the user-computer interface towards increasing use of interactive computer graphics. This evolution is still underway but the original objectives are the same. These are:

1. Minimize Manual Generation of Input Data.

   This applies both to the total amount of data necessary to define the problem and the physical act of transferring this information to the computer. The user should communicate geometrical information to his code by way of interactive graphics, e.g., a digitizing tablet and pen in conjunction with a vector refresh display terminal or a cursor and key system such as on some storage tube terminals. Only the geometrical information absolutely required for automatic mesh generation should be input in this manner.

2. Make the Programs Interactive and Adaptive.

   On request, the user should be informed of real time progress of the analysis by way of graphic displays. Moreover, he should be given the freedom to modify the course of the analysis by changing the data base while it is in progress.

3. Results Should be Displayed in a Simple and Effective Way.

   The user should be able to see graphic display of intermediate and final stress and displacement fields, load histories, crack patterns.

Automatic Remeshing

All of the programs developed at Cornell University employ automatic remeshing algorithms. This means that the programs, after computing stress intensities, interaction, angle change, and change in load or fracture length, automatically relocate each crack tip and remesh accordingly. The remeshing algorithms developed by Blandford [44] for BEFAP and Saouma [45] for FEFAP are very versatile. They accommodate mixtures of element types and allow a wide range of crack configurations to be modelled. This versatility will be evident in the examples to follow.

Example Solutions

Example #2: Simulation of the Tests Described in Example #1

Numerical Method: Finite Element and Boundary Element Solutions

User-Computer Interface: Punch Cards and Manual Remeshing for Finite Element Solution; Interactive Without Graphics for Boundary Element Solution

The author used finite elements to simulate [23,25] the behavior shown in Figure 8 for the first, and most rudimentary, example of fracture propagation modelling using the techniques described in this chapter. Each fracture increment required manual remeshing and a job resubmission. Dozens of man-hours were required to produce the results of ten primary crack increments.

More recently the same problem was analyzed by Blandford [44,46] using BEFAP. A typical mesh is shown in Figure 17. Initial data preparation required about 3 man-hours. The analysis itself, involving 7 primary crack increments and computation of domain stresses, required about 10 CPU minutes on an IBM 370/168. Still, however, the computed stress field had to be manually plotted to mark the area of secondary crack nucleation. A comparison of typical finite element, boundary element, and experimental results is shown in Figure 18.

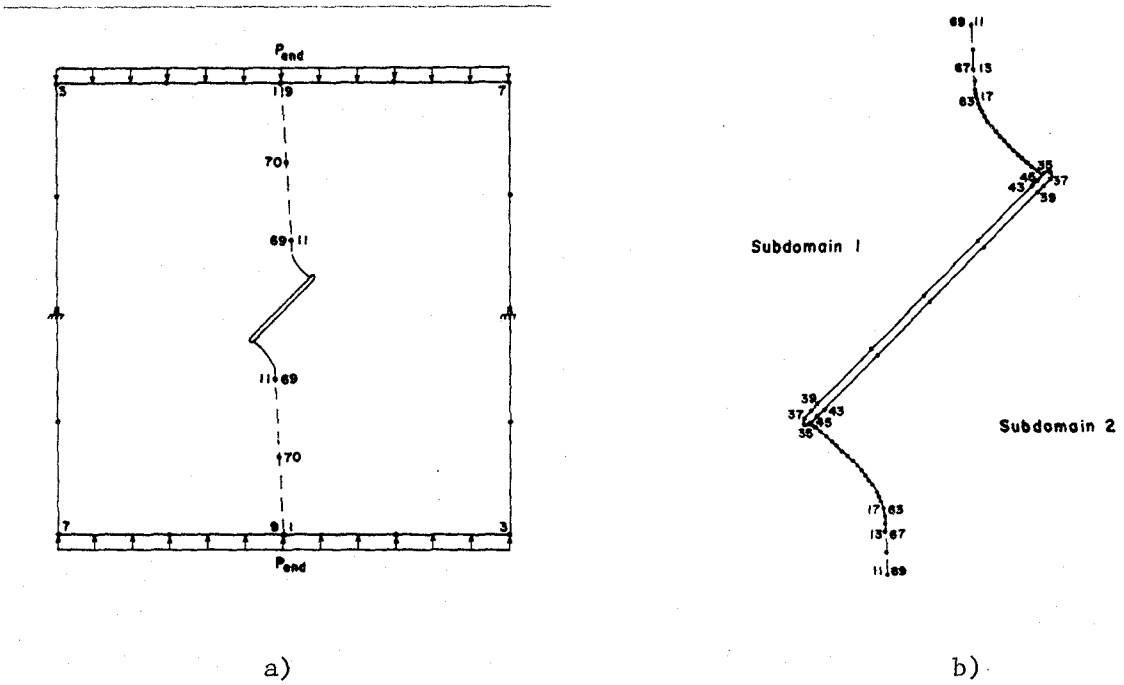

a) b)

Fig 17 a) Typical boundary element mesh for problem of example #1;
b) typical notch tip detail. From Ref. 46.

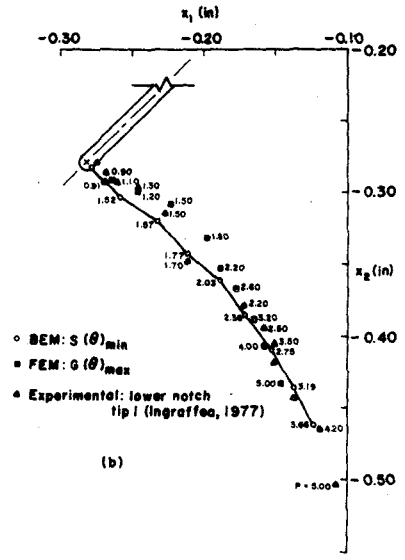

Fig. 18 Comparison of predicted and observed primary crack trajectories for problem of example #1. P in ksi. (ksi = 6.9 MPa, 1 in = 25.4 mm) From Ref. 46.

Example #3: Collapse of Underground Cavity

Numerical Method: Finite Element

User-Computer Interface: High Level Interactive Computer Graphics

The structure shown in Figure 19 represents a cross-section through a deep underground cavity loaded by overburden and horizontal stresses. The model shown was tested by Hoek [48]. An analysis of this structure was performed using the high-level interactive computer graphics facilities at the Cornell Program for Computer Graphics. An interactive graphics preprocessor [49] was used to generate the initial finite element mesh, shown in Figure 20a, and its attributes. Generation of all initial data required about 10 man-minutes.

The fracture response of this structure is similar to that of the previous example. Primary cracks initiate at crown and invert and propagate in the manner described previously with respect to Figure 16.

The initial major principal stress field is depicted in Figure 20b. Shown is a photograph taken from a color postprocessor display [50]. Regions in which the stress exceeds the postulated tensile strength are shown here in black. Such postprocessing can be performed at the end of each fracture increment; fields of principal, normal, and shear stress, strain energy density, and displacement can be quickly displayed. Moreover, no additional man-effort is required to generate an image since the postprocessor data base is common with that of the preprocessor.

Next, secondary cracks nucleate in the plate interior in a tension zone developed in response to primary crack propagation. This zone can be seen as the blackened area shown in the postprocessor image of Figure 21a. A "zoomed" detail of the final mesh showing the predicted secondary crack path is shown in Figure 21b. Experimental results for a similar problem [51] are shown in Figure 22.

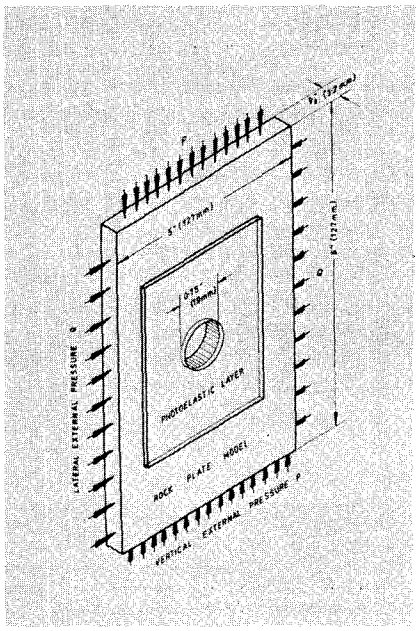

Fig. 19 Rock plate model used in experimental study of collapse of underground cavity. From Ref. 48.

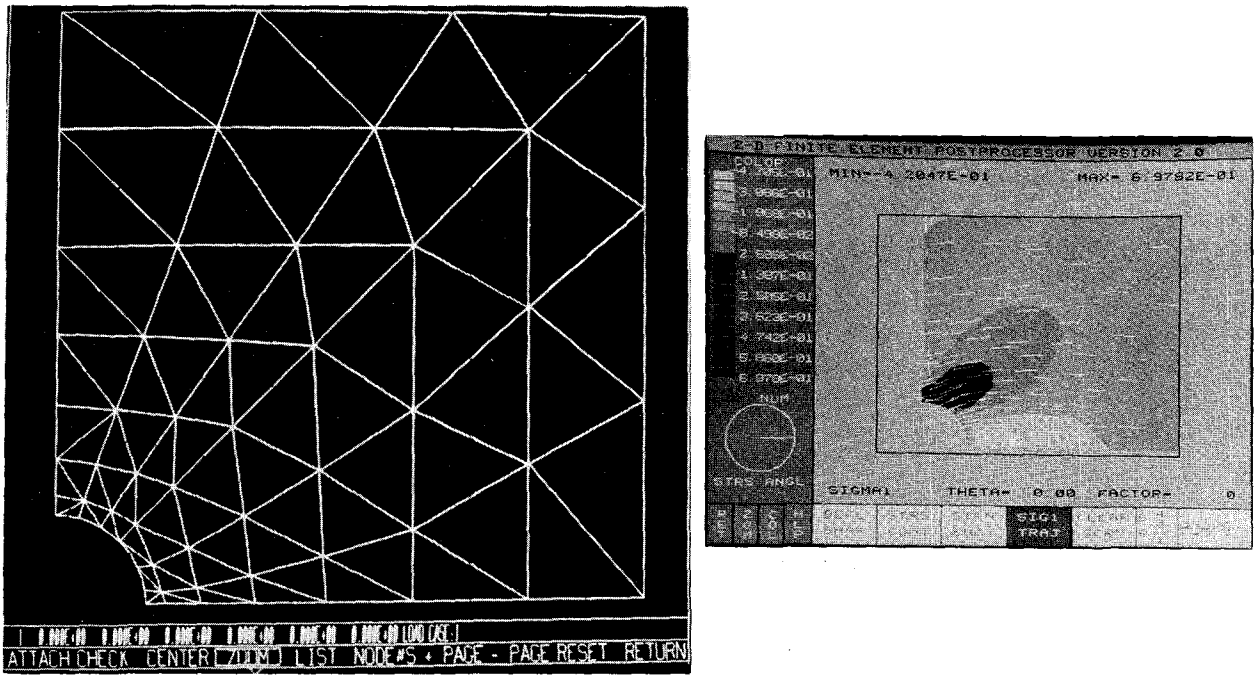

Fig. 20 a) Initial mesh for example #3; b) initial major principal field. From Ref. 29.

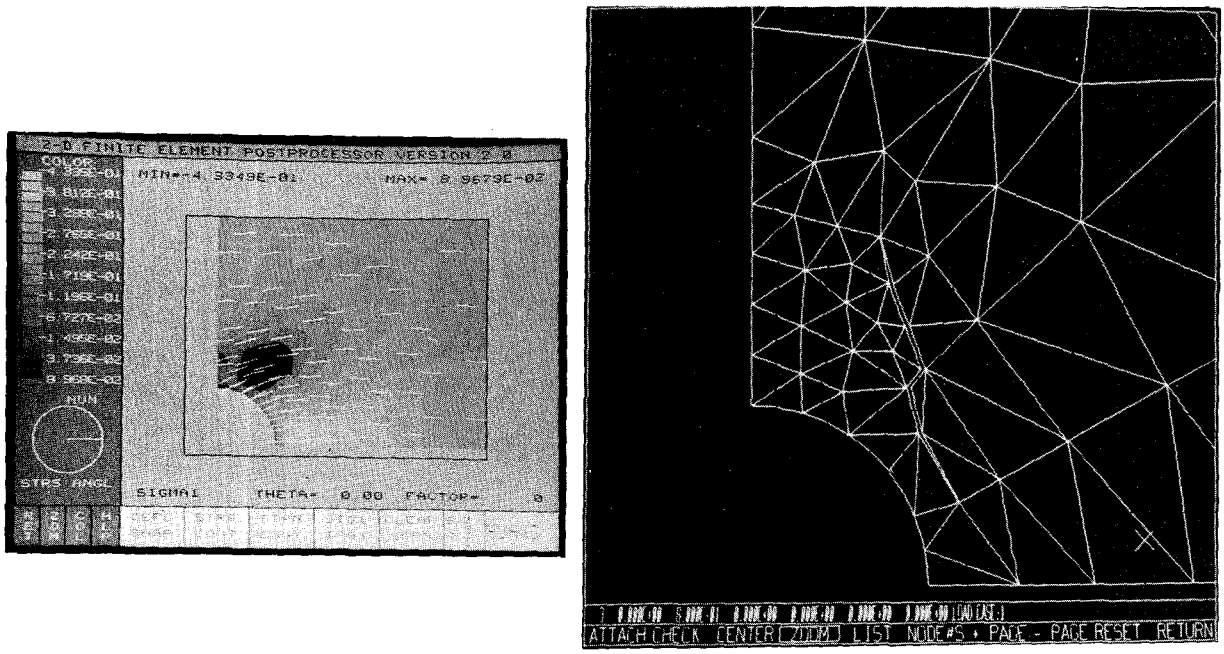

Fig. 21 a) Major principal stress field after stabilization of primary crack at point A; b) detail of final mesh. From Ref. 29.

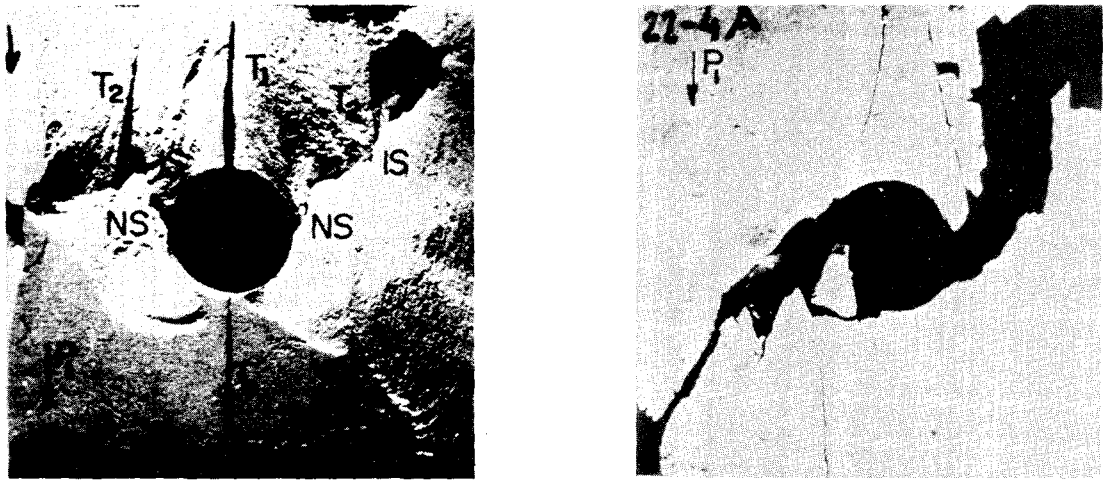

Fig. 22 Fracture patterns observed in tests on plaster models similar to the structure in Figure 19. From Ref. 51.

Example #4: Fracture Propagation Under Indentation Loading

Numerical Method: Finite Element

User-Computer Interface: Low-Level Interactive Computer Graphics

The mechanisms of fracture propagation under a tunnel boring machine roller cutter have been much studied but, in the author's opinion, are not yet completely understood. Paul [52] proposed that at the point of contact with the rock surface high bearing stresses would generate a bulb of very high hydrostatic pressure. He used finite element analysis to prove that such a condition would produce a primary radial crack as shown in Figure 23. FEFAP was used to model this occurrence as well as to predict the trajectories of the secondary radial cracks which Paul [52] surmised would occur after primary crack stabilization.

The initial and final meshes are shown in Figure 24. The predicted fracture pattern closely resembles those observed after TBM roller cutter passage over granite [53], Figure 25.

FEFAP, designed by Saouma and the author [45,47], is highly interactive and adaptive. The user receives information graphically after each analysis step, and is put in control of each subsequent step. For example, Figure 24a shows a typical fracture increment control page and its question/response dialogue. The automatic mesh modification algorithm in FEFAP can accommodate multiple cracks, a mixture of Q8, LST, and quarter-point singular elements, and interior or symmetry line cracks. The user is given the option of interactively modifying a generated mesh.

5. FRACTURE PROPAGATION MODELLING — THE FUTURE

The techniques described in this paper are certainly not the only ones available for modelling of fracture propagation. Alternative approaches can be based on other numerical methods, theories, and algorithms. However, it

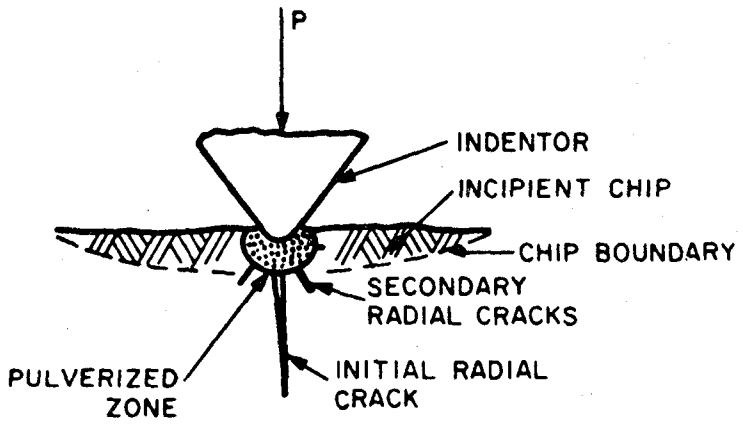

Fig. 23 Postulated fracture pattern under indentor loading. From Ref. 52.

a)

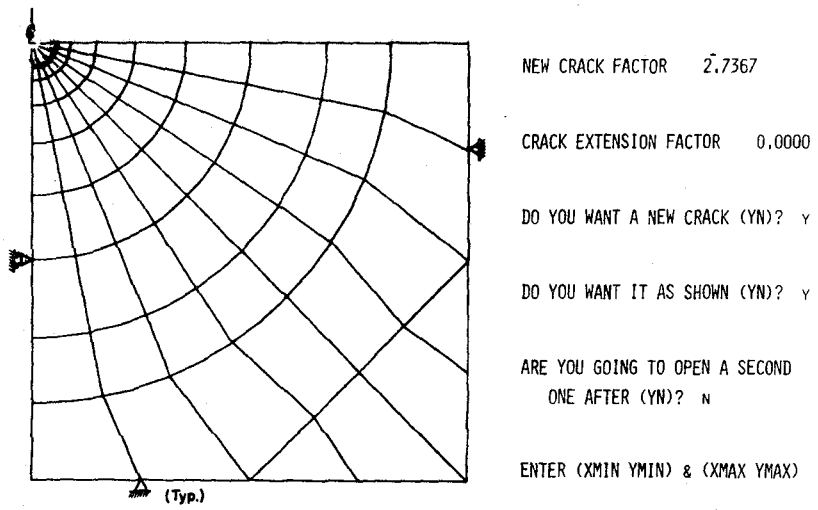

b)

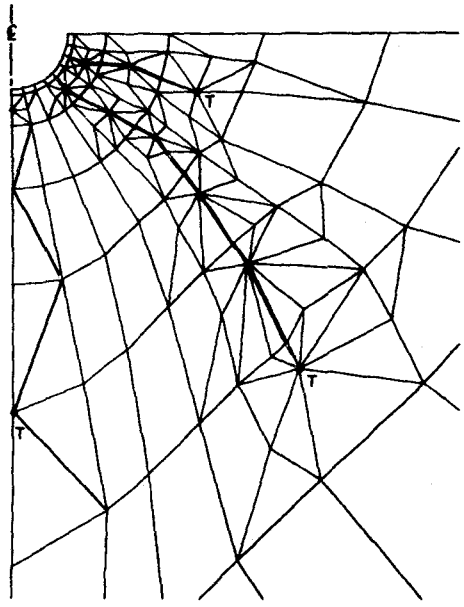

Fig. 24 Initial, a), and final, b), meshes for example #4. Crack tips are at points T.

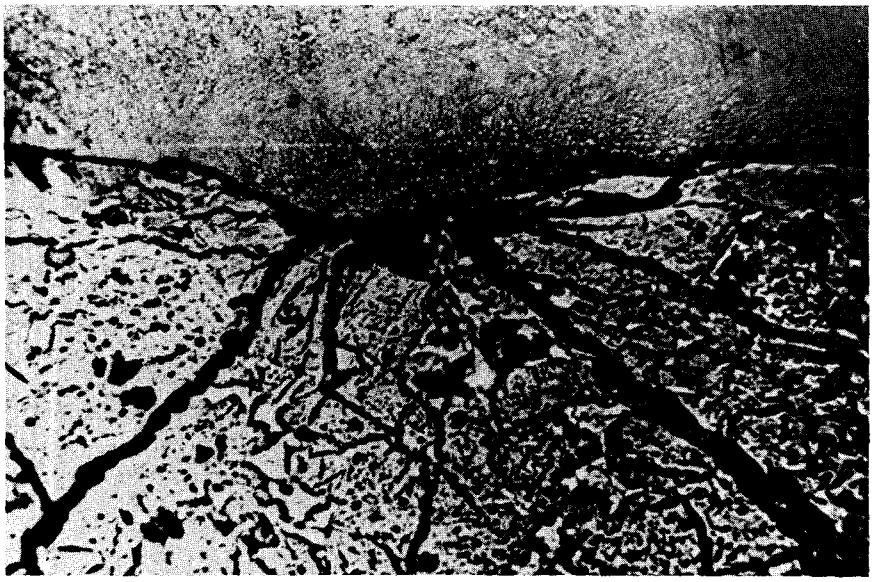

Fig. 25 Fracture patterns on cross section of granite plate after TBM cutter pass. From Ref. 53.

is the author's strongly held opinion that, regardless which model is pursued, interactive computer graphics will play a decisive role in determining the viability of and program in the marketplace of "real world" problems. The continuing, rapid revolution in graphics hardware capability and software development and the ever-increasing cost-effectiveness of fast, virtual-memory, mini-computers are the driving forces in the evolution of sophisticated fracture propagation programs.

Nowehere will this be more evident than in the area of fully three-dimensional modelling. The present high cost of performing analysis of three-dimensional structures is due largely to the human effort required to define and check geometrical data, element topology, boundary conditions, and material properties. In fact, the complexity of error detection, or even slight modification, with three-dimensional meshes can substantially reduce the cost effectiveness of a program. The user falls back onto a two-dimensional or axisymmetric model that is "good enough," sacrificing the realism of the three-dimensional problem in the face of the reality of tremendous labor cost.

However, interactive/adaptive preprocessing can eliminate a large percentage of such cost while simultaneously placing the engineer back in control of computer analysis. For example Perucchio and the author [54,55] have developed three-dimensional finite and boundary element preprocessors for use with fracture propagation codes in a high-level computer graphics environment. An example use of the boundary element preprocessor is the simulated hydrofracture propagation sequence shown in Figure 26.

Figure 26a shows the initial-stage BEM mesh, while Figure 26b shows only the fracture plane with the fracture surface removed. Figures 26c and 26d are analogous images after a fracture propagation step.

The complete boundary element mesh of Figure 26a can be rotated,

a)

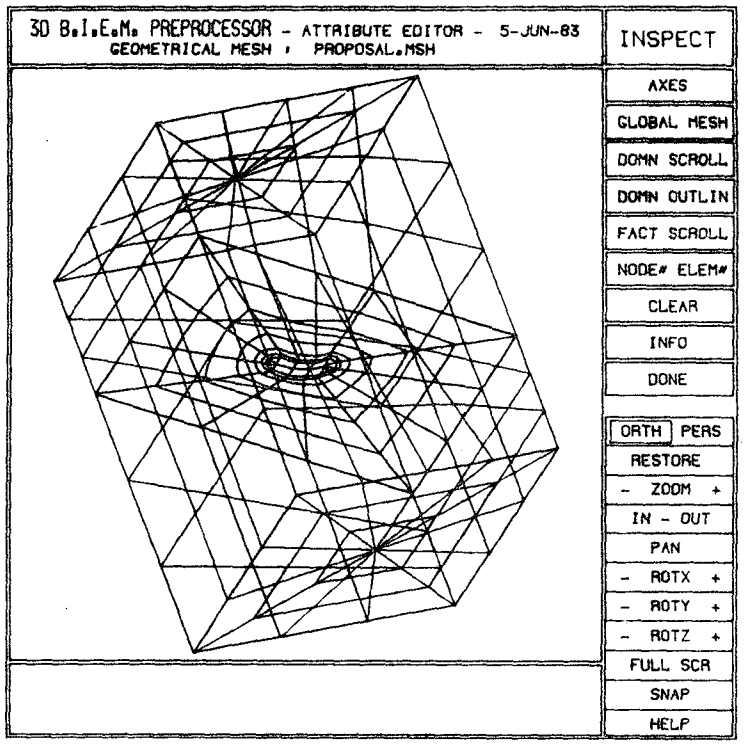

b)

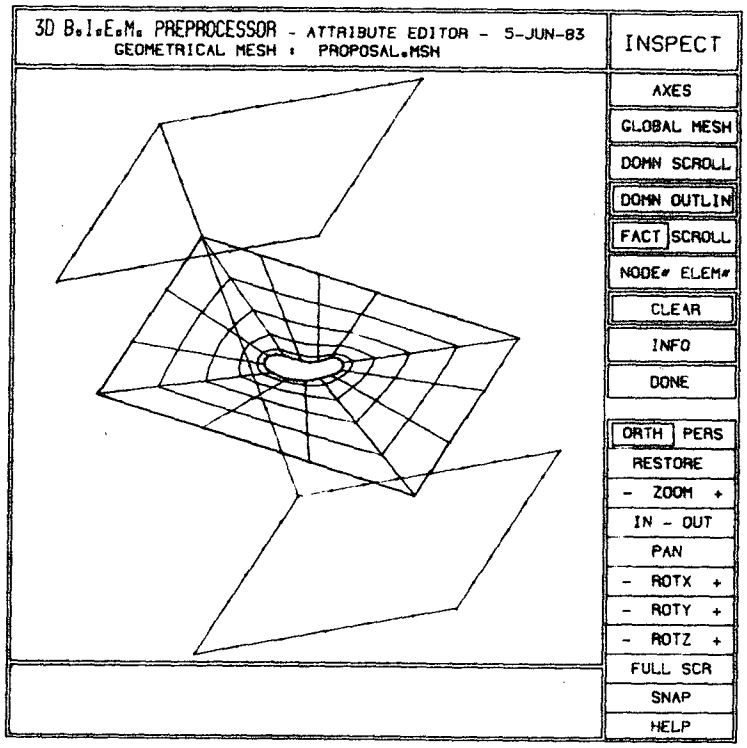

Fig. 26 Views of three-dimensional boundary element mesh for simulated hydro-fracture, a)complete mesh, b) crack plane with fracture surface removed for clarity.

c)

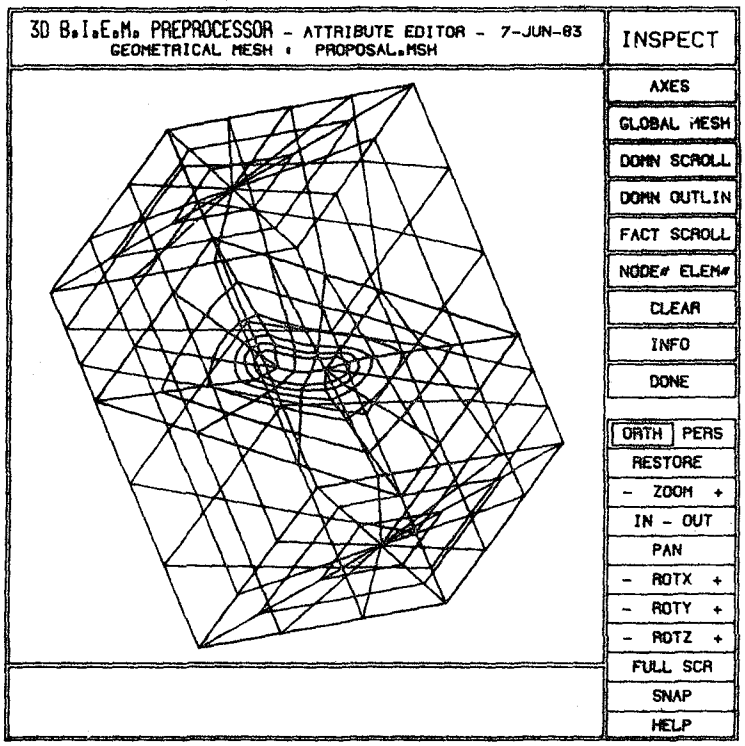

d)

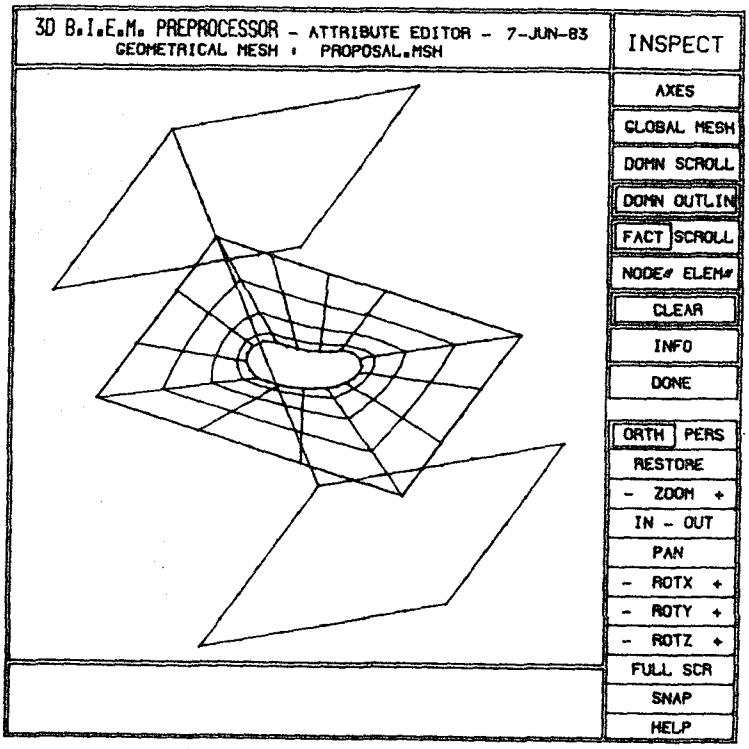

Fig. 26 continued c) complete mesh after increment of cracking, d) same as b) above, after increment.

translated, zoomed, and depth cued. The user need not sacrifice to the CPU his engineering insight into the physics of the problem. Figure 26b shows that the mesh can be taken apart to study cross-sections, sub-domains, or even elements of interest. This capability will be invaluable during the course of a fracture propagation analysis.

Given the changes in the speed and cost of computers and the increasing use of interactive graphics, the author sees the use of truly three-dimensional fracture propagation codes, with the versatility of existing two-dimensional programs, as a certainty in only a few years.

ACKNOWLEDGEMENTS

The author would like to thank the following former and present students for making the developments reported here possible: Prof. Victor Saouma, Prof. George Blandford, Dr. Corneliu Manu, Dr. Renato Perucchio, Mr. Walter Gerstle, Dr. Jay Beech, Prof. Priscilla Nelson, and Mr. Kirk Gunsallus.

The author would also like to thank Prof. Donald Greenberg, Director of the Cornell Program for Computer Graphics, for the continued use of his facility.

Research grants for the development of the techniques and programs described here came from the National Science Foundation.

REFERENCES

[1] Fairhurst, C. and Cornet, F., "Rock Fracture and Fragmentation," Proceedings of the 22nd U.S. Symposium on Rock Mechanics, MIT, June 28-July 2, 21-46, 1981.

[2] Barton, C., "Systematic Jointing in the Cardium Sandstones Along the Bow River, Alberta, Canada," Ph.D. Dissertation, Yale University, 1983.

[3] Ouchterlony, F., "Review of Fracture Toughness Testing of Rock," DS1980:15, Swedish Detonic Research Foundation, Stockholm, 1980.

[4] Abou-Sayed, A.S. and Simonson, E.R., "Fracture Toughness, K_{Ic}, of Tri-axially-loaded Indiana Limestone," Proceedings, 18th U.S. Symposium on Rock Mechanics, 2A3-1, 2A3-8, 1977.

[5] Barker, L.M., "A Simplified Method for Measuring Plane Strain Fracture Toughness," Engineering Fracture Mechanics, 9, 361, 1977.

[6] Ouchterlony, F., "A New Core Specimen for the Fracture Toughness Testing of Rock," DS 1980:17, Swedish Detonic Research Foundation (SveDeFo), Stockholm, Sweden, 18, 1980.

[7] Newman, J.C., "Stress Intensity Factors and Crack Opening Displacements for Round Compact Specimens," NASA TM 80174, Langley Research Center, Oct., 1979.

[8] Ouchterlony, F. and Zongqi, S., "New Methods of Measuring Fracture Toughness on Rock Cores," Proc. First Int. Symp. Rock Frag. Blasting, Lulea, Sweden, Aug. 22-26, 1983, in press.

[9] Beech, J. and Ingraffea, A.R., "Three-Dimensional Finite Element Stress Intensity Factor Calibration of the Short Rod Specimen," International Journal of Fracture, 18, 3, 217-229, 1982.

[10] Bubsey, R.T., Munz, D., Pierce, W.S., and Shannon, J.L., Jr., "Compliance Calibration of the Short Rod Chevron-Notch for Fracture Toughness Testing of Brittle Materials," International Journal of Fracture, 18, 2, 125-133, 1982.

[11] Ingraffea, A.R., Perucchio, R., Han, T.-Y., Gerstle, W.H., Huang, Y.P., "Three-Dimensional Finite and Boundary Element Calibration of the Short-Rod Specimen," ASTM STP from Symposium on Chevron-Notched Specimens: Testing and Stress Analysis, Louisville, Kentucky, April 21, 1983, in press.

[12] Ouchterlony, F., "Extension of the Compliance and Stress Intensity Formulas for the Single Edge Crack Round Bar in Bending," Fracture Mechanics for Ceramics, Rocks, and Concrete, editors S.W. Freiman and E.R. Fuller Jr., STP 745, ASTM, Philadelphia, 237-257, 1981.

[13] Ingraffea, A.R., Gunsallus, K.L., Beech, J.F., and Nelson, P., "A Fracture Toughness Testing System for Prediction of Tunnel Boring Machine Performance," Proceedings of the 23rd U.S. Symposium on Rock Mechanics, Berkeley, California, 463-470, August 1982.

[14] Ingraffea, A.R., Gunsallus, K.L., Beech, J.F., and Nelson, P.P., " A Short-Rod Based System for Fracture Toughness Testing of Rock," ASTM STP from Symposium on Chevron-Notched Specimens: Testing and Stress Analysis, Louisville, Ky., April 21, 1983, in press.

[15] Atkinson, B., "Subcritical Crack Growth in Geological Materials," Proceedings of Workshop on Chemical Role of Water in Crustal Deformation, April 27, 1982, in press.

[16] Ouchterlony, F., "A Simple R-Curve Approach to Fracture Toughness Testing of Rock with Sub-Size SECRBB Specimens," DS 1981:18, SveDeFo, Stockholm, Sweden, 41 pp, 1981.

[17] Barker, L. M., "Short-Rod and Short-Bar Fracture Toughness Specimen Geometries and Test Methods for Metallic Materials", ASTM STP 743, 456-475, 1981.

[18] Raju, I.S., Newman, J.C., "Three-Dimensional Finite Element Analysis of the Chevron-Notched Fracture Specimen," ASTM STP from Symposium on Chevron-Notched Specimens: Testing and Analysis, Louisville, Kentucky, April 21, 1983, in press.

[19] Barker, L.M., "Theory for Determining K_{Ic} from Small, Non-LEFM Specimens Supported by Experiments on Aluminum," International Journal of Fracture, 15, 6, 515-536, Dec. 1979. Terra Tek Report TR 78-6R, Aug. 1978.

[20] Barker, L.M., "K_{Ic} Measurements Using Short Rod Specimens - The Elastic-Plastic Case," Terra Tek Report TR 77-91R, Nov.,1977.

[21] Griffith, A.A., "The Phenomenon of Rupture and Flow in Solids," Philosophical Transactions of the Royal Society of London, Ser. A221, 163, 1921.

[22] Griffith, A.A., "Theory of Rupture," Proceedings of the First International Congress of Applied Mechanics, Delft, 55-63, 1924.

[23] Ingraffea, A.R., Discrete Fracture Propagation in Rock: Laboratory Tests and Finite Element Analysis, Ph.D. dissertation, University of Colorado, 347 p., 1977, .

[24] Ingraffea, A.R., and Ko, H.-Y., "Determination of Fracture Parameters for Rock," Proceedings of First USA-Greece Symposium Mixed Mode Crack Propagation, Sih, G.C. and Theocaris, P.S., eds., Sijithoff & Noordhoff, Alphen aan den Rijn, the Netherlands, 349, 1981.

[25] Ingraffea, A.R. and Heuze, F.E., "Finite Element Models for Rock Fracture Mechanics," International Journal of Numerical and Analytical Methods in Geomechanics, 4, 25, 1980.

[26] Cotterell, "Brittle Fracture in Compression," International Journal of Interactive Mechanics, 8, 195, 1972.

[27] Bombalakis, "Photoelastic Study of Initial Stages of Brittle Fracture in Compression," Tectonophysics, 6, 461, 1968.

[28] Hoek, E. and Bieniawski, Z.T., "Brittle Fracture Propagation in Rock Under Compression," International Journal of Fracture Mechanics, 1, 139, 1965.

[29] Ingraffea, A.R., "The Strength-Ratio Effect in Rock Fracture," Journal of the American Ceramic Society, in press.

[30] Barsoum, R.S., "On the Use of Isoparametric Finite Elements in Linear Fracture Mechanics," International Journal of Numerical Methods in Engineering, 10, 25, 1976.

[31] Barsoum, R. S., "Triangular Quarter-point Elements as Elastic and Perfectly-Plastic Crack Tip Elements, International Journal of Numerical Methods in Engineering, 11, 85, 1977.

[32] Freese, C.E., and Tracey, D.M., "The Natural Isoparametric Triangle Versus Collapsed Quadrilateral for Elastic Crack Analysis," International Journal of Fracture, 12, 767, 1967.

[33] Shih, C.F., de Lorenzi, H.G., and German, M.D., "Crack Extension Modeling with Singular Quadratic Isoparametric Elements," International Journal of Fracture, 12, 647, 1976.

[34] Ingraffea, A.R. and Manu, C., "Stress-intensity Factor Computation in Three Dimensions with Quarter-point Elements," International Journal of Numerical Methods in Engineering, 15, 10, 1427, 1980.

[35] Cruse, T.A. and Wilson, R.B., Boundary-Integral Equation Method for Elastic Fracture Mechanics, AFSOR-TR-0355, 1977.

[36] Blandford, G., Ingraffea, A.R., and Liggett, J.A., "Two-dimensional Stress Intensity Factor Calculations Using Boundary Elements Methods," International Journal for Numerical Methods in Engineering, 17, 387, 1982.

[37] Erdogan, F. and Sih, G.C., "On the Crack Extension in Plates Under Plane Loading and Transverse Shear," ASME Journal of Basic Engineering, 85, 519, 1963.

[38] Sih, G.C., "Some Basic Problems in Fracture Mechanics and New Concepts," Engineering Fracture Mechanics, 5, 365, 1973.

[39] Hussain, M.A., Pu, S.L., and Underwood, J., "Strain Energy Release Rate for a Crack Under Combined Mode I and Mode II, Frac. Analysis," ASTM STP 560, 2, 1974.

[40] Kordisch, H. and Sommer, E., "Bruchkriterien bei uberlagenden normal und scherbeanspruchung von rissen," Report W6.77, Fraunhofer-Gesellschaft, Institut fur Festkorpermechanik, Freiburg.

[41] Ingraffea, A.R., "Mixed-mode Fracture Initiation in Indiana Limestone and Westerly Granite, Proceedings 22nd U.S. Symposium on Rock Mechanics, Cambridge, MA, 186, 1981.

[42] Saouma, V., Ingraffea, A.R., and Catalano, D., "Fracture Toughness of Concrete: K_{Ic} Revisited," ASCE, Journal of the Engineering Mechanics Division, 108, 1152, 1982.

[43] Beech, J. and Ingraffea, A.R., "Three-dimensional Finite Element Stress Intensity Factor Calibration of the Short Rod Specimen," International Journal of Fracture, 18, 3, 127, 1982.

[44] Blandford, G.E., Automatic Two-Dimensional Quasi-Static and Fatigue Crack Propagation Using the Boundary Element Method, Ph.D. disseration, Cornell University, 1981.

[45] Saouma, V.E., Interactive Finite Element Analysis of Reinfored Concrete: A Fracture Mechanics Approach, Ph.D. dissertation, Cornell University, 1981.

[46] Ingraffea, A.R., Blandford, G., and Liggett, J.A. "Automatic Modelling of Mixed-Mode Fatigue and Quasi-Static Crack Propagation Using the Boundary Element Method," Proceedings 14th National Symposium on Fracture Mechanics, ASTM STP 791, I-407, 1983.

[47] Saouma, V.E. and Ingraffea, A.R., "Fracture Mechanics Analysis of Discrete Cracking," Proceedings, IABSE Colloquium on Advanced Mechanics of Reinforced Concrete, Delft, 393, 1981.

[48] Hoek, E., "Rock Fracture Around Mining Excavations," Proceedings 4th International Conference on Strata Control and Rock Mechanics, Columbia University, N.Y., 334 1964.

[49] Haber, R.B., Shephard, M.S., Gallagher, R.H., and Greenberg, D.P., "A Generalized Graphic Preprocessor for Two-dimensional Finite Element Analysis," Computer Graphics, A Quarterly Report of SIGGRAPH-ACM. 12, 3, 323, 1978.

[50] Schulman, M.A., The Interactive Display opf Parameters of Two- and Three-Dimensional Surfaces, M.S. thesis, Cornell University 1981.

[51] Lajtai, E.Z. and Lajtai, V.N., "The Collapse of Cavities," International Journal of Rock Mechanics and Mining Science, and Geomechanical Abstracts, 12, 81, 1975.

[52] Paul, B. and Gangal, M.D., "Why Compressive Loads on Drill Bits Produce Tensile Splitting in Rock," SPE 2392, Proceedings 4th Conference on Drilling and Rock Mechanics, University of Texas at Austin, 109, 1969.

[53] Wang F.-D., Ozdemir, L., and Snyder. L., "Prediction and Verification of Tunnel Boring Machine Performance," Paper presented at Euro-Tunnel, Basel, Switzerland, 1978.

[54] Perucchio, R., Ingraffea, A. R., and Abel, J. F., "Interactive Computer Graphic Preprocessing for Three-Dimensional Finite Element Analysis," International Journal of Numerical Methods in Engineering, 18, 909, 1982.

[55] Perucchio, R. and Ingraffea, A. R., "Interactive Computer Graphic Preprocessing for Three-Dimensional Boundary Integral Element Analysis," Journal of Computers and Structures, 16, 153, 1983.

FRACTURE IN CONCRETE AND REINFORCED CONCRETE

Zdeněk P. Bažant
Professor of Civil Engineering
The Technological Institute
Northwestern University
Evanston, Illinois 60201, U.S.A.

Introduction

Although cracking represents a salient feature of the behavior of concrete structures, not only under ultimate loads but also at service states, fracture mechanics has not been used in practical analysis of structures. Structural engineers had a good reason; the linear fracture mechanics was found to be inapplicable to typical concrete structures, and the premises of ductile fracture mechanics did not match material behavior. However, in various recent investigations, particularly those at the Technical University of Lund, Northwestern University, and Politecnico di Milano, it has been shown that fracture mechanics can be applied to concrete structures provided that one takes into account the effect of a large micro-cracking zone or fracture process zone that always exists at the fracture front. The objective of the present paper is to review the results of the investigations at Northwestern University, many of them carried out under a cooperative agreement with Politecnico di Milano. It is not possible to include a comprehensive review of all the work on fracture of concrete; other work may be consulted for that [1-6].

Blunt Crack Band Model

The simplest way to model cracking in a finite element program is to assume that the cracks are continuously distributed over the area of the

finite element and manifest themselves by a reduction of the elastic modulus in the direction normal to the cracks. Complete cracking corresponds to a reduction of the elastic modulus to zero. In this description, introduced by Rashid [7], the crack band front cannot be narrower than the width of the frontal finite element. At the same time, the width of the crack band front cannot be wider than a single element. Of course, one could enforce the crack front to be of a multiple-element width, however, that would not be justified mechanically since one finds that localization of strain into a single-element width generally leads to a release of elastic energy. There is a further reason why a multiple-element width at the crack front is not a correct model; if we make the loading step sufficiently small, then only one element cracks during the loading step, and this relieves the stresses in the finite element that is on the side of the element that has just cracked, thus preventing an increase of the crack front width, except if a uniform strain distribution is enforced by heavy reinforcement. Even if two finite elements at the crack front had exactly the same stress values, it would be unrealistic to assume that they both crack simultaneously since the statistical scatter of material properties will always cause one of these elements to crack before the other does. Thus, one may adopt the blunt crack band model with a single-element wide front as a realistic and numerically very convenient model for cracking in concrete [10-16]. A similar approach can be applied to rock [10, 17].

Regardless of whether the zone of microcracking at the fracture front in concrete is very wide or not, two elementary justifications may be offered for the blunt crack band model. One of them is the heterogeneity of the material. We treat the material as a smoothed, homogeneous continuum in

the macroscopic sense. In this treatment, the macroscopic stresses and strains represent the averages of the actual (microscopic) stresses and strains over a certain so-called representative volume of the material which must be at least several times the maximum aggregate size in cross section.* Obviously, the rapid and scattered variation of stresses and strains over smaller distances cannot be described by a continuum approach. Therefore, using finite elements of sizes less than several times the aggregate size would not allow any improvement in the description of the actual stress and strain fields within concrete. Even if one wishes to treat a continuous sharp crack in concrete, the blunt crack band model does not represent the reality any worse than a sharp inter-element crack model because the actual crack path is not straight but highly tortuous.

As another justification, of the blunt crack band model for describing sharp fractures in concrete, one may cite the recently documented fact that a sharp inter-element crack and a blunt crack band of single-element width yield approximately the same results for not too crude meshes (roughly when there are at least fifteen finite elements in a square mesh across the cross section). Both models give energy release rates that differ not more than a few percent from the exact elasticity solution. To illustrate it, Fig. 2 exhibits some of the numerical results from Ref. 12. In these calculations, the normal stress in the direction perpendicular to the cracks was assumed to drop suddenly to zero when the energy criterion for crack band propagation became satisfied. The finite element mesh in Fig. 2 covers a cut-out of an infinite elastic medium loaded at infinity by uniform normal stress $\bar{\sigma}$ perpendicular to a line crack of length 2a. The nodal loads applied at the mesh boundary are calculated as the resultants of the exact

*See Fig. 1

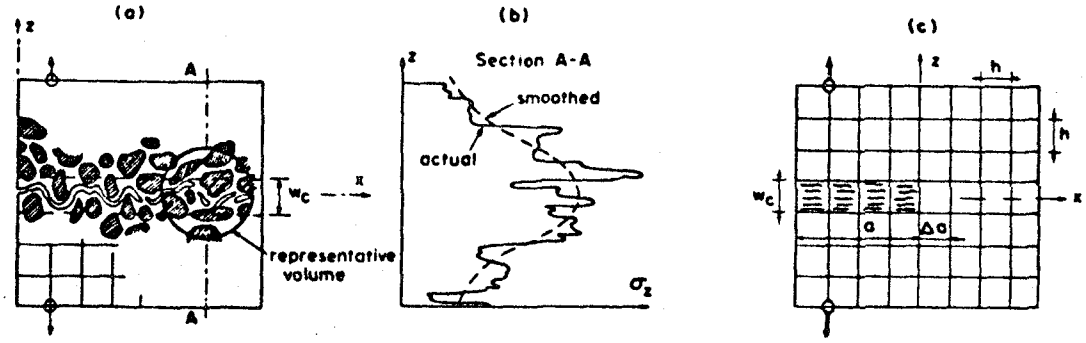

Fig. 1 - Heterogeneous Microstructure, Random Scatter of Stresses and Strains; Plots of Bažant and Cedolin (1979).

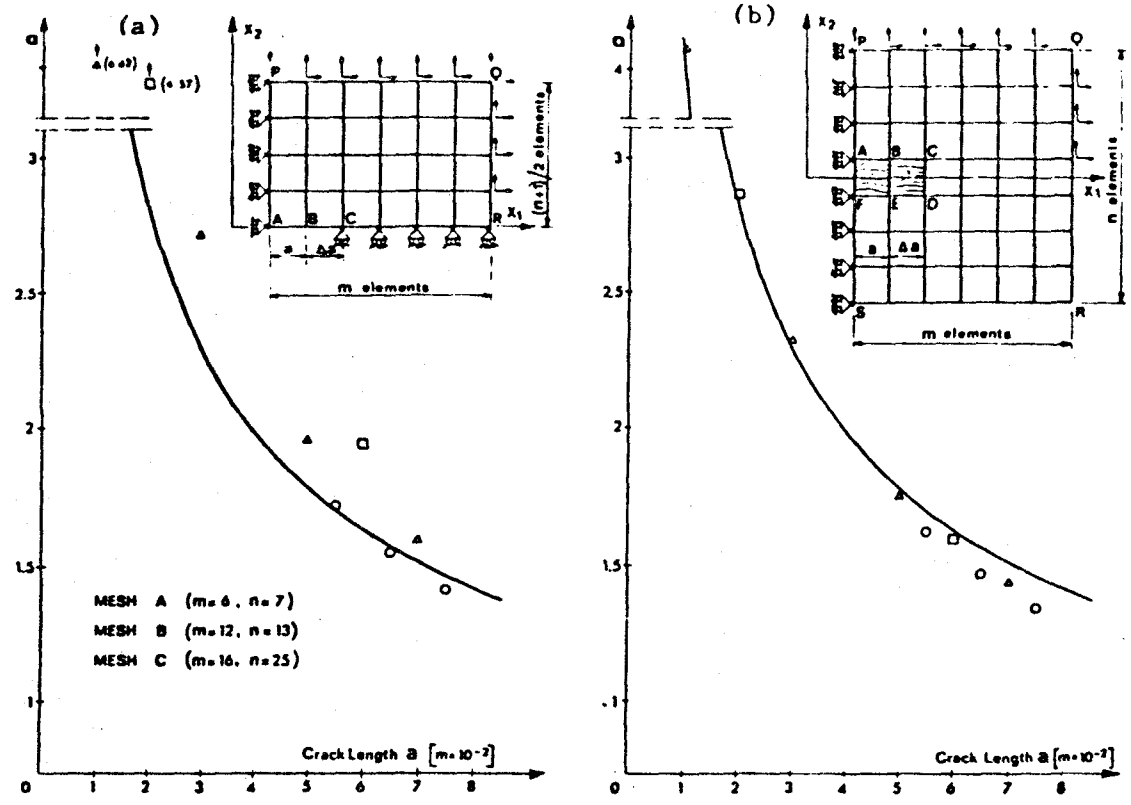

Fig. 2 - Finite Element Results of Bažant and Cedolin (1977) (for Sudden Stress Drop) Showing Equivalence of Blunt Crack Band and Sharp Crack Modeling.

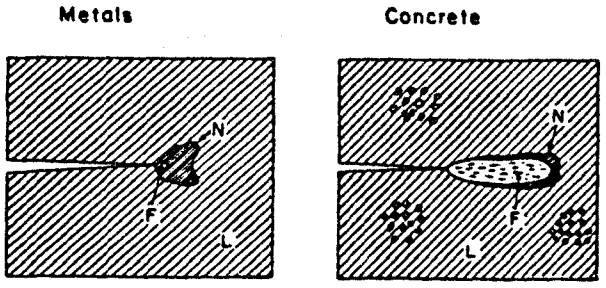

Fig. 3 - Nonlinear Zone and Fracture Process Zone for Various Materials.

stresses in the infinite medium, based on Westergaard's exact solution which is shown as a solid curve. The data points in Fig. 2 show numerical results for the square mesh shown (mesh A), as well as for finer meshes B and C (not shown) for which the element size was 1/2 and 3/8 of the element size shown, respectively. A similar equivalence of results for the sharp inter-element crack and the blunt crack band can be demonstrated when the stress is considered to drop gradually rather than suddenly to zero [11].

Aside from the foregoing justifications, the blunt crack band model appears to be more convenient for finite element analysis. When a sharp inter-element crack extends through a certain node, the node must be split into two nodes. This increases the total number of nodes and changes the topological connectivity of the mesh. Unless the nodes are renumbered, the band structure of the structural stiffness matrix is lost. Moreover, if the direction in which an inter-element crack should extend is not known in advance, one needs to make trial calculations for various possible locations of the node ahead of the crack front through which the crack should pass, in order to determine the correct direction of crack propagation. On the other hand, in the blunt crack band model, a fracture propagating in any direction through the mesh can be modeled as a zig-zag crack band with any direction of the cracks relative to mesh lines. All that needs to be done to model an oblique crack direction is to reduce the elastic stiffness in the direction normal to the cracks.

Recently, various attempts to observe the distribution of microcracks ahead of the fracture front in concrete have been made [18-20]. From strain measurements by Moiré interferometry [19, 20], it appears that the width of the

microcrack zone at the fracture front is about one aggregate size. Within this width, there is a crack concentration. However, the line along which the most dense microcracks are scattered is not straight but rather tortuous (Fig. 1), which would not be modeled by a straight inter-element crack any better than by a crack band. Correlation of the crack band model to such microscopic observation is, of course, difficult since the microcrack density varies while in the crack band it is assumed to be uniform. The question then is at which microcrack size to draw the distinction. Thus, the width of the microscopally observed crack band front depends on the definition of the width of the microcracks that are counted within the crack band.

One significant difference from ductile fracture of metals consists in the size of the fracture process zone, defined as the zone in which the material undergoes strain-softening, i.e., the maximum principal stress decreases at increasing strain. This zone is large for concrete but relatively small for metals, even in the case of ductile fracture. In the latter case, there is a large yielding zone, but the material does not soften in this zone (Fig. 3).

The stress-strain relation with strain-softening for the fracture process zone may be replaced by a strain-displacement relation if the displacement represents the integrated value of the strains across the width of the crack front. In this sense, the present blunt crack band model is equivalent to the previous line crack models with softening stress-displacement relations, introduced by Knauss, Wnuk, Kfouri, Miller, Rice and others [21-27]. For concrete this approach was pioneered by Hillerborg, Modéer and Petersson [27, 28] in their model of a fictitious sharp inter-element crack.

Let us now outline one possible form of the softening stress-strain relation for the fracture process zone. Let the virgin crack-free material be described by the elastic stress-strain relation

$$\underset{\sim}{\varepsilon} = \underset{\sim}{C}\,\underset{\sim}{\sigma} \tag{1}$$

Here, $\underset{\sim}{\sigma}$, $\underset{\sim}{\varepsilon}$ are the column matrices of the cartesian normal components of strain and stress, in cartesian coordinates $x_1 = x$, $x_2 = y$, and $x_3 = z$. $\underset{\sim}{C}$ is a 3 x 3 square compliance elastic matrix of the virgin material, with components C_{11}, C_{12},...C_{33}. For the sake of simplicity, we may now assume that all microcracks spread over the finite element are normal to axis z. Appearance of such cracks has no effect on the lateral strains ε_x and ε_y, and the only effect is an increase in the averaged normal strain ε_z in the direction perpendicular to the cracks. This may be described by cracking parameter μ introduced only in one diagonal form of the compliance matrix [10, 11], i.e.,

$$\underset{\sim}{C}(\mu) = \begin{bmatrix} C_{11} & C_{12} & C_{13} \\ & C_{22} & C_{23} \\ & & C_{33}\mu^{-1} \end{bmatrix} \tag{2}$$

The cracking parameter μ is 1 for the initial crack-free state, and approaches 0 for the final fully cracked state. It has been shown [11], that the limit of the inverse of the compliance matrix $C(\mu)$ as $\mu \to 0$ is, exactly, the well-known stiffness matrix for a fully cracked elastic material, $\underset{\sim}{D}^{fr}$. This matrix is identical to the elastic stiffness matrix for the plane state of stress, which exists in the material between the cracks.

The cracking parameter may be calibrated so as to yield the desired tensile stress-strain relation with strain-softening, $\sigma_z = EF(\varepsilon_z)$, in which

$E = 1/C_{33}$ = Young's modulus. Then one has $\mu = F(\varepsilon_z)/\varepsilon_z$. Function $F(\varepsilon_z)$ may be given as a bilinear stress-strain diagram (Fig. 4), characterized by tensile strength f_t', softening modulus E_t (negative), and limit strain ε_0 for which full cracks are formed. For computer analysis, the foregoing stress-strain relation is differentiated to obtain an incremental form to be used in a program with step-by-step loading.

The strength limit f_t', needs adjustment to take into account the effect of multiaxial stress state. In particular, the tensile strength limit is decreased due to normal compressive stresses σ_x and σ_y parallel to the crack plane. Correction may be done according to the well-known biaxial failure envelope for concrete [11].

The use of cracking parameters μ resembles the so-called continuous damage mechanics, in which damage is characterized by parameter ω which corresponds to $1 - \mu$. There is, however, a fundamental difference in that the damage due to microcracking is considered to be inseparable from a zone of a certain charasteristic width that is a material property, as we will explain later.

The energy consumed by crack formation per unit area of the crack plane, i.e.,

$$G_f = W_f w_c, \qquad W_f = \int_0^{\varepsilon_0} \sigma_z \, d\varepsilon_z \tag{3}$$

represents the fracture energy; w_c = width of the crack band front (fracture process zone), and W_f = work of maximum principal tensile stress per unit volume = area under the uniaxial tensile stress-strain curve (Fig. 4).

The magnitude of w_c is obviously an important factor. If the stress-strain relation, including its strain-softening range, is considered to be

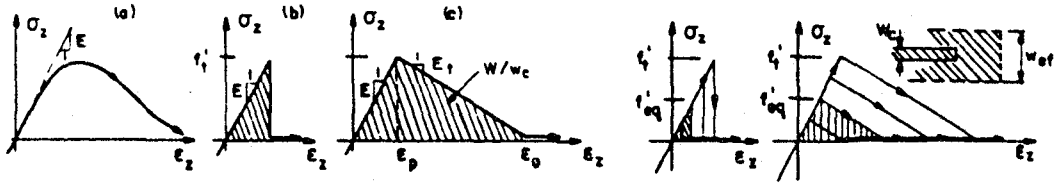

Fig. 4 - Tensile Stress-Strain Diagrams Assumed for Fracture Analysis.

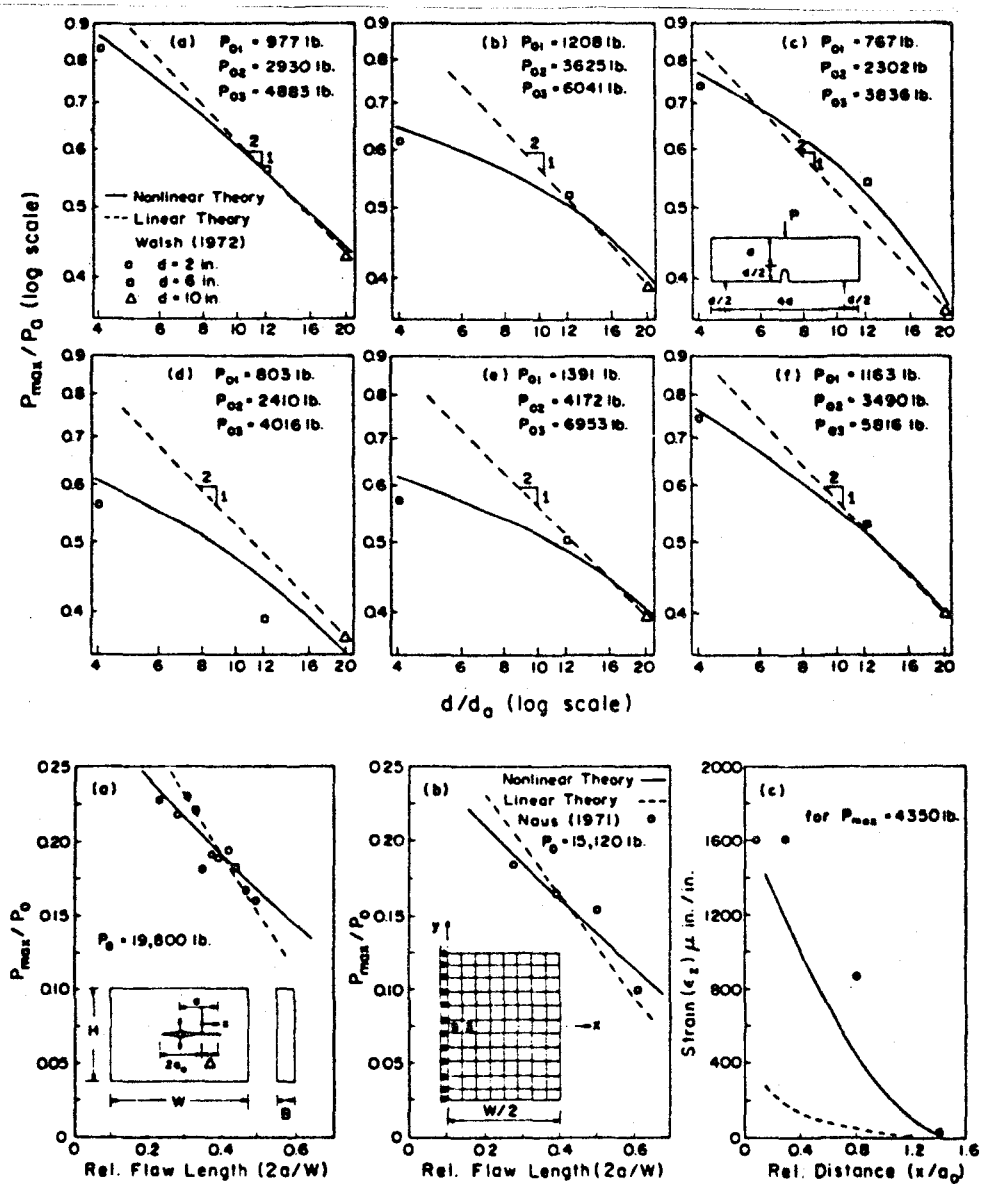

Fig. 5 - Results of Crack Band Analysis Compared With Maximum Load Test Data from the Literature (after Bažant and Oh, 1983).

a material property, which seems logical, then the larger w_c is the larger is the fracture energy G_f. However, it has been previously demonstrated [12, 13] that finite element calculations yield results independent of the choice of the element size (except for a negligible numerical error), only if the fracture energy G_f is considered as a material constant. Eq. 3 then indicates that the width w_c of the crack band front must also be a material constant, to be determined by tests. Indeed, if the value of w_c is changed without adjusting the strength limit f_t' or the strain-softening modulus E_t, the predicted values of loads needed for further crack propagation may change drastically [12, 13]. For the bilinear tensile stress-strain relation (Fig. 4), we have $W_f = \frac{1}{2}(C_{33} - C_{33}^t)f_t'^2 w_c = \frac{1}{2} f_t' \varepsilon_0$ or

$$w_c = \frac{2G_f}{f_t'^2} \frac{1}{C_{33} - C_{33}^t} \tag{4}$$

in which $C_{33}^t = 1/E_t$ (negative). Thus, the width of the crack band front may be determined by measuring the tensile strength, the fracture energy, and the softening modulus E_t. Note that Eq. 4 is similar to the well-known Irwin's expression for the size of the yielding zone. It should be also noted that determination of w_c from mechanical measurements depends on the knowledge of the strain-softening slope E_t. If this slope is changed, a different value of w_c is obtained, and fracture test data may still be fitted equally well, within a certain range of w_c. In fitting test data for concrete fracture from the literature, it has been noted that good fits could be obtained for w_c ranging from $2d_a$ ti $4d_a$ where d_a is the maximum aggregate size. The front width

$$w_c = 3d_a \tag{5}$$

was nearly optimum, and at the same time was consistent with the softening modulus E_t as observed in the direct tension tests of Evans and Marathe [32].*

Most of the important test data from the literature [33-49], have been fitted with good success using the present nonlinear fracture model [11]. Some of the fits obtained in Ref. 11 by finite element analysis using square meshes are shown in Figs. 5 and 6, in which P_{max}, representing the maximum measured load, is plotted as a function of either the crack length (flaw depth) or the specimen size. The optimum fits obtainable with linear fracture mechanics are shown for comparison in these figures as the dashed lines. The loading point was displaced in small steps in computations, and the reaction, representing load P, was evaluated at each loading step by finite elements. The same bilinear stress-strain relation was assumed to hold for all elements.

Note that the crack band approach to fracture models well not only the results for notched fracture specimens, but also the results for unnotched beams, in which the nominal bending stress at failure decreases as the beam depth increases (Fig. 5). This phenomenon is due to the fact that the large fracture process zone (strain-softening zone) cannot be fully accommodated in a small beam. The same phenomenon was previously modeled as a statistical size effect; however, explanation in terms of fracture mechanics, previously proposed by Hillerborg, appears to be the correct one.

Deviations from linear fracture mechanics have been also described for metals by the so-called R-curves (resistance curves), which represent the variation of apparent fracture energy as a function of the crack extension from a notch. Based on an original proposal by Krafft et al. [50], the R-curve may be considered for most situations as a fixed material property,

*Strain-softening in direct tensile tests of concrete has been also documented in Refs. 51-53 and 49.

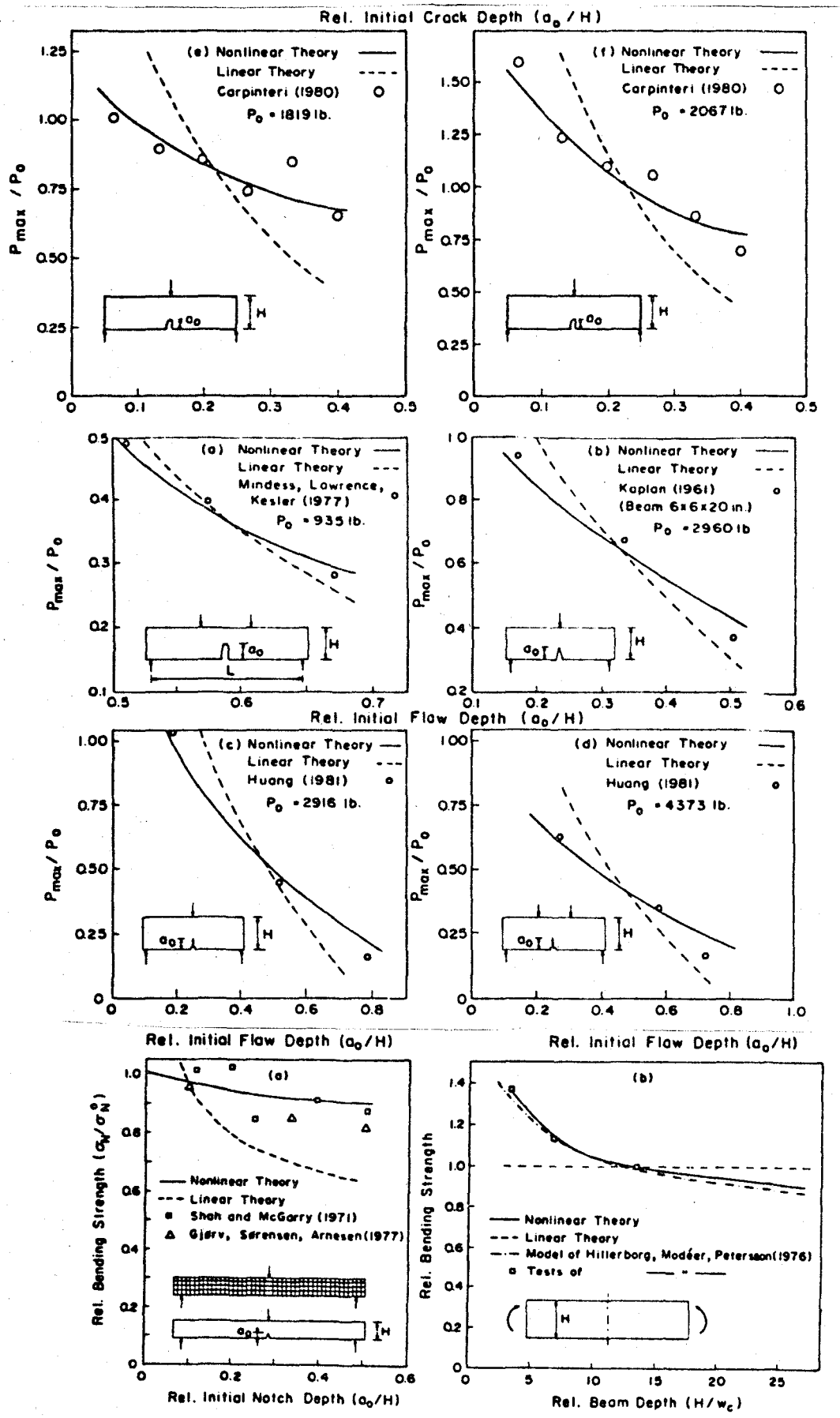

Fig. 6 - Crack Band Calculation Results Compared With Further Maximum Load Test Data From the Literature (after Bažant and Oh, 1983).

although in reality it may be such only asymptotically, for infinitely small crack extensions from a notch (for longer extensions, the R-curve should, in theory, also depend on the boundary geometry, location of the loads, crack path, etc.). It is noteworthy that the present theory achieves a good fit of test data without introducing any variation of fracture energy G_f, i.e., G_f is a constant. In fact, the present theory allows calculating the R-curves. For this purpose one needs to evaluate the work of the nodal forces acting at the crack front element during a small crack band extension. In this manner the R-curves have been calculated, using the same fracture parameters as in the previous fitting of maximum load data. These calculations have led to good fits of R-curve data reported in the literature [11]; see Fig. 7, using test data from Refs. 33, 36, 45, and 48. For the details of analysis, see Ref.11. (It is worth noting that the present theory has been also used with equal success to fit the test data for various rocks [10, 17].)

Statistical analysis of the test data available in the literature revealed that the crack band theory allows a great reduction of the coefficient of variation ω_0 of the deviations of test data from the theory. In the case of maximum load data, $\omega_0 = 0.666$, while for the best fits with linear elastic fracture mechanics, $\omega_0 = 0.267$. For the strength criterion, $\omega_0 = 0.650$. In the case of R-curves, the present crack band theory yields standard deviation for the deviations of test data from the theory as $s = 0.083$, while linear fracture mechanics with constant fracture energy yields $s = 0.317$; see Ref. 11. These are significant improvements in the error statistics, and the present crack band theory is seen to be sufficient for practical purposes. The analysis of test data from the literature allowed it also to set up an approximate

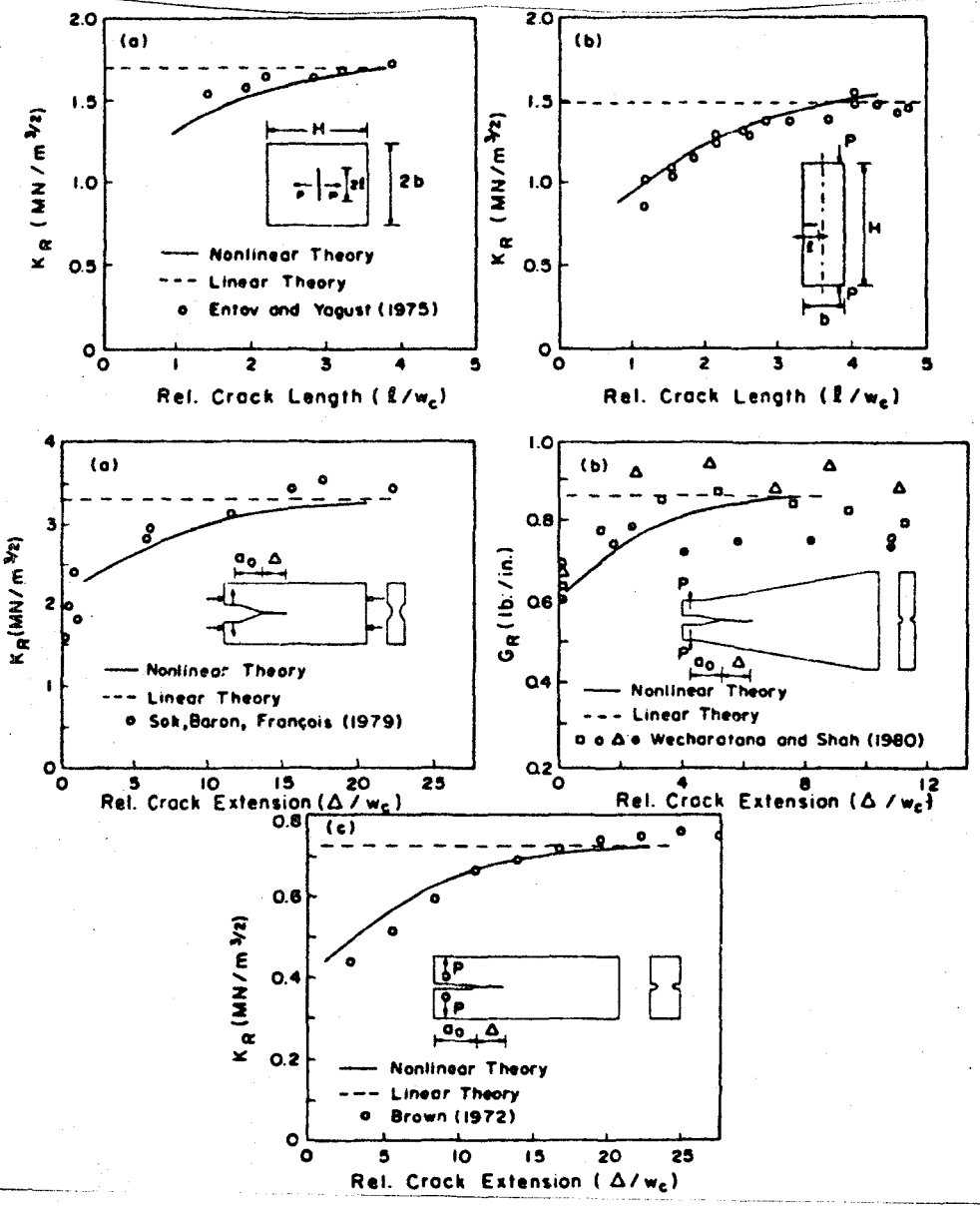

Fig. 7 - Crack Band Calculation Results Compared With Measured R-Curves from the Literature (after Bažant and Oh, 1983).

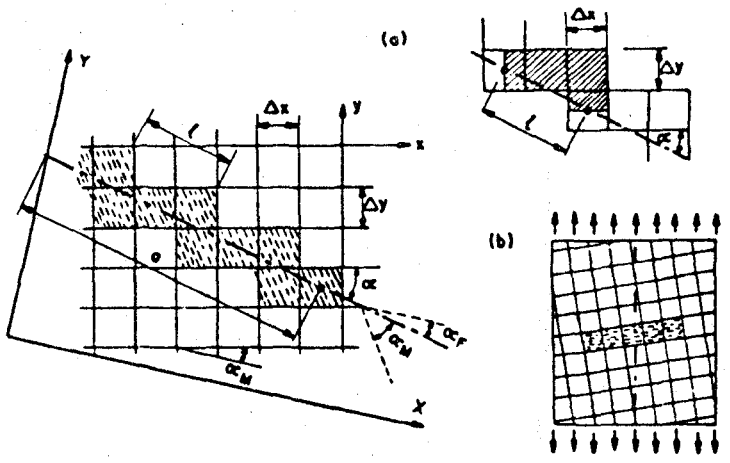

Fig. 8 - Zig-Zag Crack Band Propagation through a Square Mesh.

empirical formula for the prediction of fracture energy on the basis of tensile strength f'_t, maximum aggregate size d_a, and Young's modulus E;

$$\tilde{G}_f \simeq 0.0214(f'_t + 127)f'^2_t\, d_a/E \tag{6}$$

in which f'_t must be in psi (psi = 6895 Pa), and $\tilde{G}_f$ is in lb./in. Exploiting the relation $G_f \simeq 3d_a\, f'^2_t(E^{-1} - E_t^{-1})/2$, one can further obtain a prediction formula for the softening modulus

$$E_t \simeq \frac{-69.9E}{f'_t + 56.7} \tag{7}$$

Application in Finite Element Programs

Finite elements of size $h = w_c = 3d_a$ may be too small for many practical applications. However, we cannot simply increase the element size because according to Eq.3 the energy consumed by fracture would increase proportionally with h, other parameters remaining unchanged. Obviously, in order to maintain the same energy consumption by fracture, the area under the tensile stress-strain diagram must be changed in inverse proportion to the element width h. This may be done most conveniently by adjusting the strength limit from the actual strength f'_t to an equivalent tensile strength f'_{eq}. If we use the bilinear stress-strain diagram and keep the softening modulus E_t constant, we obtain the following expression for the equivalent strength in a square mesh in which the fracture propagates parallel to the mesh line;

$$f'_{eq} = c_f\left(1 + \frac{E}{-E_t}\right)^{-\frac{1}{2}} \left(\frac{2G_f E'}{w_h\, r_f}\right)^{\frac{1}{2}} \tag{8}$$

in which c_f is a calibration factor close to 1, depending on the type of finite element, and r_f is a correction for the compressive normal stress parallel to the crack plane ($r_f = 1 - \nu'\, \sigma_3/\sigma_1$).* We see that the tensile strength limit must be reduced in inverse proportion to the square root of element size.

*Here $\nu' = \nu/(1 - \nu)$, ν = Poisson ratio.

If the tensile strength limit is not changed when the element size changes, fracture analysis is unobjective in that the results may strongly depend on the analyst's choice of the element size. A glaring example of this was presented in Ref. 15 in which a rectangular panel, either plane or reinforced, was analyzed for propagation of a symmetric central crack band. It was demonstrated that by changing the element size four times, the calculated value of the load needed for further crack band propagation changed this by a factor of 2 (i.e., by 100%). (If the element size is much larger than w_c, the value of equivalent strength f'_{eq} is very small and may be neglected. Then one obtains the no-tension material pioneered some twenty years ago by Zienkiewicz et al.)

Keeping the strength limit the same regardless of the element size does not necessarily lead to wrong results. In fact, in many situations finite element analyses with a constant tensile strength yielded good results, in agreement with tests. The reason why this happens is that many structures are fracture-insensitive, i.e., their failure depends primarily on other phenomena such as plastic yielding of steel rather than on cracking of concrete. The flexural failure of reinforced beams is a good example. To decide whether the problem is fracture-insensitive, the analyst needs to run the finite element calculations twice: once with the actual tensile strength f'_t, and once with a zero tensile strength. If the results do not differ significantly, one may forget about adjusting the tensile strength limit.

For structures much larger than the aggregate size, the size of the fracture process zone may become negligible compared to the cross section dimensions (this is true, e.g., for gravity dams). If the finite elements are not very small, a small fracture process zone can be obtained by considering

a vertical stress drop instead of gradual strain-softening. A small fracture process zone is a prerequisite for the validity of linear elastic fracture mechanics, and indeed it is found [10, 11] that the use of a sudden stress drop after the tensile strength limit has been reached leads to results that are very close to the exact solutions of linear elastic fracture mechanics. The results with the present crack band model are just as close to the exact solution as those obtained with the sharp interelement crack model [10].

When a vertical stress drop is assumed, the energy criterion of fracture mechanics can be more closely approximated by a direct calculation of the energy release due to crack band extension, rather than the use of a specified tensile stress-strain diagram with equivalent strength. A formula for the change in potential energy due to crack band extension was given in Refs. 10 and 11. In this formula, one calculates the work of the nodal forces acting upon the frontal finite element during the fracture formation. One must also consider the differences between the initial and final strain energy within the cracked frontal finite element, as well as the work of distributed forces transmitted by reinforcement on concrete.

Instead of directly calculating the work of nodal forces on the frontal finite element, one may also obtain the exact energy release through the use of the J-integral. This method of analysis was developed by Pan and coworkers [54].

An important advantage of the blunt crack band model is that the direction of mesh lines need not be changed if the fracture runs in a skew direction. The crack band propagation criterion then requires some adjustment in order to give results that do not depend on mesh inclination.

We consider a rectangular mesh of mesh sizes Δx and Δy (Fig. 8). An inclined crack band is represented as a zig-zag crack band of overall orientation angle α_F. Let α_M be the orientation angle of the mesh lines x, and α_C be the direction of the cracks within the finite element (Fig. 9). We seek the effective width w_{ef} of a smooth crack band that is equivalent to the zig-zag band. Consider one cycle, of length ℓ, on the line connecting the centroids of the elements in the zig-zag band. The number of elements per cycle ℓ in the x-direction is $N_x = \ell \cos\alpha/\Delta x$, and the number of those in the y-direction is $N_y = \ell \sin\alpha/\Delta y$ in which $\alpha = |\alpha_F - \alpha_M|$ provided that $0 \leq \alpha \leq 90^o$. The area of the zig-zag band per cycle ℓ is $(N_x \Delta y)\, \Delta x + (N_y \Delta_x)\, \Delta y$. This area must equal the area $\ell\, w_{ef}$ of the equivalent smooth crack band, in order to assure the same energy content at the same stresses. This condition yields the effective width

$$w_{ef} = \Delta x \sin\alpha + \Delta y \cos\alpha \qquad (0 \leq \alpha \leq 90^o) \tag{9}$$

A somewhat different equation, giving similar results for $\alpha \leq 45^o$ has been used in previous work [13-15].

A different adjustment is needed when one considers a sudden stress drop and determines crack propagation directly from the energy change ΔU caused by extending the crack band into the next element. The propagation condition then is $\Delta U/\Delta a = -G_f$ where Δa is the length of extension of the crack band, which is equal to the mesh size h if the crack band propagates parallel to the mesh line [12, 13, 6]. In the case of a zig-zag band, Δa must be replaced by an effective crack band extension Δa_{ef} in the direction of the equivalent smooth crack band. We may assume Δa_{ef} to be the same for each crack band advance within the cycle ℓ in Fig. 8, whether this advance is in the x- or y-direction. Then $\Delta a_{ef} = \ell/N$ where $N = N_x + N_y$ = number of

elements per cycle ℓ. This condition yields

$$\Delta a_{ef} = \left(\frac{\cos \alpha}{\Delta x} + \frac{\sin \alpha}{\Delta y}\right)^{-1} \qquad (0 < \alpha < 90^{o}) \tag{10}$$

It has been demonstrated that the calculation results are objective not only with regard to the choice of element size but also with regard to the choice of mesh inclination relative to the fracture direction. Meshes of various inclination have been used to calculate the load— crack-length diagram for the rectangular panel considered before; they have been found to yield essentially the same results, except that the scatter (numerical errors) are somewhat larger for the zig-zag crack bands than for a smooth band; see Ref. 15.

It is one problem when the fracture direction is known and the zig-zag crack band is placed so as to conform to the average fracture direction, and another problem when the fracture direction is unknown in advance and a choice of the next element to crack must be made. The latter problem is obviously more difficult. It has been found that any finite element mesh, including a square mesh, is not entirely free of a directional bias. This bias is the strongest when the angle of fracture direction with the mesh line is small. For example, if a square mesh in the center-cracked rectangular panel is only moderately slanted (Fig. 8b), then the equivalent strength criterion with the effective width given by Eq. 8 indicates the crack band to extend straight along the mesh line, i.e., in the inclined direction, while correctly there should be side jumps so that the zig-zag band would, on the averate, conform to a horizontal direction. It appears rather difficult to avoid this type of bias. Various methods to avoid it are being studied [55-58]. Some search routines to determine which element

is the next to crack (the element straight ahead or the element on the left or on the right) are being investigated.

When concrete is reinforced, attention must also be paid to the question of bond slip of reinforcing bars embedded in concrete. It has been shown [13], that neglect of the bond slip is impossible, leading to unobjective results strongly dependent on the mesh size and converging to a physically incorrect solution. If no slip is considered to occur at the nodes between the bars and concrete, and if the element size is varied, then the stiffness of the connection between the opposite sides of a fracture changes with the mesh size and would approach infinity for a vanishing mesh size, thus preventing any crack propagation at all. In reality, due to a limit on the bond stress that can be transmitted on the surface of a steel bar, there is a certain bond slip length L_s on each side of a crack band. This length depends on the bar cross section A_b, ultimate bond force U_b', ratio n' of the elastic moduli of steel and concrete, stress σ_s in the bars at the point of crack band crossing, and the reinforcement ratio p (the bars are assumed to be spaced regularly and densely). The following expression was derived [13],

$$L_s = \frac{A_s}{U_b'} (\sigma_s - \sigma_s') \simeq \frac{A_b}{U_b'} \frac{1 - p}{1 - p + n'p} \sigma_s \tag{11}$$

For convenience of programming it is further possible to replace this actual bond slip length with an equivalent free bond-slip length L_s^* which coincides with a distance between certain two nodes within the mesh, and which permits neglecting the bond shear stresses that are difficult to model in a finite element code. The cross section area A_b must also be adjusted to a value A_b^*. The values of L_s^* and A_b^* are then determined from the condition that the extension of the steel bar over the length L_s, with bond shear stresses present, would be the same as the extension of a bar of cross section area A_b^* and length L_s^* with zero bond stresses; see Ref. 13.

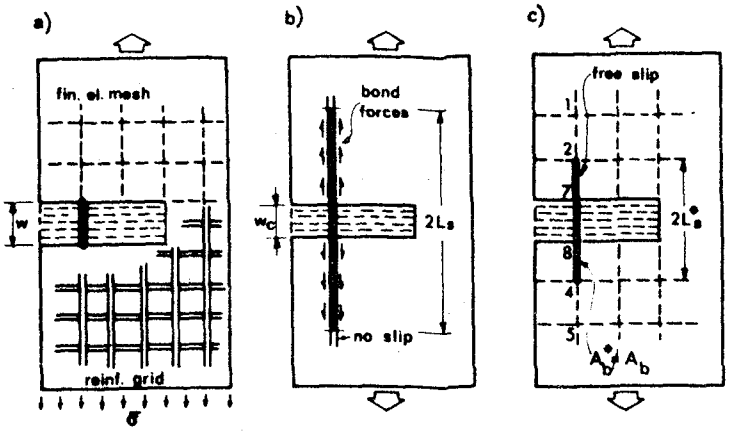

Fig. 9 - Illustrations of Bond Slip and Equivalent Free Bond Slip Length (after Bažant and Cedolin, 1980).

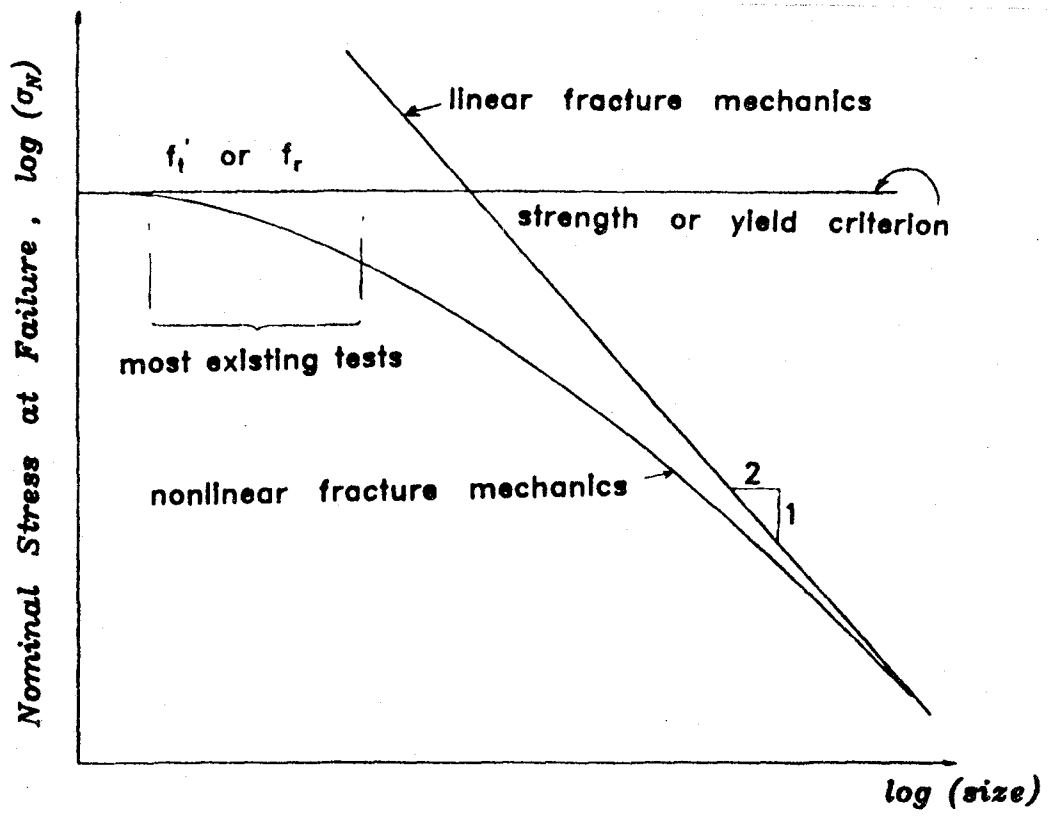

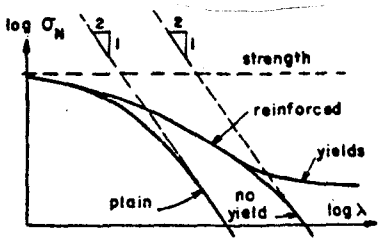

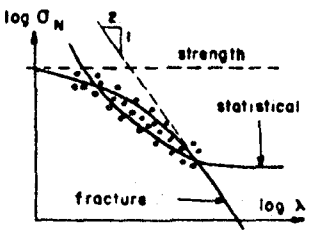

Fig. 10 - Various Theories for Structural Size Effect.

When reinforcement is used, the expression for the equivalent strength must also be adjusted. The following formula has been derived from energy release considerations [6, 15];

$$f'_{eq} = c_f \left(\frac{2G_f E_c}{w_{ef} r_f}\right)^{\frac{1}{2}} \left(1 + c_p \; n' \frac{p}{L_s^*} \cos\alpha_s\right) \qquad (12)$$

in which α_s = angle of the reinforcing bars with the normal to the crack band, and c_p is an empirical coefficient to be found by numerical calibration, i.e., comparisons of results for different mesh sizes [15].

It might be more realistic to treat reinforcement and bond slip by introducing two overlaid continuua, one representing the plane concrete, and one representing the reinforcement mesh. These continuua would be allowed to displace relative to each other and would transmit distributed volume forces from one to another, depending on the relative slip. This approach would be, however, much more complicated.

Structural Size Effect

The dispersed and progressive nature of cracking at the fracture front may be taken into account by introducing the following hypothesis [59]: The total potential energy release W caused by fracture in a given structure depends on both:

1) The length a of the fracture, and

2) The area of the cracked zone, a n d_a

in which n is a material constant characterizing the width of the cracking zone at the fracture front [11], n ≃ 3. The dependence of W upon crack length a describes that part of energy release that flows into the fracture front from the surrounding uncracked regions of the structure.

Parameters a and a_n d_a are not nondimensional. They are permitted to appear only in a nondimensional form, which is given by the following nondimensional parameters

$$\alpha_1 = \frac{a}{d}, \qquad \alpha_2 = \frac{\text{and}_a}{d^2} \tag{13}$$

They represent the nondimensional fracture length and the nondimensional area of the crack zone. Furthermore, W must be proportional to volume $d^2 b$ of the structure, b denoting the thickness, and to the characteristic energy density $\sigma_N^2/2\ E_c$ in which $\sigma_N = P/bd$ = nominal stress at failure, P = given applied load, and d = characteristic dimension of the structure. Consequently, we must have

$$W = \frac{1}{2E_c}\left(\frac{P}{bd}\right)^2 bd^2\ f(\alpha_1, \alpha_2, \xi_i) \tag{14}$$

in which f is a certain continuous and continuously differentiable positive function, and ξ_i represent ratios of the structure dimensions characterizing the shape of the structure.

To illustrate the structural size effect, we now consider structures of different sizes but geometrically similar shape, including the same ratio of fracture length to the characteristic dimension of the structure, and the same reinforcement ratio. Under this assumption, the shape parameters ξ_i are constant. Using the energy criterion for crack band propagation, $\partial W/\partial a = G_f\ b$, in which G_f is the fracture energy, we obtain (for constant ξ_i) $\partial f/\partial a = f_1(\partial\alpha_1/\partial a) + f_2\ (\partial\alpha_2/\partial a)$ where we introduce the notations $f_1 = \partial f/\partial\alpha_1$, $f_2 = \partial f/\partial\alpha_2$. Substitution of Eq. 12 into Eq. 13 then yields

$$\left(\frac{f_1}{d} + \frac{f_2\, n d_a}{d^2} \right) \frac{P^2}{2bE_c} = G_f\, b \tag{15}$$

Here the fracture energy may be expressed as the area under the tensile stress-strain curve, i.e., $G_f = n\, d_a\, (1 - E_c/E_t)\, f_t'^2/2E_c$, in which E_c is the initial Young's elastic modulus of concrete, E_t is the mean strain-softening modulus, which is negative, and f_t' is the direct tensile strength of concrete. Substituting this expression for G_f together with the relation $P = \sigma_N\, bd$* into Eq. 14, we finally obtain

$$\sigma_N = Bf_t' \left(1 + \frac{d}{\lambda_0 d_a} \right)^{\frac{1}{2}} \tag{16}$$

in which $B = [(1 - E_c/E_t)/f_2]^{\frac{1}{2}}$, $\lambda_0 = mf_2/f_1$. B and λ_0 are constants when geometrically similar structures of different sizes are considered. In the plot of log σ_N versus $\log(d/d_a)$ where d/d_a is the relative structure size, Eq. 18 is represented by the curve shown in Fig. 10. If the structure is very small, then the second term in the parenthesis in Eq. 15 is negligible compared to 1, and $\sigma_N = B\, f_t'$ is the condition characterizing failure, representing the strength criterion which in Fig. 10 corresponds to a horizontal line. This special case is obtained if W depends only on the crack-zone area but not on the fracture length. If the structure is very large, then 1 is negligible compared to the second term in the parenthesis of Eq. 15. Then $\sigma_N = \text{const.}/\sqrt{d}$. This is the type of size effect known to apply for linear elastic fracture mechanics. Thus, linear elastic fracture mechanics must always apply for a sufficiently large concrete structure. It is interesting to note also that the preceding nondimensional analysis yields this limiting case when the starting hypothesis includes only dependence of W on the fracture length but not on the cracked zone area. In Fig. 15 the limiting case of linear fracture mechanics is represented by the straight line of downward slope - 1/2.

*Here σ_N = nominal stress at failure.

The size effect in concrete structures failing due to cracking of concrete represents, as we have shown, a gradual transition from the strength criterion to the energy criterion of linear fracture mechancis. Unfortunately, among the numerous test data on fracture of plain concrete as well as on brittle failures of concrete structures, as reported in the literature, only a very small fraction involves fractures of specimens of sufficiently different sizes to check our preceding conclusion. From fracture testing of plain concrete, the size effect may be checked from the test data of Walsh [47] (Fig. 6). A very good agreement with Eq. 15 is found from these data. As for brittle failure of concrete structures, a check can be made using certain data for the diagonal shear failures of concrete beams with longitudinal reinforcement but without stirrups. Results of such tests are shown in Fig. 11 for test data from Refs. 61-67. In spite of the large scatter, due to comparing test data from different laboratories for different concretes, the declining trend is obvious. A horizontal line, corresponding to the strength criterion (as well as to the present ACI or CEB-FIP codes), is contradicted by the test data. At the same time, however, one can clearly see a substantial deviation from the straight line representing linear elastic fracture mechanics. For more detail, see Ref. 60.

In the preceding analysis we have not paid any particular attention to reinforcement. If a densely and regularly distributed reinforcement is present, one finds that the size effect is again governed by Eq. 15, however, with different constants, provided that the reinforcement remains elastic. Compared to plain concrete, the asymptotic straight line for linear elastic fracture mechanics is pushed in the plot of Fig. 10 toward the right, i.e., there exists a greater range of sizes for which the strength criterion applies.

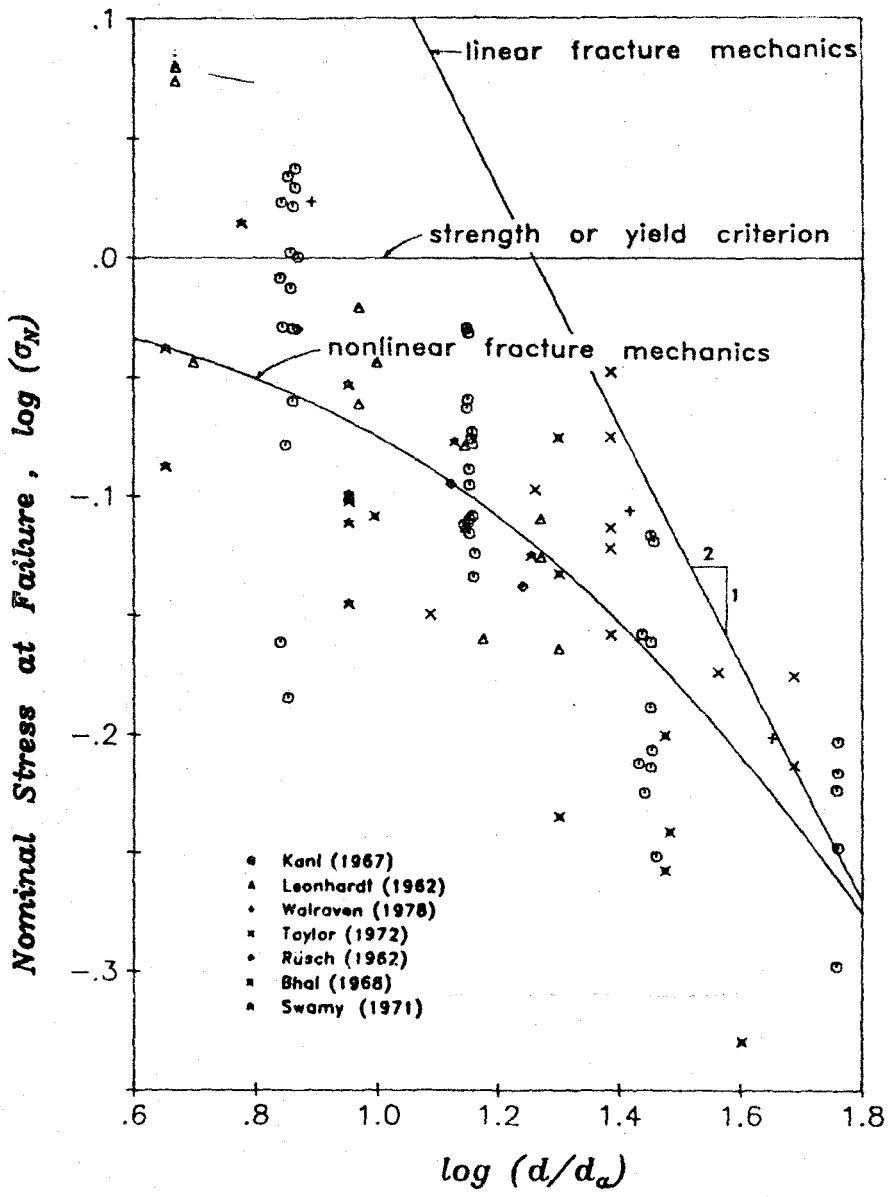

Fig. 11 - Test Data From Various Laboratories on Diagonal Shear Failure of Beams Reinforced Longitudinally but Without Stirrups (after Bažant and Kim, 1983).

Nevertheless, for sufficiently large structures, a transition to the size effect of linear fracture mechanics does occur. This conclusion, however, is true only if the reinforcement does not yield. If it does, then there is another transition in Fig. 10 to a horizontal asymptote (see Ref. 59).

The decrease of nominal stress at failure with the structure size has been explained in the past as a statistical phenomenon. The strength of concrete is randomly variable, and in a larger structure there is a greater chance of encountering a smaller strength, which could explain the size effect. However, since the random variations occur only within certain representative volumes of small size, the statistical size effect must lead to a horizontal asymptote. Thus, the asymptotic behavior is totally different from that we obtained for fracture mechanics. Needless to say, the fracture-type size effect appears to be the correct one.

Other Aspects

For some types of loading, especially those in dynamics, the principal tensile stress may initially cause only a partial cracking and fracture may be completed later under a principal tensile stress of a different direction. For such situations, a softening stress-strain relation that can be applied for a general loading path with rotating principal stress directions is needed. An attractive method to develop such a stress-strain relation is the microplane model [68, 69]. In this model, analogous to the well-known slip theory of plasticity [70, 71], one specifies the constitutive relation between the stresses and strains acting within the microstructure on a plane of any orientation. No tensorial invariance restrictions need to be satisfied by this relation, since they are satisfied subsequently by a suitable combination of microplanes of all possible orientations. It appeas that for the

modeling of progressive fracture, the strains from all microplanes must be constrained to the same macroscopic strain tensor, and requiring that the energy dissipation must be the same whether expressed macroscopically or microscopically, one finds that the inelastic stress relaxations from all microplanes must be superimposed, evaluating a certain integral over a unit hemisphere. This model has been shown [69] to be able to represent tensile strain softening of concrete. Furthermore, it was shown that the same model can describe the shear resistance of cracks and their dilatancy caused by shear [72].

While the microplane model represents a refinement of the crack band model, a simplified approach is also of interest. It has been recently investigated whether concrete fracture can be predicted by an approximate equivalent linearly elastic fracture analysis based on the concept of R-curves (resistance curves) known from fracture analysis of metals [73]. This approach is based on two hypotheses: 1) for the purpose of determining the energy release rate, the crack length a is not required to represent the actually measured crack length but permits a to be any fictitious crack length. 2) The fracture energy G_c is not a constant but varies as a function of the extension c of the fictitious crack from the body surface or a notch ($c = a - a_0$ where a_0 = notch length; Fig. 12). In the second hypothesis, the dependence of fracture energy on crack extension is supposed to be unique, as proposed for metals by Krafft et al. [50, 31]. This is certainly a simplification, since in reality the R-curve is different for different body geometries, different loading arrangements, different loading paths, etc., and indeed the R-curves calculated by finite elements from the blunt crack band theory as explained before exhibit such a dependence. Nevertheless,

for many situations, a unique curve of fracture energy versus crack extension, called the R-curve, is an acceptable approximation (Fig. 12).

In the R-curve approach, the critical state of failure is obtained when the following two conditions are satisfied [31]:

$$W'(a) = G_c(c), \qquad \frac{\partial W'(a)}{\partial a} = \frac{\partial G_c(c)}{\partial c} \tag{17}$$

in which $W'(a) = \partial W/\partial a$ = energy release rate of the body, and $c = a - a_0$. In elastic fracture mechanics, the energy release rate function has the form $W'(a) = P^2 W_1'(a)$, in which $W_1'(a)$ is the energy release rate function for $P = 1$. Substituting this relation into Eq. 16, one has two equations for two unknowns c and the failure load P. These two equations are nonlinear and have to be solved iteratively. However, if the function $G_c(c)$ is assumed to be a parabola and the function $W_1'(a)$ to be a straight line, then Eq. 15 can be reduced to a single quadratic equation for P [31].

The bulk of fracture test data was analyzed using the R-curve approach [73]. Various algebraic expressions have been used for the R-curve $G_c(c)$, including an exponential curve with a horizontal asymptote, a segment of a parabola terminating at its apex, after which a horizontal line follows, and a bilinear diagram. By statistical analysis of the test data available from the literature, it was found that the precise shape of the R-curve cannot be determined. The optimum fits were about equally good with the aforementioned expressions as well as other expressions. Only the initial value of G_c, the final value G_f and the overall slope, were found to be of importance. This conclusion implies that it makes no sense trying to develop sophisticated differential equations for determining the shape of the R-curves.

Therefore, the expression for the R-curve should be chosen from the viewpoint of convenience, and from this viewpoint the parabolic formula is probably best, since it yields a quadratic equation for P. Fig. 13 reproduces a plot from Ref. 73 of the theoretical versus measured values of P at failure, normalized with regard to the failure load P_0 calculated from the strength theory. The parabolic formula is used in this comparison. If the theory were perfect, the data points would have to fall on a straight line through the origin, of slope 1. The deviations from such a strain line are the measures of the error. Their coefficient of variation is only 0.06, which means that a very good approximation of the existing test results is possible.

The R-curve can be sufficiently characterized by three parameters, its initial and final values and the mean slope of the rising segment. These three material characteristics can be easiest determined by carrying out maximum load tests for three substantially different test specimens. Best probably are geometrically similar specimens of substantially different sizes. Measurements other than maximum load values are then not needed, which is a significant advantage of this approach. It is very difficult to measure other quantities such as the crack length and opening, loading and unloading compliancies at the critical state, etc., and it is attractive for practical applications to be able to avoid such measurements.

For concrete structures, it is of importance to model not only isolated fractures but also systems of cracks. Of particular interest is the system of parallel equidistant cracks which forms under a uniform tensile loading of a panel reinforced by a mesh of bars, or in a beam with longitudinal reinforcement subjected to tension or bending. For the parallel crack system,

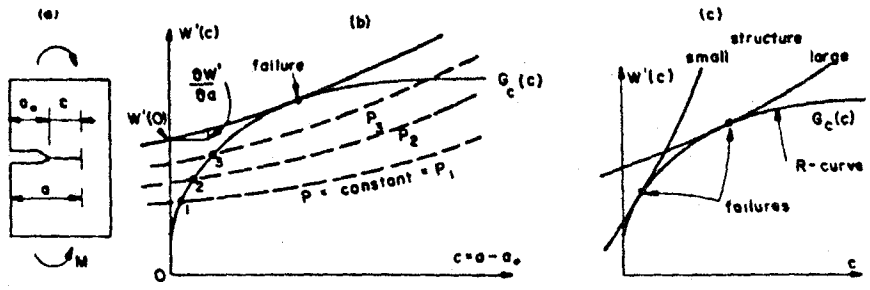

Fig. 12 - Determination of Failure with the Help of R-Curve.

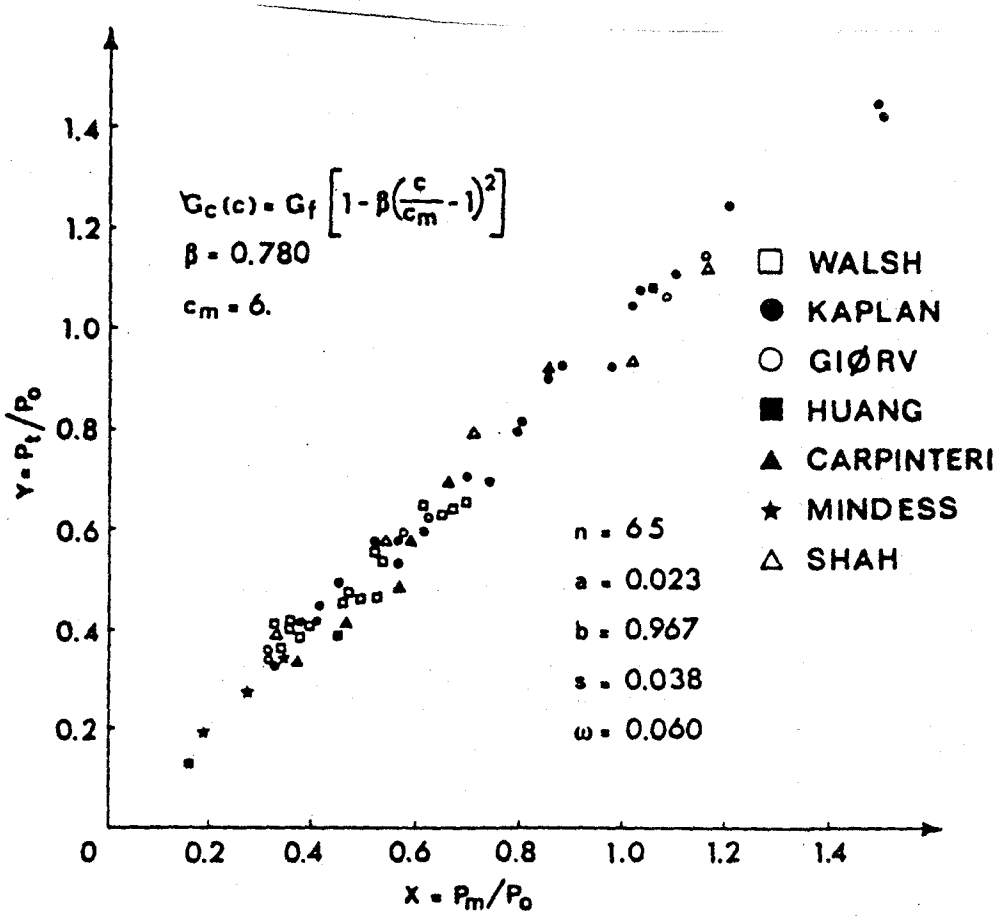

Fig. 13 - Statistical Linear Regression of Measured Failure Loads Versus Theoretical Ones.

it is necessary to determine the spacing of the cracks, after which the crack width can be estimated, and also the overall strain at which the cracks form. This problem has been traditionally analyzed on the basis of strength criteria, coupled with the conditions of bond slip. However, the strength criteria govern only the initiation of microcracking, since they pertain to the peak point of the tensile stress-strain diagram. For a complete crack formation, strain-softening must reduce the stress to zero, which means that the full strain energy under the tensile stress-strain diagram must be dissipated. Therefore, complete crack formation should properly be calculated from energy fracture criteria. This approch has been taken in Ref. 74, and simplified formulas for the crack spacing based on energy analysis were determined. Since the cracks are usually spaced rather closely compared to the maximum aggregate size, the energy balance conditions have not been written for the formation of the crack over its entire length. The formulas obtained from this fracture mechanics approach agreed reasonably well with the scant test data on crack spacing and crack width available in the literature.*

Crack width is rather important for the shear transmission capability of cracks in concrete, which is essential for the load carrying capability of concrete structures. The shear response of cracks in concrete may be characterized by an incremental relation expressing the increments of the normal and shear stress transmitted across a crack as a function relative displacement (opening) and the tangential relative displacement (slip); see Ref. 75.

---

*Aside from energy balance, the evolution of crack spacing of a growing crack system is also governed by certain stability conditions; see Ref. 76.

Conclusions

After a period of doubts regarding the applicability of fracture mechanics to concrete, it has now become clearly established that fracture mechanics does apply. However, a nonlinear form of fracture mechanics which takes into account the existance of a large fracture process zone ahead of the fracture front must be used. An attractive formulation is the crack band model, which is particularly suited for finite element analysis. Nevertheless, many questions remain open and much further research is needed.

Acknowledgment

Partial financial support from the U. S. National Science Foundation under grant CEE-8303148 is gratefully acknowledged. Mary Hill deserves thanks for her very prompt and careful typing of the manuscript.

References

1. Wittmann, F. H., (Editor), Fracture Mechanics of Concrete, Elsivier, Netherlands, 1983.

2. Mindess, S., "The Application of Fracture Mechanics to Cement and Concrete: A Historical Review," Chapter in State-of-the-Art Report of RILEM Technical Committee 50-FMC on "Fracture Mechanics of Concrete," ed. by F. H. Wittmann, Elsevier, Netherlands, 1983.

3. Ingraffea, A., chapter in "Fracture Mechanics Applied to Concrete Structures," ed. by G. C. Sih, Martinus Nijhoff Publishers, B.V., The Hague, Netherlands - in press.

4. Shah, S. P., chapter in "Fracture Mechanics Applied to Concrete Structures," ed. by G. C. Sih, Martinus Nijhoff Publishers, B.V., The Hague, Netherlands, - in press.

5. ASCE State-of-the-Art Report on "Finite Element Analysis of Reinforced Concrete," prepared by a Task Committee chaired by A. Nilson, Am. Soc. of Civil Engrs., New York, 1982.

6. Bazant, Z. P., "Mechanics of Fracture and Progressive Cracking in Concrete Structures," chapter in "Fracture Mechanics Applied to Concrete Structures," ed. by G. C. Sih, Martinus Nijhoff Publishers B.V., The Hague, Netherlands, - in press.

7. Rashid, Y. R., "Analysis of Prestressed Concrete Pressure Vessels," Nuclear Engng. and Design, Vol. 7, No. 4, April 1968, pp. 334-344.

8. Bazant, Z. P., "Instability, Ductility and Size Effect in Strain-Softening Concrete," J. of the Engineering Mechanics Division ASCE, Vol. 102, Apr. 1976, No. EM2, pp. 331-344 - Paper 12042.

9. Bazant, Z. P., and Panula, L., "Statistical Stability Effects in Concrete Failure," J. of the Engineering Mechanics Division, ASCE, Vol. 104. Oct. 1978, No. EM5, pp. 1195-1212, Paper 14074.

10. Bazant, Z. P., "Crack Band Model for Fracture of Geomaterials," Proc., 4th Intern. Conf. on Numerical Methods in Geomechanics, held in Edmonton, Alberta, Canada, June 1982, ed. by Z. Eisenstein, Vol. 3.

11. Bazant, Z. P., and Oh, B. H., "Crack Band Theory for Fracture of Concrete," Materials and Structures (RILEM, Paris), Vol. 16, 1983, in press (based on Ref. 130).

12. Bazant, Z. P., and Cedolin, L., "Blunt Crack Band Propagation in Finite Element Analysis," Journal of the Engineering Mechanics Division, ASCE, Vol. 105, No. EM2, Proc. Paper 14529, April 1979, pp. 297-315.

13. Bazant, Z. P., and Cedolin, L., "Fracture Mechanics of Reinforced Concrete," Journal of the Engineering Mechanics Division, ASCE, Vol. 106, No. EM6, Proc. Paper 15917, December 1980, pp. 1287-1306; with Discussion and Closure in Vol. 108, 1982, EM., pp. 464-471.

14. Cedolin, L., and Bazant, Z. P., "Effect of Finite Element Choice in Blunt Crack Band Analysis," Computer Methods in Applied Mechanics and Engineering, Vol. 24, No. 3, December 1980, pp. 305-316.

15. Bazant, Z. P., and Cedolin, L., "Finite Element Modeling of Crack Band Propagation," Journal of Structural Engineering, ASCE, Vol. 109, No. ST2, Feb. 1983, pp. 69-92.

16. Bazant, Z. P., Pfeiffer, P., Marchertas, A. H., "Blunt Crack Band Propagation in Finite Element Analysis for Concrete Structures," Preprints 7th Int. Conf. on Structural Mechanics in Reactor Technology, Chicago, Aug. 1983.

17. Bazant, Z. P., and Oh, B. H., "Rock Fracture via Stress-Strain Relations," Concrete and Geomaterials, Report No. 82-11/665r, Northwestern University, Evanston, Illinois, Nov. 1982.

18. Mindess, S., and Diamond, S., "A Preliminary SEM Study of Crack Propagation in Mortar," Cement and Concrete Research, Vol. 10, 1980, pp. 509-519.

19. Cedolin, L., Dei Poli, S., and Iori, L., "Experimental Determination of the Fracture Process Zone in Concrete," Cement and Concrete Research, Vol. 13, 1983 - to appear.

20. Cedolin, L., Dei Poli, S., and Iori, L., "Experimental Determination of the Stress-Strain Curve and Fracture Zone for Concrete in Tension," Proc., Int. Conf. on Constitutive Laws for Engineering Materials, ed. by C. Desai, University of Arizona, Tucson, January 1983.

21. Barenblatt, G. I., "The Formation of Equilibrium Cracks During Brittle Fracture, General Ideas and Hypothesis. Axially-Symmetric Cracks," Prikladnaya Matematika i Mekhanika, Vol. 23, No. 3, 1959, pp. 434-444.

22. Dugdale, D. S., "Yielding of Steel Sheets Containing Slits," J. Mech. Phys. Solids, Vol. 8, 1960, pp. 100-108.

23. Kfouri, A.P., and Miller, .K. J., "Stress Displacement, Line Integral and Closure Energy Determinations of Crack Tip Stress Intensity Factors," Int. Journal of Pres. Ves. and Piping, Vol. 2, No. 3, July 1974, pp. 179-191.

24. Kfouri, A. P., and Rice, J. R., "Elastic/Plastic Separation Energy Rate for Crack Advance in Finite Growth Steps," in "Fracture 1977" (Proc. of the 4th Intern. Conf. on Fracture, held in Waterloo, Ontario, June 1977), ed. by D. M. R. Taplin, University of Waterloo Press 1977, Vol. 1, pp. 43-59.

25. Knauss, W. C., "On the Steady Propagation of a Crack in a Viscoelastic Sheet; Experiments and Analysis," in The Deformation in Fracture of High Polymers, ed. by H. H. Kausch, Pub. Plenum Press, 1974, pp. 501-541.

26. Wnuk, M. P., "Quasi-Static Extension of a Tensile Crack Contained in Viscoelastic Plastic Solid," Journal of Applied Mechanics, ASME, Vol. 41, 1974, No. 1, pp. 234-248.

27. Hillerborg, A., Modéer, M., and Petersson, P. E., "Analysis of Crack Formation and Crack Growth in Concrete by Means of Fracture Mechanics and Finite Elements," Cement and Concrete Research, Vol. 6, 1976, pp. 773-782.

28. Petersson, P. E., "Fracture Energy of Concrete: Method of Determination," Cement and Concrete Research, Vol. 10, 1980, pp. 78-89, and "Fracture Energy of Concrete: Practical Performance and Experimental Results," Cement and Concrete Research, Vol. 10, 1980, pp. 91-101.

29. Knott, J. F., "Fundamentals of Fracture Mechanics," Butterworths, London, England, 1973.

30. Parker, A. P., "The Mechanics of Fracture and Fatigue, E. & F. N. Spon, Ltd. - Methuen, London, 1981.

31. Broek, D., "Elementary Engineering Fracture Mechanics," Noordhoff International Publishing, Leyden, Netherlands, 1974.

32. Evans, R. H., and Marathe, M. S., "Microcracking and Stress-Strain Curves for Concrete in Tension," Materials and Structures (RILEM, Paris), No. 1, Jan.-Feb., 1968, pp. 61-64.

33. Brown, J. H., "Measuring the Fracture Toughness of Cement Paste and Mortar," Magazine of Concrete Research, Vol. 24, No. 81, December 1972, pp. 185-196.

34. Carpinteri, A., "Experimental Determination of Fracture Toughness Parameters K_{IC} and J_{IC} for Aggregative Materials," Advances in Fracture Research," (Proc., 5th International Conference on Fracture, Cannes, France, 1981) ed. by D. Francois, Vol. 4, pp. 1491-1498.

35. Carpinteri, A., "Static and Energetic Fracture Parameters for Rocks and Concretes," Report, Instituto di Scienza delle Costruzioni-Ingegneria, University of Bologna, Italy, 1980.

36. Entov, V. M., and Yagust, V. I., "Experimental Investigation of Laws Governing Quasi-Static Development of Macrocracks in Concrete,: Mechanics of Solids (translation from Russian), Vol. 10, No. 4, 1975, pp. 87-95.

37. Gjørv, O. E., Sørensen, S. I., and Arnesen, A., "Notch Sensitivity and Fracture Toughness of Concrete," Cement and Concrete Research, Vol. 7, 1977, pp. 333-344.

38. Huang, C. M. J., "Finite Element and Experimental Studies of Stress Intensity Factors for Concrete Beams," Thesis Submitted in Partial Fulfillment of the Requirements for the Degree of Doctor of Philosophy, Kansas State University, Kansas, 1981.

39. Kaplan, M. F., "Crack Propagation and the Fracture of Concrete," American Concrete Institute Journal, Vol. 58, No. 11, November 1961.

40. Kesler, C. E., Naus, D. J., and Lott, J. L., "Fracture Mechanics - Its Applicability to Concrete," International Conference on the Mechanical Behavior of Materials, Kyoto, August 1971.

41. Mindes, S., Lawrence, F. V., and Kesler, C. E., "The J-Integral As a Fracture Criterion for Fiber Reinforced Concrete," Cement and Concrete Research, Vol. 7, 1977, pp. 731-742.

42. Naus, D. J., "Applicability of Linear-Elastic Fracture Mechanics to Portland Cement Concretes," Thesis Submitted in Partial Fulfillment of the Requirements for the Degree of Doctor of Philosophy, University of Illinois at Urbana-Champaign, 1971.

43. Shah, S. P., and McGarry, F. J., "Griffith Fracture Criterion and Concrete," Journal of the Engineering Mechanics Division, ASCE, Vol. 97, No. EM6, Proc. Paper 8597, December 1971, pp. 1663-1676.

44. Shah, S. P., chapter in "Fracture Mechanics Applied to Concrete Structures," ed. by G. C. Sih, Martinus Nijhoff Publishers, B.V., The Hague, Netherlands, - in press.

45. Sok, C., Baron, J., and Francois, D., "Mécanique de la Rupture Appliquée au Beton Hydraulique," Cement and Concrete Research, Vol. 9.

46. Swartz, S. E., Hu, K. K., Fartash, M., and Huang, C. M. J., "Stress Intensity Factors for Plain Concrete in Bending - Prenotched Versus Precracked Beams," Report, Department of Civil Engineering, Kansas State University, Kansas, 1981.

47. Walsh, P. F., "Fracture of Plain Concrete,: The Indian Concrete Journal, Vol. 46, No. 11, November 1979, pp. 469, 470, and 476.

48. Wecharatana, M., and Shah, S. P., "Resistance to Crack Growth in Portland Cement Composites," Report, Department of Material Engineering, University of Illinois at Chicago, Chicago, Illinois, Nov. 1980.

49. Petersson, P. C., "Crack Growth and Development of Fracture Zones in Plain Concrete and Similar Materials," Doctoral Dissertation, Lund Institute of Technology, Lund, Sweden, Dec. 1981.

50. Krafft, J. M., Sullivan, A. M., Boyle, R. W., "Effect of Dimensions on Fast Fracture Instability of Notched Sheets," Cranfield Symposium, 1961, Vol. I, pp. 8-28.

51. Evans, R. H., and Marathe, M. S., "Microcracking and Stress-Strain Curves for Concrete in Tension," Materials and Structures (RILEM, Paris), No. 1, Jan.-Feb., 1968, 61-64.

52. Heilmann, H. G., Hilsdorf, H. H., and Finsterwalder, K., "Festigkeit und Verformung von Beton unter Zugspanungen," Deutscher Ausschuss für Stahlbeton, Heft 203, W. Ernst & Sohn, West Berlin, 1969.

53. Rüsh, H., and Hilsdorf, H., "Deformation Characteristics of Concrete Under Axial Tension," Voruntersuchungen, Bericht Nr. 44, Munich, May 1963.

54. Pan, Y. C., Marchertas, A. H., and Kennedy, J. M., "Finite Element of Blunt Crack Band Propagation," A Modified J-Integral Approach, Preprints 7th Intern. Conf. on Structural Mechanics in Reactor Technology, Paper H, Chicago, Aug. 1983.

55. Marchertas, A. H., Kulak, R. F., and Pan. Y. C., "Performance of Blunt Crack Approach Within a General Purpose Code," in Nonlinear Numerical Analysis of Reinforced Concrete, ed. by L. E. Schwer, Am. Soc. of Mech. Engrs., New York 1982, (presented at ASME Winter Annual Meeting, Phoenix, Nov. 1982), pp. 107-123.

56. Pan, Y. C., and Marchertas, A. H., Private Communication, May 1983, at Argonne National Laboratory, Argonne, IL.

57. Bažant, Z. P., and Pfeiffer, P., "Finite Element Crack Band Analysis," in preparation.

58. Bažant, Z. P., Pfeiffer, P., and Marchertas, A. H., "Blunt Crack Band Propagation in Finite Element Analysis for Concrete Structures," Preprints 7th Int. Conf. on Structural Mechanics in Reactor Technology, Chicago, Aug. 1983.

59. Bažant, Z. P., "Size Effect in Brittle Failure of Concrete Structures," Report No. 83-2/665s, Center for Concrete and Geomaterials, Northwestern University, Evanston, Illinois, Feb. 1983.

60. Bažant, Z. P., and Kim. J. K., "Size Effect in Shear Failure of Reinforced Concrete Beams," Report No. 83-5/428s, Center for Concrete and Geomaterials, Northwestern University, Evanston, Illinois, May 1983.

61. Kani, G. N. J., "Basic Facts Concerning Shear Failure," Part I and Part II, J. of ACI, Vol. 63, No. 6, June 1966, pp. 675-692.

62. Leonhardt, F., and Walther, R., "Beiträge zur Behandlung der Schubprobleme im Stahlbetonbau," Beton-u Stahlbetonbau, Vol. 56, No. 12 (1961), Vol. 57 No. 2, 3, 6, 7, 8, (1962), Vol. 58, No. 8, 9 (1963).

63. Bhal, N. S., "Über den Einfluss der Balkenhöhe auf Schubtragfähihkeit von einfeldrigen Stahlbetonbalken mit und ohne Schubbewehrung, Dissertation, Universität Stuttgärt, 1968.

64. Walraven, J. C., "The Influence of Depth on the Shear Strength of Lightweight Concrete Beams without Shear Reinforcement," Stevin Laboratory Report No. 5-78-4, Delft University of Technology 1978.

65. Taylor, H. P. J., "The Shear Strength of Large Beams," J. of the Structural Division ASCE, Vol. 98, 1972, pp. 2473-2490.

66. Rüsch, M., Haugli, F. R., and Mayer, M., "Schubversuche an Stahlbeton Rechteckbalken mit Gleichmässig Verteilter Belastung," Deutscher Ausschuss für Stahlbeton, Heft 145, W. Ernst u. Sohn, West Berlin 1962.

67. Swamy, R. N., and Qureshi, S. A., "Strength, Cracking and Deformation Similitude in Reinforced T-Beams under Bending and Shear," Part I and II, J. of Am. Concrete Inst., Vol. 68, No. 3, 1971, pp. 187-195.

68. Bazant, Z.P., and Oh, B. H., "Microplane Model for Fracture Analysis of Concrete Structures," Proc. Symp. on the "Interaction of Nonnuclear Munitions with Structures," U. S. Air Force Academy, Colorado Springs, May 1983, pp. 49-55.

69. Bazant, Z. P., and Oh, B. H., "Model of Weak Planes for Progressive Fracture of Concrete and Rock," Report No. 83-2/448m, Center for Concrete and Geomaterials, Northwestern University, Evanston, Il., Feb. 1983.

70. Taylor, G. I., "Plastic Strain in Metals," J. Inst. Metals, Vol. 63, 1938, pp. 307-324.

71. Batdorf, S. B., and Budiansky, B., "A Mathematical Theory of Plasticity Based on the Concept of Slip," NACA TN 1871, April, 1949.

72. Bazant, Z. P., and Gambarova, P., "Crack Shear in Concrete: Crack Band Microplane Model", in preparation.

73. Bazant, Z. P., and Cedolin, L., "Approximate Linear Analysis of Concrete Fracture by R-Curves," Report No. 83-7/679a, Center for Concrete and Geomaterials, Technological Institute, Northwestern University, Evanston, Illinois, July 1983.

74. Bazant, Z. P., and Oh, B. H., "Spacing of Cracks in Reinforced Concrete," J. of Engng. Mech. ASCE.

75. Bazant, Z. P., and Gambarova, P., "Rough Cracks in Reinforced Concrete," J. of the Struct. Div., Proc. ASCE, Vol. 106, 1980, pp. 819-842; Disc. pp. 2579-2581.

76. Bazant, Z. P., Ohtsubo, H., Aoh, K., "Stability and Post-Critical Growth of a System of Cooling or Shrinkage Cracks," International Journal of Fracture, Vol. 15, No. 5., Oct. 1979, pp. 443-456.

Effect of Pore Fluid Diffusion on Deformation and Failure of Rock

by

J.W. Rudnicki
Department of Civil Engineering
Northwestern University
Evanston, Illinois 60201

INTRODUCTION

The presence of pore fluid in laboratory rock samples or fissured rock masses can substantially alter the response to applied or induced loads and the conditions for failure. Pore fluid effects have been proposed as playing a role in a wide variety of geophysical and geotechnical phenomena. These include the following: migration of aftershocks (Nur and Booker, 1972; Booker, 1974); fault creep (Rice and Simons, 1976; Rice, 1979a); earthquake precursory processes (Nur, 1972; Anderson and Whitcomb, 1975; Scholz et al., 1973; Rudnicki, 1977, 1979; Rice and Rudnicki, 1979) hydraulic fracture (Rice and Cleary, 1976; Ruina, 1978; Cleary, 1979); water level changes in wells (Johnson, et al., 1973); induced seismicity (Bell and Nur, 1978; Simpson, 1976; Raleigh et al., 1976; Ohtake, 1974; Zoback and Hickman, 1982); wave speed travel time delays (Leary et al., 1979) and migration of earthquake swarms (Johnson, 1979).

The most familiar effect of the pore fluid is to reduce the effective value of the mean normal compressive stress. This effect is usually expressed in terms of so-called effective stress laws: the effect of the pore fluid on some aspect of the mechanical behavior can be incorporated by replacing the stress by the effective stress, a linear combination of the stress and pore fluid pressure. Because the inelastic deformation of many geological materials is inhibited by an increase of hydrostatic compression, an increase in pore fluid pressure decreases the effective compressive stress and promotes further inelastic deformation. Conversely, a decrease in pore fluid pressure tends to inhibit further inelastic deformation.

Coupling of deformation with pore fluid diffusion also introduces time dependence into the response of an otherwise rate-independent solid. An elastic fluid-infiltrated solid responds more stiffly to deformations that are

rapid compared to the time scale of diffusion than for deformations that are slow compared to the diffusion time. Because many geological materials change volume when sheared inelastically, pore fluid diffusion can also be coupled to inelastic deformation. A volume increase due to microcracking and opening of pore space, as is typical of brittle rocks deformed in compression, tends to decrease the local pore fluid pressure. If the creation of new pore space occurs slowly, the tendency for the pore fluid pressure to decrease will be alleviated by fluid mass flux. If, however, new pore space is created more rapidly than fluid mass can diffuse into it, then the pore fluid pressure decreases, increasing the effective stress, and inhibiting further inelastic deformation.

This review considers the mechanical effects of pore fluid on the deformation and failure of geological and geotechnical materials. Applications to brittle rock and, more specifically, to earth faulting are emphasized. For the purpose of this article the subject is divided into those effects that can be treated on the basis of Biot's (1941a) formulation for a linear elastic fluid-infiltrated porous solid and those that arise from inelastic volume changes. Several other recent review articles also treat this subject. Reviews by Rice (1979a, 1980, 1981) on the mechanics of earthquake rupture and precursory processes have included discussion of pore fluid effects. Rudnicki (1980), in a review of fracture mechanics applied to the earth's crust, has discussed coupled deformation diffusion effects in fault propagation, and Rudnicki (1981) has reviewed the stabilizing effects of coupled deformation and diffusion on an inclusion model of faulting. Paterson (1978) has given a concise review of experimental work up to 1977.

LINEAR ELASTIC FLUID-INFILTRATED POROUS SOLID

The governing equations for a linear elastic fluid-infiltrated solid have been established by Biot (1941a). Although obviously an idealization of the behavior of rocks, this theory has proved rich enough to provide insight into a wide variety of physical phenomena. At the same time, the complexity of the equations is such that the number of solutions is not great. More elaborate theories--many derived from mixture theory--have been proposed, but they offer few advantages over the Biot approach. Uncertainties about material parameters and difficulties of solution argue against pursuing overly intricate theories at this time. Until recently, very few solutions to the fully coupled Biot equations have existed. These include solutions for surface loading of half-spaces (Biot, 1941b; Biot and Clingan, 1941; McNamee and Gibson, 1960,a,b) and for the response of planar acquifers (Verruijt, 1968) and spherically symmetric pressurized cavities (Cryer, 1963). However, the possible role of coupled deformation diffusion effects in earth faulting has provided motivation to develop additional solutions.

The next subsection reviews the governing equations of the Biot theory. Rice and Cleary (1976) have given an appealing reformulation of the Biot theory and the description to be given here closely follows their point of view. After a brief subsection discussing material parameters of the Biot theory, a sampling of recent solutions and applications is given in the succeeding subsections.

Governing Equations

Let σ_{ij} denote the total stress so that $n_i\sigma_{ij}$ is the force per unit area, including both solid and fluid phases, with unit normal n_i. Although some authors prefer to decompose the stresses into portions acting separately on the solid and fluid phases, that is unnecessary and yields no advantage.

Deformations can be described by the strains of the solid matrix ε_{ij}. Two additional variables are needed to include the effects of the pore fluid. These are chosen to be the pore fluid pressure p and the fluid mass content per unit volume m. It is often convenient to express m as the product of the mass density of homogeneous pore fluid ρ and an apparent volume fraction of voids v, i.e. $m = \rho v$. The pore fluid pressure is defined as the pressure in an imaginary reservoir of homogeneous pore fluid that would be needed to prevent any fluid mass flux to or from the reservoir when it is connected to a material element.

Linear relations for σ_{ij} and the deviation of m from an ambient value m_o have the following form:

$$\sigma_{ij} = L_{ijkl}\, \varepsilon_{kl} - M_{ij} p \tag{1}$$

$$m - m_o = R_{ij}\, \varepsilon_{ij} + Qp \tag{2}$$

where L_{ijkl} is a tensor of elastic moduli, M_{ij} and R_{ij} are additional constant constitutive tensors and Q is a scalar. The tensors L_{ijkl}, M_{ij} and R_{ij} have the symmetries derived from the symmetry of σ_{ij} and ε_{ij}. Because the response is elastic, the work increment can be expressed as a change in the Helmholtz function ϕ having the following differential form (Biot, 1941a, 1973) (at constant temperature):

$$d\phi = \sigma_{ij} d\varepsilon_{ij} + p\, d(m/\rho) \tag{3}$$

The Maxwell relation that follows from taking the mixed partial derivatives of the dual potential $\phi - pm/\rho$ with respect to ε_{ij} and p in either order is

$$\rho \frac{\partial \sigma_{ij}}{\partial p} = - \frac{\partial m}{\partial \varepsilon_{ij}} \tag{4}$$

Substituting (1) and (2) into (4) yields

$$R_{ij} = \rho M_{ij} \cdot \tag{5}$$

When the deformation is slow enough so that alterations of the pore fluid pressure from its ambient value are eliminated by fluid mass flux, conditions are said to be drained. In this case, $p = 0$ and L_{ijkl} can be identified as the tensor of elastic moduli for drained deformation. The deformation is said to be undrained when it is too rapid to allow time for fluid mass flux to or from material elements. In this case, $m = m_0$ and (2) can be solved for the pore fluid pressure to give

$$p = -Q^{-1} \rho M_{ij} \varepsilon_{ij} \tag{6}$$

where (5) has been used. Substituting (6) into (1) yields

$$\sigma_{ij} = L^{u}_{ijkl} \varepsilon_{kl} \tag{7}$$

where

$$L^{u}_{ijkl} = L_{ijkl} + Q^{-1} \rho M_{ij} M_{kl} \tag{8}$$

is the tensor of elastic moduli appropriate to undrained response.

The constitutive formulation is completed by Darcy's law. In the absence of body forces, Darcy's law can be expressed as

$$q_i = -\rho\kappa_{ij}\partial p/\partial x_j \tag{9}$$

where q_i is the mass flow rate across a unit area with normal in the i^{th} direction, and κ_{ij} is a (symmetric) permeability tensor.

When the response is isotropic, the tensors $M_{ij}(= \rho^{-1}R_{ij})$ and κ_{ij} are diagonal and, consequently, can be expressed as

$$M_{ij} = \zeta\delta_{ij} \ , \ \kappa_{ij} = \kappa\delta_{ij} \tag{10}$$

where δ_{ij} is the Kronecker delta. Furthermore, for isotropic response the tensors of elastic moduli for drained response must have the following form:

$$L_{ijkl} = G(\delta_{ik}\delta_{jl} + \delta_{il}\delta_{jk}) + (K - 2G/3)\delta_{ij}\delta_{kl} \tag{11}$$

where G and K are the shear and bulk moduli, respectively. The form of L^u_{ijkl} is the same as that for L_{ijkl} but the values of the shear and bulk moduli may be different for undrained and drained response. However, substitution of these forms for the modulus tensors and (10) into (8) reveals that the value of the shear modulus is the same for drained and undrained response and Q is given by

$$Q = \rho\zeta^2(K_u - K)^{-1} \tag{12}$$

where K_u is the bulk modulus for undrained response.

Consequently, for isotropic response, equations (1), (2), and (9) can be rewritten as follows:

$$\sigma_{ij} = (K - 2G/3)\ \delta_{ij}\ \varepsilon_{kk} + 2G\varepsilon_{ij} - \zeta p\delta_{ij} \tag{13}$$

$$m - m_0 = \zeta\rho\ [\varepsilon_{kk} + \zeta p/(K_u - K)] \tag{14}$$

$$q_i = -\rho\ \kappa\ \partial p/\partial x_i \tag{15}$$

In these equations the value of the density ρ is constant, as appropriate for a linear theory, and equal to the mass density of the homogeneous pore fluid as it exists in the reservoir imagined to be connected to the material element. The parameter ζ can be expressed as

$$\zeta = 1 - K/K_s' \tag{16}$$

where K_s' is another bulk modulus that can be identified, under some circumstances (Nur and Byerlee, 1971; Rice and Cleary, 1976), with the bulk modulus of the solid constituents. The bulk modulus for undrained response K_u satisfies $K < K_u < \infty$ where the upper limit is attained for separately incompressible solid and fluid constituents and the lower for highly compressible pore fluid. Thus, the response is elastically stiffer for undrained response. The scalar permeability κ is often expressed as $\kappa = k/\mu$ where μ is the fluid viscosity and k is a permeability with dimensions of length squared and usually given in units of darcies (1 darcy = 10^{-8}cm^2).

The bulk moduli for drained and undrained response can be used to derive Poisson's ratios for drained (ν) and undrained (ν_u) response according to the usual relation

$$\nu = (3K - 2G)/2\ (3K + G) \tag{17}$$

The limits of K_u require that the Poisson's ratio for undrained response ν_u satisfies $\nu \leqslant \nu_u \leqslant 1/2$. If (13) and (14) are combined to obtain a relation between the pore fluid pressure and the mean normal stress for undrained response, the result is

$$p = - B\sigma_{kk}/3 \tag{18}$$

where

$$B = \zeta K_u/(K_u - K). \tag{19}$$

Thus, B and ν_u can be used as alternatives to ζ and K_u. The following alternative expressions for ν_u and B can be obtained from the results of Rice and Cleary (1976):

$$\nu_u = \frac{3\nu + \zeta B\ (1 - 2\nu)}{3 - \zeta B\ (1 - 2\nu)} \tag{20}$$

$$B = \zeta[\ \zeta + v_o K\ (1/K_f - 1/K_s'')\ ]^{-1} \tag{21}$$

where K_f is the bulk modulus of the pore fluid, v_o is the apparent porosity in the the reference state and K_s'' is another bulk modulus that can, in special cases, be identified as the bulk modulus of the solid constituents.

The constitutive equations (13), (14), and (15), must be combined with field equations expressing compatibility, equilibrium of total stresses (in the absence of body forces) and fluid mass conservation. These are as

follows:

$$\varepsilon_{ij} = \frac{1}{2} \left(\partial u_i / \partial x_j + \partial u_j / \partial x_i \right) \tag{22}$$

$$\partial \sigma_{ij} / \partial x_i = 0 \tag{23}$$

$$\partial q_i / \partial x_i + \partial m / \partial t = 0 \tag{24}$$

where u_i is the displacement of the solid matrix. Substituting (15) into (24) yields, for constant ρ and κ,

$$\rho \kappa \nabla^2 p = \partial m / \partial t \tag{25}$$

where $\nabla^2(....) = \partial^2(...)/\partial x_i \, \partial x_i$. Substituting (13) into (23) and using (22) yields

$$(K + G/3) \, \partial^2 u_k / \partial x_k \, \partial x_j + G \, \partial^2 u_j / \partial x_k \partial x_k - \zeta \, \partial p / \partial x_j = 0 \tag{26}$$

Differentiating this equation with respect to x_j and adding the appropriate multiple of it to (25) reveals that the fluid mass per unit volume m satisfies the homogeneous diffusion equation

$$\nabla^2 m = \frac{1}{c} \frac{\partial m}{\partial t} \tag{27}$$

where the diffusivity c is given by

$$c = \frac{\kappa \, (K + 4G/3) \, (K_u - K)}{\zeta^2 (K_u + 4G/3)} \tag{28}$$

or, in terms of B, ν and ν_u as

$$c = \frac{2G\kappa B^2(1 - \nu)\ (1 + \nu_u)^2}{9\ (1 - \nu_u)(\nu_u - \nu)} \tag{29}$$

The formulation given here assumes that a description of the pore fluid pressure in terms of a single scalar variable is adequate. For very rapid deformations on the time scale of wave propagation, the pore fluid pressure will be different in differently oriented neighboring fissures comprising a single point in a continuum formulation. Consequently the term undrained conditions refers to response on time scales that, although short, are long enough to allow for local pressure equilibrium among neighboring fissures. Estimates of relaxation times and constitutive response at shorter time scales have been given by O'Connell and Budiansky (1977) and Cleary (1978a).

Material Parameters

Although the Biot theory introduces only two additional elastic constants, ν_u and β or K_u and ζ, there have been few detailed investigations of their values. Rice and Cleary (1976) noted that if K_s' and K_s'' are assumed to be approximately equal to K_s, the bulk modulus of the solid constituents, ν_u and B can be calculated from measured or inferred values of ν, K_f and ν_o. Using this procedure, they have tabulated results for six rocks: two granites, three sandstones, and Tennessee marble. Values of ν are about 0.25 for the granites and marble, and lower, 0.12 to 0.20, for the sandstones. The undrained Poisson's ratio ν_u ranges from 0.27 for Tennessee marble to 0.34 for Westerly granite. The value of B ranges from 0.51 for Tennessee marble to 0.88 for Ruhr sandstone. Roeloffs (1982) also discusses some measurements of the parameters in the Biot theory and quotes $\nu = 0.2$, $\nu_u = 0.34$ and $B = 0.51$ for Boise sandstone.

A measure of the magnitude of coupled deformation - diffusion effects is

the ratio

$$\eta = (1 - \nu)/(1 - \nu_u) \tag{30}$$

which figures prominently in many of the solutions to be discussed in succeeding subsections. Values for the rocks just discussed range from 1.03 for Tennessee marble and 1.04 for Charcoal granite to 1.28 for Ruhr sandstone. As noted by Rice and Rudnicki (1979), the presence of large fissures tends to increase ν_u and decrease ν so that the value of η in situ may be larger than that inferred from laboratory data, at least for low porosity rocks. They also point out that there is no direct source of the values of ν_u and ν in situ. Although measurements of seismic wave speeds can be used to obtain a value for Poisson's ratio, this value corresponds to neither ν nor ν_u (O'Connell and Budiansky, 1977; Cleary, 1978a): the deformations induced by the passage of waves at typical seismic frequencies are too rapid to allow for the establishment of local pore fluid equilibrium, as assumed in the Biot theory. As an indirect means of inferring in situ values of ν and ν_u, Rice (1979a) and Rice and Rudnicki (1979) have used the calculations of O'Connell and Budiansky (1974) for the elastic properties of cracked saturated solids. O'Connell and Budiansky (1974) give the elastic properties as a function of a crack density parameter. The value of this parameter can be inferred from observations of seismic wave speeds, and the results of the calculations can be used to obtain Poisson's ratio. Using this procedure and O'Connell and Budiansky's (1974) inference of the crack density parameter from measurements of wave speeds prior to the San Fernando earthquake, Rice and Rudnicki (1979) suggest that values of η in the range 1.10 to 1.25 may be representative of field conditions.

A characteristic time scale of these elastic coupled deformation diffusion effects is proportional to L^2/c where L is a length scale and c is

the diffusivity. Values of c inferred by Rice and Cleary (1976) from laboratory tests on intact samples range from $10^{-4} m^2/s$ for the granites and marble to $1.6\ m^2/s$ for Berea sandstone. The largest value is comparable to the value of $1.0 m^2/s$ suggested by Anderson and Whitcomb (1975) as being consistent with several field measurements in the vicinity of shallow earthquakes. Rice and Simons (1976) discuss this value in some detail and point out that it corresponds to plausible flow rates in fissured rock. Rice (1979a) has also inferred a value of $0.1\ m^2/s$ from changes in water well level observed by Kovach et al. (1975) in response to creep events on the San Andreas fault. Li (personal communication, 1983) has determined values of c from published reports of a variety of field measurements and he finds values ranging from 10^{-1} to $10^2 m^2/s$.

Plane Strain Shear Dislocation

The solution for a suddenly introduced edge dislocation was derived by Booker (1974) for incompressible constituents and by Rice and Cleary (1976) for compressible constituents. The line of the dislocation is assumed to extend infinitely in the z direction so that conditions of plane strain deformation apply and all field quantities are independent of z. The sudden introduction of an edge dislocation at the origin at time t = 0 corresponds to the following displacement continuity:

$$u_x\ (x,0^+,\ t)\ -\ u_x(x,\ 0^-,\ t)\ =\ bH(-x)\ H(t) \tag{31}$$

where u_x is the displacement in the x direction, b is the magnitude of the discontinuity and H is the unit step function. The pore fluid pressure is given by

$$p(x,y,t)\ =\ \frac{G\ b\ B\ (1\ +\ \nu_u)}{3\pi\ (1\ -\ \nu_u)}\ \frac{y}{r^2}\ [1\ -\ \exp\ (-r^2/4ct)] \tag{32}$$

where $r^2 = x^2 + y^2$ and the shear stress in the plane of the dislocation is given by

$$\tau\ (x,0,t) = \frac{Gb}{2\pi\ (1 - \nu_u)\ x}\ \mathcal{L}\ (x^2/4ct) \tag{33}$$

where

$$\mathcal{L}(\xi) = 1 - \frac{(\nu_u - \nu)}{(1 - \nu)}\ \xi^{-1}\ (1 - e^{-\xi})\ . \tag{34}$$

Because $\mathcal{L}(\xi)$ has the limits $\mathcal{L}(\infty) = 1$ for short times and

$$\mathcal{L}(0) = (1-\nu_u)/(1-\nu) = n^{-1}$$

for long times, the shear stress is reduced from its initial value by a factor n^{-1}.

Nur and Booker (1972) have pointed out that the induced pore pressure predicted by (32) could reduce the confining stress near a recently slipped fault and provide a mechanism for the generation of aftershocks. The decrease with time of the pore pressure for $y > 0$ could cause the observed decay in numbers of aftershocks with time. Johnson (1979) has also used this solution to discuss the possibility that the migration of earthquake swarms on subsidiary faults transverse to a major transform fault could be caused by time-dependent changes of shear stress and pore fluid pressure induced by slip on the transform fault.

Booker (1974) (also, Rice, (1980, 1981)) has noted that the reduction of shear stress with time predicted by (33) predicts that the coupling of deformation and diffusion will act to <u>reload</u> a fault subjected to a sudden

stress drop. This feature is made clearer by rewriting (33) as follows:

$$\Delta\tau\ (x,\ 0,\ t) = \Delta\tau\ (x,\ 0,\ 0^+)\,\mathcal{L}(x^2/4ct) \tag{35}$$

where $\Delta\tau(x,0,0^+)$ is the stress drop at $t = 0^+$ and $\Delta\tau$ has been written for τ to emphasize the interpretation as a stress drop. Because the stress drop predicted by (35) decreases with time by the factor n^{-1}, the total stress on the fault will increase, possibly contributing to the generation of aftershocks. Rice (1980, 1981) has estimated the time scale of the reloading for a slipped zone of length 2a by superimposing dislocations of opposite sign at $x = \pm 2a/\pi$. This arrangement simulates a plane strain shear crack of length 2a in the sense that, for drained response, the magnitude of the shear stress at $x = 0$ is related to b in the same way that the shear stress on the crack is related to the relative slip at the center of the crack. The magnitude of the stress drop at the center of the dislocations is then given by

$$\Delta\tau(t) = \Delta\tau(t = 0^+)\ \mathcal{L}(a^2/\pi ct)$$

Rice (1980, 1981) plots the ratio set-up as

$$\frac{\Delta\tau\ (t = 0^+)\ -\ \Delta\tau\ (t)}{\Delta\tau\ (t = 0^+) - \Delta\tau(t = \infty)} = (\pi^2 ct/a^2)[1 - \exp(-\pi^2 ct/a^2)] \tag{36}$$

versus a/ct and defines as characteristic the time at which the right hand side of (36) equals 0.5. For 2a = 4km and values of the diffusivity c in the range 0.1 m^2/s to 1.0 m^2/s, the characteristic time ranges from 3.5 to 35 days.

Stabilization of Slip on a Narrow, Weakening Fault Zone

Rudnicki (1979) has also made use of the dislocation solution to study the effects of coupling between deformation and diffusion in stabilizing rapid

slip on frictional surfaces. If the magnitude of the displacement discontinuity in (31) is time dependent, then the stress induced in the plane of the dislocation is given by the following superposition integral:

$$\tau\,(x,0,t) = \frac{G}{2\pi\,(1-\nu_u)x}\int_{-\infty}^{t}\frac{\partial}{\partial t'}(t')\,\mathcal{L}\,[x^2/4c(t-t')]dt'$$

If dislocations of opposite sign are again located at $x = \pm 2a/\pi$ to simulate a crack of length 2a and the shear stress at the center of the dislocations is added to the uniform remotely applied stress τ_∞, the result is

$$\tau_f = \tau_\infty - \frac{G}{2a(1-\nu_u)}\int_{-\infty}^{t}\frac{\partial b}{\partial t'}(t')\,\mathcal{L}\,[a^2/\pi^2 c(t-t')]dt' \qquad (37)$$

where τ_f is assumed to be a function of the slip b. If the τ_f versus b relation has a peak, then the occurrence of a rapid runaway of fault slip, interpreted as an earthquake, is possible. This runaway instability occurs when the ratio of an increment of slip to an increment of farfield stress becomes unbounded. For drained response, (37) reduces to

$$\tau_f(b) = \tau_\infty - \frac{G}{2a\,(1-\nu_u)}\,b \qquad (38)$$

Runaway instability occurs when the slope of the friction stress versus slip relation satisfies

$$\left(\frac{d\tau_f}{db}\right)_{\text{runaway}} = -\frac{G}{2a(1-\nu)} \qquad (39)$$

Rice (1979a) has given a graphical interpretation of this instability and noted that it is analogous to the instability that occurs in a soft testing

machine when the capacity of the sample to carry load decreases faster than the machine can unload. In (39) the magnitude of the right hand side is the effective stiffness of the material surrounding the slip surface. If the material surrounding the slip surface is fluid infiltrated, the rapid slip that occurs as (39) is approached induces undrained response. For undrained response, ν is replaced by ν_u. Thus, the ratio of the stiffness of the surrounding material during undrained response to that for drained response is n (see (30)). Because $\nu_u > \nu$, this ratio exceeds unity and, consequently, the slope of the τ_f vs. b curve must be more negative in order to achieve runaway instability under undrained conditions. Because the slope typically decreases with slip, the coupled deformation diffusion acts to delay instability from the point at which (39) is satisfied to that at which the corresponding relation for undrained response is met.

For simplicity, Rudnicki (1979) assumes the following parabolic relation for τ_f versus b:

$$\tau_f(b) = \tau_p - (\tau_p - \tau_r) \left[(b - b_p)/(b_r - b_p) \right]^2 \qquad (40)$$

The peak stress is τ_p, the slip at peak stress is b_p, and τ_r is the residual stress attained at slip b_r. For this τ_f versus slip law, the stabilizing effect of induced undrained response results in the following additional amount of slip prior to instability:

$$\delta_{prec} = \frac{G (b_r - b_p)^2 (\nu_u - \nu)}{4a(\tau_p - \tau_r) (1 - \nu) (1 - \nu_u)} \qquad (41)$$

The time necessary to achieve this additional slip for a constant rate of farfield stress is called the precursor time. Rapid slipping during this

precursory period may give rise to detectable effects that would make it possible to anticipate the instability.

Rudnicki (1979) has solved (37) with stress slip relation (40) numerically for slip histories in response to a prescribed constant rate of farfield stress. The calculated values of the precursor time range from less than a day to a few days for plausible ranges of the parameters. One particularly interesting feature of the results is that the precursor time can decrease with increasing length of the slip zone. Although the diffusion time $a^2/\pi^2 c$ increases with length of the slip zone and contributes to a longer precursor time, the effective stiffness of the material surrounding the slip zone is proportional to the reciprocal of the length of the zone. This decrease in effective stiffness decreases the amount of additional slip that can be achieved by pore fluid stabilization (see (41)) and, hence, tends to decrease the precursor time. Rudnicki (1981) has also discussed this effect from another point of view.

Steadily Moving Shear Dislocation

The expressions (32) and (33) can also be used to obtain the pore fluid pressure and shear stress generated by a dislocation moving steadily, but quasi-statically, at a speed V. If the step function time dependence in (31) is replaced by a Dirac delta function $\delta_{DIRAC}(t)$, the solutions are obtained from (32) and (33) by differentiation with respect to time. The result for the pore fluid pressure is

$$p(x,y,t) = \frac{B\,(1+\nu_u)}{3\pi\,(1-\nu_u)}\,Gb\,\left\{\frac{y}{x^2+y^2}\,(1-e^{-r^2/4ct})\,\delta_{DIRAC}(t) - \frac{y}{4ct^2}\,e^{-r^2/4ct}\right\} \tag{42}$$

For introduction of the dislocation at t', t is replaced by t-t' on the right hand side of (42). Then, setting x' = Vt' and x = X + Vt, and integrating from $t' = -\infty$ to $t' = t$ yields

$$p(X,y) = \frac{B}{3\pi}\frac{(1+\nu_u)}{(1-\nu_u)}\,bG\left\{\frac{y}{X^2+y^2} - \int_{-\infty}^{t}\frac{y}{4c(t-t')^2}\exp\left\{\frac{-[x+V(t-t')]^2}{4c(t-t')}\right\}dt'\right\} \tag{43}$$

The integral can be rearranged to yield

$$p(X,y) = \frac{B}{3\pi}\frac{(1+\nu_u)}{(1-\nu_u)}\,bG\,\frac{y}{X^2+y^2}\left\{1 - (VR/2c)K_1(VR/2c)\,e^{-VX/2c}\right\} \tag{44}$$

where $R^2 = X^2 + y^2$ and $K_1(Z)$ is the modified Bessel function of order 1. The following result for the shear stress in the plane of the dislocation can be obtained in similar fashion:

$$\tau(X,0) = \frac{Gb}{2\pi(1-\nu_u)X}\left\{1 - \frac{(\nu_u-\nu)}{(1-\nu)}\left[(2c/VX) - (X/|X|)\,e^{-VX/2c}\,K_1(VX/2c)\right]\right\} \tag{45}$$

The expression (45) has been derived previously by Simons (1978) using integral transform techniques and Cleary (1978b) has given a plot of the term in square brackets obtained by numerical integration of (33). Both expressions (44) and (45) approach the undrained elastic solution in the limit $V \to \infty$.

Wesson (1981) has used the solution for a steadily moving dislocation in an ordinary elastic solid to discuss observations by Johnson et al., (1973) of water well level changes in response to creep events on the San Andreas. Wesson (1981) neglects coupled deformation diffusion effects and assumes that the pore fluid pressure is equal to the mean normal stress caused by passage

of the dislocation. This is the term that remains from (44) in the limit $V \to \infty$ after replacing ν_u by ν and setting B = 1. An examination of (44) suggests, however, that coupled deformation diffusion effects can be significant. The pore fluid pressure from (44) is plotted in nondimensional form against VX/2c for three values of Vy/2c in Figure 1. For comparison, the dashed lines show the result for the limiting case $V \to \infty$, which is the same as that obtained by neglecting coupled deformation - diffusion effects. Because the solution is for steady states, reading the graph from right to left gives the pore fluid pressure history experienced by a point a fixed distance from the plane of the dislocation. Coupled deformation diffusion effects not only reduce the magnitude of the pressure change but also cause the pressure change to reverse sign behind the dislocation and to approach zero through negative values rather than positive values predicted by the ordinary elastic solution. The coupled deformation diffusion effects diminish with distance from the fault, but for c in the range 0.1 to 1.0 m^2/s and V in the range of 1 to 10 km/day, as observed for creep events on the San Andreas, Vy/2c corresponds to 1.7 to 173 meters from the fault. For ν_u = 0.4, B = 0.6 and G = 2 x $10^{10} N/m^2$ (= 2 x 10^5 bars) and V and c in the same range, the peak of the curve for Vy/2c = 1.0 corresponds to a pressure change of 1.6 to 160 mb for a slip of 1mm.

Steadily Propagating Shear Crack

Rice and Simons (1976) have examined a more realistic model of a quasi-statically propagating fault. They solve the problem of a semi-infinite, plane strain shear crack steadily moving at a speed V. The crack is loaded by shear stress τ_a applied to the crack faces over a distance L behind the crack-tip in order to simulate a finite length fault. For an ordinary elastic solid, the shear stress ahead of the crack-tip is well-known (e.g. Rice, 1968)

to have the form

$$\tau\,(X,0) = K\,(2\pi X)^{-1/2},\quad X > 0 \tag{46}$$

where K is the stress intensity factor. For the geometry and loading considered here, K is given by

$$K = \tau_a(8L/\pi)^{1/2} \tag{47}$$

Rice and Simons (1976) find that in a fluid-infiltrated elastic solid, the shear stress near the crack-tip again has the form (46) but the stress intensity factor is given by

$$K = K_{nom}\, h(VL/c) \tag{48}$$

where K_{nom} is the value in (47) and h is a function that decreases monotonically from unity at V = 0 to η^{-1} at V = ∞. Consequently, the stress at a fixed distance ahead of the crack is less in the fluid-infiltrated solid than in an elastic solid. The energy released per unit area of crack advance is related to the stress intensity factor by (Rice, 1968)

$$\mathcal{J} = (1 - \nu)\, K^2/2G \tag{49}$$

The drained value of Poisson's ratio enters (49) because the boundary condition p = 0 on the crack faces requires that the neighborhood of the crack-tip be drained (Rice and Simons, 1976; Simons, 1977). If it is assumed that the fracture continues to propagate as long as the energy released per unit crack advance equals some critical value, say $\mathcal{J}_{crit}$, then this criteria takes the form

$$(1 - \nu)K^2/2G = \mathcal{J}_{crit} \tag{50}$$

Substituting (48) and rearranging yields

$$\mathcal{J}_{nom}/\mathcal{J}_{crit} = h^{-2}(VL/c) \tag{51}$$

where $\mathcal{J}_{nom} = (1-\nu)K^2_{nom}/2G$. The limiting value of the right hand side of (50) is η^2. Because h decreases monotonically with V, the energy that must be supplied by the applied loads, $\mathcal{J}_{nom}$, must increase in order to maintain $\mathcal{J} = \mathcal{J}_{crit}$ as crack speed increases.

Rice (1966, 1979b) has emphasized that a model that idealizes the crack-tip as a singularity in the elastic stress field is appropriate only when the actual processes of material breakdown occur in a region having a size much less than any other relevant length scale. Consequently, in the fluid-infiltrated solid, the singular crack model is unsuitable at speeds for which the diffusion length c/V becomes comparable to the breakdown zone. To remedy this effect, Rice and Simons (1976) include a finite size end zone in their calculation. They then find that $\mathcal{J}_{nom}/\mathcal{J}_{crit}$ does not increase monotonically with crack speed but, instead, has a peak and then decreases. For speeds greater than that corresponding to the peak in the curve, the crack increases speed without any increase in the driving stresses and hence is unstable.

Rice and Simons (1976) discuss in detail the implications of their results for pore fluid stabilization of fault creep events and of slip surface propagation in overconsolidated clay slopes. Specifically, they note that the propagation velocities of observed creep events on the San Andreas fault in California, one to ten km per day, correspond, for realistic values of material parameters, to a range in which the curve of $\mathcal{J}_{nom}/\mathcal{J}_{crit}$ is rising stably. Furthermore, their results suggest that creep events propagating at greater velocities are not observed because they rapidly accelerate to seismic

speeds.

Simons (1977) used boundary layer analysis to study further the propagation of plane strain shear cracks in fluid infiltrated solids. Ruina (1978) has studied the tensile crack problem analogous to the problem treated by Rice and Simons (1976) and has discussed its application to hydraulic fracture. Cleary (1978b) has numerically obtained solutions for steadily propagating singularities and used these to formulate integral equations for steady propagation of finite length faults or slip zones. He gives examples for several types of loadings.

Three Dimensional Fundamental Solutions

Although few three dimensional solutions exist for the fully coupled equations, Cleary (1977) has derived the fundamental point force and fluid mass source solutions. After correcting a minor error in Cleary's expressions for a continuous fluid mass source, Rudnicki (1981b) has shown that Cleary's solution for the displacement components u_i and pore fluid pressure p due to a point force suddenly applied at the origin at t = 0 can be arranged in the following form:

$$Gu_i(x_1,x_2,x_3,t) = \frac{P_j}{16\pi r(1-\nu_u)}\left\{\frac{x_i x_j}{r^2} + (3-4\nu_u)\delta_{ij}\right\}$$

$$+ P_j \frac{\partial}{\partial x_j}\left[\frac{(\nu_u-\nu)}{16\pi(1-\nu_u)(1-\nu)}\frac{x_i}{r}\, u(r/\sqrt{ct})\right] \qquad (52)$$

$$p(x_1,x_2,x_3,t) = \frac{P_k x_k}{12\pi r^3}\frac{B(1+\nu_u)}{(1-\nu_u)} + P_k \frac{\partial}{\partial x_k}\left[\frac{B(1+\nu_u)}{12\pi(1-\nu_u)}\frac{1}{r}\,\mathrm{erfc}(r/\sqrt{ct})\right] \qquad (53)$$

where the P_j are components of the point force,

$$\operatorname{erfc}(s) = 2\pi^{-1/2} \int_s^\infty e^{-\alpha^2}\, d\alpha = 1 - \operatorname{erf}(s)$$

and

$$u(s) = \operatorname{erfc}(s/2) + 2s^{-2}\operatorname{erf}(s/2) - 2(s\pi^{1/2})^{-1}\exp(-s^2/4) \tag{54}$$

The first term in (52) has the form of the usual elastic solution with the undrained value of Poisson's ratio., For $t \to \infty$, $p = 0$ and (52) reduces to the ordinary elastic solution with the drained value of Poisson's ratio. The term in square brackets in (52) and (53) is the solution for continuous injection of fluid mass at the origin at a constant rate Q where Q is given by

$$Q = \frac{\rho c}{G}\,\frac{3}{\beta}\,\frac{(\nu_u - \nu)}{(1-\nu)\,(1+\nu_u)} \tag{55}$$

Hence, as emphasized by Rudnicki (1981b), the second term in each equation is the response to a fluid mass dipole. Cleary (1977) has derived other singular solutions, for example the point dislocation, and has outlined their use in modelling embedded regions of inelasticity.

Deformation of Spherical Cavities and Inclusions

Rice et al. (1978) have solved the problem of a spherical cavity in an infinite linear elastic fluid-infiltrated solid loaded by uniform tractions at the cavity boundary. For loading by sudden application of tractions derived from a uniform deviatoric tensor S_{ij}, the displacement at the cavity boundary $r = a$ is given by Rice et al. (1978) as

$$2Gu_i = S_{ij}x_j\,[\xi_u - f(ct/a^2)\,(\xi_u - \xi)] \tag{56}$$

where c is the diffusivity, $\xi = 2(4-5\nu)/(7-5\nu)$, and $\xi_u = 2(4-5\nu_u)/(7-5\nu_u)$. The function f depends on whether the condition on the pore fluid at the cavity boundary is no change in pore pressure ($p = 0$) or no fluid mass flux ($\partial p/\partial r = 0$) but, in either case, f has the limiting values $f(0) = 0$ and $f(\infty) = 1$. For no change in pore fluid pressure at the cavity boundary, Rice et al. (1978) give an explicit expression for and present a graph of f. If the cavity boundary is loaded by a uniform radial compressive stress σ_0 and a pore fluid pressure p_0, Rice et al. (1978) use the solution of Rice and Cleary (1976) to show that the displacement at the cavity boundary is independent of the pore fluid pressure and is given by

$$u_i = x_i(3/4G)\sigma_0. \tag{57}$$

The distribution of pore fluid pressure outside the cavity is (Rice and Cleary, 1976)

$$p = p_0(a/r)\ \text{erfc}\ [(r-a)/(4ct)^{1/2}] \tag{58}$$

The displacement of the cavity boundary in both (56) and (57) is compatible with a homogeneous deformation of the cavity interior. This feature made it possible for Rice et al. (1978) to use (56) and (57) to obtain relations for a spherical inclusion in a fluid-infiltrated elastic solid analogous to those obtained by Rudnicki (1977) from Eshelby's (1957) results for inclusions in ordinary elastic solids. These Eshelby relations connect the stress and strain in a homogeneous inclusion to the stress and strain applied in the farfield. For the fluid infiltrated solid, these relations are as follows:

$$G\,[\varepsilon_{inc}(t) - \varepsilon_{\infty}(t)] = (3/4)\,[\sigma_{inc}(t) - \sigma_{\infty}(t)] \tag{59}$$

$$G\,[\gamma_{inc}(t) - \gamma_{\infty}(t)] = \gamma_{inc}(0) - \gamma_{\infty}(0)$$

$$= \int_0^t \{\xi_u + (\xi - \xi_u)\, f\,[c(t-t')/a^2]\}[\dot{\tau}_{\infty}(t') - \dot{\tau}_{inc}(t')]dt' \tag{60}$$

where σ is the mean normal stress, ε is the volume strain, τ is a shear stress, γ is a shear strain, and the subscripts ∞ and inc refer to quantities in the farfield and inclusion, respectively. The form of (60) assumes that the response is drained at t = 0 and the generalization from (56) and (57) to (59) and (60) assumes that the inclusion is highly permeable so that it is a reasonable assumption to regard the pore fluid pressure there as uniform. A third relation, obtained by balancing the rate of increase of fluid mass in the inclusion with the mass flux through the cavity boundary computed from (58) and (59), is as follows:

$$\dot{m}_{inc}(t) = -(3\rho\kappa/a^2)\,[p_{inc}(t) - p_{\infty}(t)]$$

$$+ \int_{-\infty}^{t} \frac{a}{[\pi c(t-t')]^{1/2}}\,\{\dot{p}_{inc}(t') - \dot{p}_{\infty}(t')\}\,dt' \tag{61}$$

where it has been again assumed that the inclusion is relatively permeable.

Rice and Rudnicki (1979) have used (60) to analyze stabilizing effects of coupling between deformation and diffusion, analagous to those discussed for frictional slip, for an inclusion model of faulting (Rudnicki, 1977, 1981a). When the inclusion shear stress is given as a function of the inclusion shear strain and the farfield response is taken to be elastic, (60) becomes a relation for the inclusion shear stress as a function of the applied farfield

shear strain. Runaway instability corresponds to the possibility that an increment of farfield shear strain can induce an unbounded increment of inclusion shear strain. For purely drained conditions, runaway instability occurs when the slope at the τ_{inc} versus γ_{inc} curve satisfies the following condition:

$$\frac{d\tau_{inc}}{d\gamma_{inc}} = -\frac{G}{\xi} \tag{62}$$

The magnitude of the right hand side, G/ξ, is the effective unloading stiffness of the material surrounding the inclusion. If the response is purely undrained, the condition for runaway instability is obtained by replacing ξ by ξ_u in (62). Because $\nu < \nu_u$, $\xi_u < \xi$ and, hence, the unloading stiffness is greater for undrained response than for drained response. Consequently, the development of undrained response due to rapid straining as (62) is approached can transiently stabilize the rock mass and delay the onset of runaway instability from the time at which (62) is met until the time at which the corresponding condition is met in terms of the undrained response. This delay time is termed the precursor time and is representative of the time period during which it may be possible to observe evidence of the impending instability.

Rice and Rudnicki (1979) calculate the precursor time and time history of inclusion straining for an imposed constant farfield shear strain rate and a τ_{inc} versus γ_{inc} curve that is assumed to have the following form near peak stress:

$$\tau = \tau_p - G(\gamma-\gamma_p)^2/2\lambda \tag{63}$$

where γ_p is the strain at peak stress τ_p and λ describes the sharpness of

the peak ($\lambda^{-1} = d^2(\tau/G)/d\gamma^2$). For $\dot{\tau}_\infty$ = 1 bar/year, G = 200kbar and λ = 0.0025, Rice and Rudnicki (1979) present results for two values of ξ/ξ_u, 1.10 and 1.25, three values of the inclusion radius, a = 1, 3, and 5 km., and two values of the diffusivity, c = 0.1 and 1.0m^2/s. The results for the precursor time range from 14 to 400 days. Rice and Rudnicki (1979) note that the precursor times are a factor of two to three longer for c = 1.0m^2/s than for c = 0.1m^2/s and a factor of two to four longer for a = 5 km than for a = 1 km. Although the precursor times are much longer than those for the case of a narrow slip surface, precursor times estimated for a narrow, slitlike ellipsoidal inclusion with aspect ratio 18 to 1 range from 1.3 to 22 days.

COUPLING BETWEEN INELASTIC DEFORMATION AND DIFFUSION

Because inelastic deformation of geological and geotechnical materials often involves volume change, inelastic deformation can also be coupled to pore fluid diffusion. In brittle rocks, inelastic volume increase, or dilatancy, can result, even when all principal stresses are compressive, from microcracking in response to local tensile stresses at tips of fissures or near other inhomogeneities and from uplift in sliding over asperities on frictional surfaces (Brace, et al. 1966). Inelastic volume increase in response to shear is also observed in overconsolidated clays and can result from grain rearrangement in densely packed sands or other granular materials. Although the discussion here will emphasize inelastic volume increase, shear induced compaction is observed in very porous rocks and loosely consolidated granular materials.

The next subsection outlines a framework for describing the inelastic response of brittle rock, including the effects of pore fluids, and illustrates the hardening effect of dilatancy-induced pore pressure reductions. Succeeding subsections review results on the stability of

dilatantly hardened deformation and applications to earth faulting.

Inelastic Constitutive Law for Brittle Rock

Rice (1975) has formulated a description of inelastic deformation for the special deformation state of combined shear and uniaxial compression. Rudnicki and Rice (1975) generalized the formulation to arbitrary deformation states and magnitudes. Their framework, including the incorporation of pore fluid effects, has recently been reviewed by Rudnicki (1983a). However, it will be simplest to follow the development of Rice and Rudnicki (1979) for material subjected to shear stress τ and hydrostatic compression σ. For a stress increment $(d\tau, d\sigma)$ that involves continued inelastic deformation, the increments of shear strain $d\gamma$ and volume strain $d\varepsilon$ are as follows:

$$d\gamma = d\tau/G + d^p\gamma \tag{64}$$

$$d\varepsilon = -d\sigma/K + d^p\varepsilon \tag{65}$$

where G is the elastic shear modulus, K is the elastic bulk modulus, and $d^p\gamma$ and $d^p\varepsilon$ are the inelastic increments of shear strain and volume strain, respectively. For elastic unloading the second terms in (64) and (65) are dropped. Because an increase in hydrostatic compression inhibits inelastic deformation in brittle rock, the inelastic increment of shear strain is taken to have the following form:

$$d^p\gamma = (d\tau - \mu d\sigma)/H$$

where μ is a friction coefficient and H is an inelastic hardening modulus. For constant hydrostatic stress H is related to the slope of the τ versus γ curve by

$$\frac{d\tau}{d\gamma} = \frac{H}{1 + H/G}, \quad d\sigma = 0. \tag{66}$$

Because inelastic volume strain arises from processes that accompany inelastic shear, that is, extension of microcracks by local tensile stresses, uplift in sliding over asperities and grain rearrangement, the inelastic volume strain increment is assumed to be given by

$$d^p\varepsilon = \beta d^p\gamma \tag{67}$$

where β is the dilatancy factor. (For shear-induced compaction, $\beta<0$). In general, μ and β, as well as G, K and H may depend on the current state of deformation and even on the past history of deformation (although not on deformation increments), but for applications to brittle rocks it often suffices to assume that μ, β, G and K are constant. Laboratory observations on brittle rocks suggest values of β in the range 0.1 to 0.3 and μ in the range 0.3 to 0.6 (Rice, 1975; Rudnicki and Rice, 1975; Rudnicki, 1977).

To include the effects of pore fluid pressure, the hydrostatic stress σ is replaced by the effective stress. For elastic deformation, the form of the effective stress is, as discussed earlier, $\sigma - \zeta p$. For inelastic deformation arising from extension of sharp-tipped microcracks and frictional sliding on fissure surfaces with small contact areas Rice (1977) has shown that the appropriate form of the effective stress is $\sigma - p$. This deduction is consistent with experimental observations on inelastic properties of brittle rock (e.g. Cornet and Fairhurst, 1974; Brace and Martin, 1968). An equation for m, the fluid mass content per unit volume, is also required. As for elastic deformation, m can be expressed as ρv, but now the increment dv is separated into an elastic portion and an inelastic portion $d^p v$. The elastic portion is calculated as in the Biot theory and, for the same conditions that

$\sigma - p$ is the appropriate form of the effective stress, $d^p v = d^p \varepsilon$ (Rice, 1977). Thus, the increments of shear strain, volume strain, and fluid mass content per unit volume are as follows:

$$d\gamma = d\tau/G + [d\tau - \mu(d\sigma - dp)]/H \tag{68}$$

$$d\varepsilon = -(d\sigma - \zeta dp)/K + \beta\,[d\tau - \mu\,(d\sigma - dp)]/H \tag{69}$$

$$\rho^{-1} dm = v dp(1/K_f - 1/K_s'') - \zeta\,(d\sigma - dp)/K + d^p\varepsilon \tag{70}$$

For undrained response, the change in fluid mass content per unit volume is zero. Setting $dm = 0$ in (70) and solving for dp yields

$$dp = \frac{-\beta\, K_{eff}}{H + \mu\beta\, K_{eff}}\, d\tau \tag{71}$$

where, for convenience $d\sigma$ has been taken as zero and, using (16), K_{eff} can be written as follows:

$$1/K_{eff} = v(1/K_f - 1/K_s'') + (1/K - 1/K_s') \tag{72}$$

Hence, for dilatant inelastic deformation ($\beta > 0$) the pore fluid pressure tends to decrease. When (71) is substituted into (68), again with $d\sigma = 0$, the result is

$$d\gamma = d\tau/G + d\tau/(H + \mu\beta K_{eff}) \tag{73}$$

Because the hardening modulus has been augmented by the term $\mu\beta\, K_{eff}$, the response is stiffer and the rock mass is said to be dilatantly hardened. Dilatant hardening is a well known phenomenon in the mechanics of granular

materials and appears to have been first discussed by Reynolds (1885). Its relevance to earthquake faulting was pointed out by Frank (1965). Brace and Martin (1968) and Martin (1980) have observed dilatant hardening in axisymmetric compression tests on brittle rock.

As discussed by Rice (1975) and by Rice and Rudnicki (1979), the dilatant hardening effect can be significant for representative values of μ, β, and K_{eff}. Because the term that augments H is proportional to the product $\mu\beta$, the effect vanishes if there is no inelastic volume change or if inelastic deformation is not affected by hydrostatic stress. For highly fissured rock, K_s' and $K_s'' \gg K$ and K_f/v. Therefore, (72) reduces to

$$K_{eff} \sim K(1 + vK/K_f)^{-1}$$

If the pore fluid is liquid water (K_f = 22 kbar) and the porosity is less than 10%, $K_{eff} \sim K$. If K_f is substantially reduced by high temperatures, exsolution of trapped gas and pressure reduction,

$$K_{eff} \sim K_f/v$$

and dilatant hardening disappears in the limit $K_f \to 0$.

Stability of Dilatant Hardening

Rice (1975) has studied the stability of dilatant hardening for a layer subjected to a combination of uniaxial compression and pure shear. He finds that homogeneous dilatantly hardened deformation becomes unstable, in the sense that infinitesimal spatial nonuniformities will grow exponentially in time when the peak of the underlying drained stress-strain curve has been reached. That instability sets in at the peak of the drained stress strain curve is an artifact of the special deformation state considered: in general, dilatantly hardened homogeneous deformation will become unstable when conditions for localization of deformation (Rudnicki and Rice, 1975; Rudnicki,

1983a) are met in terms of the drained response and this may occur before or after the peak of the stress-strain curve.

Rice (1975) also noted, however, that if for a layer with an initial finite size imperfection the development of instability would depend on the time scale of deformation. Rudnicki (1983b) has explored this possibility by considering the shear deformation of a layer containing a slightly weaker sublayer. To simplify the analysis, Rudnicki (1983b) assumes that the deformations of the sublayer and of the surrounding material are homogeneous. In addition, the rate of fluid mass flux out of the sublayer is assumed to be proportional to the difference in the pore fluid pressures of the sublayer and the surrounding material. The coefficient in this relation, which must be regarded as an empirical parameter, is expressed as c/h^2 where c is a diffusivity and h is the width of the weakened sublayer. In this case, the response becomes unstable, in the sense described by Rice (1975), when the weakened sublayer reaches the peak of its underlying drained stress strain curve. However, dilatant hardening delays the onset of a catastrophic instability until the weakened sublayer reaches the peak of its undrained response curve. The time period during which the response is stabilized is again termed the precursor time.

To calculate the precursor time, Rudnicki (1983b) assumes that both the sublayer and the surrounding material have drained stress strain curves of the form (63), but that the peak stress in the weakened sublayer is slightly lower than that in the surrounding material. When the time scale of the applied deformation is much greater than that for fluid mass exchange between the layers, as appropriate for application to tectonic deformations, Rudnicki (1983b) obtains an asymptotic solution for the history of straining in the weakened sublayer. The resulting asymptotic prediction of the precursor time

is as follows:

$$ct_{prec}/h^2 = 1.48\ (c\lambda/h^2\dot{\gamma}_\infty)^{1/3}\ \alpha^{2/3}\ \Delta^{-1/6}\ [\ 1 + \alpha\ (1-(2\Delta)^{1/2})\ ]^{1/3} \quad (74)$$

where $\alpha = \mu\beta M/G$, M is an elastic modulus for one-dimensional strain, Δ is the difference in values of peak stress divided by $G\lambda$, and $\dot{\gamma}_\infty$ is the constant applied farfield strain rate. The asymptotic solution is valid for $c\lambda/h^2\dot{\gamma}_\infty >> 1$. For $\dot{\gamma}_\infty = 2.5 \times 10^{-14} s^{-1}$, on the order of measured tectonic strain rates in southern California, h = 1m, c = 0.1 m^2/s and $\lambda = .0025$, $c\lambda/h^2\dot{\gamma}_\infty = 10^{10}$. For $\Delta = 0.1$ and $\alpha = 0.3$, $t_{prec} \simeq 6$ hours. Note that the precursor time becomes arbitrarily large for $\dot{\gamma}_\infty \to 0$, but that the additional strain accumulating during this period goes to zero in the same limit.

Rudnicki (1983a) has extended this formulation to arbitrary deformation states. Although the solutions can be shown to have the same character as those for the simple case of pure shear, no explicit results are available yet.

Dilatant Hardening for an Inclusion Model of Faulting

Rice and Rudnicki (1979) have examined the effects of dilatant hardening for an inclusion model of earth faulting (Rudnicki, 1977). These effects are complementary to those due to the time dependence of the unloading stiffness discussed earlier and they are also stabilizing. Again, instability cannot occur abruptly when the condition for runaway instability in terms of the drained response is met. The rapid deformation that occurs as this condition is approached induces dilatantly hardened response of the inclusion material. Consequently, instability is delayed until (62) is met with the undrained slope of the τ_{inc} versus γ_{inc} curve entering the left-hand side of

(62). Thus, dilatant hardening delays instability by increasing the value on the left-hand side of (62) whereas the time- dependent unloading stiffness delays instability by increasing the magnitude of the right-hand side.

Rice and Rudnicki (1979) calculate strain histories and precursor times using the Eshelby relations (59) and (61) for a spherical inclusion. Because the time-dependent unloading stiffness effects are neglected, the drained form of (60), corresponding to f = 1, is used. The drained response of the inclusion material is assumed to be described by (63). For $\dot{\tau}_\infty$ = 1 bar/year, G = 200kbar, λ = 0.6, β = 0.3 and K_f = 22kbar, Rice and Rudnicki (1979) calculate precursor times ranging from 55 days for an inclusion radius a = 1km and diffusivity c = 1.0 m^2/s to 1418 days for a = 5 km and c = 0.1 m^2/s. They also note that a factor of two decrease in the dilatancy factor β reduces the precursor time by slightly more than half, whereas a tenfold decrease in the pore fluid bulk modulus K_f reduces the precursor time by slightly less than half. Although the precursor times are generally long, Rice and Rudnicki (1979) suggest that values toward the lower end of those calculated may be more appropriate.

Rice and Rudnicki (1979) also calculate the decrease from ambient value of the pore fluid pressure in the inclusion. The predicted decrease does not appear to be large enough to cause a liquid-to-vapor phase transition in the pore fluid until very near to instability. Such a phase transition would be needed to cause the substantial changes in wave speed ratios that have been suggested as precursors to earthquakes (Nur, 1972; Anderson and Whitcomb, 1975). Consequently, the calculations do not support this possibility. Nevertheless, they do indicate that transient stabilization of incipient failure by dilatant hardening, as well as by time-dependent unloading stiffness effects, could cause a period of accelerating time-dependent strain

prior to instability. Martin (1980) has observed such stabilization in axisymmmetric compression tests on saturated Westerly granite. The observations are in qualitative accord with the predictions of Rice and Rudnicki (1979) (Rudnicki, 1981), but quantitative comparison is not possible.

Dilatant Hardening Effects on Propagating Shear Fractures

Rice (1973, 1979a, 1980, 1981) has analyzed dilatant hardening effects in the endzone of a steadily propagating fracture. He assumes that a uniform uplift accompanies shear in the endzone. By assuming one dimensional diffusion of pore fluid into the endzone, Rice calculates the distribution of suctions induced on the fault plane. Because these suctions reduce the effective value of the stress normal to the fault plane, they inhibit propagation or, in other words, they increase the energy that must be supplied to continuing advancing the fractures. Although the values of material parameters entering the analysis are uncertain, Rice demonstrates that the effect can be significant. He calculates a factor of 50 as a rough upper bound on the increase of required energy for which it is possible to maintain quasistatic propagation (Rice, 1979a). But he notes that the process may be self-limiting for two reasons: the amount of uplift decreases with increasing normal stress and the induced suctions may be large enough to cause vaporization of the pore fluid or exsolution of gases.

CONCLUDING DISCUSSION

This paper has reviewed the mechanical effects of pore fluid diffusion on the quasi-static deformation and failure of brittle rock. These effects have been illustrated by applications to earth faulting. The role of pore fluid in reducing the effective value of the confining stress in bulk samples and the normal stress across frictional surfaces has been demonstrated in laboratory experiments (e.g. Brace and Martin, 1968; Byerlee and Brace, 1972) and in field studies (e.g. Raleigh et al., 1976; Zoback and Hickman, 1982). In addition, the solutions reviewed here strongly suggest that the coupling of pore fluid diffusion and deformation can introduce rate-dependence into the deformation of an otherwise rate-independent solid and make a significant contribution to the time scale of the failure process. However, few laboratory or field studies of these effects exist. Consequently, although relevant solutions of coupled-deformation and pore fluid diffusion problems have by no means been exhausted, the most pressing need is for laboratory and field data. Data are needed both to provide better estimates of material parameters and to test the accuracy of analytical predictions

Although the time dependence introduced into the failure process is evident in the solutions reviewed here, identification of these effects in situ is complicated by the presence of other time dependent processes. These include bulk viscoelastic response, coupling of crustal deformation with underlying viscous material (e.g., Anderson, 1975; Budiansky and Amazigo, 1976; Lehner et al., 1981), time dependence due to slow crack growth (e.g., Das and Scholz, 1981) and time dependent frictional slip (e.g., Dieterich, 1978). The time scales of these processes are probably different, but present uncertainties in material parameters are too great to distinguish mechanisms on this basis. Observations of water level changes in calibrated wells (e.g.,

Kovach et al., 1975) or increased use of dilatometers may be helpful in identifying coupled deformation - pore fluid diffusion. Although observations of changes in seismic wave speed ratios (Aggarwal et al., 1975; Whitcomb et al., 1973) have not proved to be as effective an earthquake precursor as had been hoped, such measurements may provide information about crack densities and saturation levels from which material parameters can be inferred. (However, Rice (1980) has emphasized that electro-kinetic effects which do not depend on degree of saturation, will be more indicative of crack density.) Moreover, there is some recent evidence (Leary et al., 1979) that extremely small changes in wave speed (~.1%) over relatively short time scales (a few days) may be caused by deformation coupled with fluid diffusion. Because of the difficulties in anticipating the time and location of spontaneous events such as earthquakes and creep, field studies in which the pore fluid pressure is actively changed by changing reservoir levels or by direct pumping (Raleigh et al., 1976) will be especially useful.

Although direct extrapolation of measurements on laboratory samples to field situations in which properties can be strongly affected by large fissures is impossible, the difficulty and expense of making relevant field observations virtually ensure that laboratory measurements will continue to contribute to understanding coupled deformation - diffusion effects. Unfortunately, most laboratory experiments have been limited to investigation of the effective stress principle for various properties and have not considered the rate dependent effects of coupling of deformation with pore fluid diffusion. As has been mentioned already, relatively few determinations exist of the parameters of even the linear Biot theory. Apparently, the only laboratory investigation of coupled deformation diffusion effects in setting a time scale for the failure process is that of Martin (1980). Although

Martin's (1980) observations agree qualitatively with the predictions of Rice and Rudnicki (1979) (see discussion by Rudnicki (1981)), the data are not extensive and there is a need for additional work in this area.

Although there are limitations on the Biot approach, most notably to linear behavior, there is general agreement that the Biot equations are a suitable approximation for many conditions of quasi-static loading. Much less agreement exists, however, for dynamic conditions. The Biot theory has been extended (Biot, 1956a,b) to describe the dynamic response of saturated porous materials and, at least in some instances, gives results in reasonable accord with observations. But it is clear that a theory that is phrased in terms of a single scalar pore pressure will be suitable for a limited frequency range. Some estimates of the time scale for which the Biot theory is applicable have been given by O'Connell and Budiansky (1977) and by Cleary (1978). Cleary (1978) has also outlined a general formulation but, as yet, the values of parameters entering this theory are largely unknown. A better understanding of the dynamic response of saturated porous media seems essential for applications to explosive loadings, interpretation of data from geophysical explorations, and ultrasonic measurements in biological materials.

The review has been limited to discussing the mechanical effects of pore fluids, but the importance of chemical effects has been increasingly recognized. Recent experiments (e.g., see Atkinson (1982), Rice (1979a, 1980) and Rudnicki (1980) for reviews) have indicated that small amounts of pore fluid can promote slow growth of cracks in rock at speeds ranging down to 10^{-10}m/s. Typically, these results are presented in relations of the following form between the crack speed V and the tensile stress intensity factor K:

$$V = AK^n \quad \text{or} \quad V = B \exp(bK)$$

where A and n or B and b are parameters depending on the environment. Small amounts of pore fluid on frictional slip surfaces may also contribute to time-dependent behavior by accelerating deformation at asperity contacts (Dieterich and Conrad, 1978). Moreover, much of the observed time-dependent behavior of brittle rocks may be due to environmentally assisted growth of microcracks. Costin and Mecholsky (1983) have successfully used laboratory results on slow growth of a single crack to predict the time dependent response of an intact specimen in uniaxial compression.

Environmentally assisted crack growth may be very important in establishing the longtime strength of crustal rocks, for example, on time scales comparable to the recurrence time of large earthquakes or the desired lifetime of nuclear waste repositories. Although it is not yet clear whether there is a threshold value of K below which no crack growth occurs, the existence of such a threshold is important for long time strength predictions. Moreover, Rice (1978) has pointed out that crack healing may be an important mechanism of strength recovery on faults. Although Rice (1978) has described a theoretical framework of analyzing environmentally assisted growth of single cracks, the analysis of these effects has not progressed to the point where they can be incorporated into the solution of relevant boundary value problems.

ACKNOWLEDGEMENT

Support during the preparation of this review from the U.S. Geological Survey Earthquake Hazards Reduction Program and the NSF Geophysics Program is gratefully acknowledged.

REFERENCES

Aggarwal, Y.P., Sykes, L.R., Simpson, D.W. and Richards, P.G. (1975). 'Spatial and temporal variations in t_s/t_p and in P wave residuals at Blue Mountain Lake, New York: application to earthquake prediction', J Geophys. Res. 80, 718-732.

Anderson, D. L. (1975). 'Time-dependent seismology', J. Geophys. Res., 80, 1497-1503.

Atkinson, B.K., (1982). 'Subcritical crack propagation in rocks: theory, experimental results and applications', J. Struct. Geology, 4, 41-56.

Bell, M.L. and Nur, A., (1978). 'Strength changes due to reservoir-induced pore pressure and stresses and application to Lake Oroville', J. Geophys. Res., 83, 4469-4483.

Biot, M.A. (1941a). 'General theory of three-dimensional consolidation', J. Appl. Phys., 12, 155-164.

Biot, M. A., (1941b). 'Consolidation settlement under a rectangular load distribution', J. of Appl. Phys., 12, 426-578.

Biot, M. A., (1956a). 'Theory of propagation of elastic waves in a fluid-saturated porous solid. I. low-frequency range', J. Acous. Soc. Am., 28, 168-178.

Biot, M. A., (1956b). 'Theory of propagation of elastic waves in a fluid-saturated porous solid. II. higher frequency range', J. Acous. Soc. Am., 28, 179-191.

Biot, M.A., (1973). 'Nonlinear and semilinear rheology of porous solids', J. Geophys. Res., 78, 4924-4937.

Biot, M. A. and Clingan, F. M. (1941). 'Consolidation settlement of a soil with an impervious top surface', J. Applied Phys., 12, 578-581.

Booker, J. R., (1974). 'Time-dependent strain following faulting of a porous medium', J. Geophys. Res., 79, 2037-2044.

Brace, W. F., Paulding, B. W., Jr. and Scholz, C. H. (1966). 'Dilatancy in the fracture of crystalline rocks', J. Geophys. Res., 71, 3939-3953.

Brace, W. F. and Martin, R. J. III, (1968). 'A test of the law of effective stress for crystalline rocks of low porosity', Int. J. Rock Mech. Mining Sci., 5, 415-436.

Budiansky, B. and Amazigo, C., (1976). 'Interaction of fault slip and lithospheric creep', J. Geophys. Res., 81, 4897-4900.

Byerlee, J. D. and Brace, W. F., (1972). 'Fault stability and pore pressure', Bull. Seismol. Soc. Am., 62, 657-660.

Cleary, M. P. (1977). 'Fundamental solutions for a fluid-saturated porous solid', Int. J. Solids, Structures, 13, 785-806.

Cleary, M. P. (1978a). 'Elastic and dynamic response regimes of fluid-impregnated solids with diverse microstructures', Int. J. Solids Structures, 14, 795-819.

Cleary, M. P. (1978b). 'Moving singularities in elasto-diffusive solids with applications to fracture propagation', Int. J. Solids Structures, 14, 81-97.

Cleary, M. P., (1979). 'Rate and structure sensitivity in hydraulic fracturing of fluid-saturated porous formations', in Proc. U.S. Symp. Rock Mech., 20th Austin, Texas, (Ed. K. Gray), pp. 127-141.

Costin, L. S. and Mecholsky J. J. (1983). 'Time dependent crack growth and failure in brittle rock', in Proc. U.S. Symp. on Rock Mechanics, 24th, College Station, Texas.

Cornet, F. H. and Fairhurst, C. (1974). 'Influence of pore pressure on the deformation behavior of saturated rocks', in Proceedings of the Third Congress of the International Society for Rock Mechanics, Vol. 1, part B, pp. 638-644, National Academy of Sciences, Washington, D.C.

Cryer, C. W., (1963). 'A comparison of the three dimensional consolidation theories of Biot and Terzaghi', Quart. J. Mech. "Appl. Math., 16, 401-412.

Das, S. and Scholz, C. H. (1981). 'Theory of time-dependent rupture in the earth', J. Geophys. Res., 86, 6039-6051.

Dieterich, J. H. (1978). 'Time-dependent friction and the mechanics of stick-slip', J. Geophys. Res., 116, 790-806.

Dieterich, J. H. and Conrad, G. (1978). 'Mechanism of unstable slip in rock friction experiments', EOS, Trans Am. Geophys. Union, 59, 1206.

Eshelby, J. D. (1957). 'The determination of the elastic field of an ellipsoidal inclusion and related problems', Proc. Roy. Soc. Ser. A., 241, 376-396.

Frank, F. C. (1965). 'On dilatancy in relation to seismic sources', Rev. Geophys. Space Phys., 3, 485-503.

Johnson, A. G., Kovach, R. L. and Nur, A. (1973). 'Pore pressure changes during creep events on the San Andreas fault', J. Geophys. Res., 78, 851-857.

Johnson, C. E. (1979). I. CEDAR - An Approach to the Computer Automation of Short-Period Local Seismic Networks. II Seismotectonics of the Imperial Valley of Southern California, PhD Thesis, California Institute of Technology, 332 pages.

Kovach, R. L., Nur, A., Wesson, R. L. and Robinson, R. (1975). 'Water-level fluctuations and earthquakes on the San Andreas fault zone', Geology 3, 437-440.

Leary, P. C., Malin, P. E., Phinney, R. A., Brocher, T. and Von Colln, R. (1979). 'Systematic monitoring of millisecond travel time variations near Palmdale, CA', J. Geophys. Res., 84, 659-666.

Lehner, F. K., Li, V. C. and Rice, J. R. (1981). 'Stress diffusion along rupturing plate boundaries', J. Geophys. Res., 86, 6155-6169.

Martin, R. J., III (1980). 'Pore pressure stabilization of failure in Westerly granite', Geophys. Res. Letters, 7, 404-406.

McNamee, J. and Gibson, R. E. (1960a). 'Displacement functions and linear transforms applied to diffusion through porous elastic media', Quart. J. Mech. Appl. Math., 13, 98-111.

McNamee, J. and Gibson, R. E. (1960b). 'Plane strain and axially symmetric problems of the consolidation of a semi-infinite clay stratum', Quart. J. Mech. Appl. Math., 13, 210-227.

Nur, A. (1972). 'Dilatancy, pore fluids, and premonitory variations of t_s/t_p travel times', Bull. Seismol. Soc. Am., 62, 1217-1222.

Nur, A. and Booker, J. R. (1972). 'Aftershocks caused by pore fluid flow?', Science, 175, 885-887.

Nur, A. and Byerlee, J. D. (1971). 'An exact effective stress law for elastic deformation of rock with fluids', J. Geophys. Res., 76, 6414-6419.

O'Connell, R. J. and Budiansky, B. (1974). 'Seismic velocities in dry and saturated cracked solids', J. Geophys. Res., 79, 5412-5426.

O'Connell, R. J. and Budiansky, B. (1977). 'Viscoelastic properties of fluid-saturated cracked solids', J. Geophys. Res., 82, 5719-5735.

Ohtake, M. (1974). 'Seismic activity induced by water injection at Matsushiro, Japan', J. Phys., Earth, 22, 163-176.

Paterson, M. S. (1978). Experimental Rock Deformation - The Brittle Field, Springer Verlag, New York.

Raleigh, C. B., Healy, J. H. and Bredehoeft, J. D. (1976). 'An experiment in earthquake control at Rangely, Colorado', Science, 191, 1230-1237.

Reynolds, O. (1885). 'On the dilatancy of media composed of rigid particles in contact, with experimental illustrations, Phil. Mag. (Reprinted in Papers on Mechanical and Physical Subjects by O. Reynolds, Vol. 2, pp. 203-216, Cambridge University Press, New York, 1901.)

Rice, J. R. (1966). 'An examination of the fracture mechanics energy balance from the point-of-view of continuum mechanics', in Proc. Int. Conf. Fract., 1st (Ed. T. Yokobori), Vol. 1, pp. 283-308, Japanese Society of Strength and Fracture, Tokyo.

Rice, J. R.. (1968). 'Mathematical analysis in the mechanics of fracture', in Fracture: An Advanced Treatise, (Ed. H. Liebowitz), Vol. II, pp. 191-311.

Rice, J. R. (1973). 'The initiation and growth of shear bands', in Plasticity and Soil Mechanics (Ed. A. C. Palmer), pp. 263-274. Cambridge University Engineering Department, Cambridge, England.

Rice, J. R. (1975). 'On the stability of dilatant hardening for saturated rock masses', J. Geophys. Res.,80, 1531-1536.

Rice, J. R. (1977). 'Pore pressure effects in inelastic constitutive formulations for fissured rock masses', in Advances in Civil Engineering Through Engineering Mechanics, pp. 360-363. American Society of Civil Engineers, New York.

Rice, J. R. (1978).' Thermodynamics of the quasi-static growth of Griffith cracks', J. Mech. Phys. Solids, 26, 61-78.

Rice, J. R. (1979a). 'Theory of precursory processes in the inception of earthquake rupture', Gerlands Beitr.Geophys., 91-127.

Rice, J. R. (1979b). 'The mechanics of quasistatic crack growth' in Proc. U. S. Nat. Congr. Appl. Mech. 8th, UCLA, June 1978 (Ed. R. E. Kelley), pp. 191-216, Western Periodicals, North Hollywood, California.

Rice, J. R. (1980). 'The mechanics of earthquake rupture', in Physics of the Earth's Interior, Proceedings of the International School of Physics "Enrico Fermi", Course 78, 1979 (Eds. A. M. Dziewonski and E. Boschi), Italian Physical Society, North Holland, pp. 555-649.

Rice, J. R. (1981). 'Pore fluid processes in the mechanics of earthquake rupture', in Solid Earth Geophysics and Geotechnology, (Ed. S. Nemat-Nasser), Applied Mech. Div. Vol. 42, American Society of Mech. Eng., New York, pp. 81-89.

Rice, J. R. and Cleary, M. P. (1976). 'Some basic stress diffusion solutions for fluid-saturated elastic porous media with compressible constituents', Rev. Geophys. Space Phys, 14, 227-241.

Rice, J. R. and Rudnicki, J. W. (1979). 'Earthquake precursory effects due to pore fluid stabilization of a weakening fault zone', J. Geophys. Res., 84, 2177-2193.

Rice, J. R., Rudnicki, J. W. and Simons, D. A. (1978). 'Deformation of spherical cavities and inclusions in fluid-infiltrated elastic solids', Int. J. Solids Struct., 14, 289-303, 1978.

Rice, J. R. and Simons, D. A. (1976). 'The stabilization of spreading shear faults by coupled deformation - diffusion effects in fluid-infiltrated porous materials', J. Geophys. Res., 81, 5322-5334.

Roeloffs, E. (1982). Elasticity of Saturated Porous Rocks: Laboratory Measurements and a Crack Problem. PhD Thesis at University of Wisconsin, Madison, 157 pages.

Rudnicki, J. W. (1977). 'The inception of faulting in a rock mass with a weakened zone', J. Geophys. Res., 82, 844-854.

Rudnicki, J. W. (1979). 'The stabilization of slip on a narrow weakening fault zone by coupled deformation - pore fluid diffusion', Bull. Seismol. Soc. Am., 69, 1011-1026.

Rudnicki, J. W. (1980). 'Fracture mechanics applied to the earth's crust', in Ann. Reviews of Earth Planetary Sciences, Vol. 8 (Ed. F. A. Donath), Annual Reviews Inc., Palo Alto, CA, pp. 489-525.

Rudnicki, J. W. (1981a). 'An inclusion model for processes preparatory to earthquake,faulting', in Solid Earth Geophysics and Geotechnology, (Ed. S. Nemat-Nasser), Applied Mech. Div. Vol. 42, American Society of Mech. Engn., New York, pp. 39-52.

Rudnicki, J. W. (1981b). 'On "Fundamental solutions for a fluid-saturated porous solid" by M. P. Cleary'. Int. J. Solids Structures, 17, 855-857.

Rudnicki, J. W. (1983a). 'A formulation for studying coupled deformation - pore fluid diffusion effects on localization', in Proceedings of the Symposium on the Mechanics of Rocks, Soils and Ice (Ed. S. Nemat-Nasser) American Society of Mechanical Engineers, New York. Publication expected in June 1983.

Rudnicki, J. W. (1983b). Manuscript in progress.

Rudnicki, J. W. and Rice, J. R. (1975). 'Conditions for the localization of deformation in pressure-sensitive dilatant materials', J. Mech. Phys. Solids, 23, 371-394.

Ruina, A. (1978). 'Influence of coupled deformation-diffusion effects on retardation of hydraulic fracture', in Proc. U. S. Symp. Rock Mech., 19th, Stateline, Nev. (Ed. Y. S. Kim), pp. 274-282.

Scholz, C. H., Sykes, L. R. and Aggarwal, Y. P. (1973). 'Earthquake prediction: a physical basis', Science, 181, 803-810.

Simons, D. A. (1977). 'Boundary layer analysis of propagating mode II cracks in porous elastic solids', J. Mech. Phys. Solids, 25, 99-116.

Simons, D. A. (1978). 'The analysis of propagating slip zones in porous elastic media' in Fracture Mechanics, Proceedings of the Symposium in Applied Mathematics of AMS and SIAM (Ed. R. Burridge), pp. 153-168.

Simpson, D. W. (1976). 'Seismicity changes associated with reservoir loading'. Eng. Geol., 10, 123-150.

Verruijt, A. (1968). 'Elastic storage of acquifers' in Flow Through Porous Media (Ed. R. J. M. DeWiest), Academic Press, New York.

Wesson, R. L. (1981). 'Interpretation of changes in water level accompanying fault creep and implications for earthquake prediction', J. Geophys. Res., 86, 9259-9267.

Whitcomb, J. H., Garmany, J. D. and Anderson, D. L. (1973). 'Earthquake prediction: variation of seismic velocities before the San Fernando earthquake', Science, 180, 632-635.

Zoback, M. D. and Hickman, S. (1982). 'In situ study of the physical mechanisms controlling induced seismicity at Monticello reservoir, South Carolina', J. Geophys. Res., 87, 6959-6974.

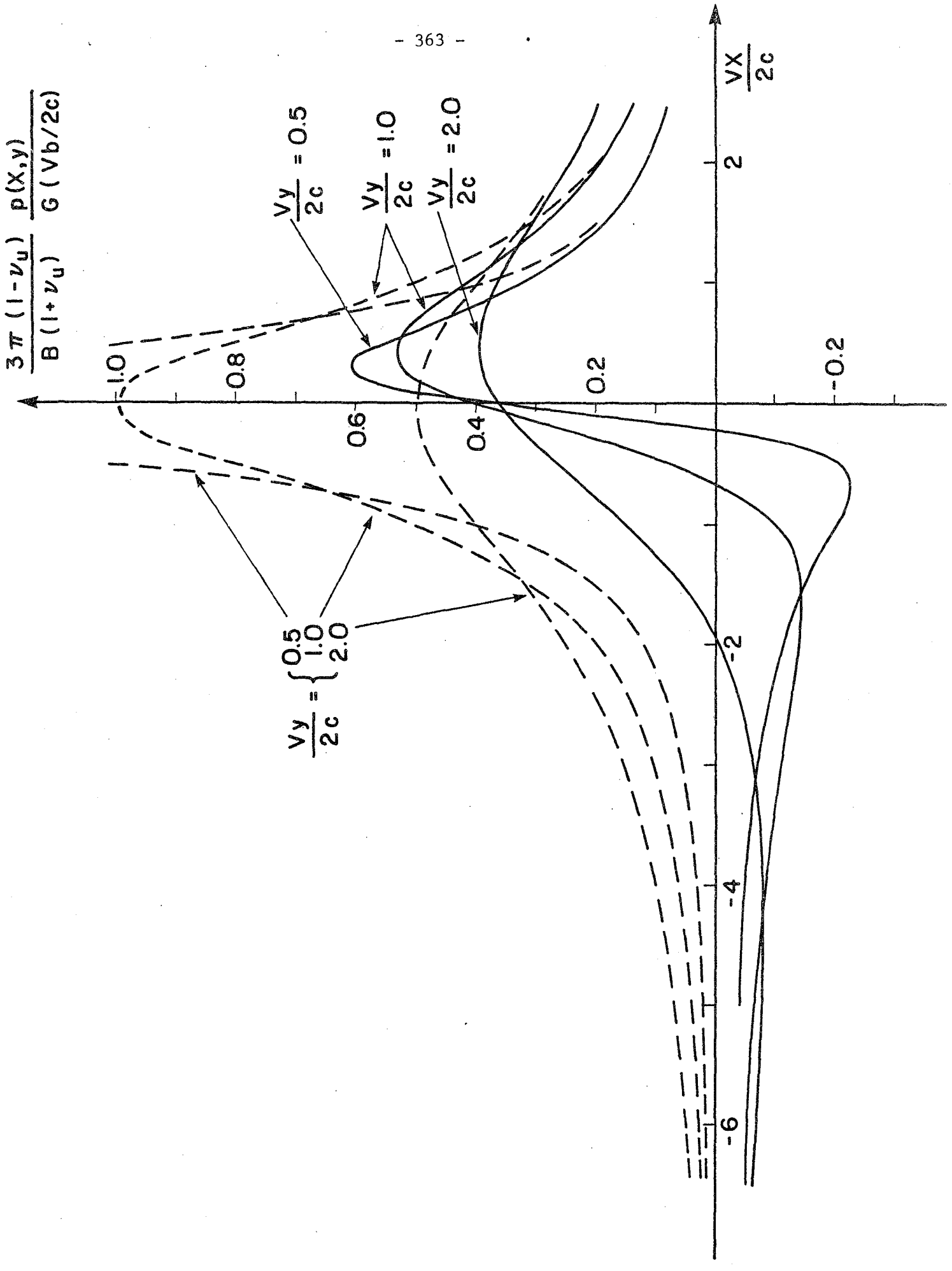
$\frac{3\pi(1-\nu_u)}{B(1+\nu_u)}\frac{p(X,y)}{G(Vb/2c)}$
$\frac{Vy}{2c}$ = 0.5
$\frac{Vy}{2c}$ = 1.0
$\frac{Vy}{2c}$ = 2.0
$\frac{Vy}{2c}$ = 0.5 1.0 2.0
$\frac{VX}{2c}$
1.0
0.8
0.6
0.4
0.2
-0.2
2
-2
-4
-6

EFFECT OF PORE WATER AND ITS DIFFUSION IN CONCRETE

G. Horrigmoe
Multiconsult Narvik A.S.
Dronningens gt.51, P.O.Box 381
8501 Narvik, Norway

1. INTRODUCTION

The mechanical behavior of porous materials, including concrete, is known to depend strongly on the distribution and history of moisture content. Material parameters affected by variations in moisture content comprise practically all the major parameters employed in the analysis and design of concrete structures , e.g. strength, modulus of elasticity thermal conductivity, moisture diffusivity and permeability [1] . Moreover, pore humidity is a key factor in long-time deformations of concrete, known as creep and shrinkage. Thus, reliable mathematical models that can predict the distribution of pore humidity in concrete structures is of major importance. While a large body of experimental information on moisture transfer in concrete has been assembled over many years of research, the development of prediction methods attracted relatively minor attention following the pioneering effort by Carlson [8] in 1937. It was not until the introduction of novel applications of concrete, especially in the form of pressure vessels

for nuclear reactors, that research in mathematical models for predicting moisture transfer gained momentum. In these structures, a correct prediction of heat and moisture transfer is a prerequisite for safe and economical desings, and this has undoubtedley been major contribution factor in the recent developments in mathematical models for diffusion of pore water in concrete.

Among the building materials in common use, concrete is the only material for which basic questions regarding mechanisms of deformation and constitutive relations remain unsettled. Whereas constitutive modelling for materials such as metals and polymers has been carried well into the nonlinear regime, most of the material research in concrete remains focused on the behaviour in the working stress range. In particular, constitutive relations for creep and shrinkage continue to be a question of considerable controversy in the literature [2]. Since the ultimate values of these time-dependent deformations are known to be several times greater than the instantaneous elastic response, their importance as the main cause of defections, redistribtion of stresses and cracking, is undisputed. However, considerable disagreement prevails regarding the the microstructural mechanisms involved in creep and shrinkage deformations. Above all, the effect of changes in pore humidity on creep and shrinkage and its constitutive modelling is far from being resolved.

The purpose of the present paper is to summarize and review the effects of diffusion of pore water in concrete, with special emphasis on mathematical models for moisture transfer. Drying of concrete under isothermal (or quasi-isothermal) condititions is a problem of widespread interest. The application of diffusion theory to model

moisture transport during drying is outlined in Section 3. Various formulations are discussed together with the effects of advancing hydration and variable temperature. The formulation of coupled heat and moisture transfer then follows in Section 4. The influence of pore humidity on creep and shrinkage and the corresponding constitutive relations are briefly examined in Section 5.

2. PHYSICAL NATURE OF PORE WATER IN CONCRETE

Concrete is formed by chemical reactions between Portland cement and water. This process is generally referred to as hydration and results in a very fine gel-type structure. Typical porosities of hardened cement paste are in the range of 0.40 - 0.55. The major part of the voids constitutes of micropores. The larger capillary pores are randomly distributed throughout the cement paste and, at least in mature and dense concretes, capillary pores can be viewed as isolated voids and not as an interconnected system. The dominant role of the micropores in cement paste produces an enormous internal surface area (of the order of $5\text{-}10^8$ m^2 per m^3, or approximately 200 000 m^2 per kg [1].

Water in concrete is held with varying degree of firmness. First, there is chemically bound water which forms a part of the hydrated compounds. Next, there is adsorbed water, i.e. water held by surface forces in the form of films on the pore walls. Due to the comparatively large size of the capillary pores, water in these pores is beyond the influence of surface forces and is referred to as free water or capillary water. The separation of water into these three categories is mainly of theoretical

value since at present there is no experimental technique available by which the various forms of water can be quantitatively determined.

A more feasible way of distinguishing between different forms of water in cement paste is to divide it into two categories: evaporable and non-evaporable. The evaporable water is by definition the amount of water which is removed from concrete upon complete drying (usually at 105°C). Similarly, the water remaining in the dried specimen after equilibrium has been achieved is the non-evaporable water.

In the pores, molecules of water vapour are attracted by surface forces that retain them at the solid surface, thus forming thin adsorbed layers of water molecules. The average thickness of the adsorbed layer increase with relative pore humidity as illustrated in Fig.2.1 for a micropore of variable thickness. The maximum layer thickness has been estimated to 5 molecules [2] ; hence, for a pore to accomodate complete adsorbed layers on two opposite walls, the pore thickness must at least be that of 10 molecules, or 26 Å. Provided that the thickness of the pore allows it and, at that the relative humidity is sufficiently high, a capillary meniscus may develop, thereby creating a certain amount of free, capillary water within the pore.

In the pores that are less than 10 molecules thick, complete adsorbed layers of water molecules cannot develop. Such films are therefore called hindered adsorbed layers. Adsorbed molecules are not held permanently but retain sufficient mobility to be able to diffuse along the layers.

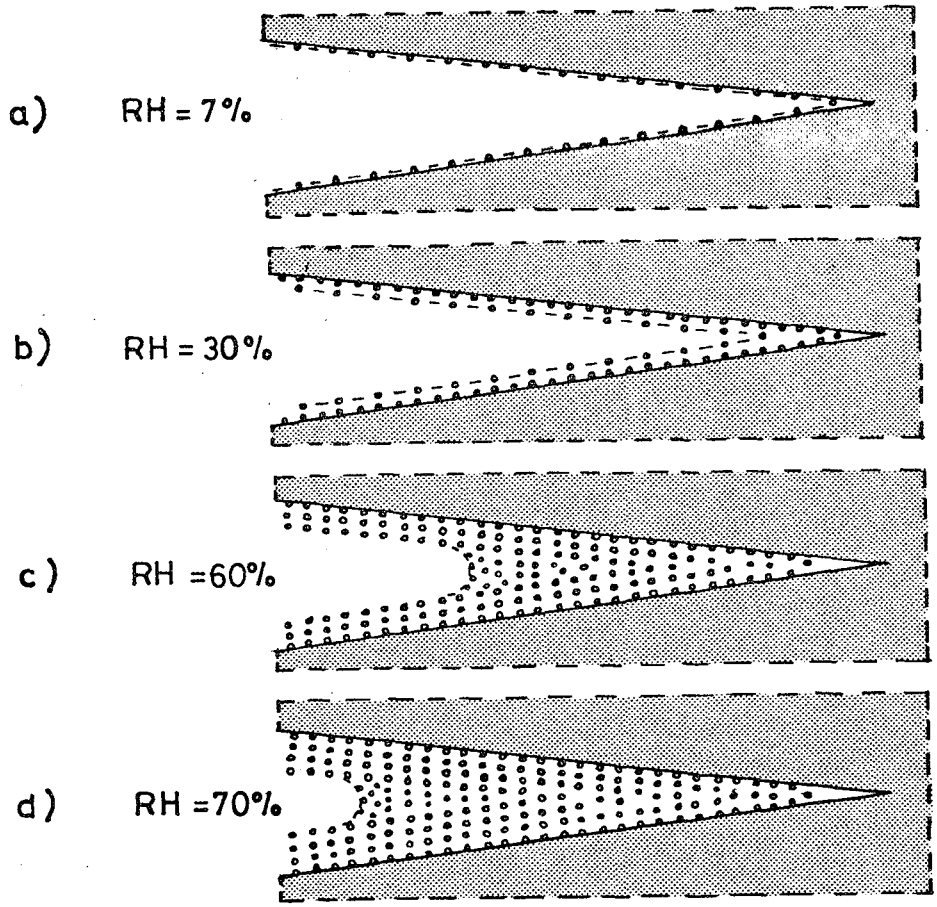

Fig. 2.1 Gradual filling of a micropore due to adsorption and capillary condensation. Source: Bažant [3].

For any porous material in equilibrium with the surrounding air there exists a definite equilibrium moisture content that increases with increasing relative humidity. For RH = 0, the mass of evaporable water is zero and at RH = 100% all pores should in principle be completely filled with water. At a given temperature the material thus processes an equilibrium curve, or a sorption isotherm, defining the amount of evaporable water retained at various relative humidities. Studies of the relationship between evaporable water content

in hardened cement paste and relative humidity of the ambient air can be found in the pioneering work of Powers and Brownyard [4] . The shape of the sorption isotherm depends on whether the material attains its equilibrium by taking up or by losing moisture, that is, by adsorption or desorption. A qualitative picture of sorption isotherms for

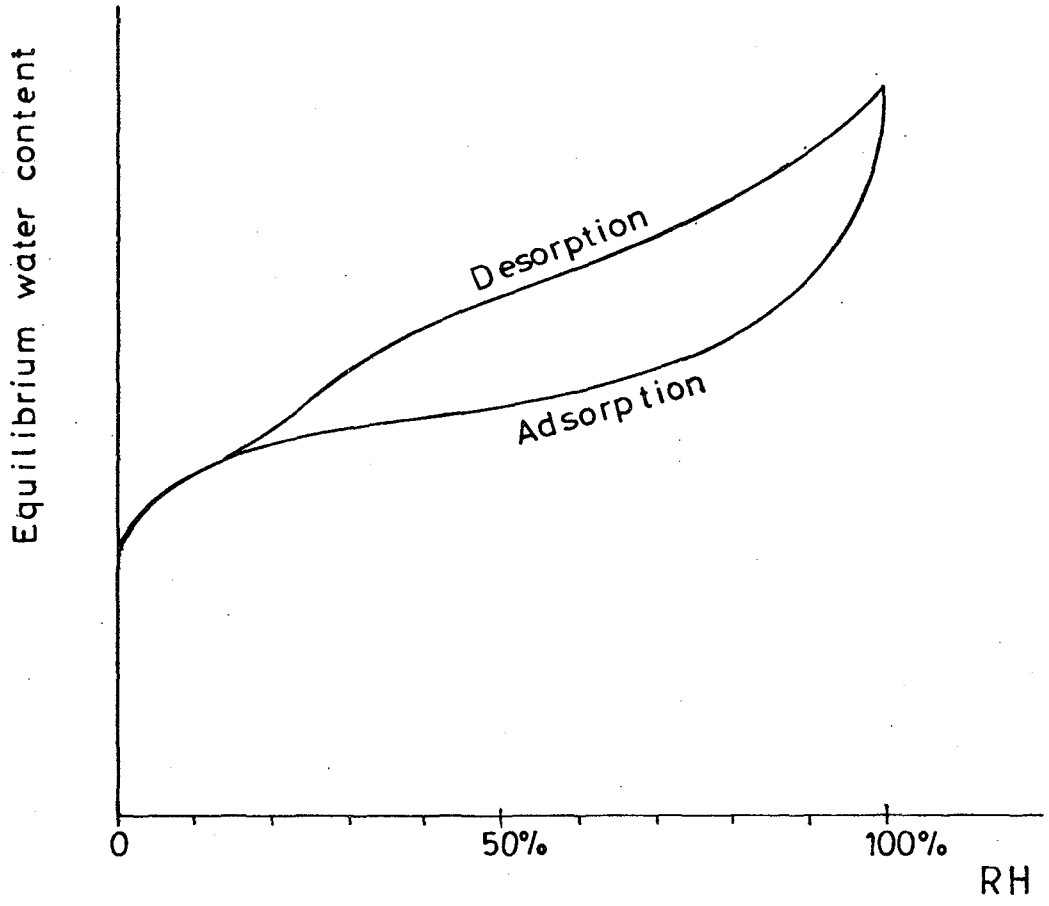

Fig. 2.2 Typical sorption isotherm of concrete.

concrete is sketched in Fig. 2.2. It is seen that the adsorption isotherm deviates from that of the preceeding desorption. This irreversibility is mainly caused by changes of the porosity of cement paste during drying [5]. The shape of the sorption isotherm depends on several factors, such as degree of hydration, water - cement ratio and temperature. It should perhaps also be noted that in actual concrete structures the material is never completely dried nor does it reach complete saturation; rather, the moisture content at a given instant is a result of successive cycles of partial drying and rewetting. Hence, the equilibrium moisture content becomes a function of the preceeding history.

3. MATHEMATICAL FORMULATION OF DIFFUSION OF PORE WATER IN CONCRETE.

Drying of concrete is a non-stationary hygro-thermal process taking place in a chemically unstable material. It is generally accepted that the theory of diffusion [6] provides an acceptable means of describing moisture transfer in concrete. However, it should be borne in mind that transport of moisture in a material with a complex structure like concrete is likely to take place by a number of different mechanisms. Consequentely, diffusion theory can only represent an approximation to the true behaviour.

In general, mass transfer in porous materials can be described by a linear relationship between the flux of the diffusing substance and the potential gradient, which represents the driving force. Thus,

$$J = - \tilde{c} \text{ grad } \mu \qquad (3.1)$$

where J represents the mass flux per unit area and time, μ is the potential and $\tilde{c}$ a transfer coefficient characterizing the diffusion properties of the material. Although the above relation is empirical, it remains valid provided the potential gradient is sufficiently small.

The second building block in the mathematical formulation of mass transfer is the conservation of mass, which reads,

$$\frac{\partial \mu}{\partial t} + \text{div } J + S = 0 \qquad (3.2)$$

Here, t denotes time and S is a source or zink term.

Generally, moisture transfer involves simultaneous transport of energy, and in some cases transfer of momentum may also be involved. These are coupled processes that require the simultaneous treatment of each transport phenomenom involved. However, under certain simplifying assumptions, diffusion of pore water in concrete can be considered independent of other transfer processes.

Isothermal drying of non-saturated concrete.

Linear diffusion theory

In mature concrete (negligible rate of hydration) under isothermal conditions, the driving force in the moisture diffusion may be taken as the moisture concentration gradient. Letting w denote the specific mass of evaporable water (mass per unit volume), Eq. (3.1) becomes

$$J = C \text{ grad } w \tag{3.3}$$

where C is the diffusivity (or diffusion coefficient). This relation is known as Fick's first law. Neglecting the source term, the balance of mass equation (3.2) reduces to

$$\frac{\partial w}{\partial t} + \text{div } J = 0 \tag{3.4}$$

The differential equation governing diffusion of moisture in concrete then directly follows by combination of Eqs. (3.3) and (3.4),

$$\frac{\partial w}{\partial t} = \text{div } (C \text{ grad } w) \tag{3.5}$$

For constant diffusivity, i.e. C = const., the above equation reduces to a second order, linear differential equation of the form:

$$\frac{\partial w}{\partial t} = C \nabla^2 w \tag{3.6}$$

where ∇^2 is the Laplacaian operator.

Because the theory of diffusion can be applied to a number of physically different transfer phenomena the solution of the above differential equation can be obtained by well documented procedures such as Fourier series, finite difference and finite element methods [7].

Equation (3.6), generally referred to as Fick's second law of diffusion, has been preferred in most of the litterature on drying of concrete. It was first used by Carlson [8] in the 1930's. Later the linear diffusion equation (3.6) has been adopted in a number of investigations [9 - 13] dealing with drying and shrinkage of concrete. The diffusion coefficients reported in these studies vary from approximately 10^{-10} to 10^{-12} m^2/s, which is a considerable difference.

An alternative formulation of the diffusion of pore water in concrete is possible. The potential μ in Eq. (3.1) may be taken as the Gibbs free energy per unit mass of evaporable water. Assuming that water vapor obeys the ideal gas equation, the potential of water can be expressed as

$$\mu = \frac{R}{M} T \ln h + \mu_{sat}\ (T) \tag{3.7}$$

where R is the gas constant, M is the molecular weight of water and T is absolute temperature. The relative pore humidity h is defined by

$$h = \frac{p}{p_{sat(T)}} \tag{3.8}$$

in which p is pore pressure and p_{sat} pore pressure at saturation, depending on temperature. Similarly, $\mu_{sat}(T)$ represents the value of Gibbs free energy corresponding to full saturation ($h = 1.0$). Assuming grad T to be negligible, it follows by substitution of Eq.(3.7) into Eq. (3.1) that the water flux can be expressed as

$$J = -\bar{a} \text{ grad } h \tag{3.9}$$

in which $\bar{a}$ is the permeability and is given by

$$\bar{a} = \frac{R}{M} \tilde{c} \frac{T}{h} \tag{3.10}$$

Diffusion of pore water in concrete is an extremely slow process and it seems reasonable to assume that thermodynamic equilibrium exsists between the various phases of water within each macropore. Thus, the relation between w and h as given by the desorption isotherm (Fig.2.2) may be taken as valid for the moisture diffusion during drying of concrete. For mature concrete and constant temperature, one may write

$$\frac{\partial w}{\partial h} = \frac{1}{k(h)} \qquad \text{or } dh = k(h)\, dw \tag{3.11}$$

in which $k(h)$ is the inverse slope of the desorption isotherm $w = w(h)$, see Fig.2.2. The variation of the coefficient k is not too large, exept for the lower humidities, which are outside the range of interest for ordinary drying. Hence, without any significant loss of accuracy, k may be taken as constant within the interval $0.95 \geq h \geq 0.25$.

Differentiating Eq. (3.11) with respect to time and substituting the result into Eqs. (3.4) and (3.9) leads to the following differential equation:

$$\frac{\partial h}{\partial t} = \text{div } (C \text{ grad } h) \tag{3.12}$$

where diffusivity C is given by

$$C = k\bar{a} \tag{3.13}$$

Equation (3.12) represents the differential equation, in terms of h, governing drying of concrete under isothermal conditions and was developed by Bažant and Najjar [14, 15]. This formulation cannot be directly applied to rewetting of concrete since the slope of the adsorption isotherm deviates significantly from that during desorption (Fig.2.2).

If the boundary condition at the surface of a drying body is that of perfect moisture transfer, this is easily implemented by requiring that

$$h = h_e \tag{3.14}$$

with h_e being the environmental humidity at the surface. For completely sealed surfaces. the normal flux water vanishes, i.e.

$$\mathbf{n} \cdot \mathbf{J} = 0 \tag{3.15}$$

where **n** is the unit outward surface normal.

The two formulations of drying defined by Eqs.(3.5) and (3.12) are equivalent provided that change of material parameters due to hydration in neglected. The formulation in terms of pore humidity makes it easier to incorporate

the effect of aging of concrete because h is directly related to Gibbs free energy μ, cfr. Eq. (3.7), which is not the case with w, see Ref. 15. Moreover, as we have already seen, boundary conditions are most conveniently defined in terms of relative humidity. Constitutive relations for creep and shrinkage depend on pore humidity, so that the distribution of h has to be known before the time-dependent deformations can be computed. For these reasons, the differential equation for drying in terms of h, Eq. (3.12), seems to have distinct advantages compared to the formulation in terms of w as defined by Eq. (3.5). It should be noted that according to the definition of pore humidity (3.8) a formulation in terms of pore pressure p would equivalent to that in terms of h.

In developing Eq. (3.12) it has been tacitly assumed that concrete may be treated as an isotropic, homogeneous material. Looking at the microstructure of concrete, this certainly seems an oversimplification. Moreover, it is obvious that in concrete structures some parts will exhibit considerable anisotropy due to the methods used for placing of concrete. Hence, in a rigorous formulation diffusivity should be treated as a tensorial quantity. However, there is no experimental data available supporting such a formulation and in view of this the use of a single scalar parameter to characterize diffusivity of concrete seems completely adequate.

The speed with which pore water migrates in concrete depends on the structure and distribution of pores in cement paste. Thus, diffusivity is a function of water-cement ratio and the degree of maturity, as evidenced by laboratory tests.

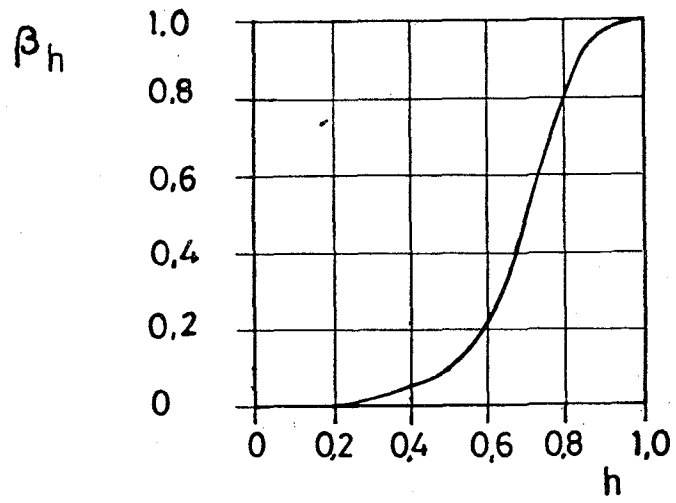

Fig. 3.1 Dependence og β_h on pore humidity h

The differential equation governing drying of concrete, including the effects of advancing hydration and variable temperature, then becomes

$$\frac{\partial h}{\partial t} = \text{div } (C \text{ grad } h) + \frac{\partial hs}{\partial t} + \kappa \frac{\partial T}{\partial t} \qquad (3.22)$$

This form of the diffusion equation is due to Bazant and Najjar [15] . It is limited to slowly varying temperatures since grad T ≈ 0 has been assumed in the derivation of Eq. (3.22). Otherwise, the temperature gradient must be included as an additional driving force in the transfer of moisture [17]. This leads to a coupling of heat and moisture transfer and will be dealt with in Section 4.

Effect of hydration

In fresh concrete, the advancing hydration calls for certain modifications of the diffusion equation. During hydration a certain amount of evaporable water is consumed by the chemical reactions. This effect can be accounted for by adding a correction term to Eq. (3.11) so that the relation between pore humidity and water content becomes

$$dh = kdw + dh_s \tag{3.16}$$

where dh_s represents the drop in pore humidity caused by hydration. The function $h_s(t)$ thus represents the so-called self-desiccation taking place in a sealed specimen. The direct effect of hydration on pore humidity is relatively small since it is somewhat counterbalanced by the simultaneous reduction in porosity.

It is clear that self-desiccation, permeability and the slope of the desorption isotherm must depend on the degree of hydration. An objective measure of the maturity or degree of hydration of cement paste is the so-called equivalent curing period t_e, defined by [2]

$$t_e = \int dt_e = \int \beta_T (T) \cdot \beta_h(h) dt \tag{3.17}$$

where β_T is assumed to obey the Arrhenius equation,

$$\beta_T = \exp \left[\frac{U_h}{R} \left(\frac{1}{T_o} - \frac{1}{T}\right)\right] \tag{3.18}$$

in which U_h is the activation energy of hydration and T_o is a chosen reference value of the current absolute temperature T. For temperatures between 0^o and 100^oC

one may use [2]

$$\frac{U_h}{R} \simeq 2500^{\circ} K$$

The actual functional dependence of h_s, $\bar{a}$ and k on t_e is not dealt with here, but it is known from experiments that the effect of curing time on permeability can be servere. It should also be noted that drying inevitably causes the distribution of t_e to be non-uniform throughout the body, cfr. the definition of β_h (3.19)

The effect og humidity on the equivalent curing period can be approximated by the empiricial formula [2]

$$\beta_h = [1 + (3.5 - 3.5h)^4]^{-1} \qquad (3.19)$$

which is shown graphically in Fig.2. It is known that the rate of hydration becomes negligible when pore humidity drops below h = 0.6 and this is well represented by Eq. (3.19).

Effect of temperature

The dependence of pore humidity on temperature can be accounted for by augmenting Eq. (3.16) by one additional term,

$$dh = kdw + dh_s + \kappa\, dT \qquad (3.20)$$

where κ is the hygrothermic coefficient,

$$\kappa = \left(\frac{\partial h}{\partial T}\right)_{w,t_e = \text{const.}} \qquad (3.21)$$

whose variation with h is shown in Fig.3.2.

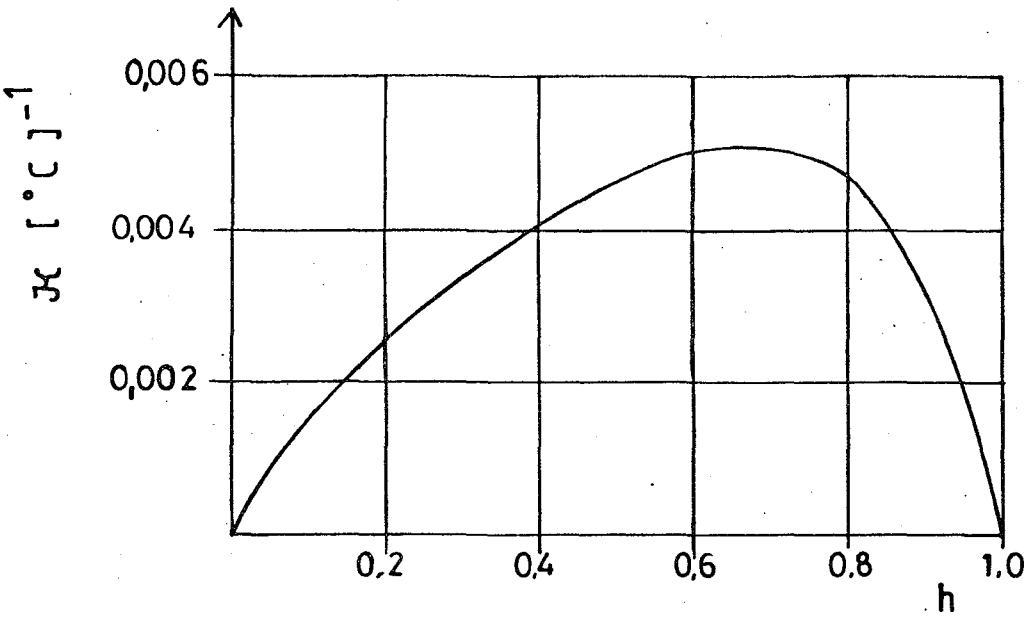

Fig. 3.2 Hygrothermic coefficient κ.
Source Bazant [16] .

Nonlinear diffusion theory

As means of obtained approximate solutions, the linear diffusion theory with constant diffusivity may be adequate for a great number of practical problems. Still, this simplified approach suffers from serious shortcomings. Assuming a constant value for the diffusion coefficient is contradictory to experimental evidence on the drying behavior of concrete. Laboratory test clearly demonstrates that in an initially fully saturated specimen subjected to drying, moisture is lost with increasing diffuculty as drying progresses. Thus, diffusivity should decrease with decreasing values of pore humidity (or specific water content). This fact was noted already in the earliest theoretical investigations of drying, see e.g. Ref. 8. Later, the dependence of

moisture conductivity on specific moisture content has been thoroughly discussed by Pihlajavaara [18 - 21] who also carried out numerical studies based on differential equation (3.5) with diffusivity taken as a linear function of moisture content w.

The alternative nonlinear formulation in terms of pore humidity (3.12) has been explored by Bazant and Najjar [14, 15] . This approach requires the diffusivity C = C(h) to be determined by fitting of test data. However, it seems that most experimental data on drying are in the form of measured weight losses and only for a very limited number of tests has the distribution of pore humidity at various stages of drying been reported. From fits of relevant data it was concluded that the following relationship provided acceptable agreement with experiments:

$$C(h) = C_1 \left[\alpha_0 + \frac{1-\alpha_0}{1 + \left(\frac{1-h}{1-h_c}\right)^n}\right] \qquad (3.23)$$

where C_1, α_0 , h_c and n are constants. In Ref.15 it was found that most of the available data could be fitted by setting $\alpha_0 = 0.05$, $h_c = 0.75$ and $n = 16$. The same formula with $n = 3$ was adopted by Argyris et al. [17]. The coefficient C_1 represents the value of diffusivity at $h = 1.0$ and is a function of temperature T and maturity t_e. A semi-empirical formula for C_1 (T, t_e) based on the activation energy concept is given in Ref.2.

The dependence of diffusivity on h is shown graphically in Fig. 3.3 which also illustrates the meaning of α_0 and h_c, and the effect of varying the value of the exponent n. It is evident from Fig.3.3 that the highly nonlinear relationship between C and h may cause serious difficulties for the numerical solution of the diffusion

equation (3.12). Thus, exstreme care should be exercised in selecting an appropriate solution algorithm as discussed by Argyris et al. [17].

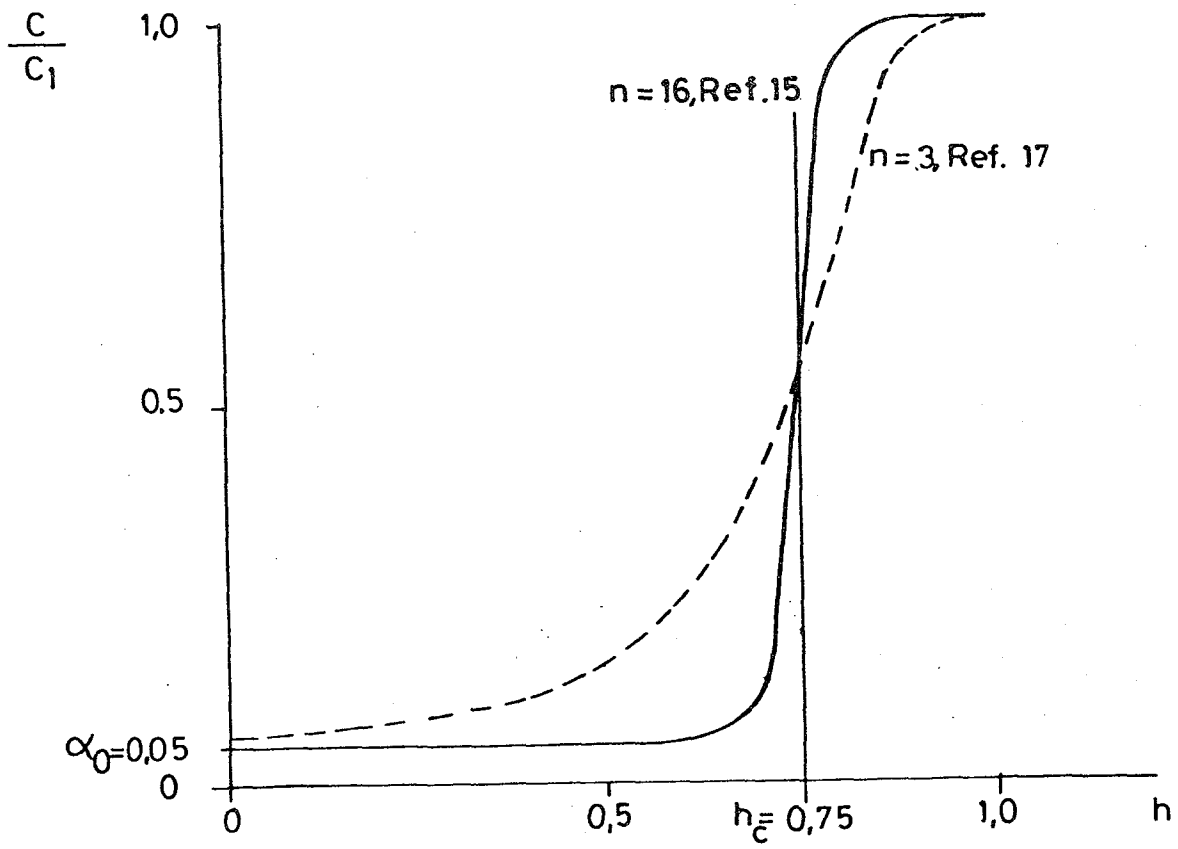

Fig. 3.3 Diffusivity C as a function of humidity h according to Eq. (3.23).

A plausible explanation of the severe reduction in diffusivity between h = 0.8 and h = 0.6 is suggested in Ref.15. At low humidities (h < 0.6) the migration of water molecules along the absorbed layers is considered to be the dominant factor in the diffusion process. For

humidities above h = 0.8 the flow of capillary water is the most important factor in the moisture transport. The interval between h = 0.6 and h = 0.8 may then be thought of as a transition zone in which flow of the less firmly held molecules in the outer layers is gradually replaced by flow of capillary water. The modelling of the transition zone is strongly dependent on the value of the exponent n, as can be observed from Fig. 3.3.

In Refs. 14,15 solutions obtained by the nonlinear diffusion equation (3.12) with C defined by equation (3.23) were compared with test data. Fig 3.4 shows some results for pore humidity in the centre of a slab subjected to drying in various environmental humidities. The experimental values plotted in Fig.3.4 were reported in Ref.22. Also shown for comparisons are the results obtained by setting C = const.

Fig. 3.5 shows the distribution of pore humidity at different times for the same experiments as in Fig.3.4. The nonlinear diffusion equation is in relatively good agreement with the test data while severe discrepancies can be observed for the results obtained from the use of a constant diffusion coefficient. Although, the numerical studies reported in Refs. 14 and 15 are limited in number, it may be concluded that prediction for drying of concrete based on nonlinear diffusion theory gives better correlation with experimental data than does the simplified linear diffusion equation.

Saturated concrete

So far, only diffusion of pore water in nonsaturated concrete has been considered. The differential equation governing diffusion in completely saturated concrete is similiar to Eq. (3.12) and can be written in the form

$$\frac{\partial p}{\partial t} = C_{sat} \nabla^2 p \qquad (3.24)$$

where p is hydraulic pressure in excess of atmospheric pressure and C_{sat} denotes diffusivity of pore water in saturated concrete, which is directly related to permeability $\bar{a}$ through the equation[23]

$$C_{sat} = \frac{\bar{a}}{\gamma g_w} \qquad (3.25)$$

Here, γ is the volumetric compressibility of capillary water and g_w the unit weight of liquid water.

With the aid of Eq. (3.25) values of diffusivity can be calculated from measured data on permeability. This conversion has been carried out by Murata [24] who reported values of C_{sat} ranging from 10^{-8} to 10^{-4} m^2/s. Compared to the normal diffusivities in nonstaturated concrete these values are several orders of magnitude higher. Hence, for structures like concrete dams in which both saturated and nonsaturated regions may exist, a discontinous jump between C and C_{sat} is to be expected at the interface between saturated and nonsaturated concrete.

Another important aspect in massive concrete structures is the water deficiency created by hydration which leads to considerably smaller values of diffusivity than that associated with a saturated state. This can be attributed to nonsaturated conditions due to air-filled voids produced by self-dessication before the arrival of the hydralic front. It should be noted that the use of air-entraining admixtures reinforces this effect. The diffusion equation (3.25) can be easily modified to account for the influence of self-dessication, see Ref.23.

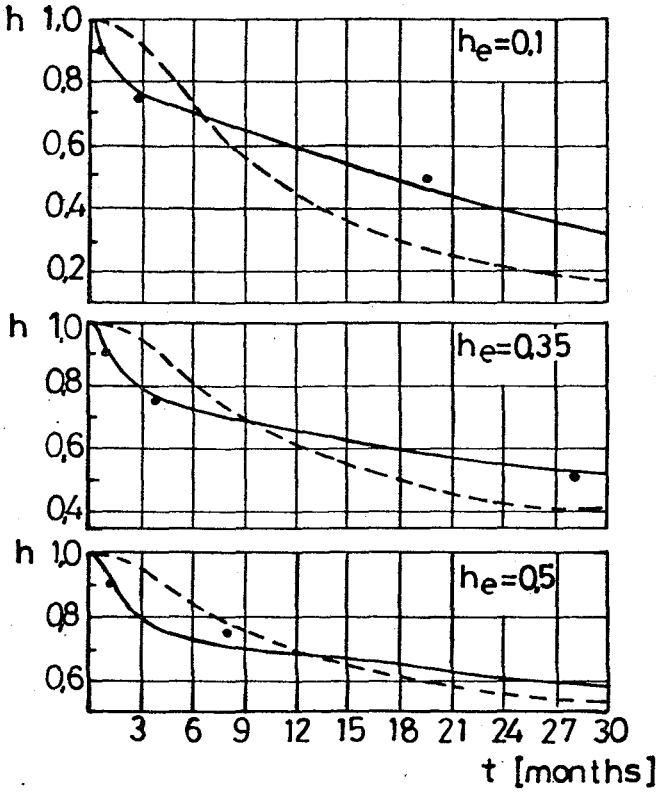

Fig. 3.4 Experimental (dots) and calculated pore humidities in centre of slab, solid line: variable C, dashed line: constant C. Source: Bažant and Najjar [14].

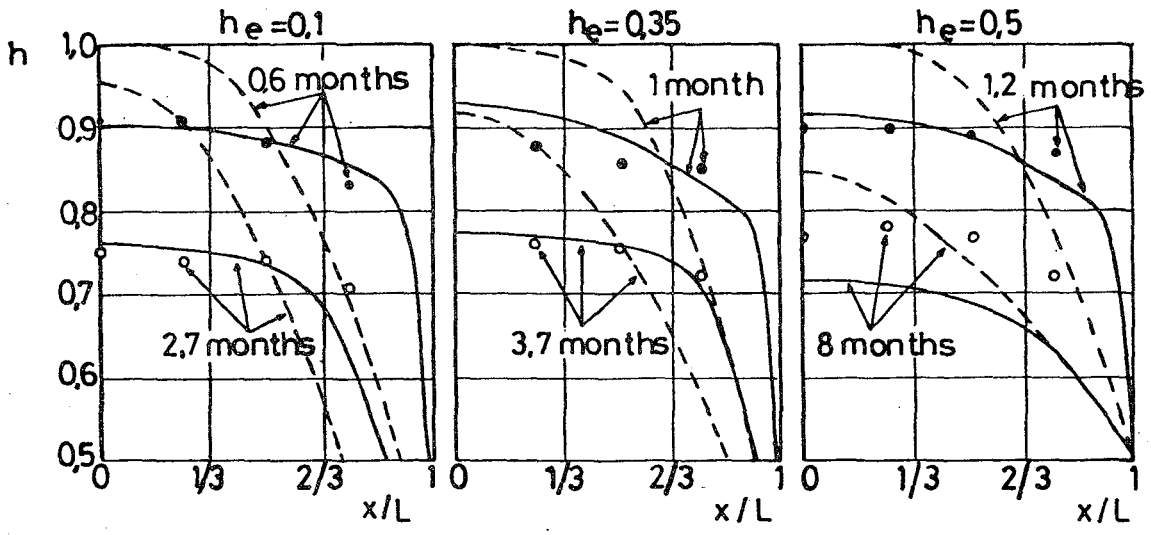

Fig. 3.5 Experimental (dots) and calculated distributions of pore humidity in drying slab; nonlinear diffusion theory (solid line) and linear diffusion theory (broken line). Source: Bažant and Najjar [14] .

4. COMBINED HEAT AND MOISTURE TRANSFER.

Heating of concrete will cause increased pressures in the pores of the material, which in turn causes migration of moisture and eventual drying. At the same time, moisture transport influences heat transfer and, hence, temperature distribution throughout the body. Moreover, the existence of temperature gradients will act as a driving force of moisture transfer in addition to the gradient of moisture concentration already discussed in Section 3. This leads to a coupling of the fluxes of

heat and mass with the gradients of temperature and moisture concentration.

Combined heat and mass transfer in concrete (and its effects on time-dependent deformations) influences structural behaviour of a variety of modern concrete structures, although this is often neglected in stress analysis and design. Of particular interest is the effect of high temperatures on the mechanical behavior of concrete in modern prestressed nuclear reactor vessels. Another problem of great concern for these structures is the radiation shielding capacity which is strongly dependent on moisture content.

Material properties.

Research on high temperature effects in concrete has traditionally been focused on evaluating fire resistance of concrete structures. A major portion of this research effort has been empirical and directed towards the study of the behavior of structural elements rather than fundamental material properties. Still, the available experimental information on high-temperature behavior of concrete is by no means insignificant, as indicated by the recent survey [25]. A complete review of the influence of temperature on material properties is beyond the scope of this paper and the reader is referred to Ref.25 for details and numerous references. In the following, only a few of the more fundamental aspects of high-temperature behavior will be discussed.

It is well known that an increase of temperature accelerates drying. At room temperature it may take years for a cylindrical specimen of 150 mm diameter to dry completely while the drying time at 100^{o}C is less than a day. It is generally assumed that all evaporable water in a specmen is removed when equilibrium has been

reached at a drying temperature of 105°C.

Another important effect of high temperatures is the gradual dehydration of cement paste. As temperature is raised beyond 120°C, both cement gel and calcium hydroxide are continuously decomposed and the chemically bound water is released into the pores. Dehydration increases with temperature and becomes complete at temperatures of approximately 600 - 850°C [26, 27]. The chemical decomposition gradually destroys the microstructure which in turn leads to increased porosity. Harmathy [26] reports that the porosity growth from 105°C to 850°C can be as much as 40 per cent.

It is to be noted that chemical changes take place in the aggregates as well. However, for ordinary aggregates this effect can be neglected for $T < 500°C$.

For the analysis of heat and mass transfer, information on heat capacity and thermal conductivity is needed. Due to the presence of various constituents in concrete (cement paste, aggregates, water, air) and the phase changes that may take place in pore water, the dependence of heat capacity and thermal conductivity on temperature and moisture content is a rather complex problem with little experimental data available. The lack of quantitative test data also holds true for moisture conductivity and permeability, although these quantities can be assumed to obey the activation energy concept up to 100°C. The accelerated drying observed for temperatures above 100°C indicates a jump upwards in diffusivity as 100°C is exceeded. This may be attributed to a possible change in the mode of moisture transfer, from migration along adsorbed layers below 100°C to flow of vaporized steam at elevated temperature [25].

Analysis of heat and mass transfer.

When concrete is subjected to high temperatures in a drying environment, one faces the problem of coupled heat and mass transfer in a porous body undergoing micro-structural and chemical changes. The general mathematical formulation of such problems is well-established within the theory of irreversible thermodynamics [28] . The influence of deformations on the fluxes of moisture and heat can be neglected,which, of course, simplifies the problem considerably. When the distribution of temperature and moisture in the body has been obtained, the resulting stresses can be calculated from the assumed constitutive relation which is a function of current values of temperature and pore humidity, and their history.

It appears that significant developments of the theory of thermal moisture transfer in porous solids have taken place in the Soviet Union. Unfortunately, very little of the results of this research has been published in western literature, except the book by Luikov [29] . A summary of the theoretical work by Soviet scientists in this area has been prepared by the same author [30] . With the introduction of powerful discretization procedures such as the finite element method the numerical solution of complex problems in heat and mass transfer has been made feasible. This includes applications to transient heat conduction [31 - 35] as well as numerical modelling of drying of porous bodies [36 - 38].

As already stated, the heat flux q depends not only on the temperature gradient but also on the gradient of moisture concentration w (Dufour effect). Similarly, the flux of moisture J is linearly related to grad w and, in addition, J is a function of the temperature gradient (Soret effect). This can be written in the

form

$$J = - a_{11} \text{ grad } w - a_{12} \text{ grad } T$$
$$q = - a_{21} \text{ grad } w - a_{22} \text{ grad } T \qquad (4.1)$$

where w is to be interpreted as the mass of all free (not chemically bound) water per unit volume of concrete. The problem is nonlinear due to the dependence of the coefficients a_{ij} (i,j = 1.2) on moisture concentration, temperature and degree of hydration. Moreover, $a_{12} \neq a_{21}$ bacause grad w and grad T are not the thermodynamic driving forces associated with the fluxes J and q , cfr. [28] .

Equation (4.1) leads to a system of coupled partial differental equations whose solution can only be obtained by sophisticated numerical procedures. The numerical solution in itself is a formidable task. Another difficulty stems from the identification of material parameters from test data. Given the limited experimental information available, it seems necessary to explore the possibility of simplifying Eq. (4.1).

One such simplification can be achieved if the moisture flux is governed by a single potential Ψ (w,T). Bažant [39] has suggested that this potential be taken as the pore water pressure p, i.e.

$$J = - \frac{a}{g} \text{ grad } p \qquad (4.2)$$

where a is the permeability (in m/s). This is equivalent to the relation used in Section 3, see Eq. (3.9), the gravity acceleration g = 9.806 m/s^2 having been included for reasons of dimensionality only.

The Dufour effect is usually of little significance for the heat flux; hence, $a_{21} \approx 0$, and consequently,

$$q = - b\,\text{grad}\ T \tag{4.3}$$

where the thermal conductivity b has been substituted for the coefficient a_{22} in Eq. (4.1).

The simplifications imbedded in Eqs. (4.2) and (4.3) may seem drastic, and, in particular, neglecting the effect of the temperature gradient on the moisture flux is not generally justified. However, the effect of grad T is implicitly included in Eq.(4.2), because we have

$$\text{grad}\ p(w,T) = \frac{\partial p}{\partial w}\,\text{grad}\ w + \frac{\partial p}{\partial T}\,\text{grad}\ T$$

Formulation of the conservation laws requires careful consideration of the physical processes involved. As already discussed, dehydration of cement paste for temperatures beyond 120°C implies that chemically bound water is released into the pores. This phenomenon must be accounted for in the conservation of mass equation, which, according to Bazant and Thonguthai[40, 41] can be expressed as

$$\frac{\partial w}{\partial t} + \text{div}\ J - \frac{\partial w_d}{\partial t} = 0 \tag{4.4}$$

where w_d is the mass of water released by the dehydration process.

The heat capacity of a multicomponent and multiphase system like concrete is not a single, well-defined quantity. However, a rigorous formulation in terms of contributions from the various components (solid microstructure, adsorbed water, capillary water, vapor) seems unnecessary complex in view of the limited experimental data presently avaliable . Thus, it may be justifiable

to consider the specific heat capacity c of concrete as a function of temperature only. The balance of heat equation them becomes [40, 41]

$$\rho c \frac{\partial T}{\partial t} - c_w \mathbf{J} \cdot \text{grad } T = - \text{div } \mathbf{q} \qquad (4.5)$$

in which ρ is the mass density of concrete and c_w is the heat capacity of liquid water. The second term on the left-hand side of the above equation represents the heat supply due to moving water and may be neglected except for situations where rapid heating occurs.

To complete the formulation, a constitutive relation between pore pressure p, water content w and temperature T in concrete is needed. An approximate, semi-empirical formula has been suggested by Bažant ang Thonguthai [40, 41]. This relation is shown diagramatically in Fig. 4.1 where the ratio of free, evaporable water content to cement content versus relative pore pressure is plotted. Below the critical point of water (374.15°C) one has to distinguish between unsaturated and saturated concrete. In Fig. 4.1 the transition from saturated to nonsaturated state is modelled by a straight line.

In general, permeability is a function of temperature and humidity, i.e. a = a (h,T). Below 100°C the dependence of permeability on temperature may be assumed to be governed by activation energy. Experimental observations [49] indicate that permeability increases approximately by two orders of magnitude for temperatures above 100°C. Below the boiling point of water permeability (like diffusivity, cfr. Section 3) decreases with decreasing relative pore humidity. Detailed expressions defining the approximate dependence of permeability on T and h can be found in Refs. 40 and 41 and only a graphical representation is included here, see Fig.4.2.

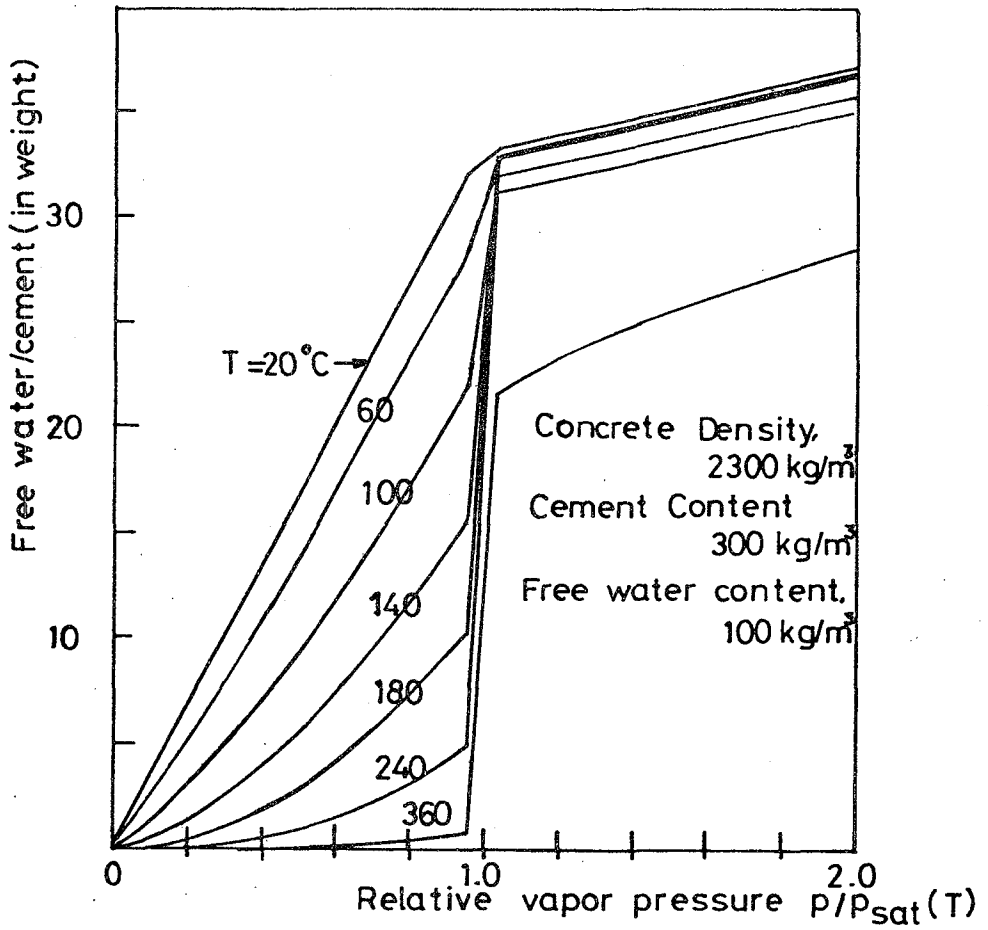

Fig. 4.1 Relation between free water w pore pressure p and temperature T.
Source: Bazant and Thonguthai [40, 41] .

Spatial discretization of the field equations (4.2) - (4.5) can be performed by means of a finite element formulation of the Galerkin procedure. Within each discrete element pore pressure and temperature are interpolated from a set of nodal values. The discretized algebraic equations of the finite element

assemblage which are computed as a sum of contributions from individual elements, can be written in the following general form:

$$\begin{bmatrix} a_{11} & a_{12} \\ a_{21} & a_{22} \end{bmatrix} \begin{bmatrix} p \\ T \end{bmatrix} + \begin{bmatrix} b_{11} & b_{12} \\ b_{21} & b_{22} \end{bmatrix} \begin{bmatrix} \dot{p} \\ \dot{T} \end{bmatrix} = \begin{bmatrix} h_1 \\ h_2 \end{bmatrix} \qquad (4.6)$$

Here, p and T are nodal values of pore pressure and temperature, respectively. A dot denotes differentiation with respect to time. Detailed expressions for the various submatrices in the above equation are available in Ref.40. In the time domain, the problem has to be solved by a step-by-step procedure. Special care must be exercized to avoid numerical instability.

Several computer programs for predicting water release and pore pressures in heated concrete already exist [40-44]. These programs are essentially similar as far as the mathematical formulation of the major mechanisms controlling heat and mass transfer are concerned but differ in the choice of material parameters and their dependence on temperature and moisture content. Differences also exist between the above programs in the selection of the spatial discretization techique (finite differences, finite elements) as well as numerical solution procedures. Comparisons of the computer programs with test data have been performed [45, 46] . Such evaluations are, however, somewhat inhibited by the relatively little amount of relevant experimental information available [40, 43, 47-49]. There seems to be considerable differences in the predictions of temperature, water release and pore pressure between the above computer programs as well as in relation to test data. The closest agreement is achieved for temperature distributions and total water release. The calculated pore pressures,

on the other hand, are relatively poor and leave room for considerable improvements.

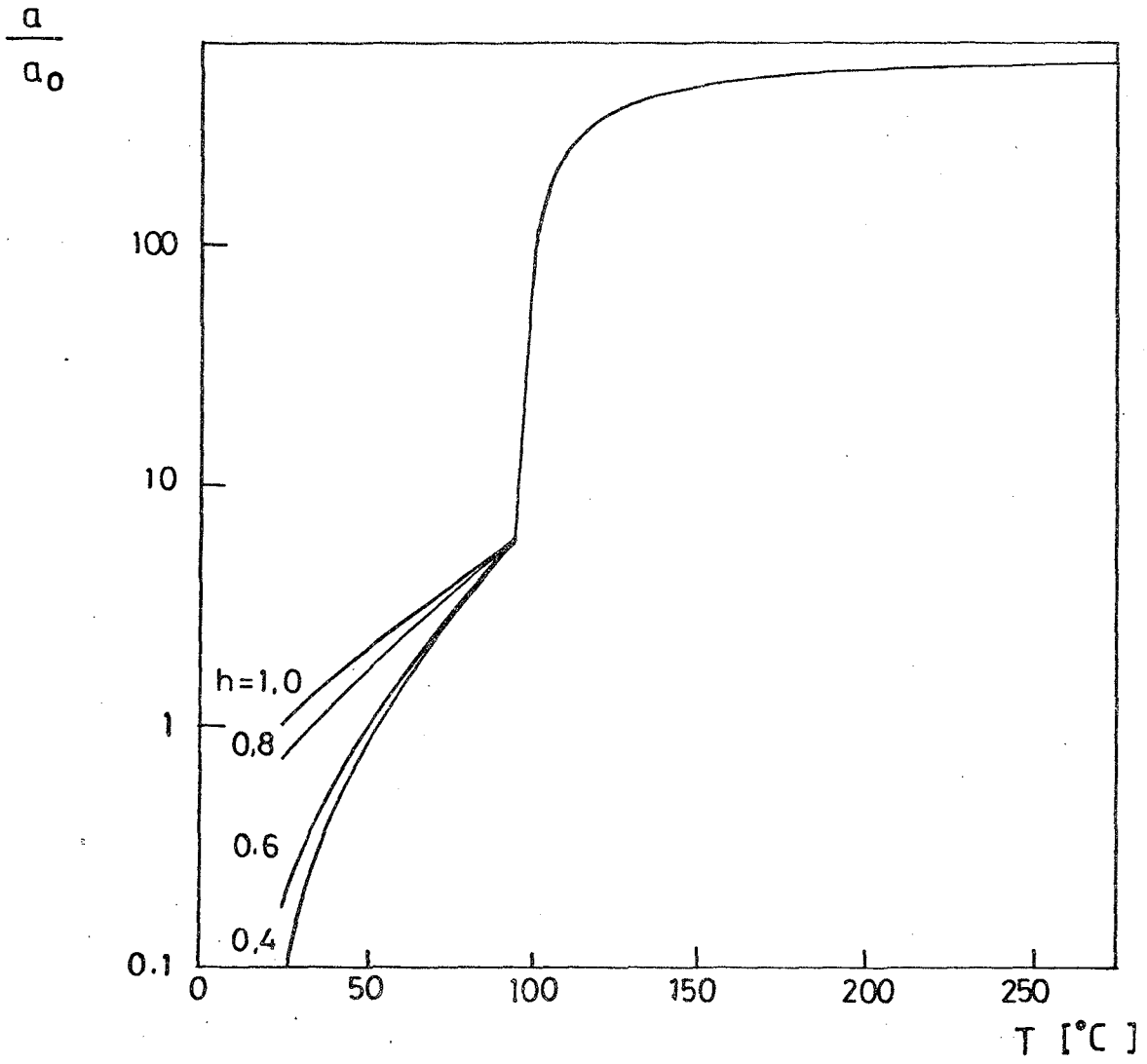

Fig. 4.2 Permeability as a function of temperature and humidity.
Source: Bažant and Thonguthai [40,41].

5. TIME-DEPENDENT DEFORMATIONS

Creep and shrinkage

Under sustained loading, deformation of concrete increases with time. This phenomenon is known as creep and the final value of creep strain can be several times as large as the instataneous elastic strain upon loading. In addition, concrete exhibits shrinkage (or swelling) which is a stress-independet deformation due to change in water content. In laboratory tests, creep is taken as the difference between the total deformation at a given time of a loaded specimen and the deformation of an "identical", unloaded companion specimen stored under the same conditions during the same period of time.

Interest in creep and shrinkage has been increasing and considerable progress has been achieved in the understanding of these phenomena. However, in spite of the extensive body of literature on this subject, many basic questions regarding the constitutive modelling of creep and shrinkage remain unsettled. Undoubtedly, this is due to the complexity of concrete as an engineering material. In particular, the strong interaction with environmental conditions (temperature and humidity) which causes migration of pore water within the material is one of the major unresolved problems in the theory of creep and shrinage. The survey papers [2,50] provide an excellent insight into the complexities involved in the development of constitutive relations for time-dependent deformations of concrete. Effects of variable temperature and humidity will be dealt with in detail by other lectures [51, 52] and the subsequent discussion is therefore restricted to a brief examination of the effects of pore water diffusion in existing mathematical models for predicting creep and shrinkage deformations in concrete.

The hydration of cement is accompained by a volumetric concentration of the system cement plus water. This reduction in volume, which takes place while concrete is still in the plastic state, is commonly referred to as plastic_shrinkage but comprise a number of different mechanisms [53] . Drying_shrinkage takes place in the hardened cement paste and is caused by a removal of water from the pores of concrete due to diffusion of moisture from the interior towards the drying surface. As outlined in Section 3, this is an extremely slow process provided severe cracking does not occur. It can also be deduced from the discussions in Section 3 that drying shrinkage increases with decreasing environmental humidity and decreases when age at the start of drying is higher.

Creep of concrete under sealed conditions (no exchange of moisture with the environment) and at constant room temperature is usually referred to as basic_creep. Due to hydration, creep deformations are reduced with increasing age at loading. Moreover, for stresses below approximately 40% of the compressive strength creep of concrete obeys the principle of superposition, which means that the strain due to a sum of stress histories is equal to the sum of the responses due to the individual stress histories. When concrete under sustained load is allowed to dry, creep is accelerated. This is the so-called drying_creep effect. Drying creep increases with decreasing environmental humidity and is accelerated by rapid changes in water content. Creep deformation of concrete under sustained temperature increases as the temperature level is raised (thermal_creep). It is also worth noting that temperature cycling leads to a sharp increase in the creep deformation rate.

Simplified prediction methods

Most of the existing mathematical models for creep and shrinkage consist of simple algebraic formulas whose main area of application is in design of ordinary concrete structures [54 - 57] . These formulas, which are usually semi - empirical, are capable of predicting average specimen or cross sectional behavior. As far as the hygro-thermal effects are concerned, approximate solutions of the nonlinear diffusion equation (3.12) are in essence incorporated in these simplified algebraic expressions. It is thus important that they are not confused with constitutive relations which are associated with local behavior (i.e. a point) of the material. It is also clear that many of the suggested formulas for predicting creep and shrinkage deformations do not comply with the principles of invariance and objectivity on which valid constitutive relations must be based.

In a recent comparison [58] of some of the suggested simplified formulas with test data it was found that these prediction methods are rather crude. Although, this may in part be attributeed to the great statistical scatter of available test data, it is felt that the accuracy of the prediction methods needs to be improved.

Constitutive relations

Nonuniform specimen behavior

A huge body of test data on creep and shrinkage of concrete has been published, especially during the last decade, Yet, this vast experimental information cannot be directly used as the basis for development of a quantitative theoretical model. The main reason for this is that laboratory specimens are not in a

uniform state of stress during the test. The outher part of the specimen will loose moisture at a higher rate than the central core, thereby producing non-uniform distributions of pore humidity and shrinkage strains over the cross section. As a result of the inhomogeneity of concrete, a complex three-dimensional state of stress is set up in the drying, load-free specimen. Depending on the environmental humidity and the duration of drying exposure, tensile stresses in the region closest to the surface may reach the tensile strength of concrete. The drying cracks thus formed cause redistribution of stresses within the specimen which alters the observed average deformation. In a recent investigation, Wittmann and Rolefstra [59] studied the effect of drying-induced cracking by a simple material model combined with pore humidity distributions determined by solving the diffusion equation (3.12). The results of these computations clearly indicate the profound effect of cracking on the time-dependent deformation of specimens subjected to drying.

In creep tests in a drying atmosphere, the external loading superimposes a uniform compressive stress on the nonuniform stresses produced by differential shrinkage deformations. This will reduce crack formation as compared to that in the companion load-free specimen used to determine pure shrinkage deformation. Moreover, in creep tests a uniform cross-sectional deformation is imposed which also causes stress redistributions that do not occur in the shrinkage specimen [60]. Hence, the companion "identical" specimens used in shrinkage and creep experiments are nor identical and, consequently the separation on the total deformation into shrinkage and creep components is invailed. Wittmamm and Roelfstra[59] , no independet mechanism of deformation may be involved in drying creep which, at least

for a major part, may be explained by crack prevention caused by the applied load.

To avoid formation of drying-induced cracks, environmental humidity must be gradually decreased so that large difference in pore humidity does not occur within the specimen. Calculations based on linear diffusion theory carried out by Bazant and Raftshol [61] indicate that the required drying rate is too slow to be practically feasible. Alternatively, the gradient in pore humidity can be eliminated by reducing the thickness of the specimen. However, the critical thickness is so small ((approximately 1.0 mm) [61, 62] that specimens have to be made of cement paste rather than concrete to avoid the formation of drying cracks.

Creep laws

Creep of concrete at h = 1.0 and constant temperature may be treated within the well-established framework of aging viscoelastic materials. Accordingly, creep strain can be expressed as a functional of the previous history of stress. To avoid storing the entire stress history a rate-type creep law i preferred. To this end, a generalized Maxwell chain model with age-dependent elastic mduli E_μ and viscosities η_μ may be selected, see Fig. 5.1. The stress σ_μ in the μth element obeys the differential equation

$$\frac{\dot{\sigma}_\mu}{E_\mu(t)} + \frac{\sigma_\mu}{\eta_\mu(t)} = \dot{\varepsilon} - \varepsilon_o \quad ; \quad \mu = 1,2,\ldots,n \tag{5.1}$$

in which ε is the total strain and ε^o is load-independent strain caused by shrinkage or thermal dilation. A general procedure for converting the integral-type creep law into above rate-type formulation is available in

Ref. 63.

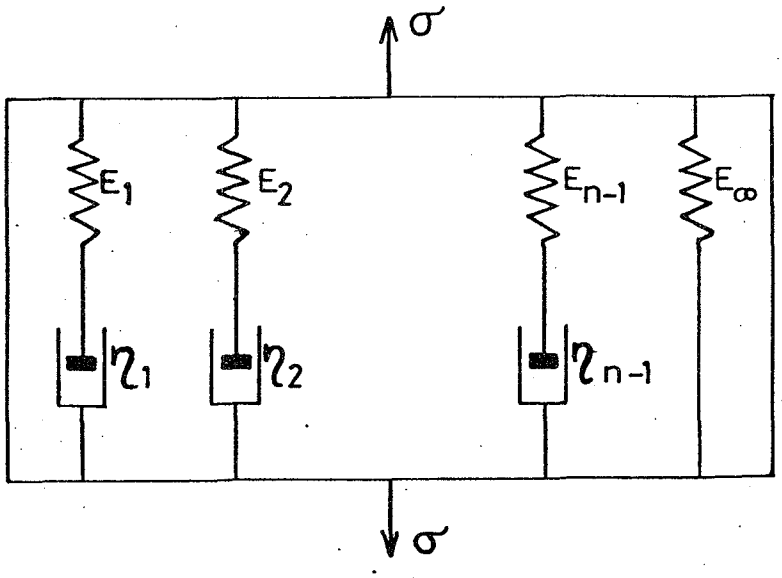

Fig. 5.1 Maxwell chalin model

A simple extension of the generalized Maxwell chain model to account for variable temperature (h = 1.0) was suggested by Bažant and Wu [64]. The effect of aging is included by making the material parameters E_μ and η_μ depend on equivalent hydration period t_e, Eq. (3.17), rather than actual time t. In Ref. 64 it was further assumed that the major creep mechanism is the diffusion of solids and water along adsorbed layers in the micro-structure. These processes can be identified by the dashport whose viscosities may then be assumed to depend on temperature through the Arrhenius equation,

$$\frac{1}{\eta_\mu} = \frac{1}{\eta_{\mu_o}} \exp\left[\frac{U_\mu}{R}\left(\frac{1}{T_o} - \frac{1}{T}\right)\right] \qquad (5.2)$$

where U_μ is the activation energy associated with the μth dashport and η_{μ_o} is a reference value of η_μ at the chosen reference temperature T_o

In a subsequent paper the same authors [65] extended their creep model to variable humidity. This was done by separating each unit of the Maxwell chain into two parts, one representing stresses σ_μ^s in solids and the other σ_μ^w representing stresses in pore water. Thus the uniaxial constitutive relation becomes

$$\dot{\sigma}_\mu^s + \phi_{ss\mu}\,\sigma_\mu^s = E_\mu^s\,(\dot{\varepsilon} - \dot{\varepsilon}^o)$$

$$\dot{\sigma}_\mu^w + \phi_{ww_\mu}[\sigma_\mu^w - f_\mu] = E_\mu^w\,(\dot{\varepsilon} - \dot{\varepsilon}^o) \qquad (5.3)$$

where the indecies s and w are associated with "solids" and "water", respectively. The rate coefficients $\phi_{ww\mu}$, characterize the microscopic diffusion fluxes of solids and water and f_μ is the value of σ_μ^w in the micropores that would be necessary for thermodynamic equilibrium with water in the adjacent capillary pores.

The above constitutive relation can be generalized to multiaxial stress and rewritten in incremental form so that it can be directly incorporated into standard finite element programs [66]. The chief drawback of this formulation is that the number of material parameters is relatively high and available experimental information does not, at present, provide a straightforward answer to the material identification problem.

Time-dependent deformations of concrete, including hygro-thermal effects, conctitute a class of problems that can be described within the context of nonlinear thermodynamic theory. Although the physical microstructural mechanisms involved in creep and shrinkage

are not yet clarified, these effects can be accounted for by the introduction of internal variables that in an average macroscopic sense represent the effects of the microstructural changes. The internal variable theory is well-established within the theory of nonlinear thermodynamics and provides a rational mathematical structure for constitutive modelling of nonlinear material problems. The adaption of this theory to creep of concrete is due to Argyris and co-workers [67 - 69] . The fundamental aspects of internal variable theory of concrete creep have thus been founded but further refinement in the form of constitutive assumptions and optimal selection of suitable internal variables as well as their identification from test data, is needed.

6. CONCLUDING REMARKS

In concrete, pore water and its diffusion plays an important role in the understanding of time-dependent deformations which are strongly influced by hygro-thermal conditions. Constitutive relations for shrinkage and creep require the spatial distribution of pore humidity to be known a priori before the deformation problem can be solved. Thus, the need for accurate and reliable mathematical models for predicting pore humidity is evident. There is ample experimental evidence supporting the use of nonlinear diffusion theory in which diffusivity depends on relative pore humidity, but further test data is required to determine the functional dependence og moisture diffusivity on pore humidity.

Heat and moisture transfer in concrete at elevated temperature can be described by standard coupled differential equations in terms of temperature and water content. The introduction of pore pressure as a variable leads to a relatively simple and computationally efficient

formulation. Constitutive assumptions regarding the relationship between pore pressure, water content and temperature will require more extensive test data to be completely verified. This is also the case with permeability and its suggested dependence on temperature.

Over the years, various mechanisms have been suggested to explain shrinkage and creep deformation of concrete, but no single mechanism has gained exclusive acceptance. Recently, attention has been focused on the effect of moisture diffusion and associated cracking for the observed time-dependent deformations of concrete specimens. The results of this research have exposed the need for a more careful evaluation of existing test data since drying specimens are in a spatial nonuniform state of pore humidity, strain and stress. This also emphasizes the importance of continued theoretical research since a constitutive theory is necessary for a proper understanding and evaluation of experiments. It is felt that significant progress in the constitutive modelling of creep and shrinkage of concrete can best be achieved by a coordinated effort that unifies experimental research, continuum mechanics and numerical analysis.

REFERENCES

1. Neville, A.M. (1977). "Properties of Concrete", Pitman Publishing Ltd., Second Edition.

2. Bažant, Z.P. (1975. "Theory of creep and shrinkage in concrete structures: A précis of recent developments", Mechanics Today Edited by S. Nemat-Nasser, Pergamon Press, Vol.2, 1-93.

3. Bažant, Z.P. (1972). "Thermodynamics of interacting continua with surfaces and creep analysis of concrete structures", Nuclear Engineering and Design, Vol.20, 477 - 505.

4. Powers, T.C. and Brownyard, T.L. (1946-47. "Studies of the physical properties of hardened cement paste", Journal of the American Concrete Institute, Vol.18, 101-132, 249-336, 469-504, 549-602, 669-712, 845-880, 933-992.

5. Young, J.F. (1982)."The microstructure of hardened Portland cement paste", Creep and Shrinkage in Concrete Structures Edited by Z.P. Bazant and F.H. Wittmann, John Wiley & Sons, 3-49.

6. Welty, J.R., Wicks, C.E. and Wilson, R.E. (1969). "Fundamentals of Heat and Mass Transfer", John Wiley & Sons, New York.

7. Cranck, J, (1975). "Mathematics of Diffusion", Oxford University Press, London.

8. Carlson, R.W. (1937). "Drying shrinkage of large concrete members", Journal of the American Concrete Institute, 33, 327-336.

9. Pickett, G. (1946). "Shrinkage stresses in concrete", Journal of the American Concrete Institute,42, 165-195 and 361-392.

10. Hancen, T.C. and Mattock, A.H. (1966). "Influence of size and shape of member on the shrinkage and creep of concrete", Journal of the American Concrete Institute, 63, 267-289.

11. Becker, N.K. and MacInnis, C. (1973). "A Theoretical method for predicting the shrinkage of concrete", Journal of the American Concrete Institute, 70, 652-657.

12. Hughes, B.P., Lowe, I.R. and Walker, J. (1966). "The diffusion of water in concrete at temperatures between 50 and 95°C", British Journal of Applied Physics, Vol.17, 1545-1552.

13. Hancox, N.L. (1968). "The role of moisture diffusion in the drying of cement paste under the influence of temperature gradients", British Journal of Applied Physics, Series 2, Vol.1, 1769-1777.

14. Bažant, Z.P. and Najjar, L.J. (1971). "Drying of concrete as a nonlinear diffusion problem", Cement and Concrete Research, 1, 461-473.

15. Bažant, Z.P. and Najjar, L.J. (1972) "Nonlinear water diffusion in nonsaturated concrete", Materials and Structures (RILEM, Paris), 5, No.25, 3-20.

16. Bažant, Z.P. (1969). "Thermodynamic theory concrete deformation at variable temperature and humidity", Department of Civil Engineering, University of California, Berkeley, Report no. 69-11.

17. Argyris, J.H., Warke, E.P. and Willam, K.J. (1977). "Berechnungen von Temperatur - und Feuchtefeldern in Massivbauten nach der Methode der Finiten Elemente", Deutscher Ausschuss für Stahlbeton, Heft 278.

18. Pihlajavaara, S.E. (1963). "Notes on the drying of concrete", State Institute for Technical Research, Helsinki, Publication No.74.

19. Pihlajavaara, S.E. and Väisänen,M. (1965). "Numerical solution of diffusion equation with diffusivity concentration dependent", State Institute for Technical Research, Helsinki, Publication No. 87.

20. Pihlajavaara, S.E. (1965). "On the main features and methods of investigation of drying and related phenomena in concrete", Ph. D. Thesis, State Institute for Technical Research, Helsinki, Publication No.100.

21. Pihlajavaara, S.E. and Kasi, S.S.H. (1969). "An approximate solution of a quasi-linear diffusion problem", State Institute for Technical Research, Helsinki, Publication No.153.

22. Abrams, M.S. and Orals, D.L. (1965). "Concrete drying methods and their effect on fire resistance", Moisture of Materials in Relation to Fire Tests, American Society for Testing Materials, STP No.385, 52-73.

23. Bažant, Z.P. (1975). "Pore pressure, uplift and failure analysis of concrete dams", Proceedings of the International Symposium on Criteria and Assumptions for Numerical Analysis of Dams, Swansea, September 8-11, 1975, 782-808.

24. Murata, J. (1965). "Studies on the permeability of concrete", Materials and Structures", (RILEM, Paris), Vol.29, 47-54.

25. Bažant, Z.P., Chern, J.C., Abrams, M.S. and Gillen, M.P. (1982). "Normal and refractory concretes for LMFBR applications, Volume 1: "Review of literature on high-temperature behavior of Portland cement and refractory concretes", Electric Power Research Institute, EPRI NP-2437.

26. Harmathy, T.Z. (1970). "Thermal properties of concrete at elevated temperatures", ASTM Journal of Materials, Vol.5, 47-74.

27. Fischer, R. (1970). "Über das Verhalten von Zementmörtel und Beton bei Hohren Temperaturen", Deutscher Ausschuss für Stahlbeton, Heft 214.

28. de Groot, S.R. and Mazur, P. (1962). "Non-Equilibrium Thermodynamics", North-Holland Publishing Company, Amsterdam.

29. Luikov, A.V. (1966). "Heat and Mass Transfer in Capillary - Porous Bodies" (Translated from Russian), Pergamon Press, Oxford.

30. Luikov, A.V. (1975). "Systems of differential equations of heat and mass transfer in capillary - porous bodies (review)", International Journal of Heat and Mass Transfer, Vol.18, 1-14.

31. Visser, W. (1965). "A finite element-method for the determination of non-stationary temperature distribution and thermal deformations", Proceedings of the First Conference on Matrix Methods in Structural Mechanics, Wright-Patterson, Air Force Base, Dayton, Ohio, AFFDL-TR-66-80, 925-943.

32. Wilson, E.L. and Nickell, R.E. (1966). "Application of the finite element method to heat conduction analysis", Nuclear Engineering and Design, Vol.4, 276-286.

33. Argyris, J.H., Balmer, H, Doltsinis, J. St. and Willam, K. (1971). "Finite element analysis of thermomechanical problems", Proceedings of the Third Conference on Matrix Methods in Structural Mechanics, Wright-Patterson Air Force Base, Dayton, Ohio, AFFDL-TR-71-160, 729-772.

34. Emery, A.F. and Carson, W.W. (1971). "An evaluation of the use of the finite-element method in the computation of temperature", Transactions of the ASME, Journal of Heat Transfer, 136-145.

35. Warzee, G. (1974). "Finite element analysis of transient heat condition, application of the weighted residual process", Computer Methods in Applied Mechanics and Engineering, Vol.3, 255-268.

36. Comini, G and Lewis, R.W. (1976). "A Numerical solution of two-dimensional problems involving heat and mass transfer", International Journal of Heat and Mass Transfer, Vol.19, 1387-1392.

37. Lewis, R.W., Strada, M. and Comini, G. (1977). "Drying-induced stresses in porous bodies", International Journal for Numerical Methods in Engineering, Vol.11, 1175-1184.

38. Lewis, R.W., Morgan, K. and Thomas, H.R. (1979). "Drying-induced stresses in porous bodies - an elastoviscoplastic model", Computer Methods in Applied Mechanics and Engineering, Vol.20, 291-301.

39. Bažant. Z.P. (1975). "Some question of material inelasticity and failure in the design of concrete structures for nuclear reactors", Preprints of the Third Conference on Structural Mechanics in Research Technology, London, September 1975, Paper No.H1/1.

40. Bažant, Z.P. anf Thonguthai, W. (1978). "Pore pressure and drying of concrete at high temperature", Proceedings of the ASCE, Journal of the Engeneering Mechanics Division, Vol.104, No.EM5, 1059-1079.

41. Bažant, Z.P. and Thounguthai, W. (1979). "Pore pressure in heated concrete walls: a theoretical prediction", Magazine of Concrete Research, Vol.31, No.107, 67-76.

42. Dayan, A. (1977). "COWAR-2 User's Manual", General Electric Company, GEFR-00090 (L).

43. McCormack, J.D., Postma, A.K. and Schur, J.A. (1979). "Water evolution from heated concrete", Hanford Engineering Development Laboratory, Report No. HDL-TIME 78-87.

44. Knight, R.L. and Beck, J.V. (1979). "Model and computer code for energy and mass transport in decomposing concrete and related materials", Proceedings of the International Meeting on Fast Reactor Safety Technology, Seattle, Washington, August 19-23, 1979.

45. Chen, K.H., Gluekler, E.L., Lam, S.T. and Shippey, V.S. (1980). "Comparison of mechanistic codes for predicting water release from heated concrete", General Eletric Company, Report No. GEFR-00521.

46. Bažant, Z.P., Chern. J.-C. and Thonguthai, W. (1981). "Finite element program for moisture and heat transfer in heated concrete", Nuclear Engineering and Design, Vol.68, 61-70.

47. England, G.L. and Ross, A.D. (1972). "Shrinkage, moisture, and pore pressure in heated concrete", Concrete for Nuclear Reactors, ACI Special Publication, SP-34, 883-906.

48. England, G.L. and Sharp, T.J. (1971). "Migration of moisture and pore pressure in heated concrete", Preprints of the First International Conference on Structural Mechanics in Reactor Technology, Berlin, 1971, Paper H2/4.

49. Chapman, D.A. and England, G.L. (1977). "Effects of moisture migration on shrinkage, pore pressure and other concrete properties", Preprints of the Fourth International Conference on Structural Mechanics in Reactor Technology, San Francisco, August 1977, Paper H5/3.

50. Bažant, Z.P. (1982). "Mathematical models for creep and shrinkage of concrete", Creep and Shrinkage in Concrete Structures Edited by Z.P. Bazant and F.H. Wittmann, John Wiley & Sons Ltd., 163-225.

51. Anderson, C.A. (1983). "Creep and thermal effects in aging materials", William Prager Symposium on Mechanics of Geomaterials: Rocks, Concretes, Soils (IUTAM) Northwestern University, Evanston, September 11-15, 1983.

52. Wittmann, F.H.(1983). "Deformation of concrete at variable moisture content", William Prager Symposium on Mechanics of Geomaterials: Rocks, Concretes, Solils (IUTAM), Northwestern University, Evanston, September 11-15, 1983.

53. Wittmann, F.H.(1982). "Creep and shrinkage mechanisms", Creep and Shrinkage in Concrete Structures Edited by Z.P. Bazant and F.H. Wittmann, John Wiley & Sons Ltd., 129-161.

54. Bažant, Z.P. and Panula, L. (1978-79). "Practical prediction of time-dependent deformations of concrete", Materials and Structures (RILEM, Paris), Part I: "Shrinkage", Vol.11, No.65, 307-316, Part II: "Basic creep", Vol.11, No.65, 317-328, Part III: "Drying creep", Vol.11, No.66, 415-424, Part IV: "Temperature effect on basic creep", Vol.11, No.66, 424-434, Part V: "Temperature effect on drying creep", Vol.12, No.69, 169-183.

55. ACI Committe 209 (1982). "Prediction of creep shrinkage, and temperature effects in concrete structures", Design for Creep & Shrinkage in Concrete Structures, ACI, SP-76, 193-300.

56. CEB-FIP (1978). "Model code for Concrete Structures, Comité Euro-International du Béton, Paris.

57. Rüsch, H., Jungwirth, D. and Hilsdorf, H. (1973). "Kritische Sichtung der Verfahren zur Berücksichtigung der Einflüsse von Kriechen und Schwinen des Betons auf das Verhalten der Tragwerke", Beton- und Stahlbetonbau, Vol.68, 49-60, 76-86, 152-158.

58. Müller, H.S. and Hilsdorf, H.K. (1982). "Comparisons of prediction methods for creep coefficients of structural concrete with experimental data", Fundamental Research on Creep and Shrinkage of Concrete Edited by F.H. Wittmann, Martinus Nijhoff Publishers, The Hague, 269-289.

59. Wittmann, F.H. and Roelfstra, P.E. (1980). "Total deformation of loaded drying concrete", Cement and Concrete Research, Vol.10, 601-610.

60. Acker, P. (1982). "Drying of concrete:Consequences for the evaluation of creep tests", Fundamental Research on Creep and Shrinkage of Concrete Edited by F.H. Wittmann Martinus Nijhoff Publishers, The Hague, 149-169.

61. Bažant, Z.P. and Raftshol, W.J. (1982). "Effect of cracking in drying and shrinkage specimens", Cement and Concrete Research, Vol.12, 209-226.

62. Chatterji, S., Thaulow, N. and Christensen, P. (1981) "Formation of shrinkage cracks in thin specimens of cement paste", Cement and Concrete Research, Vol.11, 155-157.

63. Bažant, Z.P. and Wu, S.T. (1974). "Rate-type creep law of aging concrete based on Maxwell chain", Materials and Structures (RILEM, Paris), Vol.7, 45-60.

64. Bažant, Z.P. and Wu, S.T. (1974). "Thermoviscoelasticity of aging concrete", Proceedings of the ASCE, Journal of the Engineeering Mechanics Division, Vol.100, No.EM3, 575-597.

65. Bažant, Z.P. and Wu, S.T. (1974). "Creep and shrinkage law for concrete at variable humidity", Proceedings of the ASCE, Journal of the Engineering Mechanics Division, Vol.100, No.EM6, 1183-1209.

66. Bažant, Z.P., Rossow, E.C. and Horrigmoe, G, (1981). "Finite element program for creep analysis of concrete structures", Preprints of the Sixth International Conference on Structural Mechanics in Reactor Technology, Paris, August 17-21, 1981, Paper No. H2/1.

67. Argyris, J.H., Pister, K.S. and Willam, K.J. (1976). "Thermomechanical creep of aging concrete - A unified approach", IABSE Publ. 36-1.

68. Argyris, J.H., Pister, K.S., Szimmat and Willam, K.J. (1977). "Unified concepts of constitutive modelling and numerical solution methods for concrete creep problems", Computer Methods in Applied Mechanics and Engineering, Vol.10, 199-246.

69. Pister, K.S., Argyris, J.H. and Willam, K.J. (1978) "Creep and shrinkage of aging concrete", Douglas Mc Henry International Symposium on Concrete Structures, ACI SP-55, 1-30.

CREEP AND THERMAL EFFECTS IN AGING SOLIDS

Charles A. Anderson
Los Alamos National Laboratory

I. INTRODUCTION

Professor Prager was instrumental during his lifetime in the development of simple material models to represent the behavior of solids beyond the elastic range. Thus, his name is associated closely with the development of modern theories of plasticity (for example, the perfectly plastic solid). In addition he later became interested in numerical methods and computing and how numerical techniques could be used to provide solutions to problems in the field of solid mechanics. In the last 20 years we have seen a tremendous growth in the field of computational solutions in mechanics--promoted primarily by advocates of the finite elements method--and today numerical methods allow us to solve multi-dimensional problems of solid mechanics where the materials obey complex constitutive laws. This, with the advent of numerical methods and large capacity computing machines to solve complex analytical problems, there is a reawakening to the need to develop physically based constitutive laws to represent real material behavior.

The purpose of this paper is to describe three constitutive models that have been developed for rocks, concrete and filled polymers to represent creep, thermal, stress, and aging effects. Also described in the paper are how these constitutive models are being used to numerically predict the behavior of solids in such diverse situations as aging creep of concrete structures and creeping mantle convection. In all cases low strain rate, compressive material behavior will be the main interest.

For the time-dependent behavior of concrete under long-term loads, viscoelastic models have been developed and applied to the numerical analysis of the behavior of concrete structures. A commonly applied theory for concrete structures is the linear, aging viscoelastic theory for which the superposition principle applies. Section II of the paper discusses the theory for aging concrete creep including expansion of the creep functional in a finite Dirichlet series that enables the numerical solution of practical concrete creep problems. A numerical example of calculating the creep of a concrete structure is illustrated. How the theory is altered to account for temperature amd moisture effects is also discussed.

One of the difficulties with using the viscoelastic constitutive model is its inability to handle nonlinear dependence on the stress. In both the conventional and aging viscoelastic theories the creep rate depends on the stress to the first power whereas with real materials viscoelastic creep occurs

superimposed over a rate-independent plastic behavior. Section III of the report briefly summarizes some recent work at the Los Alamos National Laboratory and Carnegie Mellon Institute concerning the development of a new viscoplastic theory for materials that exhibit a rate-dependent viscoelastic creep response together with rate-independent plastic behavior.

Section IV of this paper examines temperature and stress effects in creep of rocks with the ultimate goal of developing a capability to realistically model material flow, temperature and deformation in the Earth's crust and mantle. The major difficulty in modelling geodynamic phenomena today is the complex rheological behavior of rocks. Depending on conditions of temperature, pressure and stress, rocks can act as elastic or viscoplastic solids, brittle solids subjected to fracture, or viscous fluids. A successful predictive capability must be able to cope with these constrasting rheological properties within a single computation because the interaction between materials which behave differently (for example, the coupling of an elastic lithosphere to an underlying viscous asthenosphere) is an essential aspect to most unsolved geological problems.

The basic equations for creeping flow of rocks, including energy transport, are described in Section IV. There also is discussed the currently accepted creep models for rocks subjected to high temperature ($T > 0.5\ T_m$, where T_m is the liquidus temperature) and stress. The basic equations have been implemented in a two-dimensional finite element code, which is currently being used to study Rayleigh-Benard convection in a square box model of the Earth's upper mantle. Calculations are illustrated to show the effect of temperature on mantle creep for the cases of base heating and combined internal and base heating, which is the case most relevant to the Earth's mantle. Extension to stress and temperature dependent creep behavior of the material making up the Earth's mantle is discussed as well as how aging effects are important and can be factored into such models.

II. CREEP, THERMAL, AND AGING EFFECTS IN CONCRETE

The physical mechanisms underlying the creep of concrete, just now being fully understood, are very complex,[1,2] and their complete incorporation into numerical codes for the prediction of the creep of complex concrete structures is still impossible. Useful numerical results can often be obtained though, by using simplified creep constitutive models that do not yet

incorporate the complicating effects of moisture change, temperature change, and an extended working range of stress and strain. In this section we will first present the simplest such constitutive model, the so-called linear aging viscoelastic model, that has been proposed and often used for the numerical creep analysis of massive concrete structures. Later in the section we will discuss the effect of temperature and how this effect is accommodated in the constitutive law.

The Linear Aging Model

The characteristic of concrete that distinguishes it from the traditional viscoelastic material is the aging effect. Thus, as a function of time the constitutive law is changing through the chemical action of hydration, and it is extremely important to its creep response as to when in its lifetime an aging viscoelastic structure is loaded. Fortunately, experiments indicate that the response due to an increment in load is independent of all other past load increments, and the superposition principle applies. Thus, for small increments in stress $d\sigma = \dot{\sigma}(t')dt'$ occuring at t' measured from the time of casting, we have

$$\epsilon(t) = \int_0^t J(t,t')\,\dot{\sigma}(t')dt' \quad . \tag{2.1}$$

where $J(t,t')$ is called the creep function.

Numerical creep analysis based on the stress-strain law of Eq. (2.1) may be performed by subdividing the total time interval of interest into time steps Δt and discrete times t_r ($r = 1,2,\ldots$). The integral in Eq. (2.1) can then be approximated by finite sums involving incremental stress changes over the time steps. Details of this method, which is generally applicable to any form of the creep function $J(t,t')$, are given in Bazant.[1] Because the numerical method results in extensive storage and computational requirements, it has been superceded by methods that involve approximating the creep function $J(t,t')$ by a Dirichlet series and thus tying the constitutive model physically to Kelvin chain models (or Maxwell chain models if the relaxation function is approximated), which then yield the structural equations.

The creep function J(t,t') is approximated by a series of real exponentials of the form

$$J(t,t') = \frac{1}{E(t')} + \sum_{i=1}^{n} \frac{1}{\hat{E}_i(t')} \{1 - \exp[-(t - t')/\tau_i]\} \qquad (2.2)$$

in which τ_i are constants called retardation times and $\hat{E}_i$ are aging coefficients. When this function is introduced into the superposition integral (Eq. (2.1)) the integrand degenerates into the product of a function of t' and a function of t. The latter function does not involve the variable of integration and can be extracted from the integral, leaving only an integration of functions that are independent of t. Thus, at each new time step, it is only necessary to compute the change in value of the integral from the last time step rather than from the time of initial loading, as is required in a general case. Using this method Ref. 3 describes a completely stable numerical method for obtaining computational solutions to concrete structural creep problems.

Restricting ourselves to situations of one-dimensional stress, it can be shown that the Dirichlet series is the solution to the system of ordinary differential equations

$$\begin{aligned} \dot{\varepsilon} &= \dot{\sigma}/E + \sum_{i=1}^{n} \dot{\varepsilon}_i \\ \dot{\varepsilon}_i &= \sigma_i/\eta_i \quad i = 1,2,\ldots,n \\ \dot{\sigma} &= \dot{\sigma} + E_i\dot{\varepsilon}_i \quad i = 1,2,\ldots,n \end{aligned} \qquad (2.3)$$

when a unit step stress $\sigma(t)$ is applied at time t'. This system of equations, which corresponds to the physical system shown at the top of Fig. 1 and with variables E, E_i, η_i as shown, is called the Kelvin chain model. Since the formulation defined by Eq. (2.3) states the relations between the rates of stress and strain, it is referred to as a rate-type formulation.

Another formulation of the viscoelasticity problem is through the use of the relaxation function G(t,t') rather than the creep compliance function J(t,t'),

$$\sigma(t) = \int_0^t G(t,t')\,\dot{\varepsilon}(t')\,dt' \tag{2.4}$$

If the relaxation function is expanded in a Dirichlet series and substituted into Eq. (2.4), it can be shown that the differential equations (for one dimensional stress)

$$\sigma = \sum_{i=1}^{n} \sigma_i$$
$$\dot{\varepsilon} = \frac{\dot{\sigma}_i + \sigma_i/\tau_i}{E_i} \qquad i = 1,2,\ldots,n \tag{2.5}$$

are obtained.[4] This system of rate equations corresponds to the physical system shown at the bottom of Fig. 1 and is called the Maxwell chain model. The quantity, $\tau_i = \eta_i/E_i$, is the relaxation time of the ith unit of the Maxwell chain. As with the Kelvin chain model described previously, incremental stress-strain laws for the Maxwell chain model can be formulated. As with the Kelvin model the stress history in the incremental law is defined by a recurrence relation, and the need to sum the complete stress history at each time step is eliminated.

Kelvin and Maxwell chain models can be used interchangeably to solve creep problems provided the relaxation function G can be determined from J, or vice versa. For example if G is smooth and there is no aging effect then one can solve

$$G(0)J(t) + \int_0^t G(s)J(t-s) = 1 \tag{2.6}$$

to obtain the creep function J while for aging material the general relation Eq. (2.1) must be solved. In general, advantages accrue to the Maxwell model

when the effects of temperature and humidity change are included since these involve summing stored stress variables.

Modelling Temperature Effects in Aging Viscoelastic Solids

Accommodating the Kelvin chain model to pore moisture and temperature changes is not possible based on the underlying physics of the creep mechanism for concrete. On the other hand, as shown in Bazant,[1] incorporating the temperature effect into the creep law corresponding to the Maxwell model is rather simple. Equation (2.5) is rewritten as

$$\sigma = \sum \sigma_i \qquad \dot{\varepsilon} = \frac{\dot{\sigma}_i}{E_i(t_e)} + \frac{\sigma_i}{\eta_i(t_e)} \tag{2.7}$$

where η_i is the age-dependent viscosity associated with the ith Maxwell unit, which equals $\tau_i E_i$ at constant temperature T. Since creep is a thermally activated process, it is known from physics that η_i should depend on temperature according to the Arrhenius equation,

$$\frac{1}{\eta_i} = \frac{1}{\eta_0} \exp\left[\frac{U_i}{R}\left(\frac{1}{T_0} - \frac{1}{T}\right)\right] \tag{2.8}$$

where T_0 is the reference temperature, η_0 is the value of η at T_0, R is the universal gas constant, and U_i is the activation energy of the ith Maxwell unit. The effect of temperature on aging is represented by making E_i and η_i dependent on t_e rather than on t, where Δt_e is an equivalent hydration period that yields the same degree of hydration at temperature T as occurs during a period Δt at temperature T_0. This equivalent time is given by

$$\Delta t_e = \beta_T \Delta T \tag{2.9}$$

with

$$\beta_T = \exp\left[\frac{U_h}{R}\left(\frac{1}{T_0} - \frac{1}{T}\right)\right] \tag{2.10}$$

in which U_h equals the activation energy for hydration.

Applications

The consititutive equations for the Kelvin or Maxwell models of aging viscoelastic materials have been incorporated into several US and European concrete creep analysis computer codes. In particular Ref (5) describes how the constitutive laws are incorporated in a large finite element code for the creep analysis of complex three-dimensional concrete structures, and many examples are given. Below is illustrated one such calculation that indicates the current state of the art in concrete creep analysis. Temperature effects were not considered in this problem.

Figure 2 illustrates a concrete ring that is posttensioned by two cables on the exterior surface as shown. In this problem the steel cables are elastic whereas the concrete creeps according to the viscoelastic aging relation of the Dirichlet series form given in Eq. (2.2). A two-term approximation was used. For this example the coefficients $E_i(t')$, i = 1,2 are given by

$$\frac{1}{E_i(t)} = a_i + b_i\,(t')^{n_i} \tag{2.11}$$

where $a_1 = a_2 = 7.5 \times 10^{-9}$, $b_1 = b_2 = 0.233 \times 10^{-6}$ and $n_1 = n_2 = -0.333$. The relaxation times were taken to be $\tau_1 = 5.6$ d and $\tau_2 = 56$ d, respectively.

Figure 3 illustrates the variation of the post-tensioning strain in the cable as a function of time out of 400 d starting from an initial strain in the cable of 0.0005 applied at 90 d from concrete casting. Also shown for comparison is a shell solution to this problem for a complete composite concrete steel shell with the same geometry, material quantity, and material properties as in the finite element model. At 350 d there is a 1.3% difference in the finite element cable strain and the cable strain predicted by the shell theory solution. Further details are given in Ref. (5).

III. A NEW VISCOPLASTIC CREEP MODEL

Certain materials, in particular highly filled polymers,* exhibit uniaxial stress-strain behavior as illustrated in Fig. 4. Although a linear viscoelastic material would produce this form of stress-strain curve, a relaxation function that produces the loading curve predicts much smaller values of the offset strains ε_1, ε_2 than those observed experimentally. Alternately, an elastic-plastic material with very small yield stress and extreme work hardening would exhibit a similar stress-strain picture without the hysteresis but wouldn't show the creep and relaxation effects that these materials exhibit.

This section presents a simple model for truly viscoplastic material behavior that has been recently developed by M. E. Gurtin and W. O. Williams of Carnegie-Mellon and R. V. Browning of Los Alamos based on experimental data obtained at the Los Alamos National Laboratory.[6] The model is based on the following two hypotheses.

1. There is a constitutive quantity called the pseudo stress π, which is related to the strain through an elastic-plastic stress-strain law.
2. The true stress σ is related to π through a linear viscoelastic law.

Thus, the model combines rate-independent nonlinear plastic behavior with linear viscoelastic behavior. Experimentally determining the constituents of this viscoplastic model is of major importance to using it. Three separate creep type experiments will be shown to determine the parameters of the model.

Description of the Model

In developing the model Gurtin, Williams, and Browning first introduce the constitutive equation, which describes one-dimensional behavior of an elastic-plastic material. Thus,

$$\pi = F(\varepsilon, \varepsilon_m) \tag{3.1}$$

where $\pi = \pi(t)$ is the stress at time t, $\varepsilon = \varepsilon(t)$ is the strain at t and $\varepsilon_m(t)$ is the past maximum of the strain,

---

*Highly filled polymers are formed by a random distribution of crystals in a matrix material. In these materials there are no preferred slip directions as in metals. As for concrete and rocks, these materials are weak in tension.

$$\varepsilon_m(t) = \max_{0 \leq s \leq t} \varepsilon(s) \tag{3.2}$$

Gurtin, Williams, and Browning then introduce the terms <u>virgin</u> states (in which $\varepsilon = \varepsilon_m$) and <u>damaged</u> states (in which $\varepsilon < \varepsilon_m$). According to the terminology of plasticity the damaged state corresponds to states in which unloading has taken place. For the virgin stress-strain curve we define

$$\pi = g(\varepsilon) = F(\varepsilon,\varepsilon) \tag{3.3}$$

and rewrite (3.1) as

$$\pi = g(\varepsilon_m)\, f\,(\varepsilon,\varepsilon_m) \tag{3.4}$$

where f is the damage function and corresponds to a loading or unloading (presumed to be the same path) in the damaged region. Note that

$$f(\varepsilon_m, \varepsilon_m) = 1 \tag{3.5}$$

Figure 5 illustrates the constitutive relations representing the rate independent behavior of these solids. Note the similarity with the elastic-plastic solid with the difference being that the unloading-loading curves are not constrained to have their slopes equal to elastic modulus of the solid.

To introduce rate dependence into this model, Gurtin, Williams, and Browning redefine π of Eq. (3.1) as a pseudo-stress and they relate π to the stress σ by a linear nonaging viscoelastic law

$$\sigma(t) = \int_0^t G(t-s)\, \dot{\pi}(\sigma)ds \tag{3.6}$$

where G is a stress-relaxation function (see Eq. (2.8) for the aging form).

Conversely Eq. (3.6) can be inverted to give a relationship between π and σ

$$\pi(t) = \int_0^t J(t-s)\dot{\sigma}(s)\, ds \tag{3.7}$$

where J is the creep function (see Eq. 2.1 for the aging form). The creep formulation can be completed by writing the analogous expression for Eq. (3.4)

$$\varepsilon = k(\pi_m)\, h\, (\pi, \pi_m) \tag{3.8}$$

where π_m is the past maximum of π. The function k, which is the inverse of g, describes the virgin response while h is the damage function and represents loading-unloading states off of the virgin curve. Reference (6) establishes the validity of the inverse relation, Eq. (3.8), given Eq. (3.4).

Experimental Characterization

Here we briefly describe how the constituents of the viscoplastic theory (the functions J, g, and k) are determined from three experimental loading programs (that is, specified $\sigma(t)$). These loading programs are a standard creep test, a ramp test, and an unloading test and all are necessary to determine the parameters of the model. The three loading programs are shown schematically in Fig. 6.

First a standard creep test* is carried out. If $\sigma(t) = \sigma_0$ for all $t > 0$ then the corresponding pseudo-stress π_0 from Eq. (3.7) is

$$\pi_0(t) = \sigma_0 J(t) \tag{3.9}$$

and the strain $\varepsilon_{\sigma_0}(t)$ is

$$\varepsilon_{\sigma_0}(t) = k\,[\sigma_0\, J(t)]. \tag{3.10}$$

Now we write

$$\frac{\epsilon_{\sigma_0}(t)}{\sigma_0} = \frac{k[\sigma_0 J(t)]}{\sigma_0}$$

and taking the limit as $\sigma_0 \to 0$ and assuming that k is approximately linear for small values of its argument we will obtain J(t), the creep function.

A second experiment involving ramp loading now suffices to determine the functions k and g. Taking the creep function J found above, one may integrate it together with the experimental $\sigma(t)$ to obtain $\pi(t)$. Then a plot of $\pi(t)$ versus the experimental $\epsilon(t)$ reveals the form of g. In principle a single experiment suffices, but a useful test of the constitutive hypothesis that J encompasses the entire rate dependence is afforded by taking a series of such tests at differing rates and comparing the corresponding graphs. The function k is the inverse of the function g.

Finally, to determine the damage function it is necessary to use experiments involving unloading and, optimally, reloading processes utilizing a large selection of values of ϵ_m or π_m. For example the sawtooth loadings such as those shown in Fig. 6 may be used. From the experimental $\sigma(t)$ one uses Eq. (3.7) to compute $\pi(t)$ and then considers a π-ϵ plot over each interval on which ϵ_m is constant and $\epsilon < \epsilon_m$. The corresponding π-ϵ plots, each for a different value of π_m, may be used to construct $f(\epsilon,\epsilon_m)$ by a two-variable fitting process.

Using the above procedure a highly filled polymer was characterized. The material selected for study was only slightly viscoelastic over the time scale of the experiments carried out. After characterization the material was subjected analytically and experimentally to the loading program shown in Fig. 7. The analytical and experimental results are compared in Fig. 7. Comparisons between theory and experiment are excellent considering that the experiment involved a factor of 10 differences in loading rates.

---

*Alternately a relaxation test could be conducted for G(t) and J(t) determined from Eq. (2.6).

IV. CREEP, THERMAL, AND AGING EFFECTS IN ROCKS

There are many phenomena in the Earth that testify to the importance of long-term creep processes. These include geoidal flattening of the Earth as a whole, plate tectonic motions in the outer hundred kilometers of the earth driven by thermal creep of the underlying mantle, and episodal creep events along major faults down to grain-scale ductile flow. Fully understanding these phenomena will eventually require the development of constitutive models that take into account temperature, stress and aging effects on the creep rates of rocks and implementation of these constitutive models in numerical procedures that can predict the large scale phenomena that are being observed. These models can then be calibrated using the observed data such as surface velocity, heat transfer and surface deformation. Finally, with a well calibrated model basic questions of time history of evolution of the Earth's structure and questions of aging can be more confidently addressed. This section briefly describes constitutive laws that have been proposed for modelling high temperature creep of rocks causing mantle convection as well as detailed calculations with a finite element code that describe high Rayleigh number convection of the mantle from combined internal and base heating.

The elastic and inelastic behavior of rocks at low (near surface) stresses and temperatures is dominated by fractures on all scales. Here compaction and dilation are important processes with the resulting inelastic strains mainly due to primary and tertiary creep. However, at absolute temperatures greater than one-half the melting temperature, most large scale ductile deformation of rocks occurs as secondary or steady-state creep. Here the flow involves plastic deformation resulting from dislocation motion.[7]

Useful laboratory steady-state creep results for uniaxial stress are available for a number of rocks over wide ranges of strain-rate, temperature and driving stress. Among these are ice, halite (rock salt), marble, limestone, dolomite, anhydrite, quartzite, granite, dunite, pyrosenite, and peridotite. All of these steady-state creep results are well-fit by a relationship of the form[7,8]

$$\dot{\varepsilon} = \frac{A}{T}\ \mu \exp\left[-(Q + pV^*)/RT\right] \left(\frac{\sigma}{\mu}\right)^N \qquad (4.1)$$

where Q and V* are activation energies and volumes, μ is the shear modulus and A and N are material constants. In Eq. (4.1) R is the universal gas constant and T, p and σ are absolute temperature, pressure and octahedral shearing respectively. In many cases Eq. (4.1) can be simplified to

$$\dot{\varepsilon} = B \exp[-(Q + pV^*)/RT] \sigma^N \tag{4.2}$$

where B is a material constant. For the previously mentioned solids values of Q vary from 120 to 500 kJ/mol and N from 3 to 9. Data on V* are quite limited.

Numerical calculations using the constitutive model Eq. (4.2) have been presented for the behavior of underground cavities[9] and geotechnical structural models that represent rifts and rock folds[10,11] usually driven by direct stresses caused by material discontinuities, for instance. Also, in Ref. (12) analytical solutions are given for an underground spherical cavity for the case where the surrounding medium is a constant viscosity solid. Currently accepted models for plate tectonic motion, on the other hand, are driven not by direct stresses but by drag forces developed during slow creep of the underlying mantle. The equations describing this process of mantle creep are inherently nonlinear even for constant viscosity situations, and have in the past been solved by boundary layer or finite difference numerical techniques.[13, 14] However, these methods do not handle the physically interesting cases of nonconstant (for example, stress, temperature or pressure dependent) viscosity or the situation of internal heating of the material of the mantle caused by radioactive decay. The method of analysis described below does not possess these restrictions.

We reconsider the problem of Rayleigh-Benard convection in a square smooth box. The basic equations that describe the creep of the material of the box under thermally-induced buoyancy forces are the equilibrium equations, the constitutive law for the relation between deviatoric stresses (s_x, s_y, τ_{ty}) and velocity (u,v) gradients, the incompressibility equation, and the energy transport equation. Written with respect to an Eulerian reference frame and using the usual Boussinesq approximation, these equations are

$$\frac{\partial s_x}{\partial x} + \frac{\partial \tau_{xy}}{\partial y} - \frac{\partial p}{\partial x} = 0 \tag{4.3}$$

$$\frac{\partial \tau_{xy}}{\partial x} + \frac{\partial s_y}{\partial y} - \frac{\partial p}{\partial y} = -\rho g \alpha (T_0 - T)$$

$$\frac{\partial u}{\partial x} = \frac{1}{2\mu} s_x, \quad \frac{\partial v}{\partial y} = \frac{1}{2\mu} s_y, \quad \frac{\partial u}{\partial y} + \frac{\partial v}{\partial x} = \frac{1}{\mu} \tau_{xy} \tag{4.4}$$

where α is the bulk coefficient of expansion and where $\mu = \mu(\sigma_{ef}, T)$ is the viscosity as a function of temperature and octahedral shearing stress, which can be of a form consistent with Eqs. (4.1) or (4.2). For details see Reference 10. Also,

$$\frac{\partial u}{\partial x} + \frac{\partial v}{\partial y} = 0 \tag{4.5}$$

is the incompressibility requirement and

$$\rho C_p \left(u \frac{\partial T}{\partial x} + v \frac{\partial T}{\partial y} \right) = k \nabla^2 T + Q \ , \tag{4.6}$$

is the energy transport equation where ρ is the density, C_p is the heat capacity, k is the thermal conductivity and Q is the internal volumetric heating. In the above equations terms of the order of products of velocity have been neglected since velocities can be shown to be small ($\sim 10^{-10}$ m/s) in mantle convection.

The equations embodied in (4.3)-(4.6) have been discretized by the finite element method using a 6-node triangle with quadratically interpolated velocities and linearly interpolated pressures and implemented in a computer program.[15,16] This computer program, called MANTLE, has been compiled on the Los Alamos computer system, modified for random access memory, energy checks and balances, graphics, and other features and used in the numerical studies of creep and thermal effects in the Earth's mantle that are described below. The finite element method was chosen as the numerical approach since it possesses the advantage of allowing for a variable mesh and the concentration of elements in the thin boundary layers where the resolution is required for high

Rayleigh number flow. The nonlinear terms in Eq. (4.6) were handled by iterating between the flow equations, which determine u, v and p, and the energy transport equation, which determines T.

The problem that we have investigated is represented by a two-dimensional square box containing a creeping solid (or a very viscous fluid) that is heated on its under side and internally, cooled on the top, and insulated on the vertical sides. All boundaries are mechanically rigid and smooth. When the temperature difference between the bottom and top is small enough, energy transport occurs only by conduction in the solid. However, as the bottom temperature (or flux) is raised, a critical temperature is observed (both experimentally and analytically) at which the material in the box begins to convect heat as well as conduct it. In the absence of internal heating the critical temperature difference for onset of flow of a constant viscosity solid in a square smooth box of the length L can be determined analytically by the critical Rayleigh number R_c,

$$R_c = \frac{\alpha g L^3}{\kappa \nu} (T_B - T_0) = 779.273 \qquad (4.7)$$

where κ is the thermal diffusivity, ν is the kinematic viscosity and $T_B - T_0$ is the temperature difference. When internal heating is accounted for, the critical temperature difference must be determined numerically.

Figure 8 illustrates the problem geometry, material properties, and boundary conditions for the bottom heated convection case together with three of the finite element meshes that are being used in this study. Material properties and the dimensions of the box were selected so that a base temperature of one degree corresponds to the critical Rayleigh number. For all bottom heated cases the velocity field consisted of a single cell vortex flow. Figure 9 illustrates the horizontally-averaged temperatures in a constant viscosity convecting solid for the 18 x 18 variable mesh of Fig. 8 and where the Rayleigh numbers are 200 and 2700 times the critical value (779.293). For these Rayleigh numbers it can be seen that there are fairly narrow boundary layers along the top and bottom edges of the box (this is true of the vertical edges, also) where the temperature gradients are high, and a central core of material that is nearly isothermal and at the average temperature of the solid. Table I below summarizes the results we have obtained so far for high Rayleigh number constant viscosity

TABLE I
SUMMARY OF NUMERICAL RESULTS FOR HIGH RAYLEIGH NUMBER
BOTTOM HEATED THERMAL CONVECTION

R_a/R_c	Finite Element Mesh Spacing	Finite Element Nusselt Number	Finite Element Mesh Spacing	Finite Element Nusselt Number
100	18 x 18	9.730	48 x 48	9.625
200	18 x 18	12.162	48 x 48	11.987
300	18 x 18	13.844	---	---
500	18 x 18	16.289	80 x 80	16.153
1000	18 x 18	20.289	96 x 96	20.13
2700	18 x 18	27.698	---	---
5000	18 x 18	33.422	96 x 96	33.1
10000	18 x 18	40.765	96 x 96	40.7

convection using the 18 x 18 nonuniform mesh of Fig. 8. Also shown are the results of Jarvis and Peltier[14] for uniform finite difference meshes. The comparison is based on the Nusselt number, which is the ratio of the total heat transmitted out of the top of the box to the heat that would be transmitted if only conduction in the solid were occurring. The quantity R_a/R_c is the ratio of the actual to critical Rayleigh number.

The agreement of the finite element results with the finite difference results shown in Table I is very good particularly at the high Rayleigh numbers characteristic of Earth mantle convection. The 25 x 25 variable mesh shown in Fig. 8 will be used to calculate Nusselt numbers at extremely high Rayleigh numbers (up to 100 000) and will provide further confidence in the numerical capability.

Thermal effects on the material creep behavior were also investigated. Here the aim is a systematic study of how convection is influenced by increasingly large viscosity variations within the creeping solid. Since, as shown above, temperature variations are confined to narrow boundary layers at high Rayleigh numbers, there will be large effective viscosity variations within

these boundary layers. Again the variable mesh capability of a finite element approach is a crucial factor in resolving these large viscosity variations.

Variation of the effective viscosity of mantle rocks as a function of depth is a subject of some controversy. For our purposes we have taken a viscosity variation with temperature of the Arrhenius form (that is, of the form of Eq. (4.2) with $V^* = 0$ and $N = 1$). We have selected the parameters B and Q/R so that the effective viscosity at the top of the model, where $T = 0^oC$ in all cases, is 1.2×10^{21} Pa-s while at $T = 1000^oC$ we assumed the viscosity to be three orders of magnitude less, which is in agreement with available geophysical data on variation of rock viscosity with depth in the mantle. Calculations with MANTLE were then carried out for the bottom heated thermal convection case with base temperatures equal to 100, 200, and 300 and using the 18 x 18 variable mesh of Fig. 8. This corresponds to factors of 10, 40, and 100 decrease in viscosity from top to bottom, respectively. The results are summarized in Table II below. Here is given the average temperature of the isothermal central core, the viscosity corresponding to that temperature, and the value of R_a/R_c corresponding to the bulk solid viscosity and the base temperature as corrected by Eq. (4.7).

TABLE II

SUMMARY OF NUMERICAL RESULTS FOR BOTTOM HEATED THERMAL CONVECTION WITH TEMPERATURE DEPENDENT VISCOSITY SOLID

Bottom Temperature	Core Temperature	Average Viscosity	Nusselt Number	R_a/R_c
100	55.0	$.28 \times 10^{21}$ Pa-s	14.506	430
200	116.3	$.089 \times 10^{21}$ Pa-s	23.103	2700
300	180.5	$.037 \times 10^{21}$ Pa-s	31.589	10000

The horizontally averaged temperature profiles are shown in Fig. 10, and Fig. 11 shows the temperature profiles for the case of bottom temperature equal to 200. Comparing with the results for the constant viscosity cases shown in Fig. 9 and Table I, we see a significant difference in the form of convection caused by the temperature-dependent creep behavior of the mantle material; the

boundary layers become more concentrated at the warmer base of the model as expected, the isothermal region enlarges, and the bulk temperature of the isothermal region is higher than the mean of the base and top temperatures.

We have also carried out studies of convection of the mantle with combined heating from within and below. Here boundary layer theory doesn't apply and consequently less work has been done in this case, which is more relevant to the Earth's mantle. Here the critical Rayleigh number for convection is not known apriori and must be determined numerically. Several cases of varying ratios λ of internal heating to total heating have been investigated. Results will be illustrated for the case $\lambda = 0.6$ where the critical internal heating rate was determined to be 3.1×10^{-12} W/m^3. Table III illustrates some recent results for higher internal heating rates using the uniform mesh shown in Fig. 8.

Whereas the bottom heated case showed only a single convection cell up to very high Rayleigh numbers, the combined heating case often produced solutions composed of one or two convection cells and with two or three boundary layers respectively. Figure 12 illustrates the one and two cell temperature profiles for $R_a/R_c = 645$. Figure 13 again illustrates the horizontally averaged temperatures for the two solutions obtained at $R_a/R_c = 645$. Calculations were also carried out with the temperature-dependent creep law described previously to ascertain the effect of coupling the thermal profile to the effective viscosity of the mantle material. These results for the heating

TABLE III

SUMMARY OF NUMERICAL RESULTS FOR

COMBINED INTERNAL AND BASE HEATING $\lambda = 0.6$

		Nusselt Number	
R_a/R_c	Mesh Spacing	One Cell	Two Cell
161	20 x 20	6.208	5.335
322	20 x 20	7.198	6.487
645	20 x 20	8.204	7.812
968	20 x 20	8.781	8.690
1290	20 x 20	---	9.361
1613	20 x 20	---	9.090

conditions corresponding to R_a/R_c = 645 of Table III are shown in Figs. 14 and 15. Only the converged two-cell solution was obtained at R_a/R_c = 645. Again a significant change in the Nusselt numbers (9.311 vs 7.812) and the temperature profiles is observed.

The inclusion of thermal effects on the creep behavior of rocks will allow us to new address the lithospheric thinning problem. The erosion of the Earth's crust by a thermal plume at its base is undoubtedly an important aspect of continental rifting and the creation of oceanic swells. In this calculation a hot plume will impinge on a thick continental lithosphere and will erode the lithosphere by warming it and carrying away lithospheric material made mobile by virtue of its higher temperature. The finite element approach will allow a concentration of elements in the transition region between the lithosphere and asthenosphere to resolve the large viscosity variation across this region. Thinning rates, surface heat flow and uplift rates will be calculated as a function of plume strength; these quantities are geological observables and can accordingly be used to constrain model parameters. Figure 16 illustrates the proposed calculational model.

Incorporation of aging effects in mantle convection and its interaction with the Earth's crust would also be an important consideration. For example, the carbonate rocks thought to make up the mantle could change from the carbonate phase to a chemically reduced material with the attendant release of CO_2 which would significantly affect material (including creep) properties. Partial melt of mantle materials or precipitation of material from a molten state would also affect material properties significantly. Thus, aging effects, while difficult to incorporate into the mantle creep models, are important considerations for the prediction of the structural behavior of the Earth's mantle and crust.

ACKNOWLEDGEMENT

The author wishes to thank R. V. Browning of the Los Alamos National Laboratory and M. E. Gurtin and W. O. Williams of Carnegie-Mellon Institute for discussions with them on their manuscript dealing with the viscoplastic model for highly-filled polymers. The author also wishes to acknowledge the influence of the participants of the Viscoplasticity Workshop held at Los Alamos on September 1-3, 1982 on the content of this paper.

REFERENCES

1. Bazant, Z. P. (1975) "Theory of Creep and Shrinkage in Concrete Structures: a Precis of Recent Developments," Mech. Today, 2, 1-93.

2. Wittmann, F. H. "Creep and Shrinkage Mechanisms," in Creep and Shrinkage in Concrete Structures, J. Wiley & Sons (1982) 129-161.

3. Bazant, Z. P., and Wu, S. T. (1973), "Dirichlet Series Creep Function for Aging Concrete," J. Eng. Mech. Div. ASCE, 99, EM2, 367-87.

4. Bazant, Z. P., and Wu, S.T. (1974), "Rate-Type Creep Law of Aging Concrete Based on Maxwell Chain," Mater. Constr. (Paris)/Mater. Struct., 7, 45-60.

5. Anderson, C. A., "Numerical Creep Analysis of Structures," in Creep and Shrinkage in Concrete Structures, J. Wiley & Sons (1982) 269-303.

6. Browning, R. V., Gurtin, M. E., and Williams, W. O., "A Viscoplastic Constitutive Theory for Filled Polymers," paper submitted for publication, International J. of Solids and Structures (1983).

7. Heard, H., "Flow of Rocks at Depth," Viscoplasticity Workshop Abstracts, Los Alamos National Laboratory, September 1-3 (1982).

8. Carter, N. L., "Steady Flow of Rocks," Rev. Geophys and Space Phys. 14, (1976) 301-360.

9. Anderson, C. A., "An Investigation of the Steady Creep of a Spherical Cavity in a Half-Space," J. Appl. Mech. 98 (1976).

10. Anderson, C. A. and Bridwell, R. J., "A Finite Element Method for Studying the Transient Nonlinear Creep of Geological Structures," Int. J. for Num. and Anal. Methods in Geomechanics, 4 (1980) 255-76.

11. Bridwell, R. J. and Anderson, C. A., "Thermomechanical Models of the Rio Grande Rift," in Mechanisms of Continental Drift and Plate Tectonics, Academic Press (1981) 41-59.

12. Anderson, C. A., "Boussinesq-Papkovich Functions for Creep Around a Spherical Cavity or Rigid Inclusion in a Gravity-Loaded Half-Space," J. Appl. Mech. 28 (1981).

13. Schubert, G., Froidevaux, C., and Yuen, D. A., "Oceanic Lithosphere and Asthenosphere: Thermal and Mechanical Structures," J. Geophys. Res. 81 (1976) 3625-40.

14. Jarvis, G. T. and Peltier, W. R., "Mantle Convection as a Boundary Layer Phenomenon," Geophys. J. R. Ast. Soc. 68 (1982) 389-427.

15. Sato, A. and Thompson, E. G., "Finite Element Models for Creeping Convection," J. Comp. Phys., 22 (1976) 229-44.

16. Thompson, E. G., "MANTLE: A Finite Element Program for Thermal-Mechanical Analysis of Mantle Convection," final report on NASA Grant NGR 06-002-191 (1979).

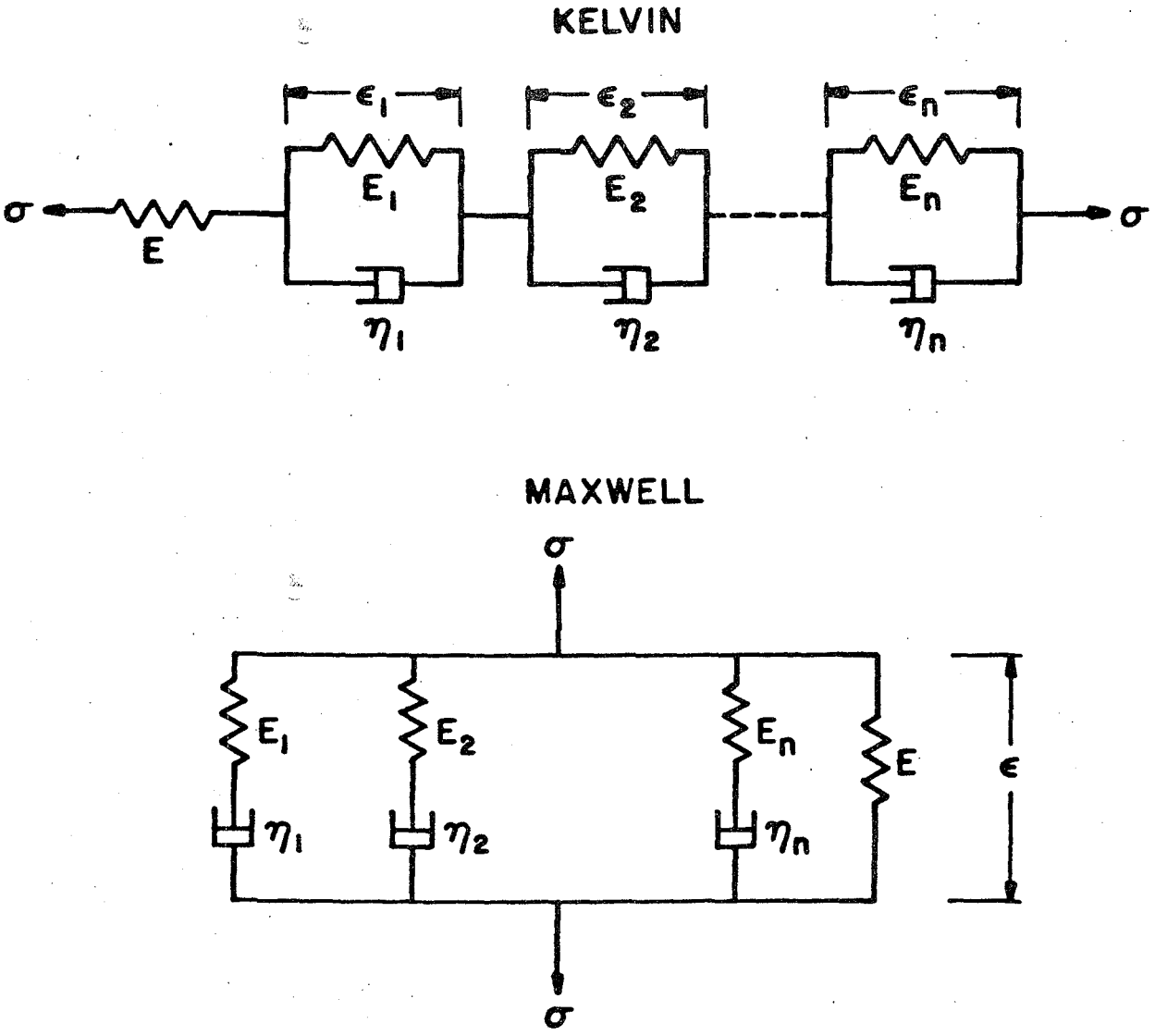

Fig. 1. Kelvin and Maxwell chains for aging viscoelastic solids.

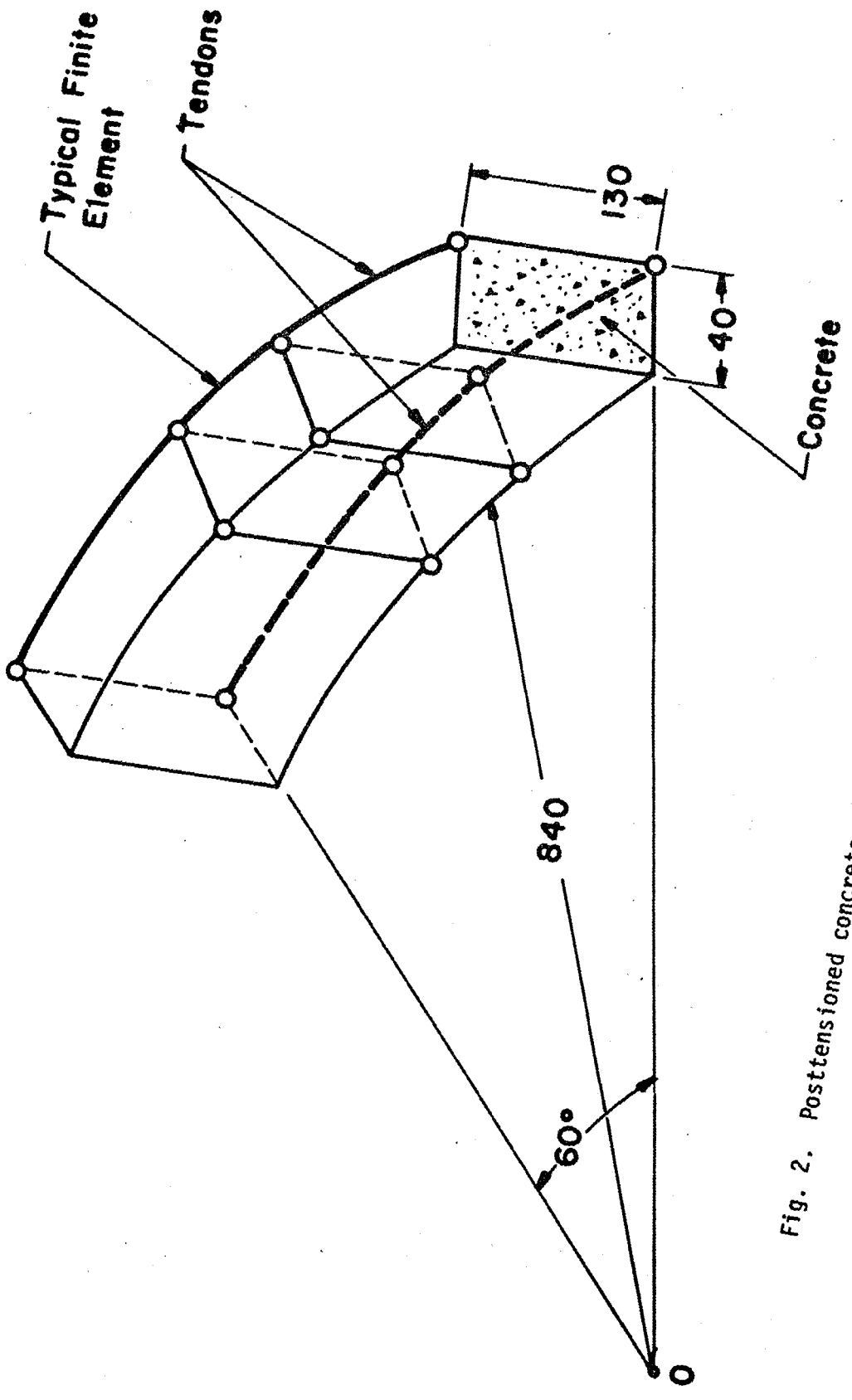

Fig. 2. Posttensioned concrete ring finite element model.

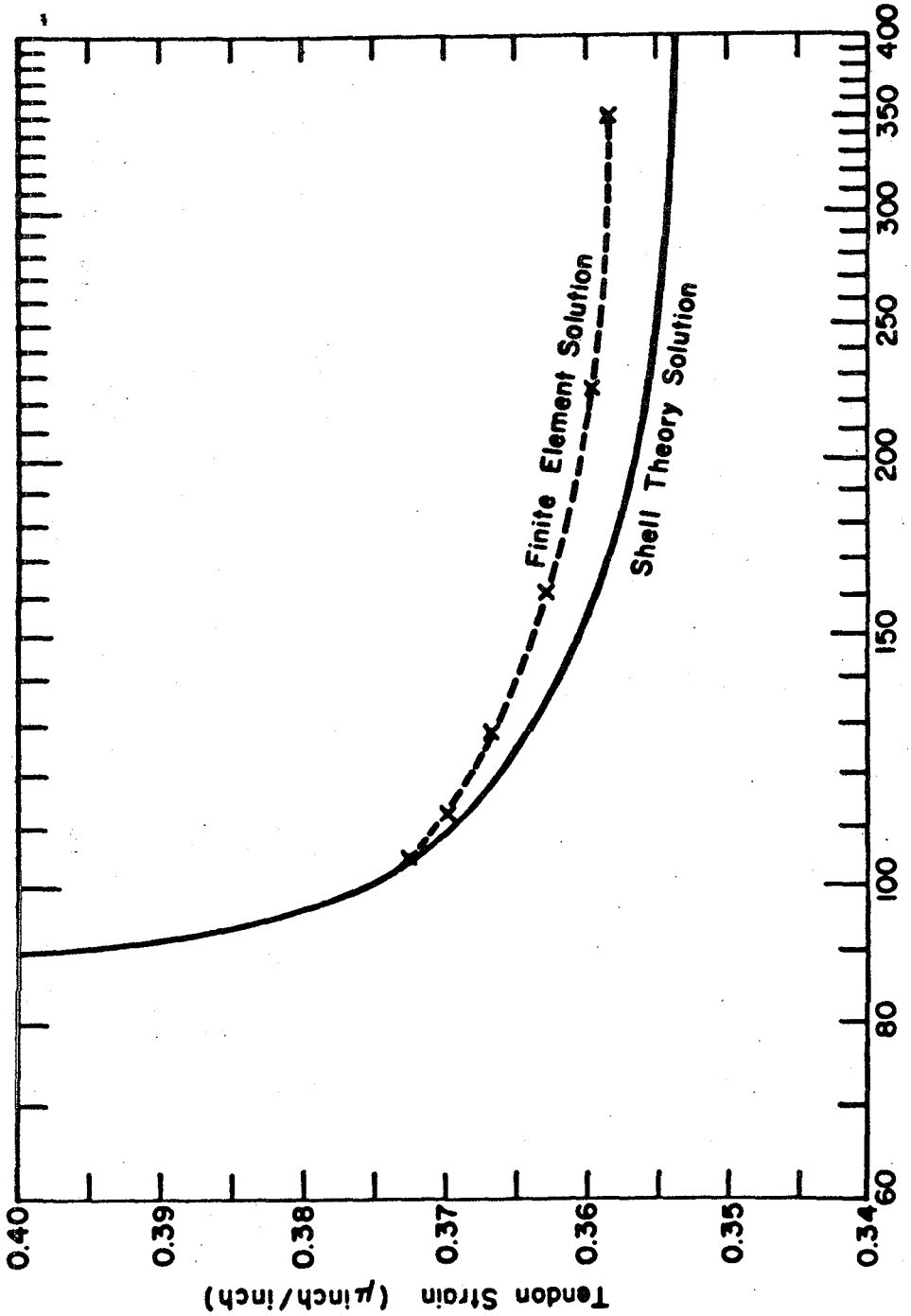

Fig. 3. Variation in posttensioning strain with time.

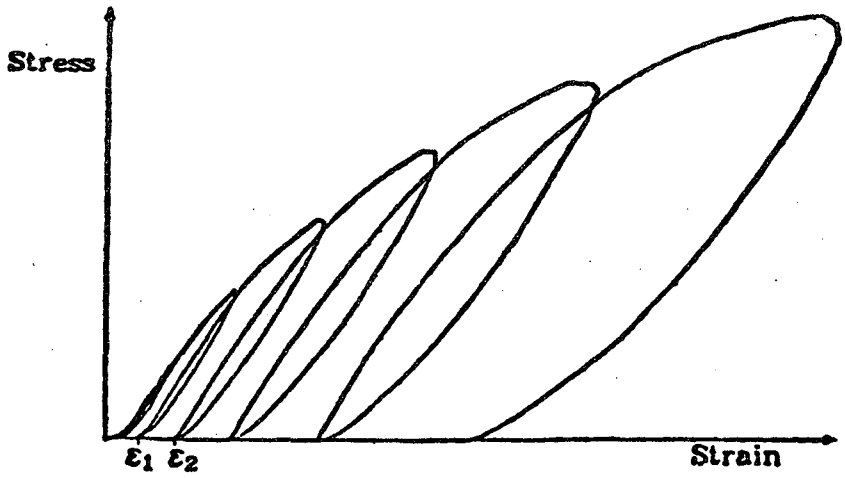

Fig. 4. A typical stress-strain diagram for a highly-filled polymer.

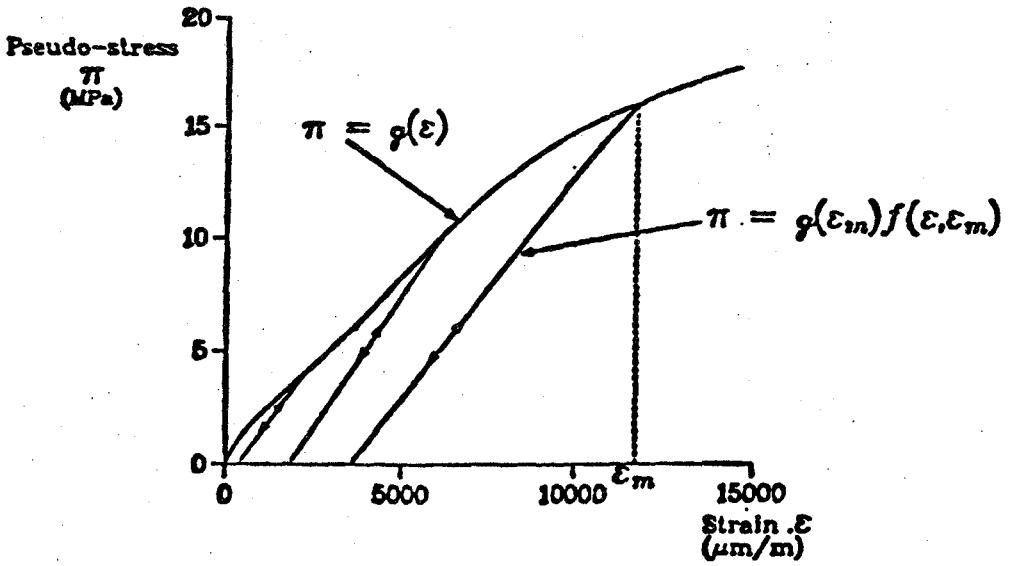

Fig. 5. Enveloping stress-strain curve and loading-unloading paths for a highly-filled polymer.

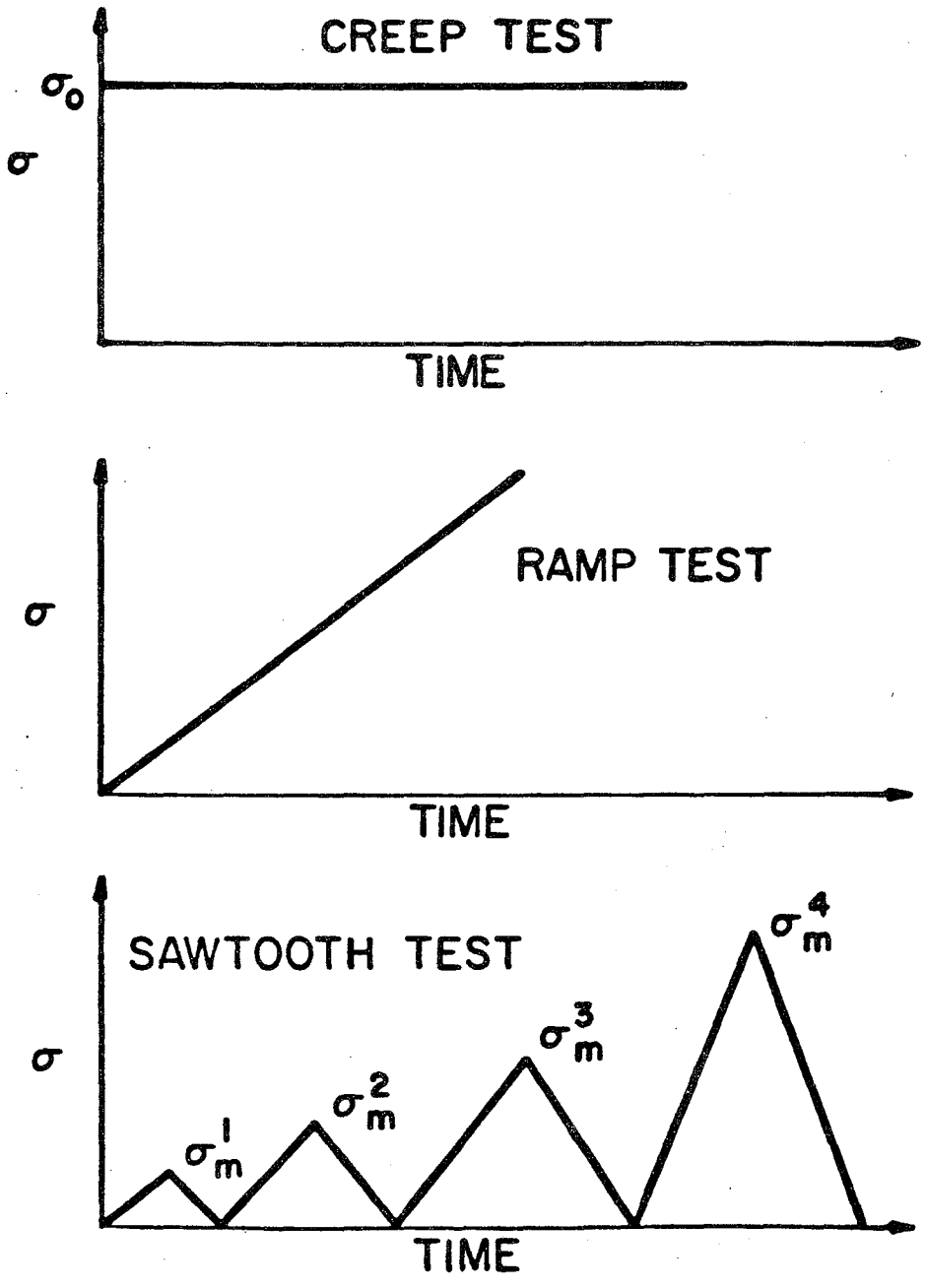

Fig. 6. Three stress-time histories used to calibrate the viscoplastic solid.

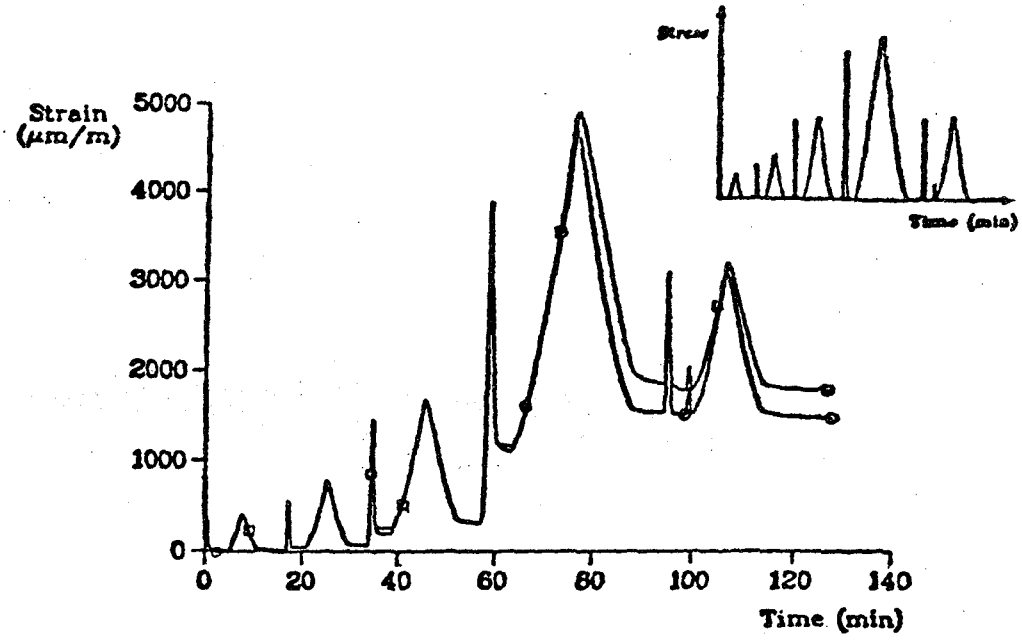

Fig. 7. Comparison of experimental (□) and calculated (o) strains for a typical filled polymer. The stress-rates are 5.0 and 0.5 MPa/min.

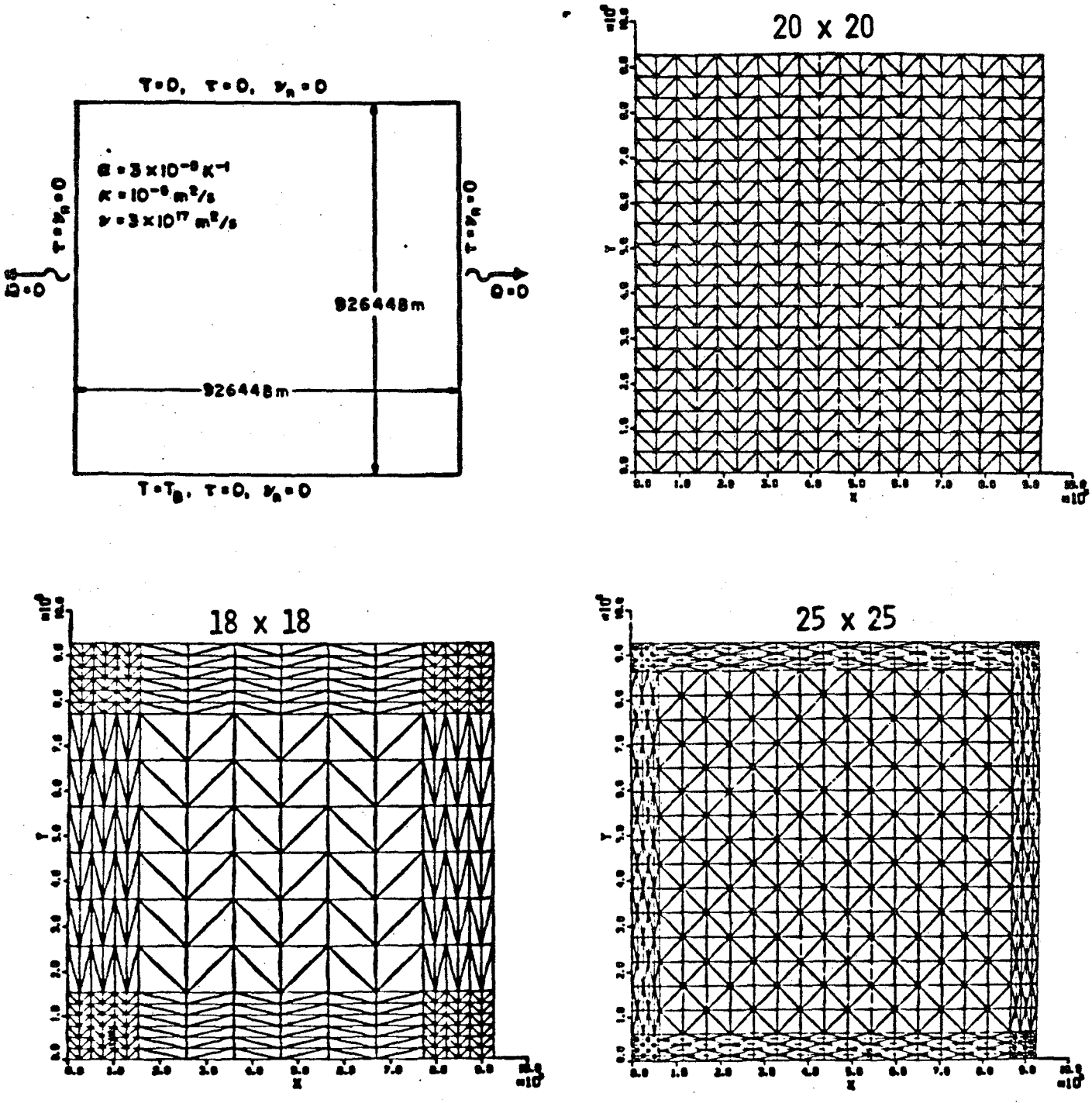

Fig. 8. Problem geometry and three finite element meshes used to study Rayleigh-Bernard convection.

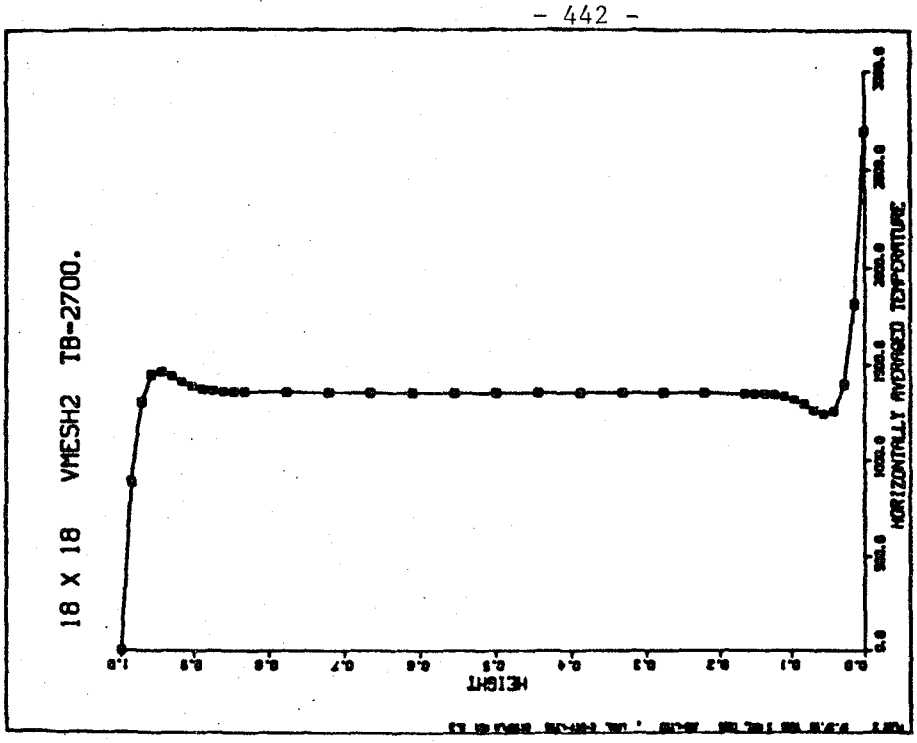

(b) R_a/R_c = 2700

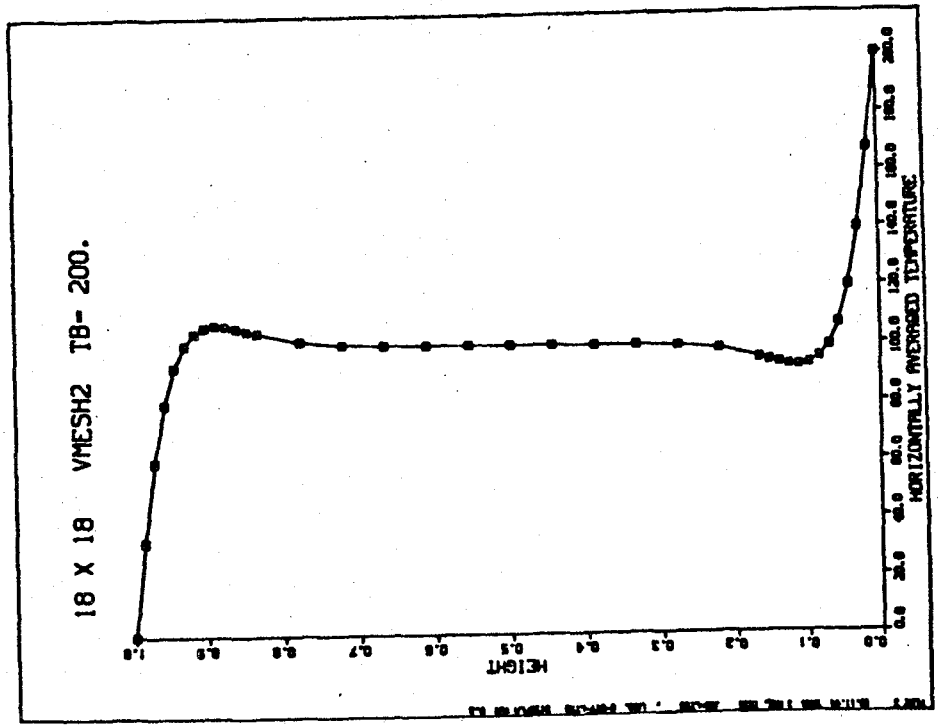

(a) R_a/R_c = 200

Fig. 9. Horizontally averaged temperature profiles for constant viscosity solid heated from below.

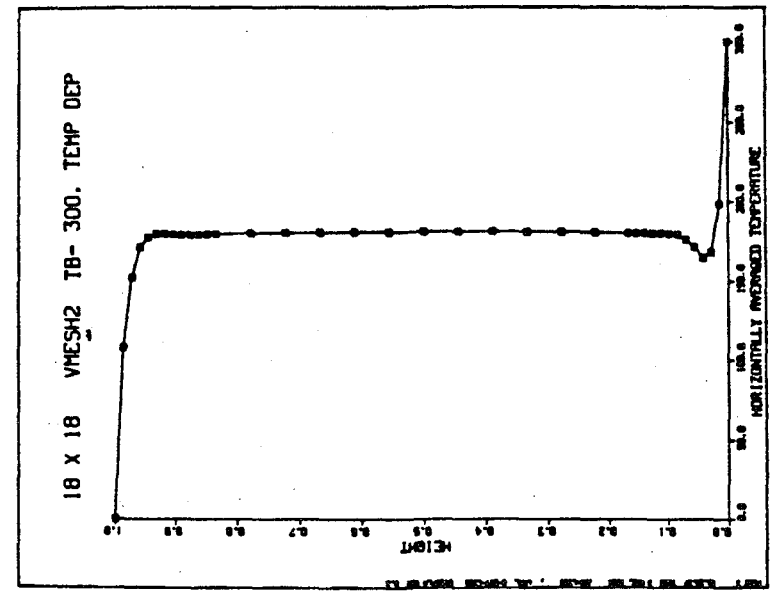

(c) $T_B = 300$

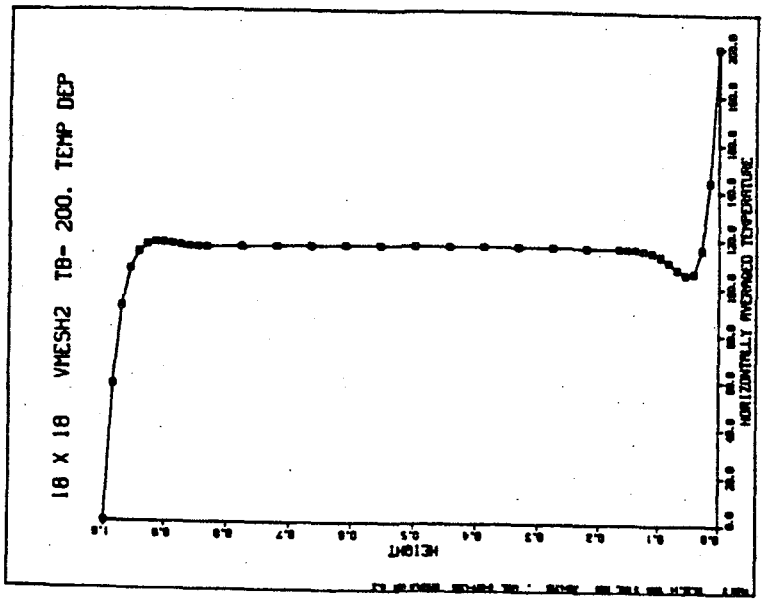

(b) $T_B = 200$

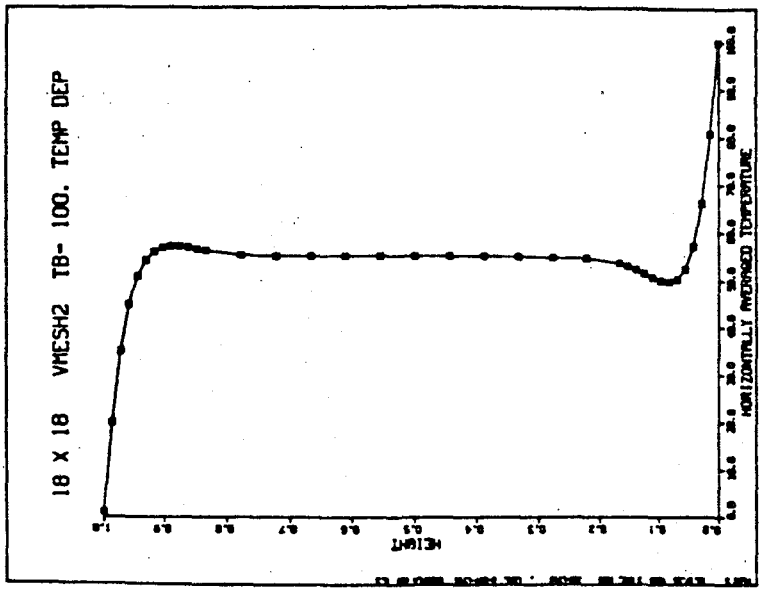

(a) $T_B = 100$

Fig. 10. Horizontally averaged temperature profiles for temperature dependent viscosity solid heated from below with base temperatures $T_B = 100$, 200, and 300 respectively.

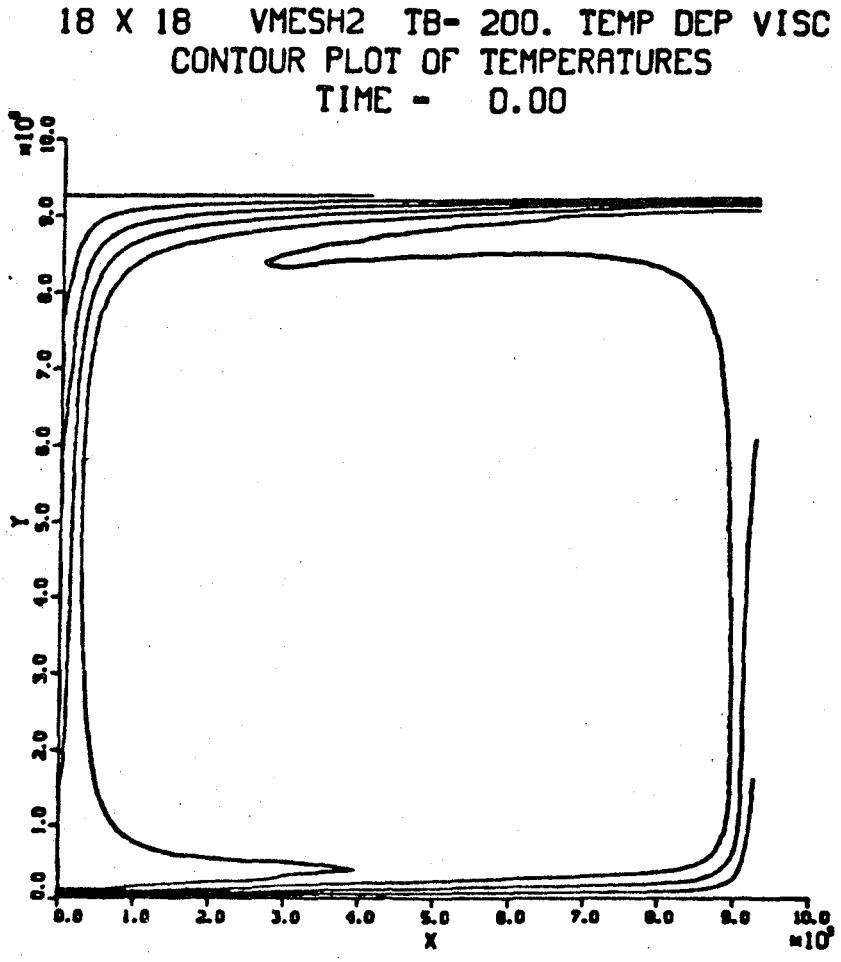

Fig. 11. Temperature profiles for temperature dependent viscosity solid heated from below with T_B = 200.

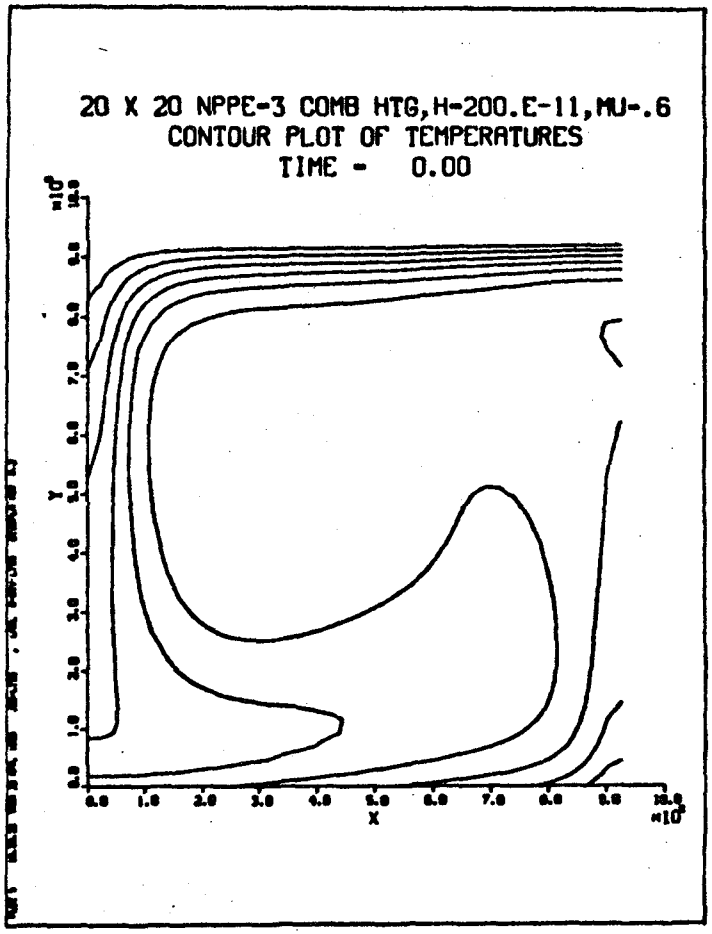

(a) Single cell

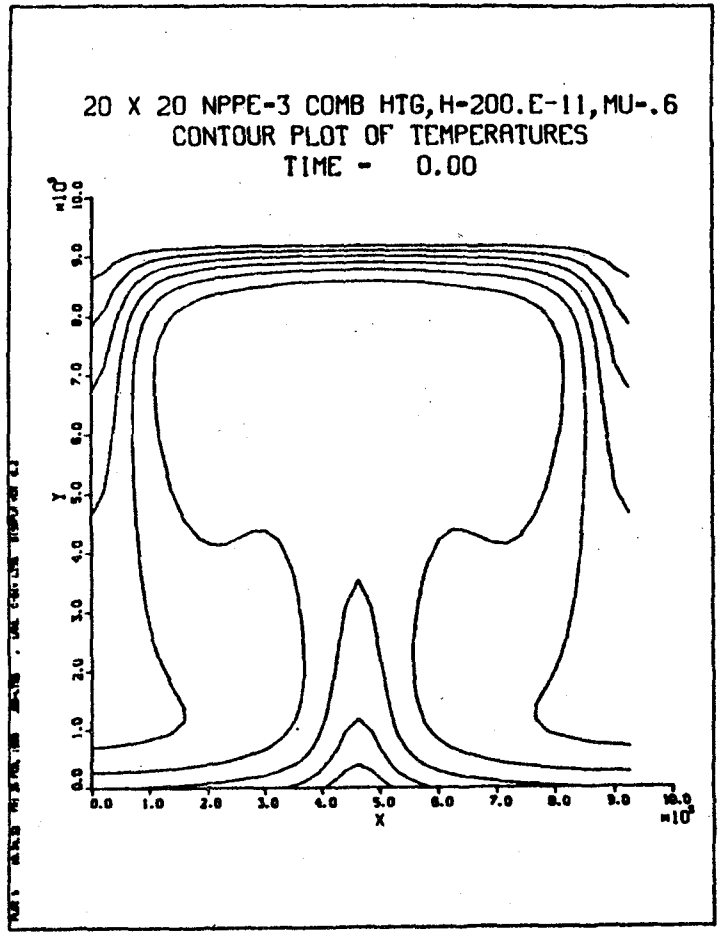

(b) Double cell

Fig. 12. One- and two-cell temperature profiles for combined internal and base heating and R_a/R_c = 645. Constant viscosity solid.

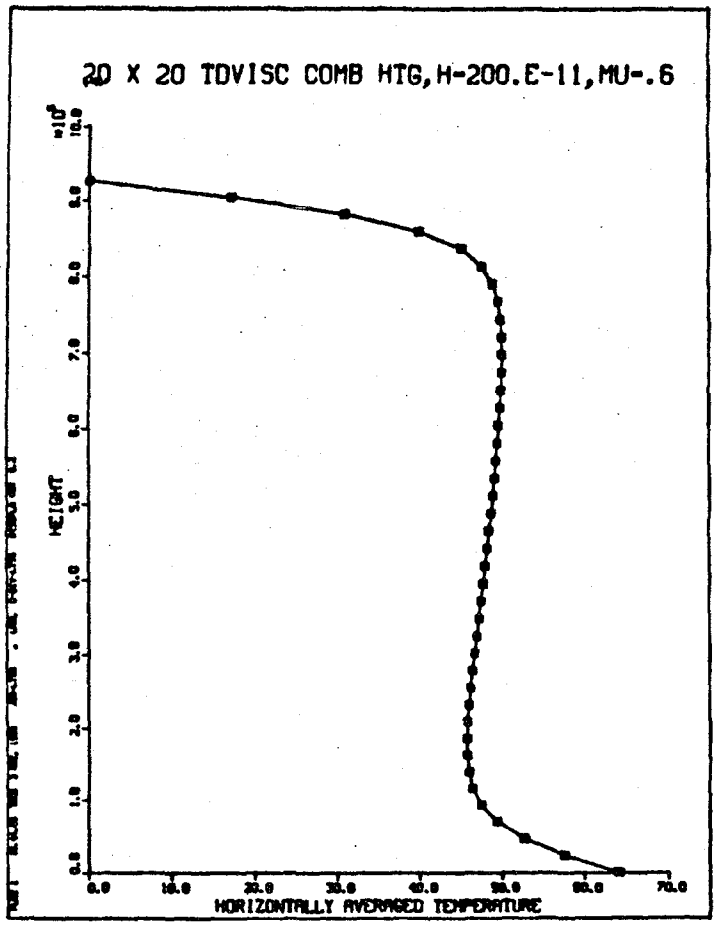

(a) Single cell

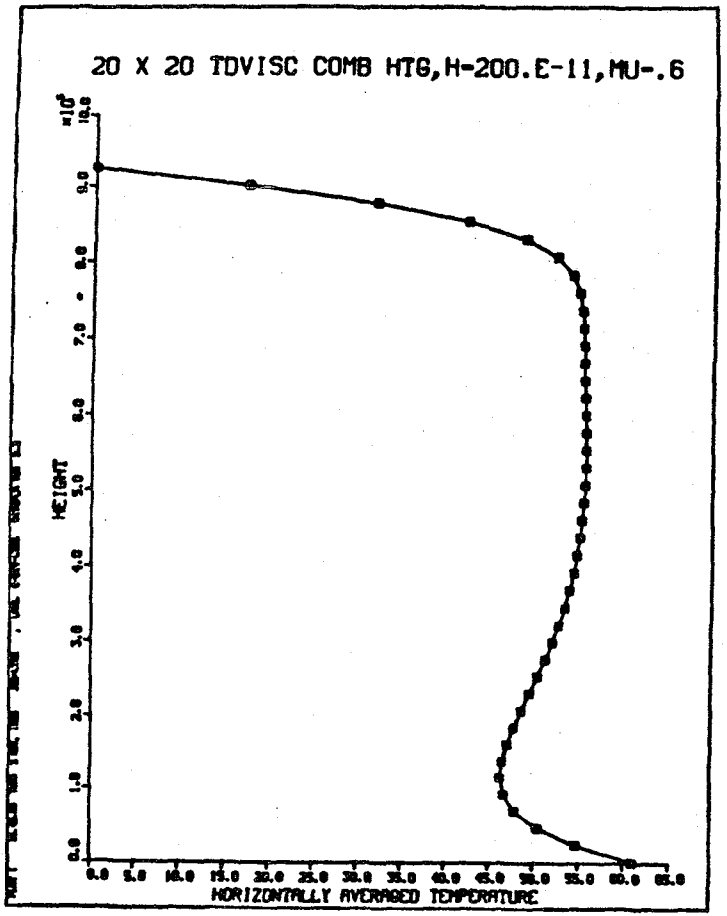

(b) Double cell

Fig. 13. Horizontally averaged temperature profiles for combined internal and base heating case with R_a/R_c = 645. Constant viscosity solid.

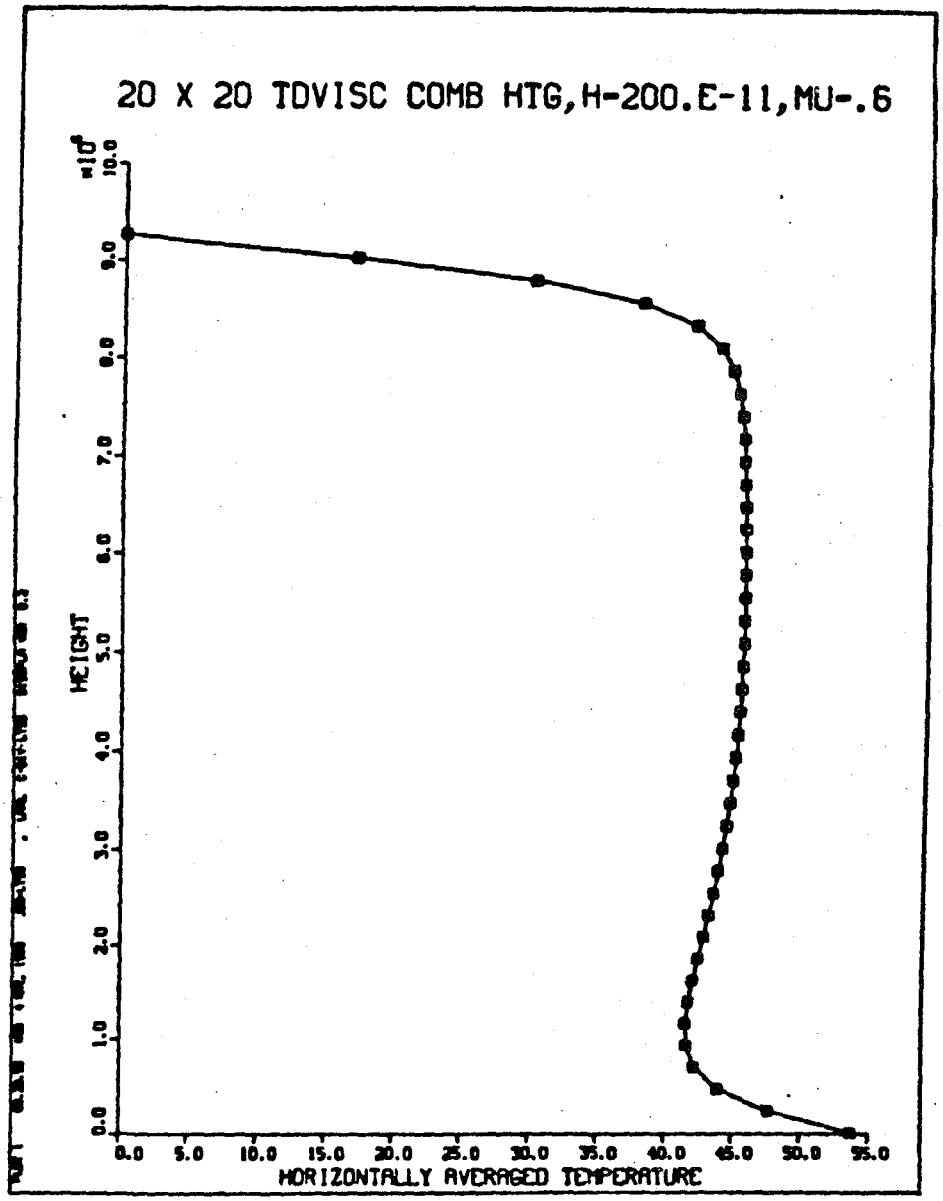

Fig. 14. Horizontally averaged temperature for combined heating case with R_a/R_c = 645. Temperature dependent viscosity solid.

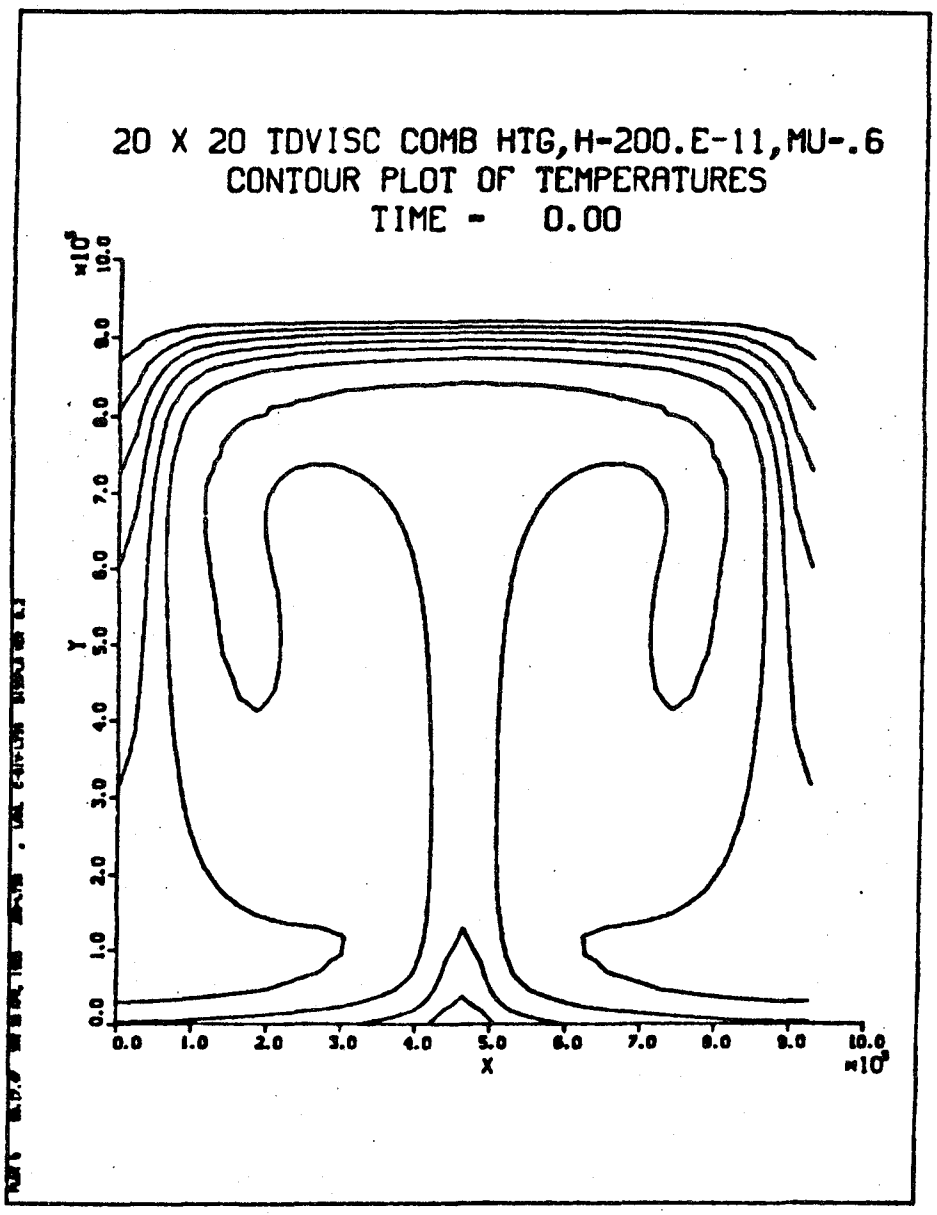

Fig. 15. Plume development for combined heating case with R_a/R_c = 645. Temperature dependent solid.

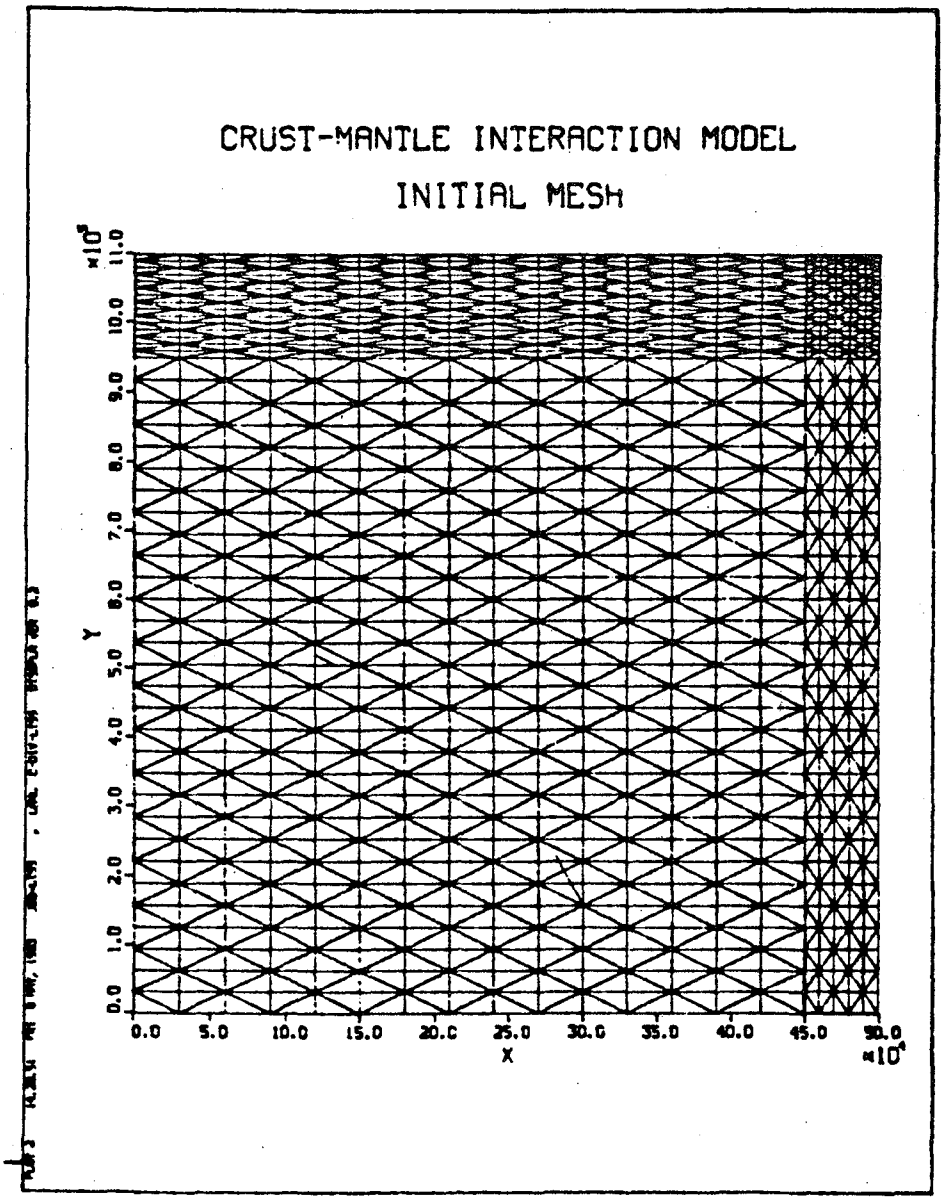

Fig. 16. Crust-mantle interaction model.

DEFORMATION OF CONCRETE AT VARIABLE MOISTURE CONTENT

F. H. Wittmann
Swiss Federal Institute of Technology Lausanne
Laboratory for Building Materials Science
Lausanne, Switzerland

Introduction

Any change of moisture content provokes a volume change of a porous material such as concrete. By means of modern numerical methods it is possible to predict hygral volume or length change if the physical processes involved are sufficiently well known. If drying takes place under load the total deformation observed is always bigger than the sum of drying shrinkage and creep. This increased deformation is often explained by special mechanisms such as drying creep or load induced shrinkage. A similar situation exists if the temperature is changed. So far, however, it is an open question if transient hygral or transient thermal creep exist or if this observation has to be explained in another way.

In this contribution we will briefly describe an approach to deduce materials behaviour from their composite structure. To do so three structural levels are introduced. Therefore this approach has been called Three Level Approach or in abreviated form TL-Approach.

TL - Approach

It can be shown that it is not possible to link processes within the structure of hardened cement paste directly with the observed behaviour of concrete. Therefore different structural levels have to be introduced.

On the microlevel we will discuss drying and shrinkage mechanisms as well as creep mechanisms which are characteristic for a xerogel such as hardened cement paste.

In real concrete additional influences such as geometry, inclusions and cracks determine the behaviour. These parameters are taken into consideration on the mesolevel. Micromechanics of composite materials is the most important tool of the mesolevel.

Finally on the macrolevel the material is considered to be homogeneous and all imperfections are treated as being smeared out over the entire specimen. The macrolevel serves essentially to collect all information available and to formulate material laws.

Creep of Hardened Cement Paste

It has been shown that creep of hardened cement paste can be satisfactorely described as a thermally activated process /1/. Time-dependence, influence of temperature, and applied load can be represented by the following equation :

$$\varepsilon = a \cdot t^K \cdot \exp(-\frac{Q}{RT}) \sinh(b \cdot \sigma) \qquad (1)$$

This equation degenerates to the well-known double-power function if temperature and load are kept constant. In addition it is only valid if the moisture content is kept constant. Equation (1) thus represents creep of hardened cement paste on the microlevel.

Drying of Hardened Cement Paste

The drying process of hardened cement paste can be adequately described by diffusion equations /2/. In this context the relative humidity H with which the microporous system is in equilibrium is often used as variable. Formally the flux of the relative humidity J_H can then be expressed by the following equation :

$$J_H = D \text{ grad } H \qquad (2)$$

In this equation D stands for the diffusion coefficient. For an infinite long cylinder the drying process can then be described by means of the following differential equation :

$$\frac{\partial H}{\partial t} = \frac{1}{r} \frac{\partial}{\partial r} Dr \frac{\partial H}{\partial r} \qquad (3)$$

It has been shown both experimentally and numerically that D depends among other factors on humidity.

$$D = f(RH) \qquad (4)$$

For this reason equation (3) has to be solved numerically.

Shrinkage of Hardened Cement Paste

Moisture loss of microporous xerogel such as hardened cement paste is always accompanied by a volume change. If an infinite thin sheet dries out instantaneous drying shrinkage is the consequence. This idealized material behaviour is called unrestrained shrinkage. It is a material property which depends on water/cement ratio, degree of hydration, type of cement, etc. In the range of 100% RH and 50% RH unrestrained shrinkage can be approximated by a straight line :

$$\varepsilon_s^u = a + bH \qquad (5)$$

where a and b are parameters which depend on the microstructure of the hardened cement paste.

If we have calculated the moisture distribution in a cylinder by means of equation (3) we get the internal state of stress by introducing equation (5). Drying shrinkage of a real specimen thus depends on the material property i.e. unrestrained shrinkage and the geometry. It has to be mentioned at this point,

that the actually observed drying shrinkage is significantly influenced by crack formation.

Behaviour of the Composite Material

So far we have limited ourselves to the discussion of the behaviour of hardened cement paste. We have to introduce the specific properties of the composite structure of concrete now.

If concrete is loaded the instantaneous deformation creates a complex state of stress in the composite structure. Most aggregates in normal concrete can be looked upon to react linearely elastic. Due to creep of hardened cement paste stresses in the structure of concrete are redistributed. By means of finite element analysis this process can be realistically simulated. It can be shown in particular that during the creep process elastic energy is stored in the aggregates. This is one of the reasons why partial creep recovery is observed on concrete after unloading.

In normal concrete aggregates can be considered to be impermeable to moisture flow. The diffusion coefficient of concrete depends on the diffusion coefficient of the porous hardened cement paste and on the aggregate volume concentration. By means of finite element analysis an effective diffusion coefficient of the composite material can be determined.

For a very long time the drying process creates an internal state of stress in concrete. The deformation of a drying specimen is the consequence of this long lasting process.

We have already mentioned that shrinkage stresses can cause cracking in the outer layers of a drying specimen. This is also true for concrete. In addition cracks are formed in drying concrete due to the fact that the inert aggregates in the shrinking matrix create additional stresses.

Simultaneous Creep and Shrinkage

Usually in a concrete structure drying shrinkage and creep occur simultaneously. It is not astonishable that there exist still diverging views on the total deformation of a loaded drying concrete specimen. The analysis and the simulation of all processes involved is far from being trivial.

Diffusion theory allows us to calculate the time dependent moisture content. We have seen that the moisture distribution creates an internal state of stress. In an unloaded specimen drying shrinkage is significantly influenced by crack formation. Application of a compressive load to a drying specimen reduces or eliminates crack formation.

As a consequence the internal state of stress of a drying specimen is changed by an applied load. It has been shown that this effect explains at least an important part if not all of what is called drying creep /3/.

Let us now consider a volume element in a drying concrete cylinder. Drying does not only create an internal state of stress but all material properties are dependent on moisture content. Creep of moist concrete for instance is much bigger than creep of dry concrete. Thus all mechanical properties of a given volume element change as the drying process proceeds. The Elastic modulus and the strength increase whereas time-dependent deformability decreases. This complex situation can be analysed and simulated by means of numerical methods.

Conclusions

Creep and shrinkage of a composite material such as concrete can only be understood on the basis of a comprehensive analysis of the different mechanisms involved and of the different superimposed stress fields. The TL-Approach has proved to be a powerful tool to deal with this problem. Subdivision of the total deformation of a loaded drying specimen into basic creep, drying shrinkage and drying creep is meaningless. To analyse and to simulate the material behaviour realistically we have to apply numerical methods.

References

1. Straub, F. and Wittmann F.H., "Activation energy and activation volume of compressive and tensile creep of hardened cement paste, Hydraulic cement pastes: their structure and properties", Proc. Conf. Sheffield, April 1976, pp. 227-229.
2. Roelfstra, P.E. and Wittmann, F.H., "Numerical analysis of drying and shrinkage", in: F.H. Wittmann (editor), Autoclaved Aerated Concrete, Moisture and Properties, Elsevier (1983).
3. Wittmann, F.H., "Creep and Shrinkage mechanisms", in: Creep and Shrinkage in Concrete Structures, by Z.P. Bazant and F.H. Wittmann (editors), John Wiley & Sons Ltd. (1982).

Numerical Modelling and Geomechanics
(Soil - Rock - Concrete)

O.C. Zienkiewicz, F.R.S.

Abstract

Numerical analysis and constitutive modelling are the essential and inseparable ingredients for the solution of problems in geomechanics. For this reason much of the progress of the last decades was achieved by collaboration or simultaneous contributions on both fronts.

This paper reviews the progress and indicates some future trends. For clarity it is devided into three parts, dealing respectively with:

a. the general formulation for analysis of porous, saturated, media

b. some aspects of numerical solution of non linear problems and

c. models of typical geomechanical materials.

In the first section we show the possible generalization of Biot's equations and various limiting situations. Here an approximate formulation with only displacement and pressure variables is given with its limits of applicability as well as the limits of purely undrained behaviour in Fig. 1.

In the second section we show that recent progress in the solution of dynamic transients will probably result in such processes as 'dynamic' or 'viscous' relaxation becoming the standard methodology for both static and dynamic solutions. Accelerated Viscous Relaxation has recently shown dramatic operations count reduction and is now being tested in a variety of problems (Figs. 2 and 3).

The third section dealing with material modelling is by necessity, selective. Here we discuss:

a. the modelling of tensile cracking behaviour and show that the simple, distributed crack, models are still the optimal approach (Fig. 7)

b. that various models can adequately give reasonable prediction for static soil mechanics problems.

c. that for cyclic (densification) modelling two relatively simple modifications allow prediction of pore pressure rise, cyclic mobility and liquefaction. Here in particular a simple boundary surface model recently introduced is efficient even with only two new physical parameters introduced.

d. that for rate sensitive, degrading, behaviour a set of new models requires to be introduced. This is of importance in dynamic loading of concrete structures.

With such models dynamic transient analysis of earthquake response of structures and their foundations becomes possible. As such analyses are at least comparable in cost to the currently used (and somewhat irrational) 'linearised' procedures we believe they will become standard practice in the near future.

Fig. 14 shows the results of a recent analysis of the San Fernando dam failure of 1971 indicating the large movements which could have occured in the first 10 seconds of the earthquake (the complete failure taking place in some 60 seconds).

Fig. 17/18 show a similar transient analysis of the Koyna dam movements and cracking which again are reasonably modelled. (1967 earthquake).

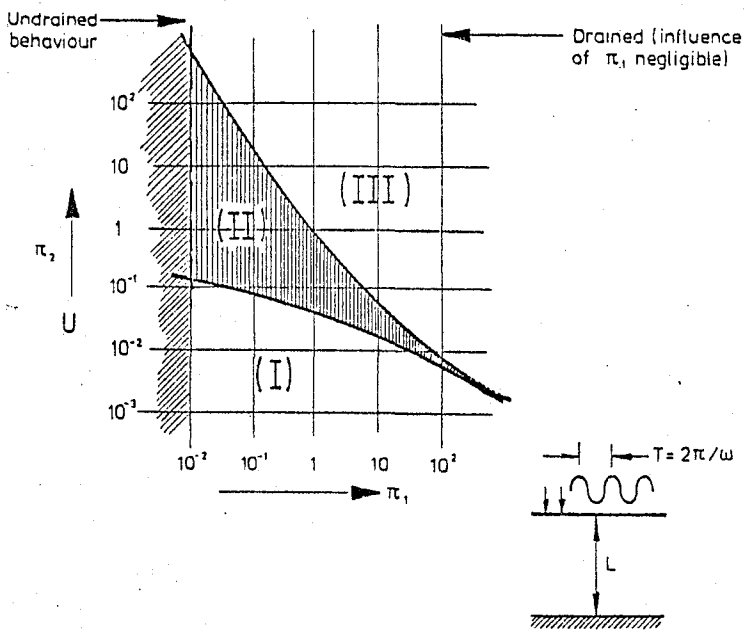

$$\pi_1 = \frac{k\rho V_c^2}{\omega L^2} = \frac{2k\rho T}{\pi \hat{T}^2} = \left(\frac{2}{\beta\pi}\right)\frac{\bar{k}}{g}\frac{T}{\hat{T}^2}$$

$$\pi_2 = \frac{\omega^2 L^2}{V_c^2} = \pi^2\left(\frac{\hat{T}}{T}\right)^2$$

$\bar{k} = \rho_f g k$ $\quad$ $\bar{k}$—kinematic permeability

$\hat{T} = 2L/V_c$ $\quad$ $V_c^2 = (D + K_f/n)/\rho$

$\approx \beta K_f/\rho_f n$

$\approx K_f/\rho_f$ (speed of sound in water)

$\beta = \rho_f/\rho$ $\quad$ $n \approx 0.33$ $\quad$ $\beta = 0.33$

U - Undrained behaviour valid
III - Full Biot type form necessary
II - u-p approximation tenable
I - u-p approximation all dynamic terms disappear (consolidation equations)

FIGURE 1 LIMITS OF APPLICABILITY OF VARIOUS ASSUMPTIONS IN SOIL-FLUID INTERACTION

Order of NOP and NSTORE for a problem of order 2m = 2

Dimension	Direct Methods		VR		AVR	
	NOP	NSTORE	NOP	NSTORE	NOP	NSTORE
1	N	N	N^3	N	N^2	N
2	N^4	N^3	N^4	N^2	N^3	N^2
3	N^7	N^5	N^5	N^3	N^4	N^3

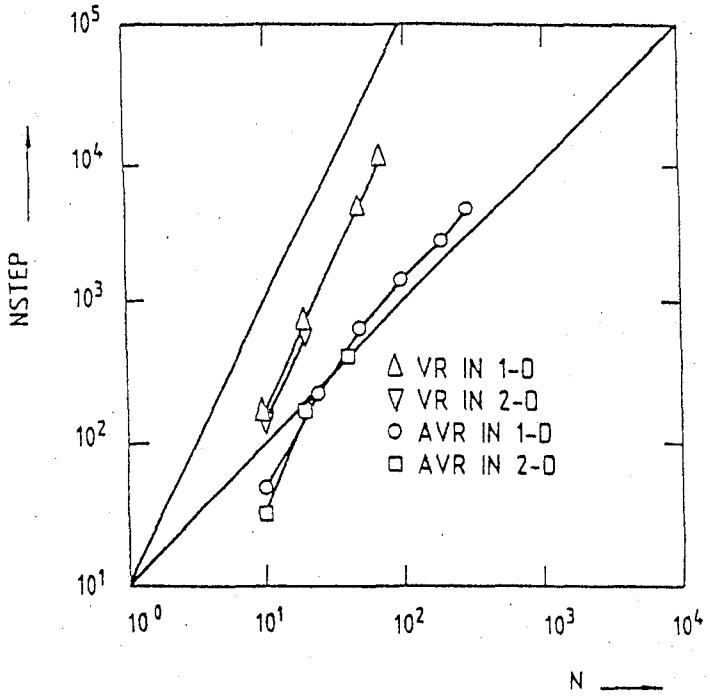

FIGURE 2 COMPARISON OF OPERATIONS (NOP) AND STORAGE (NSTORE) OR TIME STEP (NSTEP) REQUIREMENTS FOR DIRECT SOLUTION , VISCOUS RELAXATION AND ACCELERATED VISCOUS RELAXATION

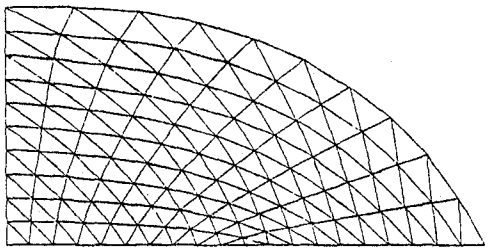

MESH

Linear
f = 1

Computime =
NSTEP =

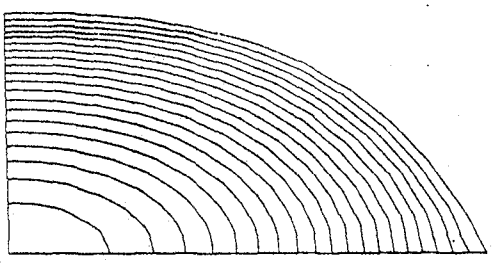

LINEAR CASE
CONTOUR INTERVAL : 0.02

Nonlinear
(softening)

Computime =
NSTEP =

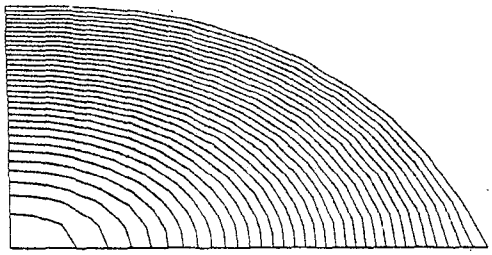

CASE : f=EXP(u)
CONTOUR INTERVAL : 0.02

Nonlinear
(hardening)

Computime =
NSTEP =

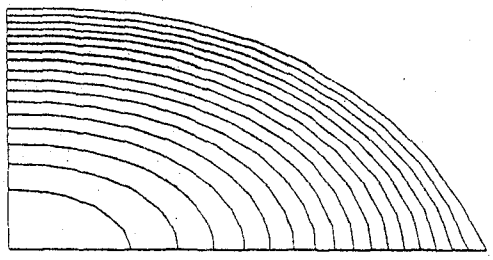

CASE : k=k(u)=1+u
CONTOUR INTERVAL : 0.02

FIGURE 3 COMPARISON OF COMPUTATION TIMES
LINEAR/NONLINEAR PROBLEM OF HEAT
CONDUCTION
$u=0$ ON BOUNDARY
$\nabla(k\nabla u)+f=0$

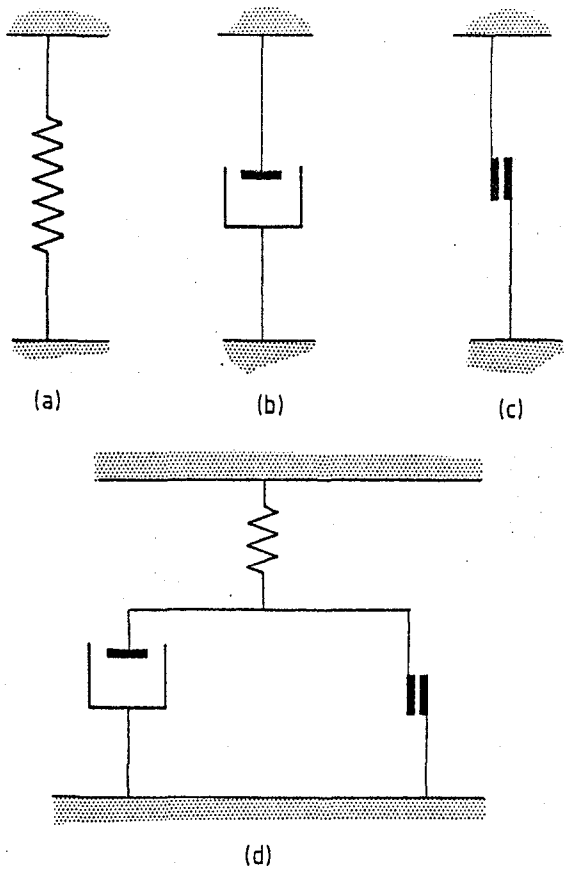

FIGURE 4 BASIC COMPONENTS FOR MATERIAL MODELS
(a) SPRING - REVERSIBLE LINEAR/NONLINEAR ELASTICITY
(b) DASHPOT - LINEAR/NONLINEAR CREEP
(c) SLIDER - PLASTIC RESISTANCE (STRAIN DEPENDANT)
(d) POSSIBLE - VISCOPLASTIC ASSEMBLY

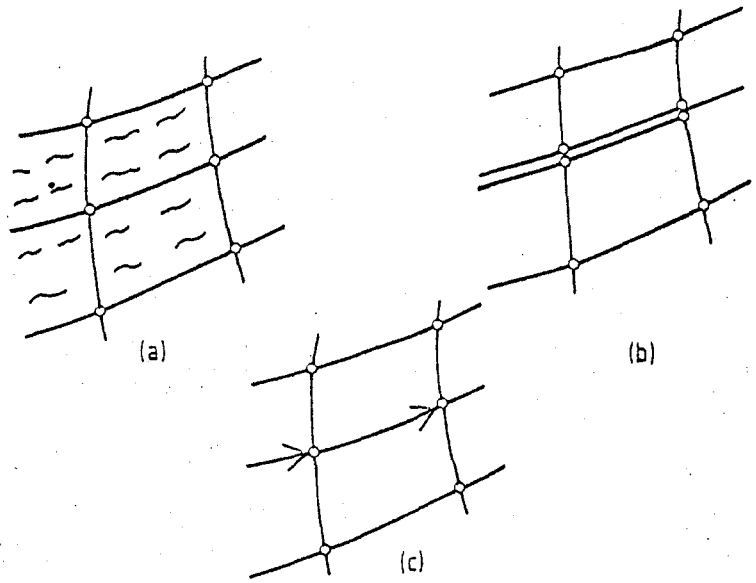

FIGURE 5 ALTERNATIVE APPROACHES TO MODELLING OF CRACKS
(a) DISTRIBUTED CRACKING
(b) CRACK ON ELEMENT INTERFACE (ELEMENT SEPARATION)
(c) FRACTURE MECHANICS - STRESS INTENSITY FACTOR APPROACH

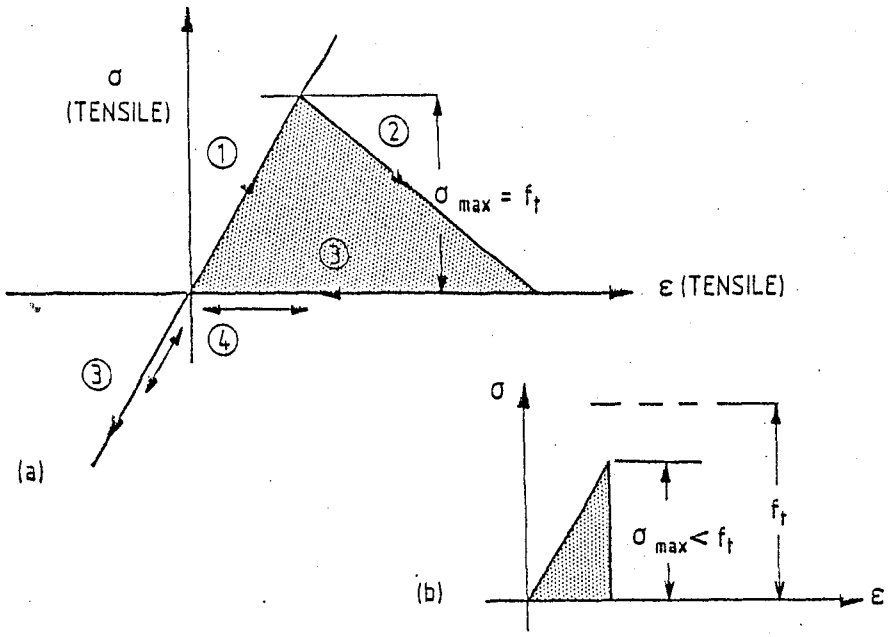

FIGURE 6 BEHAVIOUR IN UNIAXIAL TENSION
① FIRST TENSILE LOADING
② STRAIN SOFTENING
③ COMPRESSIVE RELOAD
④ SUBSEQUENT BEHAVIOUR

SHADED AREA - ENERGY DISSIPATION PER UNIT VOLUME (E)
WIDTH OF CRACK ZONE W
WE = CONSTANT IF W TOO LARGE REDUCE σ_{max} AS SHOWN IN (b)
f_t - UNIAXIAL STRENGTH IN TENSION

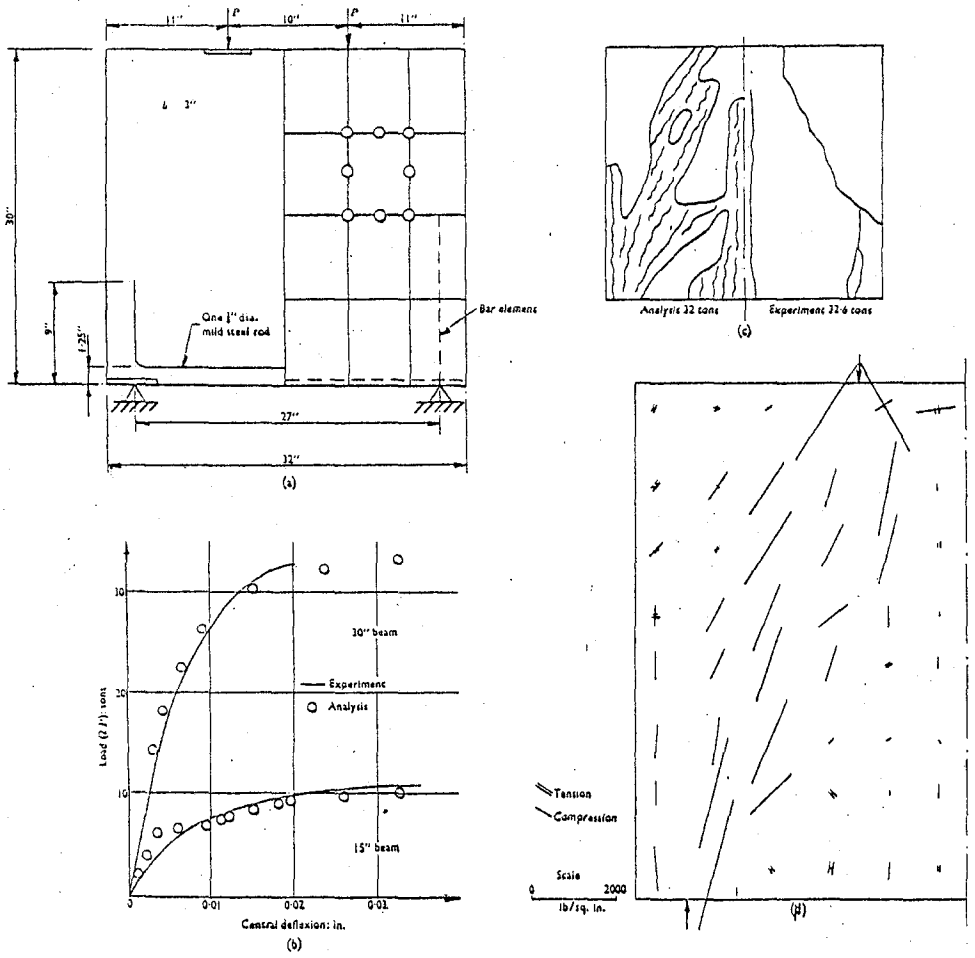

FIGURE 7 RESULTS OF ANALYSES OF DEEP BEAMS UNDER TWO POINT LOADING
(a) DETAILS AND MESH FOR 30in. BEAM
(b) LOAD-DISPLACEMENT CURVES
(c) CRACK PATTERNS NEAR FAILURE
(d) PRINCIPAL STRESSES IN 30in. BEAM AT 32 TONS
(Phillips + Zienkiewicz 1973 + 77
experiments by Remekrishnan + Anathanarayana 1968)

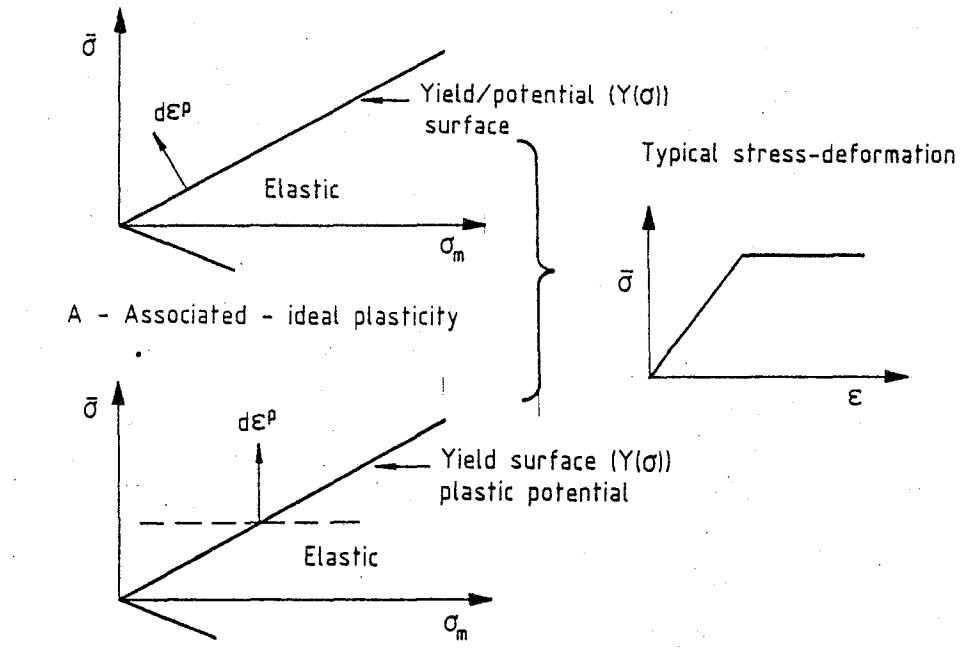

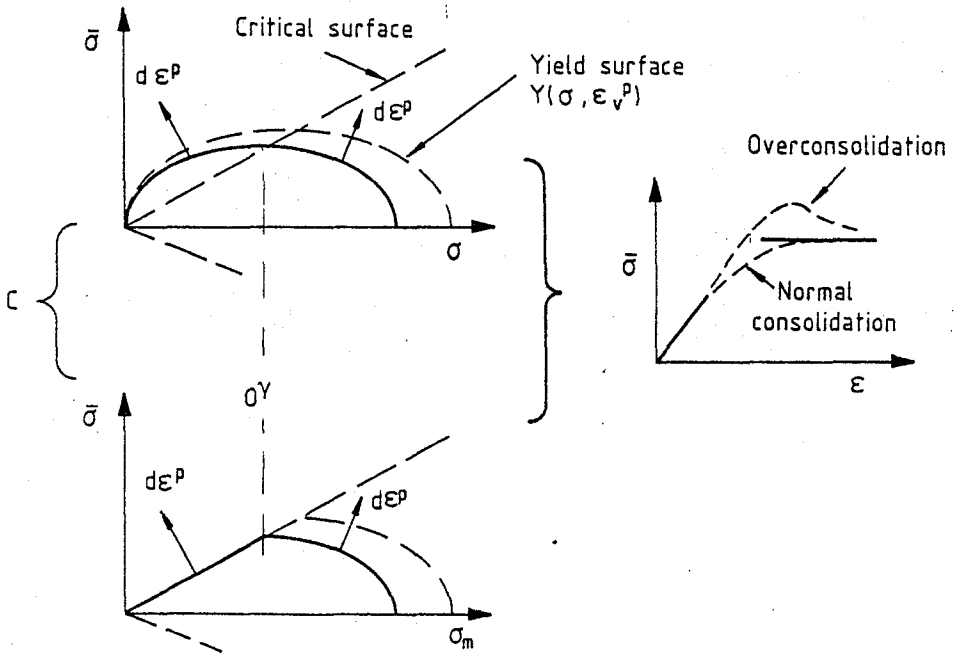

FIGURE 8 TYPICAL ELASTO-PLASTIC GEOMECHANIC MODELS IN DEVIATORIC σ/MEAN STRESS σ_m/SPACE (DEPENDENCE ON THIRD INVARIANT IMPLICATION)

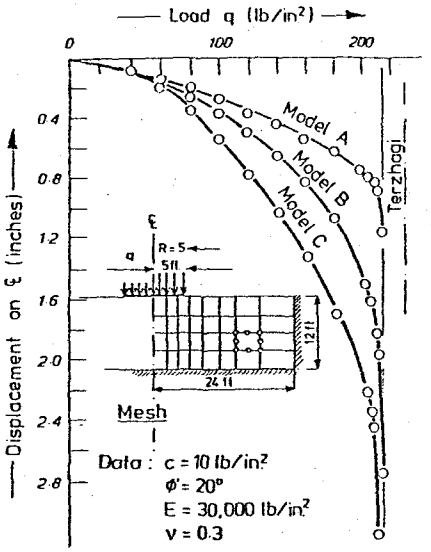

(a) AXI-SYMMETRIC FOOTING (UNIFORM LOAD) DRAINED LOAD-DEFORMATION BEHAVIOUR FOR THREE MATERIAL MODELS
(A) IDEAL ASSOCIATED PLASTICITY (MOHR COULOMB)
(B) IDEAL NON-ASSOCIATED PLASTICITY
(C) EXTENDED CRITICAL STATE

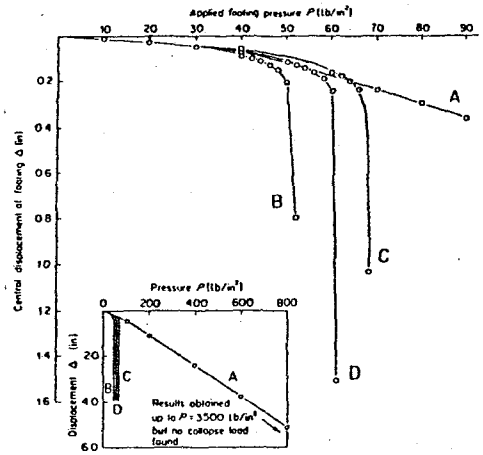

Elastic ideal plastic (Mohr-Coulomb) associative (dilatant) - Model A
Elastic ideal plastic (Mohr-Coulomb) non-associative (zero dilatancy) Model B
Elastic - strain depentent plastic Model C
Elastic - ideal plastic total stress analysis Model D

(b) LOAD DEFORMATION CHARACTERISTICS (UNDRAINED CONDITIONS) FOR PLANE FOOTING
NOTE : FOR LOCAL STRESS ANALYSIS WE USE σ_T CALCULATED BY EQUATION 4.25

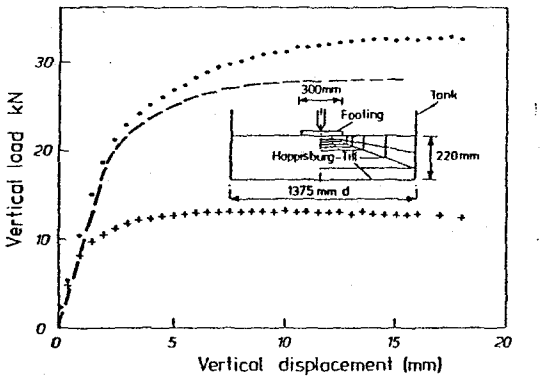

Experiment - Imperial College, M.C.R. Martins, 1977
Finite element - U.C. Swansea, L.A. Winnicki & D.J. Naylor, 1978 (Model C)
Critical state with Mohr-Coulomb cross section
Ideal Mohr-Coulomb plasticity non-associated (Model B)
E = 12000 kN/m², φ = 30°, ν = 0.3, H = 25

(c) A FOOTING ON OVERCONSOLIDATED CLAY (APPROXIMATE OVERCONSOLIDATION - 350kN/m² / 50kN/m²)

FIGURE 9 DRAINED/UNDRAINED BEHAVIOUR OF A FOOTING WITH NORMAL CONSOLIDATION AND WITH OVERCONSOLIDATED CONDITIONS

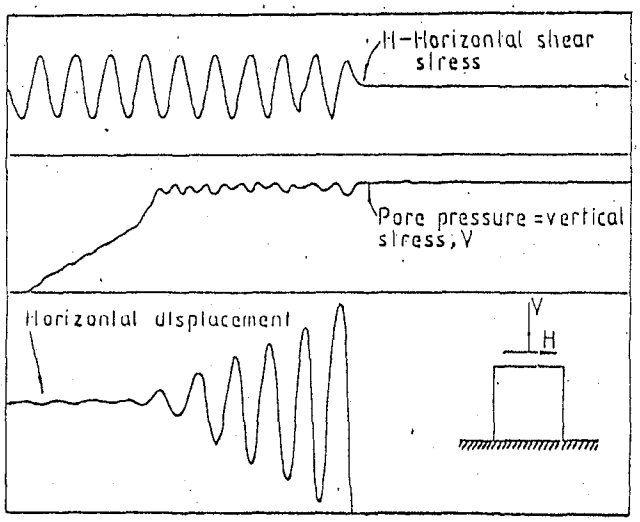

(a) Typical behaviour

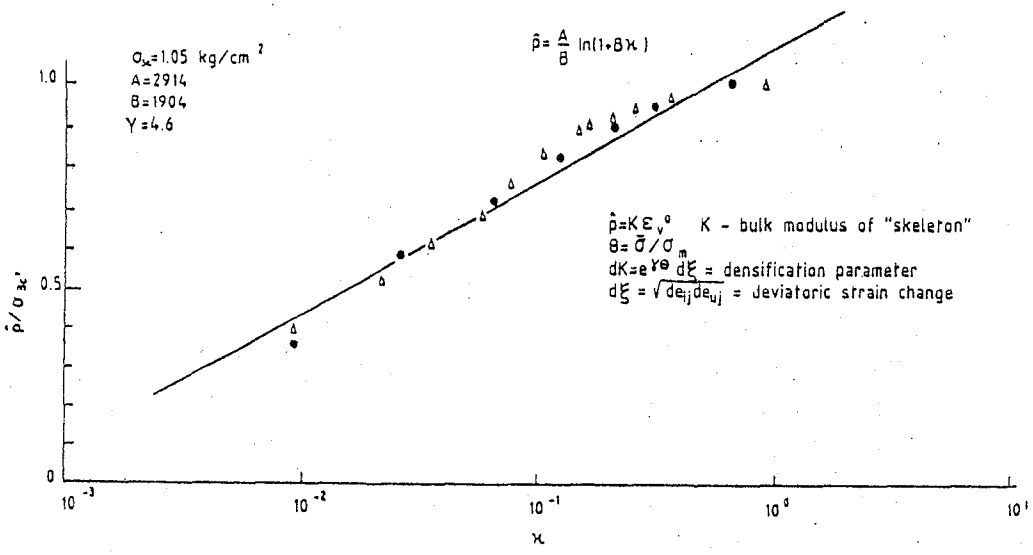

(b) Pressure changes or densification versus an endochronic parameter $\varkappa$
(Lower San Fernando Dam - Experimental data by Seed et al 1980)

FIGURE 10 DENSIFICATION OF SANDS UNDER CYCLIC LOADING

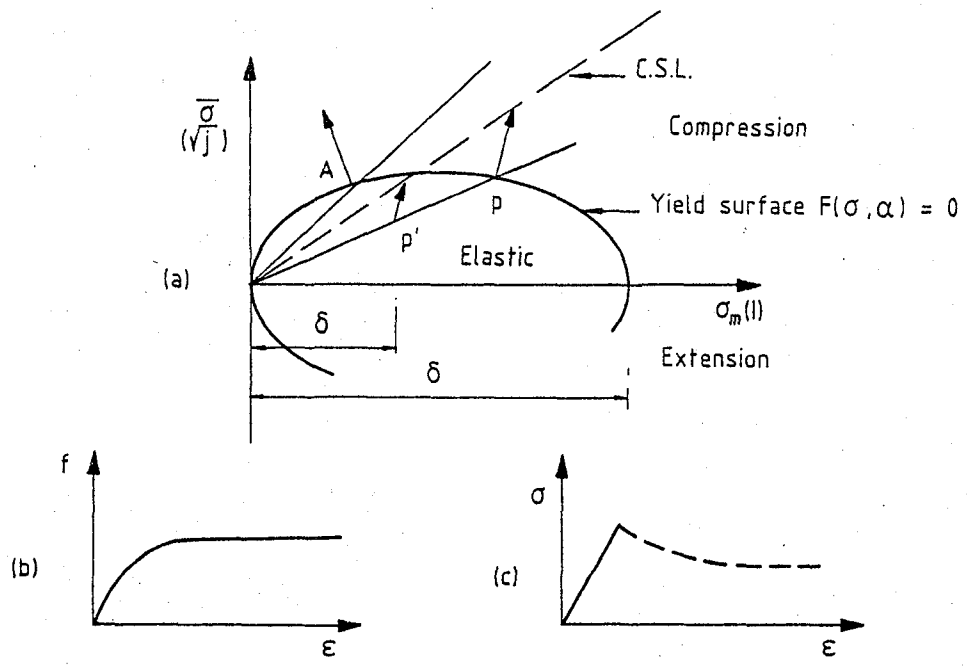

FIGURE 11 BOUNDING SURFACE PLASTICITY , CRITICAL SURFACE MODEL WITH VOLUMETRIC AND DEVIATORIC HARDENING (WILDE 1977)

$\alpha = \varepsilon_{vol}^{p} + f(\varepsilon^{-p})$

(a) Yield surface in stress space

(b) Deviatoric hardening function

(c) Stress-strain behaviour in drained loading

Plastic modulus interpolation

$K_{p'} = K_p(\frac{\delta_o}{\delta})^{\gamma}$: (γ = 1-10)

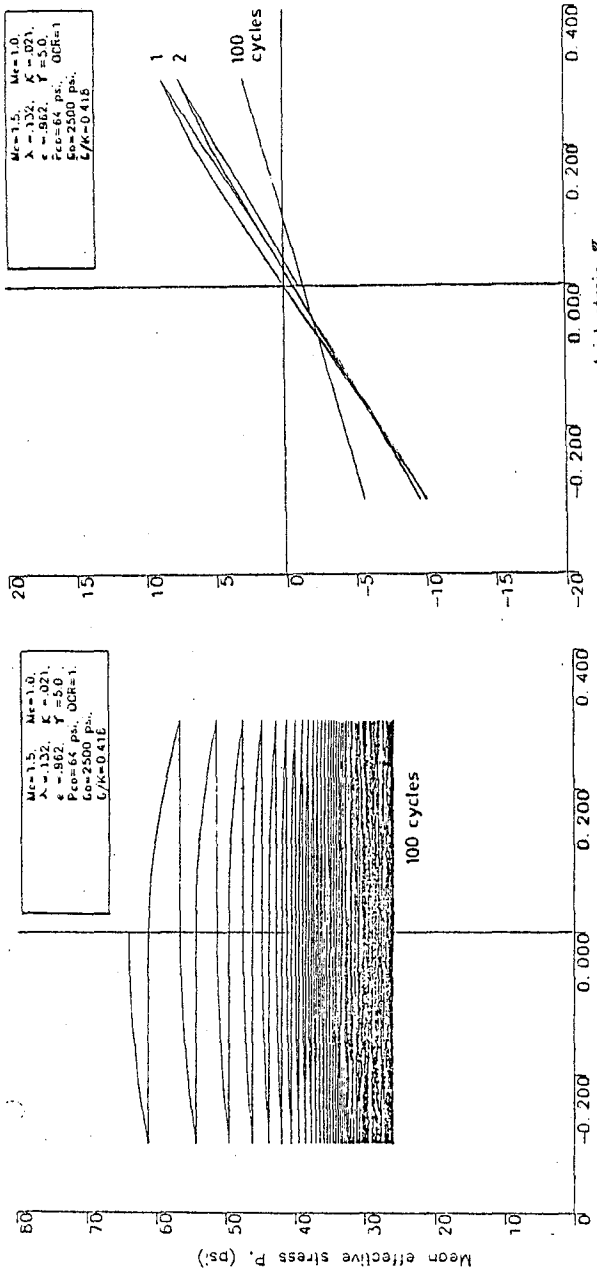

(a) Mean effective stress/axial strain (b) Axial stress/axial strain

FIGURE 12 PERFORMANCE OF BOUNDARY SURFACE MODEL UNDER CYCLIC STRAIN IN TRIAXIAL TEST
(Taylor & Bacchus 1969)
Amplitude of strain ±0.3%

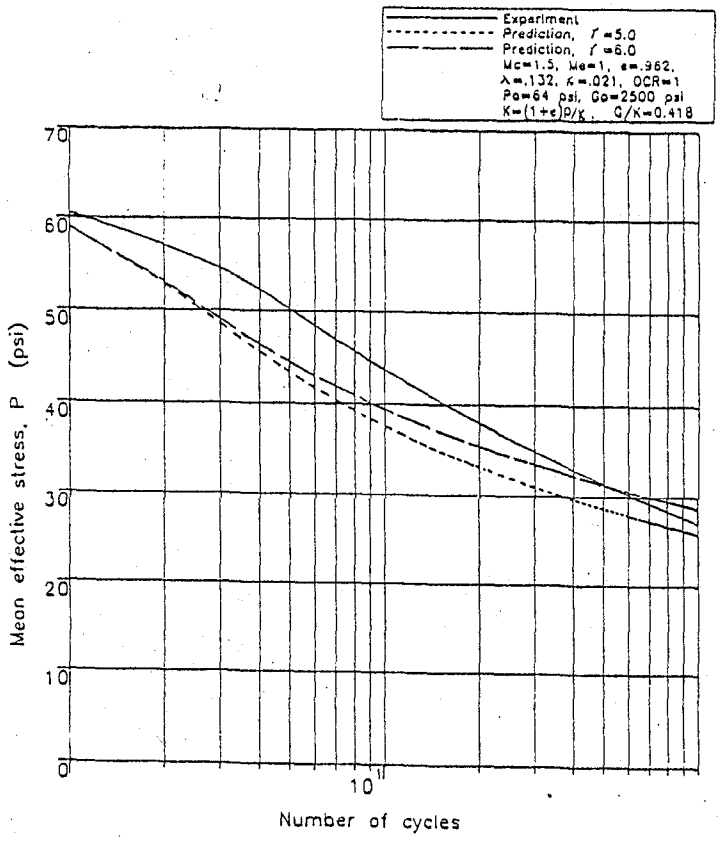

(c) Mean effective strain (pore pressure/cycles)

FIGURE 12(cont'd) PERFORMANCE OF BOUNDARY SURFACE MODEL UNDER CYCLIC STRAIN IN TRIAXIAL TEST
(Taylor & Becchus 1969)
Amplitude of strain ±0.3%

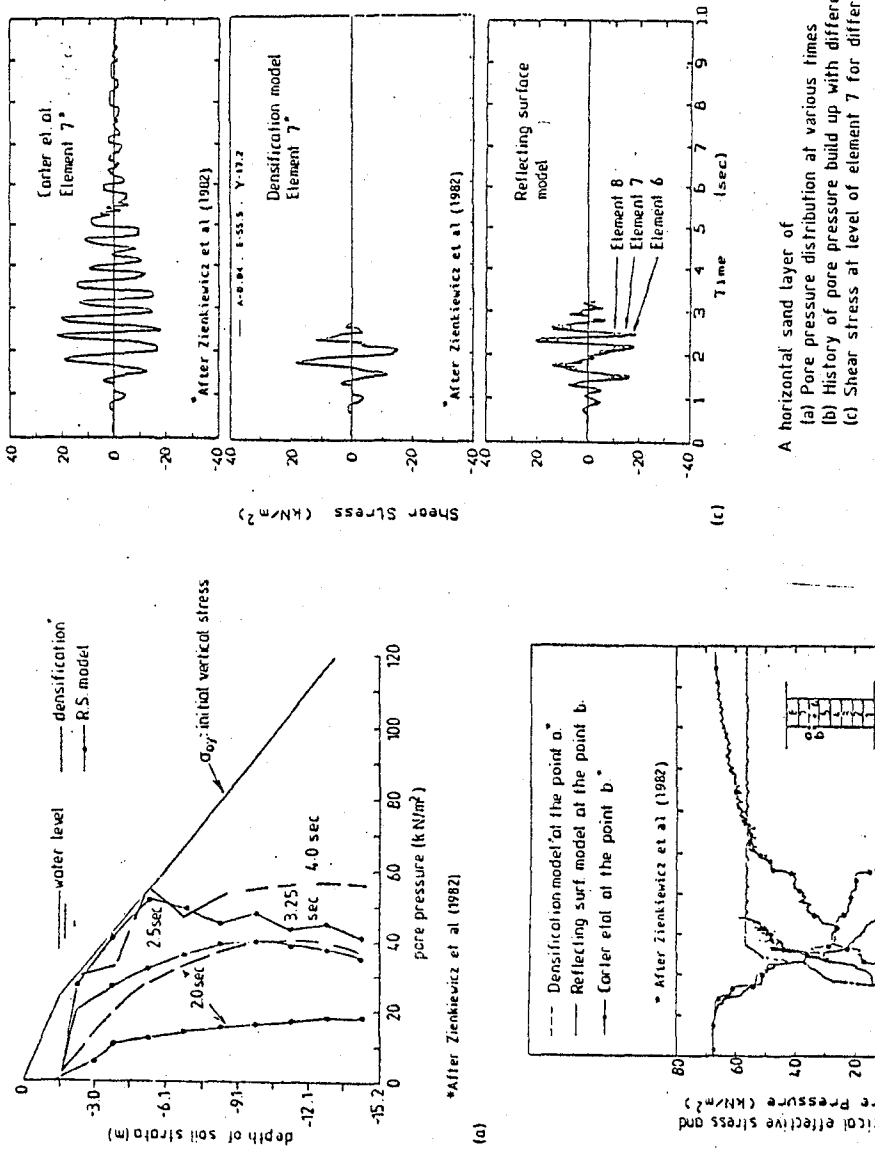

A horizontal sand layer of
(a) Pore pressure distribution at various times
(b) History of pore pressure build up with different soil models
(c) Shear stress at level of element 7 for different soil models

FIGURE 13 COMPARATIVE STUDY OF VARIOUS MODELS IN PREDICTION OF LIQUIFACTION

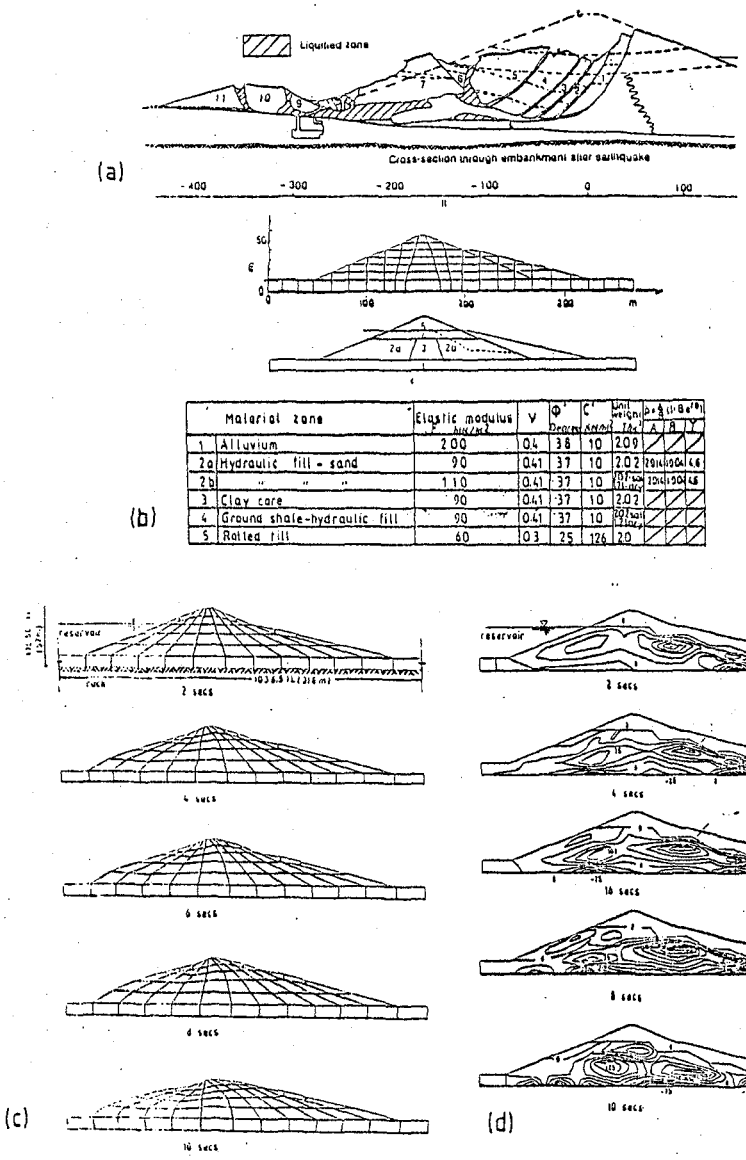

	Material zone	Elastic modulus	ν	Φ'	C'	Unit weight	Pore pressure coefficients A	B	$B\sigma_3'/\sigma_1'$
1	Alluvium	200	0.4	38	10	209			
2a	Hydraulic fill - sand	90	0.41	37	10	202	29	1.00	0.4
2b	" " "	110	0.41	37	10	202	29	1.00	0.4
3	Clay core	90	0.41	37	10	202			
4	Ground shale-hydraulic fill	90	0.41	37	10	202			
5	Rolled fill	60	0.3	25	126	20			

FIGURE 14 THE FAILURE OF LOWER SAN FERNANDO DAM . OBSERVATION AND ANALYSIS

(a) The failure (Seed et al)

(b) Finite element mesh & material properties

(c) Analysis results displacement x 5 (y node elements)

(d) Analysis of excess pore pressure build (Contour interval = 0.523kips/ft^2(25kN/m^2))

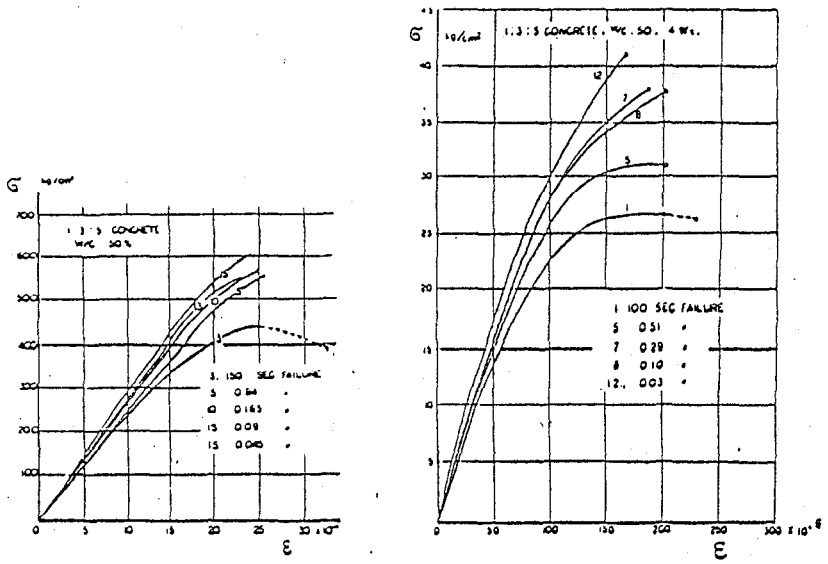

HATANO'S RESULTS FOR DIRECT COMPRESSION AND DIRECT TENSION TESTS ON 1 : 3 : 5 CONCRETE SPECIMENS (17,23)

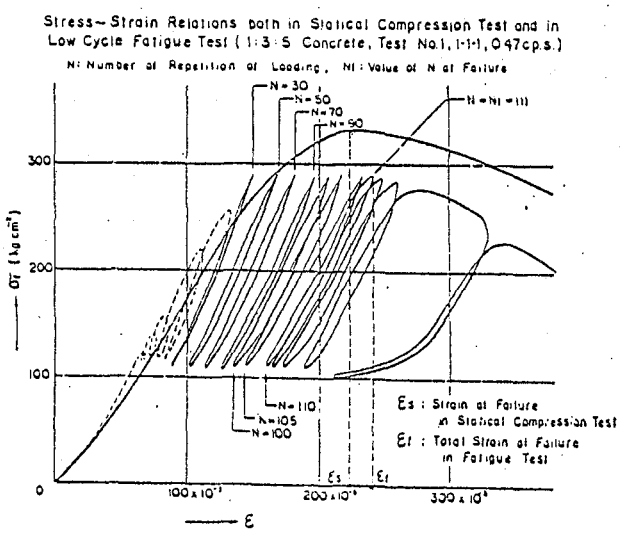

HATANO'S LOW CYCLE FATIGUE TEST IN COMPRESSION ON 1 : 3 : 5 CONCRETE SPECIMENS (27)

FIGURE 15

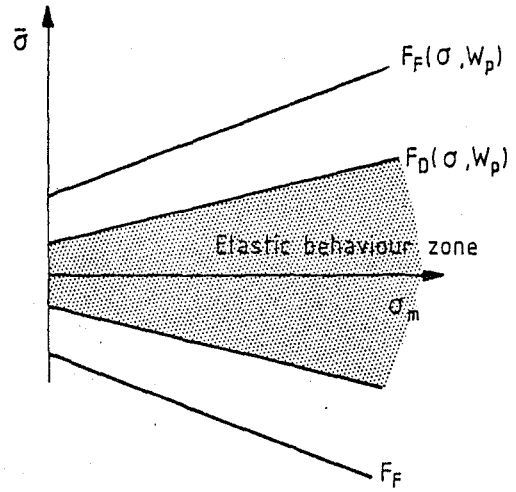

Visco-plastic model with F_D defining plastic yield at proportionality limit

$$\dot{\underline{\varepsilon}}^{vp} = \gamma \langle F - F_D \rangle \frac{\partial Q}{\partial \underline{\sigma}}$$

Q - Plastic potential

W_p - Plastic work $= \int_0^t \underline{\sigma} . \dot{\varepsilon}^{vp} \, dt$

$\gamma = \gamma(\dot{\sigma})$ $\quad F_F$ = failure monitoring surface = F

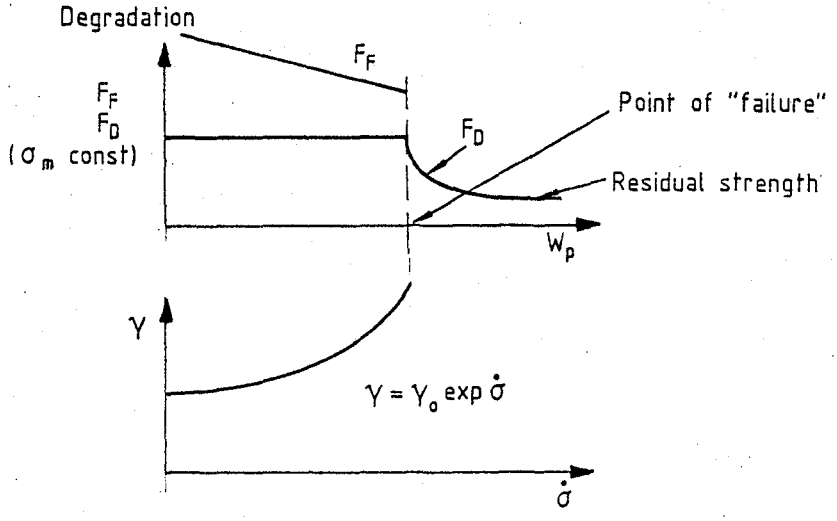

FIGURE 16 THE VISCO-PLASTIC-ELASTIC MODEL FOR RATE EFFECTS AND DEGRADATION OF CONCRETE (Bicanic et al 1980)

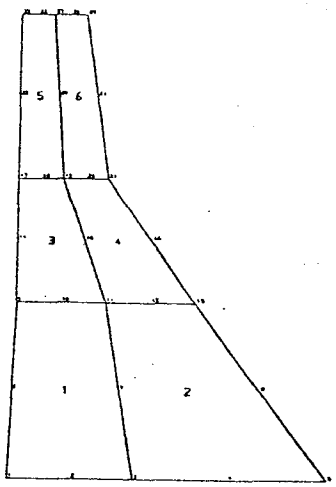

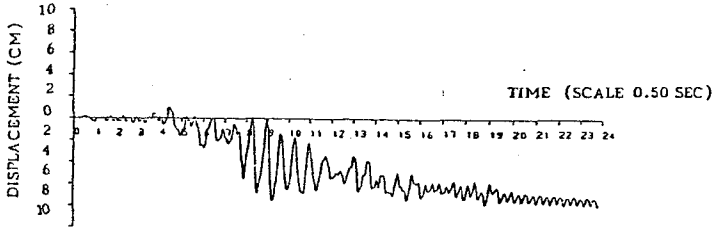

(a) Crest displacement history (horizontal direction) transversal and vertical component of Koyna earthquake

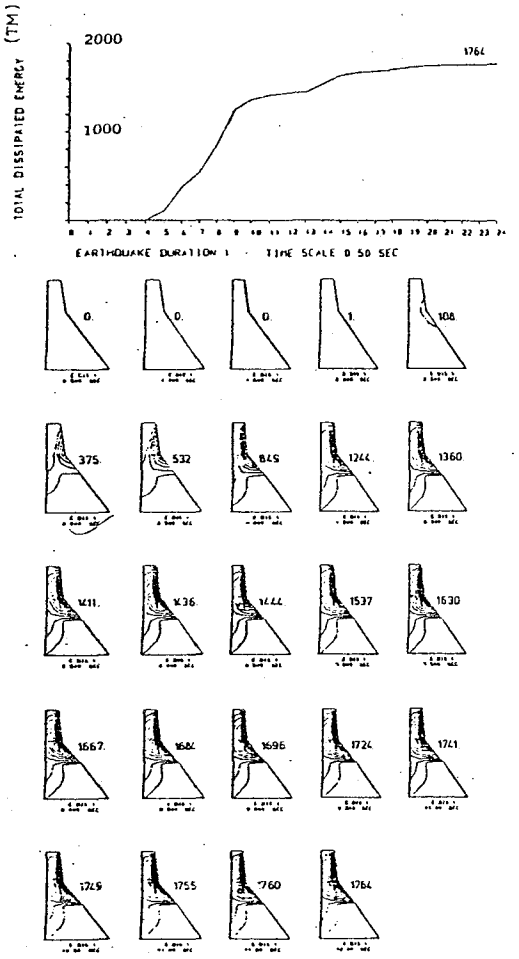

(b) Change of total dissipated energy during earthquake excitation

FIGURE 17 KOYNA DAM ANALYSIS

NUMERICAL MODELS FOR DYNAMIC LOADING

I. Sandler and M. Baron
Weidlinger Associates, New York, NY 10001

Introduction

The constitutive modeling of geological materials for applications involving dynamic loading has become a major area of interest in applied mechanics. The problem is complicated by the fact that the choice of model must depend on the application at hand: the appropriate model to be used depends on the type of material and the geometry of the problem as well as the loading rates, stress levels and periodicity or repetitiveness of the loading. In this paper some of the considerations which affect the choice of such models will be examined. The range of problems considered here is indicated by the following list:

Ground shock resulting from explosions
Soil-structure interaction under explosive loading
Ground shock under repeated loadings (multiple bursts)
Soil-structure interaction under earthquake loading.

For each of the above classes of problems, the level of sophistication in the mathematical modeling of the geological materials has risen considerably in the last two decades. The applicability of the models ranges from essentially hydrodynamic fluid behavior for the extremely high pressures (megabars) in the neighborhood of a burst point through inelastic solid material in regions at intermediate pressures to nearly linear behavior at sufficiently low pressure levels. Generally, no single model can be applied for all of the problems of interest.

Because real materials consist of variable amounts of mineral grains, air voids, and water, their mechanical behavior can exhibit wide variation and can be quite complicated. One must, however, consider carefully the scale and scope of the problems of interest since, for practical purposes, a number of essentially microscopic effects can be averaged in many cases. For large scale problems, which cover distance from tens to many thousands of feet, no practical attempt can be made to account for the interaction of the various individual constituents of materials, but averaged solid-material models which exhibit nonlinear behavior (with appropriate hysteretic effects in both pressure and shear) can be developed. Isotropy, homogeneity and rate dependence are usually assumed although experimental evidence generally indicates that the quantitative response of geological materials will be more complicated. The mathematical models are fitted, wherever possible, from experimental data corresponding to the applicable loading of the problem under consideration.

Parallel to the theoretical development of more realistic material

models have been the increasingly difficult demands on experimentalists for tests which would reproduce the behavior of the material throughout the entire range of pressures. These tests, which are an essential tool in model development, serve two major purposes: (1) to give an indication of the behavior at appropriate pressure ranges; and (2) to provide data for the evaluation of the various material constants which appear in the mathematical models. Generally static and "dynamic" laboratory tests on small samples are the major source of material property data. (Both of these tests usually are, in fact, "quasi-static" insofar as wave-propagation effects in the specimen are unimportant). Different tests are generally available for soil and rock materials. For those tests which are common to both materials, e.g., triaxial compression and proportional loading (occasionally available), different phenomena are of importance for soils than those for rocks. For example, a major effect in a soil is an irreversible volume decrease during compression (compaction), although this is generally not of major importance for rocks.

In addition to laboratory tests, there are sometimes large-scale field events which are adequately instrumented. Such tests may be viewed as material property tests, but they also serve as check results for both the modeling and the calculational procedures. The relation between the properties obtained from tests in small laboratory samples and the properties of the in situ material are also of considerable importance, but this is a question which can be appropriately answered only by carefully controlled and coordinated suites of large in situ and small scale experiments which are rarely, if ever, performed. Such questions are touched on later in this paper.

General Considerations

As noted in the introduction, a model developed for a particular class of problem may not be directly applicable to problems of an entirely different nature. For example, models developed for ground shock in which at most a few cycles of predominantly P-wave motion occur, have to be modified for use in seismic problems in which many cycles of shearing motion predominate.

It is desirable that a particular form of model be able to fit a wide class of geological materials. In this manner, the same form of model could be used for the different materials or layers found in a single problem, with only the various parameters changed. A special case of this occurs when setting certain parameters to special values (such as zero) reduces the more complex model to a simpler one.

The model should satisfy the theoretical requirements needed to prove existence, uniqueness and stability of solutions. This is necessary in order to be confident that any numerical solution is an approximation (in some sense) of the physical problem, and not nonsense that will vary widely with computer accuracy or choice of algorithm . Further, in any particular analysis dependence on unknown (or not readily available) variables must be avoided if calculations are to have any real value.

Numerous models are currently used for both explosively induced ground shock and seismic analysis. The simplest of these is the elastic model (most often linearly elastic) which also serves as the most common starting point from which other models are developed. Moreover, this simple model continues to be useful because most analytical solutions can be found only for linear problem formulations. In addition, elastic models

are often used to represent hard competent basement rock layers even when more complex models are used for the near surface materials.

Viscoelastic models are often used in seismic analysis. The hysteresis found in cyclic loading is approximated by linear viscoelasticity. The resulting linear problem may then be solved in the frequency domain. Nonlinear (strain dependent) hysteresis is approximated by an iterative scheme. During each of the successive iterations, the amount of damping in every element is adjusted to correspond to the strain amplitude found in the previous iteration for that element.

In addition, viscoelasticity can be combined with other types of models which are used to represent the plastic behavior exhibited by geological materials. These include variable moduli, cap and endochronic models, some of which will be considered in detail in subsequent sections of this paper.

Simple Plasticity Models

The early plasticity models were elastic-ideally plastic, i.e., there is a fixed yield condition

$$F(\sigma_{ij}) = 0 \tag{1}$$

which restricts the magnitude of the stress. If the material is isotropic, the yield condition can depend only on the principal stresses, or alternatively on the stress invariants

$$F(J_1, J_2, J_3) = 0 \tag{2}$$

Within the yield surface the material is elastic, i.e.

$$d\varepsilon_{ij}^{E} = \frac{1}{2G}\, ds_{ij} + \frac{1}{9K}\, \delta_{ij}\, dJ_1 \tag{3}$$

where $d\varepsilon_{ij}^{E}$ is the strain increment, ds_{ij} the increment in the stress deviator and δ_{ij} the Kronecker delta. The bulk and shear moduli are K and G, respectively.

Stresses outside the yield surface are not possible. On the yield surface, the strain increment will consist of elastic and plastic parts

$$d\varepsilon_{ij} = d\varepsilon_{ij}^{E} + d\varepsilon_{ij}^{P} \tag{4}$$

The elastic part $d\varepsilon_{ij}^{E}$ is given by Equation 3, while the plastic part is

$$d\varepsilon_{ij}^{P} = \lambda \frac{\partial \phi}{\partial \sigma_{ij}} \tag{5}$$

where λ is a non-negative scaler function, and ϕ is the plastic potential. When the plastic potential and the yield condition are the same,

$$\phi \equiv F \tag{6}$$

in which case Equation 5 becomes the associated flow rule

$$d\varepsilon_{ij}^{P} = \lambda \frac{\partial F}{\partial \sigma_{ij}} \tag{7}$$

and the plastic strain increment is normal to the yield surface at the current stress point. Furthermore, when F is convex, unique solutions are assured. When the non-associated flow rule (Equation 5 with $\phi \neq F$) is used, one cannot in general prove uniqueness. The simplest form of the yield condition is the von Mises condition

$$\sqrt{J_2'} = k \tag{8}$$

where J_2' is the second invariant of the stress deviator

$$\sqrt{J_2'} = \frac{1}{2} s_{ij} s_{ij} \tag{9}$$

and k is a constant. The von Mises condition is actually a good representation of the failure surface of many saturated clays. The von Mises yield surface is a cylinder in principal stress space, Fig. 1a.

A more realistic yield condition for granular material

$$J_2' = k + \alpha J_1 \tag{10}$$

was suggested by Drucker and Prager (1952). It is shown as the cone of Figure 1b, opening towards the positive (compressive) J_1 axis. When the

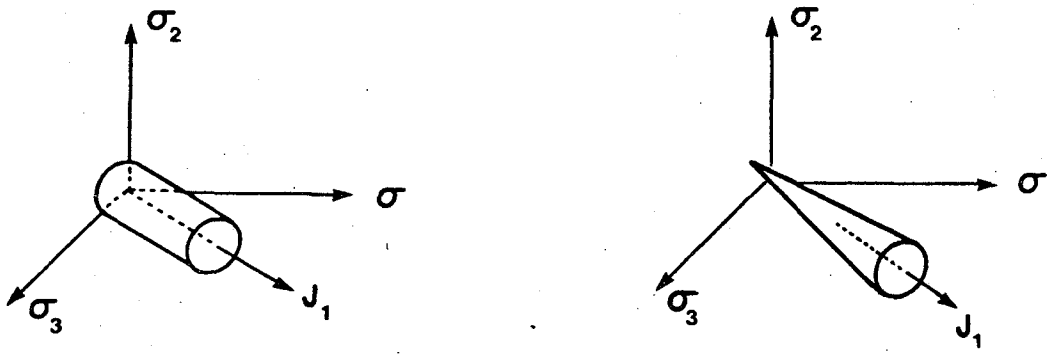

a) VON MISES (CYLINDER)

b) DRUCKER-PRAGER (CONE)

Figure 1 Simple Yield Surfaces

cohesion k is zero, Equation (10) reduces to the Mohr-Coulomb relation.

It is instructive to examine the behavior of the two simple models in uniaxial strain. This is illustrated in Figure 2 for constant elastic moduli. The stress strain curve starts with the elastic constrained modulus $K + \frac{4}{3} G$ as its slope. The stress path s_1 versus p likewise starts with its elastic slope $\frac{4G}{3K}$. At point A the yield surface is reached, and in the von Mises case (Figure 2b), the axial stress deviator cannot increase further, beyond the limiting value $\frac{2}{3} k$. Any further loading to say point B, can result only in an increase in the mean stress $p = \frac{1}{3} J$. The corresponding segment AB of the stress strain curve, Figure 2a, is parallel to the hydrostat, i.e. it has a slope K. Upon unloading at B, the stress point moves away from the yield surface, and the material behaves incrementally elastically, i.e. the lines BC and OA are parallel in both Figures 2a and 2b. At point C, the reverse side of the yield condition is reached, and s_1 is again limited, this time to $-\frac{2}{3} k$. Thus, any further unloading will be along the yield surface and the slope in the stress strain plot again will be K. The cycle is complete at point D at which $\sigma_1 = s_1 + p = 0$.

In the case of the Drucker-Prager yield condition, Figures 2c and 2d, the behavior is similar until yield is first reached at point A. As loading continues to point B, the value of s_1 increases according to the yield condition

$$s_1 = \frac{2}{3} (k + 3\alpha p) \tag{11}$$

If this value of s_1 were added to hydrostat, the slope of the resulting stress strain curve would be

$$M_{CWD} = K(1 \pm 2\sqrt{3}\,\alpha) \tag{12}$$

(with the upper sign). Equation (12) is represented by line AB_{cwd} in Figure 2c. This is not the solution for the Drucker-Prager material, which is shown as the solid line slope

$$M_{DP} = K \frac{(1 \pm 2\sqrt{3}\,\alpha)^2}{1 + 9\alpha^2\, K/G} \tag{13}$$

(again with the upper sign). The difference is explained in Figure 2d. With the associated flow rule, Equation (7), the plastic strain rate vector along AB, $\dot{\varepsilon}_A^P$, has a negative (tensile) volumetric component. Therefore, a greater stress is required (Figure 2c) to reach the same strain as compared to the case of a non-associated flow rule (one without any plastic volume change). The CWD subscript used in Equation (12) and Figure 2 refers to "Coulomb without dilatacy" and results when a von Mises plastic potential is used in conjuction with the Drucker-Prager yield condition.

Unloading from point B is again elastic with slope of $K + \frac{4}{3} G$ and $\frac{4G}{3K}$

in Figures 2c and 2d, respectively. At point C the far side of the yield condition is again reached. The stress point moves along the yield surface until $\sigma_1 = 0$ at point D in Figure 2d. In the case of the CWD material, the

VON MISES

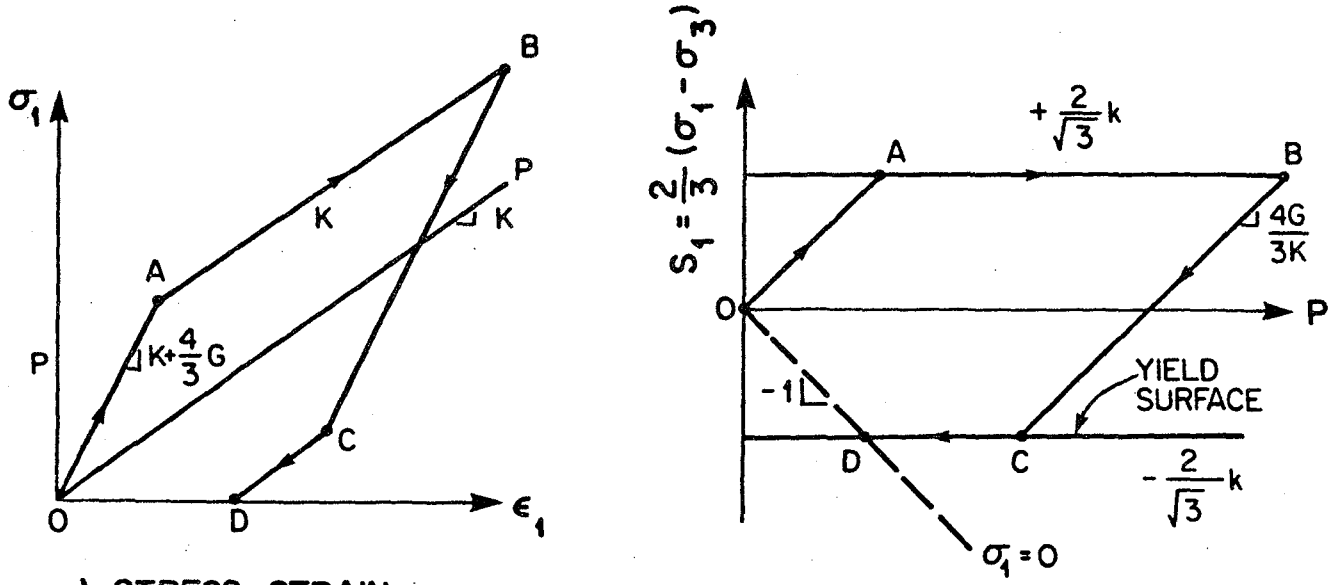

a) STRESS-STRAIN

b) STRESS PATH

DRUCKER-PRAGER

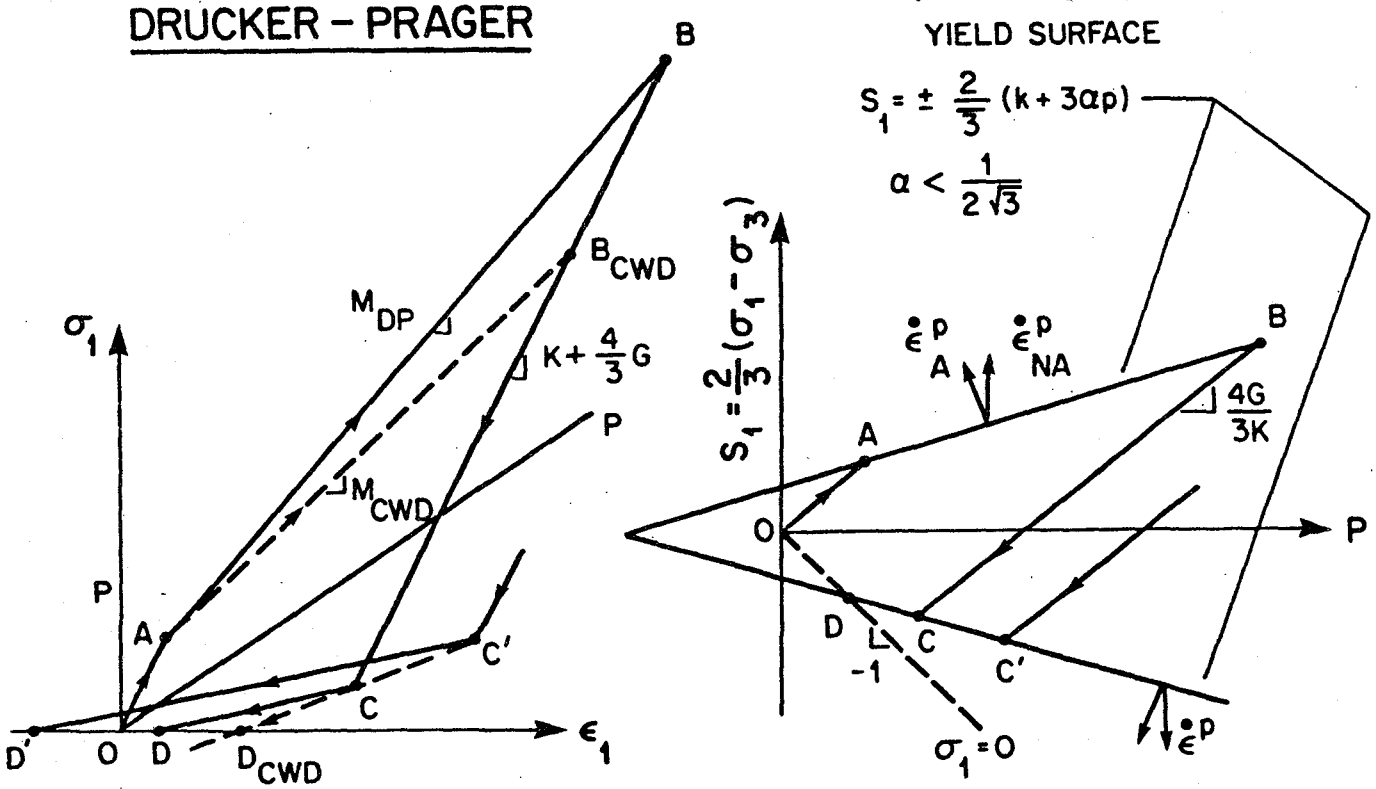

c) STRESS-STRAIN

d) STRESS PATH

Figure 2 Uniaxial Strain Behavior of simple elastic ideally plastic models

negative value of s_1 is added to the hydrostat and the resultant slope of segment CD_{CWD} in the stress strain curve is given by Equation (12) with the lower sign. In the case of the associated flow rule, there is again a volume expansion component to the plastic strain rate vector, and the resulting modulus from Equation (13), with the lower sign, is necessarily softer than that of the CWD material. While unloading from point B has resulted in a permanent compaction of the material at $\sigma_1 = 0$ (point D), unloading from some higher stress would have reached the far side of the yield surface at C', and resulted in net volume expansion, (dilatancy) at the end of the cycle at D'. This dilatancy is not observed in experiments and was the primary motivation which led to the development of more advanced EIP models. Nevertheless, to relatively low stress levels such as to those drawn in Figure 2c, the Drucker-Prager model stress strain leads to a uniaxial strain response which has many of the qualitive features observed experimentally. The model continues to be frequently used to represent "frictional" materials.

4. More Detailed Plasticity Models

In order to represent soil behavior, in which permanent compaction is usually a dominant characteristic, the simple plasticity model was expanded to include a non-linear pressure-volume relationship involving two different bulk moduli, one for initial loading, and a second for unloading/reloading. Mathematically,

$$dp = K\, d\varepsilon_{kk} \tag{14}$$

where $$K = K_L(p) \text{ for initial loading} \tag{15a}$$

and $$K = K_U(p) \text{ for unloading/reloading} \tag{15b}$$

Requiring $$K_U(p) \geq K_L(p) \tag{16}$$

insures volumetric hysteresis even in infinitesimal initial loading - unloading cycles. Another modification was the generalization of the yield condition to

$$J_2' = f(J_1) \tag{17}$$

which is sketched in Figure 3. The function $f(J_1)$ is chosen such that it is approximated by the Drucker-Prager condition, Equation (10), at low pressures, and by the von Mises condition, Equation (8), at high pressures.

The final modification involves the treatment of the deviatoric stresses within the yield surface. The incremental relation

$$ds_{ij} = 2G\, de_{ij} \tag{18}$$

is used with a variety of specifications of the shear modulus. The simplest assumption is to consider the shear modulus G to be constant. While this model (with an associated flow rule) satisfies all theoretical

requirements, the computed stress path in uniaxial strain is unrealistic when $K_U >> K_L$. If K_L increases with increasing pressure, the stress path is shown by the dashed line in Figure 4. The path would gradually approach, and finally reach, the upper yield surface. On unloading, at least in the case of soils where the unloading bulk modulus is appreciably larger than the initial loading modulus, the unloading path would not generally intersect the lower yield surface. In fact, for moderate peak pressures (and when $K_U >> K_L$), the unloading stress path would cross the loading path and intersect the upper yield surface. This behavior is not experimentally observed in most cases where stress path data is available.

An alternative simple assumption which has been used is that of a constant ratio of K/G or a constant Poisson's ratio ν. For this case, the stress path is shown by the solid line in Figure 4. It starts with a upper branch of the yield surface until a load reversal occurs. When unloading begins, the subsequent stress path is parallel to the initial loading path until the lower yield surface is encountered. The segment along the lower yield surface, until the line $s_1 + p = \sigma_1 = 0$ is reached, is associated with the tail at the bottom of the unloading segment of the stress strain curve. A variant of this approach but one which matches the data even more closely, is the use of two distinct values of Poisson's ratio, ν_L and ν_U. The choice could depend whether K_L or K_U were being

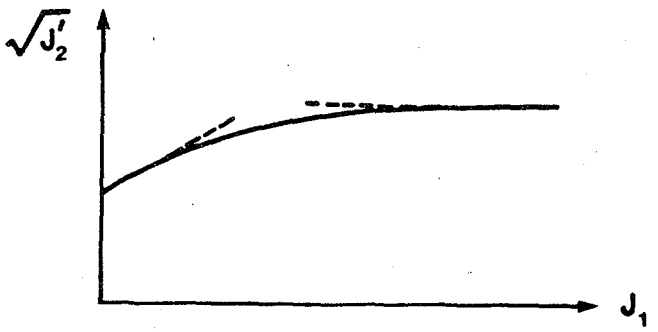

Figure 3 Yield Condition for the Advanced Elastic-Ideally Plastic Model

used, or on the sign of the incremental deviatoric work, $s_{ij}\, de_{ij}$. The corresponding stress path is illustrated as a broken dotted line in Figure 4. In either case, the stress paths agree, at least qualitatively, with experimental observations. The difference between the two simple assumptions of constant G or constant ν in loading is not of real importance. This is not true in unloading.

Unfortunately, it is possible to introduce stress paths for which a constant Poisson's ratio model (with K_U increasing with pressure) will produce energy for each load - unload cycle. The same criticism may be applied to other models which have been used in which ν was piecewise constant or in which G was a more general function of pressure.

Different constant values of G in loading and unloading have also been used. Models of this type are not subject to the above criticism. However, they fail to satisfy a continuity condition which will be discussed in conjunction with the variable modulus model in the next section.

In addition to the constant G model, another possibility which also satifies theoretical requirements and moreover, leads to stress paths which are closer to those observed experimentally, is the use of a shear modulus G which depends only upon maximum previous pressure. During initial loading, the shear modulus increases as the pressure increases. On unloading or reloading to the maximum previous pressure p_{max}, the value of $G(p_{max})$ remains constant. The uniaxial strain stress path for for such a model is shown in Figure 4 for the case when K_U increases with increasing pressure (dash-dot curve).

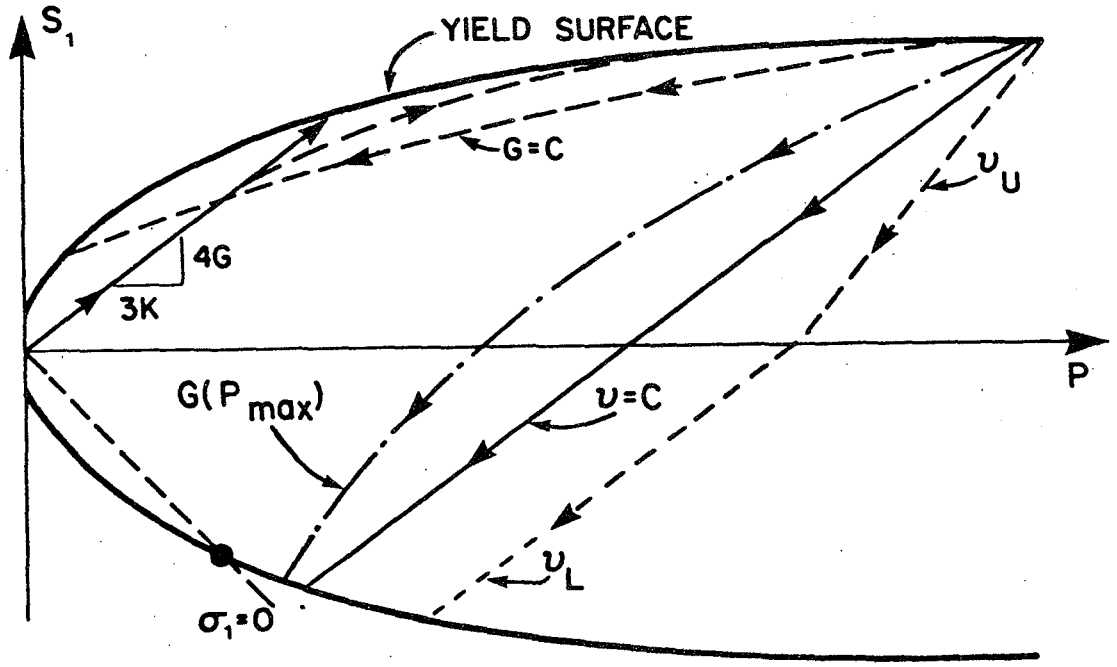

Figure 4 Loading paths for Elastic Ideally Plastic Models.

The models described above have been used extensively for ground shock in both soil and rock. In rock, the pressure-volume hysteresis is much smaller than in soils, and in competent rocks, it is often neglected entirely, i.e. a single bulk modulus is used. The use of an associated flow rule in conjunction with a pressure dependent yield condition produces dilatancy, which is generally observed in most rocks. Therefore the Drucker-Prager model is a better approximation to rock than to soil behavior at low stresses.

It is of interest to consider the triaxial behavior of advanced elastic - ideally plastic material models of the general type discussed

in this section. This is shown in Figure 5, which represents the results in the form of a $(\sigma_1 - \sigma_3)$ versus ε_1 diagram. Because of the variable bulk modulus $K_L(p)$, the initial loading curve first softens and then hardens. As the yield surface is reached (at different levels for different values of the lateral stress σ_3), the material "fails" and "flows" as represented by horizontal lines shown parallel to the strain axis. It is clear that none of the simple treatments of the shear modulus described previously can mirror the usual stress strain curves in a triaxial compression test; these are the dashed lines in Figure 5.

In order to overcome this defect and to match laboratory data from all available tests, the "variable moduli" models were introduced, Nelson and Baron (1971). In these models both the bulk and shear moduli are taken as non-linear functions of the stress and/or strain tensor invariants. Different functions are used in in loading and unloading. The variable moduli material has no unique stress strain relation, even in initial loading, but rather is defined in terms of stress rate-strain rate (incremental) relations, Equations (14) and (18). No explicit yield condition is specified. However, the behavior of the variable moduli models corresponds in many respects to that of elastic - plastic models.

The pressure volumetric strain relation is similar to that used in the advanced EIP models. Namely, one bulk modulus function of pressure (or volumetric strain) is used in initial loading ($\dot{p} > 0$ and $p = p_{max}$), and another is used in unloading ($\dot{p} < 0$) or reloading ($\dot{p} > 0$, but $p < p_{max}$). There are also different shear moduli used in deviatoric (initial) loading and unloading, i.e.

$$G = G_{LD}(p, J_2') \qquad \dot{J}_2' > 0 \qquad (19)$$

$$G = G_{UN}(p, J_2') \qquad \dot{J}_2' \geq 0 \qquad (20)$$

The condition

$$0 < G_{LD}(p, J_2') \leq G_{UN}(p, J_2') \qquad (21)$$

insures deviatoric energy dissipation in any incremental load - unload cycle.

Although there is no explicit yield surface, at any constant pressure, the (initial) loading shear moduli functions get smaller as J_2' increases. The limiting condition

$$G_{LD}(p, J_2') = 0 \qquad (22)$$

corresponds to an implicit yield condition.

Such a model was fit to a rather complete set of laboratory data for a particular soil material and good agreement for uniaxial strain triaxial compression and proportional loading tests was obtained. Moreover, it would appear that the variable moduli approach would be ideal for implicit finite element codes in which the current values of K and G in every element

would be available to construct the stiffness matrix.

The major problem with the variable moduli formulation, is qualitatively illustrated in Figure 6, where the point A lies on a surface J_2' = Constant. Consider two paths, AB and AB', arbitrarily close to each other, but on opposite sides of the surface. On the outer path AB, the shear modulus G_{LD} would apply, while on AB', G_{UN} would be used. Consequently, there will be a definite difference in strain, even when the points B and B' are infinitesimally close to one anotner.

The violation of continuity in neutral loading (J_2' = Constant) or near neutral loading is similar to that discussed by Handelman, Lin and Prager (1947), in their studies on deformation theories of plasticity. In fact, deformation theory may be considered a special case in which the rate equations of the variable moduli formulation are integrable.

In the case of proportional loading in shear, i.e., when there is a single independent stress deviator, the variable moduli approach (can be made to satisfy all theoretical requirements, including continuity. This is true for planar, or spherically symmetric problems, as well as for all of the common laboratory tests. In other problems, in which the stress history is close to proportional loading, the present theory, like deformation theory, is probably satisfactory. For problems in which the stress history involves an appreciable amount of neutral (or near neutral) loading, use of the variable moduli formulation is not recommended.

Theoretical Considerations

Continuum models intended for use in dynamic multidimensional problems should satisfy certain theoretical requirements. These requirements insure that the initial and boundary value problems involving the constitutive model, together with the equations of continuum mechanics (e.g., conservation of mass, momentum, energy), be properly posed, i.e., that such problems have solutions which exist, are unique, and depend continuously on the initial and boundary conditions. These seemingly abstract requirements are of considerable practical importance this age of numerical solutions. In particular, one should avoid attempting computer solutions for problems without solutions and, in addition, avoid problems with several solutions for fear that a non-physical, through mathematically correct, solution would be obtained. Further, because all numerical solutions are subject to several kinds of error (due to truncation or round-off, the order of accuracy associated with the chosen numerical scheme, and errors in specification of initial and boundary conditions), any solution which is unduly dependent on such errors, is highly suspect. Therefore, the continuous dependence of solutions on the input data is directly related to the confidence with which numerical solutions can be obtained for real problems.

(Continuous dependence on the data implies that a small change in the surface loading will lead to a correspondingly small change in the solution. A simple example of a discontinuous material is an elastic string with tensile strength σ_T. For loads $P < \sigma_T A$, the uniform stress will be $\sigma = P/A$ and the corresponding strain $\varepsilon = P/EA$. For loads just greater than $\sigma_T A$, the string will break and the "solution" will be entirely

different. The soil and rock models discussed up to this point have avoided any mention of the tensile stress region. Clearly natural materials, especially rocks, to fail suddenly. Yet, to allow the nature of a numerical solution to depend entirely on such artifical parameters as mesh box size, time step, or numerical algorithm is completely unsatisfactory)

The continuity problem discussed in connection with the variable moduli model constitutes a lack of continuous dependence on the input data. Slightly different input, or slightly different numerical techniques, could result in a significantly different computed results.

A major contribution to the continuum models was the introduction of Drucker's stability postulate, Drucker (1956). Non-negative work must be done by an external agent in any excursion from equilibrium. In particular, for any stress cycle, where σ_{ij}^{o} is the stress at the equilibrium state,

$$\int (\sigma_{ij} - \sigma_{ij}^{o})\, d\varepsilon_{ij} \geq 0 \tag{23}$$

The equal sign applies only for elastic or reversible paths. Satisfying Drucker's postulate is sufficient (but not necessary) to insure unique solutions, and continuous dependence on the data.

A geometric interpretation of Drucker's postulate is shown in Figure 7. By eliminating the elastic or reversible strains and by choosing σ_{ij}^{o} on the yield surface, one obtains the condition for stability in the "small" for elastic-plastic models, i.e.

$$d\sigma_{ij} d\varepsilon_{ij}^{P} \geq 0 \tag{24}$$

A consequence of Equation (24) is that the yield condition can only move outward (or not move) at a stress point, i.e., work softening or strain softening is not permitted. One may also obtain the condition for stability in the "large" for elastic-plastic materials, i.e.

$$(\sigma_{ij} - \sigma_{ij}^{o})\, d\varepsilon_{ij}^{P} \geq 0 \tag{25}$$

Equation (25) requires the normality of the plastic strain rate vector, and the convexity of the yield condition.

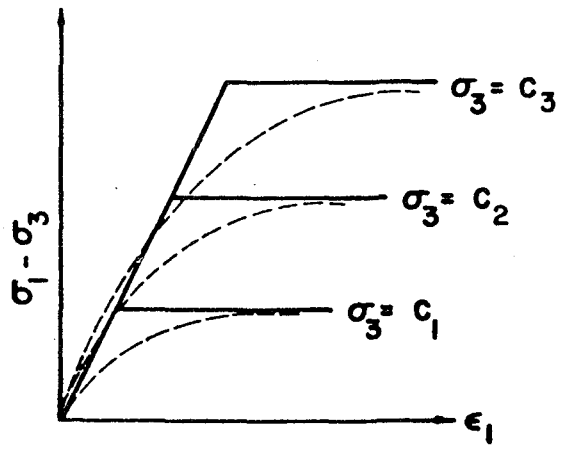

Figure 5 Triaxial Behavior of Elastic Ideally Plastic Models Compared to Real Soils

Cap Models

In order to satisfy uniqueness continuity and stability requirements, the cap model was developed. It is a continuum material model which is based on the classical incremental theory of plasticity. It has been used to represent both the high and low pressure mechanical behavior of a number of geological materials, including sands, clays and various types of rock. The model has been used primarily for computational studies of ground shock and structure medium interaction effect arising from nuclear or chemical explosions. In addition, it can be used for the study of earthquake effects; some work has already been done to apply the model to seismic problems.

The discrepancy between the observed compaction of soils and the dilatancy resulting from normality to any yield surface similar to that of Drucker-Prager, disturbed investigators for many years. Drucker, Gibson and Henkel (1957) first added a movable cap to the yield surface to eliminate this discrepancy. In the 1960's Roscoe and his coworkers at Cambridge University in England introduced the critical state model, Schofield and Wroth (1968). It had many similarities to the earlier model and to the current cap model. Finally, a group at MIT also worked on a similar model, e.g., Christian (1966).

A cap model was proposed by Dimaggio and Sandler (1971) for the representation of granular soils, and similar models have been used for many ground shock calculations. The yield surface Figure 8 is composed of a fixed failure envelope, Equation (17) and a movable cap which crosses the p axis. The combined yield surface is everywhere convex, and the associated flow rule is used throughout,i.e., the components of the plastic strain rate form a vector in stress space which is normal to the yield surface at the stress point and is outwardly directed, as shown in Figure 8. Three different modes of behavior are possible for the model: elastic, failure and cap. Elastic behavior occurs when the stress is within the failure envelope and stress changes result in recoverable deformations. Although various types of nonlinearly elastic behavior can be modeled in complex cases, the model considered here (for isotropic materials)uses a constant bulk modulus, K, and a constant shear modulus, G. During the postualated elastic behavior the volumetric and deviatoric components of stress and strain are decoupled, i.e., a purely volumetric change in strain does not affect the deviatoric stress components and a purely deviatoric strain increment produces no change in pressure.

During the failure mode of behavior, the stress point lies on the failure envelope, represented by

$$\sqrt{J_2'} = A - C \exp(3B_p) \tag{26}$$

where A, b and C are material constants. As shown in Figure 8 the associated flow rule requires that the plastic strain rate vector be directed upward to the left. Therefore, the plastic strain during failure is composed of a deviatoric or shear, component together with a volumetric, or dilatant component.

The cap mode of behavior occurs when the stress point lies on the movable cap and pushes it outward. The motion of the cap is related

to the plastic strain by means of a hardening rule. Although considerable leeway exists in the choice of the cap, an ellipical surface of the form

$$(p - p_A)^2 + \frac{1}{9} R^2 J_2' = (p_B - p_A)^2 \qquad (27)$$

is found acceptable for a wide range of geologic materials. In equation (27), p_A and p_B represent the values of p at points A and B in Figure 8, while R can be function of the position of the cap. In the simple eight parameter version of the model discused here, R is assumed to be constant.

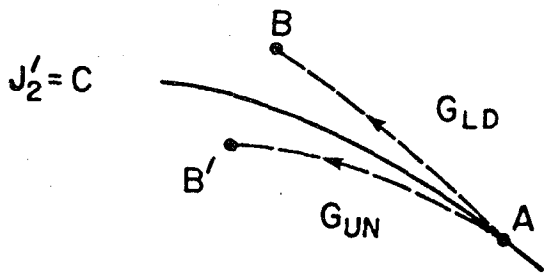

Figure 6 Example of Discontinuous Behavior in Variable Moduli Model

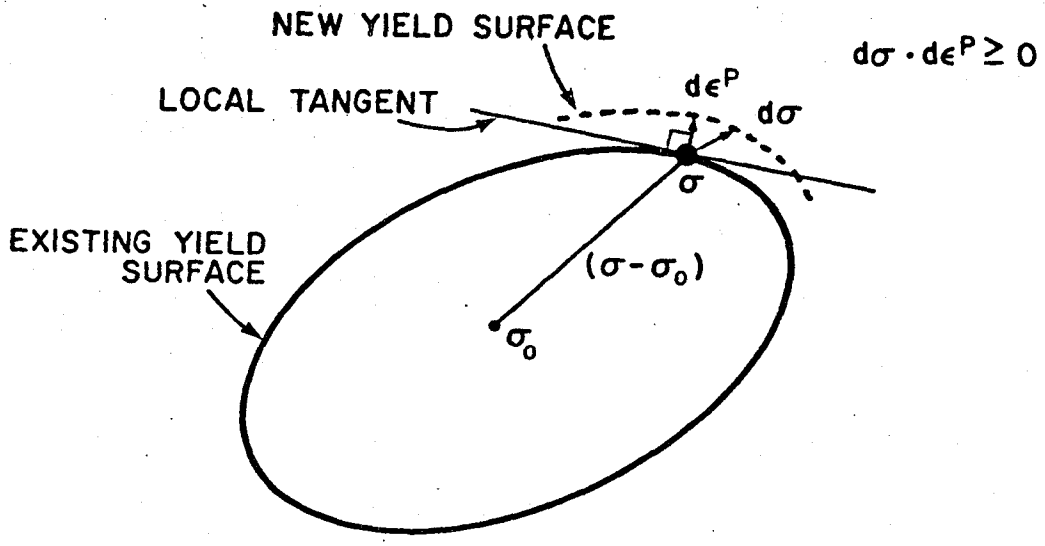

Figure 7 Geometric Interpetation of Druckers Stability Postulate

The pressures p_A and p_B which define the extent of the cap are not independent. From Figure 8, it is clear that, because point E lies on both the failure envelope and the cap,

$$\sqrt{J_{2\,E}'} = A - C \exp(-3Bp_E) \tag{28}$$

and

$$(p_E - p_A)^2 + \frac{1}{9} R^2 J_{2\,E}' = (p_B - p_A)^2 \tag{29}$$

Further, since $p_E = p_A$, Equations (28) and (29) lead to

$$p_B - p_A = \frac{1}{3} R[A - C \exp(-3Bp_A)] \tag{30}$$

for the relation between p_A and p_B. Therefore, the specification of either p_A or p_B is sufficient to describe the position of the cap.

The cap position is related to the plastic strain history of the material through a hardening rule, which, again, can be chosen with considerable leeway. For the eight parameter model discussed here, the hardening rule is assumed to be

$$\bar{\varepsilon}_v^p = W[1 - \exp(-3Dp_B)] \tag{31}$$

in which W and D are material constants and $\bar{\varepsilon}_v^p$ is related to the plastic strain history. The hardening parameter, $\bar{\varepsilon}_v^p$ depends upon the history of the dilant as well as compactive plastic strain for soils, while for rocks it depends only on the plastic strain which has been produced by cap action i.e., compaction.

As shown in Figure 8, the associated flow rule requires that during cap action the plastic strain rate vector be directed upward and to the right. This implies that the plastic strain rate produces an irreversible decrease in volume in conjunction with the irreversible shear strain. This reduction in volume is referred to as compaction and represents the volumetric hysteresis observed during compression of most geologic materials.

As the cap action proceeds, the compaction resulting from the associated flow rule leads to an increase in the cap parameter $\bar{\varepsilon}_v^p$, which, through Equation (31), leads in turn to an increase of p_B. Therefore the cap moves to the right in Figure 8, increasing the extent of the elastic region inside the new yield surface. Either p or J_2' (or both) must increase in such a way as to keep stress point on the cap in order to maintain this mode of behavior.

The cap does not move during purely elastic deformation. The behavior of the cap when the stress point lies on the failure envelope alone, however, depends upon the amount of dilatancy, or plastic volumetric expansion. This dilatacy leads to a decrease in $\bar{\varepsilon}_v^p$, resulting in the leftward movement of the cap. The cap movement is limited if and when the cap

reaches the stress point (so that the stress point lies at the corner of the yield surface.)

For most soils and for weak rocks, the low stress behavior of the model can be simplified. In the range designated as "small cap," Figure 9, the center of the elliptical cap is at the origin. The transition point is reached when the cap is large enough to intersect the failure surface, as it is shown in the figure.

The soil cap model described above was developed primarily for use in computations of explosions which usually involve much higher stress levels than are involved in earthquake-induced ground response and which are generally characterized by a single peak compressive stress followed by smaller stresses. An exception is the case of outrunning ground motion in layered soil media, which involves cyclic, low amplitude response signals similar to those of earthquakes. As a rule, however, hysteresis in cyclic loading subsequent to an initial pulse is generally viewed as having secondary importance. Hysteresis becomes quite important, however, for earthquake-induced loadings where cyclic shear is the predominant effect.

The adaptations of the cap model described below make the basic model suitable for the seismic environment. These extensions of the model represent hysteresis in cyclic shear loading and also include pore water effects in wet media.

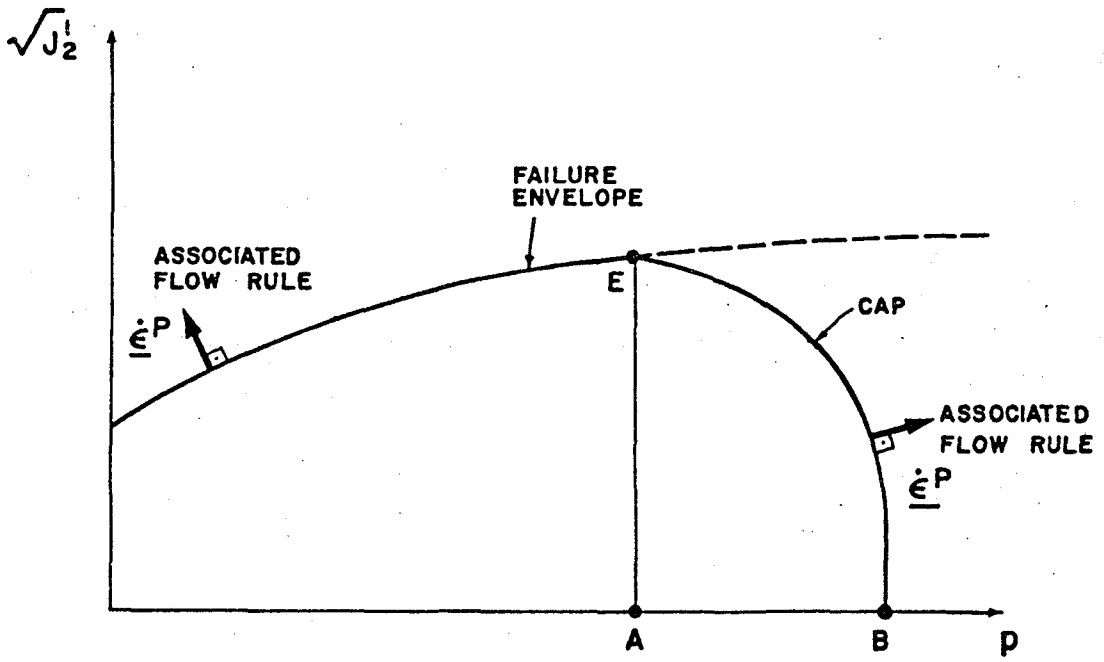

Figure 8 Yield Surface in the Cap Model

Cap Model For Cyclic Loading

A version of the cap model was developed to represent materials which exhibit viscoelastic behavior during cyclic loading. It has also been used to represent rate independent cyclic hysteresis over a limited range of loading rates.

In the viscous cap model linear viscous damping is introduced into the previously elastic portion of the cap model. For example, a standard solid was chosen to govern shear behavior within the yield surface. The parameters which define the nonplastic portion of the model are an instantaneous modulus G_F, a long term modulus $G_s < G_F$, and a relaxation rate τ. The model is shown schematically in Figure 10. The parameters G_s and τ are related to those in the figure via

$$G_s = \frac{G_F G_V}{G_F + G_V} \tag{32}$$

and

$$\tau = \mu(G_F - G_S)/G_F^2 \tag{33}$$

The deviatoric stress strain relation for the model is

$$\frac{ds_{ij}}{dt} = 2G_F \frac{de^v_{ij}}{dt} + (2G_S e^v_{ij} - s_{ij})/\tau \tag{34}$$

where e^v_{ij} is the viscoelastic deviatoric strain, i.e., the total strain minus the plastic strain.

The shear response which may be obtained from the model is illustrated by the solid line in Figure 11 where stress difference versus computed strain difference is plotted for a simulated stress-controlled triaxial compression test. The figure illustrates the qualitative behavior possible with this model. The large permanent strains in the figure during initial loading result from plastic deformation associated with the expanding cap. The small loop results from the viscoelastic behavior within the yield surface. For comparison, the response of the standard (nonviscous) cap is shown by the dashed curve. There are two effects of the modified model which are apparent in the figure. The first is the creep relative to the instantaneous cap response which increases slightly as the loading frequency decreases. The second is the hysteresis loop for each successive cycle. With appropriate parameters, both the average slope and the area of the loops are relatively insensitive to the frequency of loading (about some "centering" frequency).

The pressure-volumetric strain relation within the plastic yield surface may be chosen as elastic, or as a similar standard solid with constants K_F, K_S and τ_v. It should be noted that the instantaneous response for any level of stress and/or strain is given by the current cap model with elastic constants K_F and G_F. Therefore, implementation of this type of model in various dynamic codes becomes a relatively straightforward modification of the "elastic portion" of the subroutine.

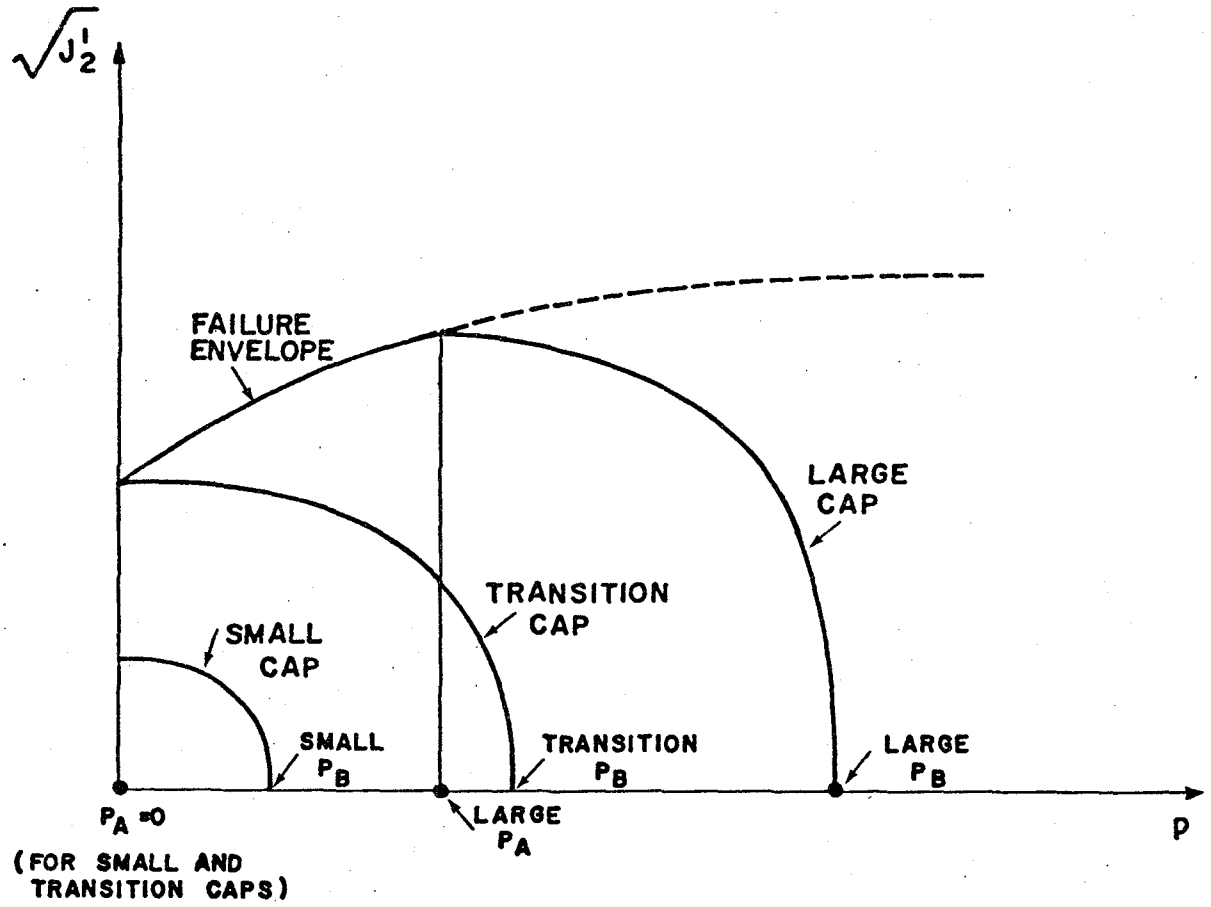

Figure 9 Some Details of the Cap Models

For situations in which experimental data suggest that the amount of hysteresis is independent of strain rate, a cap model can be constructed using kinematic hardening Prager (1966). This extended model is obtained by replacing the stress tensor σ_{ij} by the quantity $(\sigma_{ij} - \alpha_{ij})$, where α_{ij} is a tensor whose components are memory parameters defining the translation of the yield surface in stress space. Because the kinematic hardening is assumed to occur is shear only, only five of the six α_{ij} are independent, and

$$\alpha_{11} + \alpha_{22} + \alpha_{33} = 0 \tag{35}$$

This type of hardening is illustrated qualitatively in Figure 12 for the one-dimensional case in which only a single normal stress component σ' and a shear stress component τ are considered. The entire yield surface translates along the τ-axis by the amount α.

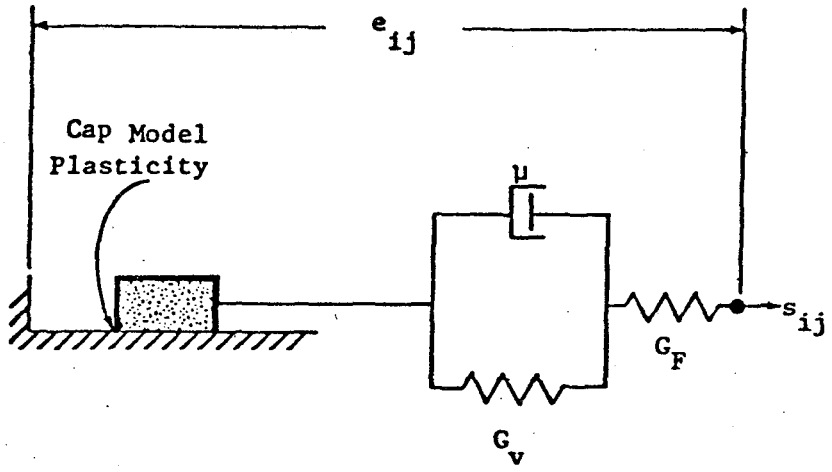

Figure 10 Schematic Representation of Viscous Cap Model

To complete the specification of the model, an evolutionary equation which governs the value of the memory parameter α_{ij} is required. This is the kinematic hardening rule which may be expressed as

$$\dot{\alpha}_{ij} = f_{ijk\ell}\,(\sigma_{ij},\ \alpha_{ij},\ \kappa,\ \varepsilon_{ij})\ \dot{e}^{p}_{k\ell} \qquad (36)$$

where $\dot{e}^{p}_{k\ell}$ are the deviatoric components of plastic strain and the usual summation convention is implied.

Obtaining the function $f_{ijk\ell}$ so as to fit the relevant available data is the key to constructing a model for a specific type of soil. Figure 13 illustrates the behavior of a kinematic cap model with a non-linear choice of function $f_{ijk\ell}$.

The stress path for a cyclic triaxial stress test is shown in Figure 13a, while the corresponding stress-strain curve is shown in Figure 13b. The material behavior illustrated in the latter figure is qualitively similar to much of the laboratory data obtained for dry sands.

As more experimental data become available, various nonlinear hardening rules such as those proposed in Mroz, Shrwastava and Dubey (1976) or Ghaboussi and Karshenas (1977) may be required to fit the behavior of any single material. Comparisons of a particular model with test data are shown in Figures 14 to 16. The model was used in computations of a structure - medium interaction experiment involving an artifically generated seismic environment.

The Modelling of Saturated Media

The introduction of substantial amounts of water into the solid matrix of soils and rocks may lead to a level of complexity above and beyond what has been discussed so far in this paper. If the migration

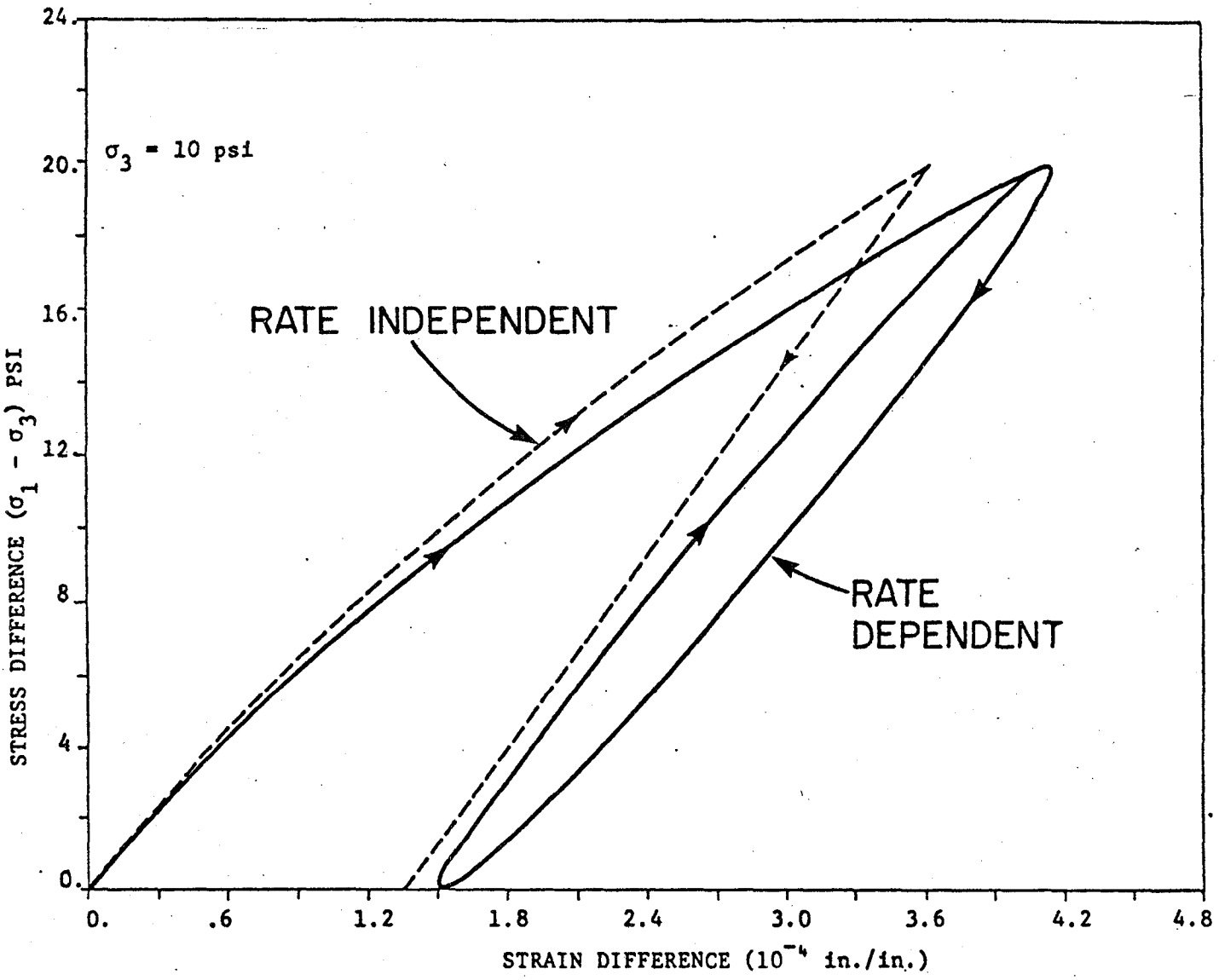

Figure 11 Comparison of Standard and Viscous Cap Models

of pore fluid is a significant factor a multiphase analysis is required; each phase must be modelled separately, and a system of individual phase conservation laws must be applied.

For excitations resulting from explosions and for short-lived seismic motions, it may be possible to neglect the migration of pore water. In such cases a single phase analysis is possible by combining the solid matrix constitive equation with a Terzaghi (1936) type of pore-pressure approach.

One such approach is described in Sandler, Dimaggio and Baron (1983) in which a laboratory remodeled kaolinite wet clay was modelled. Ordinarily such clay would be expected to be nearly isotropic. However, because the clay was K_o consolidated before the triaxial testing, and because the subsequent triaxial tests were known to exhibit substantial anisotropy, the

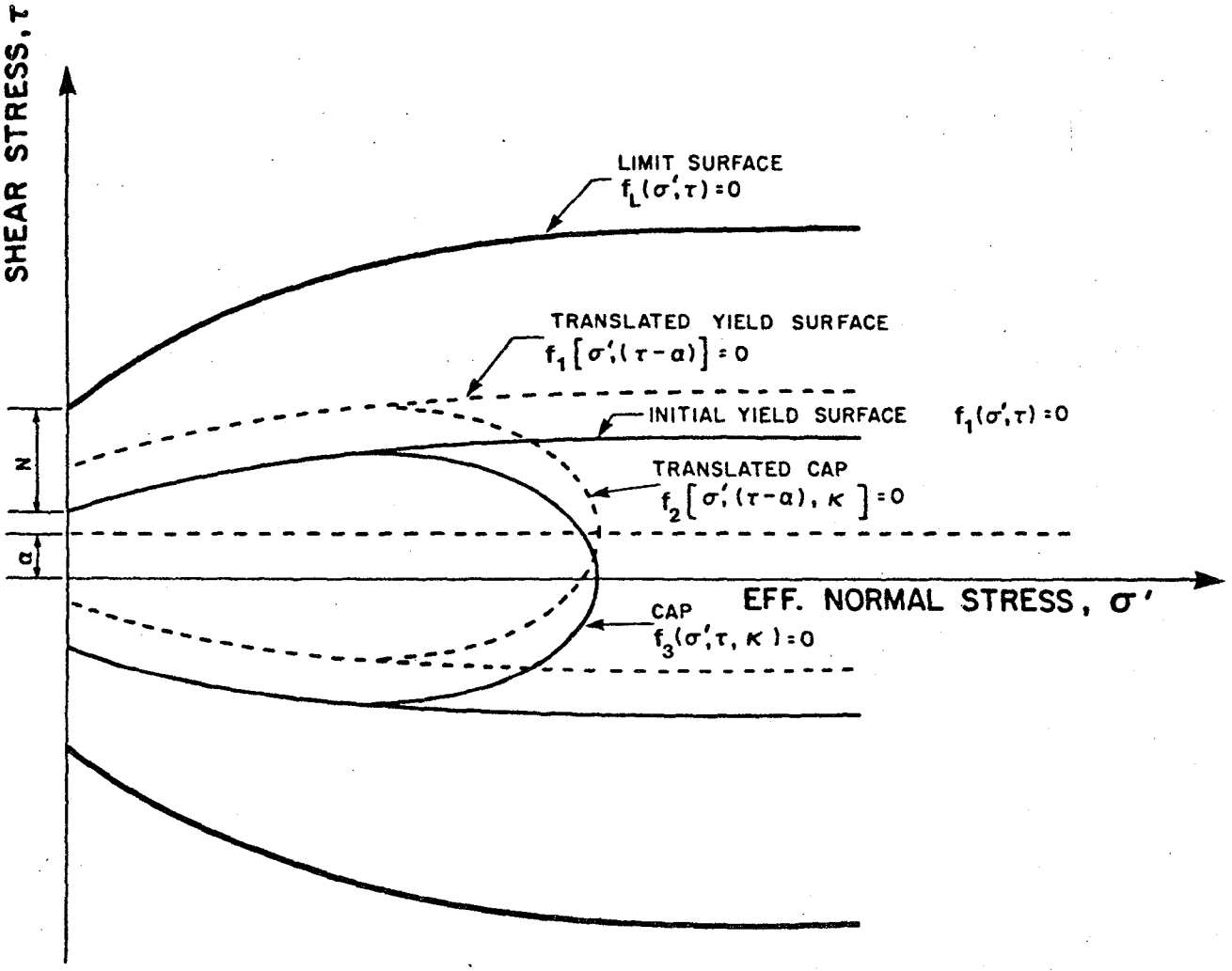

Figure 12 Kinematic Hardening Cap Model

model with a kinematically and isotropically hardening cap (where the cap has an offset in the direction of vertical compression) was utilized. In addition, the material was assumed to be incompressible under the undrained test conditions, i.e., the elastic and plastic volumetric strains were taken equal to each other in magnitude but of opposite sign.

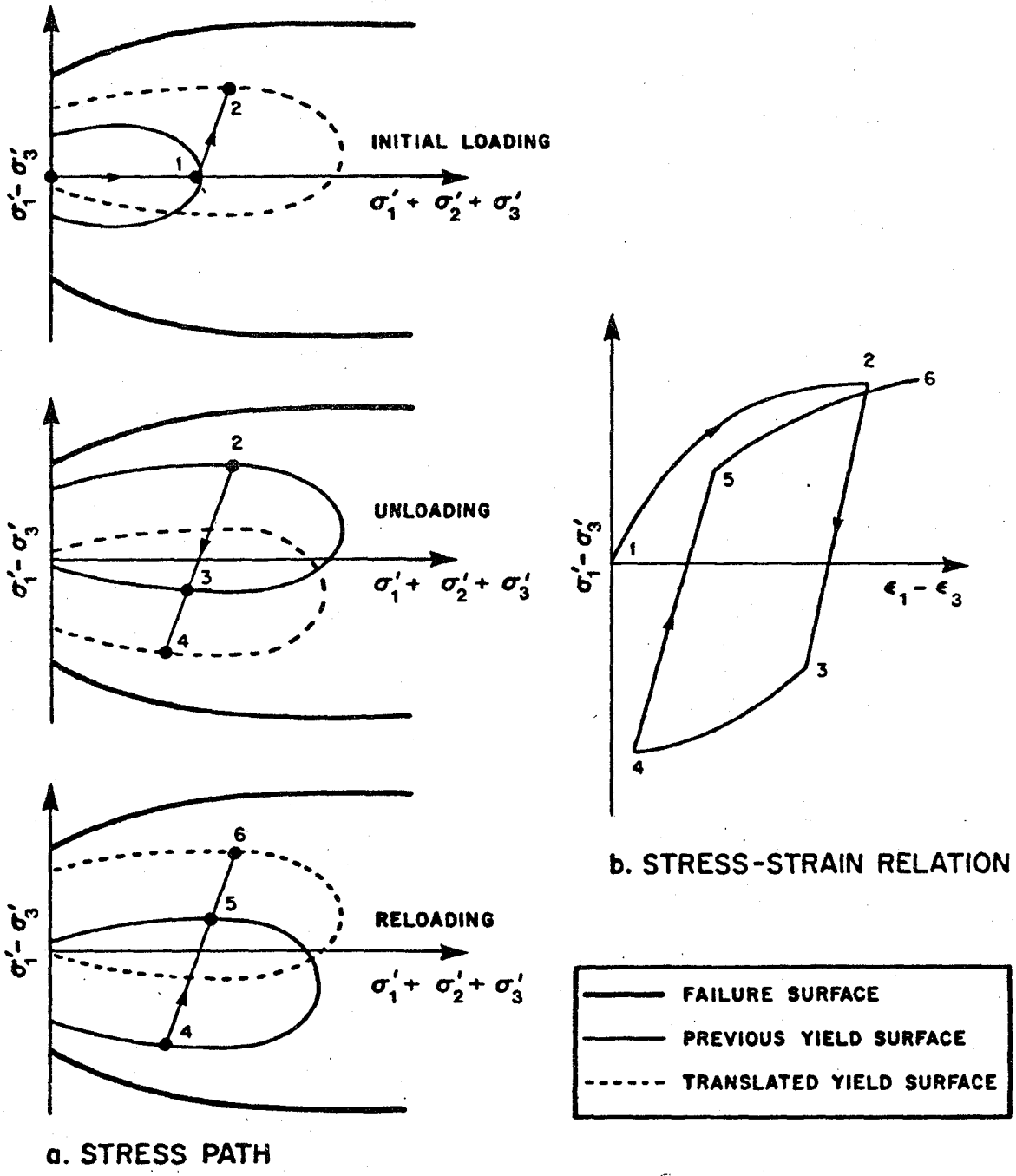

Figure 13 Triaxial Behavior of the Kinematically Hardening Cap Model

Since all the laboratory tests - those for which data was provided and those to be predicted - were performed in a narrow range of mean pressure (in the vicinity of 40 psi), a simple 9-parameter model was used with

linear failure and hardening. This made it possible to fit and exercise the undrained triaxial tests on horizontal and vertical specimens together with consolidation data. The model was exercised to predict behavior of inclined specimens under a series of stress paths. (These predictions were made before corresponding laboratory data were available for purposes of comparison.) Very good agreement between predictions and experiments was

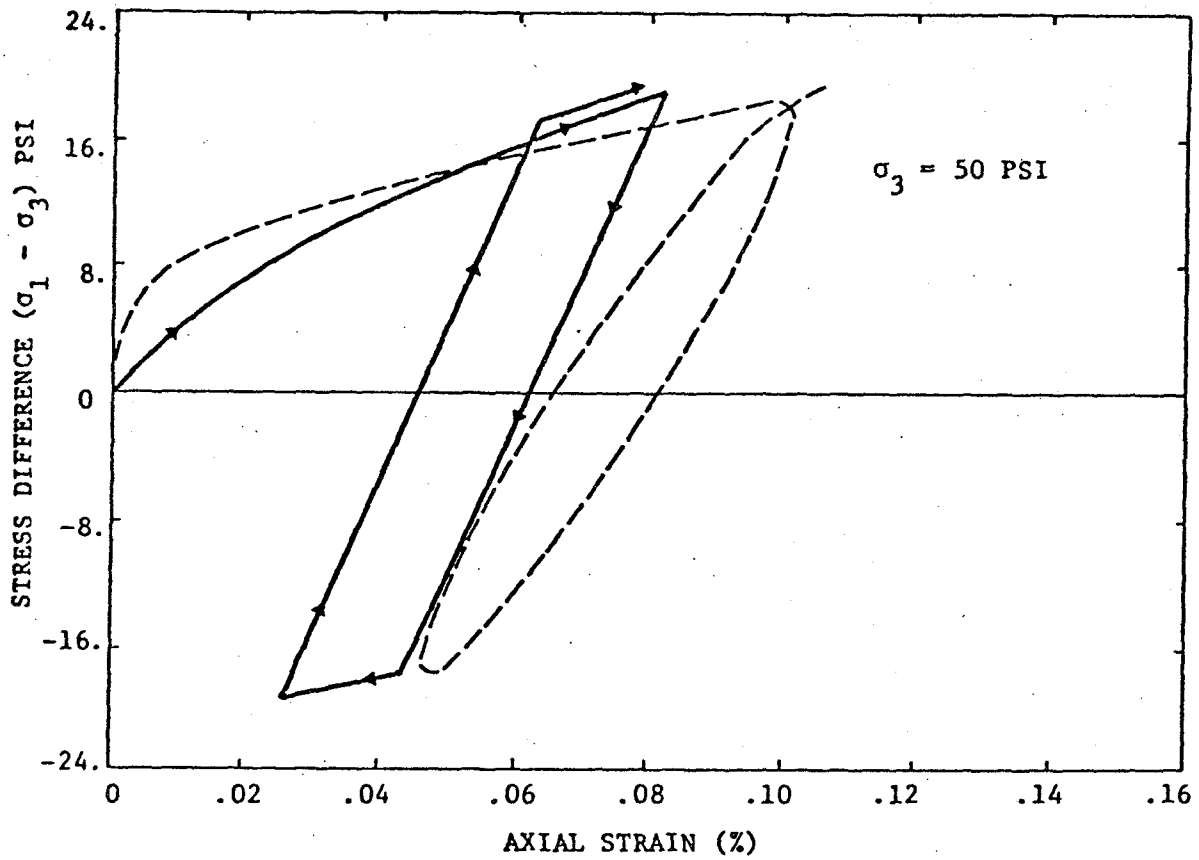

Figure 14 Fit of a Kinematically Hardening Cap Model (Low Shear)

obtained. A typical example of the pore pressure predictions of the model is shown in Figure 17. Further details may be found in Sandler, Dimaggio and Baron (1983).

Role of Insitu and Large-Scale Tests

This paper would not be complete without a discussion of the role of the material property data on the models. In order to illustrate some points of interest let us consider the problem of validation of procedures

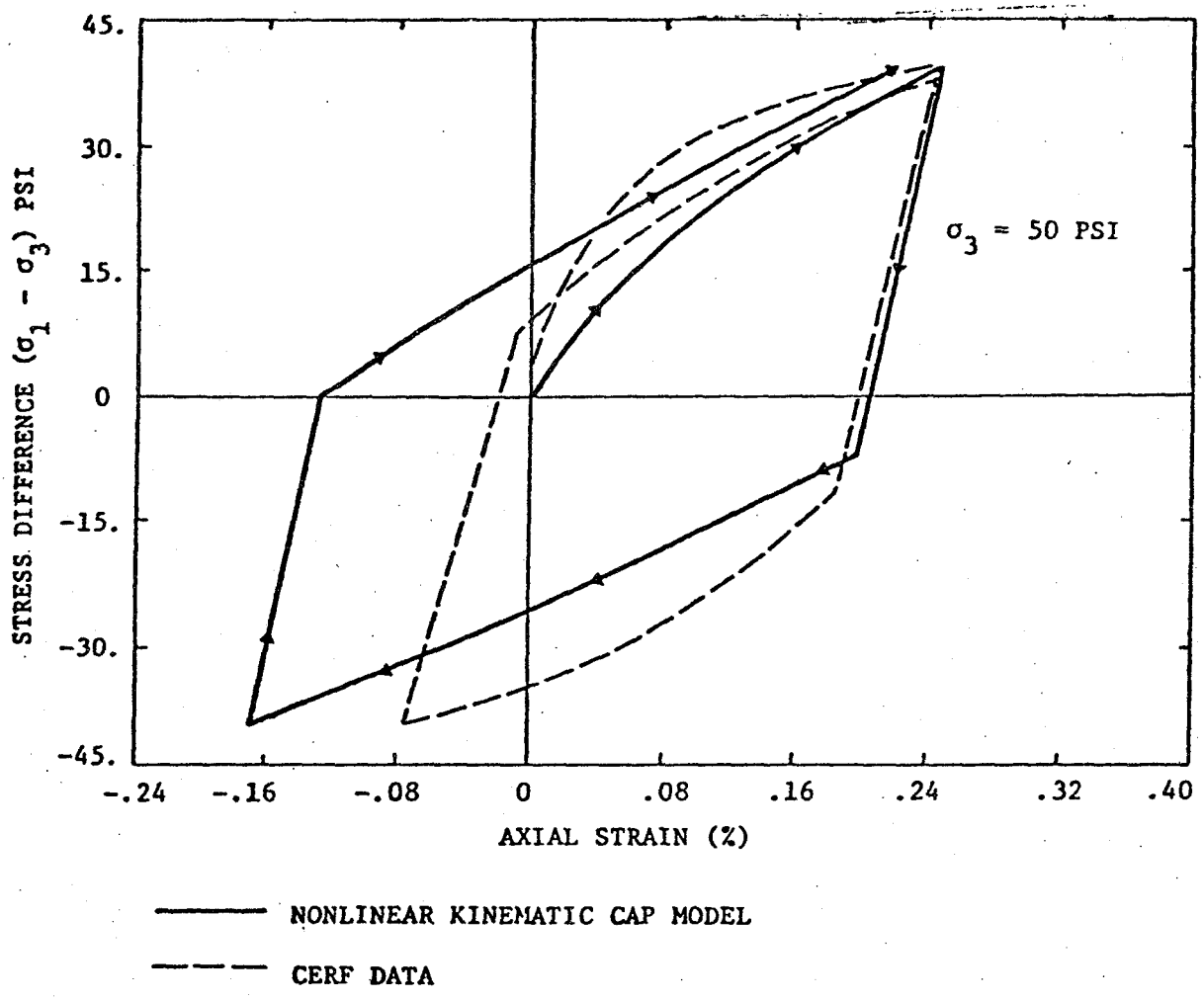

Figure 15 Fit of a Kinematically Hardening Cap Model (Moderate Shear)

used to analyze and predict explosively induced ground shock.

There were a number of large scale field tests in the U.S. in the early 1970's to test the validity of ground shock calculations. Two of the major series of events were MIDDLE GUST and MIXED COMPANY. The procedure in force at the time consisted of a site investigation and a core sampling program. Intact "undisturbed" samples would be brought to the laboratory and tested in uniaxial strain and triaxial compression. Representative property data would be chosen for each of the distinct materials or layers present at the site. The recommended properties would then be fit with constitutive model and a finite difference calculation would be run to simulate the field test.

An example of the "agreement" found between the calculational results and the field measurements is shown in Figure 18 for MIDDLE GUST - Event II, a 100 ton spherical shot of TNT. Both the small displacement LAYER code, and LAYER II (which includes transport terms) code results are very different from thet measured in the field, despite the fact that the cap model was used in the calculations.

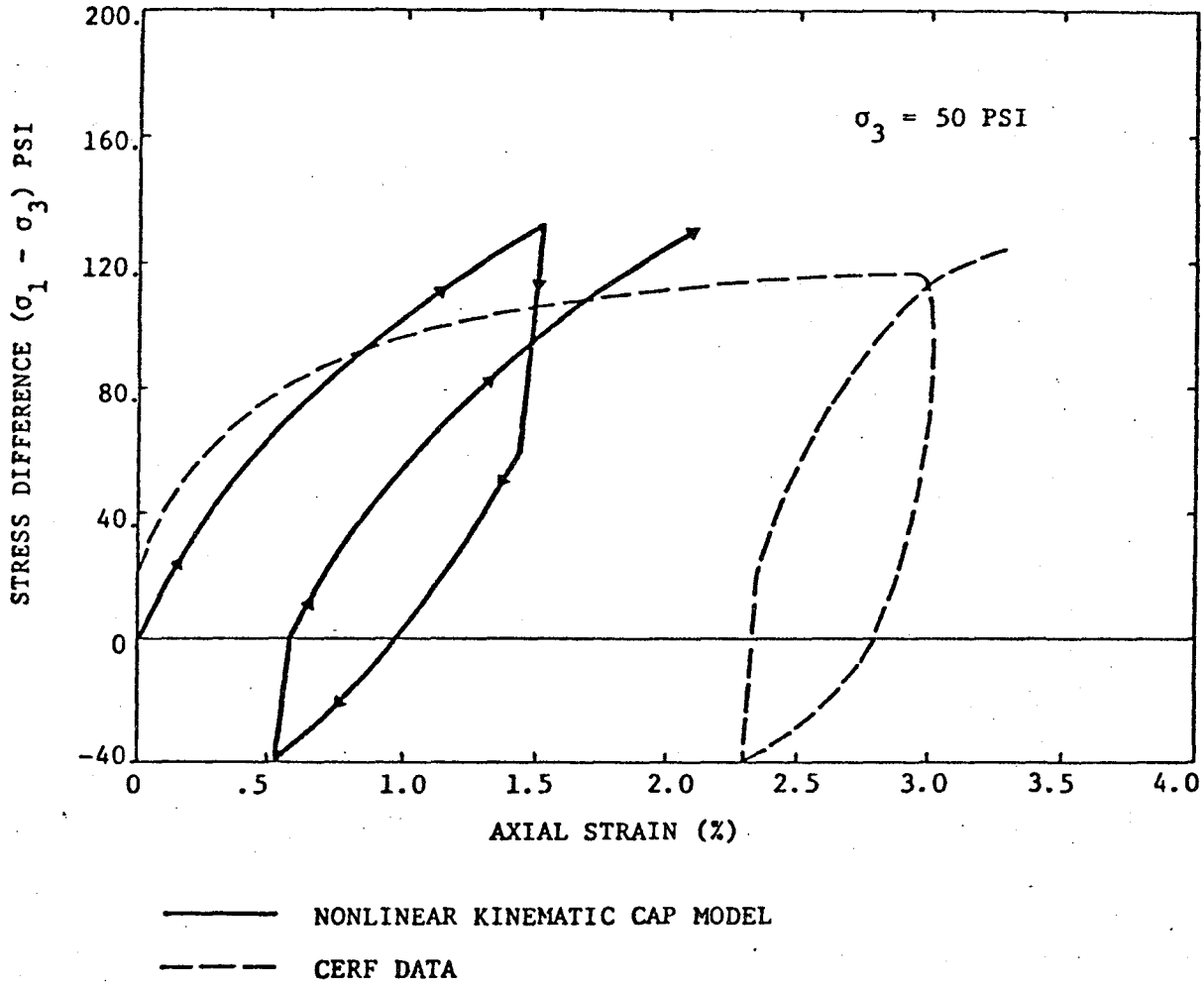

Figure 16 Fit of a Kinematically Hardening Cap Model (High Shear)

The discrepancies found in MIDDLE GUST and MIXED COMPANY were the subject of a great deal of investigation and soul searching on the part of the ground shock community. Much of the work in the area, in recent years, has been directed towards resolving these questions.

The main conclusions of these studies is that material model development cannot be based solely on laboratory tests but must also be based on the in situ behavior of the material. In many cases, the be-

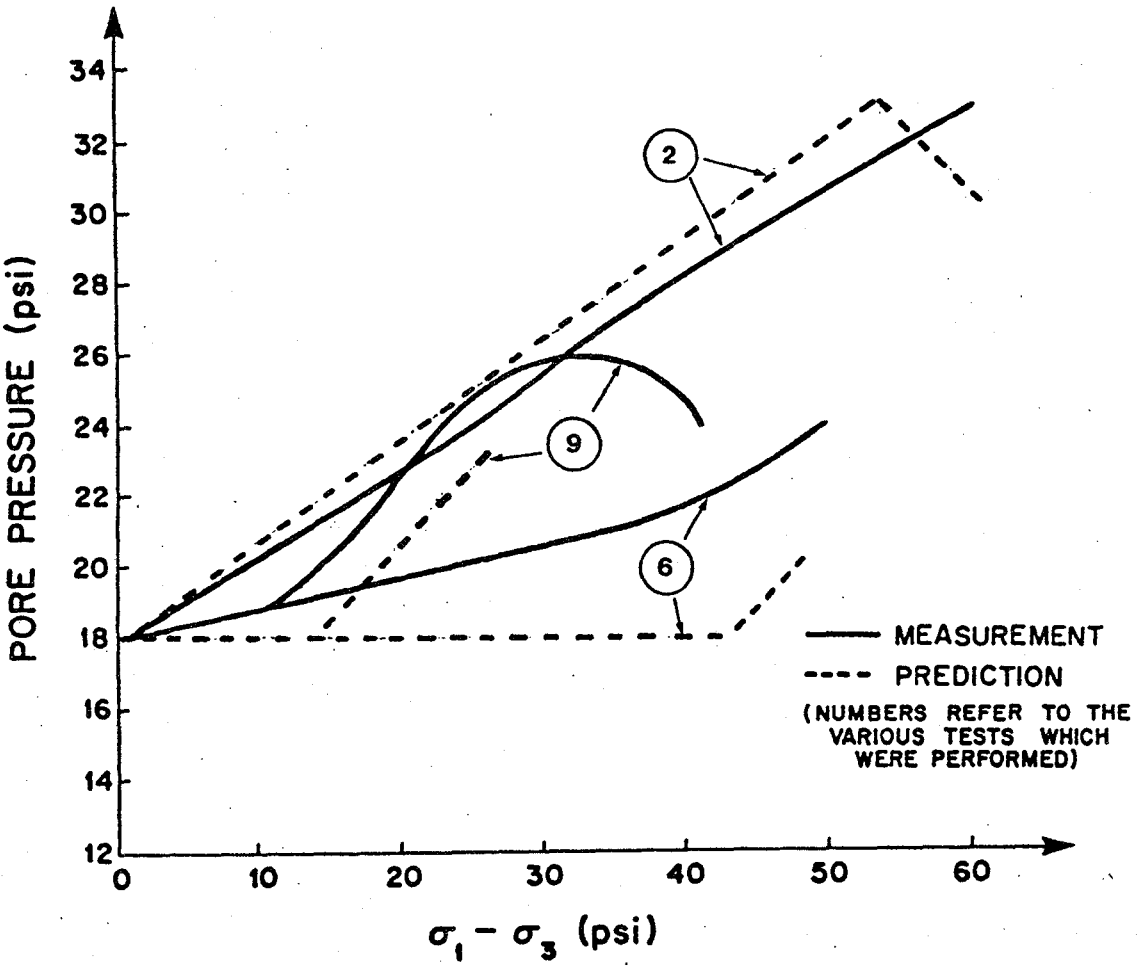

Figure 17 Comparison of Predicted and Observed Pore Pressure for Kaolinite

havior of small disturbed samples of material in the laboratory does not adequately represent the in situ behavior of the material. There are several reasons for this. For certain materials it is almost impossible to obtain truly undisturbed samples for laboratory testing. In addition, large scale inhomogeneities may make adequate smapling of the site impractical. The presence of anisotropy may lead to unrepresentative behavior in the laboratory specimens (which are almost always obtained from vertical cores). The release of lithostatic stresses of unknown magnitude, which may be significant at rock site, may alter laboratory behavior. Finally the rates at which some laboratory tests are performed may differ from those observed in ground response in explosive events.

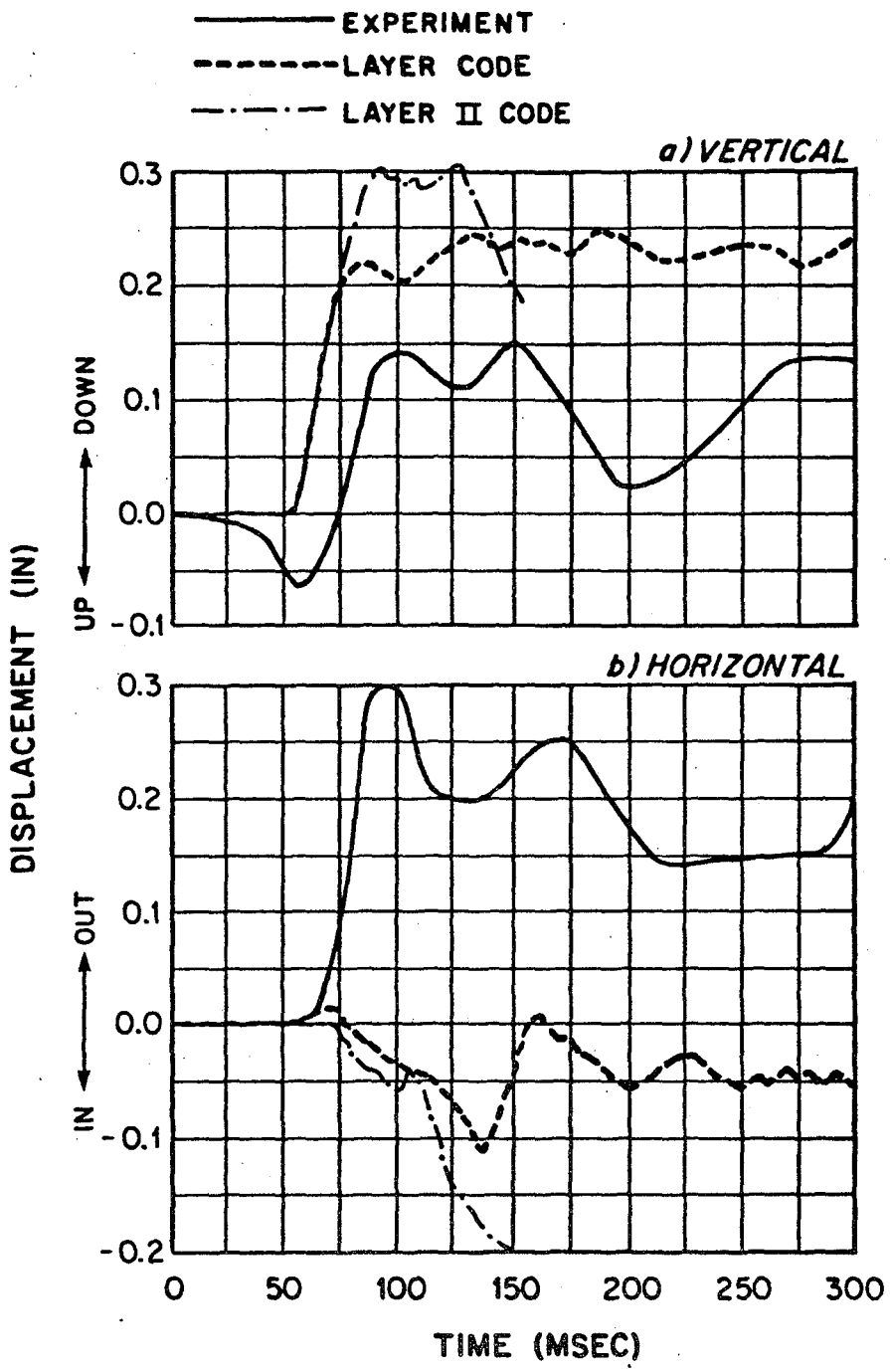

Figure 18 Comparison of Measured and Calculated Displacements for Middle Gust II

Because of the above considerations and because material models should be based on as wide a range of loading paths as possible, a number of in situ testing procedures to supplement the laboratory tests have been developed.

In addition to the field seismic survey, these in situ test include wave propagation tests with planar, cylindrical and spherical symmetry. All of the in situ tests give response data which can be interpreted only if some assumptions are made with respect to material behavior. For the relatively complicated material behavior that real geological materials exhibit, it is difficult if not impossible to obtain mathematical models based solely on the in situ tests. Consequently a preliminary mathematical model is fitted to the comprehensive data from laboratory tests as well as any situ material wave speed test that is available. This model is then used to compute the in situ test configurations and ammended so that the computed in situ response of the media mirrors the measured response. The final computational material model is thus determined by means of an iterative procedure in which both the laboratory data and the in situ data are utilized. The extremely important (and often major) role that the in situ data plays in the development of mathematical models for ground shock calculations is now widely recognized, and this iterative procedure is currently being used whenever possible.

Conclusions

An overview of some of the consideration involved in the construction of numerical models for dynamic loading of geological materials has been given. Various models appropriate for a number of physical situations of interest are presented and brief descriptions of their behavior are given.

The role of laboratory and in situ experimental data in material modeling is discussed in order to indicate how the phenomenological and practical aspects of modeling interwine. These aspects, together with the theoretical requirements, then constitute the salient points of model development.

Acknowledgement

Much of the work described herein was founded by U.S. government agencies, in particular the Defense Nuclear Agency.

The authors would like to thank their colleagues at Weidlinger Associates - especially Dr. Ivan Nelson - for their many contributions to the work described in this paper. Thanks are also due to Indy Parker for preparing the manuscript.

Bibliography

Baron, M.L., McCormick, J.M. and Nelson, I. (1969), "Investigation of Ground Shock Effects in Nonlinear Hysteretic Media, " Symposium on Computational Approaches in Applied Mechanics, American Society of Mechanical Engineers (also available in "mechanics 1970," American Acedemy of Mechanics, University Park, Pennsylvania).

Baron, M.L., Nelson, I. and Sandler, I.S. (1973) "Influence of Constitutive Models on Ground Motion Predictions," Journal of the Engineering Mechanics Division, American Society of Civil Engineers, Vol. 99, No. EM6, Proc. Paper 10210, 1181-1200.

Christian, J.T. (1966), "Plain Strain Deformation Analysis of Soil," Contract Report 3-129, Report 3, Contract DA-22-079-eng-471, Department of Civil Engineering, Massachusetts Institute of Technology.

Dimaggio, F.L. and Sandler, I.S. (1971), "Material Model for Granular Soils," Journal of Engineering Mechanics Division, American Society of Civil Engineers, Vol. 97, No. EM3, Proc. Paper 8212, 935-950.

Drucker, D.C. (1956), "On Uniqueness in the Theory of Plasticity," Quarterly of Applied Mathematics, Vol. 14, 35-42.

Drucker, D.C., Gibson, R.E. and Henkel, D.J. (1957), "Soil Mechanics and Work-Hardening Theories of Plasticity," Transactions American Society of Civil Engineers, Vol. 122, 238-346.

Drucker, D.C. and Prager, W. (1952) "Soil Mechanics and Plastic Analysis or Limit Design," Quarterly of Applied Mathematics, Vol. 10, 157-175.

Ghaboussi, J.G. and Karshenas, M. (1977), "On the Finite Element Analysis of Certain Material Nonlinearities in Geomechanics", Intl. Conf. on Finite Elements in Nonlinear Solids and Structural Mechanics Geilo Norway, Tapir Publishing Co., Trondheim, Norway.

Handelman, G.H., Lin, C.C. and Prager, W. (1947), "On the Mechanical Behavior of Metals in the Strain-Hardening Range," Quarterly of Applied Mathematics, Vol. 4, 397-407.

Mroz, Z., Shrwastava, H.P., and Dubey R.N. (1976), "A Nonlinear Hardening Model and its Application to Cyclic Loading," Acta Mechanica 25,51-61.

Nelson, I., (1978) "Constitive Models for use in Numerical Computations" Dynamic Methods in Soil and Rock Mechanics, Proceedings, Karlsruhe 1977, Vol. 2: Plastic and Long-Term Effects in Soils. Rotterdam, Balkema.

Nelson, I. and Baron, M.L. (1971), "Application of Variable Moduli Models to Soil Behavior," International Journal of Solids and Structures, Vol. 7, 399-417.

Nelson, I, Baron, M.L. and Sandler, I.S. (1971), "Mathematical Models for Geological Materials for Wave Propagation Studies," Shock Waves and the Mechanical Properties of Solids, Syracuse, New York, Syracuse University Press.

Prager W. (1966), "Models of Plastic Behavior", Proc. Fifth U.S. Cong. Applied Mechanics, 435-450.

Sandler, I.S. (1976a), "The Cap Model for Static and Dynamic Problems", Proceedings of the 17th U.S. Symposium on Rock Mechanics, Snowbird, Utah.

Sandler, I.S. (1976b) "Material Modeling Based on CIST Test and Laboratory Data," Final Report DNA 3970F, Contract DNA001-75-C0239, prepared by Weidlinger Associates for Defense Nuclear Agency.

Sandler, I.S., Dimaggio F. and Baron, M. (1983), "An Extension of the Cap Model for the Inclusion of Pore Pressure Effects and Kinematic Hardening in a Cap Model Representation of an Anisotropic Wet Clay", Mechanics of Engineering Materials, J. Wiley and Sons.

Schofield, A. and Wroth, P (1968), Critical State Soil Mechanics, London, McGraw Hill, Ltd.

Terzaghi, K. (1936), "The Shearing Resistance of Saturated Soils and the Angle Between the Planes of Shear", International Conference on Soil Mechanics and Foundation Engineering., Cambridge Mass., Vol. 1.

PART 2

DISSCUSSER'S REPORTS

CONSTITUTIVE RELATIONS FOR SOILS

Discusser's Report

W. F. Chen
School of Civil Engineering
Purdue University
West Lafayette, IN

1. INTRODUCTION

Before I go into the discussion of Professor Gudehus's paper on constitutive relations for soils, I think it is appropriate to say a few words about the historical developments of constitutive equations in soil mechanics. This discussion has to start with the historical development of analytical methods for solving problems in soil mechanics in the past. The analysis of problems in soil mechanics is generally divided into two distinct groups - the stability problems and the elasticity problems. They are then treated in two separate and unrelated ways. The stability problems deal with the condition of ultimate failure of a mass of soil problems of earth pressure, bearing capacity, and stability of slopes most often are considered in this group. The most important feature of such problems is the determination of the loads which will cause failure of the soil mass. Solutions to these problems can often be obtained by simple statics by assuming failure surface of various simple shapes - plane, circular, or logspiral and by using Coulomb failure criterion. This is known as the limit equilibrium method in soil mechanics.

The earliest contribution to this method was made in 1773 by Coulomb who proposed the Coulomb criterion for soils and also established the important concept of limiting equilibrium to a continuum and applied it to determine the pressure of a fill on a retaining wall. Later, in 1857, Rankine investigated the limiting equilibrium of an infinite body and developed the theory of earth pressure in soil mechanics. In this historical development, the introduction of stress-strain relations or constitutive relations of soils was obviated by the restriction to the consideration of limiting equilibrium and the appeal to the extremum principle. Subsequent developments by Fellenius (1926) and Terzaghi (1943), among many others, have made the limit equilibrium method a working tool with which many engineers develop their own practical solutions. Perhaps the most striking feature of this approach is that no matter how complex the geometry of a problem or loading condition, it is always possible to obtain some approximate but realistic solution.

The elasticity problems on the other hand deal with stress and deformation of the soil at working load level when no failure of the soil is involved. Stresses at points in a soil mass under a footing, or behind a retaining wall, deformations around tunnels or excavations, and all settlement problems belong in this group. Solutions to these problems are often obtained by using the theory of linear elasticity. This approach is rational for problems at short-term working load level, but limited by the assumed elasticity of the soils whose properties approach most

nearly those of a time-independent elastic material where time-dependent effects are significantly large; introducing long-term working stresses over a given period, it is obviously wrong to design a structure on the basis of this time-independent Hooke's law for soils. In this case the design must consider the influence of time on the deformations. This is known as creep. Such a behavior may be modeled as viscoelastic and the theory of viscoelasticity may be applied to obtain solutions.

Intermediate between the elasticity problems and stability problems mentioned above are the problems known as progressive failure. Progressive failure problems deal with the elastic-plastic transition from the initial linear elastic state to the ultimate failure state of the soil by plastic flow. The essential constituent in obtaining the solution of a progressive failure problem is the explicit introduction of stress-strain or constitutive relations of soils which must be considered in any solution of a solid mechanics problem.

As mentioned previously, for a long time, solutions in soil mechanics have been based upon Hooke's law of linear elasticity for describing soil behavior under working loading condition and Coulomb's law of perfect plasticity for describing soil behavior under collapse state because of simplicity in their respective applications. It is well known that soils are not linearly elastic and perfectly plastic for the entire range of loading of practical interest. In fact, actual behavior of soils is known to be very complicated and it shows a great variety of behavior

when subjected to different conditions. Drastic idealizations are therefore essential in order to develop simple mathematical constitutive models for practical applications. For example, time-independent idealization is necessary in order to apply the theories of elasticity and plasticity to problems in soil mechanics.

It must be emphasized here that no one mathematical model can completely describe the complex behavior of real soils under all conditions. Each soil model is aimed at a certain class of phenomena, captures their essential features, and disregards what is considered to be minor importance in that class of applications. Thus, a constitutive model meets its limits of applicability where a disregarded influence becomes important. This is why Hooke's law has been used so successfully in soil mechanics to describe the general behavior of soil media under short-term working load conditions, while the Coulomb's law of perfect plasticity providing good predictions of soil behavior near ultimate strength conditions, because plastic flow at this ultimate load level attains a dominating influence, whereas elastic behavior becomes of relatively minor importance.

As we can see from this historical sketch, constitutive modeling of soils has come a very long way, not only through the hundreds of years of historical developments in the older theory of earth pressure by Coulomb's and by Rankine's work, but also the establishment of the classical theory of soil mechanics by Terzaghi. During the last 15 years, the theory of soil

plasticity has been intensively developed. The modern development of soil plasticity has been strongly influenced by the modern development of somewhat older theory of metal plasticity. It is therefore appropriate to mention here the important works of Roscoe and his students (1958-63) on work-hardening theory of soil plasticity (Palmer, 1972, Parry, 1972) and also the subsequent developments and applications that mark the beginning of the modern development of a consistent theory of soil plasticity (Chen, 1975).

As a result of these and allied developments coupled with the rapid development of finite element computer programs, there are exaggerated hopes in the soil mechanics field that soil problems could soon be solved on a sound theoretical basis similar to that existing with regard to problems relating to steel structures. This limitless faith, developed in recent years, especially by the younger generation of soil mechanician, does give a strong indication of recent progress in soil mechanics today. The high hope on the application of mechanics to soil leads to the conception by some young soil mechanicians, who were trained by their curriculum in modern continuum mechanics in general and soil mechanics in particular, to insist upon the prediction of computer calculation of the settlement of a foundation with the field measurement to within an exactness of say 1 mm. Otherwise, it is to blame the constitutive model of soil for the wrong prediction.

On the other hand, soil engineer, mainly elder members of the profession with his analysis and design based primarily on experience and case history, knows well the fact that no matter how thorough a site investigation is attempted, there are always incomplete exploration and knowledge of the original conditions. It is not possible to explore, detect and measure every sand seam, loose spot or weak plane. Thus, no actual site could be completely characterized by any mathematical models, simple or complex. Even a most sophisticated theory cannot describe fully the details of an actual geotechnical problem due to the imperfectness of the laboratory investigations and the incompleteness of site investigations.

As demonstrated convincingly by Professor Leonards in his 1980 Terzaghi's lecture (1982) on several failure case studies, the actual failures of many geotechnical problems were often the result of the existence of some weak seams or loose spots that could not be detected in the exploration or that were not considered in the theories of soil mechanics, even though the defects had been detected. These painful experiences revealed clearly that these were neither due to the deficiencies of the theories, nor to the imperfectness of the laboratory investigations, but to the fact that the lack of adequate knowledge and understanding of some physical phenomena at the site that requires the establishment of a proper concept, that guides the exploration before construction, that helps to decide an appropriate rational approach and mathematical theory during the

analysis and design stage, that gives a deeper insight into the working conditions of the problem, and that provides, at the end, the engineer a clear physical picture of his problem and the range of validity of his theory and design.

As mentioned previously, the early studies in soil mechanics were based on the mathematical theory of linear elasticity and limit equilibrium of perfect plasticity. This theoretical mechanics approach has led to the rational establishment of a number of good design rules for practical applications. With the present developments in computational techniques like the finite element method, more general theory of continuum mechanics like hyper- or hypo-elasticity, classical and endochronic plasticity, and visco- elasticity and plasticity (Chen and Saleeb, 1982) have been developed to describe the very complex behavior of soils involving phenomena like inelasticity, soil-water interaction, time dependency, dynamic and cyclic loading conditions (Chen, 1983, b,c). This advanced development may produce the danger of a possible separation between the practical soil engineer and the theoretical academic engineer. This danger has been brought out to the open by Professor Gudehus' paper. In his overview on constitutive relations for soils, he pointed out clearly the shortcomings of the existing theories and the inadequacies of the existing methods. As a result, on the one hand, the academic soil engineers or mechanicians tend to generate more expert opinions that will drift far and far away from the reality of construction and their propositions and refined approaches may not

be put into practice. On the other, discouraged partly by the negative contributions of the recent achievements of modern soil mechanics and partly by the complexity of modern mathematics, continuum mechanics, and computational methods, the practicing soil engineers may be forced and driven away from this fundamental theoretical approach and try to rely more and more upon their experiences and case histories.

In the preceding discussions, I may exaggerate the trends and factors as perceived by Professor Gudehus's viewpoint on the disordered state of the present state of soil mechanics that may be detrimental for the further development of soil mechanics. However, it can be stated here that the present state of constitutive modeling in the field of soil mechanics is rather a satisfactory one and the efforts made by the soil engineers and soil mechanicians in recent years have led to a more fundamental understanding of soil behavior under different conditions. As a result, some of the constitutive models and methods that have been developed and refined in recent years to such a completeness that many practical applications have been made and good predictions with field measurements have been observed. In these later cases, it can be appreciated that these concepts, theories and methods have become working tools with which every modern engineer should be conversant. Therefore, in the following sections, some of these positive developments will be briefly summarized. Here, my emphasis is placed on a special class of simple soil plasticity models and the way in which they affect the

practical solutions.

2. CRITERIA OF MODEL EVALUATION

There exists a large variety of models which have been proposed in recent years to characterize the stress-strain and failure behavior of soils. All these models have certain inherent advantages and limitations which depend to a large degree on their particular application. Professor Gudehus has proposed some basic requirements for evaluating these models. These include tractability, material constants, economy and numerical considerations. Alternatively, we may consider the following three basic criteria for model evaluation:

1. Theoretical evaluation of the models with respect to the basic principles of continuum mechanics to ascertain their consistency with the theoretical requirements of continuity, stability and uniqueness.

2. Experimental evaluation of the models with respect to their suitability to fit experimental data from a variety of available tests, and the ease of the determination of the material parameters from standard test data.

3. Numerical and computational evaluation of the models with respect to the facility with which they can be implemented in computer calculations.

In general, the criterion for model evaluation should always consider the balance between the requirements of rigor from the continuum mechanics viewpoint, the requirements of realistic representation of soil behavior from the experimental-testing viewpoint, as well as the requirements for simplicity in application from the computation viewpoint.

For the most part, the concept of perfect plasticity has been used extensively in conventional soil mechanics in assessing the collapse load in stability problems. The standard and widely-known techniques used in conventional soil mechanics are the limit equilibrium method. However, it neglects altogether the important fact that the stress-strain relations constitute an essential part in a complete theory of continuum mechanics of deformable solids. Modern limit analysis method, however, takes into consideration, in an idealized manner, the stress-strain relations of soils. This idealization, termed normality or flow rule, establishes the limit theorems on which limit analysis is based. Within the framework of perfect plasticity and the associate flow rule assumption, the approach is rigorous and the techniques are competitive with those of limit equilibrium approach. In several instances especially in slope stability analysis and bearing capacity calculations, such a level and completeness has been achieved and firmly established in recent years that the limit analysis method can be used as a working tool for design engineers to solve everyday problems (Chen, 1975).

Most of the early applications of limit analysis of perfect plasticity to geotechnical problems have been limited to soil statics. Recent works attempt to extend this method to soil dynamics, in particular to earthquake-induced stability problems. Recent results show convincingly that the upper bound analysis method can be applied to soils for obtaining reasonably accurate solutions of slope failures and lateral earth pressures subjected to earthquake forces (Chen, 1980, 1983a, Chang and Chen, 1981, 1982).

As a further example, the Drucker-Prager type of elastic-perfectly plastic models were discussed and evaluated in the book by Chen (1975), among others. These models are computationally simple. With the proper selection of the material constants, the Drucker-Prager model can be matched with Coulomb condition. This simple model reflects some of the important characteristics of soil behavior such as: elastic response at lower loads, small material stiffness near failure, failure condition, and elastic unloading after yielding. A simple model of this type can be considered a fair first approximation in the progressive failure analysis of soil media and soil-structure interaction problems.

3. ROLE OF STRAIN-HARDENING PLASTICITY IN SOIL MECHANICS

There are several important features mentioned in the first part of Professor Gudehus's paper (Leonards, 1983)

1. There is a clear review of the stress and strain paths

associated with typical boundary value problems in soil mechanics. These paths are generally nonproportional, irreversible and nonlinear.

2. It is shown that element (uniform strain distribution) tests are:

   a. rare

   b. often do not simulate those stress paths for common boundary value problems

3. The difficulties of interpreting non-element tests close to, or beyond, the initiation of failure are emphasized.

From an academic point of view, strain-hardening models are the most attractive to model the soil, because they are inherently capable of treating conditions of unloading, stress path dependency and dilatancy as required in item (1). Furthermore, use of these models usually satisfy the rigorous theoretical requirements of continuity, uniqueness and stability. On the other hand, it is rather difficult to correlate these plasticity models with data from conventional tests as described in items (2) and (3). Thus, the difficulty is extended to the proper determination of specific values for the parameters involved.

Because real materials tested in various manners at different laboratories often do not appear to behave in any consistent and unique way, no practical model can be expected to

represent such materials in full details. The Drucker-Prager perfectly plastic model may represent a first but crude attempt to use a plasticity theory. The "cap model" represents a more refined attempt which can fit most available experimental data reasonable well (Chen, 1983c). Herein, the cap model will be used to handle and predict the complicated situations such as nonlinear, nonproportional loading and unloading, stress path dependency, and dilatancy as reviewed by Professor Gudehus on some typical boundary value problems in soil mechanics. From this numerical demonstration, it shows clearly that the "cap" type of plasticity models not only reflects some important features of soil behavior under laboratory condition, but it also provides a rather accurate prediction of some detailed soil stress-strain histories typically occurring in the ground and in field as sketched in Figs. 1.2, 1.3 and 2.2 of Professor Gudehus' paper.

4. DEMONSTRATION OF A SIMPLE CAP MODEL

The schematic shape of this simple model is drawn in Fig. 1. The model is composed of a linearly elastic region bounded by a perfectly plastic failure surface of Drucker-Prager type taking the simple form, in the usual notation

$$\sqrt{J_2} + \alpha I_1 = k \qquad (1)$$

and a strain-hardening cap taking the form of a quarter of an ellipse

$$(I_1 - L)^2 + R^2 J_2 - (X - L)^2 = 0 \qquad (2)$$

where

α, k = material constants related to c, ϕ, of Coulomb criterion.

L = value of I_1 at center of elliptic cap

R = ratio of major to minor axis of elliptic cap, taking a constant aspect ratio

X = hardening function that effectively controls material compaction and/or dilatancy, taking the simple form

$$\varepsilon_{kk}^{p} = W(e^{DX} - 1) \qquad (3)$$

The following values of the material constants were used in the present calculation made by McCarron (1983) since they were already available from previous work for a specific material (Baladi and Rohani, 1979).

$\phi = 49.1^{o}$ $\qquad$ $R = 4.33$

$c = 0$ $\qquad$ $W = 0.0075$

$\nu = 0.2736$ $\qquad$ $D = 6.78 \times 10^{-5}$ ft^2/lb

$E = 841400$ lb/ft^2

For the plane strain condition, we have:

$$\alpha = 0.2309$$

$$k = 0$$

The initial cap position is assumed at the origin of the I_1, J_2 space (Fig. 1). The numerical results are summarized in the forthcoming:

The plane strain earth pressure problem with granular soil as depicted in Fig. 1.2 of Professor Gudehus' paper was selected and solved in the following manner and the numerical results are shown in Fig. 2.

1. The material was loaded in uniaxial strain until a vertical stress of 30 psi was achieved (path 0-1, Fig. 2). During this interval the stress state is on the cap for the path.

2. Unloading (uniaxial strain) then occurred until the vertical stress was reduced to a value of 8.5 psi (path 1-2, Fig. 2). The stress-strain relation was linearly elastic along this path.

3. For the passive case a iterative procedure was used to follow the stress path (constant σ_1). The material first is linearly elastic and then elastic-plastic when loading begins on the cap (path 2-3-4, Fig. 2).

4. For the active case the stress path was also followed. The material behaved elastically until the failure surface was reached (path 2-3-4, Fig. 2). At this point the model was unable to follow the stress path.

The corresponding earth pressure problem of Fig. 1.2 with saturated clay as shown in Fig. 1.3 of Professor Gudehus's paper was also selected here and solved, and the results are summarized in the following (Fig. 3).

1. The initial loading and unloading paths are identical to those in Fig. 1.2 (path 0-1-2, Fig. 3). To simulate the saturated condition, strain paths which were volume-constant were prescribed ($\varepsilon_1 = -\varepsilon_2$, $\varepsilon_3 = 0$)

2. For the passive case the response is initially elastic until the failure surface is reached (path 2-3-4, Fig. 3). If loading continues in a constant-volume manner the state of stress eventually becomes constant (unchanged) (path 4-5, Fig. 3). For the present case loading continues along the failure surface until the state of stress coincided with the intersection of the cap and failure surface (corner loading). At this point the direction of the strain path was altered so that the volume decreased.

3. For the active case the same procedure was followed except the volume-conserving strain path was terminated before reaching the failure surface (path 2-3-4, Fig. 3). A volume-increasing path was then followed (path 4-5, Fig. 3).

If the original volume-constant path has been followed along the failure surface, the stress path would change directions so that both σ_1 and σ_2 would increase and stress path would be opposite to the curve 4-5 shown in Fig. 3(b).

As a last example, the material response given by the cap model for the four bilinear strain paths described in Fig. 2.2(a)

of Professor Gudehus' paper is show in Fig. 4. It exhibits the type of behavior that Professor Gudehus discussed, namely, that sufficiently large monotonic strain path may remove the memory of a previous stress/strain state.

The following four strain paths were used for the calculation of the corresponding stress paths shown in Fig. 4.

For Path i: The strain ratio ($\Delta\varepsilon_1 : \Delta\varepsilon_2 : \Delta\varepsilon_3$)

For Path ii: The strain ratio was (1:3:0)

For Path iii: The strain ratio was (3:-2:0)

For Path iv: The strain ratio was (1:-4:0)

Paths i, ii, and iii have continuous loading on the cap.

Path iv loads first on the cap when the strain path is parallel to Path i. When the incremental strain direction changes, the path is first elastic, then on the failure surface, then at the intersection of the failure surface and cap (or corner loading).

From these example calculations, it can be concluded that the cap model is capable of reproducing the stress-strain behavior discussed by Professor Gudehus. However, as Professor Gudehus mentioned, several practical and numerical problems may cause difficulties when solving boundary value problems. Professor Gudehus seemed particularly concerned with the following three problems:

1. Viscosity (time-effects)

2. Saturated soils (water)

3. Correct representation of the soil load history

The first point presents considerable difficulties. Considerable effort should be expected in developing the necessary constitutive relationships, computer code, and determination of the required material parameters. Perhaps a more basic problem is the requirement of a deterministic load history.

The analysis of saturated soils presents an interesting problem. The normal procedure appears to be to consider the total medium as incompressible ($d\varepsilon_{kk} = 0$). For an elastic material this may be approximated by a Poisson's ratio of $\simeq 0.5$ or an extremely large bulk modulus. If, however, the material is in an elastic-plastic state, it appears that the appropriate treatment to enforce incompressibility is to have $d\varepsilon^{e}_{kk} = -d\varepsilon^{p}_{kk}$. At the present time it seems unclear as to the best method to satisfy this relation.

Finally, the concern with correctly representing the load history of a soil history is addressed by Professor Gudehus. This aspect presents considerable practical problems in determining the past geological history of a site as well as the influence that construction activity may have in disturbing the soil mass. Professor Gudehus' concerns seem to focus on the validity of solutions obtained by say the finite element methods if the 'history' of a soil is not well represented. However, the theoretical solution does provide a rational and useful

understanding of the behavior of geotechnical problems, just one of the steps that is needed with any practical applications.

It is therefore very important to conclude here that soil mechanicians and soil engineers must have both adequate understanding and appreciation in the field of the other party. This will certainly help to contribute to the sound development of constitutive relations in soil mechanics and, as a consequence, a certain overlap in each other's development, rather than a certain separation to occur in the future.

REFERENCES

1. Baladi, G.Y., and Rohani, B., (1979), "An Elastic-Plastic Constitutive Model For Saturated Sands Subjected to Monotonic and/or Cyclic Loadings," 3rd Int. Conf. Numer. Methods Geomech. Aachen, 1979, pp. 389-404.

2. Chang, M.F. and Chen, W.F., (1982), "Lateral Earth Pressures on Rigid Retaining Walls Subjected to Earthquake Forces," Solid ~~Soil~~ Mechanics Archives, 7, Nijhoff, pp. 315-362.

3. Chen, W.F. (1975), Limit Analysis and Soil Plasticity, Elsevier, Amsterdam.

4. Chen, W.F. (1980), "Plasticity in Soil Mechanics and Landslides," J. of Engineering Mechanics Division, ASCE, 106(3), 443-464.

5. Chen, W.F. (1983a), "Soil Mechanics, Plasticity and Landslides," in Mechanics of Inelastic Materials (Eds. G.J. Dvorak and R. T. Shield), pp. - , Applied Science, London.

6. Chen, W.F. (1983b), "The Continuum Theory of Rock Mechanics," in Mechanics of Oil Shale, (Eds. K.P. Chong and J.W. Smith), pp. - , Applied Science, London.

7. Chen, W.F. (1983c), "Constitutive Modeling in Soil Mechanics," in Constitutive Laws for Engineering Materials: Theory and Applications, (Eds. C.S. Desai and R.H. Gallagher), pp. - , Wiley, London).

8. Chen, W.F., and Chang, M.F. (1981), "Limit Analysis In Soil Mechanics and Its Applications to Lateral Earth Pressure Problems," Solid Mechanics Archives, 6(3), Sijthoff & Noordhoff, pp. 331-399.

9. Chen, W.F., and Saleeb, A.F. (1982), Constitutive Equations for Engineering Materials, Vol. 1 - Elasticity and Modeling, Wiley, New York.

10. Fellenius, W.O., (1926), Mechanics of Soils, Statika Gruntov, Gosstrollzdat, 1933.

11. Leonards, G.A., (1982), "Investigation of Failures," J. Geotechnical Engineering Division, ASCE, 108(2), pp. 187-246.

12. Leonards, G.A., (1983), Private Communication.

13. McCarron, W., (1983), Private Communication.

14. Palmer, A.C., ed. (1973), Proceedings of the Symposium on the Role of Plasticity in Soil Mechanics, Cambridge University, Cambridge.

15. Parry, R.H.G., ed. (1972), Roscoe Memorial Symposium: Stress-Strain Behavior of Soils, Henley-on-Thames, Cambridge.

16. Terzaghi, K., (1943), Theoretical Soil Mechanics, Wiley, New York.

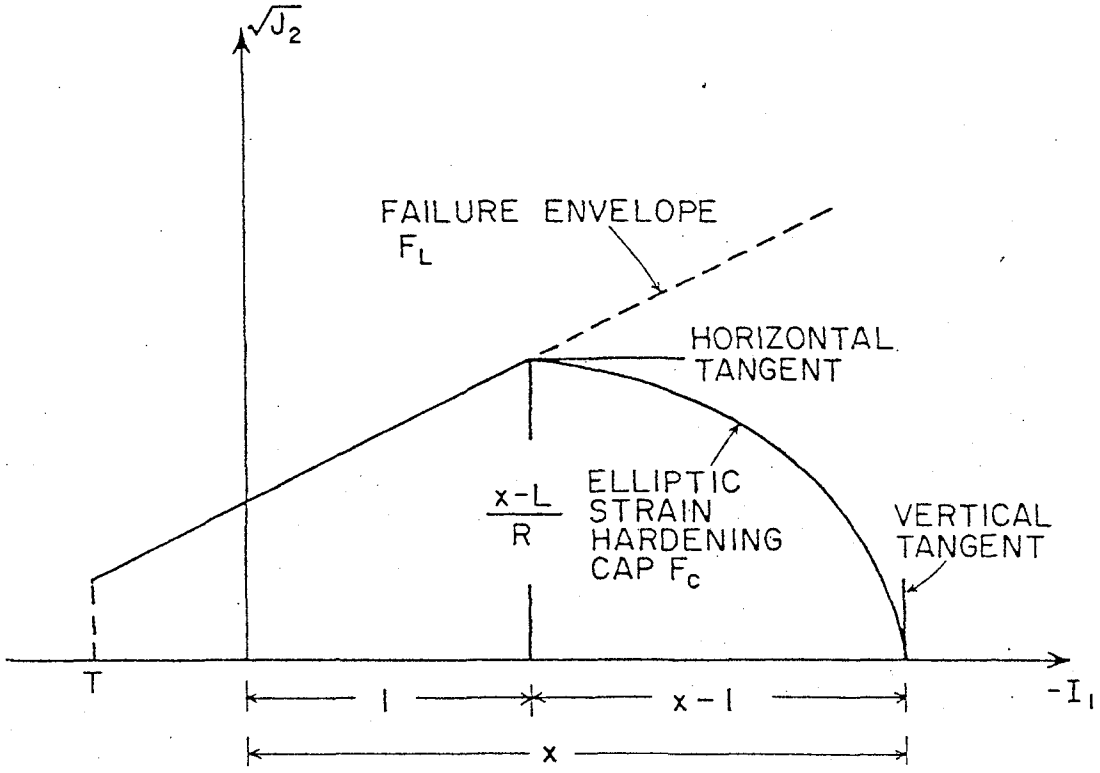

Figure 1 Elliptic Cap Model in $I_1 - \sqrt{J_2}$ Space

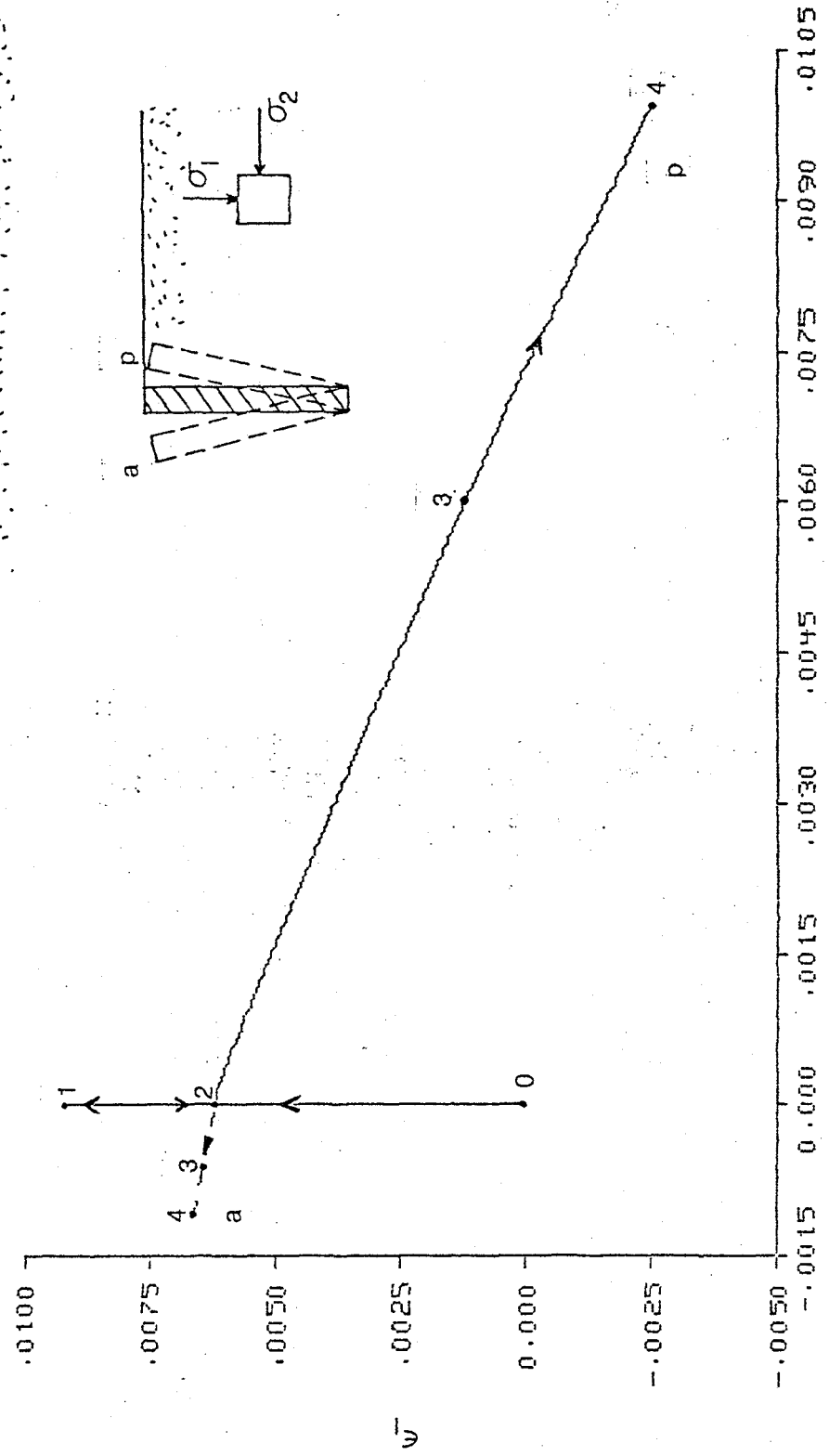

(a) Strain Paths

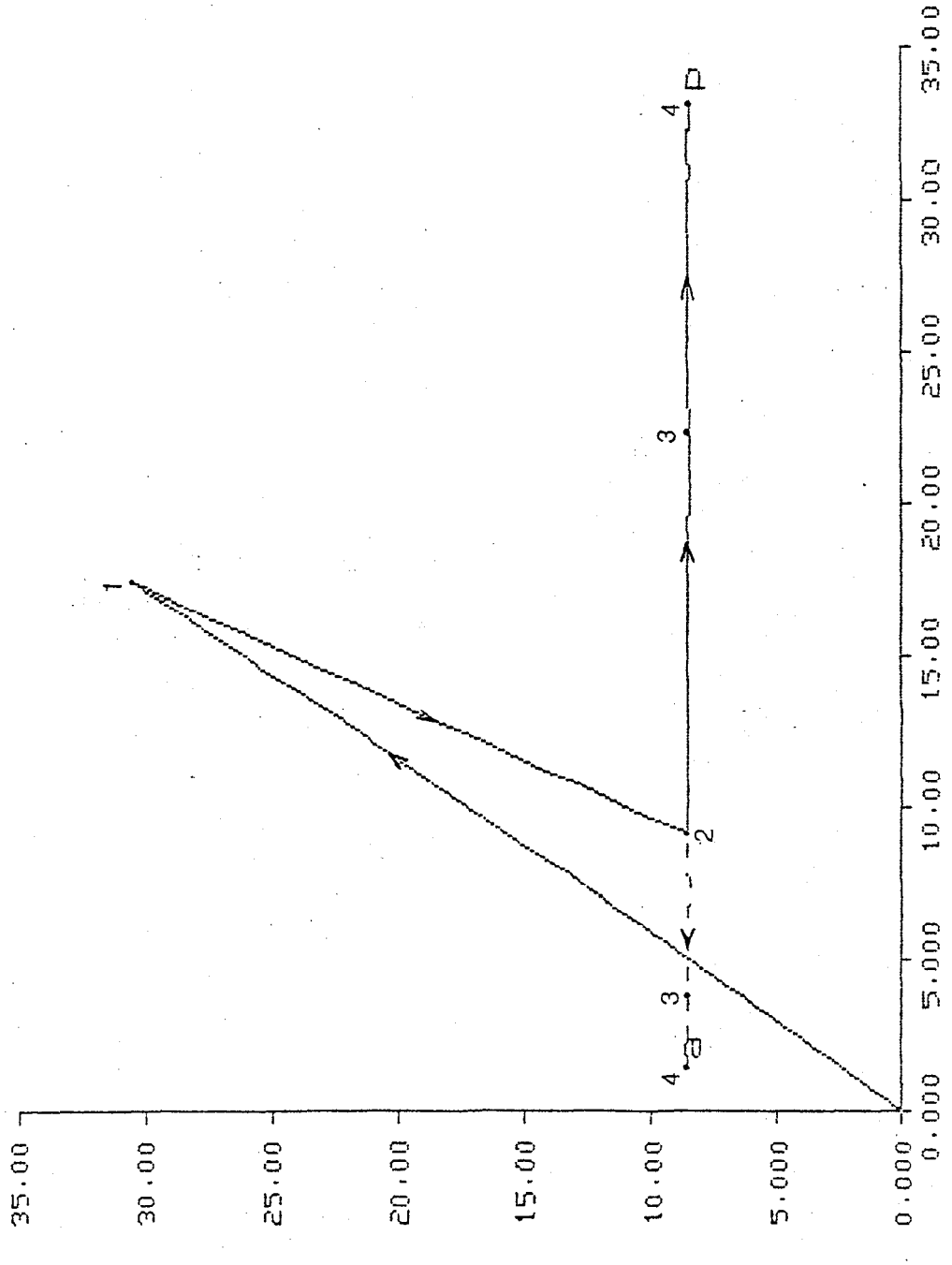

FIG. 2 EARTH PRESSURE PROBLEM WITH DRY GRANULAR SOIL CORRESPONDING TO (a) GUDEHUS'S FIG. 1.2(b) AND (b) GUDEHUS'S FIG. 1.2(c)

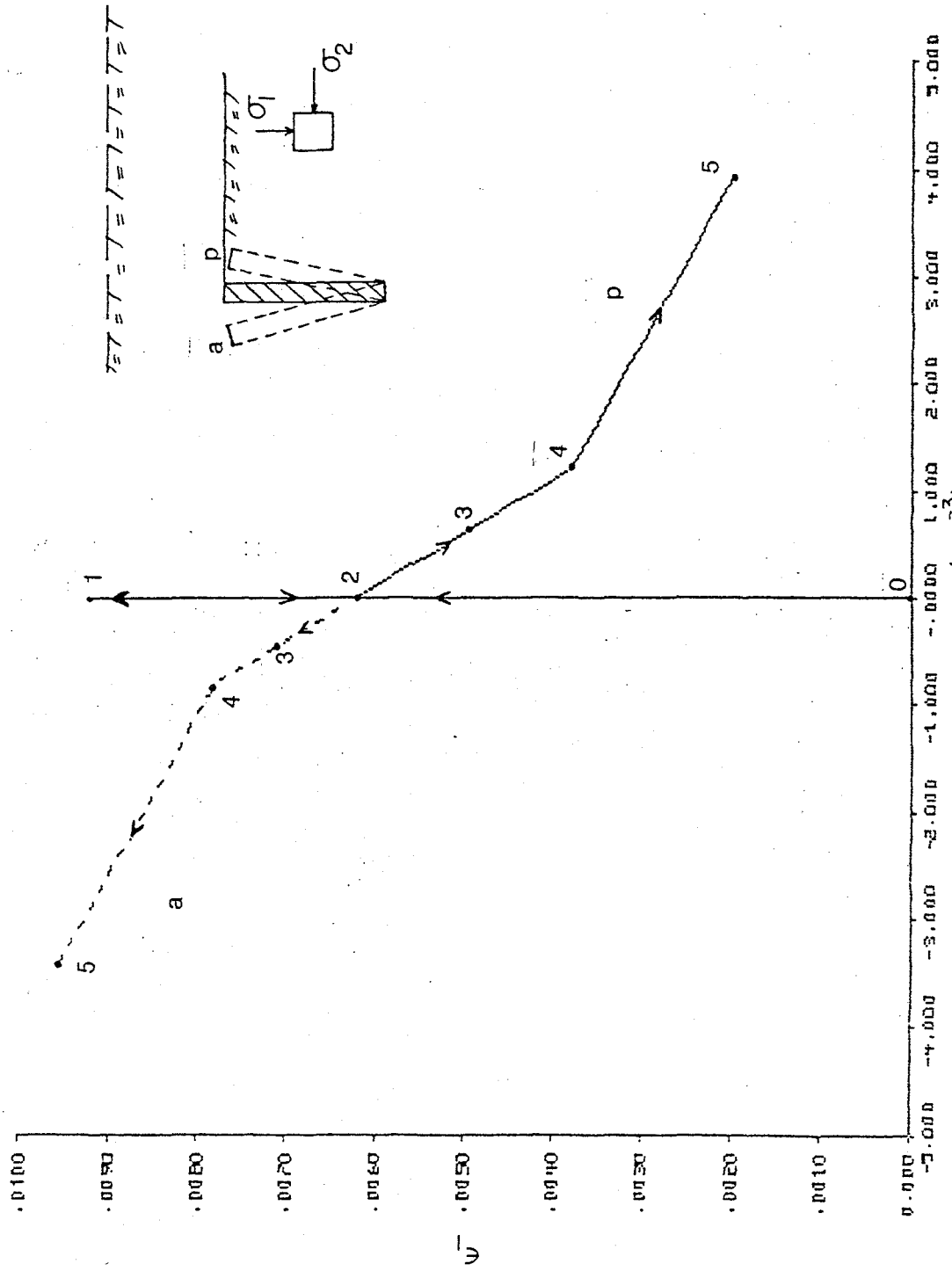

(a) Strain Paths

Fig 3

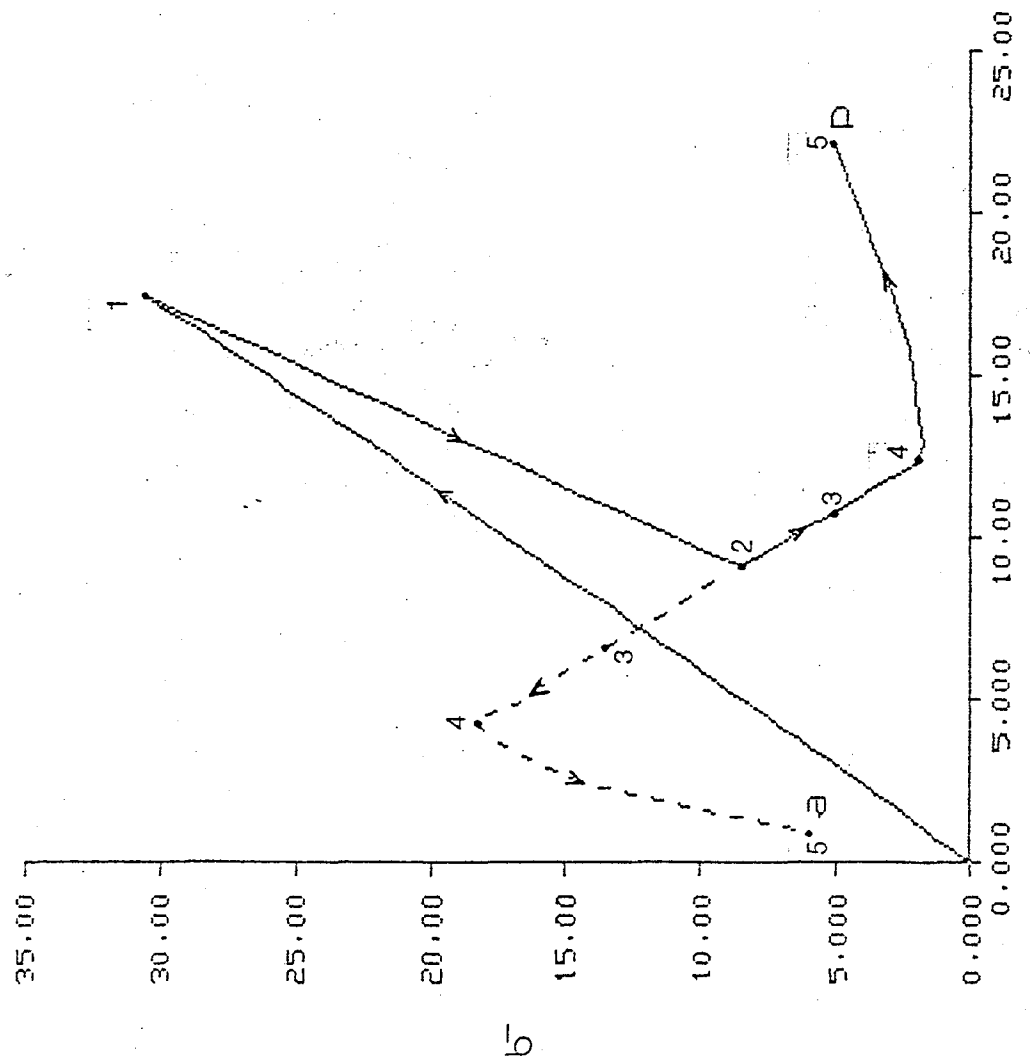

(b) Stress Paths

FIG. 3 EARTH PRESSURE PROBLEM WITH SATURATED CLAY CORRESPONDING TO (a) GUDEHUS'S FIG. I.3(b) AND (b) GUDEHUS'S FIG. I.3(c)

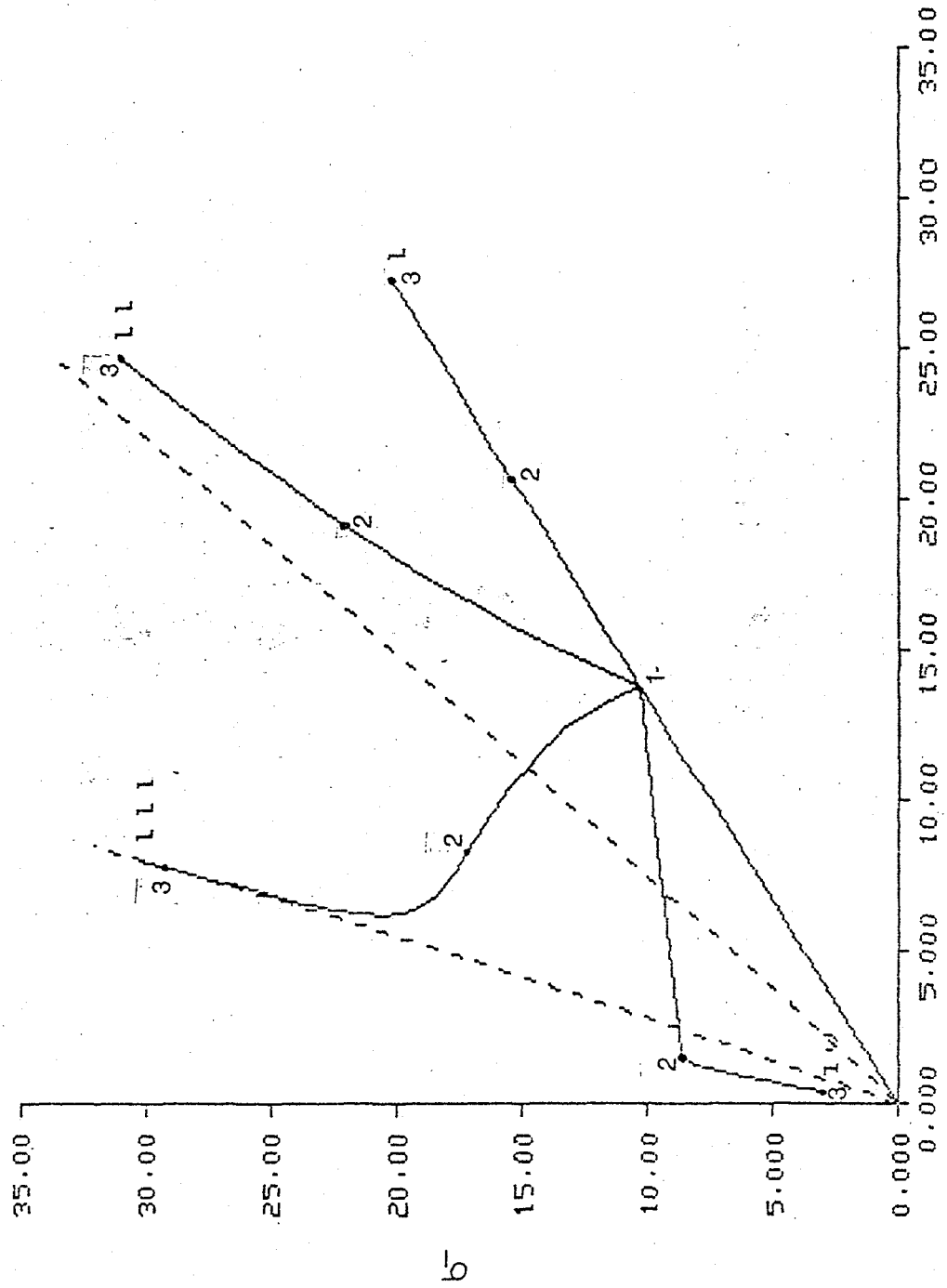

FIG. 4 STRESS PATHS CORRESPONDING TO THE FOUR BILINEAR STRAIN PATHS OF GUDEHUS'S FIG. 2.2(a)

CONSTITUTIVE RELATIONS FOR CONCRETE AND ROCK

Discusser's Report

by

W. F. Chen
School of Civil Engineering
Purdue University
West Lafayette, IN

1. INTRODUCTION

Although the applications of mechanics to reinforced concrete structures and to rock engineering are old and in many respects well established, the nonlinear deformation and ultimate load analysis of triaxially loaded concrete structures and mining problems related to rocks by means of finite element techniques is relatively recent (Chen, 1983). Different aspects of these advances were reported in several recent books, conference proceedings, and state-of-the-art reports. This includes the books by Chen (1982), Chen and Saleeb (1982, 1984), the Conference Proceedings by IABSE (1979, 1981), by U.S. Defense Nuclear Agency (1981), and the state-of-the-art reports by ASCE (1981), by Politecnico di Milano (1978), among others.

Most of the finite element studies consider concrete and rock to behavior as an elastic or elastic-plastic solid in compression and as a brittle material in tension. Simple constitutive models have been proposed and used extensively in the early studies of concrete and rock mechanics by modeling cracking in the form of tension cut-off criteria via Rankine theory of

maximum tensile stresses for tension concrete and by combining this with either a nonlinear elasticity theory or with a plasticity theory via von Mises or Coulomb yield criterion and its associated flow rule.

With the present rapid developments in computational techniques and computing capability, more general theory of continuum mechanics like hyper- or hypo-elasticity, classical and endochronic plasticity, and visco-elasticity and plasticity must be developed to describe the very complex behavior of concrete and rock materials involving phenomena like inelasticity, cracking, time dependency, and discontinuity. In Professor Dougill's paper, he has confined his presentation to the most fundamental aspects of concrete and rock mechanics, that is, the general technique used in the discussion of stress-strain laws based on the theories of elasticity and plasticity leading from modeling concrete and rock materials in the pre-failure regime to modeling the progressively fracturing solids in the post-failure range. In Professor Dougill's presentation, he has placed his emphasis on the critical subject of path dependence requirements and their implications for plasticity and fracturing and also the dual formulation in stress and strain space. In the following, I will concentrate my discussion on a number of topics that have not been covered in Professor Dougill's lecture. This includes a number of constitutive modeling techniques that were introduced in recent years to describe the nonlinear deformation as well as failure behavior of concrete or rock under triaxial conditions.

The scope is restricted to time-independent material behavior in the pre- and post-failure range which can be described on the continuum level.

2. CONSTITUTIVE MODELING

Within the framework of continuum mechanics, the behavior of real materials is generally idealized as time-independent or time-dependent. In the time-independent idealization, such as elastic and elastic-plastic models described in Professor Dougill's lecture, time effects are neglected. Time does not appear explicitly as a variable in the constitutive relations; phenomena like rate sensitivity, aging effects, and creep are not included in these modeling techniques. Further, for an ideal elastic material, the behavior is reversible and independent of the loading path, while it is irreversible and load path dependent in a plasticity-based model. On the other hand, in the time-dependent material idealization such as the viscoelastic and viscoplastic models, time effects are considered, and, therefore, they are generally capable of describing rate- and history-dependent behavior.

In concrete and rock mechanics, constitutive modeling of these materials under triaxial stress conditions is of central importance to the analyses and engineering design of triaxially load concrete structures and mining systems. Elastic modeling has been used most widely and is well understood, but irreversible deformation is not. This is an area of great importance for

concrete and rock materials. The principles of continuum mechanics provide the needed general guidelines for characterization of these materials, a field of increasing importance for sophisticated analyses.

It must be emphasized here that the previous idealizations and subsequent classification of the constitutive modeling techniques are only for mathematical convenience in describing the actual complex behavior of real materials. Nothing can compel the material to behave according to any of these idealized models. Indeed, for concrete and rock materials, the actual material response will exhibit the behavior characteristics of most of these models under certain conditions of stresses, temperatures, vibration, and strain rates. Therefore, in any practical problem, it is essential that we determine the limits and conditions under which the material can sensibly be assumed to exhibit the dominant characteristics of a particular type of the idealized models. Furthermore, since any idealized model has its own shortcomings, all the results obtained must be interpreted carefully in terms of these shortcomings.

3. FAILURE CRITERIA

The failure of concrete or rock in three-dimensional state of stress is extremely complicated. Numerous criteria have been devised to explain the conditions for failure of a material under such a loading state. These models can be classified as one-parameter models including the Rankine or Griffith criterion of

maximum tensile stress failure and the Tresca criterion of failure at maximum shear stress, two-parameter models including the Mohr-Coulomb criterion of shear failure, three-parameter models including the well-known Mohr-Coulomb criterion with a small tension cut-off, and four- and five-parameter models with a nonlinear relation between octahedral normal and shear stresses ($\sigma_{oct} - \tau_{oct}$) as well as noncircular cross sections on the deviatoric plane (Fig. 1).

In all these strength models, two basic postulates are adopted; isotropy, and convexity in the principal stress space. The first assumptions is mainly introduced because of the inherent simplification of the failure model. It is certainly true some concrete especially rocks exhibit significant anisotropy with respect to their strength which requires the formulation of the failure surface in the six-dimensional stress space instead of the three-dimensional space of principal stresses. For concrete and many rocks, however, the assumption of isotropy is reasonable. On the other hand, convexity is an assumption which is supported by global stability arguments in plasticity (see for example, Chen and Saleeb, 1982). Clearly, there are some questions on the validity of this postulate, and in fact, there is strong indication that the failure envelope for rocks, for example, over a wide range of hydrostatic (confining) pressures may be non-convex with respect to the hydrostatic axis.

Most of these three-, four-, and five-parameter models give a close estimate of the relevant experimental data, contain all

the three stress invariants for an isotropic material, reflect all the required characteristics concerning smoothness, convexity, symmetry, curved meridians, etc. as shown in Fig. 1. But the Willam-Warnke´s five-parameter model includes most of the earlier one-, two- and three-parameter models as special cases and therefore becomes increasingly popular in recent years (Chen and Han, 1983a). The five-parameter failure model of Willam-Warnke may be adopted as the basic surface for further development of elastic-plastic-fracture model for concrete (Chen and Han, 1983b).

4. PRE-FAILURE RANGE

Linear elasticity for isotropic and transversely isotropic materials constitutes the oldest and simplest approach to modeling the stress-strain behavior of concrete and rocks under low deforming loads. However, for higher loads or for rocks with large pore space such as the weaker sedimentary rocks, the stress-strain curve is generally nonlinear, and any analysis based on linear elasticity would not be realistic. Such nonlinear behavior may be characterized by variable stress-strain moduli. The simplest approach to formulate such nonlinear models is to simply replace the elastic constants in the linear stress-strain relations with secant moduli dependent on the stress or strain invariants.

These models are mathematically and conceptually very simple. The models account for two of the main characteristics of

concrete and rock behavior; nonlinearity and the dependence on the hydrostatic stress. The main disadvantage of the models is that they describe a path-independent behavior. Therefore, their application is primarily directed towards monotonic or proportional loading regimes.

A more rigorous approach in formulating secant stress-strain models for concrete and rocks can be developed on the basis of hyperelasticity theory. This type of formulation can be quite accurate for concrete and rock in proportional loading. They satisfy the rigorous theoretical requirements of continuity, stability, uniqueness, and energy consideration of continuum mechanics. However, here, as noted previously, this type of models fail to identify the inelastic character of concrete and rock deformations, a shortcoming that becomes apparent when the material experiences unloading. The main objection to the hyperelastic formulations is that it often contains too many material parameters. For instance, a third-order isotropic model requires nine constants; while 14 constants are needed for a fifth-order isotropic hyperelastic model. A large number of tests is generally required to determine these constants, which limit the practical usefulness of the models.

The path-independent behavior implied in the previous secant type of stress-strain formulation can be improved by the hypoelastic formulation in which the incremental stress and strain tensors are linearly related through variable tangent material response moduli that are functions of the stress or strain state.

In the simplest case of hypoelastic models, the incremental stress-strain relations are formulated directly as a simple extension of the isotropic linear elastic model with the elastic constants replaced by variable tangential moduli which are taken to be functions of the stress and/or strain invariants. Models of this type are attractive from both computational and practical viewpoints. They are well suited from both computational and practical viewpoints. They are well suited for implementation of finite element computer codes. The material parameters involved in the models can be easily determined from standard laboratory tests using well defined procedures; and many of these parameters have broad data base. However, the application of this type of hypoelastic models should be confined to loading situations which do not basically differ from the experimental tests from which the material constants were determined or curve-fitted. Thus, the isotropic models should not be used in cases such as non-proportional loading paths or cyclic loadings.

A general description of hyper- and hypo-elastic formulations has been given in Professor Dougill's paper. Here, I would like to add the following two comments on problems associated with the hypoelastic modeling. The first problem is that, in the nonlinear range, the hypoelastic models exhibit stress induced anisotropy. This anisotropy implies that the principal axes of stress and strain are different, introducing coupling effect between normal stresses and shear strains. As a result, a total of 21 material moduli for general triaxial conditions have to be

defined for every point of the material loading path. This is a difficult task for practical application. The second problem is that under the uniaxial stress condition, the definition of loading and unloading is clear. However, under multiaxial stress conditions, the hypoelastic formulation provides no clear criterion for loading or unloading. Thus, a loading in shear may be accompanied by an unloading in some of the normal stress components. Therefore, assumptions are needed for defining loading-unloading criterion. Furthermore, the material tangent stiffness matrix for a hypoelastic model is generally unsymmetric which results in a considerable increase in both storage and computational time. As a result of this, uniqueness of the solution of boundary value problems cannot generally be assured.

The mechanics of concrete and rocks in the elastic range is well developed. Predictions of acceptable accuracy based on some of these models mentioned previously have been made to many practical problems. However, elastic analyses do not account for the important phenomenon of irreversible deformations of materials. In general, it is this inelastic, irreversible range of deformation that is of great concern in a nonlinear deformation and ultimate load analysis of concrete structures and mining problems. Plasticity theory is well established with a long history of successful application to metals. For concrete or rock materials, the internal microcracks developed and grown during loading can be considered as a irreversible behavior. Figure 2 shows a typical uniaxial stress-strain diagram for plain concrete

in the compression range. The material exhibits an almost linear behavior up to the proportional limit at point A, from which the material constitution is progressively weakened due to internal micro-cracking up to failure at point D. The nonlinear deformations are essentially inelastic, since upon unloading only the portion of ε^e can be recovered from the total deformations $\varepsilon = \varepsilon^e + \varepsilon^p$. It is clear that this phenomenon corresponds exactly to the behavior of a work-hardening elastic-plastic solid.

The plasticity-based models can account for in principle, path-dependent irreversible inelastic deformations. Using a properly choosing pressure-dependent yield function, a hardening rule, and a flow rule, the models developed can fit rather well to the triaxial stress-strain test data of concrete. The material parameters involved can also be determined relatively easily.

The theory of plasticity enables one to go beyond the elastic range in a time-independent but theoretically consistent way, because the theory satisfies the conditions of uniqueness, continuity, stability, and thermodynamic laws. Consistency is admirable and the practicability of the theoretical situation is something that cannot be avoided. Thus, where it is possible, efforts should be made to introduce theoretical concepts and mathematics to concrete and rocks. If this is not possible, an empirical and engineering treatment may be introduced. However, experiments for determining the stress-strain diagrams beyond the

elastic range for general two- and three-dimensional states of stress are difficult to perform, especially for concrete and rock type of materials. Little has been done in the area of cyclic loading, rate-dependency, nonproportional loading, and post-failure response. The question of modeling strain softening in the post-failure range using plasticity theory is highly controversial. This can, to some extent, be rectified by introducing the concept of progressively fracturing solids, a subject very much emphasized in Professor Dougill's lecture. The formulation of a purely fracturing material is completely analogous to that of flow plasticity.

As apparent from the preceding discussion, it is necessary to include many complex effects in the material model in order to describe the behavior of concrete and rock properly. An important step in the direction of developing a more unified and comprehensive material model for concrete or rock is the generalization of the theory of viscoplasticity by introducing the measure of intrinsic time (Valanis, 1971). This is known as the endochronic theory of viscoplasticity. This theory offers a possibility to accurately model concrete or rock behavior in a wide range of loading conditions. The theory has been adopted with good success to concrete materials (Bazant, 1971), but there seems to be no application to rock yet either in static or dynamic loading conditions.

The concept of intrinsic time provides a good measure of the irreversible damage caused by the internal microcracks that

contribute directly to the inelastic strains. In this theory the degradation of material stiffness is obtained directly from the evolution of the damage function without recourse to the loading-unloading conditions. This type of models can represent many features of concrete behavior. However, the models generally involved many functions and parameters which are obtained by a rather complicated fitting procedure. Also, some of these models are incrementally nonlinear, and thus they may require excessive programming and computer effort.

5. POST-FAILURE RANGE

Concrete fails or fractures in extremely complex modes. It is known that concrete or rock material can be roughly as brittle at one extreme and ductile at another extreme, depending on the confining pressure or hydrostatic pressure. Thus, strictly speaking, we should speak of the "brittle state" or "ductile state" of materials, rather than of "brittle materials" or "ductile materials." Nevertheless, in the following discussion, we shall consider concrete or rock as a brittle material under ordinary load condition and it approaches a ductile material under extreme high hydrostatic pressure condition.

To this end, we classify the mode of failure into three types, namely, the cracking, crushing and a mixture of cracking and crushing. Documented test results for tension-tension or tension-compression biaxial conditions show the cause of fracture is primarily a brittle splitting in the plane normal to the

maximum tensile strain direction. This phenomenon should be studied within the framework of fracture mechanics correlating the propagation of discrete cracks to the stress concentration at the crack tip. Here, in the concrete community, a contrary continuum point of view is generally adopted, in which distinct cracks are smeared or distributed evenly within a finite element. It is then assumed that the cracked concrete element becomes an orthotropic (or more accurately, transversey isotropic) elastic material, with one of the material axes being oriented along the direction of cracking, such formulations easily allow for gradual build-down of strength in the direction of tension (tension softening or stiffening). Also shear-strength reserves due to aggregate interlocking and dowel action of reinforcement can be accounted for by retaining a positive shear modulus. The continuous model with a tension cut-off criterion (maximum tensile stress or strain) for cracking has been used in most of the computational models for analysis of reinforced concrete structures.

It is known (Bazant, 1976) that the strength criterion for crack formation over a finite element is unobjective and leads to incorrect results when the stress concentrations near the front of the fracture are calculated with more and more refined finite element meshes. It has been found that the overall stiffness of a structure and the predicted load-carrying capacity reduced with the decrease of the size of the element meshes. If the characteristic length of the problem is large (say, 0.34m, as suggested by Nilson, 1982), the brittle fracture model based on a strength

criterion can be used. For smaller size structures or for small element meshes, the softening cracking model based on an energy criterion should be used.

In the mixed failure range, the material fails in the form of cracking and sliding due to excessive tension and shear. Since microcracks are not oriented regularly, but rather randomly in this region, softening of materials would occur in all stress components. Such a multiaxial softening behavior may be treated by the fracturing theory (Dougill, 1976). A further improvement may be made by combining the plasticity and fracturing theories to model the softening behavior of fractured concrete due to cracking and sliding in the mixed failure zone (Bazant and Kim, 1979).

In summary, there are no brittle or ductile materials, the medium is only subjected to loading conditions which cause brittle or ductile response in the post-failure range. For concrete or rock type of materials, hydrostatic confinement plays the key role in distinction between different failure modes by the state of stress. Other factors such as the rate of loading, the composition of concrete, the amount of reinforcements have also important effects on the post-failure response of this material. Therefore, the perfectly brittle and the perfectly ductile models for the two extreme hydrostatic pressure cases combined with the plastic-fracturing model for the transition range form a good modeling basis for the actual post-failure behavior of fractured concrete or rock material. The difficulty of this approach is

that good softening data for concrete or rock are lacking. So, the shape and the expansion of the fracturing surface required in the progressively fracturing theory can not be easily defined. Further investigations are therefore urgently needed on the following topics: post-failure behavior, unconventional loading paths including cyclic response phenomena, rate effects, composite behavior and numerical algorithms.

REFERENCES

1. ASCE Committee on Concrete and Masonry Structures, (1981). A State-of-the-ArtReport on Finite Element Analysis of Reinforced Concrete, Task Committee on Finite Element Analysis of Reinforced Concrete Structures, ASCE, Spec. Publication, New York.

2. Bazant, Z.P., (1976). Instability, Ductility, and Size-Effect in Strain-Softening Concrete, J. Engrg. Mech. Div., ASCE, 102 (EM2),April, 331-344.

3. Bazant, Z.P., (1978). Inelasticity and Failure of Concrete: A Survey of Recent Progress, Proc. Spec. Sem. Anal. Reinforced Concr. Struct.Means Finite Element Method, Milan, 5-59.

4. Bazant, Z.P. and Kim, S.S., (1979). Plastic-Fracturing Theory of Concrete, J. Engrg. Mech. Div., ASCE, 105 (EM3), June, 407-428.

5. Chen, W.F., (1982). Plasticity in Reinforced Concrete, McGraw-Hill, New York.

6. Chen, W.F., (1983). The Continuum Theory of Rock Mechanics, in Mechanics of Oil Shale, K.P. Chong and J.W. Smith, Eds., Applied Science, Amsterdam.

7. Chen, W.F., and Han, D.J., (1983a). Failure Criteria for Concrete Materials," Proc. of Colloq. Failure Criteria of Structured Media, Grenoble, France.

8. Chen, W.F., and Han, D.J., (1983b). A Five-Parameter Mixed-Hardening Model for Concrete Materials, Proc. Int. Sym. Plasticity Today, Udine, Italy.

9. Chen, W.F., and Saleeb, A.F., (1982,1984). Constitutive Equations forEngineering Materials, Vol. 1 - Elasticity and Modeling, Vol. 2 - Plasticity and Modeling, Wiley, New York.

10. Dougill, J.W. (1976). On Stable Progressively Fracturing Solids, Zeitschrift Angewandte Mathematik und Physik, 27, Fsac. 4, 423-437.

11. IABSE, (1979). Proceedings Int. Assoc. Bridge Structr. Engrg. Colloq. PlasticityReinforced Concrete, Vol. 28, Introductory Report and Final Report, Lyngby, Copenhagen, Zurich.

12. IABSE, (1981), Proc. Int. Assoc. Bridge Structr. Engrg. Colloq.Adv. Mech. of Reinforced Concr., Vol. 34, Introductory Report and Final Report, Delft, Zurich.

13. Nillsson, L. (1982). Nonlinear Wave Propagation in Plastic Fracturing Materials - A Constitutive Modelling and Finite Element Analysis, Proc. IUTAM Symposium Nonlinear Deformation Wave, Tallin, August.

14. Politecnico di Milano, (1978). Proceedings Spec. Sem. Anal. ReinforcedConcr. Struct. Means Finite Element Method, Milan.

15. Schreyer, H.L., and Jeter, Jr., J.W., Eds., (1981). Proceedingsof Workshop on Constitutive Relations for Concrete, U.S. Defense Nuclear Agency, Albuquerque.

16. Valanis, K.C., (1971). A Theory of Viscoplasticity Without a Yield Surface, Archiwum Mechaniki Stossowanej, (Archives of Mechanics), Warszaw, 23, 517-551.

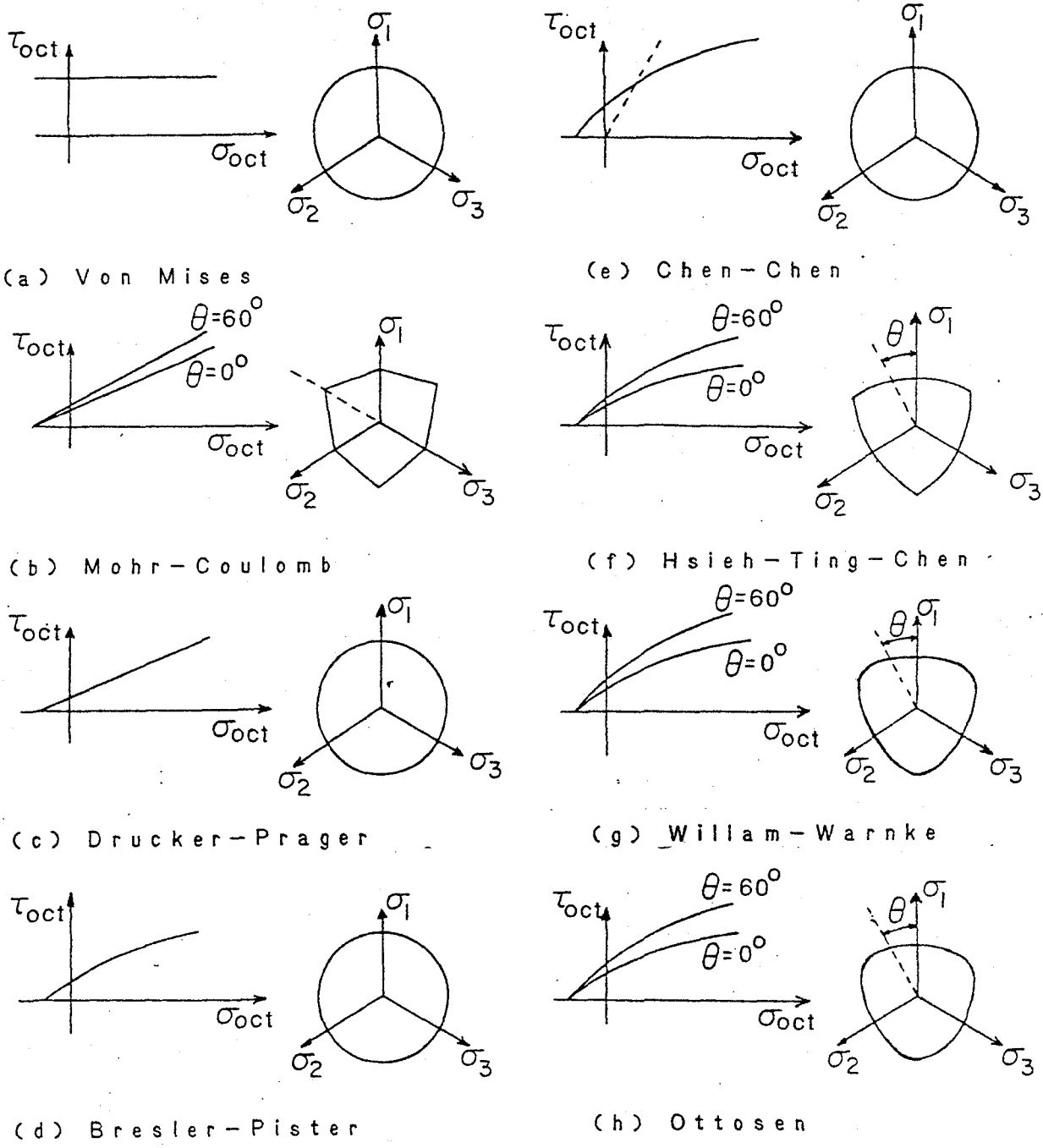

FIG. 1 FAILURE MODELS

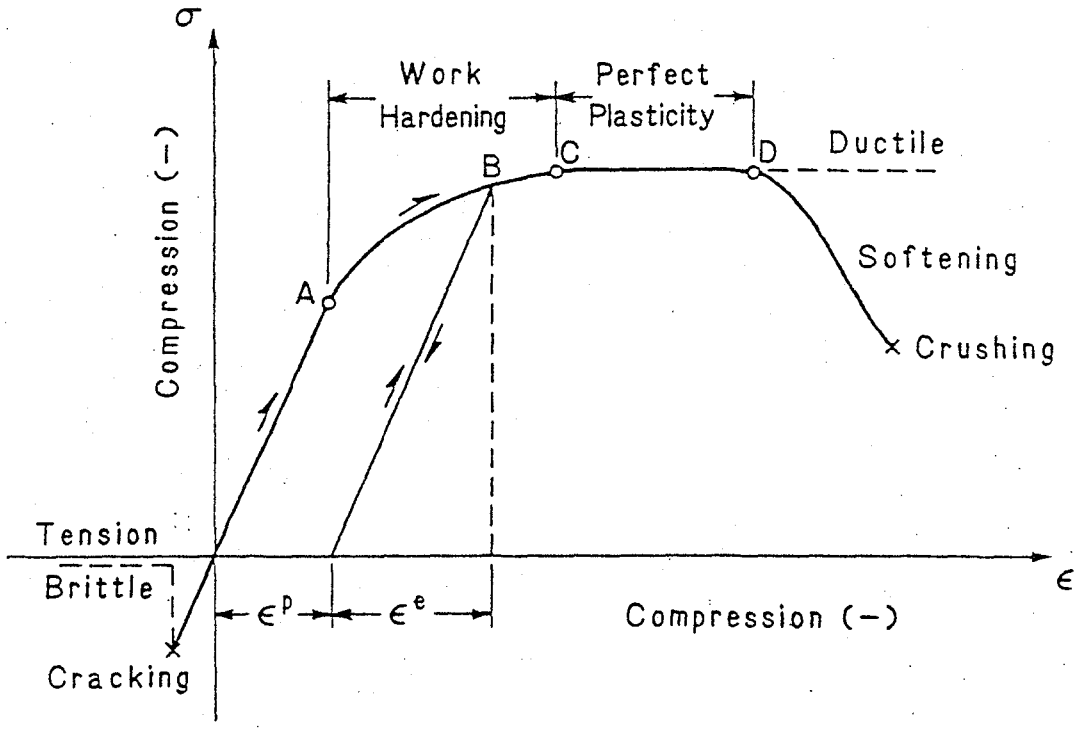

FIG. 2 SCHEMETIC UNIAXIAL STRESS-STRAIN CURVE FOR PLAIN CONCRETE

BEHAVIOUR OF SOLIDS WITH A SYSTEM OF CRACKS

DISCUSSER'S REPORT

A. EHRLACHER

LABORATOIRE DE MECANIQUE DES SOLIDES
ECOLE POLYTECHNIQUE
91128 PALAISEAU CEDEX
(France)

INTRODUCTION

The two papers dealing with "the Behaviour of Solids with a System of Cracks" cover the main fields of the matter.

The first one, "Inelastic Properties of Solids with Random Crack" of Professor Zaitsev (1983) is concerned with the quasi-static problems.

The second one, "The Mechanics of Fracture Under High-Rate Stress Loading" of Professor Grady (1983) is concerned with the dynamic problems.

Zaitsev insists on the randomness of the distribution of cracks and inhomogeneities in the solids. A difference is made between rocks and hardened cement paste which are quasi-homogeneous at the scale of the problem, and concrete which is significantly inhomogeneous.

Grady deals with four problems. In the first part he investigates the strain rate dependence of the critical traction stress of a solid. In the second part, he shows how kinetic energy considerations can predict the size of particles produced in dynamic fragmentation without reference to the initial distribution of flaws. In the third part, he looks at the dynamic fragmentation with a statistical point of view, and in the last part, he uses a damage parameter D with an appropriate rate equation to produce a continuum modelling of dynamic fracture.

First of all, let us underline the fact that concerning solids with a system of cracks the question we may have to answer are significantly different if we consider a static loading or a dynamic loading.

Let us look at the stress intensity factor K_I at the crack tip of a crack with a characteristic dimension a.

If we apply a static loading, K_I is proportionnal to $\sqrt{a}$, while if we apply a dynamic loading with a constant strain rate, for example, the stress intensity factor is independent of the crack size and proportionnal to $t^{3/2}$ for small time t in comparison with a/c_s (c_s is the shear were velocity).

Let K_{IC} be the toughness of our material. In the static case the K_I of the greatest cracks reaches K_{IC} at first and only those cracks propagate.

In the dynamic case, with a constant strain rate $\dot{\varepsilon}_0$, all the cracks with a characteristic size a greater than a certain value a_0 will have the same stress intensity factor K_I, and then a lot of cracks will reach the critical value K_{IC} and propagate at the same time, giving a fragmentation of the solid.

The value a_0 is decreasing with the strain rate as $\dot{\varepsilon}_0^{-2/3}$.

Because of these qualitatively different behaviours of the system of cracks, we shall discuss them separately.

In the first part, we shall discuss about the quasi-static problems. The dynamic problems will be discuss in the second part.

I - QUASI-STATIC PROBLEMS

Among, the quasi-static problems dealing with microcracked solids, at least three questions arise naturally.

The first one is about the influence of the presence of microcracks on the macroscopic behaviour.

The second one is about the consequences on the macroscopic behaviour of the propagation of these microcracks.

The third one is about the coalescence of microcracks which produces a macrocrack and leads to the failure of the solid.

The numerous references given in the paper of Zaitsev (1983) show that there is a lot of method to try to answer these questions, at least in the quasi-homogeneous case.

Before we discuss the Monte-Carlo method proposed by Zaitsev, we shall comment the macroscopic thermodynamical approach, and the homogenization technic which are two among the most classical ways to tackle that sort of questions.

a- Macroscopic thermodynamical approach :

It is possible to account for the macroscopic experimental results directly by the use of a set of thermodynamical internal state variables, with some of them characterizing the microstructure of the material. Then a thermodynamical potential (the free energy for example) and a dissipative pseudo-potential or rate equations satisfying thermodynamic restrictions (see, for example, Germain (1973) or Nguyen (1981)) can define the macroscopic behaviour of the material.

The difficulty of that approach is to postulate a good choice for the internal state variables and the potentials. To do that, one generally makes a simplified physical model for the microstructure. The crossing from the microlevel to the macrolevel is often done using homogenization technic.

In the case of microcracked bodies the use of damage parameters as internal variables summarizing the effects of microcracks on the macroscopic behaviour has been done extensively.

Kachanov (1958), Lemaitre (1978, 1979) or Mazars (1982) use for example a scalar damage parameter D(t) to explain the decreasing of the elastic modulus (for experimental results see, for example, Terrien (1980)).

$$E(t) = (1 - D(t))\, E_0 \qquad (1)$$

That damage parameter, the value of which increases from zero to one is physically bounded with the fraction of flaws surface in a section of the solid.

Some solution for brutal damage in elastic brittle solids where parameter D can take only two values, D = 0 for the sane material, D = 1 for the totally damaged material, has been given by Bui and al. (1980), (1981), (1983).

Shah and al (1983a), (1983b) gives a thermodynamic approach with a vectorial representation for damage to account for the planar nature of microcracks.

If we want to account for the non isotropic natures of the microcracking process, it is possible to have a tensorial representation for damage $\underline{D}(t)$, to change the initial elastic matrix $\underline{E_0}$ in the actual one $\underline{E}(t)$, (Bui, Dang Van, Stolz, (1982)).

$$\underline{E}(t) = (\underline{I} - \underline{D}(t))\, \underline{E_0} \qquad (2)$$

where $\underline{I}$ is the identity tensor.

The thermodynamic force associated with the rate of damage $\dot{D}$ is the elastic strain energy W (Lemaitre, (1978)) and then generally $\dot{D}$ is postulated as a function of W.

That approach with damage parameters is especially suitable for traction. When dealing with traction and compression, the formulation is far more complex because of the microcrack closure which can restore the initial elasticity matrix in compression.

It is then possible to use instead of damage parameters other internal state variables such as a fracturing strain (Bažant (1980)). That choice can account for the sliding of the two lips of closed microcracks.

b- Homogenization technic :

The second very classical way to look at quasi-homogeneous solids is to consider that each point at the macroscale represents a small solid at the microlevel which would be in an uniform stress state if it included no flaw or other inhomogeneity.

The size and position of flaws or inhomogeneities are characterized by a finite number of parameters at the macroscale.

The value of the fields at each point at the macroscale is the mean value of the same field at the microlevel in the volume of the microelement, there fields being characterized by a finite number of parameters.

The coherence needs some additional condition, "the localisation condition" which may be the classical Hill-Mandel condition (Mandel (1964), Hill (1967)), or a periodicity hypothesis, or other conditions (see, for example, Suquet (1982)).

Generally the use of that homogenization technic needs some hypothesis on the microstructure. For example, shall we consider only one crack in the microelement, or two interacting cracks, or more ... ?

One we have chosen our microstructure and our "localisation condition", we have to solve a finite loading parameters problem on the microelement. If we have such a solution, the mean value of the fields and the rate of the characteristic parameters give us the macroscopic behaviour.

A very good application of that technic for the microcracked bodies has been recently done by Andrieux (1983), which looked at a single cracked microstructure in plane strain and used a solution depending on two parameters

characterizing the discontinuities of displacements on the crack lips.

He deduced then the macroscopic behaviour of a microcracked body which seems to well approximate the experimental results in compression and in traction for concrete.

From the solution of two interacting cracks, it is possible to apply the same technic to a more sophisticated microstructure.

That homogenization technic is often the first stage of a macroscopic thermodynamic approach. It permits to construct a continuum modelling with a set of internal state variables at the macrolevel and their rate equations from a simple model of the microstructure, the behaviour of which is known.

Then from a given state of the solid, it is to say from a given initial field of internal variables, we can calculate the evolution of the fields for a given loading. When no more solution exists, the failure occurs.

The important point we must underline in view of Zaitsev's paper (1983) is that we must know the initial field of internal variables to know the further evolution.

In certain problems, such as plasticity problems for example, the initial value of internal variables is, to a certain extent , of little importance, and can be given the value zero.

On the contrary, when dealing with microcracked bodies, it is generally not possible to hypothesize that the initial distribution of flaws is zero, and that initial distribution is of the greatest importance since the damage concentrates in the weakest zone.

We must then account for the initial random distribution of flaws or internal variables in the case of a continuum modelling.

c- *The Monte-Carlo method* :

Zaitsev chooses to investigate the influence of the initial random distribution of flaws in a quite interesting manner.

He numerically simulates the evolution of a system of microstructures, the behaviour of which is known.

Dealing with different problems, he chooses different microstructures with different behaviour, as in his figures (7, 17, 23) (Zaitsev (1983)).

Each microstructure being characterized by a finite number of parameters, he chooses some statistical laws for the initial value of these parameters, and he generates a random macrostructure with the help of a computer.

The behaviour of each microstructure being well known, he can simulate a loading and compare the results for different initial distributions of flaws and experimental data.

His first simulation (Zaitsev (1980), Zaitsev and Wittmann (1981)) is done with cracks, the center, the length, and the orientation of which being statistically uniformly distributed, and he considers the interaction between two neighbouring cracks.

His second simulation Zaitsev (1981), Wittmann and Zaitsev (1981) has been done with a microstructure made with pores and cracks. Each pore has two coplanar preexisting cracks. The position, length and orientation of the microstructure is statistically uniformly distributed.

Then he made simulations with circular inclusions with one preexisting interfacial crack and preexisting cracks in the matrix, another simulation for concret with polygonal inclusions with one preexisting bond crack and for hightweight concrete he made a simulation with round inclusions and small pores.

For each simulation the calculation gives the global $\sigma - \varepsilon$ curve and the macrocrack loading to the failure of the sample.

Let us notice that he does not use a continuum modelling of his microcracked sample because he generates directly some microstructure, but there is no essential difference with a random generation of initial internal variables values through a finite element method for a continuum modelling.

In both cases the Monte-Carlo method provides an efficient tool to study the qualitative response of a sample to a certain loading, the influence of the parameters of the random distribution, and a global statistical characterization of the behaviour of the sample.

But, before answering these questions we must determine how many microstructure or finite elements are needed to have significant results (Zaitsev (1983) chooses 50 microelements) and how many numerical simulations are sufficient to deduce statistically satisfying results (Zaitsev (1983) makes twenty realisations of the Monte-Carlo method to deduce the results of his figure 19).

Then the influence of the parameters of the random distribution may be quite easily simulated, while a statistical characterization of the global behaviour is not a simple question and we have a quite similar problem when we want to deduce the behaviour of a material from experimental data.

Nevertheless that method is very efficient since it can be adapted to a lot of problems simply by changing the microelement or the interaction between microelements as it can be seen in the Zaitsev's paper (1983).

Especially that method can be used to give a probabilistic response to the problem of determining the risk of failure of a complex structure submitted to a complex quasi-static loading.

II- DYNAMIC PROBLEMS

We have already underlined the fact that while under a static loading only one or a few macrocracks appear in the solid, with a dynamic loading all the microcracks the length of which is upper than a certain size a_0 can propagate, leading to the dynamic fragmentation of the solid (a_0 is decreasing with the strain rate as $\dot{\varepsilon}_0^{-2/3}$).

a- Dynamic stress intensity factor :

The dynamic stress intensity factors for a single crack has been extensively studied in a lot of paper among which we can mention, De Hoop (1958), Craggs (1963), Broberg (1960), Baker (1962), Cotterel (1964), Eshelby (1969), Achenbach (1970), Achenbach and Nuismer (1971), Glennie and Willis (1971), Chen and Sih (1973), Bui (1978), and especially Kostrov (1966), (1975) and Freund (1972a), (1972b), (1973), (1974).

Atkinson and Eshelby (1968), Kostrov and Nikitin (1970), Freund (1972) and Bui, Ehrlacher and Nguyen (1980) have studied the problems bounded with the energy release rate at the crack tip.

From these works we can deduce, in the single case of a non propagating crack and for small time in comparison with a/c_s (where a is the crack length and c_s the shear wave velocity) that, for constant strain rate loading, the stress intensity factor at the crack tip is independent of the crack-size and dependent with time as $t^{3/2}$ (Kipp and al (1980)).

If we hypothesize that the crack tip will propagate as soon as the stress intensity factor will reach the critical value K_{IC}, we can deduce the fracture time and the strain rate dependent fracture stress as $\dot{\varepsilon}_0^{1/3}$.

Grady hypothesizes that for a system of crack under constant strain rate loading all the cracks the length of which is sufficiently high behave in the same way, and he deduces the general strain rate dependence of the fracture stress as $\dot{\varepsilon}_0^{1/3}$ for the sufficiently flawed material (that seems not to be the case for Solenhofen Limestone (Grady and Lipkin (1980)).

Then he demonstrates that other classical dynamic fracture criteria such as those of Tuler and Butcher, Birkimer, Steverding and Lehnigk or even Von Rittinger give similar results.

b- The fragment size :

In view of applications the most important question is to determine the fragment size occuring in the dynamic fracture process.

There are three ways to approach the average fragment size d.

The simplest one is a relation between the fragment size and the number of activated cracks. If we note N the number of activated cracks per unit volume, the fragment size d is of order $N^{-1/3}$.

If we recall the order of the characteristic size of the activated cracks given by Grady.

$$a_0 \sim (c_s K_{IC} / E \dot{\varepsilon}_0)^{2/3} \qquad (3)$$

and if we hypothesize that the number of cracks per unit volume, the size of which is upper than a_0 is of order :

$$N(a_0) \sim \alpha / a_0^3 \qquad (4)$$

where α is a non dimensional parameter, we find that the fragment size d would be of the order of :

$$d \sim \alpha^{-1/3} a_0 \sim \alpha^{-1/3} (c_s K_{IC} / E \dot{\varepsilon}_0)^{2/3} \qquad (5)$$

The second way to approach the fragment size is to consider the strain energy stored in the solid before the fragmentation occurs.

When the cracks propagate, that strain energy is transformed in surface energy for one part and in kinetic energy for the other part. It is well known that more rapid is the crack propagation, more important is the second part.

For example, if we consider a single cracked body under a static loading. If the crack does not propagate, there is a static energy release

rate G^{stat} which characterizes the fields near the crack tip. If suddenly the crack propagates at speed $\dot{a}$, then the energy release rate is

$$G = g_I(\dot{a}) \cdot G^{stat} \qquad (6)$$

where $g_I(\dot{a})$ is a universal function of the crack tip velocity decreasing from one to zero when $\dot{a}$ increases from zero to the Rayleigh wave velocity C_R. (Atkinson and Eshelby (1968), Kostrov and Nikitin (1970), Freund (1972), Ehrlacher (1980)).

The function $g_I(\dot{a})$ can be analyticaly written in a complicated manner, but is very well approximated by the linear function

$$G_I(\dot{a}) \approx 1 - \dot{a}/C_R \qquad (7)$$

Then, $\dot{a}\ g_I(\dot{a})\ G^{stat}$ is the rate of the dissipated energy through the crack tip propagation and $\dot{a}(1 - g_I(\dot{a}))\ G^{stat}$ is the rate of transformation of strain energy in kinetic energy.

As, in general, during fragmentation process, the velocity of the crack tips are of the order of the Rayleigh wave velocity ($\dot{a}/C_R \sim 0.6 - 0.7$) the most important part of the strain energy is transformed in kinetic energy.

Then the fragment size is not of order of $(K_{IC}/\sigma_c)^2$ as an energy balance neglecting the kinetic energy would have suggested, but is one or more order of magnitude greater.

That point is reinforced by the fact that the energy needed to create a new surface is not constant but seems to be an increasing function of the crack tip velocity because the dissipative mechanisms are more complex for rapid cracks.

On the contrary kinetic energy considerations instead of strain energy considerations give quite interesting and applicable results (Grady (1983)). The order of fragment size which can be deduced (equation 19 of Grady (1983)) shows the same dependence in tenacity K_{IC} and strain rate $\dot{\varepsilon}_0$ as in the flaws distribution approach.

As it can be seen on figure 3 of Grady (1983), the experimental data seem to be well predicted by a strain rate dependence as $\dot{\varepsilon}_0^{-2/3}$.

c- *Continuum modelling approach* :

From the work of Davison and Stevens (1973) the continuum modelling approach for dynamic fragmentation seems to be an interesting way.

Grady's paper (1983) shows very well the variety of the continuum modelling approach through numerous references.

The model proposed by Grady and Kipp uses a classical scalar damage parameter D with an appropriate rate equation deduced from physical considerations on statistical concepts.

The comparison of his figures (6.a) and (6.b) (Grady (1983)) shows very well how effective such a direct continuum approach can be with the use of a wave propagation code.

Those types of continuum modelling give a good approximation of the shape of the boundary between the sane zone and the fragmentation zone, and a good agreement between the value of the calculated damage parameters in the fracture zone and the experimental measures of the fragment size.

Perhaps can we hope that a continuum modelling will describe, through a good choice of internal state variables and rate equations, the statistical nature of the fragment size at each point at the macroscale.

CONCLUSION

The quasi-static and the dynamic behaviour of a microcracked solid is quite different, since in the static case only the more susceptible microcracks can propagate and coalesce to induce the failure of the solid in two or a few pieces, while in the dynamic case a lot of microcracks propagate at the same time inducing the fragmentation of the solid.

In the quasi-static case the behaviour of the solid is very sensitive to the initial distribution of flaws and then the Monte-Carlo method proposed by Zaitsev is a very powerful tool to compare the experimental results to numerical simulations, and to predict the risk of failure of a complex structure under complex loading.

When dealing with dynamic problems the initial distribution and size of flaws may be important to predict the fragment size in the failed material, but the Grady's approach from the kinetic energy point of view can give quite predictive results without referring to that initial distribution.

In both static and dynamic loadings, it seems that a continuum modelling with the help of damage parameters and appropriate rate equations can provide a relatively simple and quite efficient tool in view of applications.

REFERENCES

Achenbach J.D., (1970), Z.A.M.P. 21, 887-900.

Achenbach J.D. and Nuismer R., (1971), Int. J. Fract. Mech., 23.6, 969-976.

Andrieux S., (1983), Thesis, Ecole Nationale des Ponts et Chaussées, Paris.

Atkinson C. and Eshelby J.D., (1968), Int. J. Fract. Mech., 4, 3-8.

Baker B.R., (1962), J. Appl. Mech. 29, 449-458.

Bažant Z.P., (1980), J. of Eng. Mech. Div., Prof. of the ASCF, V. 106.

Broberg K.B., (1960), Arkiv för Fisik, 18, 159-192.

Bui H.D., (1978), Mécanique de la Rupture Fragile, Masson, Paris.

Bui H.D., Dang Van K., Stolz C., (1981), C.R.A.S., 292, série II, p. 251.

Bui H.D., Dang Van K., Stolz C., (1982), C.R.A.S., 294, série II, p. 1155.

Bui H.D., Ehrlacher A., (1980), Int. Conf. on Fracture, ICF 5, Cannes, vol. 2, pp. 533-553.

Bui H.D., Ehrlacher A., Nguyen Q.S., (1980), J. de Mécanique, 19, 697-723.

Bui H.D., Ehrlacher A., Renard C., (1983), Cong. Franç. de Méca., Lyon.

Chen E.P. and Sih G.C., (1973), Int. J. Solids Struc., 9, 897-919.

Cotterel B., (1964), J. Appl. Mech., 31, 177-199.

Craggs J.W., (1963), Fracture of Solids, D.C. Drucker and J. Gilman (Ed.), Wiley, New York.

Davison L. and Stevens A., (1973), J. Appl. Phys., 44, 588-672.

De Hoop A.I., (1958), Doctoral dissertation, Technische Hogeschool, Delft.

Ehrlacher A., (1980), Int. Conf. on Fracture, ICF 5, Cannes.

Eshelby J.D., (1969), J.M.Ø.S., 17, 177-199.

Freund L.B., (1972), J. of Elasticity, 2, 341-349.

Freund L.B., (1972a), J.M.Ø.S., 20, 129-140.

Freund L.B., (1972b), J.M.Ø.S., 20, 141-152.

Freund L.B., (1973), J.M.Ø.S., 21, 47-61.

Freund L.B., (1974), J.M.Ø.S., 22, 137-146.

Germain P., (1973), Cours de Mécanique des Milieux Continus, Masson, Paris.

Glennie E.B. and Willis J.R., (1971), J.M.Ø.S., 19, 11-30.

Grady D.E., (1983), IUTAM Prager Symposium on Mechanics of Geomaterials : Rocks, Concretes, Soils, Northwestern University, Evanston.

Grady D.E. and Lipkin J., (1980), Geophys. Res. Letters 7, 255-258.

Hill R., (1967), J.M.Ø.S., 15, p. 79.

Kachanov LM (1958), Inv. Ak. N.S.S.R. 8, p. 26.

Kipp M.E., Grady D.E., Chen E.P., (1980), Int. J. Fract., 16, 471-478.

Kostrov B.V., (1966), P.M.M. 30, 6, 1042-1049.

Kostrov B.V., (1975), Int. J. Fract., 11, 47-56.

Kostrov B.V., Nikitin L.V., (1970), Arch. Mech. Stos. 22, 749-776.

Lemaitre J., Chaboche J.L., (1978), J. Mécan. Appl., 2, n° 3, p. 317.

Lemaitre J., Cordebois J.P., Dufailly J., (1979), C.R.A.S., 288, série B, 391.

Mandel J., (1966), Proc. 11th Int. Cong. Appl. Mech., Munich, p. 502.

Mazors J., Lemaitre J., (1982), Annales I.T.B.T.P., n° 401.

Nguyen Q.S., (1981), IUTAM Symp. on "3 dim. Const. Rel. and Ductile Fracture", North-Hall. Pub., 315-330.

Shah S.P., Suaris W., (1983a), A.S.C.E.-EMD, Spec. Conf., Purdue Univ.

Shah S.P., Suaris W., (1983b), SMIRT 7 Conf. Chicago.

Suquet P., (1982), Thesis, Univ. P. et M. Curie, Paris.

Terrien M., (1980), Bul. de Liaison L.C.P.C., Vol. 105.

Wittmann F.H., Zaitsev Y.V. (1981), Int. Conf. on Fract., ICF 5, Cannes.

Zaitsev Y.V., (1980), Proc. 7th Int. Conf. on Chemistry of Cement, IV, 176-180.

Zaitsev Y.V., (1981), Int. Conf. on Fract., ICF 5, Cannes.

Zaitsev Y.V., (1983), IUTAM Prager Symp. on Mechanics of Geomaterials : Rocks, Concretes, Soils, Northwestern University, Evanston.

Zaitsev Y.V., Wittmann F.H., (1981), Matériaux et Constructions, vol. 14, pp. 357-365.

FRACTURE PROPAGATION AND FRACTURE ENERGY*

by

Michael P. Cleary, Department of Mechanical Engineering

Massachusetts Institute of Technology
Cambridge, Massachusetts 02139

*(Discussers Report for the IUTAM William Prager Symposium on Mechanics of Geomaterials, Sept.1983)

SUMMARY

The discussion in this paper is divided into four main combinations of categories:

1.1 Phenomenology and observations of fracture in the microscale.

1.2 Modelling of (brittle) fracture processes on the microscale.

2.1 Experimental investigation of fracture on the macroscale.

2.2 Analysis of (brittle) fracture for testing and structural design.

A brief review is given of representative research and development in each of these areas, with particular emphasis on the relation to perceived reality. Major unresolved problems are posed for future investigation.

INTRODUCTION AND BACKGROUND

An understanding of fracture is essential to the whole spectum of human fabrication activities, and has finally gained its rightful role in engineering research and development over the past three decades or so. The essential ingredients in fracture mechanics of materials are:

A. A detailed knowledge of the stress distribution in the body of interest, at all scales of interest - often divided into micro and macro for convenience of reference, although scales obviously merge into each other asymptotically.

B. A reliable estimate of the material response to the local stress level at any point, including the effects of temperature and stress history; especially, conditions for rupture instability (which may have to be viewed as non-local) must be well determined.

The central aspects of these ingredients are the constitutive relations for unruptured response of the materials (for any relevant loading history) and adequate criteria for the onset and propagation of rupture processes - which we comprehensively refer to as fracture. The most common parameters employed are the (perhaps incremental) material moduli for stress analysis and the fracture energy required to grow the rupture; the former have attracted considerable theoretical and experimental attention in solid mechanics for many decades (especially from the group spearheaded by William Prager, as other contributions in this Symposium Proceedings will attest) but detailed resolution of the issues involved in fracture growth/direction criteria has been slower, despite intense scrutiny over the past decade especially (e.g. Liebowitz, 1968- , Erdogan, 1976).

A major cause of this contrast is certainly the additional geometry-dependence (non-local) character of the fracture process, which tends to produce a greater variety of phenomenology and especially a strong size-effect in the response of a material sample. Although this size-effect has also been more recently realized to haunt the development of adequate constitutive relations for materials with hierarchies of microstructure (especially "natural" materials such as rock, cement, concrete and perhaps even ceramics), as aqainst more homogeneous processed materials which have been solidified from a uniform (liquid) melt, it has its source of aggravation mainly in fracture-related processes: moduli dependence on scale is more readily incorporated in analyses and design.

It is thus appropriate for us to concentrate especially on the mechanics of fracture, since the major complexities of materials response must be implicitly embedded in any such study: if intrinsic materials behavior is integrated with the presence or development of rupture processes, we should be able to deduce the overall (so-called microscale) material response - which can then be embedded in a larger-scale (so-called macroscopic) structural analysis, perhaps including the presence of a fracture which has evolved from linkage of the small-scale ruptures. This logic is the motivation for the sequence of sub-division presented next.

1.1 PHENOMENOLOGY AND OBSERVATIONS OF FRACTURE ON THE MICROSCALE

The process involved here can be very complex but, essentially, they require some nuclei at which initiation and growth can take place. These can be stress concentration points (e.g. granular/asperity contact), inclusions such as hard or soft second phases, dislocation pile-up sites, or just weak grain-boundaries in polycrystals. Many reviews have been done on the melt-processed construction materials (e.g. Chalmers et al., 1954-) but much less has been done on the more "natural" materials. The reasons for this may be found in the more complex and precise requirements of the expensive melt-processed materials (metals, polymers and composites): they must withstand all conceivable states of loading, including cycles of temperature and stress (which can ratchet eventual fatigue in even the toughest materials) whereas the "natural" materials have had lower imposed expectations - and fail even these in all too many circumstances! Cracked pavements, mine roof falls and earthquake-proof conventional buildings illustrate the poor structural response of such solid-bonded compositions, so they are rightly the focus of much recent work, described by Bazant(1983) for instance.

The most basic problem with materials produced by solid mixing and bonding (albeit with some chemical reactions in the cementing process) is that they typically contain intrinsic flaws (e.g. pores and cracks) and other sources of stress concentration (e.g. asperity contacts). The cementing bond can also be quite weak, but some researchers (e.g.Birchall and Kelly, 1983) claim dramatic increases in strength and toughness, even up to levels comparable with melt-processed materials, when intrinsic flaws are removed. In any case, the presence of inhomogeneity sites is clearly

central and it presents two major aspects for study:

a) How do we determine the response (and hence the strength/toughness reduction) associated with any particular/generic site?

b) How do we characterize the distribution and interaction of such sites?

Experimental evidence to resolve these questions is not very abundant, especially on details of response around inhomogeneity sites. Some deductions can be made from macroscopically-observed crack patterns (e.g. Jaegar and Cook, 1979) and more detailed electron microscopy studies have been conducted by others (e.g. Tapponier & Brace, 1976) for nominally macroscopically homogeneous stressing conditions. Actually, of course, it is well known that stresses are not uniform in testing of samples with conventional apparatus and thus the interpretations assigned can be quite misleading; in the Resource Extraction Laboratory at MIT we have been developing various techniques to achieve more uniform conditions and have especially done extensive testing (plus electron microscopy studies) on a technique called pore-pressure-induced-cracking (PPIC), in which the porous sample has internal pressure higher than confining stress-hence a tensile effective stress (which governs rupture onset). This technique, combined with detailed analysis of pore-fluid diffusions, promises to allow a detailed study of microcrack onset and population evolution for the first time(e.g.Hess, 1983).

The formation of a linked-up macroscopic fracture, and the associated development of crack patterns, have been observed by some researchers (e.g. Hoagland et al, 1973), and an attempt has been made to relate these processes to the observed macroscopic crack growth (Ingraffea, 1983 and overall reviews by Argon, 1982 and Bazant, 1983). However, although broad features seem consistent, there are serious shortcomings in the level of associated prediction:

1.2 ANALYSIS OF FRACTURE PROCESSES ON THE MICROSCALE

Two major questions have been posed for experimental and theoretical analysis hopefully toward more general predictions, without the need for as much experimentation, in the future.

The first question has been chiefly regarded as a study in classical solid mechanics: the site is identified as a pore or crack or asperity in an otherwise homogeneous region and the isolated effect is worked out, using an estimated tensile strength or critical stress-intensity factor to decide on initiation/propagation of a crack from the nucleating site. Indeed, various estimates of strength reduction have been worked out, with some success (e.g. McClintock and Argon, 1968; Sikarsie, 1973), on the basis of this approach and size-effects (e.g. strength varying as sample size to a power between 0.5 and 1.0) seem to support such mechanisms as brittle cracking and effective dislocation pile-ups.

The second question has generated a greater variety of approaches. Chief among these as been a smearing out of the influence created by surrounding sites, best represented by the "self-consistent" technique (e.g. Cleary, Chen and Lee, 1980); the technique can be made arbitrarily precise in principle, but is practically limited by the few available solutions for interaction between sites: special cases like two spheres are available, but an infinite 3-D array would be more useful (e.g. as used by Barr and Cleary, 1982, for a 2-D array of surface cracks in the context of thermal or shrinkage cracking, see also Bazant, 1983). Actually, our computer programs are now reaching the stage (e.g. Narendran and Cleary, 1982) where quite complex arrays of growing cracks can be studied and are are being compared with experimental patterns observed in the

laboratory (see also Sec. 2.2 later). Thus, techniques are becoming available to correctly analyse the response of a continuum element containing a representative distribution of microcracks, if such a model (e.g. Kachanov,1982) is useful, e.g. up to the onset of site/crack coalescence and macroscopic rupture formation.

A complementary approach, also needed to decide on onset of fracture at any particular site, is to assign a statistical distribution of strength to various well-defined site locations, such as grain-boundaries (e.g. McClintock and Mayson, 1976). Then, by using many available techniques such as dipole dislocation representations of each cracking event, the stress-field can be computed at each instant/load and the crack pattern can evolve in a combined deterministic/stochastic fashion. Results of this method in 3-D are still to be obtained (McClintock, private comm.,1983) but the expectation seems to have the right trend in helping to explain size-effects as due to (statistical) sample size as well as micro-fracture mechanics, which Bazant(1983) seems to regard as exclusively rationalising the observed data for concrete.

2.1 EXPERIMENTAL INVESTIGATION OF FRACTURE ON THE MACROSCALE

The essential features of this activity are:

a) Choice of a suitable geometry for crack growth observations
b) Analysis of stress distributions for the chosen geometry
c) Determination/classification of conditions for fracture onset and growth
d) Relation of observations to mechanisms operative on the microscale

Many possible choices have evolved for specimen geometry; these are summarized in Ingraffea(1983) and Ouchterlony(1982), but we should add some others that we have found useful in the Resource Extraction Laboratory at MIT. A diametrally-loaded core ("Brazilian" test, Jaegar and Cook, 1979) can be modified to include a diametral crack of various lengths - cast into

artificial specimens or cut from a central hole in rock cores. This loading is simpler to apply than the internal pressure in the notched annular core (NAC), and may have more potential under confining pressure, but it does not have the desirable insensitivity to crack length in deducing toughness from the critical load at which unstable crack growth sets in.

A common attribute of these samples is the facility for stress analysis and deduction of some appropriate crack-tip-loading parameter. Extensive lists of solutions exist in the literature (e.g. Ouchterlony,1982) for linear isotropic materials response and may anisotropic nonlinear analyses are also being conducted (e.g. Cleary and Miller, 1983 for the NAC and the compact tensile specimen used extensively by us, Switchenko and Cleary, 1979). Great attention must be paid to ensure that the crack near tip stress field is not influenced in character by the boundaries, and then its amplitude (expressed as stress-intensity factor K or energy-release-rate J) can be regarded as critical in deciding fracture onset or growth for other geometries where the same near-tip field applies-hence the name fracture toughness testing.

2.2 ANALYSIS OF (BRITTLE) FRACTURE GROWTH IN TYPICAL STRUCTURES

The essence of such analysis are two distinct features:

a) Determination of the stress distribution in the (cracked) structure.

b) Evaluation/imposition of an appropriate criterion for fracture onset.

Both aspects have produced a variety of approaches, some of which are discussed by Ingraffea(1983). It may be worth summarizing the major methodologies here.

a. Two separate approaches have developed, one based on the Finite Element Method (e.g. Rice, 1981) and another on the so-called Boundary Integral Method (e.g. Ingraffea, 1983). The BIM has the advantage of requiring discretion only along boundaries, but is practically limited to linear/isotropic response of simple regions; whereas the FEM allows

arbitrary nonlinearity and severe inhomogeneity, but requires a volume discretisation and complete remeshing for any charge of boundaries. To avoid the weakness of either method, we have combined the two techniques (Annigeri and Cleary, 1983) to get a most effective scheme for analysis of fractures growing through structures (as against stationary dracks for which FEM may be the best approach, Cleary and Miller, 1983): we have modified the conventional BIM to a Surface Integral Equation, allowing more natural representation of growing cracks and their near-tip singularities, without extensive remeching, and we have interfaced with FEM - which naturally picks up all nonlinearity and inhomogeneity (including boundaries). Available general 2-D analysis codes (e.g. Narendran and Cleary, 1983) are now being extended to 3-D fracture problems (e.g. Cleary, Kavvadas and Lam, 1983).

b. The criteria for brittle crack growth seem now to be conventionally accepted as that of a critical value for the opening stress-intensity-factor K_I at onset of propagation and that of $K_{II} = 0$ for the direction of incremental growth. We have used these criteria successfully to trace the growth of fractures observed in our laboratory apparatus (e.g. Papadopoulos, Narendran and Cleary, 1983). Other criteria for directions have been proposed (such as maximum strain-energy density and maximum energy release rate J for a probe in the new direction of growth), but these seem to often give quite similar results (e.g. Ingraffea, 1983). When the near-crack-tip stress field is no longer $1/\sqrt{r}$, then a more general J criterion must be used and even that will break down if the near-tip field has interference from boundaries or other mechanisms set in (such as slip-bands in large-scale yielding of ductile materials); such considerations are now the main concern of the extensive research effort in elastic-plactic fracture mechanics(e.g. Rice, 1981), which may require much more adaptation for application to fracture of "natural" materials.

References

Annigeri, B., and M.P. Cleary, (1982)"Surface Integral Finite Element Hybrid (SIFEH) Method for Fracture Mechanics", in Reports of Research in Mechanics and Materials, Dept. of Mech. Eng., MIT, REL-82-21.(see also MIT, Ph.D. Thesis "Surface Integral Finite Element Hybrid Method for Localized Problems in Continuum Mechanics", by B. Annigeri, expect Fall 1983)

Argon, A.S.,"Fracture in Compression of Brittle Solids" report of Committee of the National Materials Advisory Board. National Academy of Sciences, sponsored by DOD/NASA, contract No. MDA 903-78-C-0038, 1982.

Bazant,Z., "Fracture in Concrete and Reinforced Concrete", Proc. William Prager Symposium on Mechanics of Geomaterials, Wiley & Sons, Sept. 1983.

Birchall, J.D. and A.Kelly, "New Organic Materials", Scientific American Vol. 245, No.5, pp 104-115, May 1983.

Chalmer, B., J.W. Christian and T.B. Massalski,"Progress in Materials Science", An International Review Journal, 1954.

Cleary,M.P., "Applications of Rock Fracture Mechanics", at the Symposium on Fracture Mechanics, Sendai, Japan, Nov.1982.

Cleary, M.P., "Modelling and Development of Hydraulic Fracturing Mechanics", in Rock Fracture Mechanics (ed. H.P. Rossmanith),Springer-Verlag, Udine, 1982-83.

Cleary M.P., I.W. Chen and S.M. Lee, "Self-Consistent Techniques for Heterogeneous Media",ASCE, 106, EM5, 1980.(Also see articles by M.M. Carroll and G. Dvorak)

Cleary M.P., Michael Kavvadas, and K.Y.Lam, "Development of a Fully Three-Dimensional Simulator for Analysis and Design of Hydraulic Fracturing", Paper No. SPE/DOE 11631, presented at Symposium on Low Permeability, Denver, March 1983.

Cleary, M.P., "Elastic and dynamic response regions of fluid-impregnated solids with diverse miscrostructures", Intl. J. Solids and Structures, 14, 795-819, 1978.

Cleary, M.P. and B. Miller, "Finite Element Analysis for Fracture Toughness Testing", in Journal of Eng. Mechanics, June 1983.

Erdogan, F.,(ed.) Fracture Mechanics, published by ASME, 1976.

Hoagland, R.G.,G.T.Hahn and A.R. Rosenfield, "Influence of Microstructure on Fracture Propagation in Rock", in Rock Mechanics, 5, 77-106, 1973.

Ingraffea, A.R., "Fracture Propagation in Rock", Proc. William Prager Symposium on Mechanics of Geomaterials, Wiley & Sons, Sept. 1983 (see also contribution, (Springer-Verlag)"Numerical Modelling of Fracture Propagation" in Rock Fracture Mechanics, ed. H.P. Rossmanith).

Jaegar and N.Cook,"Fundamentals of Rock Mechanics",1979.

Kachanov, M.L., "Continuum Model of Medium with Cracks", Special issue of the Jounral of the Engineering Mech. Div. of ASCE, Mechanics of Heterogeneous Media, May 1980.

Liebowitz, H.(ed.) Treatise on "Fracture", Academic Press, 1968.

McClintock, F.A. and A.S. Argon, "Mechanical Behavior of Materials", Addison-Wesley, 1968.

McClintock, F.A. and H. Mayson, "Principal stress effects on brittle crack statistics", in "The Effects of Voids on Material Deformation", ed. S.C. Cowin and M.M. Carrol) pp. 31-45, ASME, New York, 1976.

Narendran, V.M. and M.P. Cleary, "Analysis of Growth and Interaction of Multiple Hydraulic Fractures", in Reports of Research in Mechanics and Materials, Dept. of Mech. Eng., MIT, REL-82-11, Nov. 1982.(also Paper No. 12272, to be presented at SPE Reservoir Simulation Symposium, San Francisco Nov. 1983).

Ouchterlony, F., "Review of Fracture Toughness Testing Rock", Stockholm Sweden, Sweden Detonic Res. Found., 1982.

Papadopoulos, J.M., V.M. Narendran and M.P. Cleary, "Laboratory Simulations of Hydraulic Fracturing", Paper No. SPE/DOE 11618, presented at Symposium on Low Permeability, Denver, March 1983.

Rice, James R., "Elastic-Plastic Crack Growth", in the Rodney Hill 60th Volume, (ed. H.G. Hopkins and M.J. Sewell) May 1981.

Sikarsie, D.(ed.), "Rock Mechanics Symposium", ASME, 1973.

Switchenko, P.M. and M.P. Cleary, "The Thermomechanical Response of Oil Shale", in Reports of Research in Mech. and Materials, Dept. of Mech.Eng., MIT, Aug. 1979. (NSF Report #ENG-77-18988-1).

Tapponier, P. and W.F. Brace, "Development of Stress-Induced Microcracks in Westerley Granite", Intl. Jour. Rock Mech.Min. Sci., Vol. 13, pp 103-112, 1976.

PART 3

CONTRIBUTED PAPERS

CONSTITUTIVE EQUATIONS FOR CONCRETE UNDER PLANE STRESS CONDITIONS

Koichi MAEKAWA
Assistant Lecturer of Civil Engineering
Technological University of Nagaoka
Niigata, Japan

Hajime OKAMURA
Professor of Civil Engineering
University of Tokyo
Tokyo, Japan

1. Equivalent Stress - Strain Relationship

In case of concrete under plane stress conditions, there exists an elastic zone on a stress space or a strain space, where the stress or the strain is very small. When strained beyond the boundary of the elastic zone, additional irreversible deformation occurs and the elastic zone expands correspondingly (See Fig.1.). A subsequent elastic zone is developed even in the strain softening conditions. Within this newly developed elastic zone, we found the linear relationship between the equivalent stress S and the equivalent elastic strain Ee as

$$S = Eo\ K\ Ee \tag{1}$$

where Eo is a constant corresponding to the initial stiffness and K is the ratio of linear elastic stiffness to the initial one. The equivalent stress and the equivalent elastic strain is defined as

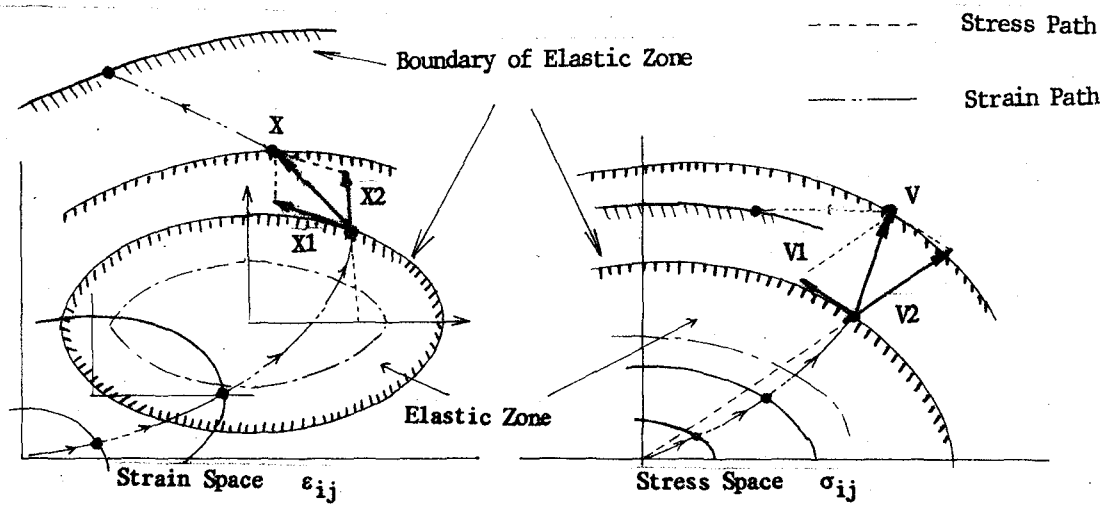

Fig. 1 Elastic Zones on Stress and Strain Spaces

$$S = \sqrt{\left(\frac{0.60\,\sigma_o}{fc}\right)^2 + \left(\frac{1.30\,\tau_o}{fc}\right)^2} \qquad Ee = \sqrt{\left(\frac{0.62\,\varepsilon_o}{\varepsilon_{oo}}\right)^2 + \left(\frac{0.98\,\gamma_o}{\varepsilon_{oo}}\right)^2}$$

$$\sigma_o = \sqrt{2}\,\frac{\sigma_{xx} + \sigma_{yy}}{2} \qquad \varepsilon_o = \sqrt{2}\,\frac{\varepsilon_{exx} + \varepsilon_{eyy}}{2}$$

$$\tau_o = \sqrt{2\left(\left(\frac{\sigma_{xx} - \sigma_{yy}}{2}\right)^2 + \sigma_{xy}^2\right)} \qquad \gamma_o = \sqrt{2\left(\left(\frac{\varepsilon_{exx} - \varepsilon_{eyy}}{2}\right)^2 + \varepsilon_{exy}^2\right)}$$

(2) (3)

where fc is the uniaxial compressive strain and ε_{oo} is the corresponding compressive strain.

Then the boundary should be defined as Ee equal to Eemax and the corresponding equivalent stress Smax shall be

$$Smax = Eo\ K\ Eemax \tag{4}$$

In the plastic theory, K is considered constant and the relation between the both boundaries on the stress and strain spaces is unchanged. However, in case of concrete, K is not constant and from the experimental results of biaxial unloading paths, we have found the K values shall be calculated by

$$K = \exp(-0.73Emax(1-\exp(-1.25Emax)))$$

$$E = \int \frac{\partial Ee}{\partial \varepsilon_{eij}}\, d\varepsilon_{ij} \tag{5}$$

as shown in Fig.2, where E is a strain path-dependent index E called as the total equivalent strain. This nonlinearity is because the local buckling due to the extension of microcrackings and disappearance of some volume in which the strain energy is reserved. The parameter K expresses this behavior and accordingly we call this parameter as a fracture parameter.

When the subsequent elastic zone is expanded, it also moves on the strain space according to the kinematic shift of plastic strains. The effective plastic strain defined as

$$\varepsilon_{pls} = \int \sqrt{d\varepsilon_{pij}\ d\varepsilon_{pij}} \tag{6}$$

cannot be applied for concrete under compression - tension stress state as shown in Fig.3. We have newly introduced the equivalent plastic strain Ep representing the shift of the elastic zone on the strain space. We formulated Ep as the function of the total equivalent strain

$$Ep = \int \frac{\partial Ee}{\partial \varepsilon_{eij}}\, d\varepsilon_{pij} \qquad E = Ee + Ep$$

$$Ep = Emax - \frac{20}{7}(1-\exp(-0.35Emax)) \tag{7}$$

based on the test results shown in Fig.2.

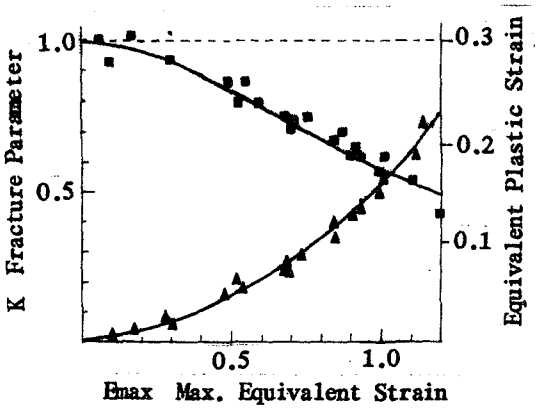

Fig.2 Fracture Parameter and Equivalent Plastic Strain

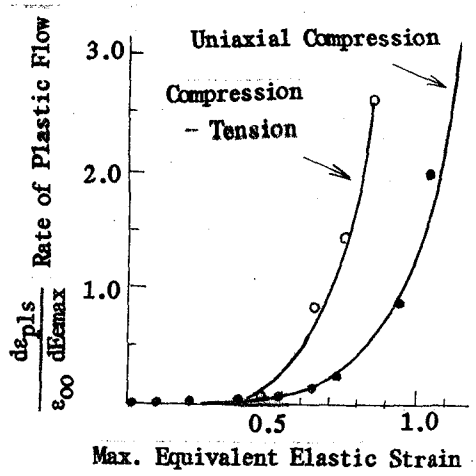

Fig.3 Effective Strain in the Plastic Theory

2. Flow Rule

In completing the system of constitutive equations, it is required to formulate the directional correlation between the stress and strain invariant vectors and the principal stress direction under an arbitrary strain path. Within the elastic zone, the directional relationship can be assumed isotropic and symmetric as

$$\begin{bmatrix} \varepsilon_o \\ \gamma_o \end{bmatrix} = \frac{1}{E^*} \begin{bmatrix} 1-\nu & 0 \\ 0 & 1+\nu \end{bmatrix} \begin{bmatrix} \sigma_o \\ \tau_o \end{bmatrix} \qquad E^* : \text{Proprotional coefficient} \tag{8}$$

The Poisson's ratio was experimentally obtained as shown in Fig.4. When the strain moves within the elastic zone, two stress invariants can be obtained by solving Eq.1 and Eq.8 simultaneously.

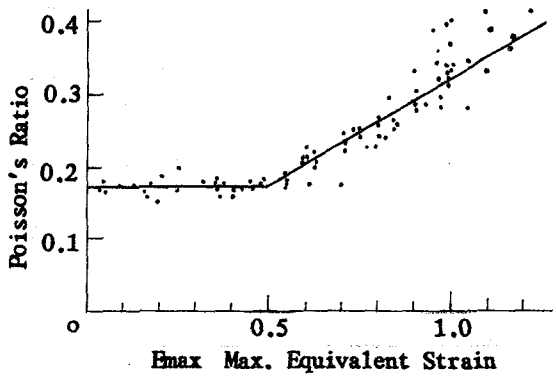

Fig.4 Poisson's Ratio in Elastic Zone

To formulate the flow rule governing the direction of the plastic rate vector, we introduced the directional correlaton between stress invariant rate and total strain invariant rate. The stress invariant rate can be divided into two components, V1 and V2 as

$$V = \begin{bmatrix} d\sigma_o \\ d\tau_o \end{bmatrix} = V1 + V2 = \begin{bmatrix} -\frac{\partial S}{\partial \tau_o} \\ \frac{\partial S}{\partial \sigma_o} \end{bmatrix} dj + \begin{bmatrix} \sigma_o \\ \tau_o \end{bmatrix} d1 \qquad (9)$$

where the first term V1 is the tangential component to the stress surface of constant S and the second term V2 is the parallel component to the stress invariant vector. The total strain invariant rate has two components X1 and X2, corresponding to V1 and V2 respectively as shown in Fig.1.

The direction of X1 must coincide with the tangential vector on the boundary of strain space due to the continuity condition. The direction of X2 was obtained from the experiments including non-proportional loading paths as shown in Fig.5 which indicates all the component X2 of the same strain surface converge to the same point. Accordingly, we get the total strain invariant rate X expressed by

$$X = \begin{bmatrix} \frac{\partial \varepsilon_o}{\partial \varepsilon_{eij}} d\varepsilon_{ij} \\ \frac{\partial \gamma_o}{\partial \varepsilon_{eij}} d\varepsilon_{ij} \end{bmatrix} = X1 + X2 = \begin{bmatrix} -\frac{\partial Ee}{\partial \gamma_o} \\ \frac{\partial Ee}{\partial \varepsilon_o} \end{bmatrix} dk + \begin{bmatrix} \varepsilon_o - \alpha(Ee) \\ \gamma_o - \beta(Ee) \end{bmatrix} dm \qquad (10)$$

The flow direction of plastic strain invariants is now obtained from Eq.8, 9 and 10. Typical cases are shown in Fig.6. For low stress level, the direction is approximately parallel to the normal vector as the normality rule indicates. On the contrary, for the high stress level the direction tilts from the normal vector, especially in the compression - tension stress state. This is the result of the anisotropic behavior of concrete.

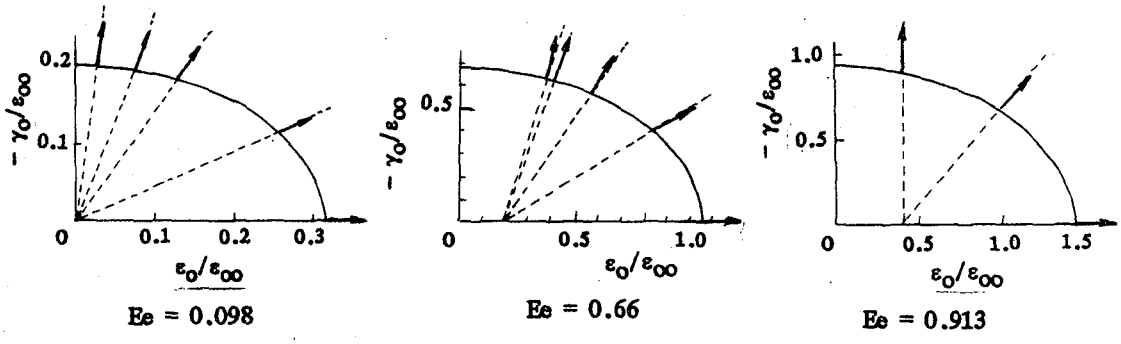

Fig.5 The Direction of Component X2 on Strain Space

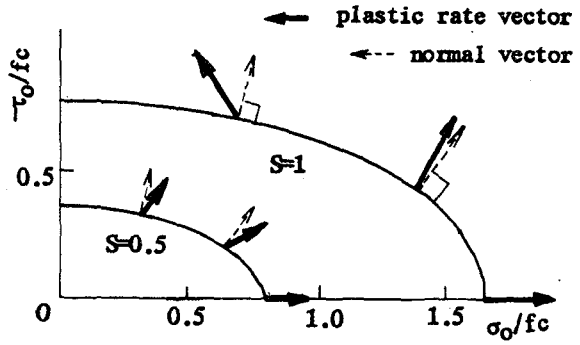

Fig.6 The direction of Plastic Rate Vector

ENDOCHRONIC DESCRIPTION OF SAND BEHAVIOR

Han C. Wu
Professor of Civil Engineering
The University of Iowa
Iowa City, Iowa 52242, U.S.A.

The endochronic theory of plasticity [1] has been applied to describe the mechanical behavior of drained sand. In this application, the endochronic constitutive equations have been modified to account for special features of sand behavior [2]. They read

$$\underset{\sim}{\varepsilon} = \frac{1}{3}\left(A\,\sigma + \sum_{h} B^{h} q^{h} + \sum_{d} C^{d} q^{d}\right)\underset{\sim}{\delta} + E_2\,\underset{\sim}{s} + \sum_{s} F_2^{s}\,\underset{\sim}{p}^{s} \qquad (1)$$

in which $\underset{\sim}{\varepsilon}$ is the strain; σ is the hydrostatic stress; $\underset{\sim}{s}$ is the deviatoric stress; $\underset{\sim}{\delta}$ is Kronecker's delta; q^h, q^d, and $\underset{\sim}{p}^s$ are r number of internal variables such that $r = h + d + s$; A, B^h, C^d, E_2, and F_2^s are material constants.

The values of these internal variables grow as the internal structures of materials change by deformation. The r internal variables are divided into three groups, each being active only for a specific function. Thus, h number of internal variables q^h are active in the representation of hydrostatic response, s internal variables $\underset{\sim}{p}^s$ are responsible for deviatoric response and d number of internal variables q^d are related to volume change (densification or dilation) due to shearing. The last group, q^d, distinguishes granular materials from other continua such as metals or concrete.

The rate of change (or evolution) of each group of internal variables is a material property and depends on the material that the model is presumed to describe. Therefore, the evolution equation may be linear or nonlinear depending on the material at hand. In [2], it has been found that a nonlinear evolution equation for q^h, and linear evolution equations for $\underset{\sim}{p}^s$ and q^d are satisfactory for the sands considered.

The evolution equations may be integrated resulting in expressing the current state of internal variables in terms of deformation histories leading up to the present state. By substituting these expressions for the internal variables into Eq. 1, and thereby eliminating the internal variables from the equation, an explicit equation relating the current stress to the deformation history is obtained. It is remarked that the form of this equation is highly dependent upon the form of the evolution equations, even though the internal variables do not appear explicitly in this equation.

In the present model for drained sand, three intrinsic (endochronic) times are used and denoted by z_H, z_S and z_D respectively for hydrostatic response, deviatoric response, and densification (and/or dilation). The evolution of internal variables is with respect to these intrinsic times.

This constitutive equation has been applied to model sand behavior under various loading conditions. Discussion would include: 1) the nonlinear volumetric response at isotropic consolidation, 2) the deviatoric response and its dependence on the normal stress, 3) densification and dilation due to change in the deviatoric state, and 4) effects of unloading, reloading and cyclic loading.

The theoretical results are compared with experimental data found in the literature.

Acknowledgements

The author wishes to express his appreciation to the National Science Foundation for support under Grant CEE-8213569.

References

1. Valanis, K.C. (1980), "Fundamental Consequences of a New Intrinsic Time Measure - Plasticity as a Limit of the Endochronic Theory", Archives of Mechanics, 32, 171.

2. Wu, H.C., Wang, T.P. (1983), "Endochronic Description of Sand Response to Static Loading", Journal of the Engineering Mechanics Division, ASCE, 109, August, paper No. 18162.

REMARKS ON SOME INCREMENTALLY NON-LINEAR CONSTITUTIVE RELATIONS

F. Darve
Institut de Mécanique de Grenoble
B.P. 68 - 38402, Saint Martin d'Hères Cedex
France

Introduction

The conventional elasto-plastic theories are not well adapted to describe the soil behaviour for several physical reasons such as :

1. A virgin soil has no elastic domain, but a previous strain history induces nearly elastic range in the vicinity of the previous loading path : the elastic limit is very complex and strongly dependent on the strain history.

2. It is particularly difficult to exhibit experimentally a general three-dimensional loading-unloading criterion.

3. The elastic portion of strain increments depends mainly on the number and the kind of contacts between the particles. The plastic strains influence very much these contacts. Therefore, the elastic strain increment can not be expressed independently of the previous plastic deformations.

We propose rather to study directly the relationship between $d\underset{\sim}{\varepsilon}$ and $d\underset{\sim}{\sigma}$ (for rate-independent materials) : $d\underset{\sim}{\varepsilon} = \underset{\sim}{F}(d\underset{\sim}{\sigma})$. We will see briefly three main properties of $\underset{\sim}{F}$, then the general formulation of a new class of incremental constitutive laws and finally a simple law of this kind.

Properties of the incremental constitutive relation

1. The rate-independent behaviour of the medium implies that $\underset{\sim}{F}$ is homogeneous of degree one : $$\forall \lambda \geqslant 0 \ , \ \underset{\sim}{F}(\lambda\, d\underset{\sim}{\sigma}) = \lambda\, \underset{\sim}{F}(d\underset{\sim}{\sigma}) \ .$$

2. The plastic irreversibilities induce the non-linearity of $\underset{\sim}{F}$: $\underset{\sim}{F}(-d\underset{\sim}{\sigma}) \neq -\underset{\sim}{F}(d\underset{\sim}{\sigma})$

3. The structural anisotropy of a deformed sample implies the mechanical anisotropy of $\underset{\sim}{F}$.

We consider the six-dimensional vectors $\{d\varepsilon_\alpha\}$ and $\{d\sigma_\beta\}$. According to property 1, the six functions F_α verify Euler's identity for homogeneous functions :

$$F_\alpha(d\sigma_\beta) = \frac{\partial F_\alpha}{\partial(d\sigma_\beta)}\, d\sigma_\beta = M_{\alpha\beta}\, d\sigma_\beta \ ,$$

where the thirty-six functions $M_{\alpha\beta}$ are homogeneous functions of degree zero of $d\sigma_\gamma$. Therefore these functions depend only on the unit vector $\{u_\gamma\}$ defined by :

$$u_\gamma = d\sigma_\gamma / \| d\underset{\sim}{\sigma} \| \ , \qquad (1)$$

with : $\|\underset{\sim}{d\sigma}\| = \sqrt{d\sigma_\alpha\, d\sigma_\alpha} = \sqrt{d\sigma_{ij}\, d\sigma_{ji}}$, norm of $\underset{\sim}{d\sigma}$.

The general formulation of the incremental rate-independent laws is then given by (Darve and Labanieh [1]) :

$$d\varepsilon_\alpha = M_{\alpha\beta}(u_\gamma)\, d\sigma_\beta \ . \qquad (2)$$

Study of the constitutive tensor $\underset{\sim}{M}(\underset{\sim}{u})$

Let us consider one of the thirty-six functions $M_{\alpha\beta}$. We can have an approximate expression of $M_{\alpha\beta}$ by its Mac Laurin series development (for functions of several variables) :

$$M_{\alpha\beta}(u_\gamma) = M^1_{\alpha\beta} + M^2_{\alpha\beta\gamma}\, u_\gamma + M^3_{\alpha\beta\gamma\delta}\, u_\delta u_\gamma + \cdots \qquad (3)$$

With the definition (1) of $\underset{\sim}{u}$, the relation (3) allows us to write (2) under the following form :

$$d\varepsilon_\alpha = M^1_{\alpha\beta}\, d\sigma_\beta + \frac{1}{\|\underset{\sim}{d\sigma}\|} M^2_{\alpha\beta\gamma}\, d\sigma_\gamma\, d\sigma_\beta + \frac{1}{\|\underset{\sim}{d\sigma}\|^2} M^3_{\alpha\beta\gamma\delta}\, d\sigma_\delta\, d\sigma_\gamma\, d\sigma_\beta + \cdots \qquad (4)$$

or in a concise manner :

$$d\varepsilon_\alpha = \sum_{n=1}^{p} \frac{1}{\|\underset{\sim}{d\sigma}\|^{n-1}} M^n_{\alpha\beta_1\cdots\beta_n}\, d\sigma_{\beta_1} \cdots d\sigma_{\beta_n} \ , \qquad (5)$$

where : $\begin{cases} \alpha, \beta_1, \ldots, \beta_n \in \{1, 2, \ldots, 6\} \\ p \geqslant 1 \text{ is the choose order of the development.} \end{cases}$

The case $p = 1$ in the constitutive law (5) gives the trivial solution of the elasticity : $d\varepsilon_\alpha = M^1_{\alpha\beta}\, d\sigma_\beta$,

but, for $p > 1$, we can describe by (5) the plastic irreversibilities, because this relation is non-linear in $\underset{\sim}{d\sigma}$ and not because of a change of $\underset{\sim}{M}^1$ with a loading-unloading criterion as in elasto-plasticity.

The case $p = 2$, which gives the simplest incrementally non-linear constitutive law, has been called by Darve [2] and Darve, Thanopoulos [3] "incremental law of second order" and its general form is :

$$d\varepsilon_\alpha = M^1_{\alpha\beta}\, d\sigma_\beta + \frac{1}{\|\underset{\sim}{d\sigma}\|} M^2_{\alpha\beta\gamma}\, d\sigma_\gamma\, d\sigma_\beta \ . \qquad (6)$$

Determination of the constitutive tensors $\underset{\sim}{M}^1$ and $\underset{\sim}{M}^2$

For the law (6), $\underset{\sim}{M}^1$ and $\underset{\sim}{M}^2$ are only dependent on the loading history and the second main basis of the law is to determine $\underset{\sim}{M}^1$ and $\underset{\sim}{M}^2$ by identifying the behaviour given by (6) with the real behaviour of the soil for "generalized triaxial paths". This particular set of paths is defined, in fixed principal axes of stress and strain, by the increase (compression) or decrease (extension) of one of the principal stresses, the other two remaining constant but not necessarily equal (as for conventional triaxial paths).

With the assumption of orthotropy for the incremental law and with some simplifications of the general expression of $\underset{\sim}{M}^2$, the knowledge of the responses of the soil to the six incremental paths :

$$\underset{\sim}{d\sigma} = \begin{Bmatrix} \pm 1 \\ 0 \\ 0 \\ 0 \\ 0 \\ 0 \end{Bmatrix} , \begin{Bmatrix} 0 \\ \pm 1 \\ 0 \\ 0 \\ 0 \\ 0 \end{Bmatrix} , \begin{Bmatrix} 0 \\ 0 \\ \pm 1 \\ 0 \\ 0 \\ 0 \end{Bmatrix}$$

(which belong to the set of generalized triaxial paths) allow us to write $\underset{\sim}{M}^1$ and $\underset{\sim}{M}^2$ as functions of the current states of stress and strain, the current value of the void ratio, and others material parameters depending on the previous load history (Darve and Labanieh [4] , Darve [5]).

For this reason this law can be called "incremental law of the interpolation-type" since once the two matrices $\underset{\sim}{M}^1$ and $\underset{\sim}{M}^2$ are obtained from the basic tests, any other stress increment gives the interpolated strain increment by relation (6).

Conclusion

The framework of the conventional elasto-plasticity seems to be not able to describe the main characteristics of the soils behaviour particularly for cyclic loadings. We propose a different way which is based essentially on an incrementally non-linear constitutive relation (see (6)) whose matricial coefficients are determined by the experimental knowledge of the behaviour for generalized triaxial paths. Our formulation is three-dimensional, valid in cyclic loadings and the constitutive constants are given by conventional drained triaxial tests.

References

1. Darve, F. Labanieh, S. (1982), "Incremental constitutive law for sands and clays. Simulations of monotonic and cyclic tests", Int. J. for Num. and Anal. Meth. in Geomech., 6, 243-275.
2. Darve, F. (1980), "Une loi rhéologique incrémentale non-linéaire pour les solides", Mech. Res. Comm., 7, n° 4, 205-212.
3. Darve, F., Thanopoulos, I. (1982), "Simulation of cyclic behaviour of sands with an incremental non-linear constitutive law", proceedings of IUTAM-symposium Deformation and Failure of Granular Materials, A.A. BALKEMA, 201-212.
4. Darve, F., Labanieh, S. (1982), "An incremental non-linear constitutive law and cyclic behaviour of sands", proceedings of Int. Symp. on Numerical Models in Geomechanics, A.A. BALKEMA, 90-99.
5. Darve, F. (1984), "An incrementally non-linear constitutive law : assumptions and predictions", proceedings of Int. Workshop on Constitutive Behaviour of Soils, A.A. BALKEMA.

CONSTITUTIVE RELATION FOR ROCK-LIKE MATERIAL, BASED ON A SHEAR CRACK MODEL

H. Lippmann
Lehrstuhl A fuer Mechanik, Technische Universitaet,
P.O. Box 202420, D-8000 Muenchen 2, FRG.

Introduction

In a previous paper [1] elastic-plastic constitutive equations were developed for u n i a x i a l compression of rock-like material. In this paper they will under certain assumptions be generalized to plane strain, or even to 3-dimensional deformation.

Fundamentals

At the beginning let us consider the u n i a x i a l stress (σ) - strain (ε) diagram only, of a rock-like material under compression as shown in Fig. 1 in which, σ and ε are counted positive. Up to the level σ_0, ε_0 the behaviour be completely elastic. Thereafter growing arrays of crack faces give rise to internal friction so that the deformation, now being referred to as crack-"plastic" or "clastic" becomes dissipative. After the so-called point of failure is reached, i.e. the maximum of the curve $\sigma = \sigma(\varepsilon)$ the weakening influence of the cracks prevails. In this "post-failure" regime the curve drops down to a constant state of residual strength σ_R which is adopted if $\varepsilon \geqslant \varepsilon_R$, or otherwise asymptotically (i.e. $\varepsilon_R \to \infty$).

Based on a rheological model the "elements" of which incorporate linear or non-linear elasticity, "sticking-friction" until fracture occurs, and afterwards slipping-friction along crack-faces, the following loading equation was derived in ref. [1],

$$\sigma(\varepsilon) = S\left\{\int_{-\infty}^{\tau} \tau\, f(\tau,\varepsilon)\,d\tau + J[1 - F(1,\varepsilon)]\right\} \qquad (1)$$

In it, S is a dimensional factor proportional to the number of elements used in the model. The constant ratio J denotes the mean stress in those elements which already slip, related to their limit stress at fracture. For each pre-strain $\varepsilon \geqslant 0$ given, $F(\tau,\varepsilon)$ is the overall statistical distribution function, and $f(\tau,\varepsilon)$ the corresponding distribution density of dimension-less elastic stress τ of the model elements, standardized in such a manner that $\tau = 1$ represents the limit of the fracture. f and F fulfil among other conditions, also

$$F(\tau,\varepsilon) = f(\tau,\varepsilon) = 0 \quad \text{if} \quad \varepsilon \geqslant \varepsilon_R \qquad (2)$$

Besides (1), also uniaxial unloading and reloading conditions have been derived in [1], and been illustrated by applicational examples.

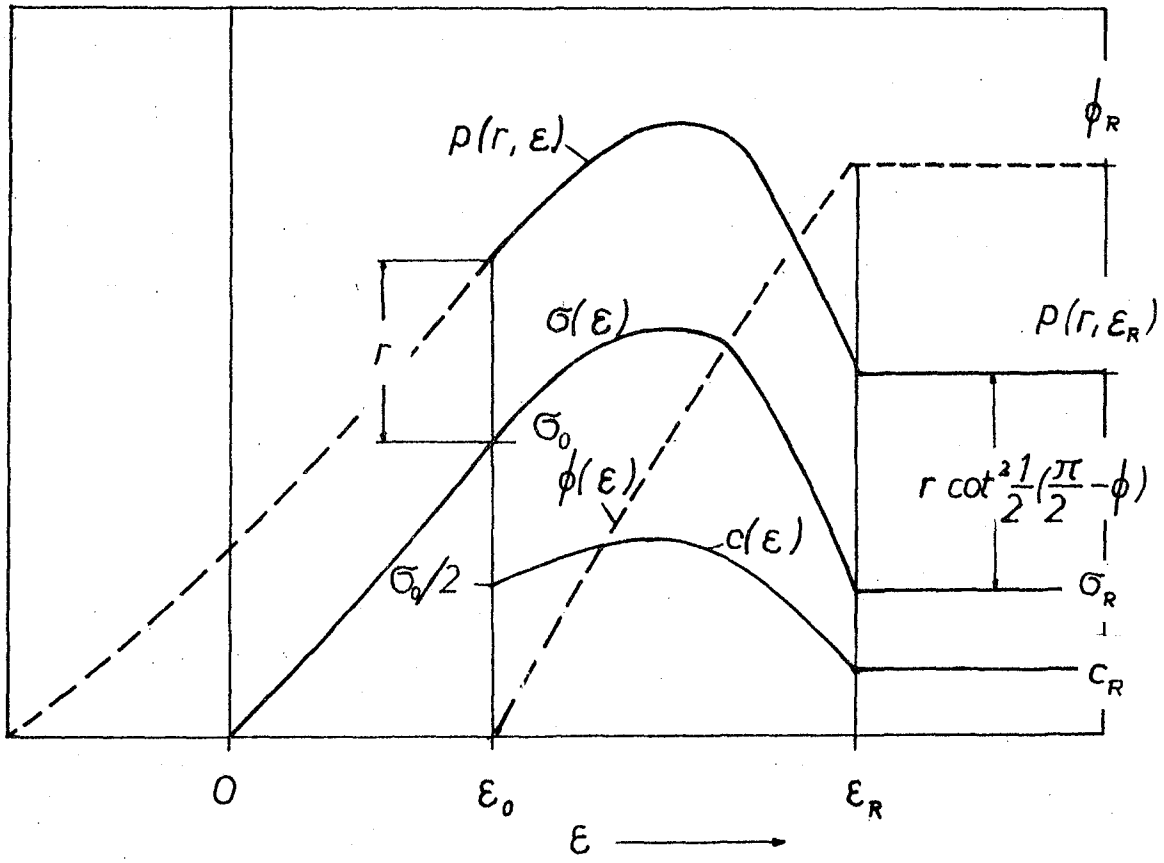

Fig. 1 - Stress, Angle of Int. Friction, and Cohesion vs. Strain

Biaxial State of Strain

We now assume that for plane strain loading, also a lateral principal pressure r acts so that the vertical principal pressure $p = p(r, \varepsilon)$ may become different from σ. The direction called "vertical" belongs to the larger pressure i.e.,

$$0 \leq r \leq p(r, \varepsilon) \tag{3}$$

and the "equivalent" deviatoric strain ε due to the overshooting stress $p - r$ only, is also measured vertically. Then we make the following assumptions:

a) The number S of the model elements is independent of r.

b) The loading (or limit, yield) condition for the residual state be described using a given function g_R, by means of the equation

$$p - r = g_R(r) \tag{4}$$

c) The functions f, F to refer to the deviatoric state of elastic shear in the model elements only, are independent of a superimposed hydrostatic pressure.

Assumption (c) holds rigorously if as an example, material is linear elastic or elastically incompressible, elastically isotropic, and the individual fracture limits of the model elements are statistically independent of r.

Analysis

We first apply the lower pressure r as a hydrostatic one, and then superimpose the deviatoric pressure $p - r$ in vertical direction so that by virtue of assumptions (a, c) equ. (1) can be written as follows,

$$\frac{p - r}{S} = \int_{-\infty}^{1} \tau\, f(\tau, \varepsilon)\, d\tau + J[1 - F(1, \varepsilon)] \tag{5}$$

Then it holds for any loading path in the (abstract) p, r - plane provided that $p - r$ never becomes negative. J being independent of ε, is obtained using (2), (4) if $\varepsilon \geqslant \varepsilon_R$ to yield,

$$J = \frac{p - r}{S} = \frac{1}{S}\, g_R(r) \tag{6}$$

Therefore equ. (5) becomes,

$$p - r = g(r, \varepsilon) = S \int_{-\infty}^{1} \tau\, f(\tau, \varepsilon)\, d\tau + [1 - F(1, \varepsilon)]\, g_R(r) \tag{7}$$

From it the integral as well as S can be eliminated if (7) would after substituting $r = 0$, i.e. $p = \sigma$ be written down again, and then substracted from equ. (7) to yield,

$$p - r = g(r, \varepsilon) = \sigma(\varepsilon) + [1 - F(1, \varepsilon)][g_R(r) - g_R(0)] \tag{8}$$

Equ. (7) or (8) is the bi-axial loading condition searched for. Besides g_R the two functions $\sigma(\varepsilon)$, $F(1, \varepsilon)$ have to be determined experimentally.

Using (6) also the conditions for unloading and reloading, given in [1] may be transformed correspondingly though the resulting expressions then become less simple. Of course for $\varepsilon = \varepsilon_o$ or $\varepsilon = \varepsilon_R$ respectively, a continuous transition takes place.

In order to formulate the conditions (7), (8) or its generalizations invariantly one has to observe that,

$$r = \frac{1}{2}(p + r) - \frac{1}{2}(p - r)$$

Then for isotropic material $p + r$ or $p - r$, respectively must be replaced by,

$$p - r = \left| \sqrt{(\sigma_1 - \sigma_2)^2 + 4\sigma_{12}^2} \right|, \qquad p + r = \sigma_1 + \sigma_2$$

Here σ_1, σ_2, σ_{12} denote the pressures or the shear stress, respectively in orthogonal coordinates x_1, x_2. Correspondingly ε becomes, using the associated strain rates $\dot{\varepsilon}_1$, $\dot{\varepsilon}_2$, $\dot{\varepsilon}_{12}$, and time t to start with t_o,

$$\varepsilon = \int_{t_o}^{t} \dot{\varepsilon}\, dt\,; \qquad \dot{\varepsilon} = \frac{1}{2} \left| \sqrt{(\dot{\varepsilon}_1 - \dot{\varepsilon}_2)^2 + 4\dot{\varepsilon}_{12}^2} \right|.$$

All equations could be extended to the 3-space if p , r would be taken as the maximum or minimum principal pressure, and no influence would be attributed to the intermediate principal pressure.

Whether the flow rule belonging to the yield criterion (8) is an associate one or not, has not yet been examined.

Example

Let the residual state obey a COULOMB-MOHR loading condition i.e.,

$$g_R(r) = 2\,\frac{r\sin\phi_R + c_R\cos\phi_R}{1-\sin\phi_R}$$

in which ϕ_R denotes the internal angle of friction and c_R the cohesion. Then the right-hand side of equ. (7) also represents a COULOMB-MOHR criterion i.e.,

$$g(r,\varepsilon) = 2\,\frac{r\sin\phi + c\cos\phi}{1-\sin\phi}$$

in which the instantaneous angle of friction ϕ and the cohesion c are no longer constants. Rather they depend on pre-strain ε according to,

$$\begin{aligned}\cot^2\tfrac{1}{2}\left(\tfrac{\pi}{2}-\phi\right) &= 1+\left[\cot^2\tfrac{1}{2}\left(\tfrac{\pi}{2}-\phi_R\right)-1\right]\left[1-F(1,\varepsilon)\right]\\ c &= \tan\tfrac{1}{2}\left(\tfrac{\pi}{2}-\phi\right)\left\{\frac{S}{2}\int_{-\infty}^{1}\tau\, f(\tau,\varepsilon)\,d\tau + c_R\left[1-F(1,\varepsilon)\right]\cot\tfrac{1}{2}\left(\tfrac{\pi}{2}-\phi_R\right)\right\}\end{aligned} \qquad (9)$$

Therefore $\phi = \phi(\varepsilon)$ varies because of equ. (2) , from the value $\phi_o = \phi(\varepsilon_o) = 0$ if $\varepsilon = \varepsilon_o$ (elastic limit) up to $\phi_R = \phi(\varepsilon_R)$ if $\varepsilon \geq \varepsilon_R$ (residual state). This is qualitatively shown in Fig. 1 .

From the COULOMB-MOHR criterion it follows directly that,

$$c(\varepsilon) = \tfrac{1}{2}\,\sigma(\varepsilon)\tan\tfrac{1}{2}\left[\tfrac{\pi}{2}-\phi(\varepsilon)\right]$$

while equ. (8) yields regarding (9) that,

$$\tfrac{1}{r}\left[p(r,\varepsilon)-\sigma(\varepsilon)\right] = \cot^2\tfrac{1}{2}\left[\tfrac{\pi}{2}-\phi(\varepsilon)\right]$$

Both relations are also qualitatively illustrated in Fig. 1 .

References

1. H. Lippmann: Ductility Caused by Progressive Formation of Shear Cracks. In: Three-Dimensional Constitutive Relations and Ductile Fracture (S. Nemat-Nasser, editor). Amsterdam: North-Holland Publ. Comp. 1981, pp. 389-404.

Acknowledgment: Sponsorship by VOLKSWAGEN FOUNDATION having granted an Academy Fellowship to the author, is gratefully acknowledged.

DEFORMATION AND THERMODYNAMIC RESPONSE DURING BRITTLE FRACTURE*

R. B. Stout
Lawrence Livermore National Laboratory
P. O. Box 808, L-200, Livermore, CA 94550

Introduction

In 1920, Griffith [1] introduced concepts to analyze an idealized crack in an elastic continuum at thermodynamic equilibrium. Griffith's analysis applied Gibbs' concepts [2] and was a global balance between the change in surface energy of the idealized crack and the change in elastic energy of the surrounding body during a variation of crack length. The following briefly describes extensions of Griffith's and other continuum mechanics concepts to obtain a discontinuum model of the deformations and thermodynamics during brittle fracture [3]. The model describes crack density with a statistical mechanics approach, and makes an analogy between a crack and a dislocation. Thus, a scalar crack density function can be defined analogous to a scalar dislocation density function [4]. The scalar crack density is a function argument in a functional representation for the relative deformations between atoms. The relative deformation functional has a lattice structure deformation that is represented by a function as in continuum mechanics and a crack deformation that is represented by a functional somewhat analogous to the discontinuum mechanics for dislocations [5,6]. The thermodynamics is almost analogous to that for dislocations [5,6], except for the surface dependence during crack propagation and crack opening. The next section briefly outlines the deformation and thermodynamic modelling.

Deformations and Thermodynamics

A species of crack can be identified by attributes analogously to the way species of dislocations can be identified. For this purpose, consider a point on a crack and let $\underline{\xi}$ denote the tangent vector to the crack tip line, $\underline{\zeta}$ denote a vector in the plane of the crack, $\underline{\nu}$ denote the velocity of the crack relative to the local lattice structure, $\underline{V}]$ denote the opening rate between atoms at the crack tip, and $\underline{U}]$ denote the current opening displacement between atoms at the crack tip. For shorthand purposes, let $\underline{\phi}$ denote the set of vectors $\{\underline{\xi}, \underline{\zeta}, \underline{\nu}, \underline{V}], \underline{U}]\}$; then $\underline{\phi}$ identifies a crack species and is a point in a hyperspace domain Φ of crack attributes. Applying concepts from statistical mechanics, a scalar crack density function denoted by $\Gamma(\underline{x},\tau,\underline{\phi})$ can be defined as the probable number of cracks in a spatial volume neighborhood of point $\underline{x}$ and in a hyperspace volume neighborhood of point $\underline{\phi}$ at time τ. There is an evolution equation for Γ which is a statistical transport statement for each species and has been described elsewhere [3].

*Work performed under the auspices of the U.S. Department of Energy by the Lawrence Livermore National Laboratory under contract No. W-7405-ENG-48.

The crack density function describes displacements across crack tips; to describe the displacement between two arbitrary atoms in a body a continuum contribution away from crack tips is also necessary. This total relative deformation between two atoms, say A and B, is a functional and is denoted by

$$\underline{\chi}\}(A\rightarrow B,t) = \underline{X}_I(A\rightarrow B) + \underline{u}_I(A\rightarrow B,t) + \underline{u}]\,(A\rightarrow B,t) \tag{1}$$

where $\underline{\chi}\}$ is the total relative deformation between atoms A and B at time $\tau = t$; $\underline{X}_I$ is the initial deformation at time $\tau = 0$; and $\underline{u}_I$ is the lattice displacement function; and $\underline{u}]$ is the crack displacement functional. The crack displacement functional depends on the crack density function and is given by

$$u_i](A\rightarrow B,t) = \int_0^t \int_{\underline{\chi}(A,\tau)}^{\underline{\chi}(B,\tau)} (\dot{T}_{ij}\Gamma + T_{ij}\dot{\Gamma} + T^*_{ij}\,\dot{\bar{\Gamma}})\,dx_j(A\rightarrow B,\tau)\,d\tau \tag{2}$$

where tensor operators on domain $\underline{\Phi}$ are given by

$$\dot{\underline{T}}() = \dot{T}_{ij}() \equiv \int_{\Phi} V_i]\,e_{jk\ell}\xi_k\zeta_\ell()\,d\underline{\phi} \tag{3a}$$

$$\underline{T}() = T_{ij}() \equiv \int_{\Phi} u_i]\,e_{jk\ell}\xi_k\nu_\ell()\,d\underline{\phi} \tag{3b}$$

$$\underline{T}^*() = T^*_{ij}() \equiv \int_{\Phi} u_i]^*\,e_{jk\ell}\xi_k\zeta_\ell()\,d\underline{\phi} \tag{3c}$$

and the crack density change with respect to time is

$$\dot{\bar{\Gamma}} \equiv \partial_\tau\Gamma + \underline{\nabla}\cdot(\underline{\bar{v}}\Gamma) \tag{3d}$$

In equation (2), the first integrand gives the relative displacement from crack opening rates, the second integrand gives the relative displacement from crack propagation, and the third integrand gives the relative displacement from changes in the crack density function at points on a line between atoms A and B. From equation (2), various kinematic measures of relative deformation can be defined. The kinematic measures are necessary for the representations of external work and of thermodynamic internal energy [3]. For quasi-static modelling, the kinematic measures are for a total relative strain tensor that decomposes into a strain tensor function as in continuum mechanics and a strain tensor functional from the crack density dependent term; a relative velocity that has a lattice structure relative velocity function and a crack density dependent relative velocity functional; and a relative rate of deformation tensor that has an interatomic gradient operator on the lattice structure relative velocity function and the crack dependent relative velocity functional. The kinematic functional representations follow formally the kinematic concepts of continuum mechanics.

The thermodynamic modelling assumes that an internal energy functional, ε, exists that depends smoothly on the arguments of the entropy function $\eta(\underline{x},\tau)$; the lattice structure strain function, $\underline{\gamma}(\underline{x},\tau)_I$; the crack density

function, $\Gamma(\underline{x},\tau,\underline{\phi})$; and the mass density function, $\rho(\underline{x},\tau)$; and for a subset $R+\partial R(\overline{\tau})$ of a closed body R for all times τ in $[o,t]$ and points $\underline{\phi}$ in domain Φ. With this assumption, an incremental change in the internal energy can be represented as an integral over subset R that has terms for internal energy changes from entropy changes, from lattice strain changes, from crack density changes, from mass density changes, and from surface area changes resulting from crack propagation and crack opening rates. Then, using the first law of thermodynamics, the internal energy change expression can be combined with expressions for external work and heat changes to obtain

$$\{\int_R (\Delta_\eta\varepsilon\dot{\eta} - \dot{\bar{H}} + (\underline{\Delta}_\gamma\varepsilon - \bar{\underline{g}}):\dot{\underline{\gamma}} + (\Delta_\Gamma\varepsilon - \underline{g}\cdot\underline{\underline{T}}^*)\dot{\bar{\Gamma}} + (\underline{\Delta}_{\nu\Gamma}E - \underline{g}:\underline{\Delta}_\nu\dot{\underline{\underline{T}}})\cdot\underline{V}]\Gamma \tag{4}$$

$$+ (\underline{\Delta}_{\nu\Gamma}E + \underline{\nabla}(\Delta_\Gamma\varepsilon) - \underline{g}:\underline{\Delta}_\nu\,\underline{\underline{T}})\cdot\underline{\nu}\Gamma)d\underline{x}\}\Delta t = 0$$

At thermodynamic equilibrium, Gibbs' methodology [2] for reversible thermodynamic processes leads to the following equilibrium thermodynamic potentials:

$T \equiv \Delta_\eta\varepsilon$ ... thermodynamic equilibrium temperature for reversible heat transport $\dot{\bar{H}}$

$\bar{\underline{g}} \equiv \underline{\Delta}_\gamma\varepsilon$ ... net mechanical stress equals the thermodynamic potential for strain;

$\underline{g}:\underline{\underline{T}}^* \equiv \Delta_\Gamma\varepsilon$ ... stress work on a crack equals the thermodynamic potential for crack kinetics;

$$\underline{g}:\underline{\Delta}_\nu\dot{\underline{\underline{T}}} = \sigma_{ij}\int_\Phi \varepsilon_{jk\ell}\xi_k\zeta_\ell()\,d\underline{\phi}$$

$\equiv \underline{\Delta}_{\nu\Gamma}E$ ... surface stress at the crack equals the thermodynamic potential for surface strain; and

$$\underline{g}:\underline{\Delta}_\nu\underline{\underline{T}} = \sigma_{ij}\int_\Phi U_i]e_{jk\ell}\xi_k()d\underline{\phi}$$

$\equiv \Delta_{\nu\Gamma}E + \underline{\nabla}(\Delta_\Gamma\varepsilon)$... stress work during crack propagation equals the thermodynamic potential for surface, $\underline{\Delta}_{\nu\Gamma}E$, plus the spatial gradient of the thermodynamic potential for crack kinetics.

In the above equilibrium definitions, the operators $\underline{\Delta}_{V\Gamma}E$ and $\bar{\Delta}_{V\Gamma}E$ are derived from the internal energy functional, ε, by functional analysis of the surface dependence. At thermodynamic nonequilibrium, none of the equality definitions need be true and a consistent thermodynamic formalism such as that of Onsager [7] has to be applied [3]. However, from the equilibrium thermodynamics considered, a thermodynamic potential for crack kinetics, a thermodynamic potential for surface straining at the crack tip, and an extension of Griffith's conditions for the thermodynamic potential of surface all emerge. The thermodynamic potential for crack kinetics is interpreted as a condition for incipient fracture. This means that fracture properties of various brittle materials can be classified by a thermodynamic potential, which is a material characteristic. This would be an immense improvement over current fracture classification methods that use stress intensity factors which are dependent on the geometry and the boundary conditions of the test specimen.

Acknowledgment

The author wishes to thank L. Burrow for the excellent typing.

References

1. Griffith, A.A., Phil. Trans. Roy. Soc. London, A221, pp 163, 1920.

2. Gibbs, J.W., The Scientific Papers of J. Willard Gibbs, Vol. 1, Dover Pub. Inc., NY, 1961.

3. Stout, R.B., to be published in Eng. Fract. Mech., 1983.

4. Stout, R.B., Crystal Lattice Defects, Vol. 9, pp 47, 1980.

5. Stout, R.B., Crystal Lattice Defects, Vol. 9, pp 65, 1981.

6. Stout, R.B., Rheol. Acta, Vol. 21, pp 659, 1982.

7. Onsager, L., Phys. Rev., Vol. 37, pp 405 and Vol. 38, pp 2265, 1931.

COMPUTATIONAL STABILITY AND UNIQUENESS OF STRAIN-SOFTENING MATERIALS

K. J. Willam
Professor of Civil Engineering
University of Colorado, Boulder
Boulder, Colorado 80309, U.S.A.

Introduction

An on-going controversy among eminent researchers has recently focused on the predictive value of numerical studies with strain-softening materials. On one hand most materials exhibit limited ductility and toughness which must be accommodated by a realistic computational procedure for contained damage accumulation within the structure. On the other hand, the continuum-oriented material formulations are restricted by thermodynamic requirements of irreversible processes and the ensuing stability and uniqueness conditions e.g. of elasticity and elasto-plasticity.

These fundamental questions are further obfuscated by two aspects:

(i) The problematic concepts of extracting "objective" strain-softening formulations from strain-controlled test data, and

(ii) The contiguous numerical problem of developing solution techniques which are sufficiently robust to survive the formation and propagation of contained material instabilities within the structure, and which are at the same time sufficiently sensitive to detect overall structural failure without undue delay.

Strain Softening Model

The controversy above has its origin in the attempt to monitor contained fracturing within the structure by an "equivalent" degradation process of strength and stiffness within the traditional constitutive concepts for non-linear continua. Similar to the theory of plasticity which provides a phenomenological model for the highly discontinuous propagation of line defects on the micromechanical level, the so-called "smeared" approach describes the propagation of tensile crack and frictional slip defects on the macromechanical level. Clearly, the different scale of these defects in concrete and geomaterials introduces a size effect into the softening formulation which results from the localization of fracture within the so-called fracture process zone. If we assume that this process zone is a material property, then it follows that the fracture energy is released only within failure bands of constant width. Consequently, the identification of the material softening branch introduces a crack width parameter "d" which results from the homogenization of fracture propagation within the material test sample in the

post-peak regime. In this sense, the softening regime is not a "proper" material property, but rather the result of a size-dependent averaging procedure of the fracture discontinuties which control the degrading post-peak behavior of a particular test specimen loaded to failure under strain control.

Computational Strategy

It is of little surprise that the numerical results of boundary value problems for softening materials are extremely sensitive and depend to a large extent on the computational strategy. Starting from the spatial discretisation with rank-deficient or locking finite elements to the incremental quasistatic time history analysis of the inelastic fracture process, and the iterative enforcement of stress transfer within truly finite time intervals a successful solution centers around a strain-controlled driving strategy in analogy to strain - rather than load-controlled testing. Similar to the strain-space formulation of plasticity, the evolution law for the inelastic fracture strains must be expressed in terms of total strains rather than stresses in order to stabilize the solution procedure. In spite of its slow convergence, the initial load strategy provides a convenient computational scheme for softening material properties because of the underlying splitting of the well-conditioned positive definite elastic operator (implicit elastic stiffness format) from the potentially ill-conditioned fracture operator (explicit initial load format). For a proper appreciation of the computational task, the structural analyst must be aware that the contained fracture analysis attempts to trace the entire evolution of local material instabilities and the ensuing stress redistribution mechanism up to the point of overall instability when the redistribution capacity of the structure is exhausted. Clearly, the success of such an analysis depends to a large extent on the close tracing of the fracture process and the efficient stress transfer due to localized softening within truly finite increments.

Direct Shear Test

In order to explore the limitations of the smeared approach, the contained fracture propagation in concrete and mortar specimens was studied with the large capacity servo-controlled direct shear apparatus at CU, Boulder. For the various ratios of normal to tangential loading, both contained tensile cracking and frictional slip modes of fracture were mobilized within the specimen which is in reality a "mini-structure". Some of the preliminary results were summarized in ref. [1]. The identification of the crack-width parameter "d" from triaxial Hoek-cell tests was described in the recent report [2] in which the computational predictions of the smeared approach were also compared with the experimental results of the direct shear test indicating little sensitivity with regard to mesh size because of the high confinement of the shear box.

References

1. Christensen, J., Ickert, K., Stankowski, T., Sture, S. and Willam, K., 1983, "Numerical Modeling of Strength and Deformation Behavior in the Direct Shear Test," Proc. Int. Conf. Constitutive Laws of Engineering Material, C.S. Desai and R.H. Gallagher eds., Tucson, AZ, (1983), pp. 537-544.

2. Christensen, J.D., (1983), "Computational and Experimental Investigation of Concrete Failure in Shear," M.S. Thesis, CEAE Department, University of Colorado, Boulder.

ANALYTICAL MODELS FOR CRACKING OF CONCRETE SUBJECT TO SHEAR

Pietro G. Gambarova
Professor of Structural Engineering
Politecnico di Milano
Milan, Italy

Nature of the problem

Cracking in concrete elements affects the mechanical characteristics in such a way that both the shear strength and the shear stiffness markedly decrease compared to solid concrete. However, although reduced, these characteristics may still be important on condition that the confinement action across the cracks is significant.

Both shear strength and stiffness of cracked concrete are mostly ensured by the roughness of crack surfaces (Aggregate Interlock Mechanism). Consequently, a first approach to the description of the behaviour of cracked concrete subject to shear should be based on Aggregate Interlock Properties. Nevertheless, a more general approach is needed to describe not only the shear transmission capabilities of existing cracks, but also the process of formation of the cracks themselves.

Within these different approaches, two constitutive models to describe how cracked concrete behaves are here presented.

The first (Rough Crack Model) refers to a system of existing parallel cracks and is based on finite stress-strain relations between the stresses at the crack interface and the "equivalent" strains produced by cracking itself.

The second (Model of Weak Planes or Microplane Model) assumes that the non linear behaviour in tension (up to cracking, which is introduced by means of equivalent strains) is the result of the concrete behaviour along randomly distributed "weak planes" (or "microplanes"). A one-to-one functional dependence is assumed between the normal stress and the normal strain in each weak plane; cracking is represented in each plane by the tail of the $\sigma_n(\varepsilon_n)$ function, characterized by large strain values and by zero stress values.

Rough Crack Model

The Rough Crack Model describes the Aggregate Interlock Mechanism, Fig.1 /1/, starting from some simple micromechanical models (Fig.2) and from the available test data (mostly those by Paulay and Loeber /4/). Total stress-total displacement relations are worked out at the crack interface /1,3/. These relations can be regarded as constitutive laws of the material (cracked concrete) if the following assumptions are introduced: the cracks are linear, parallel and densely spaced; solid concrete deformations between two contiguous cracks are negligible; crack displacements can be replaced with equivalent strains obtained by smearing the displacements over a length equal to crack spacing s. The stress-strain relations are formulated as follows:

$$\sigma^c_{nt} = \tau_o \left(1-\sqrt{\frac{2\delta_n}{d_a}}\right) r \frac{a_3 + a_4 |r|^3}{1+a_4 r^4}, \quad \sigma^c_{nn} = -\frac{a_1 a_2 r \sqrt{\delta_n}}{(1+r^2)^{0.25}} \sigma^c_{nt} \qquad (1,2)$$

where a_1, a_2, a_3, a_4 are constants, $\tau_o = 0.25\text{-}0.30\, f'_c$, $r = \delta_t/\delta_n = \gamma_{nt}/\varepsilon_n$. At constant crack dilatancy (Fig.3a,b, $\delta_n/\sigma^c_{nt} = 0.0725$ mm^3/N or $\sigma^c_{nt}/\delta_n = 13.8$ N/mm^3) both the stiffness coefficients $E_{33} = \partial\sigma^c_{nt}/\partial\gamma_{nt}$ and $E_{31} = \partial\sigma^c_{nt}/\partial\varepsilon_n$ have large values, and so also the shear-opening coupling, represented by E_{31}.

Microplane Model

Because of the nature of concrete, which is a brittle aggregate material with hard inclusions and a weak matrix (Fig.4), the stresses are far from uniform at the local level, having sharp extremes in the thin cement-paste layers between two contiguous aggregate particles (these layers are called weak planes or microplanes). Assume now that in each microplane the static behaviour is characterized by a uniaxial law $\sigma_n = C_n(\varepsilon_n)\cdot\varepsilon_n$, where n is the normal to the microplane (Figs.5, 6); the shear stiffness is negligible; the normal strain ε_n is equal to the resolved macroscopic tensor ε_{km} for the same plane ($\varepsilon_n = n_k n_m \varepsilon_{km}$, with k,m=1,2 in two dimensions); the law $\sigma_n(\varepsilon_n)$ has a softening branch (Fig.6); the microplanes have a random distribution at the macroscopic level (Fig.5). For the loading in tension of the microplanes the following intrinsic law has been adopted: $\sigma_n = E_n \varepsilon_n e^{-\varepsilon_n/\varepsilon_o}$. Superimposing the responses of all microplanes, the stresses σ_{ij} and the coefficients E_{ijkm} of the stiffness matrix of the material can be obtained as follows:

$$\sigma_{ij} = \frac{1}{\pi}\int_0^\pi C_n n_k n_m n_i n_j \varepsilon_{km}\, d\phi, \quad E_{ijkm} = \frac{1}{\pi}\int_0^\pi (C_n + dC_n/d\varepsilon_n)\, n_i n_j n_k n_m\, d\phi \qquad (3,4)$$

With a suitable formulation for C_n, the elastic behaviour can also be described, with $\nu = 0.33$ (plane stresses), which can easily be corrected to 0.18-0.20 /2/. The formulation of the laws $\sigma_n(\varepsilon_n)$ for loading in tension and in compression, and for unloading, can be based on the results of Aggregate Interlock tests /4/, see Fig.7, where δ_t and δ_n have to be smeared over a "crack band width" w_c equal to a multiple of the maximum aggregate size d_a (for instance $w_c = d_a$). Although the constitutive law of the microplanes is path-independent, the superposition of the responses is path-dependent.

Comparison with test results, and conclusions

Both models give shear-slip curves (under imposed strain histories) which are in good agreement with the experimental results, Figs.8,10 (here reference is made only to Aggregate Interlock Tests, see the test set-up in Fig.9).

The fitting obtained with the Rough Crack Model is even better, but the Microplane Model is much more general and can describe the overall behaviour of concrete in tension and shear. Both models can usefully be introduced into FEM programs, for updating the stiffness characteristics of cracked concrete.

References

1. Bazant,Z.P., Gambarova,P.G., "Rough Cracks in Reinforced Concrete", Journal of the Structural Division, ASCE, Vol.106, No.ST4, Proc.Paper 15330, April 1980, pp.819-842.

2. Bazant,Z.P., Gambarova,P.G., "Crack Shear in Concrete : Crack Band Microplane Model", Report, Center for Concrete and Geomaterials, Northwestern University, Evanston, Illinois, 1983.

3. Gambarova,P.G., Karakoç,C., "A new approach to the analysis of the confinement role in regularly cracked concrete elements", 7th Int.Conf. on Structural Mechanics in Reactor Technology (SMiRT 7),Paper H5/7, Chicago, August 83.

4. Paulay,T., Loeber,P.J., "Shear Transfer by Aggregate Interlock", Special Publication SP42, American Concrete Institute, 1974, pp.1-15.

5. Reinhardt,H.W., Walraven,J.C., "Cracks in Concrete Subject to Shear", Journal of the Structural Division, ASCE, Vol.108, No.ST1, Proc.Paper 16802, January 1982, pp.207-224.

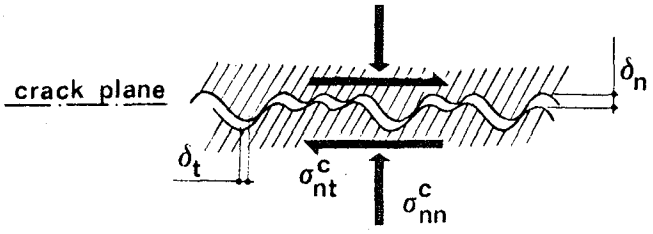

Fig.1 - Crack morphology (plane stresses).

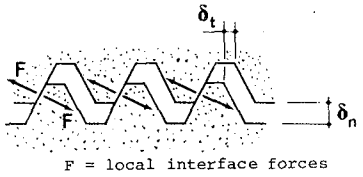

Fig.2a - Wedge effect : crack response depends on the ratio $r = \delta_t/\delta_n$.

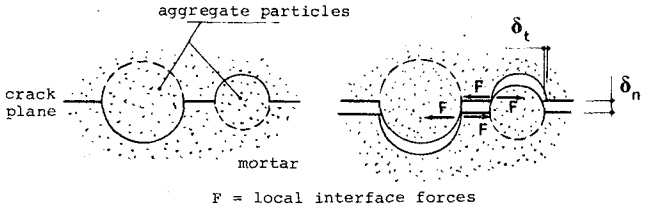

Fig.2b - At small crack openings, a limited confinement action is required.

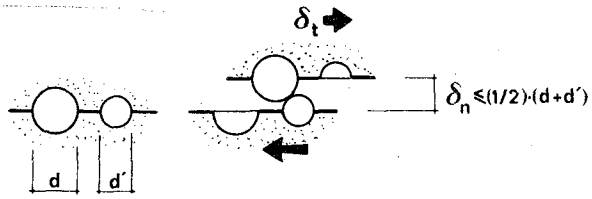

Fig.2c - The local contact is lost when $\delta_n > (1/2)(d+d')$. A more strict condition (here adopted) is $\delta_n > (1/2)\ d$.

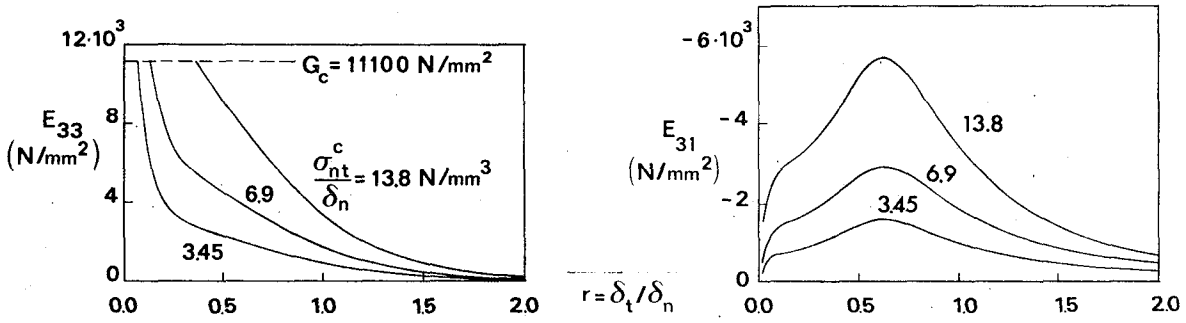

Fig.3 - Curves of the stiffness coefficients E_{33} and E_{31} (from Eqs.1 and 2), for different values of the crack dilatancy. $f'_c = 31\ N/mm^2$, $d_a = 19$ mm, s = 190 mm.

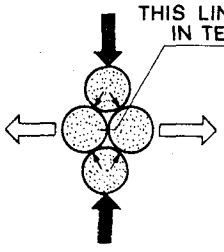

Fig.4 - Simplified model for concrete, with weak planes in tension and in compression.

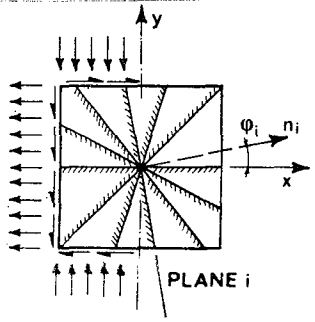

Fig.5 - Weak planes (microplanes) in the bidimensional case.

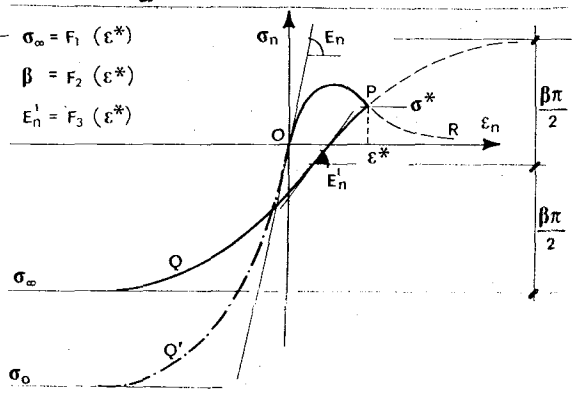

Fig.6 - Loading in tension (OPR), unloading in tension (PQ), loading in compression (OQ').

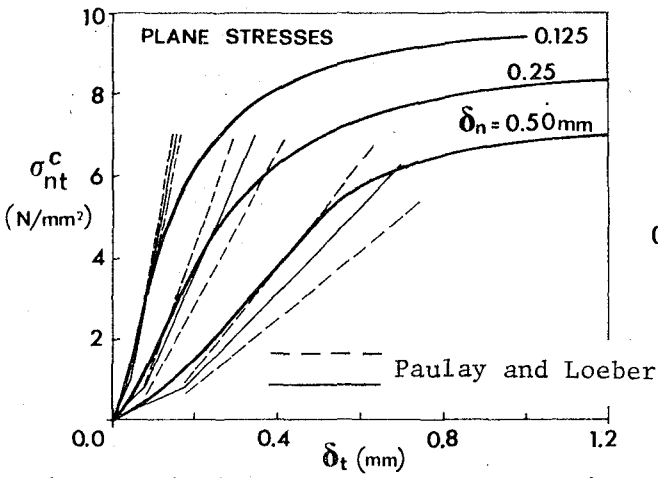

Fig.7 - Fitting of Paulay and Loeber' test results at constant crack opening /4/, by means of the Microplane Model. f'_c = 31 N/mm^2, d_a = 19 mm.

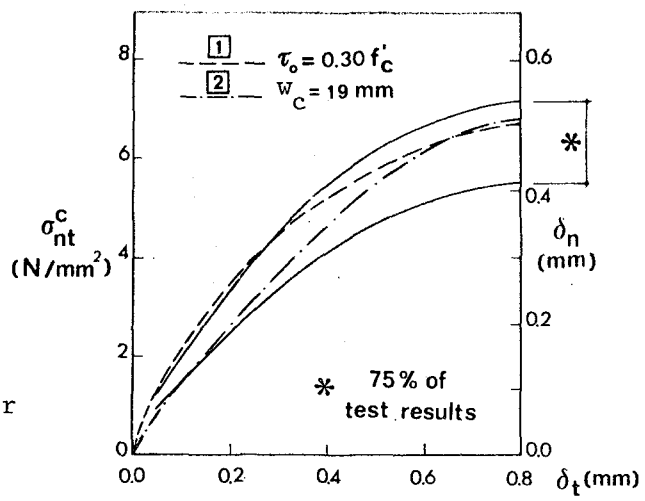

Fig.8 - Fitting of Paulay and Loeber' test results at constant crack dilatancy /4/ δ_n/σ^c_{nt}=0.0725 mm^3/N : 1 = Rough Crack Model, 2 = Microplane Model.

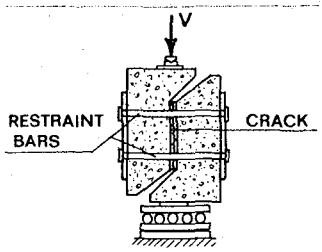

Fig.9 - Typical test set-up for Aggregate Interlock tests. The confinement action is exerted by external bars.

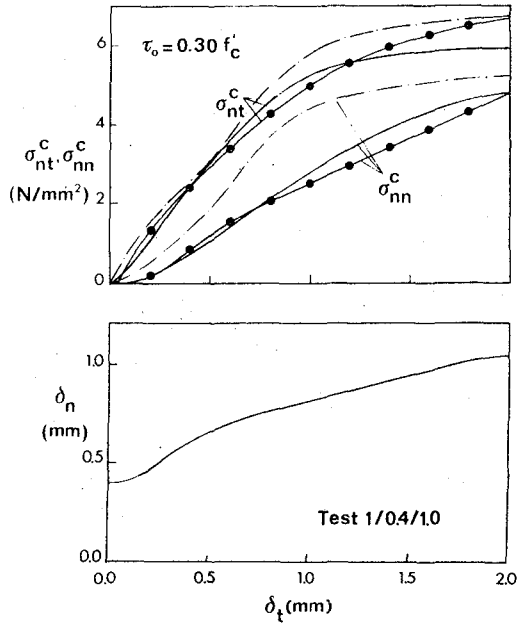

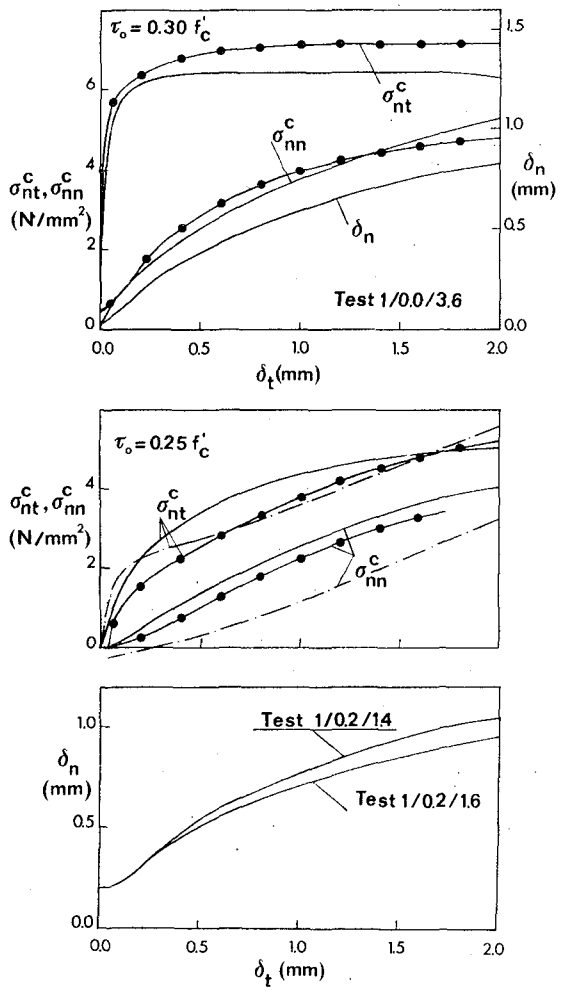

Fig.10 - Fitting of Reinhardt and Walraven' test results /5/ (curves with solid circles) : Rough Crack Model solid curves, Microplane Model dash-dotted curves. f'_c = 31.2 N/mm^2 (average value), d_a = 16 mm.

CRACK GROWTH IN CEMENT BASED COMPOSITES

R. Ballarini, Graduate Student

and

S. P. Shah and L. M. Keer
Professors of Civil Engineering

Northwestern University
Evanston, Illinois 60201, USA

Introduction

In cement-based composites there is a zone surrounding a crack tip within which a significant amount of microcracking and other inelastic deformations occur. Furthermore, because cracks in these materials are tortuous, mechanical interlock occurs between opposing crack surfaces. In concrete this interlock arises from aggregate bridging, and in fiber-reinforced mortar it arises from fiber bridging. The portion of the crack which is traction free is referred to as the actual stress-free crack and the zone within which mechanical interlock and microcracking occur is referred to as the process zone. The sum of these two lengths is referred to as the effective crack length. Figure 1 shows schematically these regions. The process zone can be large and can greatly affect the fracture process.

Kaplan [1] applied LEFM concepts to the study of fracture in concrete and mortar. He observed that strain energy release rate (G_{Ic}) values increased with increasing beam size. Kaplan pointed out that these discrepancies were a result of slow crack growth prior to instability. This study was the first to indicate that the effect of slow crack growth prior to brittle fracture should be included in theoretical models used to predict crack growth in cement-based composites. More recently models have been proposed [2,3,4] which include the effect of the process zone. These models replace the aggregate interlock and microcracking in the process zone with a closing pressure which resists crack opening. It has been concluded that these models give a more realistic and accurate description of fracture than other models which do not include the process zone. All the models used approximate analytical techniques to calculate the stress intensity factor produced by the loading and the closing pressure. Furthermore, the crack profile was assumed. In this investigation the physical model proposed by Wecharatana and Shah [4] is used, and a more accurate analytical technique is developed to calculate all physical quantities. The effect of the process zone and the range of crack lengths for which this zone makes a significant contribution to the fracture process is determined.

Analytical Model

A significant amount of experimental work has been performed using three

point and four point bending specimens. To predict crack growth in this structure, it is necessary to understand the stress and displacement fields arising from the external loading and from any loading which might exist along the crack surfaces. This is done by solving the elastostatics problem shown in Figure 2. The solution was obtained using the principle of superposition. This scheme is shown in Figure 2. By finding the stresses produced by a single dislocation in an infinite space on the lines y=0 and y=h and applying the negative of these as well as concentrated forces to a layer, the solution for a layer containing a dislocation and loaded as shown in Figure 2 is obtained by adding the dislocation solution to the layer solution. The crack is modelled by replacing the single dislocation with a distribution of dislocations given by

$$B(c) = \frac{\partial}{\partial c} (u_x^+ - u_x^-) , \tag{1}$$

integrating the effect of each, and imposing the proper stress boundary condition on the crack surfaces. In equation (1) u_x^+ and u_x^- represent the x-displacements of material points to the left and to the right of the point (0,c) respectively. The general solution to the problem of a layer with prescribed tractions on its surfaces can be found using Fourier Transform techniques (see Sneddon [5]). Applying this method to this particular problem leads to the following nonlinear integral equation for the unknown dislocation density B(c)

$$\frac{2\mu}{\pi(\kappa+1)} \int_o^d B(c) \left\{ \frac{1}{c-y} + \frac{2}{c+y} - \frac{(3c+y)}{(c+y)^2} + \frac{4cy}{(c+y)^3} + K_1(c,y) \right\} dc$$

$$= RHS(y) - \hat{\sigma} \qquad 0 \leq y \leq d \tag{2}$$

where $\hat{\sigma}$ is the closing pressure function which models the mechanical interlock and other inelastic deformations in the process zone. $K_1(c,y)$ and RHS(y) are not given here. Equation (2) was solved by the method of successive approximations. The crack opening displacements and stress intensity factor are given by

$$u_x^+ - u_x^- = \eta = \int_y^d B(c)dc$$

$$K_I = \lim_{y \to d} \sqrt{2\pi(y-d)} \frac{2\mu}{\pi(\kappa+1)} \int_o^d \frac{B(c)dc}{c-y} \tag{3}$$

Hence the problem of finding the stress and displacement fields is solved.

Fiber-Reinforced Mortar

The closing pressure function for fiber-reinforced mortar was approximated by the following function [6,7,8]

$$\hat{\sigma} = \sigma_{max} \left(1 - \frac{\eta}{\eta^f_{max}}\right)^2 \tag{4}$$

where σ_{max} is the maximum post-cracking stress for the material in uniaxial tension, η is the crack opening displacement, and η^f_{max} is the maximum pulled out distance of the fibers. η^f_{max} is taken as one-half the fiber length. To test the proposed model, experimental work performed by Valezco et al. [8] was analyzed. By using the reported values of load and crack length, the proposed model was

used to predict the crack mouth opening displacement (CMOD). In modeling fiber-reinforced mortar, it was assumed that the process zone was the zone in which the fibers had not pulled out of the matrix. Other inelastic deformations around the crack tip were ignored, since the crack opening was resisted for the most part by the fibers. For these beams the crack opening displacements were always less than one-half the fiber length (1/2 inch), so that the fibers never pulled out of the matrix. This means that fiber bridging occurred throughout the length of the cracks and that this process zone increased as the crack lengths increased. Figure 3 is a comparison of predicted and observed CMOD values. It can be seen from this graph that the proposed model describes the effects of the fibers quite adequately. Even though they are not presented here, it was observed that for a given effective crack length, the stress intensity factors are higher for the beam with a shorter initial notch length. This is a result of the process zone being longer for this beam at any given effective crack length. It can be concluded that the fibers make the material much tougher.

Concrete

The closing pressure function for concrete was assumed as

$$\hat{\sigma} = f_t \left(1 - \frac{\eta}{\eta_{max}}\right) \tag{5}$$

where f_t is the uniaxial tensile strength of the concrete, η is the crack opening displacement, and η_{max} is the displacement which separates the actual stress-free crack and the process zone (Figure 1). Two models were used to predict the CMOD for a particular load and crack length. The first model (Model 1) assumes that the measured crack length is the effective crack length. That is, the measured crack carried tractions up to a critical value of the crack opening displacement. To test this model, experiments performed by Catalano and Ingraffea [3] were analyzed. As seen in Figure 4, by using this model a significant error in the predicted CMOD's is obtained in the short crack region. The reason for this is that for the short cracks, the nonlinear deformations occurring ahead of the crack tip will have a large influence on the fracture process, and this model assumes these nonlinear deformations do not exist. A second model (Model 2) was used in which the measured crack length is assumed to be stress free, and a process zone exists ahead of the stress-free region. For this model the actual stress-free crack is plotted in Figure 4, and, as seen from this plot, by using Model 2 a good correlation exists between experimental and predicted values of CMOD for all crack lengths. Even though they are not presented here, it was observed that the length of the process zone decreased as the crack lengths increased. This was also observed by Wecharatana and Shah [4]. This result is reasonable, since for the long cracks the displacements are so large that the length of the zone within which interlocking occurs decreases.

Conclusions

1. For fiber-reinforced concrete the effect of the process zone must be included to predict results for all crack lengths, especially for the longer crack lengths, since the fiber bridging zone in these cases may be equal to the whole length of the effective crack.

2. In concrete, the process zone ahead of the visible crack tip where microcracking and other inelastic deformations occur must be included to predict results in the short crack region, since the length of this zone may be on the same order as the stress-free length. Long cracks tend to behave as stress-free cracks.

3. Critical stress intensity factors are a function of the crack length.

4. Accurate analytical procedures should be employed whenever testing a physical model. This will eliminate errors in the calculations, and will result in a better understanding of whether the physical model is satisfactory.

5. Experimental programs should be tailored so they can be used in conjunction with mathematical models. Any physical quantity which is associated with the fracture process which is included in the mathematical model should be measured in experiments, especially the slow crack growth and crack opening displacements.

Acknowledgement

The research reported here was supported by a grant from the Air Force Office of Scientific Research (AFOSR-820243).

References

1. Kaplan, M. F., (1961), "Crack Propagation and the Fracture of Concrete," Journal of the American Concrete Institute, 58, 591-610.
2. Hillerborg, A., Modeer, M., and Petersson, P. E., (1976), "Analysis of Crack Formation and Crack Growth in Concrete by Means of Fracture Mechanics and Finite Elements," Cement and Concrete Research, 6, 773-782.
3. Catalano, D. M. and Ingraffea, A. R., (Nov. 1982), "Concrete Fracture: A Linear Elastic Fracture Mechanics Approach," Report No. 82-1, Department of Structural Engineering, Cornell University.
4. Wecharatana, M. and Shah, S. P., "Predictions of Nonlinear Fracture Process Zone in Concrete," to appear in Proceedings of ASCE Engineering Mechanics Division.
5. Sneddon, I. N., (1951), Fourier Transforms, McGraw-Hill, N.Y.
6. Shah, S. P., Stroeven, P., Dalhuisen, D., and van Stekelenberg, P., (Sept. 1978), "Complete Stress-Strain Curves for Steel Fiber Reinforced Concrete in Uniaxial Tension and Compression," Proceedings, International Symposium, RILEM-ACI-ASTM, Sheffield, 339-408.
7. Naaman, A. E., Moavenzadeh, F., and McGarry, F. J., (1974), "Probabilistic Analysis of Fiber Reinforced Concrete," Proceedings of ASCE Engineering Mechanics Division, 100, No. EM2, 397-413.
8. Velazco, G., Visalvanich, K., and Shah, S. P., (1980), "Fracture Behavior of Fiber Reinforced Concrete Beams," Cement and Concrete Research, 10, 41-51.

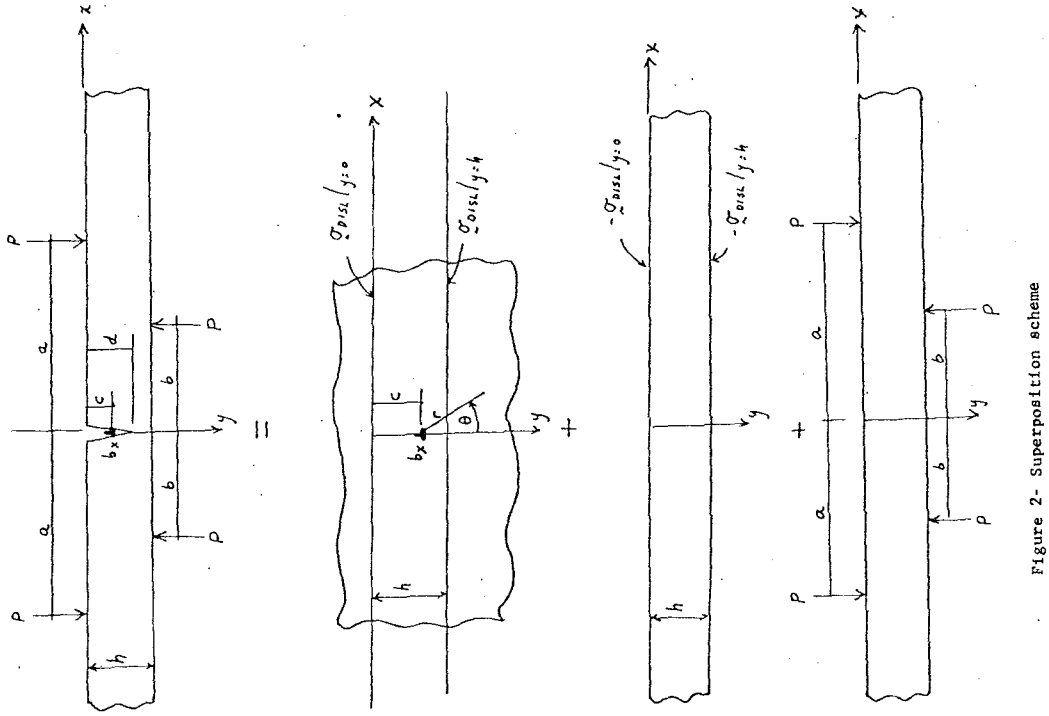

Figure 2- Superposition scheme

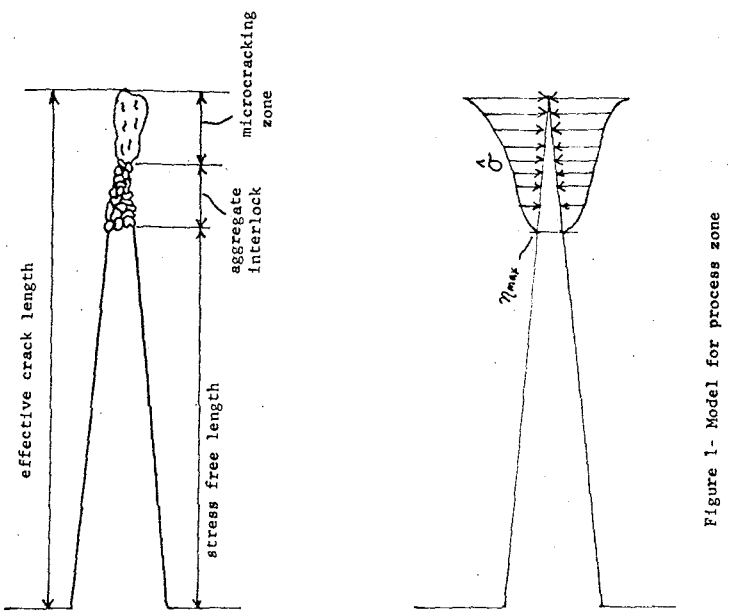

Figure 1- Model for process zone

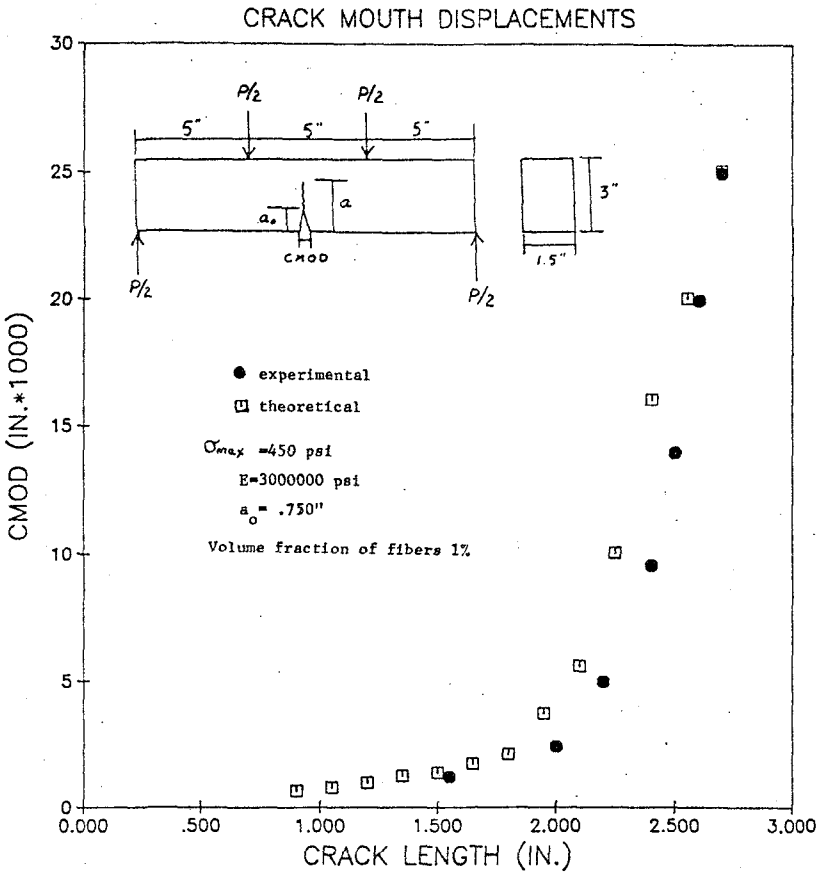

Figure 3- Velazco's Fiber Reinforced Mortar Specimen 1-8

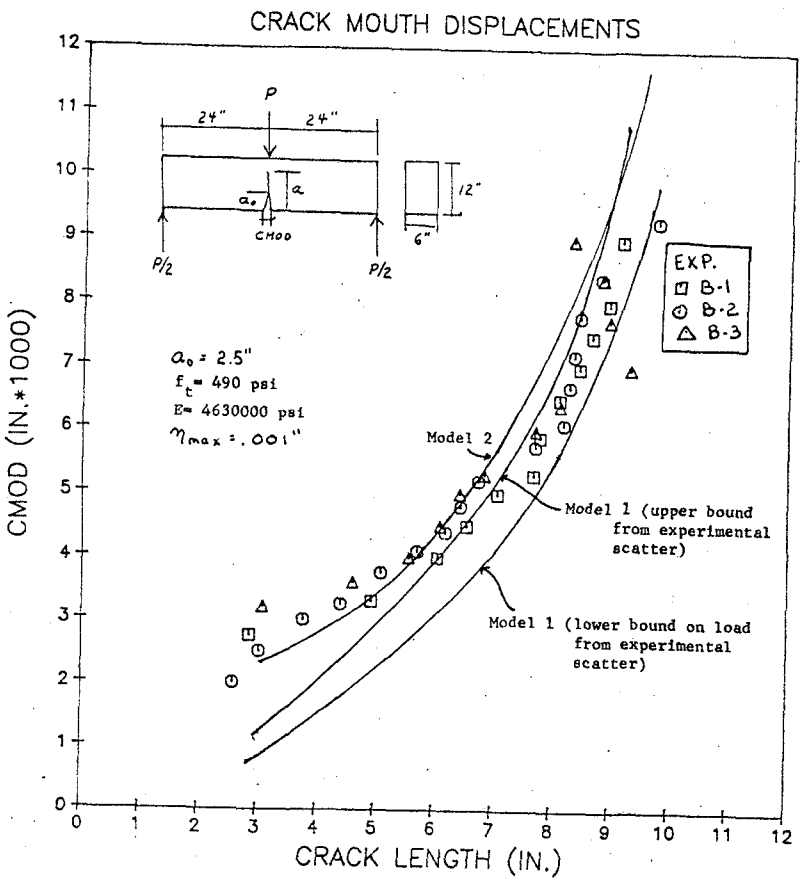

Figure 4- Catalano and Ingraffea B-series beams

EXAMPLES OF PRACTICAL RESULTS ACHIEVED BY MEANS OF THE FICTITIOUS CRACK MODEL

A. Hillerborg
Professor of Building Materials
Lund Institute of Technology
P.O.Box 725, S-220 07 LUND, Sweden

Introduction

By means of the fictitious crack model /1, 2, 3/ it is possible to analyse all types of tensile fracture in concrete, rock and other materials. Some examples of results will be demonstrated. The analyses are based on the simplifying assumption that the σ-w-curve is either one single straight line (S.L) or two straight lines imitating the properties of concrete (C), Fig 1. The σ-w-curve shows the relation between the additional deformation w of the fracture zone and the stress across this zone. The area below the σ-w-curve represents the fracture energy G_F per unit newly formed crack area.

From the material properties E = elastic modulus, f_t = tensile strength, and G_F, it is suitable to calculate a material property l_{ch}, called the characteristic length of the material

$$l_{ch} = EG_F/f_t^2$$

The value of l_{ch} is often about 10 mm for cement paste, 200 mm for mortar and 400 mm for concrete.

Analysis of fracture mechanics tests

The entire behaviour in a test can be analysed and simulated, e.g. complete load-deformation curves, crack opening displacements, crack growth etc. Consequently the probable result of a test can be calculated.

Fig 2 shows the calculated G_c-values (and the corresponding K_{Ic}-values), which can be expected in a three point bend test, if the evaluation is made by means of linear elastic fracture mechanics. The lower curves are valid if the crack length at maximum load is assumed to be equal to the notch depth a, whereas the upper curves are valid if the crack length at maximum load is calculated from the compliance.

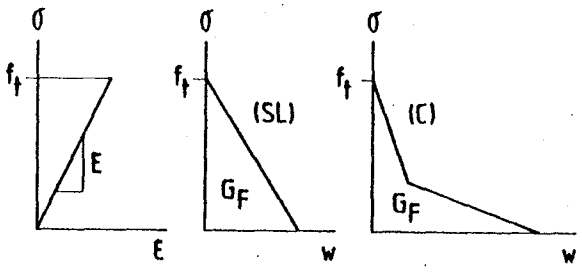

Fig. 1.

Fig 3 shows the notch sensitivity, i.e. the change in net bending strength with the notch depth /3/. From this figure it is evident that the notch sensitivity is not a material property, but that it depends on

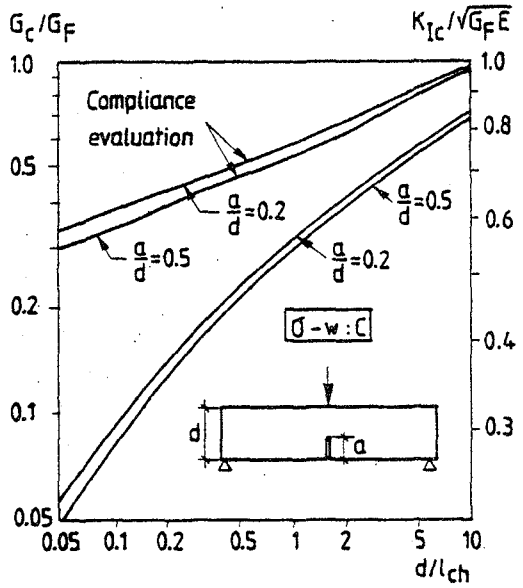

Fig. 2.

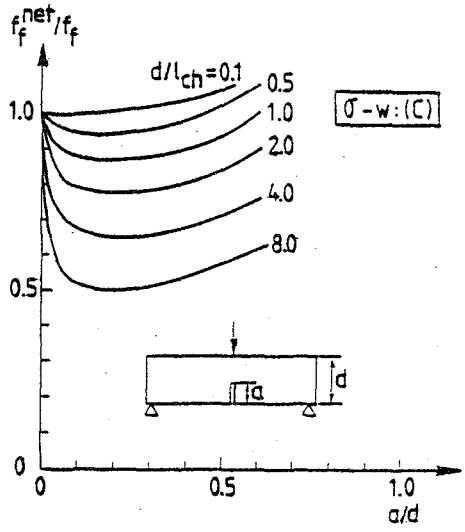

Fig. 3.

the ratio d/l_{ch}.

Fig 4 shows theoretical K_R-curves for a beam with different initial notch depths and with the assumption that the crack tip is situated where w = 0.01 mm /3/. From this figure it might be concluded that the K_R-curve can be regarded as a material property. Fig 5 /3/ however shows that this is not the case, as the curve varies considerably where different beam depths are concerned.

In the same way as has been illustrated in Figs 3-5 all kinds of fracture mechanics test can be analysed, e.g. double cantilever beams, compact tension tests, ring tests, chevron notch tests etc. The double torsion test has been analysed /4/ with the conclusion that the ordinary evaluation method is valid only if a concrete specimen is very large, about 0.6 x 3 m.

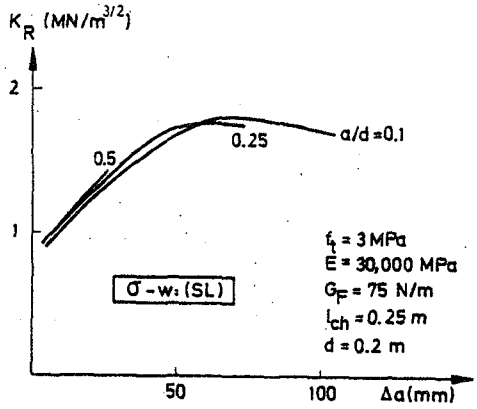

Fig. 4.

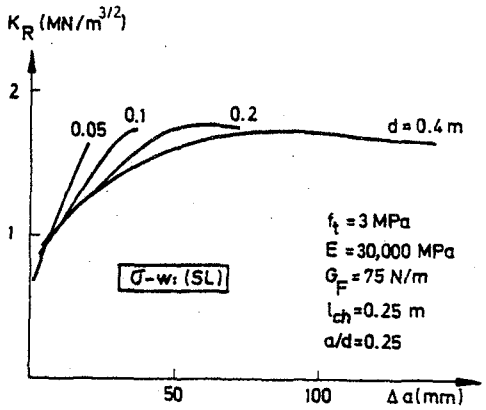

Fig. 5.

Structural design

The fictitious crack model can be applied to uncracked (unnotched) specimens as well as to cracked, as opposed to conventional fracture mechanics, which can only be applied where cracks already exist.

The first application of the model was the calculation of the ratio between the flexural strength f_f (modulus of rupture) and the tensile strength /1/. A result of such an analysis is shown in Fig 6, where the influence of the choice of the shape of the σ-w-curve is also demonstrated. The dashed line shows the influence of shrinkage in an indoor climate. It is evident that this influence increases very much with the beam depth d. The flexural strength is of importance for the transition from the uncracked to the cracked state in a reinforced beam.

The model has been applied to unreinforced concrete pipes by Gustafsson /5/. The pipes can fail in bending acting as a beam or as a ring. The theoretical failure load has been calculated in these two cases and the corresponding maximum stress at failure according to the ordinary elastic theory has been determined. This stress is a formal flexural strength, and it is denoted by f_f. The results are given in Figs 7 and 8 for a concrete quality with l_{ch} = 380 mm. It can be seen that the formal strength for ring failure is much higher than that for beam failure. The results are in agreement with test results. The diagrams are now used by concrete pipe manufacturers for the design of pipes, and they

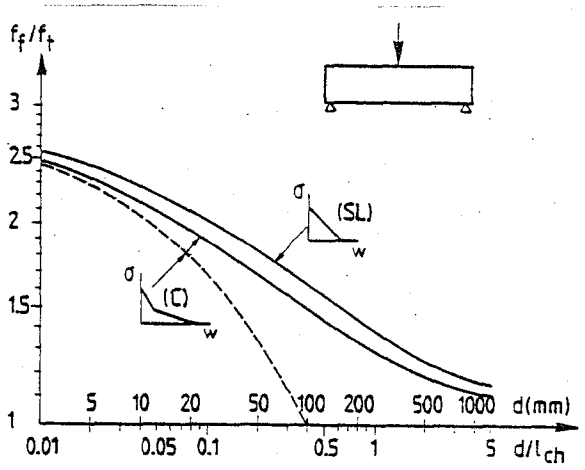

Fig. 6.

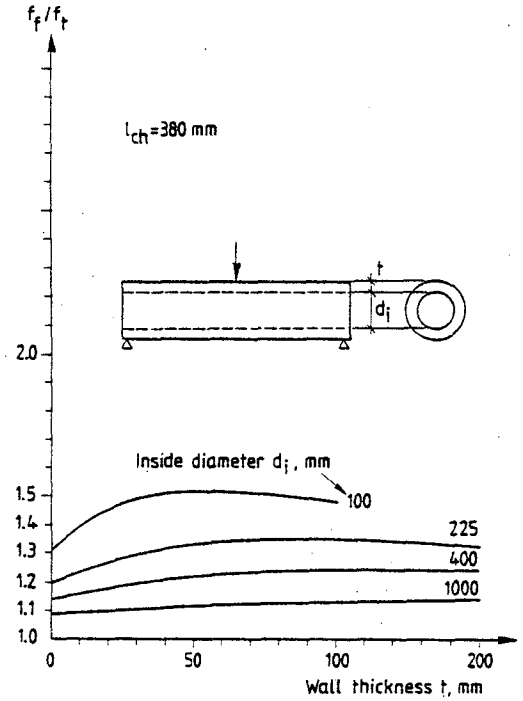

Fig. 7.

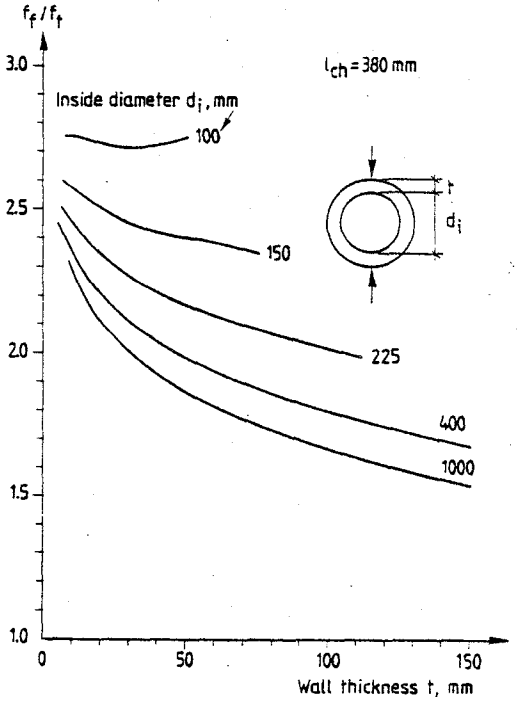

Fig. 8.

are an example of the application of the fictitious crack model in design.

The most advanced application so far is the analysis of shear fracture of concrete beams with longitudinal reinforcement, performed by Gustafsson /6, 7/. Some results are shown in Fig 9. The upper scale on the horizontal axis is valid for a concrete quality with l_{ch} = 250 mm. On the whole the theoretical results agree well with the test results, e.g. regarding the influence of span/depth-ratio, reinforcement percentage ρ_ℓ, and beam depth. The theoretical values are however lower than the test values, because aggregate interlock and reinforcement dowel action have not yet been included in the analysis. It is possible to do this in principle, but there are practical numerical problems as well as a lack of knowledge of some of the material properties.

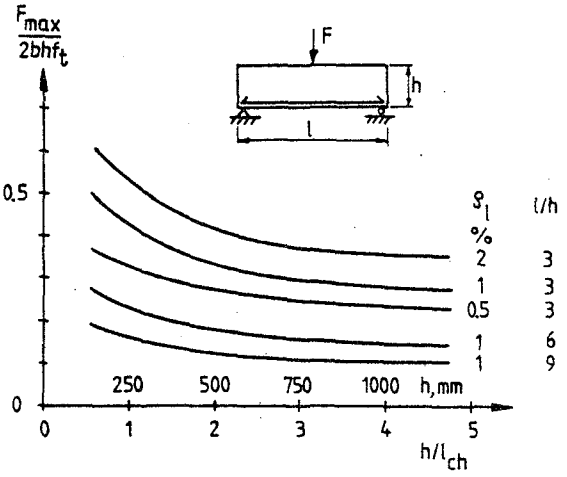

Fig. 9.

References

1. Hillerborg, A., Modéer, M., Peterson, P.E., (1976), "Analysis of crack formation and crack growth in concrete by means of fracture mechanics and finite elements", Cement and Concrete Research, 6, 773-782.
2. Modéer, M., (1979), "A fracture mechanics approach to failure analysis of concrete materials", Report TVBM-1001, Div of Building Materials, Lund Inst of Techn., Sweden.
3. Peterson, P.E. (1981), "Crack growth and development of fracture zones in plain concrete and similar materials", Report TVBM-1006, Div of Building Materials, Lund Inst of Techn., Sweden.
4. Hillerborg, A. (1983), "Theoretical analysis of the double torsion test", Cement and Concrete Research, 13, 69-80.
5. Gustafsson, P.J. (1983), "Oarmerade betongrörs böjbrottlast och ringbrottlast", Report TVBM-3012, Div of Building Materials, Lund Inst of Techn., Sweden.
6. Peterson, P.E., Gustafsson, P.J. (1980), "A model for calculation of crack growth in concrete-like materials", Second Int. Conf. on Numerical Methods in Fracture Mechanics, Swansea, Proc., 707-719.
7. Gustafsson, P.J., Private communication.

VIBROTHERMOGRAPHY OF GRANULAR SOILS

M.P. LUONG

Maître de Recherche C.N.R.S.
LABORATOIRE DE MECANIQUE DES SOLIDES
ECOLE POLYTECHNIQUE
91128 PALAISEAU, France

Introduction

Rheological properties of granular soils subjected to vibratory and transient loading can be interpreted at the granular level where the solid particles interact leading to a global aggregation (contractancy) or disaggregation (dilatancy) according to the following main deformation mechanisms.

Deformation mechanisms

A cohesionless granular material can be considered as a grain assembly. Observed macroscopic deformations are derived essentially from their structural modifications, i.e. rearrangements of the constitutive grains inducing irreversible contractive or dilative volume changes :

- Consolidation mechanism corresponding to the mutual tightening of solid particles inducing a contractive behaviour ;
- Distortion mechanism due to irreversible grain slidings leading initially to a contractive behaviour followed by a dilative behaviour when the deviatoric stress level $\eta = q/p$ exceeds the grain interlocking threshold called characteristic state (stationary volume change) ;
- Attrition mechanism subsequent to asperity breakage and grain crushing modifying the relative density under high stresses. The resulting effect is a contractive behaviour.

Characteristic threshold

The characteristic threshold is revealed by the appearance of a dilatancy loop when the load cycle exceeds the deviatoric stress level η_c (Fig. 1.a and 1.b). Such observations enable the determination of the entanglement capacity of a granular material [2].

Below the characteristic threshold, the intergranular contacts are

stable. The limited slidings tend to a maximal aggregation. In this subcharacteristic domain or contractancy zone, a hysteresis loop occurs when reloading. The mechanical behaviour depends upon the load history.

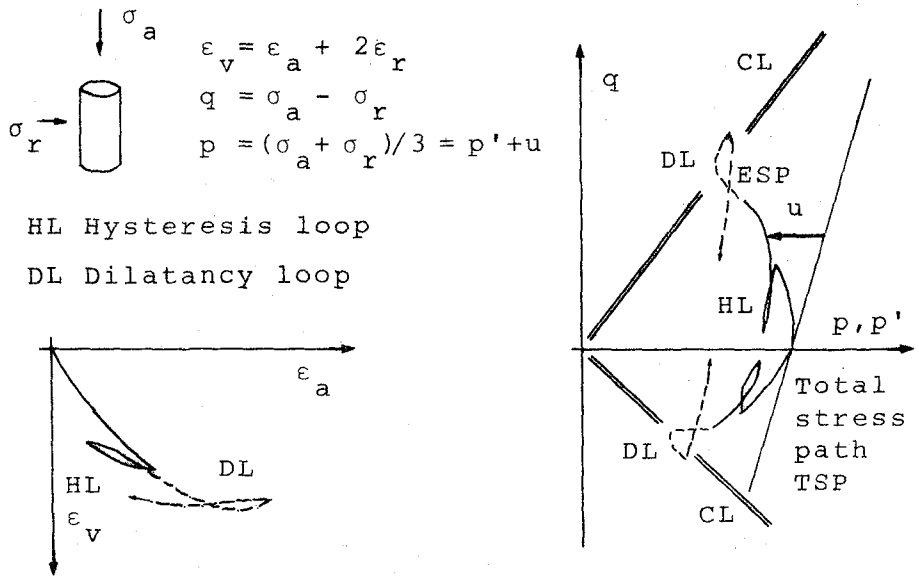

(1.a) Under drained condition. (1.b) Under undrained condition.

Figure 1 : Dilatancy loop observed after a load cycle crossing the characteristic line CL.

Above the characteristic threshold, the grain contacts become unstable, leading to significant slidings due to interlocking breakdown. A reload shows a dilatancy loop with memory loss of load history and a softening phenomenon occurs.

Heat generated by friction

When a siliceous sand grain slides against another one, there occurs a motion resistance called friction. What is the cause and what really happen on the contact surface ?

Bowden and Tabor [1] demonstrated that when quartz or glass surfaces slide over one another in the dark, small sparkling points of light can be seen at the interface.

The friction between grains generates heat in the same fashion as when prehistoric man used silex stones to generate fire.

In the conventional triaxial test, if the load is cycled within the subcharacteristic domain under the characteristic threshold η_c, the deformation work (a) given by the hysteresis loop in the (q,ε_a) diagram is very small. On the contrary, if the characteristic threshold is exceeded, a very large dissipation of energy (B) occurs as shown in the Figure 2.

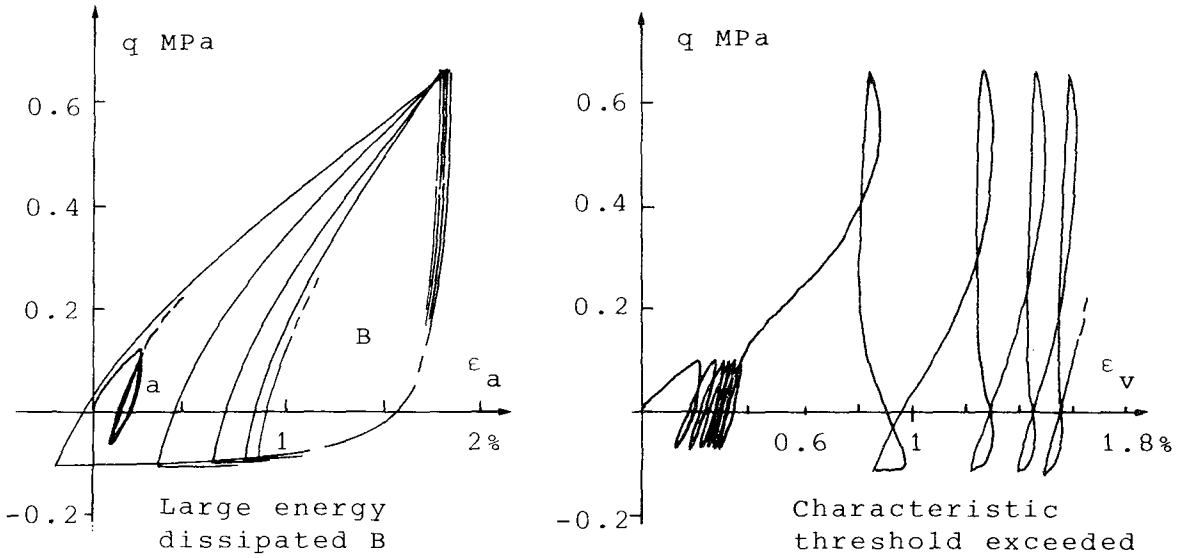

Figure 2 : *Conventional triaxial test (Fontainebleau sand γ_d = 15.7 kN/m^3)*

At the Laboratoire de Mécanique des Solides, infrared videothermography is used in real time with an infrared detector which treats the detected infrared signals and displays these upon a television monitor with colour series of 1°C. for each step with the aid of a colourer.

Experimental set-up and Results

The behaviour of a Stampian sand (Fontainebleau sand) is studied when subjected to two types of vibratory loading.

a- *Conventional triaxial loading : Indirect shearing*

A cylindrical sand sample (dry unit weight γ_d = 15.7 kN/m^3 ; void ratio e = 0.720 ; relative density I_D = 0.62) confined under a constant isotropic pressure of 100 kPa is subjected to a vibratory force generated by a steel mass located at the top of the specimen excited by an electrodynamic vibrator.

When the frequency reaches 87 Hz, with a controlled displacement of 1mm at the base, the specimen (70 mm diameter - 150 mm high) is in resonance and presents a striction zone where the deviatoric stress level exceeds the characteristic threshold of interlocking breakdown of the granular structure, (Fig. 3.a).

b- *Cylindrical loading : Direct shearing*

A tubular sand sample at the same initial density confined under a pressure of 50 kPa is directly sheared by a concentric steel cylinder excited in an axial vibratory motion by the electrodynamic generator.

In this case of loading, the principal stress axes rotate during loading. At the frequency of 80 Hz and with a controlled displacement of 1mm, the characteristic threshold is reached and hot colours due to heat production by friction appear as shown in the figure 3.b.

Concluding remarks

Infrared vibrothermography demonstrates the thermal dissipation of sheared granular material characterizing the sliding mechanism of grains when the granular interlocking structure breaks down on exceeding the characteristic threshold.

This non-destructive testing technique allows records and observations in real time of heat patterns produced by the dissipation of energy due to friction between grains.

The infrared vibrothermographic test couples mechanical and thermal energy. Additionally it offers the potential of directly monitoring the stress state of particle rearrangements or characteristic threshold and of predicting the degradation or damage of granular materials by active heating.

References

[1] Bowden F.P., Tabor D., (1959), "Friction et lubrification", Monographies Dunod, Paris.

[2] Luong M.P., (1980), "Stress-strain aspects of cohesionless soils under cyclic and transient loading", Proc. Int. Symp. on S.U.C.A.T.L., Swansea, Jan. 1980, U.K.

[3] Reifsnider K.L., Henneke E.G., Stinchcomb W.W. (1980), "The mechanics of vibrothermography" in Mechanics of Nondestructive Testing ed. by W.W. Stinchcomb, pp. 249-276.

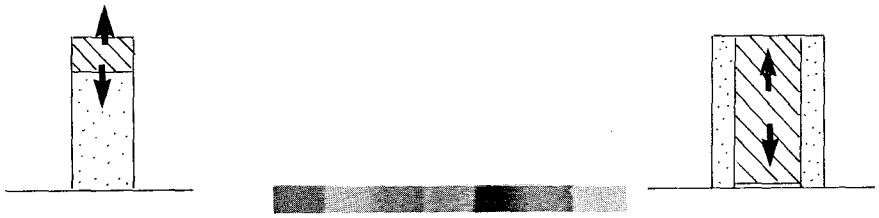

Each colour band corresponds to one degree Celsius

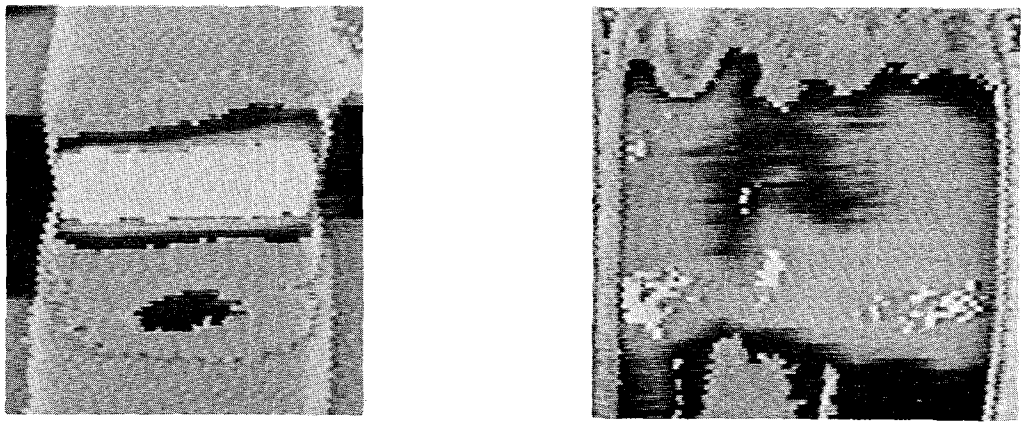

a. Indirect shearing *b. Direct shearing*

Figure 3 - *Heat production by vibratory shearing.*

GRAVITY FLOW OF BULK SOLIDS

Andrew W. Jenike
Consultant to Jenike & Johanson Inc
No. Billerica, Massachusetts 01862 - U.S.A.

The term bulk solids is used to describe ores from mines and quarries, grains from farmers' fields and all therefrom derived particulate solids which are transported, stored and handled in bulk. The annual tonnage of these solids moved from the ground to their destination is in the billions.

The characteristics of these solids vary widely: the particle size and composition varies from micron size titanium dioxide to meter-size blocks of mine-run ores, the strength of the particles from that of cornflakes to steel balls, the frictional and cohesive properties from those of lubricated polyethylene pellets to slimy ores.

Our interest is in the flow of these solids into, through and particularly out of flow channels, such as mine shafts and storage vessels.

The theory of flow, which is over twenty years old [1,2,3], is based on two characteristics which all flowing solids have in common:

1. While flowing, particles slide on each other hence, the bulk solid is in a limiting, i.e. plastic state of stress.

2. When an obstruction to flow occurs and flow in a channel ceases, it is because the cohesive and frictional surface properties of the particles are sufficiently high to sustain the stresses acting within the obstruction. An obstruction may be in the form of an arch across the channel or a crater around the outlet of the vessel. In both types of obstruction the critical factor is the unconfined compressive strength, fc, which the solid has at the surface of the arch or crater.

Flow criterion

It follows that a bulk solid will flow through a channel provided that, everywhere within the channel, the strength fc is less than the unconfined compressive stress $\bar{\sigma}_1$ acting within the solid at the surface of a potential obstruction:

$$fc < \bar{\sigma}_1 \qquad (1)$$

The design for assured flow from vessels requires the knowledge of those two parameters and the satisfaction of inequality (1).

Unconfined Yield Strength, fc

The strength fc of a solid at a given temperature and surface moisture is a function of the major pressure σ_1 which has consolidated the solid and the time of action of that pressure while the solid was at rest. Obstructions to flow caused by the interlocking of particles, which are large with respect to the width of the channel, will not be discussed here. Let us consider a typical operation of a storage silo, Figure 1. The rate of outflow is controlled by a feeder. Assume that the silo is filled with solid with negligible impact. The pressures within the solid are those due to gravity. Under the action of these pressures material consolidates, its density increases. As particles are brought closer together, cohesive forces increase. They usually increase also with the time of consolidation at rest under constant pressure. The relation $fc(\sigma_1)$, where σ_1 is called the major consolidating pressure, is referred to as the flow-function of a solid. Typical flow functions are shown in Figure 2. The higher the location of the curve, the greater the strength of the bulk solid and, hence the lower its flowability.

When the feeder is started and the solid flows, a limiting state of stress develops within the converging part of the channel. The ratio of the major pressure σ_1 to the minor pressure σ_2 assumes a practically constant value

$$\frac{\sigma_1}{\sigma_2} = \frac{1 + \sin \delta}{1 - \sin \delta} \tag{2}$$

for a sufficiently small range of σ_1. δ is called the effective angle of friction of a solid and is a vital characteristic of bulk solids.

In most industrial applications the outflow velocity is small and the effects of acceleration can be ignored. The equations of equilibrium in polar coordinates r,θ for plane strain (m=0) and in spherical coordinates r,θ,α for axial symmetry (m=1) are

$$\frac{\partial \sigma_r}{\partial r} + \frac{1}{r}\frac{\partial \tau_{r\theta}}{\partial \theta} + \frac{1}{r}\left[\sigma_r = \sigma_\theta + m(\sigma_r - \sigma_\alpha) + m\tau_{r\theta} \cot \theta\right] + \gamma \cos \theta = 0. \tag{3}$$

$$\frac{\partial \tau_{r\theta}}{\partial r} + \frac{1}{r}\frac{\partial \sigma_\theta}{\partial \theta} + \frac{1}{r}\left[m(\sigma_\theta - \sigma_\alpha) \cot \theta + (2 + m)\tau_{r\theta}\right] - \gamma \sin \theta = 0. \tag{4}$$

Substitute, as follows:

$$\sigma r = \gamma\ r\ s(1 + \sin\delta\ \cos\ 2\Psi) \tag{5}$$

$$\sigma\theta = \gamma\ r\ s(1 - \sin\delta\ \cos\ 2\Psi) \tag{6}$$

$$\tau r\theta = \gamma\ r\ s\ \sin\delta\ \sin\ 2\Psi \tag{7}$$

$$\sigma\alpha = \gamma\ r\ s(1 + \sin\delta) \tag{8}$$

to obtain

$$\frac{\partial s}{\partial\theta} + s\ f(r,\theta) + g(r,\theta) = 0, \tag{9}$$

$$r\ \frac{\partial s}{\partial r} + s\ h(r,\theta) + j(r,\theta) = 0, \tag{10}$$

where

$$f(r,\theta) = 2(\frac{\partial\psi}{\partial\theta} + 1)\frac{\sin\delta}{\cos^2\delta}\ \sin\ 2\psi + 2r\ \frac{\partial\psi}{\partial r}\ \frac{\sin\delta}{\cos^2\delta}(\sin\delta + \cos\ 2\psi) +$$

$$+ \frac{1}{\gamma}\ \frac{\partial\gamma}{\partial\theta} + m\ \frac{\sin\delta}{\cos^2\delta}(1 + \sin\delta)[\sin\ 2\psi - \cot\theta(1 + \cos\ 2\psi)], \tag{11}$$

$$g(r,\theta) = -\ \frac{\sin\delta}{\cos^2\delta}\ \sin\ (\theta + 2\psi) - \frac{\sin\theta}{\cos^2\delta}, \tag{12}$$

$$h(r,\theta) = 1 + 2(\frac{\partial\psi}{\partial\theta} + 1)\ \frac{\sin\delta}{\cos^2\delta}(\cos\ 2\psi - \sin\delta) - 2r\ \frac{\partial\psi}{\partial r}\ \frac{\sin\delta}{\cos^2\delta}\ \sin\ 2\psi +$$

$$+ \frac{r}{\gamma}\ \frac{\partial\gamma}{\partial r} + m\ \frac{\sin\delta}{\cos^2\delta}(1 + \sin\delta)(\cot\theta\ \sin\ 2\psi + \cos\ 2\psi - 1), \tag{13}$$

$$j(r,\theta) = -\ \frac{\sin\delta}{\cos^2\delta}\ \cos(\theta + 2\psi) + \frac{\cos\theta}{\cos^2\delta}. \tag{14}$$

Now consider that as the solid flows toward the outlet, r becomes small and in order to obtain an approximate expression for the stresses at the outlet assume r=0 and density γ = constant. This produces the following set of two ordinary differential equations which define a radial stress field independent of the top boundary condition of the converging channel.

$$\frac{d\psi}{d\theta} = F(\theta,\psi,s) =$$

$$= -\ 1 - [m\ s\ \sin\delta(1 + \sin\delta)(\cot\theta\ \sin\ 2\psi + \cos\ 2\psi - 1) + \cos\theta -$$

$$- \sin\delta\ \cos(\theta + 2\psi) + s\ \cos^2\delta]/2\ s\ \sin\delta(\cos\ 2\psi - \sin\delta), \tag{15}$$

$$\frac{ds}{d\theta} = G(\theta,\psi,s) =$$

$$= \frac{s \sin 2\psi + \sin(\theta + 2\psi) + m\, s \sin \delta[\cot\theta(1 + \cos 2\psi) - \sin 2\psi]}{\cos 2\psi - \sin \delta} \qquad (16)$$

Such convergence is a common characteristic of hyperbolic systems of PDE's. The above simplifications raise the obvious question of the rapidity of convergence and, hence, of the validity of the results to be obtained. Analytical evidence of convergence of general fields to radial is presented in references 3, 7 and 8. More importantly, a method of design based on these assumptions has been used - all over the world - for the past twenty-five years, and is still being used.

The effective angle of friction δ and the unconfined yield strength fc are measured as a function of the major consolidating pressure σ_1 on a shear tester [2,3,9], Figure 3.

The other side of inequality (1), stress $\bar{\sigma}_1$, is obtained from an analysis of stresses in a self-sustaining, unloaded arch spanning the channel [5]. Stress σ_1 as well as stress $\bar{\sigma}_1$ are computed at the wall of the channel. With the assumption of a radial stress field, both these stresses increase linearly with the width of the channel and their ratio, called the flow-factor,

$$ff = \frac{\sigma_1}{\bar{\sigma}_1} \qquad (17)$$

determines the flowability of a channel. ff is a function of m,δ, the channel slope angle θ' and the wall friction angle ϕ'. Values of the flowfactor have been computed for a range of the above parameters. Examples are given in Figure 4 for $\delta=50°$. In axial symmetry (m=1) the range of wall conditions (θ_c',ϕ') within which flow can occur is bounded and depends on δ.

In the proess of design the flowfunction, FF, Figure 2, is measured for the prescribed solid and operating condition (moisture, temperture, time of storage at rest) and is superimposed over the appropriate flow-factor (m,δ,θ',ϕ'), Figure 5. The two lines intersect at a value fcrit = fc. For conditions above the point of intersection, inequality (1) is satisfied and gravity flow obtains. The point of intersection thus determines the minimum outlet dimension

$$B = fcrit \times H(m,\theta')/\gamma \qquad (18)$$

The design method is fully described in reference [9] which contains a series of charts of ff, function $H(m,\theta')$ and others.

References

1. Jenike, A. W. and Shield, R. T. (Dec 1959), "On the Plastic Flow of Coulomb Solids Beyond Original Failure," J. of Appl. Mech. V. 27, 599-602.

2. Jenike, A. W., Elsey, P. J. and Woolley, R. H. (1960), "Flow Properties of Bulk Solids," Proceedings, A.S.T.M., V. 60, 1168-1181.

3. Jenike, A. W. (Oct 1961), "Gravity Flow of Bulk Solids," Bul. 108, Utah Engineering Experiment Station, University of Utah, Salt Lake City, Utah.

4. Jenike, A. W. (1962), "Gravity Flow of Solids," Trans. of the Institution of Chemical Engineers, V. 40, n 5, 264-271.

5. Jenike, A. W. and Leser, T. (Aug 1963), "A Flow-No Flow Criterion in the Gravity Flow of Powders in Converging Channels," Fourth International Congress on Rheology, Brown University.

6. Jenike, A. W. (1964), "Steady Gravity Flow of Frictional-Cohesive Solids in Converging Channels," J. of Appl. Mech., V. 31, Series E, n 1, 5-11.

7. Johanson, J. R. (Sept 1964), "Stress and Velocity Fields in the Gravity Flow of Bulk Solids," J. of Appl. Mech., Series E, V. 86.

8. Jenike, A. W. (1965), "Gravity Flow of Frictional-Cohesive Solids - Convergence to Radial Stress Fields," J. of Appl. Mech., Series E, V 32, 205-207

9. Jenike, A. W. (Nov 1964), "Storage and Flow of Solids," Bul. 123, Utah Engineering Experiment Station, University of Utah, Salt Lake City, Utah.

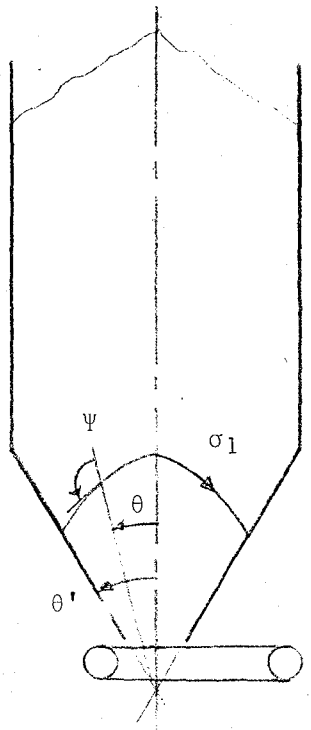

Figure 1 - Silo

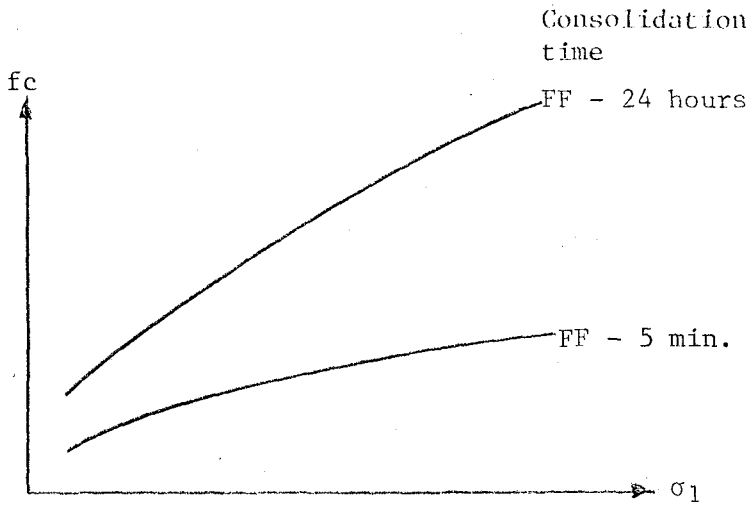

Figure 2 - Flow-functions

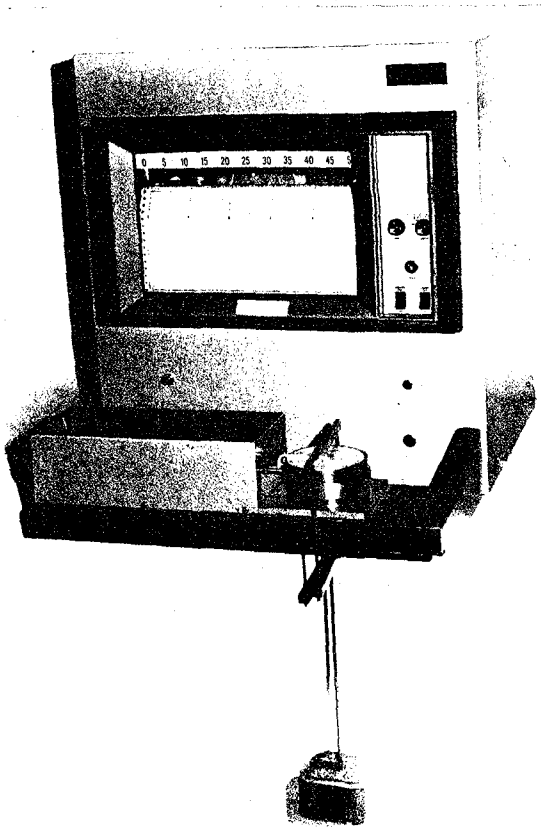

Figure 3 - Shear tester

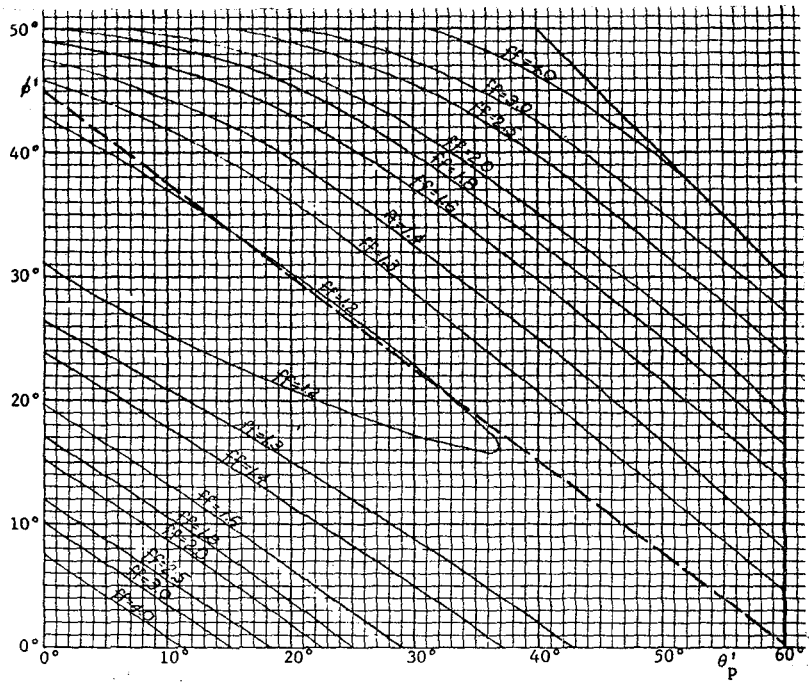

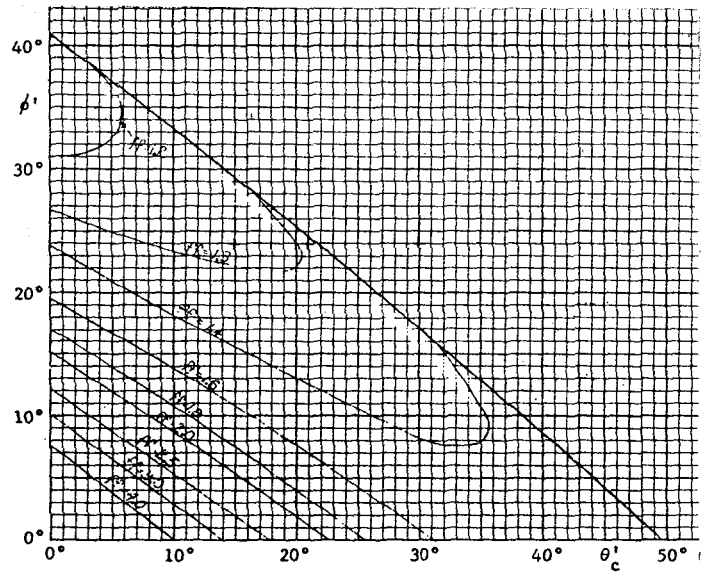

Figure 4 - Flow-factor contours for $\delta = 50°$

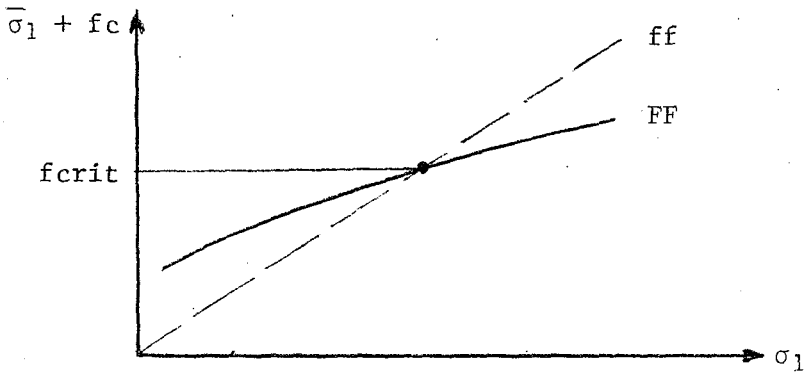

Figure 5 - Minimum outlet diameter

MECHANICAL MODELING OF THE SHRINKING AND SWELLING OF POROUS SOLIDS

S. C. Cowin
Professor of Mechanics
Department of Biomedical Engineering
Tulane University
New Orleans, LA 70118

Introduction

The purpose of this note is to point out that the theory of elastic materials with voids [1,2] can be used to model the swelling and shrinking observed in hydroscopic solids. Hydroscopic solids are discussed first, then modeling of the swelling and shrinking of these materials. Examples of hydroscopic materials include natural materials such as geological materials and plant and animal tissues and many man made composites. Examples of the effects of swelling and shrinking of plant and animal tissue include the warping and cracking of drying lumber and swelling of animal tissue in solutions of different salinity. Examples of the effects of swelling and shrinking of geological materials include soil heaving due to permafrost and the cracks that appear in the sundried gumbo at the bottom of a former mud puddle. There are numerous industrial processes which involve either the drying or wetting of geological materials and plant and animal tissues.

The fluid in the hydroscopic materials is classified here as either fluid that is free or fluid that is structural. The free fluid can move freely in the pores of the material body and its movement does not involve changes in the volume of the solid matrix of the material. On the other hand, the movement of water designated as structural does involve changes in the volume of the solid matrix. In the literature on wood drying, for example, free water is as defined above and the additional moisture content of a wood specimen is said to be "bound" water; i.e. water that is chemically bound within cell walls. When the moisture content of wood is progressively reduced, the moisture content at which the cell walls are completely saturated (that is to say all the bound water is retained) but no water exists in the cell cavities (no free water) is called the "fiber saturation point". For wood the fiber saturation point is about 30% moisture content. The fiber saturation point is generally considered to be the moisture content below which the physical and mechanical properties of wood begin to change as a function of moisture content. In the literature on soils and animal tissue the definitions employed by writers are not clear and consistent as they are in the literature on wood. Thus the words structural and free have been chosen to distinguish between the water that changes the volume of the solid matrix in which it is contained, and the water that does not cause volume changes, respectively.

There is not a theory among the traditional continuum theories which permits a porous body to enlarge or reduce the overall volume it occupies in the

absense of body tractions and gravitation. There is such a mechanism, however, in the theory of elastic materials with voids [1, 2]. In this theory there is a field representation of the balance of self-equilibrated force systems at each point in the continuum. Examples of self-equilbrated force systems include the force system surrounding a slightly larger sphere is a regular array of close packed identical spheres under compression, or the force system induced in the surrounding material by the swelling of freezing water in a closed pore of the material. In the classical theory of elasticity there are singular solutions associated with self-equilibrated force systems. These are called "centers of dilation or compression" or "double forces without moments". In the theory of linear elastic materials with voids these self-equilibrated force systems are assumed to exist at every point in the medium and are not associated with singularities. The purpose of this note is to point out that continuously distributed centers of dilation and compression can be used to model the swelling and shrinking of porous materials under no surface tractions or gravitational force.

In the next section the theory of elastic materials with voids is briefly summarized and, in the following section, an example of the theory's predictions in the case of homogeneous swelling or shrinking is presented. In the final section directions for the development of complete theories of swelling and shrinking are suggested.

The Linear Theory of Elastic Materials with Voids

The basic concept underlying this theory is that of a material for which the bulk density ρ is written as the product of two fields, the density field of the matrix material γ and the volume fraction field ν ,

$$\rho = \gamma\nu \quad . \tag{1}$$

This representation of the bulk density of the material introduces an additional degree of kinematic freedom in the theory, the solid volume fraction ν . The linear theory of elastic materials with voids deals with small changes from a reference configuration of a porous body. In the reference configuration (1) can be written as $\rho_R = \gamma_R \nu_R$ and it is assumed here that ν_R is spatially constant. As is customary in linear elasticity the reference configuration is assumed to be stress free and strain free.

The independent kinematic variables in the linear theory are the displacement field $u_i(\underset{\sim}{x},t)$ from the reference configuration and the change in volume fraction from the reference volume fraction, $\phi(\underset{\sim}{x},t)$,

$$\phi(\underset{\sim}{x},t) = \nu(\underset{\sim}{x},t) - \nu_R \quad , \tag{2}$$

where $\underset{\sim}{x}$ is the spatial position vector in cartesian coordinates and t is time. The infinitesimal strain tensor $E_{ij}(\underset{\sim}{x},t)$ is determined from the displacement field u_i by the relation

$$E_{ij} = \tfrac{1}{2}(u_{i,j} + u_{j,i}) \quad , \tag{3}$$

where the comma followed by a lower case Latin letter indicates a partial derivative with respect to the indicated coordinate axes.

The equations of motion governing a linear elastic continuum with voids are the balance of linear momentum,

$$\rho \ddot{u}_i + T_{ij,j} + \rho b_i \quad , \tag{4}$$

and the balance of equilibrated force,

$$\rho k \ddot{\phi} = h_{i,i} + g + q \quad , \tag{5}$$

where T_{ij} is the symmetric stress tensor, b_i is the body force vector, h_i is the equilibrated stress vector, k is the equilibrated inertia, g is the intrinsic equilibrated body force and q is the extrinsic equilibrated body force. The extrinsic equilibrated body force q, which was denoted by $p\ell$ in [1] and [2], is of major importance in the problem at hand. The interpretation of q is as a force system like a center of dilation in classical elasticity, but it is a center of dilation that exists at every point in the medium and which either acts at a distance or is externally controllable. Jenkins [3] suggested that q be interpreted as an externally controlled pore pressure. In modeling the swelling and shrinking mechanism q is an internal, self-equilibrated, pore pressure field that exerts no external surface tractions.

The constitutive equations for the linear isotropic theory of elastic materials with voids relate the stress tensor T_{ij}, the equilibrated stress vector h_i and the intrinsic equilibrated body force g to the strain E_{ij}, the change in volume fraction ϕ, the time rate of change of the volume fraction $\dot{\phi}$, and the gradient of the change in volume fraction $\phi_{,i}$; thus

$$T_{ij} = \kappa \delta_{ij} E_{kk} + 2\mu (E_{ij} - \frac{1}{3} \delta_{ij} E_{kk}) + \beta \phi \, \delta_{ij} \tag{6}$$

$$g = -\omega \dot{\phi} - \xi \phi - \beta E_{kk} \text{ and } h_i = \alpha \phi_{,i} \quad . \tag{7}$$

The coefficients μ, α, β, ξ, ω and $\kappa = \lambda + \frac{2}{3}\mu$ all depend upon ν_R and μ, α, ξ, ω and κ must be positive and β must satisfy the inequality

$$\kappa \xi \geq \beta^2 \quad . \tag{8}$$

This inequality is incorrectly reported in [1], where a factor of four multiplies β^2 on the right hand side.

Prediction of Homogeneous Swelling or Shrinking

Within the context of the linear theory of elastic materials with voids a very simple case of homogeneous deformation is considered here in order to illustrate the swelling or shrinking mechanism implicit in the theory. The simple case is characterized not only by steady homogeneous stress, strain and volume fraction, but also by a neglect of gravitational forces and the rate effect in the theory (by setting the coefficient ω equal to zero). In

addition it is assumed that the body is under a uniform hydrostatic pressure at the boundary, $T_{ij} = -p\delta_{ij}$. Since the deformation is assumed to be homogeneous, the shape of the body is immaterial, but, to fix ideas, it could be taken as a unit cupe or unit shpere. Equations (4) and $(7)_2$ are satisfied identically and equations (6) and a combination of (5) and $(7)_1$ yield the following equations relating E_{ij} and ϕ to p and q:

$$\kappa\delta_{ij}E_{kk} + 2\mu(E_{ij} - \frac{1}{3}\delta_{ij}E_{kk}) + \beta\phi\delta_{ij} = -p\delta_{ij} \quad , \tag{9}$$

$$q = \xi\phi + \beta E_{kk} \quad . \tag{10}$$

The solution of these equations for E_{ij} and ϕ is

$$E_{ij} = -\delta_{ij}\frac{1}{3}\left(\frac{\xi p + \beta q}{\kappa\xi - \beta^2}\right), \quad \phi = \left(\frac{\beta p + \kappa q}{\kappa\xi - \beta^2}\right) \quad . \tag{11}$$

In the absence of external tractions, that is to say when the external pressure p is zero, E_{ij} and ϕ are given by

$$E_{ij} = -\delta_{ij}\frac{1}{3}\left(\frac{\beta q}{\kappa\xi - \beta^2}\right) \ , \ \phi = \frac{\kappa q}{\kappa\xi - \beta^2} \quad . \tag{12}$$

This result shows that the self equilibrated pressure q can cause volumetric deformation in the absence of surface tractions. This is the basic mechanism that is needed in a model of swelling or a model of shrinking. In the following section the formation of such models are discussed.

Toward the Development of Complete Theories of Swelling and of Shrinking of Elastic Bodies

The mechanism for swelling and shrinking implicit in the theory of ealstic materials with pores was illustrated in the previous section. In order to develop complete theories of shrinking or initial swelling, two more ingredients are necessary. First, a constitutive equation relating the self equilibrated pressure q to the moisture content is required. Second, a theory for moisture transfer in non-saturated porous bodies is needed. This type of theory is already under development [4, 5].

The problem of osmotically induced swelling due to varying concentrations of say, salt, in the pore fluid will require a different approach. In this case the porous medium is fully rather than partially saturated and the constitutive equation for q must depend upon the concentration of a particular species in the pore fluid, rather than upon the moisture content.

Acknowledgement

This work was supported by the National Science Foundation.

References

1. Cowin, S. C., Nunziato, J. W. (1983), "Linear Elastic Materials with Voids", J. Elasticity, 13, 125-147.

2. Nunziato, J. W., Cowin, S. C. (1979), "A Nonlinear Theory of Elastic Materials with Voids", Arch. Rat. Mech. Anal., 44, 175-201.

3. Jenkins, J. T. (1975), "Static Equilibrium of Granular Materials", J. Appl. Mech., 42, 603-608.

4. Harmathy, T. Z. (1969), "Simultaneous Moisture and Heat Transfer in Porous Systems with Particular Reference to Drying", I & EC Fundamentals, 8, 92-103.

5. Whitaker, S. (1977), "Toward a Diffusion Theory of Drying", Ind. Eng. Chem. Fundam., 16, 408-414.

STRESS-STRAIN CURVES OF CONCRETE UNDER MULTIAXIAL LOAD HISTORIES

Kurt H. Gerstle and Hon-Yim Ko
Department of Civil, Environmental,
and Architectural Engineering
University of Colorado
Boulder, CO 80309 U.S.A.

Reliable analytical predictions of the behavior and strength of reinforced concrete structures depend largely on our understanding, and appropriate analytical formulation, of the response of the plain concrete to applied stresses. A vast body of such analytical formulations has appeared in the literature in recent years. For their calibration and verification, these studies have depended on available test data for plain concrete under bi- and triaxial stresses. Almost all of the multiaxial tests available in the literature are under proportional, monotonically increasing loading to failure. Such tests are inadequate for the verification of comprehensive constitutive theories intended to account for stress histories consisting of arbitrary load paths, unloading, stress reversals, and reloading. Any element of a real structure could be expected to be exposed to such load sequences during its lifetime.

To provide some experimental data about the response of concrete to such general compressive load histories, a test program was undertaken at the University of Colorado during 1981 and 1982, sponsored by the N.S.F., utilizing the well-proven test cell which uses fluid pressure to apply arbitrary compressive principal stresses to a 4 inch cubical specimen. The results of these tests are to be collected in the form of a report to be made available to interested researchers. It is the purpose of this presentation to outline the contents and format of this report.

Sixty-five multiaxial load history tests were carried out. Stresses were applied in appropriate steps, and principal strains were measured and recorded for each load step, so that complete stress-strain curves could be drawn. Details of the test program are contained in Refs. 1 and 2.

The test program can be divided into the following series:

1. A series of 12 cyclic triaxial tests, consisting of cyclic hydrostatic preloading to various stress levels, followed by proportional deviatoric stress cycles without reversal along triaxial compression, simple shear, and triaxial extension paths.
2. A series of 8 cyclic triaxial tests consisting of hydrostatic preloading, followed by proportional deviatoric stress cycles with reversal along the same deviator paths as in Series 1.
3. A series of 13 tests consisting of hydrostatic loading, followed by proportional stress deviation, followed by a circular stress path within the deviatoric plane. (Fig. 2)
4. A series of 22 axisymmetric triaxial tests to explore load path effects; in addition to proportional and hydrostatic-deviatoric paths, this series contained staircase-type loadings to explore convergence to the proportional path, tests with hydrostatic stress increments with and without hydrostatic preloading, and tests under non-proportional loadings. (Fig. 3)
5. A series of 6 tests within the deviatoric plane, as well as a number of other tests specifically designed to check the meaning of loading and unloading. (Fig. 4)
6. A series of 4 tests of piecewise-biaxial loadings. (Fig. 5)

The presentation of the test results tries to avoid any analytical bias; accordingly, the information provided in the report consists only of the primary

test data, arranged for each test in the following sequence:

1. Plot of stress path.
2. Principal strains plotted against corresponding principal stress, as, for example, in Fig. 6.
3. Tabulation of applied principal stresses and measured principal strains in three directions for each load step, as also shown in Fig. 6.

It is hoped that these data will provide useful experimental information for scholars of concrete behavior.

References:

1. Scavuzzo, Robert, "Behavior of Concrete Under Multiaxial Load Histories". M.S. Thesis, C.E.A.E. Dept., University of Colorado, Boulder, 1982.

2. Stankowski, Thomas, "Concrete Under Multiaxial Load Histories", M.S. Thesis, C.E.A.E. Dept., University of Colorado, Boulder, 1983.

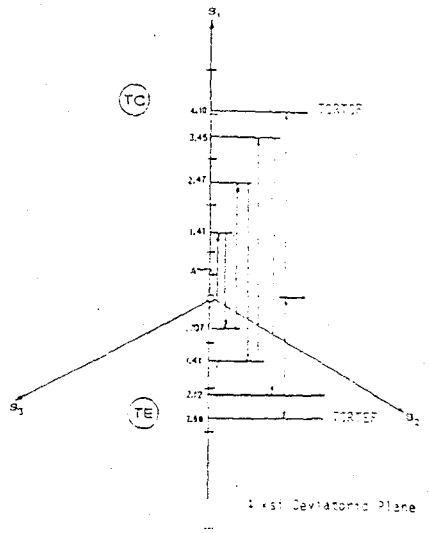

Fig.1
Series 2: Deviatoric Stress Cycles

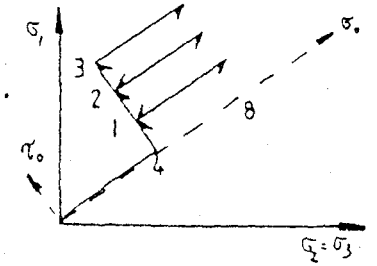

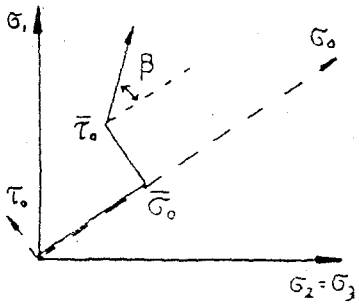

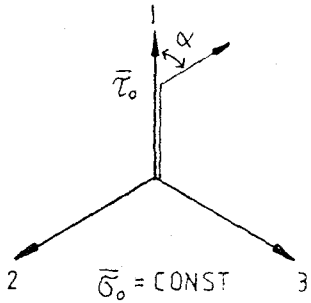

Fig.4
Series 5: Non-Proportional Loads in Deviator Plane

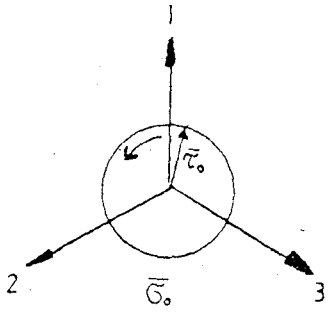

Fig.2
Series 3: Circular Stress Paths

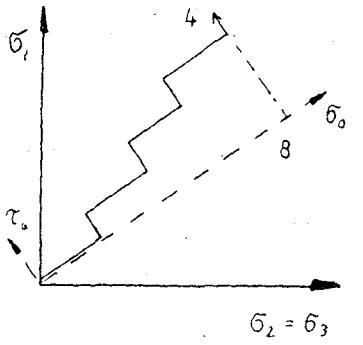

Fig.3
Series 4: Axisymmetric Non-Proportional Stress Histories

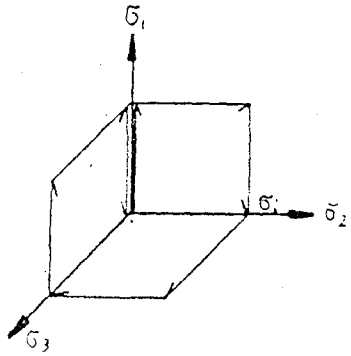

Fig.5
Series 6: Piecewise-Biaxial Stress Histories

Fig.6 Typical Presentation of Test Results

Test 1 - 10 : Cyclic Triaxial Compression in 8 ksi Plane

RD-EP #	SIG X (PSI)	EPS X +1000 (IN/IN)	SIG Y (PSI)	EPS Y +1000 (IN/IN)	SIG Z (PSI)	EPS Z +1000 (IN/IN)
	0	0.0000	0	0.0000	0	0.0000
	500	-0.0382	500	0.0011	500	0.1211
	1500	0.1184	1500	0.2084	1500	0.2739
	3000	0.4571	3000	0.7181	3000	0.6232
	4000	0.7341	4000	1.0828	4000	0.9109
	3500	0.6444	3500	0.9773	3500	0.8367
	3000	0.5585	3000	0.8558	3000	0.7437
	1000	0.1542	1000	0.3129	1000	0.2906
	500	0.0075	500	0.1279	500	0.1720
	0	-0.0370	0	0.0842	0	0.0860
	1000	0.1173	1000	0.2385	1000	0.2596
	3000	0.5100	3000	0.7808	3000	0.7002
	5000	1.1356	5000	1.5950	5000	1.3259
	6000	1.5157	6000	2.1438	6000	1.7403
	5000	1.1942	5000	1.8827	5000	1.5730
	4000	1.1442	4000	1.5654	4000	1.3217
	3000	0.7536	3000	1.3124	3000	1.1494
	1000	0.1775	1000	0.7690	1000	0.7245
	500	0.1358	500	0.5382	500	0.5711
	0	0.1007	0	0.4188	0	0.3570
	2000	0.6876	2000	0.9115	2000	0.8659
	4000	1.1770	4000	1.9419	4000	1.3306
	6000	1.6327	6000	2.2379	6000	1.8468
	8000	2.5939	8000	3.5527	8000	2.9309
	7850	2.6882	7850	3.5859	8300	3.1158
	7700	2.6106	7700	3.5105	8600	3.3277
	7600	2.6817	7600	3.4725	8800	3.5018
	7500	2.6838	7500	3.4263	9000	3.5994
	7600	2.6829	7600	3.4791	8800	3.6171
	7700	2.6141	7700	3.5422	8600	3.6010
	7850	2.6861	7850	3.6336	8300	3.5092
	8000	2.7337	8000	3.7281	8000	3.4636
	7500	2.6185	7500	3.5175	9000	3.7296
	7000	2.4520	7000	3.2738	10000	4.5284
	6500	2.3447	6500	3.0175	11000	5.8254
	6750	2.3158	6750	3.1454	10500	5.8273
	7500	2.5055	7500	3.4612	9000	5.4892
	8000	2.6750	8000	3.6955	8000	5.2463
	7000	2.3955	7000	3.2521	10000	5.6971
	6000	2.0130	6000	2.7564	12000	7.2839
	5500	1.8215	5500	2.5591	13000	9.3061
	6000	1.8543	6000	2.5192	12000	9.3604
	7000	2.2131	7000	3.0069	10000	8.4296
	8000	2.6229	8000	3.6042	8000	8.9623
	7000	2.1454	7000	3.0615	10000	8.3183
	6000	2.1814	6000	2.8300	12000	9.3429
	5500	1.9825	5500	2.5720	13000	9.6772
	5000	1.4333	5000	2.0339	14000	11.0956
	4550	0.8279	4550	1.1076	14900	13.3301
	4250	0.4632	4250	0.4813	15000	15.4502

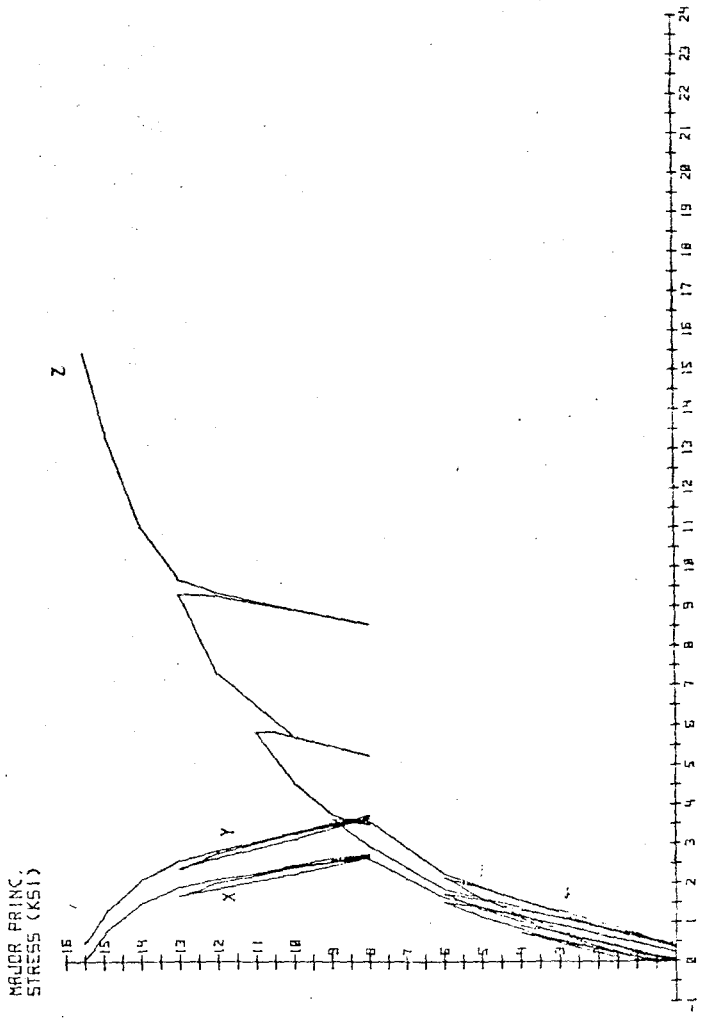

PLAIN CONCRETE IN UNIAXIAL POST-PEAK CYCLIC TENSILE AND TENSILE-COMPRESSIVE LOADING

H.W. Reinhardt
Professor of Structural Engineering
Stevin Laboratory of Delft University of Technology
Stevinweg 4, 2626 CN Delft, The Netherlands

Introduction

Usually, fatigue of concrete is treated by empirical relations such as S-N-curves and Goodman diagrams. However, the mechanism of degradation is not yet well understood. Because it is believed that crack propagation is an essential feature of fatigue a rational approach should start from cracking behaviour of concrete.

Modelling

The idea of cohesive forces (Barenblatt, Dugdale) is applied to the softening zone in front of a real crack. The distribution of cohesive stresses σ is described by

$$\frac{\sigma}{f_t} = 1 - \left(\frac{c-x}{c-a}\right)^n \qquad (1)$$

with f_t tensile strength, 2a real crack length, (c-a) length of softening zone.

The length of the softening zone is determined by the requirement that the stress singularity at x = c vanishes. This condition can be fulfilled by equating the stress intensity factors due to the cohesive forces, K_s, and due to the remote stress σ_o in an infinite panel with a central crack, K_σ:

$$K_s = 2\sqrt{\frac{c}{\pi}} \int_0^c \frac{\sigma(x)}{\sqrt{c^2 - x^2}}\, dx \qquad (2)$$

$$K_\sigma = \sigma_o \sqrt{\pi c} \qquad (3)$$

The results of numerical integration are plotted in fig. 1. The vertical axis is a measure of the length of the softening zone whereas the horizontal axis is the ratio between the remote stress and the tensile strength. The graph shows the very distinct influence of the exponent n of eq. (1) on the size of the softening zone.

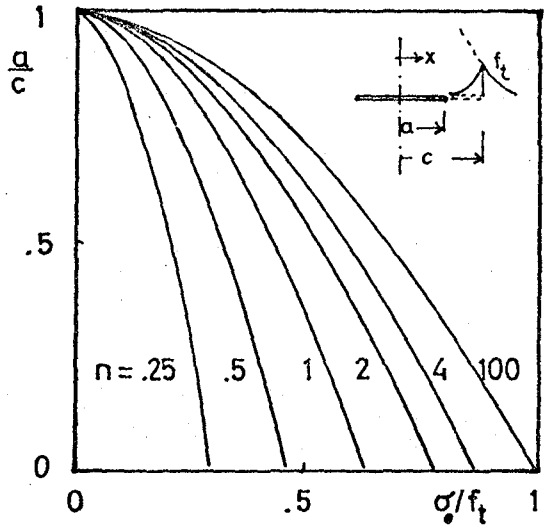

Fig. 1 - Softening zone length vs. stress-strength ratio

Regarding a/c = 0 as a failure criterion the apparent strength f_t (in a tensile test) is lower the smaller n, compared to the real strength f^* which follows from $f^*/f_t = f_t/\sigma_{o(a/c=o)}$.

To use the model, the exponent n should be known as a function of concrete composition and loading history. Furthermore, n can be split up into two parameters k and l governing the stress-deformation relation of concrete in uniaxial tension and the opening shape of the softening zone, respectively, according to

$$\frac{\sigma}{f_t} = 1 - \left(\frac{\delta}{\delta_o}\right)^k \tag{4}$$

$$\frac{\delta}{\delta_o} = \left(\frac{c-x}{x-a}\right)^l \tag{5}$$

with δ deformation of the softening zone and δ_o deformation where stresses cannot longer be transferred.

Experiments

In order to establish the values of k and l experiments are being carried out on concrete cylinders ø 110 mm and panels in deformation controlled uniaxial loading with three types of loading, fig. 2. The concrete cube strength is 45 N/mm^2, the tensile splitting strength 2.9 N/mm^2, the maximum aggregate grain size 16 mm.

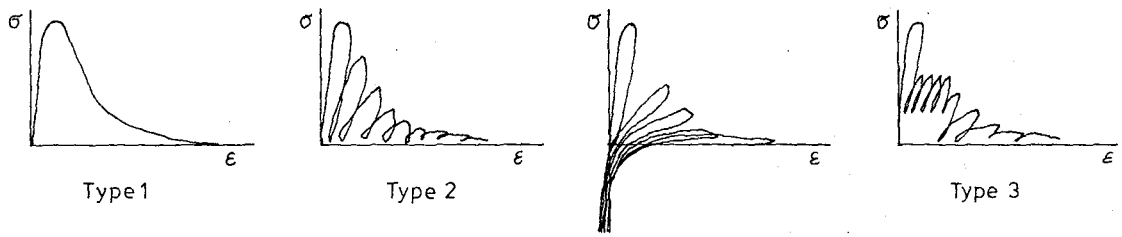

Fig. 2 - Types of loading

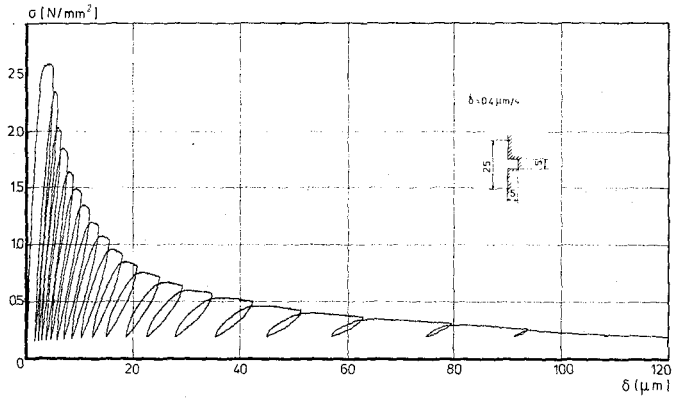

Fig. 3 - Stress-deformation curve under cyclic tensile loading

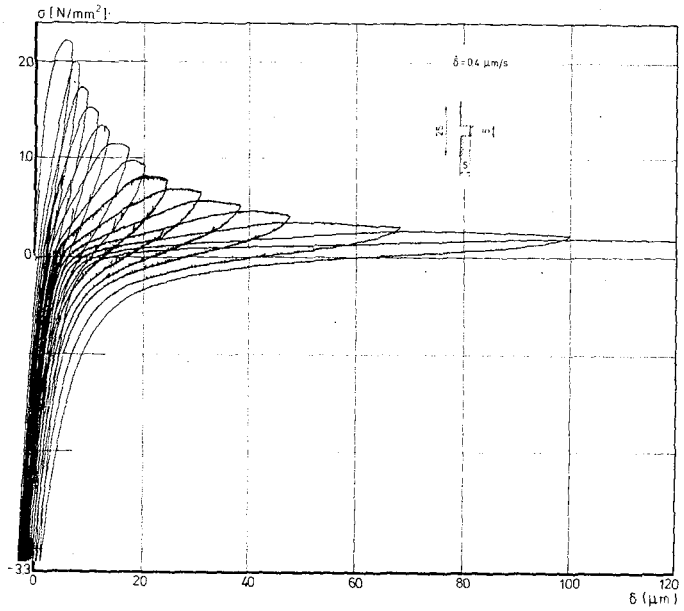

Fig. 4 - Stress-deformation curve under alternating loading

Fig. 3 and 4 show typical results of the cylinder test in cyclic loading. From 50 experiments it can be concluded that the stress-deformation curve seems to be unique, i.e. not affected by the type of loading. Furthermore, there is an indication that the residual strength is less after a certain number of cycles the lower the stress at unloading (i.e. compressive).

The panel tests (300x250x50 mm) shall provide an answer to the deformation of the softening zone in front of a real crack. Results will be presented during the symposium.

Conclusion

The present state of the investigations allows the following conclusions:

1) The tensile post-peak stress-deformation curve of concrete seems to be unique.
2) The lower stress at unloading affects strength more the lower that stress is.

THE USE OF THE ROUGH CRACK MODEL OF WALRAVEN AND THE FICTITIOUS CRACK MODEL OF HILLERBORG IN F.E. ANALYSIS

J. Blaauwendraad
Professor Civil Engineering
Delft University of Technology
The Netherlands

F.J.M. van den Berg
Research Assistent
Delft University of Technology
The Netherlands

P.J.G. Merks
Research Assistent
Rijkswaterstaat
NL - Utrecht

Program Micro/1

Structures of reinforced and unreinforced concrete in the cracked stage are analyzed numerically in two ways, either with discrete single cracks, or using the concept of smeared cracks. This paper regards applications of the program MICRO/1 for plane stress problems with discrete cracks. A finite element method is used which is based on an assumed stress field and natural boundary displacement (Lagrangian multipliers for the boundary tractions). So, differently from the standard FEM programs of the compatible type, the program MICRO is an equilibrium model, using boundary displacements as degrees of freedom. Essentially two different types of elements are used, namely triangular elements for the concrete and straight linear elements for the reinforcement. A reinforcement bar never crosses a triangular element, but instead is always positioned in between two elements. Bond behaviour is counted for by a nonlinear spring between the concrete and the reinforcement. Stresses in the triangles vary linearly over the region of the element. This corresponds with linearly varying boundary displacements, linearly varying bond stresses between the triangles and the straight reinforcement bars,and hence a parabolic distribution of the normal force in the bars.
Discrete cracks do not occur between the triangular elements, but run across the elements. In such a case a triangle is split in two parts, and additional degrees of freedom appear in the crack, namely for the crack opening and for the sliding of the two crack faces. In a cracked triangle the stresses can become discontinuous if necessary, and the same applies for the bond shear stress along the edge of a cracked element.

The constitutive relations of the concrete correspond with the model of Link, which has been extended with an appropriate tension cut-off criterion. The bond mechanism is a nonlinear spring, which behaves elastically up to a maximum shear stress, and shows softening for increasing slip behind that state. The behaviour of cracks can be discribed with the rough crack model

of Walraven and the fictious crack model of Hillerborg, Peterson c.s. The latter tension-softening concept has been adopted as the fracture mechanics option to account for the process zone of micro cracks around the crack "tip". This model is especially active if no reinforcement is applied.

Shear failure of reinforced concrete beams

The program has been applied to simulate the behaviour of reinforced concrete beams under shear loading. We consider the case in which main reinforcement is applied to carry the bending moments, but no shear reinforcement (stirrups) has been used. Furthermore we concentrate on the well-known fact that for such beams the shear capacity depends on the actual depth of the beam. Our starting point is a series of experiments which was carried out at the Stevin Laboratories of Delft University of Technology. From this series we selected two beams which correspond to each other such that the slendernes ratio a/h in the shear part of the beam has the same value (namely 3), however the depths differ considerably (respectively 125 mm and 720 mm). The beams have been shown in fig. 1. If model laws would apply, these beams should show the same ultimate nominal shear stress τ_u, which is the average shear stress at failure. The experiment however shows a value $\tau_u = 1.2$ *Mpa* for the shallow beam, and $\tau_u = 0.7$ *MPa* for the deep beam. So the shallow beam behaves far better. In fact this beam can be loaded until the main reinforcement starts to yield because the full plastic moment has been reached, producing a ductile failure behaviour. The deep beam cannot be loaded that far. Long before the reinforcement yields, brittle failure occurs in the shear part of the beam. The two beams are welcome bench-mark problems because of their expected simularity and still so different behaviour.

The wanted material properties of the concrete to be fed in the program MICRO/1 are the cylindrical compression strength, the tensile strength, the modulus of elasticity and Poissons ratio. These quantities have been taken from the experimental data. The rough crack model of Walraven is related to the cube compression strength, which is also known from the experiment. The fictituous crack model of Hillerborg has not been applied in these analyses. Due to the presence of the crack arresting main reinforcement, the fictituous crack model is less important in this case. The data for bond have been chosen on basis of experience. The adopted data are regularly used values for normal concrete and ribbed reinforcement bars. In this short note we just show a comparison between the load-deflection diagrams found in the test and resulting from the analysis (fig. 1). The ductile and brittle failure is produced satisfactorily. Crack patterns, not shown here, do also correspond quite well.

Mixed mode fracture in unreinforced notched beam

The program has also been applied to the problem of crack propagation in an unreinforced beam. Starting point in this case is a series of tests at Cornell University for mixed mode crack propagation in notched beam under pure shear. One of the tests is shown in fig. 2. A curvilinear crack develops and a typical diagram occurs for the load versus the crack mouth sliding displacement (CMSD).

In the analysis we used data for the tensile strength, compression strength, elasticity modulus and Poisson's ratio which are derived from the experiment. For the fracture mechanics release energy G_f two values $35\ ^{N}/_{m}$ and $100\ ^{N}/_{m}$ have been adopted. The results (fig. 2) show that the ultimate load can be computed rather accurately, but not the softening branch. Part of the difference between the test and the analysis may be due to different definitions of CMSD.

Conclusions

The rough crack model of Walraven in F.E. Analysis of the shown reinforced concrete beams yields good computational results. Used in combination with the fictitious crack model of Hillerborg also promising results were reached for failing unreinforced notched beams.

References

1. Grootenboer, H.J., Leijten, S.F.C.H., Blaauwendraad, J.: Concrete Mechanics, Numerical models for reinforced concrete structures in plane stress, Heron, vol. 26, 1981, no. 1c.

2. Walraven, J.C., Reinhardt, H.W.: Concrete Mechanics, Theory and experiments on the mechanical behaviour of cracks in plain and reinforced concrete subjected to shear loading, Heron, vol. 26, 1981, no. 1a.

3. Hillerborg, A. and Petersson, P.E.: Fracture mechanical calculations, test methods and results for concrete and similar materials. Advances in Fracture Research, 5th international conference of fracture, Cannes (ed.C.Francois), p. 1515-1522 (1981).

4. Walraven, J.C.: Het afschuifdraagvermogen van grindbeton en lichtbetonliggers zonder schuifwapening, Cement nr. 1, 1979.

5. Arrea, M., Ingraffea, A.R.: Mixed-mode crack propagation in mortar and concrete, Report 81-13 Cornell University, 1982.

6. Van den Berg, F.J.M., Merks P.J.G.: Interaction of rough crack model and fictitious crack model in program MICRO/1. F.E. Analysis of beams subjected to shear. Report BSW 83- Rijkswaterstaat, Structural Research, Utrecht, Netherlands, 1983.

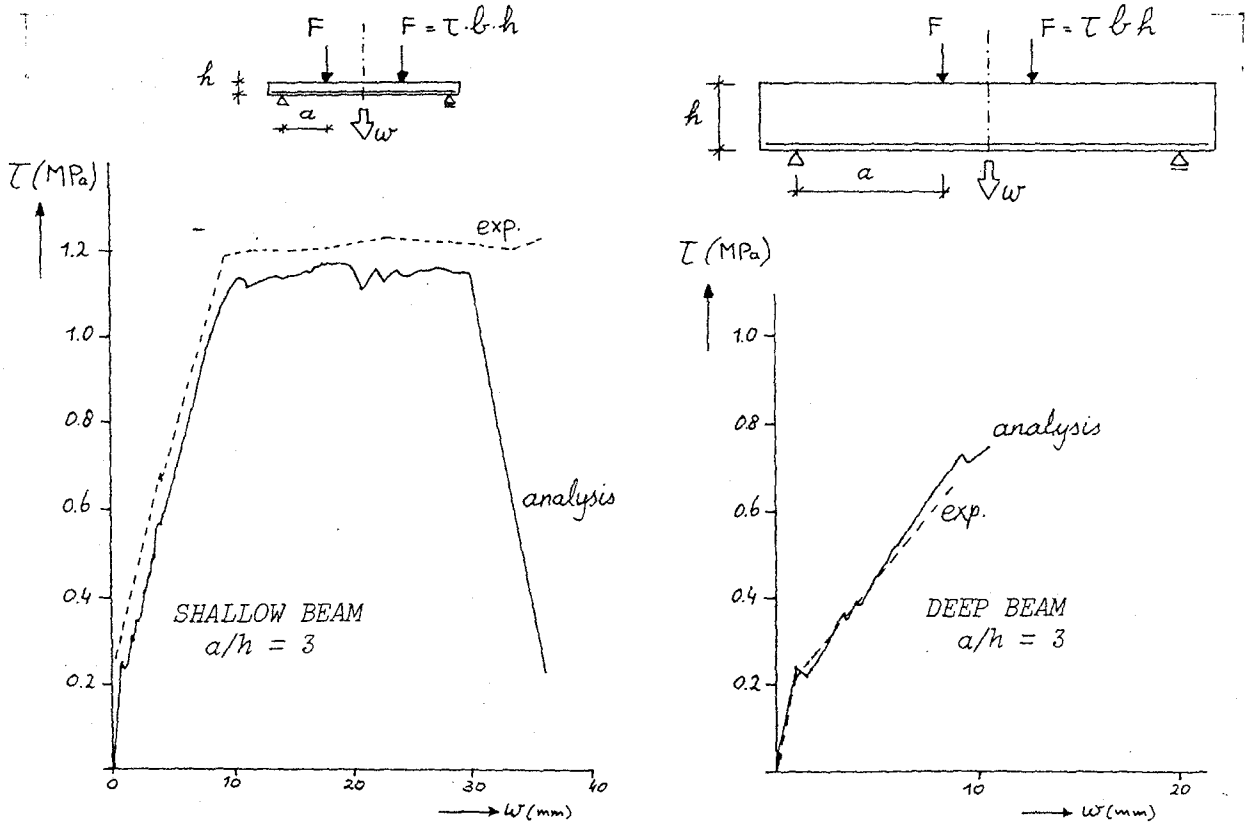

Figure 1 Two beams with the same shear slenderness $a/h = 3$, but the actual depths of the beam differ about a factor 6. The failure type is ductile for the shallow beam and brittle for the deep beam.

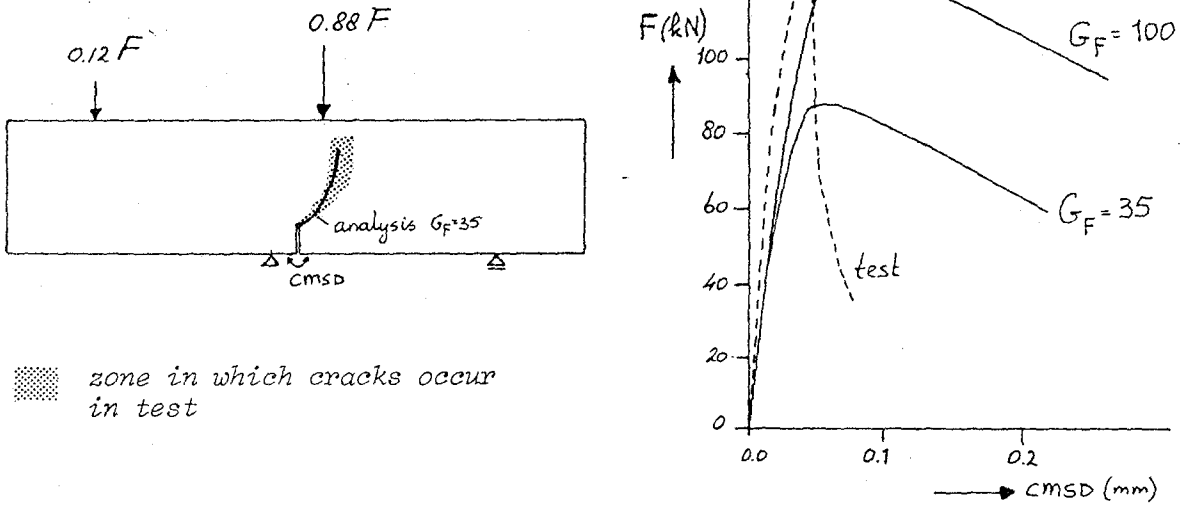

Figure 2 Unreinforced notched beam in pure shear. In this mixed mode fracture problem a curved crack trajectory occurs.

PLASTICITY-BASED ANALYSIS OF REINFORCED CONCRETE STRUCTURES

E. C. Ting and M. Yener
Professor and Assistant Professor of Civil Engineering
Purdue University
West Lafayette, Indiana 47907, U.S.A.

Introduction

Plasticity concepts have been widely adopted in the modeling and code development for the finite element analysis of concrete structures. A wide variety of theories has been proposed, and some have already been incorporated in general-purpose codes for practical applications. In this paper, we report a comparative study of the advantages and the suitability of various plasticity-based concrete models, regarding their tractability in numerical implementation and their accuracy in predicting concrete behavior under different loading conditions.

Plasticity-Based Modeling of Concrete Behavior

One of the critical topics of concern in concrete plasticity is to select accurate yet sufficiently simple yielding and loading functions to describe the physically nonlinear, irreversible behavior prior to macrocracking. For convenience and consistency, it is common to assume a loading function having the same form as the failure criterion. The validity of this assumption was studied by considering five fracture criteria, namely the functions proposed by (a) Mises, (b) Drucker and Pager (DP), and (c) Bresler and Pister (BP), along with (d) the four-parameter model (4P) proposed by Hsieh, Ting, and Chen, and (e) the five-parameter model (5P) by Willam and Warnke.

In this study, two sets of biaxial data and two sets of triaxial data were utilized for the purpose of comparison. Based on each criterion considered, the test data for different loading conditions were evaluated to compute the hardening parameter as a function of the effective plastic strain. Comparison of the results has indicated that the hardening parameters for 4P and 5P models are in close agreement with each other. However, they vary considerably for different stress ratios for the biaxial loading condition. On the other hand, for triaxial loading induced by large confined pressure, both models yield approximately the same hardening parameter. Furthermore, the limiting values of the parameter resulting from these models do not converge to the compressive strength, f'_c, in the biaxial stress condition. However, they approach f'_c in the presence of large confined pressure.

The behavioral pattern predicted by the Mises and DP criteria is essentially opposite to that exhibited by the 4P and 5P models. Both the Mises and DP models yield nearly identical hardening parameters with limiting value approaching f'_c for biaxial loading conditions. However, they fail to give good agreement in triaxial conditions. In contrast, results using the BP function show large discrepancy for all loading conditions considered.

On the basis of the argument above, the Mises criterion appears to be better suited in a plasticity-based formulation in the absence of large hydrostatic pressure. However, modifications of the criterion regarding dilatancy should be included when the confined pressure is dominant. In our study, we have proposed the following modifications: $\sqrt{J_2}/|1+\gamma\sigma_m|$, where $\gamma=1$ when all principal stresses are compressive and $\gamma=0$ otherwise. In this expression, J_2 is the second deviatoric stress invariant and σ_m is the mean stress. The proposed modification reduces to the Mises criterion for the plane stress condition and results in nearly identical hardening parameters for the two sets of triaxial test data considered. This function not only considerably simplifies the hardening formulation, but also yields results which are as accurate as those predicted by the more complex 4P and 5P models.

For further comparison of the theories, an elastic-plastic finite element analysis was carried out. The associated flow rule, the normality condition, and a mixed hardening rule comprised of isotropic hardening and Ziegler-type kinematic hardening were assumed. Implementing the 4P and 5P models has indicated that both models yield nearly identical results regarding plastic deformation. The hardening parameter was determined from uniaxial compression tests, and reasonable correlations were obtained for uniaxial compressive strains. Larger discrepancies were observed in the biaxial conditions, and the predictions were unacceptable in the tensile region. In particular, the predicted strain values for the simple tension condition were several times larger than the recorded values. The discrepancies may be traced to the fact that both the 4P and 5P models seem to overestimate the hardening effect in compression and underestimate it in tension. This behavior appears to be caused by the inclusion of large dilatancy effects in the functional forms of both models.

Suppressing the effect of hydrostatic pressure in the loading function improves the prediction. Using the Mises function yields accurate predictions in all biaxial cases considered. For the triaxial stress conditions, the 4P and 5P models both give good predictions. The modified Mises function yields slightly larger discrepancies, but the results appear to be acceptable.

We also utilized a non-associated flow rule by suppressing the first stress invariant in the 4P function. In so doing, the prediction was improved considerably for the biaxial cases. A refined model containing two separate loading surfaces for the volumetric and deviatoric plastic deformations was also implemented. In this model, the Mises criterion was assumed for the deviatoric strain, and a linear function of the mean stress was taken for the volumetric strain. Among the classical plasticity models we considered, the model with two loading surfaces seems to give the best correlation with both the biaxial and triaxial data.

The viscoplasticity theories based on the endochronic concept have received considerable attention in recent years. Despite some shortcomings, the endochronic theory has shown great potential as an alternative approach in plasticity-based modeling of concrete behavior. The advantages of the models based on the endochronic theory lie in the flexibility in curve fitting and in the convenience in numerical implementation.

The original and the advanced versions of the endochronic theory for concrete, both developed by Bazant and his associates, were examined in our preliminary work. Essentially, our study focused on the accuracy of each model and its ability to describe the general behavior of concrete under various loading conditions. The behavior is normalized by only one control parameter, namely f'_c. Our experience has indicated that the simpler original version predicts concrete behavior under uniaxial and biaxial conditions

quite well, based on two different sets of test data. If the uniaxial compressive stress-strain response is controlled by strain increment, strain softening can be obtained. We have also evaluated the sensitivity of the constants assumed in the models. The results have indicated that, despite the large number of constants required in the curve fitting scheme, varying the coefficients does not change the predicted behavior significantly.

The main drawback of the original version appears to be in its application to cyclic behavior. This seems to be one of the primary reasons why the advanced version was developed. In addition to the well-documented flaw that the original version fails to form a hysteresis loop, hence resulting in negative energy dissipation, the predicted unloading and reloading slopes in the uniaxial stress-strain response are not satisfactory.

Among the many improvements in the advanced version, the most important appears to be the introduction of the concept of jump kinematic hardening. This concept introduces discontinuities in the constitutive formulation, which somewhat detracts from the original advantage of the continuous plasticity theory. However, it predicts the cyclic behavior quite well. Furthermore, the advanced theory provides good predictions regarding the stress-strain relationship for monotonic uniaxial and biaxial loading conditions. However, the improvements over the original version were not significant.

As verified in our study, the hysteresis loops, modulus degradation, and the softening in the envelope of the stress-strain cycles appear to be quite satisfactory. However, it should be noted that including the jump kinematic condition does not appear to guarantee the formation of a hysteresis loop. When the reloading generates more inelastic strain than the unloading, the stress-strain response does not form a loop.

One of the difficulties we encountered was that the advanced theory exhibited some discrepancies between the responses based on a stress-controlled increment and a strain-controlled increment. No significant difference was found when the original version was employed. In addition, the complex functional form of the advanced theory was much more difficult to implement in a finite element code, as compared to the original version.

If one's interest is focused on the concrete behavior prior to cracking, a possible approach is to introduce the jump kinematic hardening in the original version of the endochronic theory in order to adjust its drawbacks regarding cyclic response. The resulting constitutive formulation was simpler and easier to implement. Our results have also shown that the predicted uniaxial cyclic behavior is nearly as good as that predicted by the advanced version. It should be noted, however, that due to the lack of accurate cyclic test data, a quantitative comparison cannot be made at this time.

Finite Element Analysis Implementation

Modeling for finite element analysis of concrete structures is very complicated in view of the fact that it should include accurate criteria for cracking and post-cracking behavior. Thus, selection of a proper finite element code for analysis and verification of results becomes the critical question in the development of plasticity-based models. Two general purpose programs have been developed in our study. Based on an imporved version of NONSAP, a computer code, NFEAP, was developed earlier. Because the basic algorithm is derived from the total or updated Lagrangian formulation, an enormous number of iterations is required. Incorporating a complete model into the code requires considerable streamlining in its structure, and the finished code is rather inefficient. Similar difficulties have also been reported by other investigators.

Recently, a new code, STRAW-P1, has been developed based on a version of STRAW originated at Argonne National Laboratory. The code employs explicit integrations for transient large deformation analysis. Using the dynamic relaxation technique, static response can be obtained. The code is convenient for implementing complicated material models and has been shown to be efficient and reliable. Our experience has indicated that the development effort and CPU time for STRAW-P1 are about 1% of that required by NFEAP. We have since implemented five different concrete plasticity models in addition to the cracking and post-cracking models. Presently, three different versions of endochronic viscoplasticity models are also being implemented.

The verification of computer codes for concrete is an extremely difficult task due to the lack of complete test results. In particular, little information regarding the development of cracks is available for the validation of cracking behavior models. We have considered the standard split tension test, pull-out test, and a plain concrete cylinder subjected to implosion pressure as the basis for a preliminary comparison study. Our limited results have shown that to predict the total failure of a concrete structure, both large deformation and plastic deformation should be considered. However, because of the domination of cracking, the selection of plasticity model and failure criterion makes very little difference as far as load-deformation relations and the ultimate strength of the structure are concerned. Using any of the plastic-fracture theories which are considered in this study, good agreement between predictions and test results can be obtained. All models implemented in the computer code have indicated that the crack patterns also appear to be quite reasonable.

A GENERALIZED BASIS FOR MODELLING PLASTIC BEHAVIOR OF MATERIALS

C. S. Desai
M. O. Faruque
Department of Civil Engineering and Engineering Mechanics
University of Arizona
Tucson, Arizona 85721 U.S.A.

Introduction

Further developments toward evaluation and implementation of a general approach for developing plasticity-based constitutive models will be presented. The approach shows promise of handling isotropic, anisotropic hardening and nonassociative behavior.

Proposed Model

An expression for yield function, F, can be written as

$$F\ (J_i,\ I_i^p,\ K_j,\ \alpha_m) = 0 \tag{1}$$

where J_i (i = 1, 2, 3) = invariants of the stress tensor, I_i^p (i = 1, 2, 3) = invariants of the plastic strain tensor, K_j (j = 1, 2, 3, 4) = joint invariant of stress and plastic strain tensors and α_m (m = 1, 2, ...n) = internal state variables. As discussed in Refs. 1 and 2, F in Eq. (1) can be expressed as a complete polynomial in J_1, $J_2^{1/2}$, and $J_3^{1/3}$, from which a series of truncated forms can be developed. For instance, the following

$$F \equiv J_{2D} + \alpha_1 J_1^2 - \beta_1 J_1 J_3^{1/3} - \gamma_1 J_1 - k_1^2 = 0 \tag{2a}$$

$$F \equiv (J_{2D})^2 + \beta_2 J_1 J_3 - \gamma_2 J_1^3 - k_2^4 = 0 \tag{2b}$$

$$F \equiv (J_{2D})^3 + \beta_3 J_1^3 J_3 - \gamma_3 J_1^5 - k_3^6 = 0 \tag{2c}$$

$$F \equiv J_{2D} + \beta_4 J_1 J_3^{1/3} - \gamma_4 J_1^2 - k_4^2 = 0 \tag{2d}$$

Here J_{2D} = second invariant of deviatoric stress tensor.

where α_i, β_i, γ_i and k_i (0 = 1, ...4) are material parameters to be determined. The foregoing functions plot continuous and convex in the stress spaces, e.g., $\sqrt{J_{2D}}$ - J_1 and principal stress space.

Hardening Behavior

The hardening behavior is defined by using the following expression:

$$\beta = \beta(\xi) = \beta_u \left[1 - \frac{\bar{\beta}_a}{f_o + f(\xi r)}\right] \tag{3}$$

where β = hardening or growth function, β_u = ultimate value of β [= 3α, Eq. (2a)], $\bar{\beta}_a$ = hardening constant, f_o = material constant related to the initial size of the yield surface, and $\xi = \int (d\epsilon_{ij}^p \, d\epsilon_{ij}^p)^{1/2}$. The parameter, r, is given by

$$r = \sqrt{r_v^2 + r_D^2} \tag{4}$$

where $r_v = \xi_v/\xi$, $r_D = \xi_D/\xi$, and ξ_v, ξ_D = volumetric and deviatoric parts of ξ.

Nonassociative behavior is handled by expressing plastic potential function, Q, as the sum of the yield function and a correction function (1, 2). Induced anisotropy is included by adding the joint invariant(s) in F (2, 3).

The presentation will include results on the analysis and implementation of F in Eq. (2a) and hardening behavior, Eq. (3), with some applications of the nonassociative and (induced) anisotropy models.

References

1. Desai, C. S., "A General Basis for Yield, Failure and Plastic Potential Functions in Plasticity," Int. J. Num. and Analyt. Meth. in Geomech., Vol. 4, 1980, pp. 361-375.

2. Desai, C. S. and Faruque, M. O., "A Generalized Basis for Modelling Plastic Behavior of Materials," Proc., Int. Conf. Const. Laws for Eng. Materials: Theory and Appl., Tucson, AZ, 1983, Vol. II, John Wiley & Sons, U. K., in press.

3. Baker, R. and Desai, C. S., "Induced Anisotropy During Plastic Straining," Int. J. Num. Analyt. Meth. in Geomech., under publication.

A MODELLING OF THE NONLINEAR MECHANICAL RESPONSE AND FAILURE OF SOLIDS

A. Sawczuk
Professor of Applied Mechanics
Université Aix-Marseille III and Laboratoire
de Mécanique et d'Acoustique du C.N.R.S.
13402 - Marseille Cédex 09, B.P. 71,France*

Summary

1. Mathematical descriptions of complex material behaviors are frequently proposed generalising known material laws formulated for uniaxial stress, or developing often ingenious models when stimulated by observations and synthetising particular experimentally noticed facts. Nonlinear mechanical response to external and/or internal agencies, and concerning the phenomena like creep, plasticity, fissuration or internal damage growth deserves a study based on general principles governing the tensorial variables involved in constitutive or evolution laws. This appears to be of particular importance for materials with oriented, inborn or developing under straining, internal structure exhibiting directional properties like oriented damage, deformation induced hardening or softening. Similarly, it can be of pertinence in presence of mechanical couplings with other physical or chemical phenomena which should be accounted for in equations regarding mechanical response. The constitutive relations concern thus not solely stress and strain or their rates, and accelerations, say but also equations governing evolution of couplings,continuous damage and alike. At hoc models even dexteriously developed, might not fully account for the real material response, particularly as to the number of independent variables to be considered when studying oriented solids both within their deformability as well as failure.

2. It seems appropriate, before particularisations are made regarding specific mechanical models, to reflect upon usefulness of the basic principles governing independent and dependent second order tensors, vectors and scalars involved in the constitutive, evolution or failure equations concerning any macroscopic mechanical behavior. Such principles exists in the mathematical theory of tensor valued functions of tensor variables.

3. A tensor valued function of second order tensors, vectors and scalars can, in principle be expressed in its canonical form, thus as a linear combination of the basic, form invariant tensor generators specific for the class of internal symmetries of the material considered. The number of basic tensor generators as well as that of basic invariants are known for isotropic materials as well as for a large class of anisotropic materials, thus those

---

* on leave from the Institute of Fundamental Engineering Research IPPT, Polish Academy of Sciences, Warsaw, Poland.

possessing or developing internal orientations of the mechanical, thermal or other material response. The coefficients staying at the generators are scalar valued functions of the set of basic invariants of all the dependent tensors involved, including those accounting for the material symmetries. Our attention is focussed on polynomial representations of tensor valued tensor functions and on their applications to be mathematical modelling of materials response.

4. For isotropic materials when the response is governed by one independent second order tensor the representations approach was long ago applied by PRAGER when formulating the general law of plastic behavior. With respect to the criteria of failure of plastic solids essentially the same approach was used by THOMAS. Mathematical aspects of the polynomial representations were originally studied by RIVLIN and ERICKSEN, as well as by SEDOV and LOKHIN and continued by SPENCER, SMITH, WANG and, particularly for orthotropic materials, by BOEHLER. An isotropic tensor valued tensor function of one tensor variable has three basic invariants and three tensor generators. This allows to formulate any law for isotropic behavior as a polynomial containing three terms. For anisotropic materials vectors or tensors specifying the material privileged directions enter the constitutive or the structure variations laws. The number of tensor generators appropriately increases and mixed invariants of the independent tensors appear. Representations are then more involved, but their properties allow to arrive at the most general form of constitutive or evolution equations. In this sense, for a response studied, the building blocks are available as well as principal rules allowing to construct a theory of mechanical response. Using other mathematical requirements as regards e.g. regularities of the stress-strain relations, time independence in case of plasticity and, in general thermodynamical restrictions, specific laws can be constructed. Symplifications can be made in order to retain in the equations the essential terms as regards to their pertinence for the behavior in question. It is then possible to arrive at wieldy theories with the full knowledge of what type of effects is then neglected. Specific linearisations of the constitutive relations lead to the classical theories of material response, e.g. to the linear elasticity where the independent tensor variable being, say, linear strain, the stress is expressed accordingly, the nonlinear term of the representation being neglected.

5. Polynomial tensor functions representations were used to specify the law for anisotropic plasticity, e.g for rocks, composite materials or soils It comes out quite evidently that the flow law, in general, is not necessarily associated with a yield condition. The yield condition appears in this approach as a consequence of the requirement that plastic flow is insensitive on the time scale change. This requirement gives an additional relation between the stress and mixed stress-anisotropy tensors. Comparisons between the associated flow law which assumes first the existence of a yield locus with that following from the representation theory is discussed. General forms of yield criteria for anisotropic plastic material including anisotropic strain hardening are given and the associated failure modes discussed. A description of the plastic strains induced oriented hardening is given.

6. Applications of the tensor function approach to creep are presented Specific creep laws can be proposed without any necessity, at this stage, to use the dissipation potential. A simple theory is compared with experiments on materials plastically prestrained before creep. The theory allows to describe the pertinence of experimentally observed hardening on subsequent creep. The same approach is used when describing the dynamic response of solids, when both strain and strain rates are, to some extent, independent. This allows to ac-

count for the rate sensitivity of materials.

7. An oriented continuous damage is studied, when the damage patterns posess certain symmetries. Experimentally simulated damage is considered both as to respect to the macroscopic response of a homogenized material as well as regarding the law of oriented damage growth, similarly expressed in terms of a tensor function representation. Mechanics of perforated sheets is studied both analytically and experimentally and the respective comparisons are given, as to the deformation laws and failure modes.

8. The method is used as well in a study of deformation and failure of porous solids, both sintered metals and fissurated rocks. Results concerning a theory of anisotropic consolidation are also given. In this case the material porosity is specified by a permeability tensor not necessarly isotropic and all the equations regarding deformation, fluid outflow and fluid-structure couplings are expressed in form of relevant representations. The results of analysis are compared to the existing theories of consolidation of fluid saturated anisotropic soils.

9. The paper recalls the basis of the representations of tensor functions and specifies their applications for concrete modes of materials response. It is application oriented and might appear useful when proposing specific, engineering oriented models as it attempts to give an information about the number and type of the tensor generators and tensor invariants involved in the behavior in question. This gives a possibility to make a suitable choice of variables to be entered in a specific, applicable theory. Further necessity for introducing specific mathematical and mechanical principles in order to specify the theories is commented upon.

PLASTICITY IN REINFORCED CONCRETE - POTENTIAL AND LIMITATIONS

Peter Marti
Associate Professor of Structural Engineering
University of Toronto
Toronto, Ontario, M5S 1A4, CANADA

Introduction

During the past three decades, limit analysis methods were increasingly applied to reinforced and prestressed concrete. Thorough comparisons with experiments revealed that satisfactory strength predictions are obtained in a wide range of practical applications. Earlier attempts to predict the static strength of reinforced concrete beams and slabs, such as Ritter's and Moersch's truss models and Johansen's yield line theory were extended, unified and generalized. Most codes of practice now contain ultimate strength provisions which are partly based on plasticity concepts.

The majority of all reinforced concrete members are under-reinforced. Their strength is essentially determined by the yield strength of the reinforcement. The concrete properties have not a pronounced influence. The ductile behaviour justifies the application of limit analysis methods and the simplicity, transparency and adaptability of these methods explains their practical importance.

Limit analysis methods have also been applied to over-reinforced members. Their strength is partly or fully governed by the concrete. Effective concrete strength values are determined from comparisons with experiments. Thus, the limited ductility and the brittleness of the concrete and other factors are empirically taken into account. While the theory is kept very simple it is necessarily restricted. However, in spite of the fundamental deficiencies a series of useful results have been obtained.

Rigid-plastic models provide a reasonable basis for the ultimate strength design of common reinforced and prestressed concrete structures. Usually, a normal in-service performance is observed if an adequate safety margin against failure is chosen and if the reinforcement is well detailed and abrupt changes of the geometry and of the reinforcement are avoided. Simple checks of certain global deformations are often sufficient. However, general non-linear elastic-plastic models are needed to investigate the behaviour of structures with unusual or particularly critical geometrical or loading conditions, to determine the limits of applicability of rigid-plastic models, etc. Unfortunately, all elastic-plastic calculations suffer from the fact that the initial strains and stresses are practically unknown. Generally, only rough estimates of their magnitude can be made. This problem is often overlooked in elaborate analyses.

Rigid - Plastic Models

The concrete is frequently modelled as an isotropic, perfectly plastic material governed by the Coulomb-Mohr criteria $4|\tau|+3\sigma \leq f_c$ and $\sigma \leq 0$ and the associated flow rule is assumed to be valid. For uniaxial and plane stress states, these criteria reduce to the no-tension and no-crushing criterion $0 \geq \sigma \geq -f_c$. The effective compressive strength f_c is smaller than or equal to the cylinder compressive strength f'_c. The reinforcing bars are usually assumed to be perfectly plastic and to carry stress in their original direction only. Their distribution and anchorage are supposed to be such that their action can be described by equivalent average stresses. Furthermore, rigid bond is assumed between concrete and reinforcement.

Introducing suitable generalized variables yield criteria for reinforced concrete elements can be obtained by considering first the yield surfaces for the unreinforced concrete element and for the reinforcement separately. The yield surface for the reinforced element is the envelope of all linear combinations of stresses in the concrete and in the reinforcement which do not violate the respective yield criteria. It is obtained by translating the yield surface for the concrete with its origin moved within the yield surface for the reinforcement or vice versa.

Instead of treating concrete and reinforcement together as a reinforced concrete continuum, it is often advantageous to introduce bond forces, transverse forces due to curved reinforcing bars and anchorage forces as body and boundary forces acting on the concrete continuum.

The lower-bound method of limit analysis provides a possible equilibrium system of internal forces throughout a structure under ultimate loads. It is directly applicable in reinforced concrete design and detailing. For arbitrary geometrical and loading situations the concrete dimensions and the dimensions, the distribution and the details of the reinforcement can be determined based on consistent equilibrium and ultimate strength considerations by developing plane and spatial truss models and corresponding stress fields consisting of struts, strut connections, fans and arches. Fans and arches can always be replaced by statically equivalent struts or strut systems. The necessary minimum dimensions of the struts are determined by the effective concrete compressive strength f_c. It is suggested to assume an average value $f_c = .6 \cdot f'_c$. Deviations from this value may be indicated depending on the required redistribution of the internal forces, the detailing of the reinforcement, the effect of any lateral confinement and on similar influences.

The upper-bound method is generally best suited for analyzing an existing design and it is indispensable for a proper interpretation of experiments.

Elastic - Plastic Models

Generally, there are pre-existing cracks in reinforced concrete elements due to imposed deformations (resulting from shrinkage, creep, temperature effects, etc.) and/or previously applied loads. Under a certain loading process, some of the existing cracks tend to open and propagate while others

tend to close and new cracks occur in general. In this way, new structural systems consisting of concrete bodies and reinforcing bars are successively created. The concrete bodies are bounded by crack surfaces, have finite dimensions, are deformable and have a certain strength, in particular, a non-vanishing tensile strength. The crack surfaces are irregular and rough. Finite relative displacements occur between any couple of initially neighbouring points which are separated by a crack. Along certain parts of the crack surfaces the concrete bodies are in contact. There, forces may be transferred and the roughness of the crack surfaces may gradually be destroyed. The reinforcing bars which connect the concrete bodies are also three-dimensional deformable bodies. At the bar surfaces within the concrete relative displacements occur and forces are transferred similar to the situation at the crack surfaces.

Four groups of constitutive relations are needed for an appropriate treatement of the concrete, the reinforcement, the aggregate interlock between the concrete bodies and the bond between concrete and reinforcement. Unfortunately, the presently available test data do not yet allow a general incremental plasticity formulation of the aggregate interlock and bond-slip relationships. Therefore, different simplifying assumptions are normally made. A very powerful yet questionable assumption is to consider continuously distributed or smeared cracks. In fact, this assumption eliminates theoretically the bond problem and it implies that the stresses in the solid concrete between the cracks must be constant if body forces are neglected and all reinforcing bars are straight. If in addition, the concrete tensile strength is neglected and the relative displacements between the crack surfaces are restricted to an orthogonal crack opening, one arrives at the basic assumptions of the so-called compression field theory. According to this theory the cracked concrete is replaced by a fictitious continuous material with coinciding principal stress and strain axes which can adapt to carry uniaxial compressive stress in an arbitrary direction.

Conclusions

There is a considerable potential for further developments in the field of plasticity in reinforced concrete. Rigid-plastic models should be further advanced and their limits of applicability should be better investigated by comparisons with experiments and with elastic-plastic models. The progress of elastic-plastic models is linked with a better understanding of the aggregate interlock and bond characteristics. A suitable combination of fracture mechanics and continuum mechanics concepts should be rather fruitful.

References

1. IABSE - Colloquium "Plasticity in Reinforced Concrete", Copenhagen 1979. Introductory Report, IABSE Reports of the Working Commissions Vol. 28, Zurich, 1978, 172 pp.; Final Report, IABSE Reports of the Working Commissions, Vol. 29, Zurich, 1979, 360 pp.

2. Chen, W.F., "Plasticity in Reinforced Concrete", McGraw Hill, New York, 1982, 474 pp.

3. Thuerlimann, B., Marti, P., Pralong, J., Ritz, P. and Zimmerli, B., "Anwendung der Plastizitaetstheorie auf Stahlbeton" (Application of the Theory of Plasticity to Reinforced Concrete"), Institute of Structural Engineering, ETH Zurich, 1983, 252 pp.

PLASTIC ANALYSIS OF STRUCTURAL CONCRETE

M. W. Braestrup
M. Sc., Ph. D. (Struct. Eng.)
Dept of Structural Engineering, Technical University of Denmark
DK 2800 Copenhagen Lyngby, Denmark

Introduction

To make realistic predictions about the behaviour of structures under load, it is necessary to describe the material response from first loading to failure. However, if only the ultimate load is sought it is possible to make a short-cut, using the bounding theorems of plasticity, valid under certain idealized constitutive assumptions. Thus it is proposed to regard structural concrete as a rigid, perfectly plastic material.

Constitutive Model for Concrete

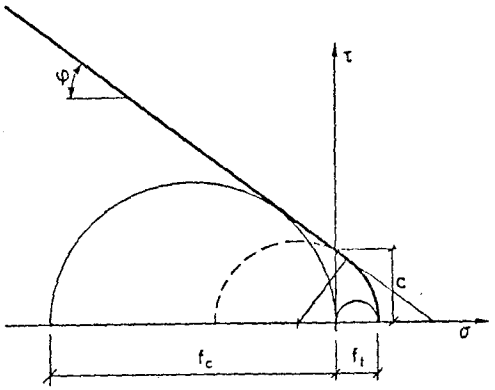

Fig. 1

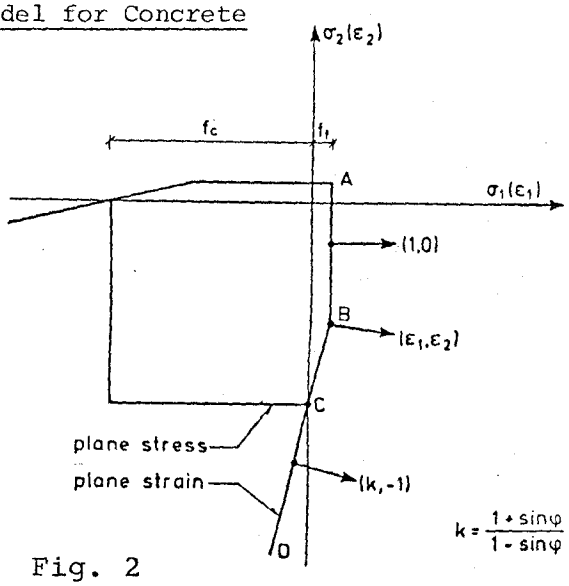

Fig. 2

A major problem in applying plasticity to structural concrete is the formulation of a suitable description of concrete. Traditional analyses are based upon the square yield locus for plane stress, which may be generalized into the modified Coulomb criterion. The latter model has during the last decade been applied by a research group at the Technical University of Denmark to treat a number of non-classical problems, involving shear in plain and reinforced concrete.

In the σ, τ -plane, the modified Coulomb criterion is a failure envelope for The Mohr's circles of stresses on sections in concrete (Fig. 1). Adoption of the criterion as a yield condition results in a yield surface in principal stress space, the corresponding yield loci for plane stress and strain being shown in Fig. 2. The associated flow rule implies that the dilatancy angle at sliding failure is identified with the angle of friction.

Thus the constitutive model for concrete endeavours to describe the strength properties and the deformations at ultimate by means of just three material parameters: tensile strength f_t, compressive strength f_c, and angle of internal friction φ, determining the parameter k. For most practical purposes, however, the tensile strength is neglected, and the standard value $\varphi = 37^o$ (k = 4) is adopted for the angle of friction. Thus a particular concrete quality is characterized alone by its compressive strength, as is the case with the square yield locus.

Yield Lines in Concrete

Fig. 3

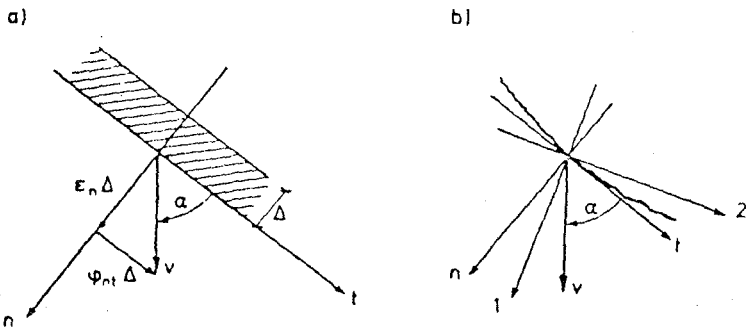

A yield line is a kinematical discontinuity separating two rigid body parts which are moving at the relative velocity v, inclined at the angle α (Fig. 3b). Regarding the yield line as an idealization of a narrow deforming zone (Fig. 3a), we can determine the principal strain rates and directions, which are coaxial with the principal directions of stress. It appears that the first principal axis bisects the angle between the relative velocity vector and the yield line normal. The stress state which is capable of producing this deformation is determined by the flow rule and the yield condition (Fig. 2). Multiplying the stresses by the strain rates, we compute the dissipation D, and introducing the parameters:

$$l = 1 - (k-1)\, f_t/f_c \qquad \text{and} \qquad m = 1 - (k+1)\, f_t/f_c, \qquad \text{we find:}$$

$$\varphi \leq \alpha \leq \frac{\pi}{2} : D = \tfrac{1}{2}\, v\, f_c\, (l - m \sin\alpha), \quad - \frac{\pi}{2} \leq \alpha \leq \varphi : D = \tfrac{1}{2}\, v\, f_c\, (1 - \sin\alpha)$$

The latter formula is valid for plane stress only, the normality condition imposing the lower limit $\alpha = \varphi$ upon the deformation in yield lines under plain strain conditions.

The dissipation describes the resistance of concrete to the formation of a yield line, and it depends upon the angle α. A yield line with normal deformation only ($\alpha = \pi/2$) is called a collapse crack, and in this case the dissipation reduces to $D = v\, f_t$. Thus the resistance to simple splitting is minimal, but as soon as tangential deformations are present, the resistance picks up, and the compressive strength becomes dominant. For pure shearing ($\alpha = 0$) in plane stress, the resisting shear stress is equal to $f_c/2$. Thus in order to minimize the internal work dissipated, concrete tends to fail in collapse cracks, or at least in yield lines with large normal components of the deformation rate. This entails dilation of the body, and the efficiency of reinforcing bars is not so much due to the directly carried applied load as to the resistance offered against the expansion of the deforming concrete.

Applications

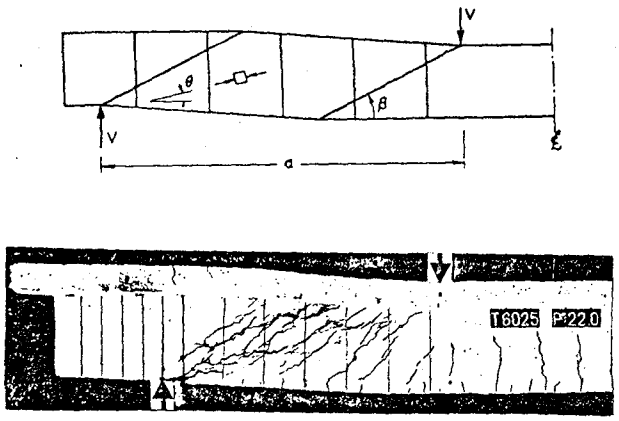

Fig. 4

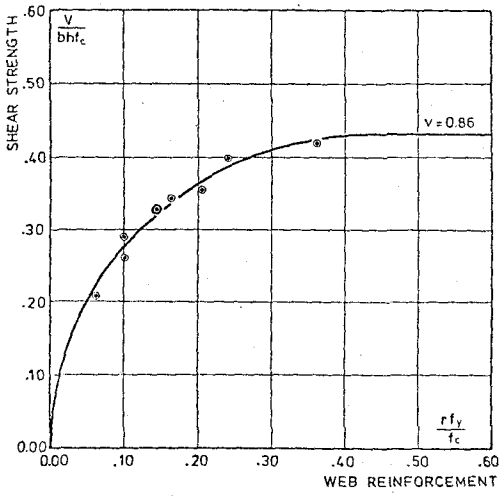

Fig. 5

Although the material model is quite primitive, it provides a decent description of concrete at ultimate. A particular important application is the shear failure of beams. Theoretical and observed failure mechanisms are shown in Fig. 4, and Fig. 5 compares the predicted relationship between the nominal ultimate shear stress and the degree of vertical stirrup reinforcement with the results of a test series. The shear failure is characterized by the fact that the deformations are constrained by the non-yielding longitudinal reinforcement, resulting in sliding failure of the concrete. The corresponding stress state is a diagonal compression field with a strut inclination θ which is half the yield line inclination β. The tensile concrete strength is neglected, which means that the concrete is potentially cracked in all sections. Under loading, cracks form perpendicular to the first principal direction of concrete stress, i.e. initially at an inclination of 45°. As the stirrups pick up load, the inclination of concrete compression - and cracking - decreases until it reaches the strut inclination $\theta = \beta/2$ at ultimate. The solution is easily extended to beams with inclined stirrups or distributed loading, and to beams with little or no stirrup reinforcement.

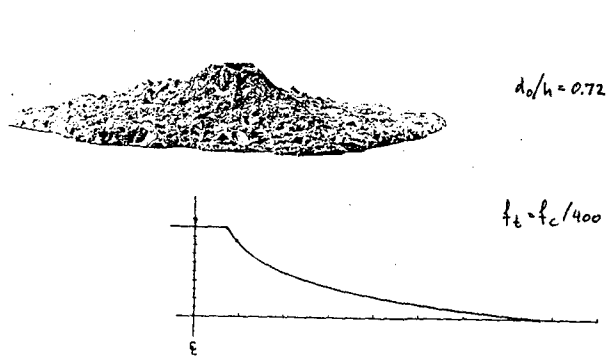

Fig. 6

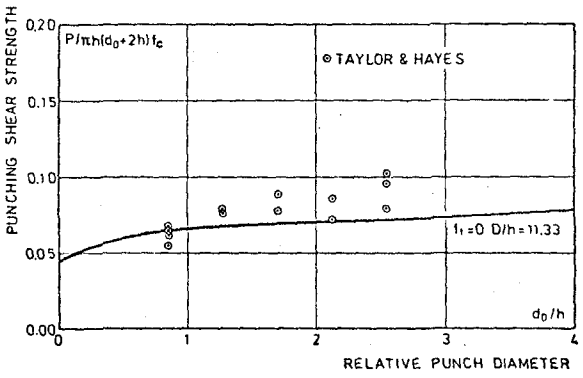

Fig. 7

Plane stress is assumed for shear in beams. The plane strain solution is topical for shear strength analysis of construction joints or cracks. A more demanding application of the model is the pull-out of embedded bolts. This has the appearance of a brittle phenomenon, and plastic analysis would not seem to be meaningful. Yet the upper bound technique yields a reasonable description of the shape of the failure surface, as seen in Fig. 6. The solution also applies to punching shear failure of slabs, and Fig. 7 shows the predicted strength compared with test results.

Other promising applications of the theory include anchorage and bond failure of reinforcing bars in concrete.

Discussion

It is not the intention to claim that concrete is a perfectly plastic material with an associated flow rule, but only to point out that the simple plastic model offers possibilities which are well worth exploring. The merits of the approach should then be judged by the agreement of predictions with reality. Minor objections may be raised concerning the shape of the failure envelope, which is not realistic for substantial hydrostatic compression. An attractive way of improving the model without introducing additional parameters would be to replace the straight line of Fig. 1 by a parabola (Fig. 8). With a zero tension cut-off, the plane stress solutions would be unaffected, whereas different - presumably more realistic - predictions would be obtained under conditions of plane or axisymmetric strain. So far, this approach has not been pursued further.

Fig. 8

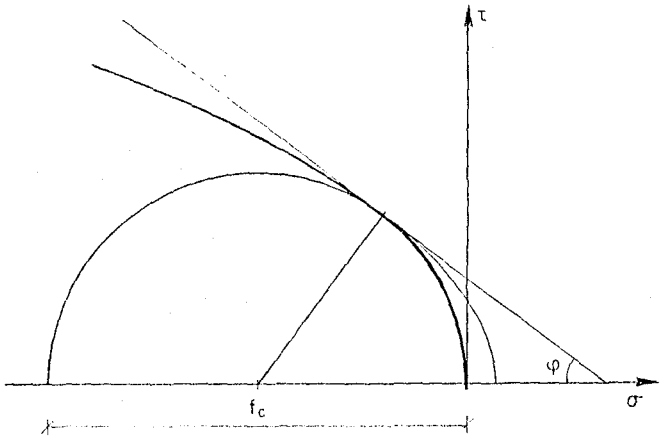

References

1. Nielsen, M.P. (1983), "Limit Analysis and Concrete Plasticity", Prentice-Hall (in press).
2. Braestrup, M.W., Nielsen, M.P. (1983), "Plastic Methods of Analysis and Design", Handbook of Structural Concrete, Ch. 20, Pitman/McGraw-Hill

3. Braestrup, M.W. (1981), "Structural Concrete as a Plastic Material, IABSE, Reports of the Working Commissions, 34, 3-16.
4. Braestrup, M.W. et al. (1978), "Plastic Analysis of Shear in Concrete", ZAMM, 58, 6, 3-14.
5. Nielsen, M.P. et al. (1978), "Concrete Plasticity. Beam Shear-Punching Shear - Shear in Joints", Danish Society for Structural Science and Engineering.